Springer Series in Advanced Manufacturing

R. Venkata Rao

Advanced Modeling and Optimization of Manufacturing Processes

International Research and Development

Springer

Springer Series in Advanced Manufacturing

For further volumes:
http://www.springer.com/series/7113

R. Venkata Rao

Advanced Modeling and Optimization of Manufacturing Processes

International Research and Development

Springer

Dr. R. Venkata Rao
Mechanical Engineering Department
S.V. National Institute of Technology
Ichchhanath, Surat
Gujarat 395 007, India
Tel.: +91-0261-2201697
e-mail: ravipudirao@gmail.com

ISSN 1860-5168

ISBN 978-0-85729-014-4 e-ISBN 978-0-85729-015-1

DOI 10.1007/978-0-85729-015-1

Springer London Dordrecht Heidelberg New York

British Library Cataloguing in Publication Data
A catalogue record for this book is available from the British Library

Library of Congress Control Number: 2010937562

Cover design: eStudio Calamar, Berlin/Figueres

Printed on acid-free paper

Springer is part of Springer Science+Business Media (www.springer.com)

Dedicated to my parents (*Lakshmi Narayana and Jayamma*), *dearest wife* (*Sujatha Rao*), *and beloved daughter* (*Jaya Lakshmi*)

Preface

Manufacturing includes various types of processes and today's manufacturing processes are caught between the growing needs for quality, high process safety, minimal manufacturing costs, and short manufacturing times. In order to meet the demands, manufacturing process setting parameters have to be chosen in the best possible way. The selection of optimum process parameters plays a significant role to ensure quality of product, to reduce the manufacturing cost and to increase productivity in computer controlled manufacturing process. For such optimization it is necessary to represent the manufacturing process in a model. However, the primary challenge for manufacturing process optimization often stems from the fact that the procedure is typically highly constrained and highly non-linear. Additionally, manufacturing process models are likely discontinuous, non-explicit, or not analytically differentiable with the design variables. Due to the enormous complexity of many manufacturing processes and the high number of influencing parameters, conventional approaches to modeling and optimization are no longer sufficient. Advanced modeling and optimization techniques are needed to be developed and used as modeling and optimization of manufacturing process is becoming increasingly important in industry in the drive towards 'agile manufacturing'.

The purpose of this book is to present a comprehensive review on latest research and development trends at international level for modeling and optimization of various manufacturing processes, particularly the machining processes which are the most frequently analyzed manufacturing processes. Using examples of various processes, the possibilities for process modeling and optimization with advanced modeling and optimization techniques are demonstrated. The book presents thorough literature of various manufacturing processes, mathematical models, traditional and non-traditional optimization techniques, real case studies, results of applications of the proposed methods, and highlights the best modeling and optimization strategies to achieve best process performance. The algorithms and computer codes for meta-heuristic optimization techniques included in the book will be very much useful to the readers.

The book is expected to be very useful to the designers and manufacturing engineers in the manufacturing sector who are responsible for the technical aspects of realizing a product as it presents new models and optimization techniques to make their tasks easier, logical, efficient and effective. The book is intended for designers, manufacturing engineers, practitioners, managers, institutes involved in design and manufacturing related projects, applied research workers, academics, and graduate students in mechanical, industrial, and manufacturing engineering.

I am grateful to Anthony Doyle and Claire Protherough of Springer-Verlag, London, for their support and help in producing this book. I wish to thank various researchers and the publishers of international journals for giving me the permission to reproduce certain portions of their published research works. I gratefully acknowledge the support of my research scholars Mr. P. J. Pawar, Mr. B. K. Patel, and Mr. V. K. Patel. My special thanks are due to the Director, Registrar (Mr H. A. Parmar) and my colleagues at S.V. National Institute of Technology.

While every attempt has been made to ensure that no errors (printing or otherwise) enter the book, the possibility of these creeping into the book is always there. I will be grateful to the readers if these errors are pointed out. Suggestions for further improvement of the book will be thankfully acknowledged.

Surat, June 2010 R. Venkata Rao

Contents

Chapter 1
Overview

1.1 Manufacturing Processes

Manufacturing is the backbone of any industrialized nation. Its importance is emphasized by the fact that, as an economic activity, it comprises approximately 20–30% of the value of all goods and services produced. A country's level of manufacturing activity is directly related to its economic health. In general, the higher the level of manufacturing activity in a country, the higher the standard of living of its people.

Manufacturing can be defined as the application of mechanical, physical, and chemical processes to convert the geometry, properties, and/or appearance of a given starting material to make finished parts or products. This effort includes all intermediate processes required for the production and integration of a product's components. The ability to produce this conversion efficiently determines the success of the company. The type of manufacturing performed by a company depends on the kinds of products it makes. Manufacturing is an important commercial activity carried out by the companies that sell products to customers. In the modern sense, manufacturing involves interrelated activities that include product design and documentation, material selection, process planning, production, quality assurance, management and marketing of products. These activities should be integrated for producing viable and competitive products.

The manufacturing processes of today have become extremely complex owing to the technological advances in last three decades. The status of the modern manufacturing processes is one of the extreme complexity and technological sophistication. The materials and processes first used to shape the products by casting and hammering have been gradually developed over the centuries, using new materials and more complex operations at the increasing rates of production and higher levels of quality.

The manufacturing processes can be classified into five main categories as follows:

R. V. Rao, *Advanced Modeling and Optimization of Manufacturing Processes*,
Springer Series in Advanced Manufacturing, DOI: 10.1007/978-0-85729-015-1_1,

1. Processes used to change the shape of the material: these processes apply mechanical force or heat or other forms and combinations of energy to effect a change in the geometry of the work material. These processes include casting, hot and cold forming (such as forging, extrusion, rolling, drawing, squeezing, roll forming, magnetic forming, electroforming, etc.), sheet metal working (such as piercing, bending, shearing, drawing, etc.), powder metal forming, plastic molding, etc.
2. Processes used for machining parts to fixed dimensions: these processes include traditional machining (such as turning, shaping, drilling, boring, reaming, broaching, milling, grinding, hobbing, lapping, honing, polishing, etc.) and non-traditional machining processes. According to nature of energy employed in machining, non-traditional machining processes are further classified into the following groups:
   - Mechanical processes like ultrasonic machining, abrasive jet machining, water jet machining, abrasive water jet machining, etc.
   - Chemical and electro chemical processes like electro chemical machining, electro chemical grinding, electro chemical honing, etc.
   - Thermal and electro thermal processes like electric discharge machining, laser beam machining, plasma arc machining, ion beam machining, etc.
   - Finishing processes like abrasive flow machining, magnetic abrasive finishing, etc.
3. Processes used for surface treatment: these processes include cleaning operations to remove dirt, oil, and other surface contaminants, surfacing operations such as shot peening, sand blasting, diffusion, ion transplantation, etc., coating operations such as electroplating, anodizing, etc., and thin film deposition processes such as physical vapor deposition, chemical vapor deposition, etc.
4. Processes used for joining the parts: products requiring the assembly of two or more parts are usually joined by the processes like welding, soldering, brazing, sintering, pressing, riveting, screw fastening, adhesive joining, etc.
5. Processes used to enhance the properties of work materials: There are various processes in which the physical and mechanical properties of the materials are changed by the application of an elevated temperature or by rapid or repeated stressing of the material. Processes by which the properties are changed include heat treatment operations such as annealing, normalizing, hardening, tempering, sintering, etc.

1.2 Need for Modeling and Optimization of Manufacturing Processes

Manufacturing includes various types of processes and today's manufacturing processes are caught between the growing needs for quality, high process safety,

minimal manufacturing costs, and short manufacturing times. In order to meet the demands, manufacturing process setting parameters have to be chosen in the best possible way. In today's manufacturing environment many large industries use highly automated and computer-controlled machines as their strategy to adapt to the ever-changing competitive market requirement. Due to high capital and manufacturing costs, there is an economic need to operate these machines as efficiently as possible in order to obtain the required pay back**.** The success of the manufacturing process depends upon the selection of appropriate process parameters. The selection of optimum process parameters plays a significant role to ensure quality of product, to reduce the manufacturing cost and to increase productivity in computer controlled manufacturing process. For example, in the case of milling operation the significant parameters that need to be optimized are cutting speed, radial and axial depths of cut, feed, and number of passes. In the case of ultrasonic machining operation, optimum selection of amplitude of vibration, frequency of vibration, mean diameter of abrasive grain, volumetric concentration of abrasive particles in slurry and static feed force significantly affect the material removal rate and surface quality. In the case of cold forging operation, optimum selection of parameters such as perform diameter, maximum number of forming operations, area reduction in each pass, the included angle in the extrusion and upset die significantly minimize the possibility of fracture. In the steady state problem of wire drawing and rolling, the optimal scheduling of passes is an important task. In deep drawing processes, the decision about the proper blank-holder force in order to avoid tearing and wrinkling forms an optimization problem.

Modeling and optimization of process parameters of any manufacturing process is usually a difficult task where the following aspects are required: knowledge of manufacturing process, empirical equations to develop realistic constrains, specification of machine capabilities, development of an effective optimization criterion, and knowledge of mathematical and numerical optimization techniques. A human process planner selects proper parameters using his own experience or from the handbooks. Performance of these processes, however, is affected by many factors and a single parameter change will influence the process in a complex way. Because of the many variables and the complex and stochastic nature of the process, achieving the optimal performance, even for a highly skilled operator is rarely possible. An effective way to solve this problem is to discover the relationship between the performance of the process and its controllable input parameters by modeling the process through suitable mathematical techniques and optimization using suitable optimization algorithm.

The first necessary step for process parameter optimization is to understand the principles governing the manufacturing process by developing an explicit mathematical model which may be mechanistic and empirical [1]. The model in which the functional relationship between input–output and in-process parameters is determined analytically is called mechanistic model. However, as there is lack of adequate and acceptable mechanistic models for manufacturing processes, the

empirical models are generally used in manufacturing processes. The modeling techniques of input–output and in-process parameter relationships are mainly based on statistical regression, fuzzy set theory, and artificial neural networks.

The optimization algorithms can be classified in two distinct types:

1. Traditional optimization algorithms: these are deterministic algorithms with specific rules for moving from one solution to the other. These algorithms have been in use for quite some time and have been successfully applied to many engineering design problems. The examples of these algorithms include non-linear programming, geometric programming, quadratic programming, dynamic programming, etc. However, the optimization problems related to manufacturing are usually complex in nature and characterized by mixed continuous–discrete variables and discontinuous and non-convex design spaces. Hence, the traditional optimization methods fail to give global optimum solution, as they are usually trapped at the local optimum. Also these techniques are usually slow in convergence. To overcome these problems, researchers have proposed non-traditional methods for optimization of process parameters of various manufacturing processes.
2. Non-traditional optimization algorithms: these algorithms are stochastic in nature, with probabilistic transition rules. These algorithms are comparatively new and gaining popularity due to certain properties, which the deterministic algorithms do not have. These methods are mainly based on biological, molecular, or neurological phenomenon that mimics the metaphor of natural biological evolution and/or the social behavior of species. To mimic the efficient behavior of these species, various researchers have developed computational systems that seek fast and robust solutions to complex optimization problems. Examples of these algorithms include simulated annealing (SA), genetic algorithm (GA), particle swarm optimization (PSO), artificial bee colony (ABC), shuffled frog leaping (SFL), harmony search (HS), etc.

1.3 Some Important Modeling and Optimization Techniques

1.3.1 Statistical Regression Technique

The data collected through experiments usually exhibits a significant degree of error or a "noise." In such a case, there is no need to intersect every point as the individual data points may be incorrect. Rather, the curve is designed to follow the pattern of points taken in group. This approach is known as statistical regression [2]. Regression is conceptually simple technique for investigating functional relationship between output and input decision variables of a process and may be useful for manufacturing process data description, parameter estimation and control.

The criteria for fitting the best line through the data in simple linear regression is to minimize the sum of squares of residuals (S_r) between the measured values of response and the values of response calculated with the regression model. The linear fit is expressed as:

$$Y = a_0 + a_1 X \tag{1.1}$$

where Y is the value of response and X is the value of variable. The coefficients a_0 and a_1 are obtained by differentiating "S_r" with respect to a_0 and a_1, respectively, and setting these derivatives equal to zero as the aim is to minimize the error. To test whether the data are well fitted in model or not, the values of standard error of estimates (S) of the regression analysis and the values of standard deviation are calculated (S_y) are determined as given by Eqs. 1.2 and 1.3, respectively.

$$\text{Standard error of estimate}(S) = (S_r/n-2)^{1/2} \tag{1.2}$$

where n = number of data points.

$$\text{Standard deviation, } \left(S_y\right) = (S_t/n-1)^{1/2} \tag{1.3}$$

where S_t = total sum of squares of the residuals between data points and the mean.

$S < S_y$ indicates that the regression model has merit. The actual extent of improvement, by using regression analysis rather than describing data as an average value, is quantified by coefficient of determination (R^2) which varies from 0 to 1. Value of $R^2 = 1$ indicates perfect fit and $R^2 = 0$ indicates no improvement.

Although linear regression provides a powerful technique for fitting the best line to data, it is predicted on the fact that the relation between the independent and dependant variables is linear. However, this is not true in many practical situations. If the data is ill suited for the linear regression, non-linear regression can be used. Various standard forms of non-linear relationships like exponential, power, saturation growth rate model, etc. can be linearized easily. In other cases either polynomial regression or Guass–Newton method can be used. Multiple linear regression is the useful extension of the linear regression when the response is a linear function of two or more independent variables which is the case in many practical applications.

Although statistical regression may work well for modeling, this technique may not describe precisely the underlying non-linear complex relationship between the decision variables and responses. A prior assumption regarding functional relationships (such as linear, quadratic, higher order polynomial, and exponential) between output and input decision variables is a prerequisite for regression equation based modeling. Prediction of outputs for an unknown set of inputs based on regression technique is valid only over the region of the regression variable contained in the observed data. It is only an aid to confirm the cause–effect relationship and does not imply a cause and effect relationship. Moreover, error components of regression equation need to be mutually independent, normally distributed having constant variance [2, 3].

1.3.2 Fuzzy Set Theory

The fuzzy set theory plays an important role in input–output and in-process parameter relationship modeling [4]. The theory on fuzzy set admits the existence of a type of uncertainty in process decision variables due to vagueness rather than due to randomness alone and many decisions in process control are in fuzzy environment [5]. Fuzzy set theory-based modeling is generally preferred when subjective knowledge or opinion of process experts plays a key role in defining objective functions and decision variables [6]. In order to fully capture the knowledge of the expert, a distribution (membership function) over the feasible interval of parameter needs to be specified. The closer the value of this membership function of a variable to 1, the more that variable belongs to the fuzzy set.

The conventional optimization methods deal with the selection of design variables that optimize an objective function subject to the satisfaction of the stated constraints. For a fuzzy system, this notion of optimization has to be revised. Since the objective and constraint functions are characterized by the membership functions in a fuzzy system, the decision can be viewed as an intersection of the fuzzy objective and constraint function [7].

The optimization problem of a fuzzy set is thus stated as follows:

$$\begin{aligned} &\text{Minimize } f(x) \\ &\quad \text{subject to: } g_j(x) \in G_j \quad j = 1, 2, \ldots\ldots, m. \end{aligned} \tag{1.4}$$

where m is the number of constraints, G_j denotes the fuzzy interval to which $g_j(x)$ belongs. The feasible region "S" which denotes the intersection of all G_j is defined by the membership function:

$$\mu_s(x) = \min\left\{\mu_{Gj}\left[g_j(x)\right]\right\} \tag{1.5}$$

Since the design vector is considered feasible when $\mu_s(x) > 0$, the optimum design is characterized by the maximum value of the intersection of the objective function and the feasible domain $\mu_D(x^*)$ as given by:

$$\mu_D(x^*) = \max\{\min(\mu f(x), \mu_s(x))\} \tag{1.6}$$

where x^* denotes the optimum level of parameter.

The fuzzy set-based techniques can be quite effective in converting subjective knowledge/opinion of the skilled operator into a mathematical framework [6]. In the literature, predominantly the fuzzy set theory has been used in three ways. In the first type of applications, fuzzy set theoretic operations help to arrive at certain decision. For example, if the membership grades of certain solutions in two conflicting objectives are known, then the optimum solution can be chosen as the one providing the highest membership grade in the intersection set of two objectives. The second type of application makes use of fuzzy arithmetic, which deals with fuzzy numbers. A fuzzy number is a generalization of an interval number, in which various intervals may have different membership grades. For example,

the most likely estimate of friction may be assigned a membership grade 1 and the lower and upper estimate may be assigned a membership grade 0.5. With these three points, a triangle can be constructed to represent friction as a fuzzy number. Fuzzy arithmetic computations are useful when the input parameter values, for example friction and material properties, are not known precisely. In the third type of application, fuzzy logic is used for making inferences based on the input values. The fuzzy set-based prediction system takes input data and carries out "fuzzification." In the fuzzification process, the input data undergo some translation in the form of linguistic terms such as "low feed," "average cutting speed," "high depth of cut," "very high cutting force," etc. The translated data are sent to an inference engine, which applies a set of predefined IF–THEN rules. The output of inference system in linguistic form will go through defuzzification process, which converts it to numerical data [8].

Fuzzy set theory-based modeling is thus a suitable technique for manufacturing problems when multiple quality characteristics exist and hierarchy of importance of each objective is not clearly defined. However, fuzzy set theory suffers from few shortcomings such as that the rules developed are based only on experts' knowledge and their prior experiences and opinions are not easily amenable to dynamic changes of underlying manufacturing process. It also does not provide any means of utilizing analytical models of manufacturing processes [9].

1.3.3 Artificial Neural Networks

Traditionally, the term neural network had been used to refer to a network or circuit of biological neurons. The modern usage of the term often refers to artificial neural networks, which are composed of artificial neurons or nodes. Artificial neural network is a powerful data modeling tool that is able to capture and represent complex input–output relationships. A primary motivation for study of neural networks was man learning from nature especially about how animal brains learn based on experience. Such learning is known to have features such as: robustness, gradual degrading failure rather than catastrophic failure, distributed intelligence, achievement of significant stability as well as plasticity in learning new things (without forgetting all the past things and yet perceiving newness and updating internal capture of knowledge).

Neural networks are composed of simple elements operating in parallel. These elements are inspired by biological nervous system. As in nature, the network function is determined largely by the connection between elements. Neural network can be trained to perform a particular function by adjusting the values of connections (weights) between elements. Commonly, neural networks are adjusted or trained so that a particular input leads to a specific target output. The network is adjusted based on a comparison of an output and the target until the network matches the target. Typically, many such input–target pairs are used in this supervised learning to train a network.

Neural networks are systems that can acquire, store, and utilize knowledge gained from experience. An artificial neural network (ANN) is capable of learning from an experimental data set to describe the nonlinear and interaction effects with great success. It consists of an input layer used to present data to the network, output layer to produce ANN's response, and one or more hidden layers in between. The input and output layers are exposed to the environment and hidden layers do not have any contact with the environment. ANNs are characterized by their topology, weight vectors, and activation function that are used in hidden and output layers of the network. A neural network is trained with a number of data and tested with other set of data to arrive at an optimum topology and weights. Once trained, the neural networks can be used for prediction [10].

The most commonly used neural network model is the multilayer perceptron (MLP). This type of neural network is known as a supervised network because it requires a desired output in order to learn. The goal of this type of network is to create a model that correctly maps the input to the output using historical data so that the model can then be used to produce the output when the desired output is unknown.

The back-propagation is a popular learning method of the multi-layered neural network. The forward path computing of the multi-layered neural network is performed with each layer fully connected to the next layer as shown in Fig. 1.1 for a maximum "p" layered network. The state vector $X(t) = [x_1(t), \ldots\ldots, x_{N(t)}(t)]^t$ for a particular layer "t" is formed from the input vector $Y(t-1) = [y_1(t-1), \ldots\ldots, y_{N(t-1)}(t-1)]^t$, that is output of the previous layer (layer $t-1$) of the network, by the following equation:

$$X(t) = W(t)Y(t-1) \text{ with } 1 \leq t \leq P \tag{1.7}$$

where $W(t) = [w_{ij}(t)]_{N(t)N(t-1)}$; $w_{ij}(t)$ is the weight between the ith neuron of layer t and the jth neuron of layer $t-1$; $N(t)$ and $N(t-1)$ are the number of neurons in layer t and $t-1$, respectively.

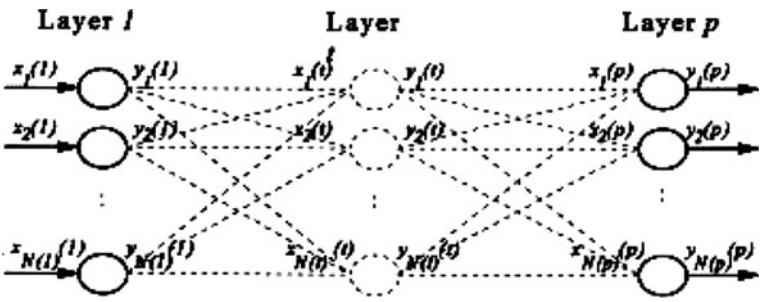

Fig. 1.1 Multi-layered feed-forward neural network (from [83]; reprinted with permission from Elsevier)

The output vector $Y(t-1)$ of layer $t-1$, i.e., the input vector of layer t is calculated by the following equation:

$$y_j(t-1) = f\left(x_j(t-1)\right) \text{ with } 1 \le j \le N(t-1) \tag{1.8}$$

where a typical form $f(\cdot)$ is the sigmoid activation function.

$$f\left(x_j(t-1)\right) = 1 \Big/ \left(1 + \mathrm{e}^{-xj(t-1)}\right) \tag{1.9}$$

To finish computation of the output of the feed-forward path, the back-propagation learning can be carried out using the so-called δ learning rule as follows:

$$\delta_j(t-1) = \left[1 - y_j(t-1)\right] y_j(t-1) \beta_j(t-1) \text{with } 1 \le j \le N(t-1) (\text{hidden layer}) \tag{1.10}$$

with

$$\beta(t-1) = W^{\mathrm{t}}(t)\delta(t) \tag{1.11}$$

where the superscript t denotes transposed matrix or vector with $\beta(t-1) = [\beta_1(t-1), \ldots \beta_{N(t-1)}(t-1)]^{\mathrm{t}}$, $\delta(t) = [\delta_1(t), \ldots \delta_{N(t)}(t)]^{\mathrm{t}}$ and

$$\delta_j(t) = (d_i(t) - y_i(t))(1 - y_i(t)) y_i(t) \text{ with } 1 \le i \le N(t) \text{ (output layer)} \tag{1.12}$$

where $d_i(t)$ is the teaching signal.

The weight $w_{ij}(t)$ is updated according the following equation:

$$\Delta w_{ij}(t) = \eta \delta_i(t) y_j(t-1) \text{ with } 1 \le i \le N(t);\ 1 \le j \le N(t-1) \tag{1.13}$$

where η is the learning rate.

The MLP and many other neural networks learn using back propagation algorithm. With back propagation, the input data is repeatedly presented to the neural network. With each presentation, the output of the neural network is compared to the desired output and an error is computed. This error is then fed back (back propagated) to the neural network and used to adjust the weights such that the error decreases with each iteration and the neural model gets closer and closer to producing the desired output. This process is known as "training."

The true power and advantage of using neural networks lies in their ability to represent both linear and non-linear relationships and in their ability to learn these relationships directly from the data being modeled. Traditional linear models are simply inadequate when it comes to modeling data that contains non-linear characteristics. The learning ability of non-linear relationship in manufacturing operations without going deep into the mathematical complexity, or prior assumptions on the functional forms of the relationship between inputs, in-process parameters and outputs, makes ANN an attractive alternative choice for many researchers to model various manufacturing processes. However, ANNs have the following limitations [3, 11]:

- Model parameters may be un-interpretable for non-linear relationship.
- It is dependent on voluminous data set, as sparse data relative to number of input and output variables may result in over fitting or terminate training before network error reaches optimal or near-optimal point.
- Identification of influential observations, outliers, and significance of various predictors may not be possible.
- There is always an uncertainty in finite convergence of algorithms used in ANN-based modeling technique, and generally convergence criteria are set based on prior experiences gained from earlier applications.
- No universal rules exist regarding choice of a particular ANN technique for any typical metal cutting process problem.

1.3.4 Gray Relational Analysis (GRA)

In real world problems the situation can never be perfectly black (with no information) or perfectly white (with complete information). Situations between these extremes are described as being gray, hazy, or fuzzy. Therefore, a gray system means that a system in which a part of information is known and a part of information is unknown [12, 13]. With this definition, information quantity and quality form a continuum from a total lack of information to complete information—from black through gray to white. Since uncertainty always exists, one is always somewhere in the middle, somewhere between the extremes, somewhere in the gray area. In the middle, gray systems will give a variety of available solutions. Gray relational analysis, based on this theory, can be further effectively adapted for solving the complicated interrelationships among the designated performance characteristics. Through this analysis, the gray relational grade is favorably defined as an indicator of multiple performance characteristics for evaluation. In recent years, the gray relational analysis has become the powerful tool to analyze the processes with multiple performance characteristics. It also provides an efficient solution to multi-input and discrete data problems. In gray relational analysis, the complex multiple response optimization problem can be simplified into a optimization of single response gray relational grade. The procedure for determining the gray relational grade is discussed below:

Step 1: Data pre-processing: if the number of experiments is "m" and the number of responses (i.e. performance characteristics) is "n," then the ith experiment can be expressed as $Y_i = (y_{i1}, y_{i2}, \ldots, y_{ij}, \ldots, y_{in})$ in decision matrix form, where y_{ij} is the performance value (or measure of performance) of response j ($j = 1, 2, 3, \ldots, n$) for experiment i ($i = 1, 2, 3, \ldots, m$). The general form of decision matrix D is given as,

$$D = \begin{bmatrix} y_{1l} & \cdots & y_{1j} & \cdots & y_{1n} \\ \cdots & \cdots & \cdots & \cdots & \cdots \\ y_{il} & \cdots & y_{ij} & \cdots & y_{in} \\ \cdots & \cdots & \cdots & \cdots & \cdots \\ y_{ml} & \cdots & y_{mj} & \cdots & y_{mn} \end{bmatrix} \tag{1.14}$$

The term Y_i can be translated into the comparability sequence $X_i = (x_{i1}, x_{i2}, \ldots, x_{ij}, \ldots, x_{in})$, where x_{ij} is the normalized value of y_{ij} for response j ($j = 1, 2, 3, \ldots, n$) of experiment i ($i = 1, 2, 3, \ldots, m$). After normalization, decision matrix D becomes normalization matrix D', is given as follows:

$$D = \begin{bmatrix} \mathrm{x}_{1l} & \cdots & x_{1j} & \cdots & x_{1n} \\ \cdots & \cdots & \cdots & \cdots & \cdots \\ x_{il} & \cdots & x_{ij} & \cdots & x_{in} \\ \cdots & \cdots & \cdots & \cdots & \cdots \\ x_{ml} & \cdots & x_{mj} & \cdots & x_{mn} \end{bmatrix} \tag{1.15}$$

The normalized values x_{ij} are determined by use of the Eqs. 1.16–1.18, which are for beneficial type, non-beneficial type and target value type responses, respectively. They are described as follows for $i = 1, 2, \ldots, m$ and $j = 1, 2, \ldots, n$:

1. If the expectancy of the response is larger-the-better (i.e. beneficial response), then it can be expressed by

$$x_{ij} = \left(y_{ij} - \min\left(y_{ij}\right)\right) / \left(\max\left(y_{ij}\right) - \min\left(y_{ij}\right)\right) \tag{1.16}$$

2. If the expectancy of the response is smaller-the-better (i.e. non-beneficial response), then it can be expressed by

$$x_{\mathrm{ij}} = \left(\max\left(y_{ij}\right) - y_{ij}\right) / \left(\max\left(y_{ij}\right) - \min\left(y_{ij}\right)\right) \tag{1.17}$$

3. If the expectancy of the response is nominal-the-best (i.e. closer to the desired value or target value), then it can be expressed by

$$x_{ij} = 1 - \left(\left|y_{ij} - y_j^*\right|\right) / \left(\max\left(\max\left(y_{ij}\right) - y_j^*, y_j^* - \min\left(y_{ij}\right)\right)\right) \tag{1.18}$$

where y_j^* is closer to the desired value of jth response.

Step 2: Reference sequence: in comparability sequence all performance values are scaled to [0, 1]. For a response j of experiment i, if the value x_{ij} which has been processed by data pre-processing procedure is equal to 1 or nearer to 1 than the value for any other experiment, then the performance of experiment i is considered as best for the response j. The reference sequence X_0 is defined as $(x_{01}, x_{02}, \ldots, x_{0j}, \ldots, x_{0n}) = (1, 1, \ldots, 1, \ldots, 1)$, where x_{0j} is the reference value for jth response and it aims to find the experiment whose comparability sequence is the closest to the reference sequence.

Step 3: Gray relational coefficient: gray relational coefficient is used for determining how close x_{ij} is to x_{0j}. The larger the grey relational coefficient, the closer x_{ij} and x_{0j} are. The gray relational coefficient can be calculated by Eq. 1.19.

$$\gamma\left(x_{0j}, x_{ij}\right) = \left(\Delta_{\min} + \xi\Delta_{\max}\right)/\left(\Delta_{ij} + \xi\Delta_{\max}\right) \quad \text{for } i = 1, 2, \ldots, m \text{ and } j = 1, 2, \ldots n \tag{1.19}$$

In Eq. 1.19, $\gamma(x_{0j}, x_{ij})$ is the gray relational coefficient between x_{ij} and x_{0j} and

$$\begin{aligned}
\Delta_{ij} &= \left|x_{0j} - x_{ij}\right|, \\
\Delta_{\min} &= \min\left\{\Delta_{ij}, i = 1, 2, \ldots, m; \quad j = 1, 2, \ldots, n\right\} \\
\Delta_{\max} &= \max\left\{\Delta_{ij}, i = 1, 2, \ldots, m; \quad j = 1, 2, \ldots, n\right\} \\
\xi &= \text{distinguishing coefficient}, \ \xi \in (0, 1]
\end{aligned}$$

Distinguishing coefficient (ξ) is also known as the index for distinguishability. The smaller ξ is, the higher is its distinguishability. It represents the equation's "contrast control." The purpose of ξ is to expand or compress the range of the grey relational coefficient. Different distinguishing coefficients may lead to different solution results. Decision makers should try several different distinguishing coefficients and analyze the impact on the GRA results [14].

Step 4: Gray relational grade: the measurement formula for quantification in gray relational space is called the gray relational grade. A gray relational grade (gray relational degree) is a weighted sum of the grey relational coefficients and it can be calculated using Eq. 1.20.

$$\Gamma(X_0, X_i) = \sum_{j=1}^{n} w_j \cdot \gamma\left(x_{0j}, x_{ij}\right) \quad \text{for } i = 1, 2, \ldots, m \tag{1.20}$$

where $\sum_{j=1}^{n} w_{jj} = 1$

In Eq. 1.20, $\Gamma(X_0, X_i)$ is the gray relational grade between comparability sequence X_i and reference sequence X_0. It represents the level of correlation between the reference sequence and the comparability sequence. w_j is the weight of response j and usually depends on decision makers' judgment. The gray relational grade indicates the degree of similarity between the comparability sequence and the reference sequence. If an experiment gets the highest gray relational grade with the reference sequence, it means that comparability sequence is most similar to the reference sequence and that experiment would be the best choice [15].

Several values of distinguishing coefficient can be considered to find the rankings of given experiments. Each distinguishing coefficient gives its own ranking. To get the final GRA ranking "Mode principle" can be applied, which considers the effect of all distinguishing coefficient values. The "Mode" is the

value that occurs most often. In "Mode principle," the experiment having mode number at rank 1 position is selected and given final GRA rank as 1. Similarly, the experiment having mode number at rank 2 position is selected and given final GRA rank as 2 and so on.

However, for solving the problems with multiple performance characteristics with gray relational analysis, the weighting values of the performance characteristics or responses while calculating the gray relational grade are determined based on subjective estimation. This approach may not reveal the relative importance for various performance characteristics. An analytic hierarchy process (AHP) method may be used for systematically deciding the weights of relative importance of the responses [16, 17]. Fuzzy logic can also be used to calculate the weighting values.

1.3.5 Taguchi Robust Design Method

Taguchi methods have been used widely in engineering analysis to optimize performance characteristics by means of settings of design parameters [18]. Taguchi method is a combination of mathematical and statistical techniques used in an empirical study. It is economical for characterizing a complicated process. It uses fewer experiments required in order to study all levels of all input parameters, and filters out some effects due to statistical variation. Taguchi method can also determine the experimental condition having the least variability as the optimum condition. The variability of a property is due to "noise factor," which is a factor difficult to control. On the contrary, the factor easy to control is called "control factor."

Taguchi robust design method is a strong tool for the design of high quality systems. To optimize designs for quality, performance, and cost, Taguchi robust design method presents a systematic approach that is simple and effective [19]. Taguchi method involves the stages of system design, parameters design, and tolerance design. System design involves the application of scientific and engineering knowledge required in manufacturing a product, parameter design is employed to find optimal process values for improving the quality characteristics, and tolerance design consists of determining and analyzing tolerances in the optimal settings recommended by parameter design [20].

Taguchi method of robust parameter design is an off-line statistical quality control technique in which the level of controllable factors or input process parameters are so chosen to nullify the variation in responses due to uncontrollable or noise factors such as humidity, vibration, and environmental temperature. The objective of Taguchi approach is to determine the optimum setting of process parameters or control factors, thereby making the process insensitive to the sources of variations due to uncontrollable or noise factors [21, 22]. In this method, main process parameters or control factors which influence process results are taken as input parameters and the experiment is performed as per specifically designed orthogonal array. The selection of appropriate orthogonal array is based on total degree of freedom (DOF) which is computed as,

$$\begin{aligned}\text{DOF} = {} & (\text{number of levels} - 1)\text{for each factor} + (\text{number of levels} - 1) \\ & \times (\text{number of levels} - 1)\text{for each interaction} + 1 \end{aligned} \tag{1.21}$$

The variability of the quality characteristic can be expressed by signal to noise (S/N) ratio. The terms "signal" and "noise" represent the desirable and undesirable values for the characteristic, respectively. Taguchi method uses the S/N ratio to measure the characteristic deviating from the desired value. The experimental condition having the maximum S/N ratio is considered as the optimal condition, as the variability of characteristic is in inverse proportion to the S/N ratio. The (S/N) ratio (η) represents the quality characteristic for the observed data in the Taguchi's design of experiments (DOE) and mathematically it can be computed as,

$$\eta = -10\log(\text{MSD}) \tag{1.22}$$

where MSD is the mean square deviation and commonly known as quality loss function. Depending on the experimental objective, the quality loss function can be of three types: lower-the-better (LB), higher-the-better (HB), and nominal-the-best (NB) type. These quality loss functions are computed as follows:

$$\text{MSD} = (1/\text{n})\sum_{\text{i}=1}^{\text{n}} \text{y}_\text{i}^2 \tag{1.23}$$

where y_i is the observed data of quality characteristic at the ith trial and n is the number of repetitions at the same trial. The S/N ratio represents the desired part/undesired part and aim is always to maximize the S/N ratio whatever be the nature of quality characteristics. From the S/N ratio, the effective parameters having influence on process results can be seen and the optimal sets of process parameters can be determined. In addition to the S/N ratio, a statistical analysis of variance (ANOVA) can be employed to indicate the impact of process parameters on surface roughness. In this way, the optimal levels of process parameters can be estimated.

Taguchi method is a widely accepted method of DOE. It has proved to be an effective methodology for producing high-quality products at relatively low cost. This approach has been applied successfully in many US, Japan, and European manufacturing firms, especially in automobile, electronics, food processing, and medical equipment industries. Taguchi method is also suitable for both continuous and discrete responses and is independent of intrinsic modeling approach. However, the orthogonal array design suggested by Taguchi is limited in number and may fail to adequately deal with many important interaction effects within the domain of the design proposed. Also Taguchi proposes a short term, one-time improvement technique to reduce the number and cost of experimentations, which may eventually lead to sub-optimal solutions. Taguchi method for multi-objective problems is purely based on judgmental and subjective process knowledge.

1.3.6 Taguchi Fuzzy-Based Approach

Taguchi fuzzy-based approach is the fuzzy logic analysis coupled with Taguchi methods for optimization in case of multiple performance characteristics. In Taguchi method, for single process response, the optimum level of the process parameters is the level having highest S/N ratio. However, optimization of multiple responses is not as straightforward as that of the optimization of a single process response. A higher S/N ratio for one process response may correspond to a lower S/N ratio for another process response. As a result, an overall evaluation of S/N ratios is required for the optimization of multi-process response. To solve this problem, fuzzy logic analysis is introduced into Taguchi method for optimization of multi process response. Fuzzy logic is used to develop the fuzzy reasoning of multiple performance characteristics. The loss function corresponding to each process response is fuzzified and then a single fuzzy reasoning grade is obtained by fuzzy inference and defuzzification. A fuzzy logic unit comprises of a fuzzifier, a membership function, a fuzzy rule base, an inference engine and a defuzzifier. First, the fuzzifier uses membership functions to fuzzify the signal to noise (S/N) ratios obtained by Taguchi method. Next, the inference engine performs the fuzzy reasoning on fuzzy rules to generate a fuzzy value. Finally, the defuzzifier converts the fuzzy value into a multi-response performance index. A fuzzy logic system is thus used to investigate relationships between responses for determining the efficiency of each parameter design of the Taguchi dynamic experiments. From the fuzzy inference process, the optimal process conditions can be easily determined.

1.3.7 Factorial Design Method

It is a method that researchers can use to design the experiments. An experiment using factorial design allows one to examine simultaneously the effects of multiple independent variables and their degree of interaction. In statistics, a full factorial design is a design of experiment consisting of two or more factors, each with discrete possible values or levels, and whose experimental units take on all possible combinations of all these levels across all such factors. Such an experiment allows studying the effect of each factor on the response variables, as well as the effect on interaction between factors on the response variable [23]. For majority of the experiments, each factor has only two levels. Such a design is called as 2^k design with k number of factors. A 2^2 design with two factors P and Q and having two levels -1 and $+1$ has four test conditions as shown in Table 1.1.

In Table 1.1, each test condition is given a coded value such that -1 is used when a factor is at its low value and $+1$ is used when a factor is at its high value. Such coded levels can be derived from the formula:

Table 1.1 A 2^2 full factorial design

Test	Coded test condition	
	P	*Q*
i	−1	−1
ii	1	−1
iii	−1	1
iv	1	1

$$\text{Coded test condition} = (\text{ATC} - \text{MTC})/((\text{range of test conditions})/2) \quad (1.24)$$

where ATC = actual test condition and MTC = mean test condition.

A full factorial experiment allows all factorial effects to be estimated independently and is commonly used in practice. However, it is often too costly to perform a full factorial experiment. For example, if we have 8 factors to investigate and each factor has two levels, we need to have $2^8 = 256$ runs. Instead, a fractional factorial design, which is a subset or fraction of a full factorial design, is often preferred because much fewer runs are required. The half fractional factorial design requires 2^{k-1} tests to be carried out. When this fraction is properly selected, the resulting design can estimate the maximum number of factorial effects of interest with maximum precision.

Factorial design can be used when there are more than two levels of each factor. However, the number of experiments required for such designs will be considerably greater than their two level counterparts. Factorial designs are therefore less attractive if a researcher wishes to consider more than two levels. A factorial experiment can be analyzed using ANOVA or regression analysis. Other useful exploratory analysis tools for factorial experiment includes main effects plots, interaction plots, and normal probability plots for the estimated effects. When the factors are continuous, two-level factorial design assumes that the effects are linear. If a quadratic effect is accepted for a factor, a more complicated experiment should be used such as central composite design. Optimization of factors that could have quadratic effects is the primary goal of response surface methodology.

1.3.8 Response Surface Methodology

Response surface methodology (RSM) is a collection of statistical and mathematical methods that are useful for the modeling and optimization of the engineering science problems. In this technique, the main objective is to optimize the responses that are influenced by various input process parameters. RSM also quantifies the relationship between the controllable input parameters and the obtained responses. In modeling and optimization of manufacturing processes using RSM, the sufficient data is collected through designed experimentation.

In general, a second-order regression model is developed because first-order models often give lack-of-fit [23]. According to RSM, all the input process parameters are assumed to be measurable and the corresponding responses can be expressed as follows:

$$y = f(x_1, x_2, \ldots, \mathrm{x}_k) + \varepsilon \tag{1.25}$$

where y is the response which is required to be optimized, f is the unknown function of response, x_1, x_2, …, x_k denote the independent parameters or variables, also called natural variables, k is the number of the independent variables and finally ε is the statistical error that represents other sources of variability not accounted for by f. These sources include the effects such as the measurement error. It is generally assumed that ε has a normal distribution with mean zero and variance [24].

It is possible to separate an optimization study using RSM into three stages. The first stage is the preliminary work in which the determination of the independent parameters and their levels are carried out. The second stage is the selection of the experimental design and the prediction and verification of the model equation. The last one is obtaining the response surface plot and contour plot of the response as a function of the independent parameters and determination of optimum points.

It is assumed that the independent variables (input process parameters) are continuous and controllable by experiments with negligible errors. It is also required to find a suitable approximation for the true functional relationship between independent variables and responses. Usually, a second-order regression model as given below is utilized in RSM.

$$y = b_0 + \sum_{i=1}^{k} b_i x_i + \sum_{i=1}^{k} b_{ii} x_i^2 + \sum_{j>1}^{k} b_{ii} x_i x_j \tag{1.26}$$

where "y" is the response and the x_i (1, 2, …, k) are the coded levels of k quantitative variables. The coefficient b_0 is the free term, the coefficients b_i are the linear terms, the coefficients b_{ii} are the quadratic terms, and the coefficients b_{ij} are the interaction terms. The equations relating the response with the variables are then derived by determining the values of the coefficients using the method of least squares (MLS). MLS is a multiple regression technique [25].

Response surface methodology (RSM) has several advantages compared to the classical experimental or optimization methods in which one variable at a time technique is used. First, RSM offers a large amount of information from a small number of experiments. Indeed, classical methods are time consuming and a large number of experiments are needed to explain the behavior of a system. Second, in RSM it is possible to observe the interaction effect of the independent parameters on the response. The model equation easily clarifies these effects for binary combination of the independent parameters. In addition, the empirical model that related the response to the independent variables is used to obtain information

about the process. With respect to these, it may be said that RSM is a useful tool for the optimization of manufacturing processes.

On the other hand, the major drawback of RSM is to fit the data to a second order polynomial. It cannot be said that all systems containing curvature are well accommodated by the second order polynomial. To overcome this, the data can be converted into another form that can be explained by the second order model. For example, logarithmic transformations and other linearization methods can be used for this purpose. Although these transformations may be useful, it is not possible to say that these transformations give desirable results for all systems. In addition, the transformation of response or inputs is time consuming and sometimes it is difficult to know which form of the transformation is the best. Alternatively, if the system is hardly explained by a second order model, one should choose a smaller range of independent parameters. It is possible to increase the accuracy of the model equation by working in a narrow range of independent parameter but it should be remembered that working in a narrow range reduce the possibility of determination of the stationary point. Preliminary work becomes more critical for the determination of the independent parameter range.

Response surface methodology (RSM) is unsuitable for solving highly nonlinear, multi-modal functions and also in case of multiple objectives [26]. Moreover, objective function needs to be continuously differentiable, which may not be the case in many complex physical processes.

1.3.9 Knowledge-Based Expert Systems

Knowledge-based expert systems (KBES) are computer programs embodying knowledge about a narrow domain for solving problems related to that domain. An expert system usually comprises two main elements, a knowledge base and an inference mechanism. The knowledge base contains domain knowledge which may be expressed as any combination of "IF–THEN" rules, factual statements, frames, objects, procedures, and cases. The inference mechanism is that part of an expert system that manipulates the stored knowledge to produce solutions to problems. A human expert uses knowledge and reasoning to arrive at conclusions, so does an expert system. The reasoning carried out in an expert system attempts to mimic human experts in combining pieces of knowledge. Thus, the structure or architecture of an expert system partially resembles how a human expert performs. Thus, there is an analogy between an expert and an expert system [27, 28].

Once the domain knowledge to be incorporated in an expert system has been extracted, the process of building the system is relatively simple. The ease with which expert systems can be developed has led to a large number of applications. The effect is to arrive at a solution to a given problem, as far as possible, the same reasoning process as that of human expert. The knowledge contained within the database of an expert system is normally elicited from various sources

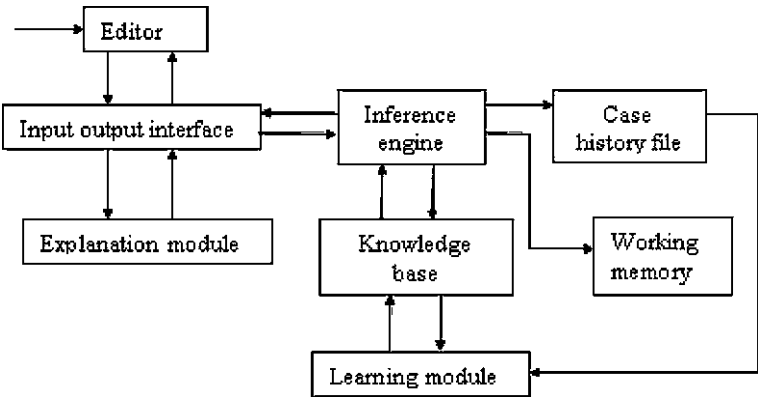

Fig. 1.2 Schematic of a typical rule based system

but is specific to the type of problem under investigation. In response to the interrogation by the user, the expert system must take the relevant information from its knowledge base and then by means of reasoning process (inference engine) produce an appropriate solution. A common form of architecture used in expert system is rule-base approach. A typical rule based system is shown in Fig. 1.2.

Using this approach, the decision to be made in arriving at the solution of a given problem is based on the set of IF–THEN rules which embody knowledge specific to the problem. Each rule represents a small element of a knowledge related to a given area of expertise. Collectively the number of related rules may correspond to the chain of inferences which lead from some initial known facts to some useful conclusions. These conclusions are reached by moving recursively through the rules either in a forward or backward direction. Typically, the inference process is carried out in an interactive mode.

The knowledge contained in the system has been compiled from two main sources: from human experts working in the field of manufacturing and from the technical documents, catalogues, or handbooks of various companies. The success of an expert system is hidden in its expandable structure like a human expert who adds every new solution he comes across to his knowledge and uses this knowledge in his future analyses. Since the system has a separate and modular knowledge base, it is very easy indeed to update the system by simply getting into the database and editing the knowledge files. The more information the system contains, the more problems it can handle. Knowledge base is the heart of the system, therefore it is the task of a few people who are responsible from the manufacturing to add, delete, or modify it. Editor allows the new problems, picture and information files related to the problems, causes and the remedies of the problems to be added to the knowledge base. Besides, it is possible to add new causes to the problems, or new remedies to the causes that already exist in the knowledge base.

In the development of an expert system a number of approaches can be used. One can adopt a high level artificial intelligence oriented language such as PROLOG, or LISP [29].

1.3.10 Principal Component Analysis (PCA)

Principal component analysis (PCA) involves a mathematical procedure that transforms a number of possibly correlated variables into a smaller number of uncorrelated variables called principal components. The first principal component accounts for as much of the variability in the data as possible, and each succeeding component accounts for as much of the remaining variability as possible. Depending on the field of application, it is also named the discrete Karhunen–Loève transform (KLT), the Hotelling transform or proper orthogonal decomposition (POD).

Principal component analysis (PCA) was introduced in 1901 by Pearson [30] and further developed by Hotelling [31]. Now it is mostly used as a tool in exploratory data analysis and for making predictive models. PCA involves the calculation of the eigenvalue decomposition of a data covariance matrix or singular value decomposition of a data matrix, usually after mean centering the data for each attribute. The results of a PCA are usually discussed in terms of component scores and loadings.

Principal component analysis (PCA) is a multivariate statistical method, which allows the representation of the original dataset in a new reference system characterized by new variables called principal components. Each principal component has the property of explaining the maximum possible amount of variance obtained in the original dataset. PCA can thus gather highly correlated independent variables into a principal component and all principal components are independent of each other. All it does is to transform a set of correlated variables to a set of uncorrelated principal components. A weighting factor for a principal component is determined based on its contribution percentage to total variance. Then, for multiple objectives the index can be formulated by integrating all principal components through the weighting methods. The procedure of PCA can be described as follows [32]:

1. The S/N ratios of each quality characteristic obtained from Taguchi Method are normalized as:

$$x_i^*(j) = \left(x_i(j) - x_i^-(j)\right) / \left(x_i^+(j) - x_i^-(j)\right) \tag{1.27}$$

where $x_i^*(j)$ is the normalized S/N ratio for jth quality characteristic in ith experimental run, $x_i(j)$ is the S/N ratio for jth quality characteristic in ith experimental run, $x_i^-(j)$ is the minimum and $x_i^+(j)$ is the maximum S/N ratio for jth quality characteristic in all experimental runs.

2. The normalized multi-response array for m experimental runs and n quality characteristics can be represented by matrix X^* as,

$$X^* = \begin{bmatrix} x_1^*(1) & x_1^*(2) & \dots & x_1^*(n) \\ x_2^*(1) & x_2^*(2) & \dots & x_2^*(n) \\ \dots\dots & \dots\dots & \dots & \dots\dots \\ \dots\dots & \dots\dots & \dots & \dots\dots \\ x_m^*(1) & x_m^*(2) & \dots & x_m^*(n) \end{bmatrix} \tag{1.28}$$

3. The correlation coefficient array (R_{jl}) of matrix D^* is evaluated as follows:

$$R_{jl} = \operatorname{cov}\left(x_i^*(j), x_i^*(1)\right) \Big/ \left(\sigma_{xi^*(j).}\sigma_{xi^*(l)}\right) \quad \text{for } j = 1, 2\ldots n;\ 1 = 1, 2\ldots, n \tag{1.29}$$

where cov ($xi^*(j)$, $xi^*(l)$) is the covariance of sequences $xi^*(j)$ and $xi^*(l)$, and $\sigma_{xi^*(l)}$ is the standard deviation of the sequence $xi^*(l)$.

4. The Eigen values and eigenvectors of matrix R_{jl} are calculated from the correlation coefficient array.

$$(R - \lambda_k \mathrm{I}_m)V_{ik} = 0 \tag{1.30}$$

where λ_k are the Eigen values, and

$$\sum_{k=1}^{n} \lambda_k = n \tag{1.31}$$

$V_{ik} = [a_{k1}, a_{k2}, \ldots, a_{kn}]^{\mathrm{T}}$ are the eigenvectors corresponding to the Eigen value λ_k.

5. The uncorrelated principal components are then computed as follows:

$$Y_{mk} = \sum_{i=1}^{n} x_m^*(i) \cdot V_{ik} \tag{1.32}$$

The principal components are created in order of decreasing variance, and therefore the first principal component, Y_{m1}, accounts for most variance in the data. The components with an Eigen value greater than one are chosen to replace the original responses for further analysis.

6. The coefficient of determination is calculated by the following equation:

$$C_k = \lambda_k / n, \quad \text{for } k = 1, 2, \ldots, n \tag{1.33}$$

The coefficient of determination, C_k, represents the weight of the principal component, P_{mk}.

Ding et al. [33] presented an adaptive kernel principal component analysis (AKPCA) method, which has the flexibility to accurately track the kernel principal components (KPC). First, KPC are recursively formulated to overcome the batch nature of standard kernel principal component analysis (KPCA). This formulation

is derived from the recursive Eigen decomposition of kernel covariance matrix and indicates the KPC variation caused by the new data. Second, kernel covariance matrix is correctly updated to adapt to the changing characteristics of data. In this adaptive method, the KPC is adaptively adjusted without re-Eigen decomposing the kernel Gram matrix. This method not only maintains constant update speed and memory usage as the data-size increases but also alleviates sub-optimality of the KPCA method for non-stationary data. The results demonstrated that this approach yields improvements in terms of both computational speed and approximation accuracy.

Sârbu and Pop [34] applied a fuzzy principal component analysis (FPCA) method for robust estimation of principal components. The efficiency of the new algorithm was illustrated on a data set concerning the quality of the Danube River. The FPCA method achieved better results mainly because it is more compressible than classical PCA, i.e., the first fuzzy principal component accounts for significantly more of the variance than their classical counterparts. These facts (greater accounting for total variance and shaper delineation of principal components) should encourage the application of fuzzy principal components analysis methodology to other areas. Using fuzzy principal component analysis, it is possible to explain some of the discrepancies, found in the literature, relating to multivariate analysis of data in terms of efficiency, goodness-of-fit, predictive power and robustness.

1.3.11 Mathematical Iterative Search Methods

Iterative search techniques may be described in terms of their structures, computational procedures, and important decision problems formulated as minimization or maximization of a mathematical function of several variables having a number of constraints. In these approaches, there is no need to construct an actual physical model of the manufacturing process under consideration, which is mostly replaced by an empirical mathematical model describing the actual process.

In any general linear programming (LP) optimization technique, both objective function and constraint equations are linear functions, and the most popular search algorithm in LP is simplex. As manufacturing process problems are mostly complex and non-linear in nature, LP techniques does not provide an adequate answer, or may not be appropriate for many such problems [3]. Multi-modal functions and consideration of multiple non-linear response functions justify the use of non-linear programming (NLP) solution techniques in this case. In any NLP manufacturing process optimization problem formulation, either the objective function(s) or at least one of the constraints is non-linear in nature, and a particular combination of process conditions is optimal, if and only if, all of Kuhn-Tucker conditions [35] with other convexity assumptions on response functions are satisfied. Some of the mathematical iterative search techniques are described below.

1.3.11.1 Dynamic Programming

In mathematics and computer science, dynamic programming is a method of solving complex problems by breaking them down into simpler steps. It is applicable to problems that exhibit the properties of overlapping sub-problems and optimal sub-structure. Top–down dynamic programming simply means storing the results of certain calculations, which are then re-used later because the same calculation is a sub-problem in a larger calculation. Bottom–up dynamic programming involves formulating a complex calculation as a recursive series of simpler calculations.

Dynamic programming developed by Bellman [36] is a well suited mathematical tool for optimization of multistage decision problems. The multistage decision problem is the one in which number of single stage processes are connected in series so that the output of one stage is the input of the succeeding stage. The multistage decision problems can be classified into three categories:

1. Initial value problem in which the initial state variable is prescribed.
2. Final value problem in which the final state variable is prescribed. However, the final value problem can be transformed into initial value problem by reversing the direction of state variables.
3. Boundary value problem in which the values of both input and output variables are specified.

The dynamic programming decomposes the multistage decision problem as a sequence of single stage problems. Thus, an N-variable problem is represented as a sequence of N single variable problems that are solved successively. These N sub-problems are obviously simpler to solve than original problem. The decomposition to N sub-problems is done in such a manner that the optimal solution of the original N-variable problem can be obtained from the optimal solution of N one-dimensional problems.

The procedural steps for solving a problem by dynamic programming can be summarized in the following manner:

Step 1: Identify the decision variables and specify objective function to be optimized under certain limitations, if any

Step 2: Divide the given problem into a number of smaller sub-problems or stages. Identify the state variables at each stage and write down the transformation function as a function of the state variables and decision variables at the next stage.

Step 3: Write down the general recursive relationship for computing the optimal policy. Decide whether top-down or bottom-up method is to follow to solve the problem.

Step 4: Construct appropriate stages to show the required values of the return function at each stage.

Step 5: Determine the overall optimal policy or decision and its value at each stage. There may be more than one such optimal policies.

For multistage decision problems, the dynamic programming is preferred over classical optimization techniques as classical optimization techniques can solve multistage decision problems only when:

1. The number of variables is very small.
2. The functions involved are continuous and continuously differentiable.
3. Optimum points are not lying on the boundary points.
4. The problem is relatively simple so that the set of resultant equations can be solved either analytically or numerically.

Dynamic programming on the other hand can deal with the discrete variables, non-convex, non-continuous, and non-differentiable functions. It can also take into account stochastic variability by a simple modification of the deterministic procedure. Dynamic programming thus can solve both continuous and discrete variables and yield a global optimal solution. The applications of dynamic programming for the solution of a linear programming problem has a serious limitation due to the dimensionality restrictions. The number of calculations needed will increase very rapidly as the number of decision variables and state parameters increases. However, despite these disadvantages, this technique is very suitable for the solution of a wide range of complex problems in several areas of decision making.

1.3.11.2 Goal Programming

Goal programming [37, 38] is one of the methods developed for solving multi-objective optimization problems. In this method, the designer sets the goal for each objective that must be achieved. The optimum solution is then defined as the one that minimizes the deviations from the set goals. Thus, the goal programming formulation of a multi-objective optimization problem leads to:

$$\text{Minimize:} \left(\sum_{J=1}^{k} \left(d_j^+ + d_j^- \right)^p \right)^{1/p}, \quad p \geq 1 \tag{1.34}$$

where k is the number of objectives, d_j^+ and d_j^- are the underachievement and overachievement of the jth objective. Value of p is based on utility function chosen by the designer.

$$\text{Subject to: } g_j(x) \leq 0 \quad j = 1, 2 \ldots, m \tag{1.35}$$

where $g_j(x)$ is the jth constraint expressed in terms of variables x, m is the number of constraints.

$$d_j^+ \geq 0, \quad j = 1, 2, \ldots, k \tag{1.36}$$

$$d_j^- \geq 0, \quad j = 1, 2, \ldots, k \tag{1.37}$$

$$d_j^+ d_j^- = 0, \quad j = 1, 2, \ldots, k \tag{1.38}$$

$$f_j(x) + d_j^+ - d_j^- = b_j, \quad j = 1, 2, \ldots, k \tag{1.39}$$

where $f_j(x)$ is the fitness value of the objective j, b_j is the goal set by the designer for the jth objective. The value of b_j for jth objective is obtained by obtaining the minimum function value of the particular objective while satisfying all constraints.

A goal programming model performs three types of analysis. First, it determines the input requirements to achieve a set of goals. Second, it determines the degree of attainment of the defined goals with given resources, and third, it provides the optimum solution under the varying inputs and goal structures. In sum total, the salient feature of goal programming is its capability to handle managerial problems that involve multiple incompatible goals according to their importance as fixed up by the management. The important advantage of goal programming is its flexibility, which allows model simulation with numerous variations of constraints and goal priorities. But it may be mentioned here that the limitations of linear programming technique in terms of assumptions, namely proportionality, additivity, and divisibility are attributable to goal programming also. However, there are non-linear goal programming problems reported in the literature.

1.3.11.3 GRG Method

Generalized reduced gradient (GRG) procedure is one of a class of techniques called reduced-gradient or gradient projection methods which are based on extending methods for linear constraints to apply to non-linear constraints. They adjust the variables so the active constraints continue to be satisfied as the procedure moves from one point to another. The ideas for these algorithms were devised by Wilde and Beightler [39] using the name of *constrained derivatives*, by Wolfe [40] using the name of the *reduced-gradient method* and extended by Abadie and Carpenter [41] using the name *generalized reduced gradient*. According to Avriel [42], if the economic model and constraints are linear this procedure is the Simplex Method of linear programming, and if no constraints are present it is gradient search. There are many possible GRG algorithms [43].

The GRG method has been proven to be a precise and accurate method for solving non-linear programming problems. The idea of GRG is to convert the constrained problem into an unconstrained one by using direct substitution. The various steps in this algorithm are discussed below:

Step 1: Choose the initial solution $x^{(0)}$. Set termination factor $\in$. Set t = 0. Transform all inequality constraints by adding slack variables.

Step 2: Calculate the factor $y_i^{(t)}$ for all variables $i = 1, 2 \ldots, n$ as follows:

$$y_i^{(t)} = \min\left\{\left(x_i^{(t)} - x_i^{(\mathrm{L})}\right), \left(x_i^{(\mathrm{U})} - x_i^{(t)}\right)\right\} \Big/ \left(x_i^{(\mathrm{U})} - x_i^{(\mathrm{L})}\right) \tag{1.40}$$

where $x_i^{(U)}$ and $x_i^{(L)}$ are the upper and lower bounds for the ith variable, respectively.

Step 3: Arrange $y_i^{(t)}$ in the descending order of magnitude. Choose first k variables as basic variables. Remaining $(n - k)$ are non-basic variables.

Step 4: Calculate the matrix A, which is $k \times k$ matrix of vector ∇a. The vector ∇a is calculated by differentiating the kth constraint with respect to the basic variables.

Step 5: Calculate the matrix B, which is $k \times (n - k)$ matrix of vector ∇b. The vector ∇b is calculated by differentiating the kth constraint with respect to the non-basic variables.

Step 6: Calculate the GRG ∇f as follows:

$$\nabla f = \nabla f_1 - \nabla f_2 A^{-1} B \tag{1.41}$$

where ∇f_1 is the part of gradient vector of the objective function that corresponds to non-basic variables evaluated at the point $x^{(t)}$. Similarly, ∇f_2 is the rest of the gradient vector of the objective function.

Step 7: Compute a feasible descent direction "d_1" by projecting ∇f on the feasible domain such that,

$$\begin{aligned} &\text{if } \nabla f \leq \in;\ \text{Terminate} \\ &\text{if otherwise, } d_1 = -\nabla f_1 \end{aligned} \tag{1.42}$$

$d_2 = -A^{-1} B d_1$; d_2 is the column vector.

$$\text{and } d = [\, d_1 \quad d_2 \,]^{\mathrm{T}} \tag{1.43}$$

Step 8: Find $\alpha^{(t)}$ such that $f(x^{(t)} + \alpha^{(t)} d)$ is minimum.Now update $x^{(t)}$ as,

$$x^{(t+1)} = x^{(t)} + \alpha^{(t)} d \tag{1.44}$$

Step 9: Go to Step 2.

The procedure is repeated until the termination criterion is met.

The main computational burden associated with the GRG algorithm arises from the Newton–Raphson iterations during line search. Strictly speaking, the gradients of constraints need to be recalculated and the Jacobian matrix B needs to be inverted at every NR iteration during the line search. This is prohibitively expensive. Another difficulty is to select a feasible starting point. Special algorithms must be used to handle arbitrary starting points.

1.3.11.4 Geometric Programming

Geometric programming developed by Duffin et al. [44] is an optimization technique applicable to solve non-linear models with a posynomial or signomial objective functions subject to constraints of same type. Posynomial functions are

the functions having positive coefficients and variables and real exponents. In the geometric programming method, the original optimization problem (supposedly in posynomial form) is known as primal problem. If the problem is not in posynomial form, variable substitution may be used to convert the original problem into a primal form. Thereafter, the primal problem is converted into an equivalent dual problem expressed in terms of set of dual variables. This transformation is achieved using arithmetic–geometric-mean equality principle. Once the optimal dual variables are found by solving the dual non-linear programming problem, the primal solution can be obtained by solving the set of simultaneous equations formed. The optimization method for this depends on the degree of difficulty.

The degree of difficulty (dd) is expressed as,

$$\mathrm{dd} = T - N - 1 \tag{1.45}$$

where T is the number of equations and N is number of unknown variables. If $\mathrm{dd} < 0$, a feasible solution may not exist as the number of equality constraints is more than the number of variables. If the solution exists, any T equality constraints can be used to find optimal solution. On the other hand if $\mathrm{dd} > 0$, number of constraints is less than the number of variables. Thus, some of the dual variables can be eliminated using the equality constraint. In such a case an optimization method known as GRG may be used to find the optimal dual variables. When $\mathrm{dd} = 0$, the simultaneous equations can be easily solved by Gauss-elimination method, as the number of equations is exactly equal to the number of unknowns.

Geometric programming method differs from other optimization technique in the emphasis it places on relative magnitude of the terms of the objective functions rather than variables. Instead of finding optimal values of design variables first, geometric programming first finds the optimal of objective function. This feature is especially advantageous in situations where the optimal value is of only interest. This eliminates the need of calculation of optimum design vectors. Another advantage of geometric programming is that it often reduces the complicated optimization problem to one involving the set of simultaneous liner algebraic equations. GP inherits some drawbacks. However, the main disadvantages of GP lie in the fact that it requires the objective functions and constraints in the form of posynomials/signomials.

1.3.11.5 Quadratic Programming

The quadratic programming problem has a quadratic objective function and linear constraints and is convex. Hence the quadratic programming problem can be solved by suitably modifying the linear programming technique. Sequential quadratic programming method developed by Schittkowski [45] is widely used method in manufacturing optimization as this optimization method has been considered to be an excellent approach for handling constrained optimization problems.

The basic concept of sequential quadratic programming is quite simple. The approximation function, instead of the original non-linear function, is used for optimization. First, a second order Taylor series approximation of the objective function and constraints functions with respect to the design variables (x_i, $I = 1$, 2 …, n) is constructed. The search direction vector "S" for optimization can be determined by the matrix of the second derivatives of the approximation function. Once the search direction vector "S" is chosen, an optimal scalar step length parameter α is calculated through the quadratic interpolation. Therefore, the design vector x_{k+1} during iteration can be expressed as:

$$x_{k+1} = x_k + \alpha_k S \tag{1.46}$$

where k is the iteration number.

In other words, the sequential quadratic programming method consists of three main stages, i.e.:

1. Find the search direction vector "S,"
2. Find the scalar step length parameter "α," and
3. Test for convergence to the optimum and terminate if convergence is achieved.

The main limitation of quadratic programming is that the convergence to an optimal solution depends on the chosen initial solution. Also the algorithm tends to get stuck to the local optimal solution.

1.3.11.6 Integer Linear Programming

Integer programming is used in problems where optimal solution is sought in terms of integral values of variables as non-integral answers not being meaningful in the context of situation which gives rise to the problem (e.g., finding optimum number of teeth on gears). Conventionally, integer linear problems can be solved by cutting plane method and branch and bound method. However, as the cutting plane method has a serious drawback of round-off error which arise during numerical computations, branch and bound method has been widely used in practical applications.

The branch and bound method is very effective in solving the mixed-integer linear and non-linear programming problems. The method was originally developed by Land and Doig [46] to solve integer linear programming problems and was later modified by Dakin [47]. In branch and bound method, the integer problem is not directly solved. Rather, the method first solves the continuous problem obtained by relaxing the integer restrictions on the variables. If the solution to the continuous problem happens to be an integer solution, it represents the optimum solution of integer problem. Otherwise at least one of the integer variable, x_i, must assume a non-integral value. If "x_i" is not an integer, we can always find an integer $[x_i]$ such that $[x_i] < x_i < [x_i] + 1$. The two sub-problems are formulated, one with additional upper bound constraint and another with the lower bound constraint. The process of finding these sub-problems is called "branching."

The branching process eliminates some portion of the continuous space that is feasible for integer problem while ensuring that none of the integer feasible solutions are eliminated. Each of these two sub-problems is solved again as a continuous problem.

The process of branching and solving the sequence of continuous problems is continued until an integer feasible solution is found for one of the two continuous problems. When such integer feasible solution is found, the corresponding value of objective function becomes an upper bound on the minimum value of the objective function. At this stage we can eliminate from further considerations all continuous solutions whose objective function values are larger than the upper bound. The solutions which are eliminated are said to have been fathomed because it is not possible to find a better integer solution from these solution spaces than what we have now. The value of upper bound on the objective function is updated whenever the better bound is obtained. The algorithm continues to select solution for further branching until all the solutions are fathomed. At that stage, the particular fathomed solution that has the integer feasible solution with the lowest value of objective function gives the optimum solution of the original linear integer programming problem.

Branch and bound algorithms can be (and often are) slow, however. In the worst case they require effort that grows exponentially with problem size, but in some cases the methods converge with much less effort.

1.3.12 Meta-Heuristics

1.3.12.1 Genetic Algorithms

Genetic algorithms (GAs) are search algorithms based on mechanics of the natural selection and the natural genetics [48]. GA exploits the idea of the survival of the fittest and the interbreeding population to create a novel and innovative search strategy. A population of the strings representing solution to the specified problem are maintained by GA, which then iteratively creates the new population from the old by ranking the strings and interbreeding the fittest to create the new strings, which are closer to the optimum solution to a specified problem.

Genetic algorithms (GAs) is very appealing for single and multi-objective optimization problems [49], and some of its advantages are given below:

- As it is not based on gradient-based information, it does not require the continuity or convexity of the design space.
- It can explore large search space and its search direction or transition rule is probabilistic, not deterministic, in nature, and hence, the chance of avoiding local optimality is more.
- It works with a population of solution points rather than a single solution point as in conventional techniques, and provides multiple near-optimal solutions.

- It has the ability to solve convex, and multi-modal function, multiple objectives and non-linear response function problems, and it may be applied to both discrete and continuous objective functions.

The three basic operators in the GA, i.e., reproduction, crossover, and mutation are discussed below.

Reproduction

The reproduction operator allows individual strings to be copied for possible inclusion in the next generation. The chance that a string will be copied is based on the strings fitness value. The different types of reproduction operators include proportional selection, tournament selection, truncation selection, linear ranking selection, and exponential ranking selection. The selection of the particular scheme depends on the problem domain being explored.

Crossover

Crossover refers to the blending of chromosomes from the parents to produce new chromosomes for the offspring. The GA selects two strings at a random from the mating pool. It is then decided whether to crossover using a parameter called crossover probability. If the crossover takes place then a random slicing point is chosen in the string. The sliced regions are then mixed to create two new strings.

Mutation

Although crossover can generate a staggering amount of different strings, there may not be enough variety of stings to ensure that the entire problem is covered. This may lead to converging on strings that are not quite close to the optimum it seeks. To overcome this problem a mutation operator is introduced into a GA. For each string element in each string in the mating pool the algorithm checks to see if it should perform mutation or not. If it should then the string element is flipped (in case of binary strings). The mutation thus helps to prevent the population from stagnation and maintains the diversity throughout the iterations. However, the mutation probability should be kept very low as a high mutation rate will destroy fit strings and degenerate the algorithm into a random walk.

The operation of a basic GA is shown in Fig. 1.3.

The performance of the GA thus mainly depends on population size, number of generations, crossover rate, and mutation rate. GAs are preferred when near optimal improved conditions are acceptable for implementation by the manufacturer instead of costly exact optimum solution. It is a derivative free approach for

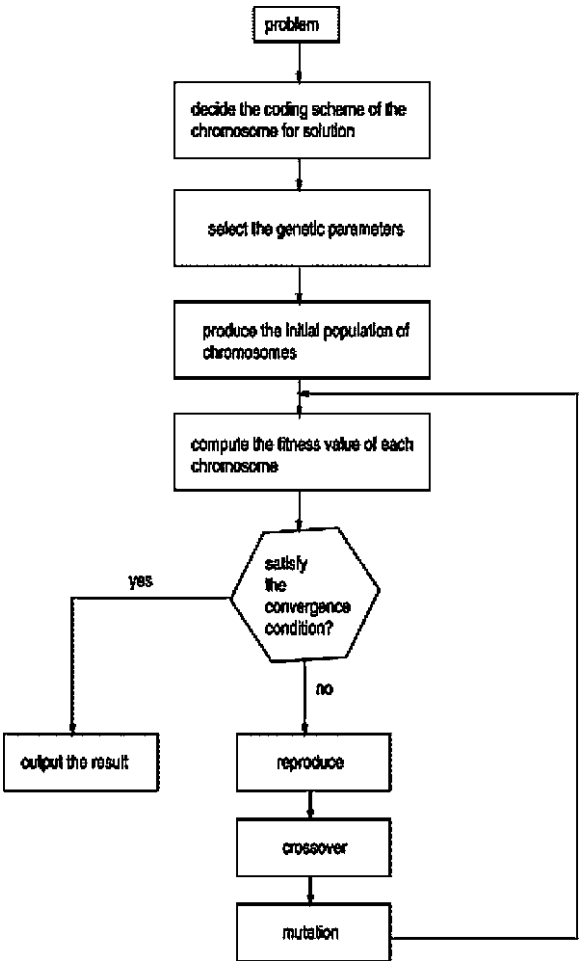

Fig. 1.3 Operation of basic genetic algorithm (from [84]; reprinted with permission from Elsevier)

near optimal points search direction and may be applied to continuous or discrete response function.

Although GA has advantages over the traditional techniques, it has following limitations:

- All offsprings are accepted and their parent strings are abandoned at the end of every generation regardless of their fitness values. This gives rise to a risk that a good parent string may be replaced with its deteriorated child string. Thus, the improvement on the average performance of child population over parent population cannot be always guaranteed.
- Only good parent strings are given chance to produce offspring without any consideration of the possibilities of generating better offspring by others.
- Not efficient when convergence speed is taken into consideration.
- No guarantee of optimal solution.

To overcome the above limitations, the basic GA is modified to give rise to few more algorithms like non-dominated sorting GA [49], differential evolution approach (DE), memetic algorithm (MA), etc.

1.3.12.2 Simulated Annealing

The SA algorithm developed by Kirkpatrick et al. [50] resembles the cooling process of molten metals through annealing. At high temperatures, the atoms in the molten metal can move freely with respect to each another, but as the temperature is reduced, the movement of the atoms gets restricted. The atoms start to get ordered and finally form crystals having the minimum possible energy. However, the formation of crystal mostly depends on the cooling rates. If the temperature is reduced at very fast rates, the crystalline state may not be achieved at all; instead, the system may end up in polycrystalline states, which may have a higher energy state than the crystalline state. Therefore, in order to achieve the absolute minimum energy state, the temperature needs to be reduced at a slower rate.

The SA algorithm simulates this process of slow cooling of molten metal to achieve the minimum function value in the minimization problem. The cooling phenomenon is simulated by controlling a temperature like parameter introduced with the concept of Boltzman probability distribution. According to Boltzman probability distribution, a system in a thermal equilibrium at a temperature "T" has its energy distributed probabilistically according to the following expression:

$$P(E) = \exp(-E/KT) \tag{1.47}$$

where "K" is Boltzman constant. This expression suggests that a system at high a temperature has almost uniform probability of being at any energy state. Therefore, by controlling the temperature, "T," and assuming that the search process follows Boltzman probability distribution, the convergence of an algorithm can be controlled. At any current point, $X(t)$, the new value of the variables for the successive iterations is calculated using the formula,

$$X(t+1) = X(t) + \sigma\left(\sum_{i=1}^{N} R_{\mathrm{i}} - 0.5N\right) \tag{1.48}$$

where $\sigma = (X_{\max} - \mathrm{X}_{\min})/6$, R is random number and N is number of random numbers used.

Using the Metropolis algorithm [51], the probability of the next point being accepted at $X(t + 1)$ depends on the difference in the function value at these two points or on $\Delta E = E(t + 1) - E(t)$ and is calculated using the Boltzman probability distribution:

$$P(E(t+1)) = \min(1, \exp(-\Delta E/KT)) \tag{1.49}$$

If $\Delta E \leq 0$, this probability is one and the new configuration is always accepted. In the function minimization context, this makes sense because if the functional value at new configuration is better than the old one, the point new configuration must be accepted. The interesting situation happens when ΔE is bigger than zero, which implies that the function value at new configuration is worst than at previous configuration. According to many traditional algorithms, the point should not be chosen. According to the Metropolis algorithm, there is some finite probability of selecting the new configuration even though it is worst than the previous one. However, the probability is not same in all situations. This probability depends on the magnitude of ΔT and T values.

If the parameter T is large, this probability is more or less high for points with largely disparate functional values. Thus, any point is almost acceptable for a large value of T. On the other hand, if the parameter T is small, then the probability of accepting an arbitrary point is small. Thus, for small values of T, the points with only small deviation in the function values are accepted [52].

Simulated annealing (SA) is a point-by-point method. The algorithm begins with an initial point and a high temperature T. A second point is created at random in the vicinity of the initial point and the difference in the function values, ΔE, at these two points is calculated. If the second point has a smaller function value, the point is accepted, otherwise the point is accepted with the probability of exp $(-\Delta E/KT)$. This completes an iteration of this SA procedure. In the next generation, another point is created at random in the neighborhood of the current point and the Metropolis algorithm is used to accept or reject the point. In order to simulate the thermal equilibrium, at every temperature the number of points (n) are usually tested at a particular temperature, before reducing the temperature. The algorithm is terminated when a sufficiently small temperature is obtained or a small enough change in function value is found. An estimate of the initial temperature can be obtained by calculating the average of the function values at a number of random points in the search space. A suitable value of "n" can be chosen (usually between 2 and 100) depending on the available computational resource and the solution time. Decrement factor is left to the choice of the user. The flowchart for SA algorithm is shown in Fig. 1.4. In this figure, Ts corresponds to starting temperature, C_T corresponds to the decrement factor, X corresponds to $X(t)$, Xn corresponds to $X(t + 1)$, Δobj corresponds to ΔE, and Te corresponds to the termination criterion.

Some of the features of the SA algorithm are given below:

- Because of the discrete nature of the function and construction evaluations, the convergence or transition characteristics are not affected by the continuity of differentiability of the function.
- The convergence is also not influenced by the convexity status of the feasible space.
- The design variables need not to be positive.
- The method can be used to solve mixed-integer, discrete, or continuous problems.

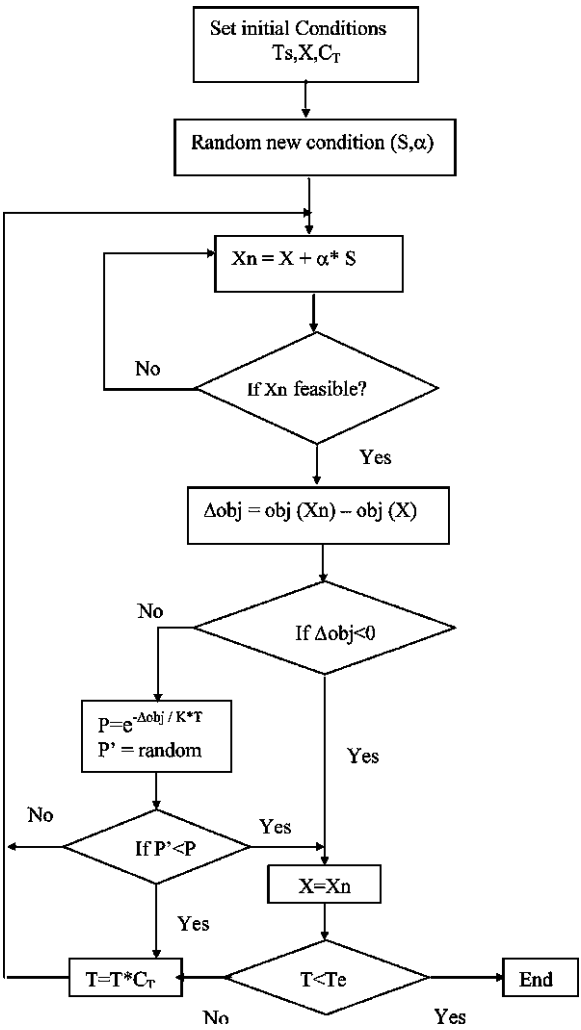

Fig. 1.4 Flow chart of simulated annealing algorithm

- Not all combinational optimization problems can be annealed to given satisfactory solutions (e.g., the time taken to get a decent answer may prove to be unreasonable).

1.3.12.3 Tabu Search

Tabu search [53] is a generalized, problem independent, easy to implement technique that may be applied virtually to any kind of process optimization model.

It is a derivative free approach and may be applied to multi-minima (or maxima), linear (or non-linear), and discrete (or continuous) response function.

Tabu search is an extension of classical local search method. A local search method is an iterative search procedure that, starting from an initial feasible solution progressively improves it by applying series of local moves. However, the local search technique encounters a local optimum and is time consuming. To overcome this limitation, tabu search not only keeps the track of local information (like the current value of the objective function) but also information related to the exploration process which guides to select the subset of best solutions in the neighborhood. To escape from a local minimum, iterative exploration process in some instances accepts the non-improving moves also. As soon as non-improving are possible, the risk of visiting again a solution (referred as cycling) is present. To prevent cycling, tabus are used. Tabus are stored in the short term memory of search called tabu list. When a best vector is determined from the sample of decision vectors in the neighborhood of the current decision vector, a move is made from current decision vector to the best decision vector not in the tabu list. The tabu list contains a certain number of last decision vectors visited. The best decision vector replaces the oldest vector in the tabu list and the survival vectors in the list are given tabu active status. Tabu active vectors are forbidden to create the sample of decision vectors in the neighborhood. The tabu active status of a decision vector can be overridden only based on certain aspiration level criteria. Length of the tabu list is an important decision. If the length of the list is too small then its role to prevent cycling might not be achieved. Conversely, too long size creates too many restrictions to the search process and may lead to significantly longer computational time.

In a search process, it is sometimes fruitful to intensify the search in some region as it may contain some acceptable solution. Such intensification can be carried out by giving high priority to the solutions which have common features with the current solution. This can be done with the introduction of an additional term in the objective function which will penalize the solutions far from the present one. As against intensification, sometimes diversification is essential to avoid a large region of state space graph remains completely unexplored. This can be achieved by penalizing the performed moves or solutions often visited. The penalty is set large enough to ensure the escape from the current region. It is also possible to use penalty on frequently performed moves during the whole search procedure. The algorithm is terminated after some number of iterations without any improvement in the objective function value or when objective reaches a prespecified threshold value.

The convergence of algorithm for multi-modal objective function in a finite number of steps, however, is not guaranteed like other meta-heuristics. The choice of tabu list size always influences the end solution of the problem. Also with tabu search, complexity is not only present in the problems but in the technique itself.

1.3.12.4 Particle Swarm Optimization

Particle swarm optimization (PSO) is an evolutionary computation technique developed by Kennedy and Eberhart [54]. It exhibits common evolutionary computation attributes as given below:

- It is initialized with a population of random solutions,
- It searches for optima by updating generations, and
- Potential solutions, called particles, are then "flown" through the problem space by following the current optimum particles.

The particle swarm concept was originated as a simulation of a simplified social system. The original intent was to graphically simulate the graceful but unpredictable choreography of a bird flock. Each particle keeps track of its coordinates in the problem space, which are associated with the best solution (fitness) it has achieved so far. This value is called "pBest." Another "best" value that is tracked by the global version of the PSO is the overall best value, and its location obtained so far by any particle in the population. This location is called "gBest." The PSO concept consists of, at each step, changing the velocity (accelerating) each particle toward its "pBest" and "gBest" locations (global version of PSO). Acceleration is weighted by a random term, with separate random numbers being generated for acceleration toward "pBest" and "gBest" locations. The updates of the particles are accomplished according to the Eqs. 1.50 and 1.51. Equation 1.50 calculates a new velocity for each particle (potential solution) based on its previous velocity the best location it has achieved ("pBest") so far, and the global best location ("gBest") the population has achieved. Equation 1.51 updates individual particle's position (X_i) in solution hyperspace. The two random numbers "r_1" and "r_2" in Eq. 1.50 are independently generated in the range [0,1].

$$V_{i+1} = w^* V_i + c_1^* r_1^* (\text{pBest}_i - X_i) + c_2^* r_2^* (\text{gBest}_i - X_i) \tag{1.50}$$

$$X_{i+1} = X_i + V_{i+1} \tag{1.51}$$

The acceleration constants "c_1" and "c_2" in Eq. 1.50 represent the weighting of the stochastic acceleration terms that pull each particle towards "pBest" and "gBest" positions. "c_1" represents the confidence the particle has in itself (cognitive parameter) and "c_2" represents the confidence the particle has in swarm (social parameter). Thus, adjustment of these constants changes the amount of tension in the system. Low values of them allow particles to roam far from target regions before being tugged back, while high value results in abrupt movement toward, or past through target regions [55]. The inertia weight "w" plays an important role in the PSO convergence behavior since it is employed to control the exploration abilities of the swarm. While the large inertia weights allow wide velocity updates allowing to globally explore the design space, the small inertia weights concentrate the velocity updates to nearby regions of the design space. The optimum use of the inertia weight "w" provides improved performance in a number of applications [56].

Particle's velocities on each dimension are confined to a maximum velocity, V_{max}, which is a parameter, specified by the user. If the sum of accelerations would cause the velocity on that dimension to exceed V_{max}, then the velocity on that dimension is limited to V_{max}. Although the heuristics are developed to determine the inertia weights and acceleration constants for guaranteed convergent trajectories, it is mainly applicable to single objective optimization. It is very difficult to obtain the values of inertia weights and acceleration constants for multi-objective optimization problems, due to inherent conflicting nature of objectives to be optimized. To overcome this problem, a time variant PSO was described by Tripathi et al. [57]. The algorithm is made adaptive in nature by allowing its vital parameters, i.e., inertia weights and acceleration constants to change with iterations. This adaptiveness helps the algorithm to explore the search space more efficiently. A mutation operator is also included to overcome the premature convergence. The performance of the algorithm is then measured with respect to four main performance measures, i.e., convergence rate, diversity, purity, and minimal spacing. The flow chart of PSO algorithm is shown in Fig. 1.5.

As both the GA and PSO are evolutionary algorithms, they share some common features as given below:

- Both algorithms start with randomly generated population.
- Both algorithms evaluate the population with fitness value.

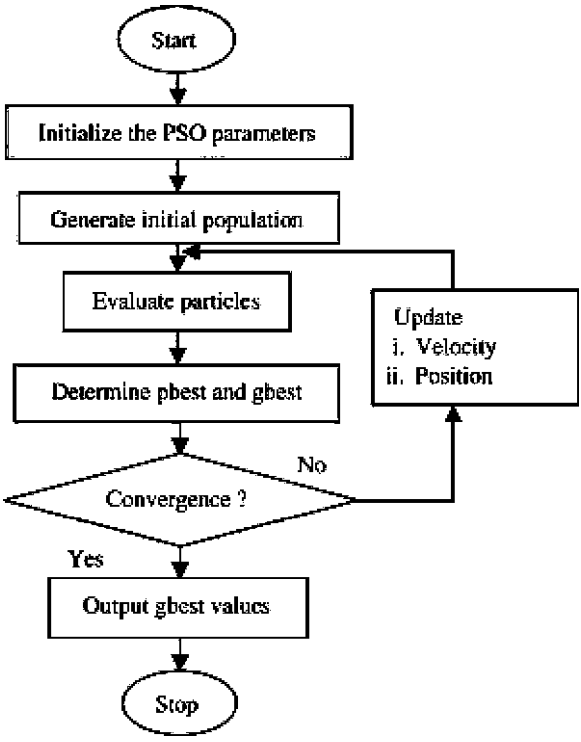

Fig. 1.5 General flow chart of PSO algorithm (from [85]; reprinted with permission from Elsevier)

- Both algorithms update the position and search with random techniques.
- Both algorithms do not guarantee optimal solution.

However, the PSO algorithm differs from GA with respect to the following points:

- Unlike GA, PSO does not need complex encoding and decoding process and special genetic operator. It takes real number as a particle in the aspect of representation solution.
- PSO does not need genetic operators like cross over and mutation. The particles update themselves with internal velocity. However, modified versions of PSO uses mutation operator to avoid the premature convergence.
- The information sharing mechanism is totally different. In GA the chromosomes share information with each other and hence the whole population moves like a one group towards an optimal area. In PSO, only "gBest" gives out information to the other. Hence it is a one-way information sharing mechanism. The evolution looks only for the best solution.
- All particles tend to converge to the best solution.
- In PSO, it is difficult to keep the diversity of the population. The search rates are relatively low and hence it may require more computation time while solving the complex optimization problem.

1.3.12.5 Ant Colony Optimization

Similar to PSO, ant-colony optimization (ACO) algorithms evolve not in their genetics but in their social behavior. ACO was developed by Dorigo et al. [58] based on the fact that ants are able to find the shortest route between their nest and a source of food. This is done using pheromone trails which ants deposit whenever they travel as a form of indirect communication.

When ants leave their nest to search for a food source, they randomly rotate around an obstacle, and initially the pheromone deposits will be the same for the right and left directions. When the ants in the shorter direction find a food source, they carry the food and start returning back, following their pheromone trails, and still depositing more pheromone. An ant will most likely choose the shortest path when returning to the nest with food as this path will have the most deposited pheromone. For the same reason, new ants that later starts out from the nest to find food will also choose the shortest path. Over time, this positive feedback (auto catalytic) process prompts all ants to choose the shorter path. Implementing the ACO for a certain problem requires a representation of "S" variables for each ant, with each variable "i" has a set of "n_i" options with their values "l_{ij}," and their associated pheromone concentrations $\{t_{ij}\}$; where $i = 1, 2, \ldots, S$, and $j = 1, 2, \ldots, n_i$. As such, an ant is consisted of "S" values that describe the path chosen by the ant. Gajpal and Rajendran [59] proposed modified ant colony algorithm incorporating a local search to improve the solution. In the ACO, the process starts

by generating m random ants (solutions). An ant k represents a solution string, with a selected value for each variable. Each ant is then evaluated according to an objective function. Accordingly, pheromone concentration associated with each possible route (variable value) is changed in a way to reinforce good solutions, as follows:

$$C_{ij}(t) = \rho C_{ij}(t-1) + \Delta C_{ij}; \quad t = 1, 2, \ldots\ldots, T \tag{1.52}$$

where T is the number of iterations (generation cycles); $C_{ij}(t)$ is the revised concentration of pheromone associated with option l_{ij} at iteration t, $C_{ij}\ (t-1)$ is the concentration of pheromone at the previous iteration $(t-1)$; ΔC_{ij} = change in pheromone concentration; and ρ = pheromone evaporation rate (0–1). The reason for allowing pheromone evaporation is to avoid too strong influence of the old pheromone to avoid premature solution stagnation. In Eq. 1.53, the change in pheromone concentration ΔC_{ij} is calculated as:

$$\begin{aligned} \Delta C_{ij} &= \Sigma_k R/\text{Fitness}_k, && \text{if option is chosen} \\ &= 0, && \text{if option is not chosen} \end{aligned} \tag{1.53}$$

where R is a constant called the pheromone reward factor; and fitness_k is the value of the objective function (solution performance) calculated for ant k. It is observed that the amount of pheromone gets higher as the solution improves. Therefore, for minimization problems, Eq. 1.53 shows the pheromone change as proportional to the inverse of the fitness. In maximization problems, on the other hand, the fitness value itself can be directly used. Once the pheromone is updated after iteration, the next iteration starts by changing the ants' paths (i.e. associated variable values) in a manner that respects pheromone concentration and also some heuristic preference. Ant colony optimization algorithm is, however, best suited for discrete optimization problems only.

1.3.12.6 Artificial Bee Colony Algorithm

Artificial bee colony (ABC) algorithm is developed to model the intelligent behavior of honeybee swarms [60]. The honeybee swarms consists of three essential components: food sources, employed foragers, and unemployed foragers, and defines two leading modes of the behavior: recruitment to a nectar source and abandonment of a source.

- Food sources: the value of a food source depends on many factors, such as its proximity to the nest, richness, or concentration of energy and the ease of extracting this energy. For the simplicity, the "profitability" of a food source can be represented with a single quantity. For example, there are two discovered food sources, A and B, in Fig. 1.6.
- Employed foragers (EF): they are associated with a particular food source, which they are currently exploiting or are "employed" at. They carry with them information about this particular source, its distance, and direction from the nest

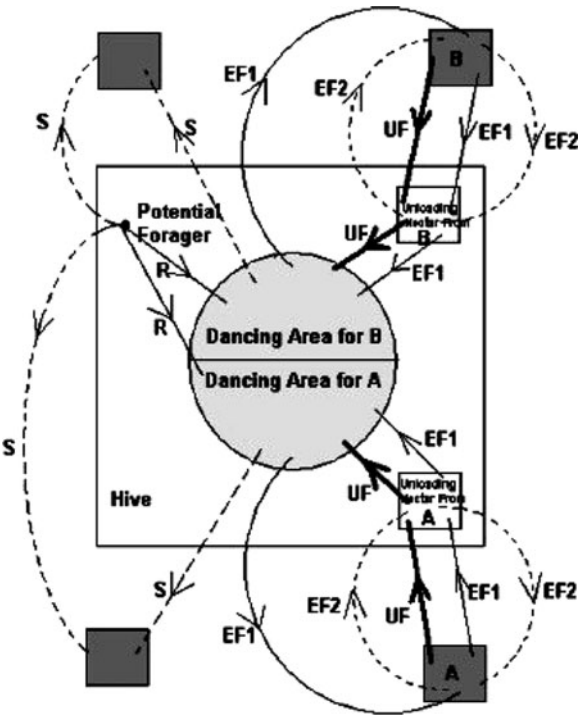

Fig. 1.6 Behaviour of honeybee foraging for nectar (from [60]; reprinted with permission from Elsevier)

and the profitability of the source and share this information with a certain probability.

- Unemployed foragers (UF): they are looking for a food source to exploit. There are two types of unemployed foragers: "scouts (S)" searching the environment surrounding the nest for new food sources and "onlookers" waiting in the nest and finding a food source through the information shared by employed foragers, i.e., "recruit (R)".

The exchange of information among bees is the most important occurrence in the formation of collective knowledge. While examining the entire hive, it is possible to distinguish some parts that commonly exist in all hives. The most important part of the hive with respect to exchanging information is the dancing area. Communication among bees related to the quality of food sources occurs in the dancing area. The related dance is called waggle dance. Since information about all the current rich sources is available to an onlooker on the dance floor, she probably could watch numerous dances and choose to employ herself at the most profitable source. There is a greater probability of onlookers choosing more profitable sources since more information is circulating about the more profit able sources. Employed foragers share their information with a probability, which is proportional to the profitability of the food source, and the sharing of this

information through waggle dancing is longer in duration. Hence, the recruitment is proportional to profitability of a food source.

At the very beginning, a potential forager will start as unemployed forager. That bee will have no knowledge about the food sources around the nest. There are two possible options for such a bee: (i) it can be a scout and starts searching around the nest spontaneously for a food due to some internal motivation or possible external clue; or (ii) it can be a recruit after watching the waggle dances and starts searching for a food source.

After finding the food source, the bee utilizes its own capability to memorize the location and then immediately starts exploiting it. Hence, the bee will become an "employed forager." The foraging bee takes a load of nectar from the source and returns to the hive, unloading the nectar to a food store. After unloading the food, the bee has the options of (i) becoming an uncommitted follower after abandoning the food source (UF), (ii) dancing and then recruiting nest mates before returning to same food source (EF1), and (iii) continues foraging at the food source without recruiting after bees (EF2). However, all bees do not start foraging simultaneously. The new bees begin foraging at a rate proportional to the difference between the eventual total number of bees and the number presently foraging.

At the first step, the ABC generates a randomly distributed initial population P_{initial} of N solutions, where N denotes the size of population. Each solution x_i ($i = 1, 2, \ldots, N$) is an H-dimensional vector where H is the number of optimization parameters (decision variables). After initialization, the population of the solutions is subjected to repeated cycles, $C = 1, 2, \ldots, G$, of the search processes of the employed bees, the onlooker bees and scout bees. An employed bee produces a modification on the solution in her memory depending on the local information. If the objective function value (fitness) of the new solution is higher than that of the previous one, the bee memorizes the new position and forgets the old one. Otherwise, she keeps the position of the previous one in her memory. After all employed bees complete the search process; they share the nectar information of the food sources and their position information with the onlooker bees on the dance area. An onlooker bee evaluates the fitness information taken from all employed bees and chooses a food source with a probability related to its fitness value. An onlooker bee also produces a new solution and it memorizes the new position if its fitness value is better than the previous position. An artificial onlooker bee chooses a food source depending on the probability value associated with that food source, p_i, calculated by Eq. 1.54.

$$p_i = F_i \Big/ \sum_{n=1}^{N_b} \mathrm{F}_n \tag{1.54}$$

where F_i is the fitness value of the solution i which is proportional to the nectar amount of the food source in the position i and N_b is the number of food sources which is equal to the number of employed bees. In order to produce a candidate food position from the old one in memory, the ABC uses Eq. 1.55,

$$v_{ij}=x_{ij}+R_{ij}\left(x_{ij}-x_{kj}\right) \tag{1.55}$$

where $k \in \{1,2,\ldots,N\}$ and $j \in \{1,2,\ldots,D\}$ are randomly chosen indexes. Although k is determined randomly, it has to be different from i. R_{ij} is a random number between (−1, 1) and it controls the production of neighbor food sources around x_{ij} and represents the comparison of two food positions visually by a bee. As can be seen from Eq. 1.55, as the difference between the parameters of the x_{ij} and x_{kj} decreases, the perturbation on the position x_{ij} gets decrease, too. Thus, as the search approaches to the optimum solution in the search space, the step length is adaptively reduced.

If the position of the food source cannot be improved for some predetermined number of cycles, then that food source is abandoned. The abandoned food source is replaced with a new food source by the scouts. In ABC, this is simulated by producing a position randomly and replacing it with the abandoned one. The value of predetermined number of cycles is an important control parameter of the ABC algorithm, which is called "limit" for abandonment. The value of limit is generally taken as the number of employed bees. If the abandoned source is x_i and $j \in \{1,2,\ldots,D\}$, then the scout discovers a new food source to be replaced with x_i. This operation can be defined as in Eq. 1.56.

$$x_i^j=x_{\min}^j+\text{rand}\ [0,1]\left(x_{\max}^j-x_{\min}^j\right) \tag{1.56}$$

It is clear from the above explanation that there are three control parameters used in the ABC: The number of food sources which is equal to the number of employed or onlooker bees (N), the value of limit, and the maximum cycle number (G).

The flow chart of ABC algorithm is shown in Fig. 1.7.

The performance of ABC algorithm in terms of convergence rate and accuracy of the solution is found superior over other non-traditional algorithms such as GA, PSO algorithm, etc. in few recent applications [61, 62]. ABC algorithm combines both, the stochastic selection scheme carried out by onlooker bees, and greedy selection scheme used by onlookers and employed bees to update the source position. Also the neighbor source production mechanism in ABC is similar to the mutation process, which is self-adapting. The random selection process carried out by the scout bees maintains diversity in the solution. The ABC algorithm is thus flexible, simple, and robust optimization algorithm which can be used effectively in the optimization of multimodal and multi-variable problems.

1.3.12.7 Artificial Immune Algorithm

The immune system is the basic and remarkable defence system against bacteria, viruses, and other disease-causing organisms. It can produce millions of antibodies from hundreds of antibody genes and can protect animals which are infected by foreign molecules. The artificial immune system (AIS) or artificial immune

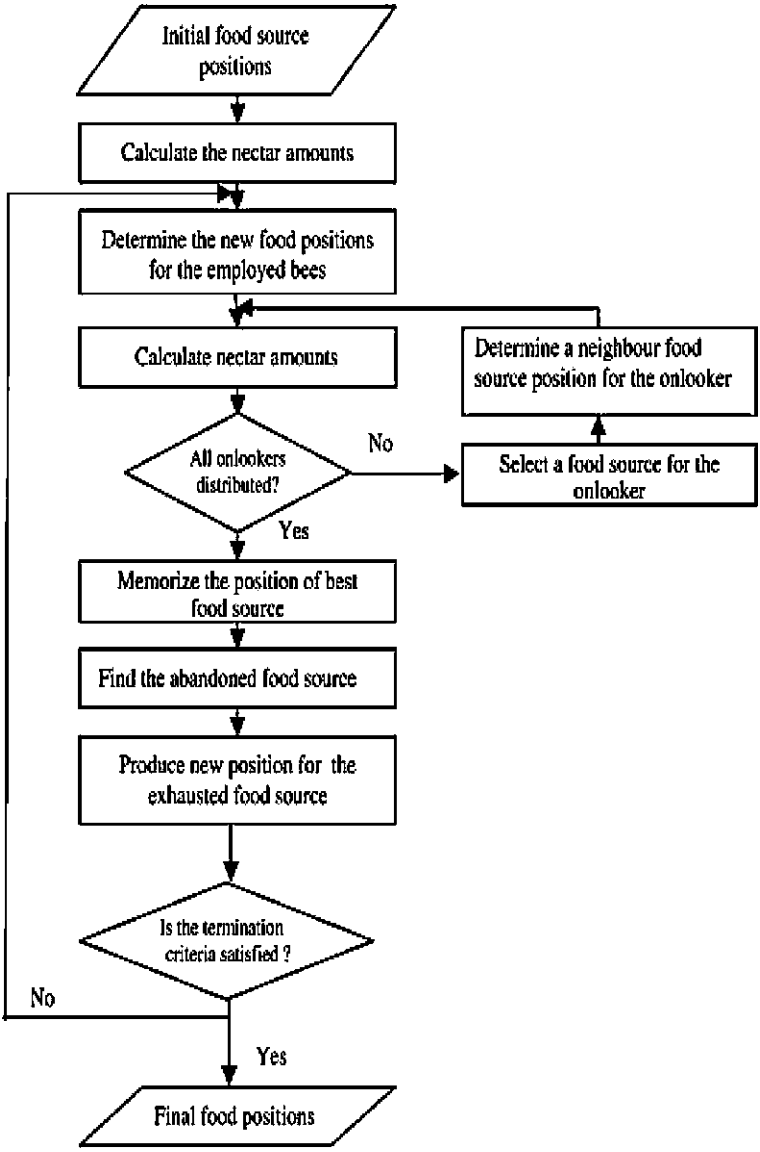

Fig. 1.7 Flow chart of the ABC algorithm (from [86]; reprinted with permission from Elsevier)

algorithm (AIA) was inspired by the immune system. In AIA, the objective function and constraints operate as the antigens, and the solutions to the objective function operate as the antibodies. Similar to GA, AIA starts by creating antibodies randomly in a feasible space, and finally reaches the optimum via natural selection, crossover, and mutation. The field of artificial immune system is concerned with abstracting structure and function of immune system to computational system, and

investigating the application of these systems towards solving computational problems from engineering [63–66].

The immune system defends the body against harmful diseases and infections. B-cells recognize the antigens which enter into the body that circulate through the blood. Each antigen has a particular shape that is recognized by the receptors present on the B-cell surface. B-cells synthesize and carry antibodies on their surfaces molecules that act like detectors to identify antigens. A B-cell with better fitting receptors and binding more tightly the antigen, replicate more and survive longer. This process of amplifying, using proliferation, only those cells that produce a useful B-cell type is called clonal selection. Clones are not perfect, but they are subjected to somatic permutations that result in children having slightly different antibodies from the parent. Clonal selection guarantees that only good B-cells (i.e., with higher affinity with the antigen) can be cloned to represent the next generation. However, clones with low affinity with antigen do not divide and will be discarded or deleted. Hence, the clonal selection enables the body to have sufficient numbers of antigen-specific B-cells to build up an effective immune response. The immune response represents solutions and antigens represent the problem to solve. More precisely, B-cells are considered as artificial agents that roam around and explore an environment.

The AIA starts with a random population which mimics antibodies (Ab) and affinity of the antibody is calculated from its objective function value. n highest antibodies are selected and cloned depending on their affinities. Generally n is kept same as N (number of antibodies). These antibodies are cloned depending on its affinities. If the affinity is more for the particular antibody it will have more number of clones. It is calculated as,

$$N_c = \sum_{i=1}^{n} \text{round}(\beta N/i) \tag{1.57}$$

where N_c is the number of clones generated, β is the multiplying factor controlling the number of clones, and N is the total number of antibodies.

These generates repertoire C_j. Repertoire C_j undergoes affinity maturation process Eq. 1.58 which is inversely proportional to its antigenic affinity. If the affinity is high the mutation rate is low.

$$x_{i,m} = x_i + A(\text{rand}[-1, 1])(x_{\max} - x_{\min}) \tag{1.58}$$

where A is a factor depending on the affinity and decreases as affinity increases. Replace low affinity antibodies with new randomly generated antibodies given by,

$$x_i = x_{\min} + \text{rand}(0.1)(x_{\max} - x_{\min}) \tag{1.59}$$

Compared with GAs, AIA has an affinity calculation function, which can describe the relationship not only between the antigen and the antibody but also between antibodies. That gives AIA the unique characteristic of guaranteeing the survival of variant offspring that can match the antigen better. The higher the

affinity, the stronger the binding, and thus the better the immune recognition and response. The algorithms based on AIA have much better performance than conventional probabilistic optimization algorithms. However, it usually takes long time for the binary coding AIA to obtain convergence. Furthermore, it is very difficult for AIA to break away from the local optimal value, which can restrict the search process to the zone around this value and can easily lead to premature termination of the process. Qiao et al. [67] proposed an improved affinity calculation approach by combining the Euclidean distance with the difference between fitness values, and make the threshold value a dynamic parameter in order to overcome the drawback of the tendency of GA and AIA towards local optimum value and premature completion. Simulation results showed that the proposed approach is more efficient than the GA and the real-value coding artificial immune algorithm.

1.3.12.8 Shuffled Frog Leaping Algorithm

Shuffled frog leaping (SFL) algorithm is a meta-heuristic for solving discrete optimization problems. SFL algorithm is a population based, cooperative search metaphor inspired by natural memetics. The algorithm uses memetic evolution in the form of infection of ideas from one individual to another in a local search. The local search is similar in concept to PSO. A shuffling strategy allows for the exchange of information between local searches to move toward a global optimum. Thus, the SFL algorithm combines the benefits of the genetic-based Memetic Algorithm (MA) and the social behavior-based PSO algorithms [68, 69]. The SFLA consists of a set of interacting virtual population of frogs partitioned into different memeplexes. The virtual frogs act as hosts or carriers of memes where a meme is a unit of cultural evolution. The algorithm performs simultaneously an independent local search in each memeplex. The local search is completed using a PSO-like method adapted for discrete problems but emphasizing a local search. To ensure global exploration, the virtual frogs are periodically shuffled and reorganized into new memplexes in a technique similar to that used in the shuffled complex evolution algorithm. In addition, to provide the opportunity for random generation of improved information, random virtual frogs are generated and substituted in the population. The algorithm parameters to set are: population size (P), number of memeplexes (m), and number of frogs in each memeplex (n).

The steps of SFL algorithm are given below:

1. Generate randomly an initial population (P) of frogs (solutions). For H-dimensional problems (H variables), a frog "i" is represented as $X_i = (x_{i1}, x_{i2}, \ldots, x_{iS})$.
2. Calculate the fitness value of each frog (solution).
3. Sort the frogs in a descending order of their fitness values.

4. Divide the entire population into "m" memeplexes, each containing "n" frogs. Thus, $P = m \times n$.
5. Allocate the frogs to the memeflexes such that first frog goes to the first memeplex, the second frog goes to the second memeplex, ….., frog "m" goes to the mth memeplex, and frog "$m + 1$" goes back to the first memeplex, etc.
6. Within each memeplex, the frogs with the best fitness (X_b) and the worst fitness (X_w) are identified.
7. Apply the local search within memeplex using the following equation:

$$X_{i+1} = X_i + r \times (X_b - X_w) \tag{1.60}$$

   r = random number between 0 and 1
   If "X_{i+1}" is better than "X_i", replace current frog position "X_i" with new position "X_{i+1}". Else go to Step 8.
8. Identify the frog with the global best fitness (X_g) and apply global search using following equation:

$$X_{i+1} = X_i + r \times \left(X_g - X_w\right) \tag{1.61}$$

   If "X_{i+1}" is better than "X_i," replace current frog position "X_i" with new position "X_{i+1}". Else go to Step 9.
9. Generate new frog position "X_i" randomly to replace the worst frog.

$$X_{i+1} = X_{\min} + r \times (X_{\max} - X_{\min}) \tag{1.62}$$

   $X_{\min} = (x_{\min 1}, x_{\min 2},., x_{\min S})$ and $X_{\max} = (x_{\max 1}, x_{\max 2},., x_{\max S})$
10. Does the termination criteria met? If yes then stop. Else go to Step 2.

Compared with a GA, the likelihood of convergence to a global optimal solution and the solution speed are better in the case of SFL algorithm and hence it can be used as an effective tool for solving combinatorial optimization problems.

1.3.12.9 Harmony Search Algorithm

The harmony search (HS) algorithm which is a meta-heuristic optimization algorithm was developed by Geem et al. [70]. This algorithm is conceptualized from the musical process of searching for a perfect state of harmony, such as jazz improvement. The jazz improvisations seeks the best state (fantastic harmony) determined by an estimation performed by set of pitches played by each instrument.

The steps in the procedure of HS are discussed below:

1. Determine algorithm parameters: In this step, the optimization problem is specified in terms of objective functions, constraints, and decision variables along with their upper and lower bound values. The HS algorithm parameters are also specified in this step. These are the harmony memory size (HMS), or

the number of solution vectors in the harmony memory; harmony memory considering rate (HMCR); pitch adjusting rate (PAR); number of decision variables (N) and the number of improvisations (NI), or stopping criterion. The harmony memory (HM) is a memory location where all the solution vectors (sets of decision variables) are stored. This HM is similar to the genetic pool in the GA. The HMCR and PAR are parameters that are used to improve the solution vector

2. Initialize the harmony memory: The HM matrix is filled with as many randomly generated solution vectors as the HMS:

$$\mathrm{HM} = \begin{bmatrix} x_1^1 & x_2^1 & x_3^1 & \cdots & x_N^1 \\ x_1^2 & x_2^2 & x_3^2 & \cdots & x_N^2 \\ x_1^3 & x_2^3 & x_3^3 & \cdots & x_N^3 \\ \cdots & \cdots & \cdots & \cdots & \cdots \\ \cdots & \cdots & \cdots & \cdots & \cdots \\ x_1^{\mathrm{HMS}} & x_2^{\mathrm{HMS}} & x_3^{\mathrm{HMS}} & \cdots & x_N^{\mathrm{HMS}} \end{bmatrix} \tag{1.63}$$

3. Improvise a new harmony: A new harmony vector is generated based on three rules: (1) memory consideration, (2) pitch adjustment, and (3) random selection. Generating a new harmony is called "improvisation." In memory consideration stage, the value of the first decision variable (x_1) for the new vector is chosen from any of the values in the specified HM range ($x_1 - x_{\mathrm{HMS}}$). Values of the other decision variables are chosen in the same manner. The HMCR, which varies between 0 and 1, is the rate of choosing one value from the historical values stored in the HM, while (1-HMCR) is the rate of randomly selecting one value from the possible range of values, as shown by the following equation:

$$\text{If HMCR} > \text{rand}\,(), x_{\mathrm{i}}^{'} \in \left\{x_i^1, x_i^2, \ldots, x_i^{\mathrm{HMS}}\right\};\ \text{else}\, x_i^{'} \in X_i \tag{1.64}$$

where rand () is a random number between 0 and 1. Every component obtained by the memory consideration is examined to determine whether it should be pitch-adjusted. This operation uses the PAR parameter, which is the rate of pitch adjustment as follows:

$$\text{If PAR} > \text{rand}\ (), x_i^{'} = x_i^{'} \pm \text{rand}().\text{bw};\ \text{else}\, x_i^{'} = x_i^{'} \tag{1.65}$$

where bw is an arbitrary distance bandwidth. In this step, harmony memory consideration and pitch adjustment is applied to each variable of the new harmony vector one by one.

4. Update harmony memory: If the new harmony vector has better fitness function than the worst harmony in the HM, the new harmony is included in the HM and the existing worst harmony is excluded from the HM.
5. Check terminating criterion: The HS algorithm is terminated when the terminating criterion (e.g. maximum number of improvisations) has been met. Otherwise, Steps 3 and 4 are repeated.

The flow chart of HS algorithm is shown in Fig. 1.8.
There are few drawbacks of the HS algorithm as given below:

- HS algorithm requires large number of iterations to improvise upon the previous best solution.
- The selection of the appropriate bandwidth is a difficult task, due to which there is a chance that the decision variable may lie outside their boundary values.

To overcome the above drawbacks of the existing HS algorithm a modified HS algorithm is developed. In the modified HS algorithm (HS_M), new harmony

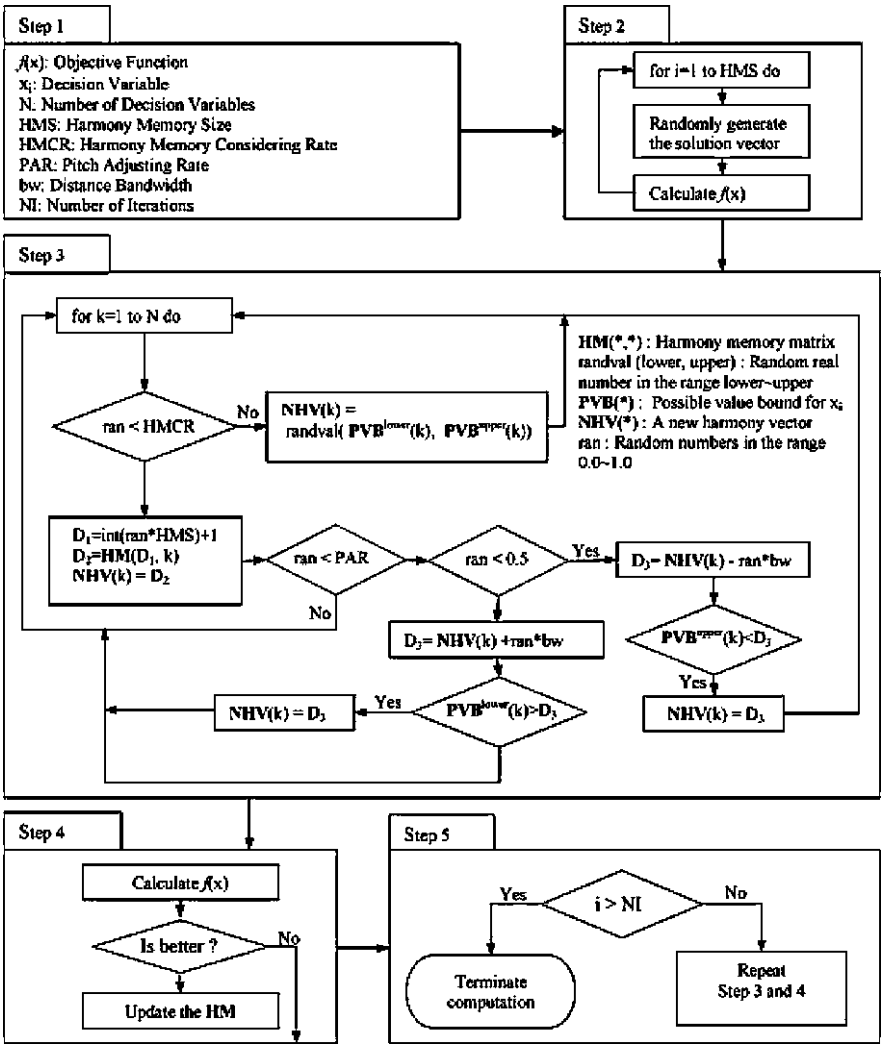

Fig. 1.8 Flow chart of harmony search algorithm (from [87]; reprinted with permission from Elsevier)

vector is based on four rules: (1) memory consideration, (2) previous best vector, (3) pitch adjustment, and (4) random selection. In the modified HS algorithm, Eqs. 1.64 and 1.65 take the forms of Eqs. 1.66 and 1.67, respectively.

$$\text{If HMCR} > \text{rand}(), x_i^{'} \in \left\{x_i^1, x_i^2, \ldots, x_i^{\text{HMS}}\right\}; \text{ else } x_i^{'} \in x_i^{\text{best}} \tag{1.66}$$

$$\text{If PAR} > \text{rand}(), x_i^{'} = x_i^{'} \pm \sigma(\text{rand}() - 0.5); \text{ else } x_i^{'} = x_i^{'} \tag{1.67}$$

where σ is the standard deviation. The remaining steps of the modified HS algorithm are same as that of HS algorithm.

1.3.12.10 Hybrid Algorithms

Modern search methods for optimization consider hybrid evolutionary algorithms those employing evolutionary algorithm and local optimizers working together. The hybridism comes from the balancing of global and local search procedures. The inspiration in nature has been pursued to design flexible, coherent, and efficient computational models. The main focuses of such models are real world problems, considering the known little effectiveness of canonical GAs in dealing with them. Investments have been made in new methods, which the evolutionary process is only part of the whole search process. Due to their intrinsic features as global solver, GAs are employed as a generator of search areas, which are more intensively inspected by a heuristic component.

The motivation to develop hybrid algorithms is derived from the observation that certain intelligent techniques would produce good results for one problem but not for others. This is because each intelligent technique has computational properties that make it attractive for particular problems. Even techniques with lower performance have useful features. For example, SA has a powerful method of allowing a restricted number of uphill moves to escape from non-local minima and for gradually decreasing that number as the optimization progresses towards the global optimum. Also, tabu search has an efficient tabu checking mechanism and a special memory structure to guide and constrain the search process. These advantageous features can be made use of in a hybrid technique combining ideas from existing algorithms.

Two or more basic non-traditional algorithms are combined to form hybrid algorithms to improve the performance of individual algorithms. For example, genetic simulated annealing algorithm (GSA) combines benefits of GA and SA algorithms [71]. GA and SA are both independently valid approaches toward problem solving with certain strengths and weaknesses. GA can begin with a population of solutions in parallel, but it suffers from poor convergence properties. By contrast, SA has better convergence properties if the starting temperature is sufficiently high and the temperature cooling rate is low. However, the higher temperature and the lower cooling rate reduce the performance of SA. In addition, parallelism cannot be easily exploited in SA. In GSA, individuals with higher

fitness values have a greater probability of surviving into the next generation. However, those with less fitness values are not discarded. Instead, a local selection strategy of SA is applied to select them with a probability related to the current temperature (as in SA).

Hybrid immune algorithm combines the benefits of artificial immune algorithm and hill climbing local search algorithm [72]. Memetic algorithm [73] is also a hybrid algorithm in which the GA is combined with the heavy local search. In this algorithm, an initial population is created at random similar to the GA. Afterwards, a local search is performed on each population member to improve its experience and thus obtain a population of local optimum solutions. Then, crossover and mutation operators are applied to produce offsprings. These offsprings are then subjected to the local search so that local optimality is always maintained.

Recently many variants of GAs have been investigated for improving the learning and speed of convergence. For some problems, the user often has to be satisfied with local optimal or suboptimal solutions. Sadegheih [74] proposed a novel hybrid approach consisting of a GA, SA, and tabu search and the better performance of the hybrid approach was illustrated using various test iterations. Oysu and Bingul [75] applied heuristic algorithms such as SA, GA and hybrid algorithm (hybrid-GASA) to tool-path optimization problem for minimizing air-time during machining. Many forms of SA rely on random starting points that often give poor solutions. The problem of how to efficiently provide good initial estimates of solution sets automatically is still an ongoing research topic. The authors had proposed a hybrid approach in which GA provides a good initial solution for SA runs. The three algorithms were tested on three-axis-cartesian robot during milling of wood materials and their performances were compared based on minimum path and consequently minimum airtime. In order to make a comparison between these algorithms, two cases among the several milling operations were considered. Hybrid algorithm was reported better than other heuristic algorithms alone.

Zhang and Tang [76] presented a novel hybrid ant colony optimization approach to solve the vehicle routing problem. The main feature of the hybrid algorithm is to hybridize the solution construction mechanism of the ant colony optimization (ACO) with scatter search (SS). The experimental results showed that the proposed hybrid method is competitive to solve the vehicle routing problem in terms of solution quality. Ho et al. [77] used an adaptive network-based fuzzy inference system (ANFIS) with the genetic learning algorithm to predict the workpiece surface roughness for the end milling process. The hybrid Taguchi-genetic learning algorithm (HTGLA) was applied in the ANFIS to determine the most suitable membership functions and to simultaneously find the optimal premise and consequent parameters by directly minimizing the root-mean-squared-error performance criterion. Experimental results showed that the HTGLA-based ANFIS approach outperforms the ANFIS methods given in the Matlab toolbox in terms of prediction accuracy.

Liao [78] presented two hybrid differential evolution algorithms for optimizing engineering design problems. One hybrid algorithm enhances a basic differential

evolution algorithm with a local search operator, i.e., random walk with direction exploitation, to strengthen the exploitation ability, while the other adding a second metaheuristic, i.e., HS, to cooperate with the differential evolution algorithm so as to produce the desirable synergetic effect. All algorithms incorporated a generalized method to handle discrete variables and parameter-less penalty method for handling constraints. Fourteen engineering design problems selected from different engineering fields were used for testing. The test results showed that: (i) both hybrid algorithms outperform the differential evolution algorithms; (ii) among the two hybrid algorithms, the cooperative hybrid outperforms the other hybrid with local search; and (iii) the performance of hybrid algorithms can be further improved with some effort of tuning the relevant parameters.

Luis et al. [79] proposed a hybrid optimization approach. In the first stage, a multi-objective version of differential evolution was used to generate an initial approximation of the Pareto front. In the second stage, rough set theory was used to improve the spread and quality of this initial approximation. Hui [80] proposed a multi-objective optimization method based on adaptive simulated annealing genetic algorithm. Wang et al. [81] developed three hybrid HS algorithms, namely, hybrid harmony search (hHS) algorithm, hybrid globalbest harmony search (hgHS) algorithm and hybrid modified globalbest harmony search (hmgHS) algorithm for solving the flow shop scheduling with blocking to minimize the total flow time. Computational results showed the effectiveness of the hybrid harmony search algorithms, especially the (hmgHS) algorithm.

Lozano and Martínez [82] reported on hybrid meta-heuristics with evolutionary algorithms specializing in intensification and diversification. The use of evolutionary algorithms specializing in intensification and diversification for building hybrid meta-heuristics becomes a prospective line of research for obtaining effective search algorithms.

References

1. Box GEP, Draper NR (1987) Empirical model-building and response surface. Wiley, New York
2. Montgomery DC, Peck EA (1992) Introduction to linear regression analysis. Wiley, New York
3. Mukherjee I, Ray PK (2006) A review of optimization techniques in metal cutting processes. Comput Ind Eng 50:15–34
4. Zadeh LA (1965) Fuzzy sets. Inf Control 8:338–353
5. Zimmerman HJ (1976) Description and optimization of fuzzy system. Int J Gen Syst 2:209–215
6. Zadeh LA (1973) Outline of a new approach to the analysis of complex systems and decision processes. IEEE Trans Syst Man Cybern, SMC 3:28–44
7. Rao SS (1987) Description and optimum design of fuzzy mechanical systems. J Mech Transm Autom Des 109:126–132
8. Chandrasekaran M, Muralidhar M, Krishna CM, Dixit US (2010) Application of soft computing techniques in machining performance prediction and optimization: a literature review. Int J Adv Manuf Technol 46:445–464

9. Shin YC, Vishnupad P (1996) Neuro fuzzy control of complex manufacturing processes. Int J Prod Res 34:3291–3309
10. Dixit PM, Dixit US (2008) Modeling of metal forming and machining processes: by finite element and soft computing methods. Springer-Verlag, London
11. Coit DW, Jackson BT, Smith AE (1998) Static neural network process models: considerations and case studies. Int J Prod Res 36:2953–2967
12. Deng JL (1989) Introduction to grey system theory. J Grey Syst 1:1–24
13. Deng JL (2005) The primary methods of grey system theory. Huazhong University of Science and Technology Press, Wuhan
14. Kuo Y, Yang T, Huang GW (2008) The use of grey relational analysis in solving multi attribute decision making problems. Comput Ind Eng 55:80–93
15. Fung CP (2003) Manufacturing process optimization for wear property of fiber-reinforced polybutylene terephthalate composites with grey relational analysis. Wear 254:298–306
16. Rao RV (2007) Decision making in the manufacturing environment using graph theory and fuzzy multiple attribute decision making methods. Springer-Verlag, London
17. Saaty TL (2000) Fundamentals of decision making and priority theory with AHP. RWS Publications, Pittsburg
18. Taguchi G (1962) Tables of orthogonal arrays and linear graphs. Maruzen, Tokyo
19. Taguchi G (1990) Introduction to quality engineering. McGraw-Hill, New York
20. Oktem H, Erzurumlu T, Col M (2006) A study of the Taguchi optimization method for surface roughness in finish milling of mold surfaces. Int J Adv Manuf Technol 28:694–700
21. Phadke MS (1989) Quality engineering using robust design. Prentice-Hall, Englewood Cliffs, New Jersey
22. Ross PJ (1988) Taguchi techniques for quality engineering. McGraw-Hill, New York
23. Montgomery DC (1997) Design and analysis of experiments. Wiley, New York
24. Baş D, Boyacı IH (2007) Modeling and optimization I: usability of response surface methodology. J Food Eng 78:836–845
25. Myers RH, Montgomery DC (1995) Response surface methodology: process and product optimization using designed experiments. Wiley, New York
26. Carlyle WM, Montgomery DC, Runger GC (2000) Optimization problems and method in quality control and improvement. J Qual Technol 32:1–17
27. Cakir MC, Cavdar K (2006) Development of a knowledge-based expert system for solving metal cutting problems. Mater Des 27:1027–1034
28. Chrysslouris G, Wright K (1986) Knowledge based systems in manufacturing. CIRP Ann Manuf Technol 35:437–440
29. Osakada K, Kado T (1988) Application of AI techniques to process planning of cold forging. CIRP Ann Manuf Technol 37:239–242
30. Pearson K (1901) On lines and planes of closest fit to systems of points in spaces. Philos Mag Ser 6(2):559–572
31. Hotelling H (1933) Analysis of a complex of statistical variables into principal components. J Educ Psychol 24:417–441
32. Fung CP, Kang PC (2005) Multi-response optimization in friction properties of PBT composites using Taguchi method and principal component analysis. J Mater Process Technol 170:602–610
33. Ding M, Tian Z, Xu H (2010) Adaptive kernel principal component analysis. J Signal Process 90:1542–1553
34. Sârbu C, Pop HF (2005) Principal component analysis versus fuzzy principal component analysis: a case study: the quality of Danube water (1985–1996). Talanta 65:1215–1220
35. Hillier FS, Liebermann GJ (1999) Operations research. CBS Publishers, New Delhi
36. Bellman RE (1957) Dynamic programming. Princeton University Press, Princeton, New Jersey
37. Phillips DT, Ravindran A, Solberg JJ (1976) Operations research: principles and practice. Wiley, New York
38. Rao SS (1978) Optimization theory and applications. Wiley Eastern Limited, New York

39. Wilde DJ, Beightler CS (1967) Foundations of optimization. Prentice-Hall, Englewood Cliffs, New Jersey
40. Wolfe P (1963) Methods of nonlinear programming. McGraw Hill, New York
41. Abadie J, Carpenter J (1969) Generalization of the Wolfe reduced gradient method to the case of nonlinear constraints. Academic Press, London
42. Avriel M (1976) Nonlinear programming: methods and analysis. Prentice-Hall, Englewood Cliffs, New Jersey
43. Lasdon LS, Waren AD, Jain A, Ratner M (1978) Design and testing of a generalized reduced gradient code for nonlinear programming. ACM Trans Math Software 4:34–39
44. Duffin RJ, Peterson E, Zener C (1967) Geometric programming. Wiley, New York
45. Schittkowski K (1986) NLPQL: a FORTRAN subroutine solving constrained non-linear programming problem. Ann Oper Res 5:485–500
46. Land AH, Doig A (1960) An automatic method for solving discrete programming problems. Econometrica 28:497–520
47. Dakin RJ (1965) A true search algorithm for mixed integer programming problems. Comput J 8(3):250–255
48. Holland JH (1975) Adaptation in neural and artificial systems. University of Michigan Press, Ann Arbour
49. Deb K (2002) Multi-objective optimization using evolutionary algorithm. Wiley, Chichester
50. Kirkpatrick S, Gelatt C, Vecchi M (1983) Optimization by simulated annealing. Science 220:671–680
51. Metropolis N, Rosenbluth A, Rosenbluth M, Teller A, Teller E (1953) Equation of state calculations by fast computing machines. J Chem Phys 21:1087–1092
52. Rao RV, Pawar PJ, Davim JP (2010) Optimization of process parameters of mechanical type advanced machining processes sing a simulated annealing algorithm. Int J Mater Prod Technol 37(1/2):83–101
53. Glover F (1986) Future paths for integer programming and links to artificial intelligence. Comput Oper Res 13:533–549
54. Kennedy J, Eberhart R (1995) Particle swarm optimization. Proc IEEE Int Conf Neural Netw 4:1942–1948
55. Dong Y, Tang J, Xu B, Wang D (2005) An application of swarm optimization to nonlinear programming. Comput Math Appl 49:1655–1668
56. Bergh F, Engelbrecht AP (2006) A study of particle swarm optimization particle trajectories. Inf Sci 176:937–971
57. Tripathi P, Bandopadhyay S, Pal SK (2007) Multi-objective particle swarm optimization with time variant inertia and acceleration coefficients. Inf Sci 177:5033–5049
58. Dorigo M, Maniezzo V, Colorni A (1996) Ant system: optimization by a colony of cooperating agents. IEEE Trans Syst Man Cybern 26:29–41
59. Gajpal Y, Rajendran C (2006) An ant colony optimization algorithm for minimizing the completion time variance of jobs in flowshops. Int J Prod Econ 101:259–272
60. Karaboga D, Basturk B (2008) On the performance of artificial bee colony (ABC) algorithm. Appl Soft Comput 8:687–697
61. Rao RV, Pawar PJ (2010) Parameter optimization of a multi-pass milling process using non-traditional optimization algorithms. Appl Soft Comput 10:445–456
62. Rao RV, Pawar PJ (2009) Modeling and optimization of process parameters of wire electric discharge machining. J Eng Manuf 223:1431–1440
63. de Castro LN, Timmis J (1996) Artificial immune systems: a new computational intelligence approach. Springer-Verlag, London
64. de Castro LN, Von Zuben FJ (2002) Learning and optimization using clonal section principle. IEEE Trans Evol Comput 6:239–251
65. Emma H, Jon T (2008) Application areas of AIS: the past, the present and the future. Appl Soft Comput 8:191–201

66. Rodin V, Benzinou A, Guillaud A, Ballet P, Harrouet F, Tisseau J, Le Bihan J (2004) An immune oriented multi-agent system for biological image processing. Pattern Recognit 37:631–645
67. Qiao Z, Xu X, Liang YC (2006) An improved artificial immune algorithm with a dynamic threshold. J Bionic Eng 3:93–97
68. Elbeltagi E, Hegazy T, Grierson D (2005) Comparison among five evolutionary-based optimization algorithms. Adv Eng Inf 19:43–53
69. Eusuff M, Lansey K, Pasha F (2006) Shuffled frog-leaping algorithm: a memetic meta-heuristic for discrete optimization. Eng Optim 38:129–154
70. Geem ZW, Kim JH, Loganathan GV (2001) A new heuristic optimization algorithm: harmony search. Simulation 76(2):60–68
71. Wang ZG, Rahman M, Wong YS, Sun J (2005) Optimization of multi-pass milling using parallel genetic algorithm and parallel genetic simulated annealing. Int J Mach Tools Manuf 45:1726–1734
72. Yildiz AR (2009) A novel hybrid immune algorithm for optimization of machining parameters in milling operations. Rob Comput Integr Manuf 25:261–270
73. Moscato P (1989) On evolution, search, optimization, genetic algorithms and martial arts: towards memetic algorithms. Technical Report 826. California Institute of Technology, Pasadena, CA
74. Sadegheih A (2009) Optimization of network planning by the novel hybrid algorithms of intelligent optimization techniques. Energy 34:1539–1551
75. Oysu C, Bingul Z (2009) Application of heuristic and hybrid-GASA algorithms to tool-path optimization problem for minimizing airtime during machining. Eng Appl Artif Intell 22(3):389–396
76. Zhang X, Tang L (2009) A new hybrid ant colony optimization algorithm for the vehicle routing problem. Pattern Recognit Lett 30(9):848–855
77. Ho WH, Tsai JT, Lin BT, Chou JH (2009) Adaptive network-based fuzzy inference system for prediction of surface roughness in end milling process using hybrid Taguchi-genetic learning algorithm. Expert Sys Appl 36(2):3216–3222
78. Liao TW (2010) Two hybrid differential evolution algorithms for engineering design optimization. Appl Soft Comput. doi:10.1016/j.asoc.2010.05.007
79. Luis VSQ, Alfredo GHD, Julián M, Coello CAC, Caballero R (2010) DEMORS: a hybrid multi-objective optimization algorithm using differential evolution and rough set theory for constrained problems. Comput Oper Res 37(3):470–480
80. Hui S (2010) Multi-objective optimization for hydraulic hybrid vehicle based on adaptive simulated annealing genetic algorithm. Eng Appl Artif Intell 23(1):27–33
81. Wang L, Pan QK, Tasgetiren MF (2010) Minimizing the total flow time in a flow shop with blocking by using hybrid harmony search algorithms. Expert Sys Appl. doi:10.1016/j.eswa.2010.04.042
82. Lozano M, Martínez CG (2010) Hybrid metaheuristics with evolutionary algorithms specializing in intensification and diversification: overview and progress report. Comput Oper Res 37:481–497
83. Song Q, Kho KP, See KH (1999) Implementation of two-dimensional systolic algorithms for multi-layered neural networks. J Syst Arch 45(14):1209–1218
84. Lin XH, Kwok YK, Lau VKN (2003) A genetic algorithm based approach to route selection and capacity flow assignment. Comput Commun 26(9):961–974
85. Sakthivel VP, Bhuvaneswari R, Subramanian S (2010) Multi-objective parameter estimation of induction motor using particle swarm optimization. Eng Appl Artif Intell 23(3):302–312
86. Karaboga N (2009) A new design method based on artificial bee colony algorithm for digital IIR filters. J Franklin Inst 346(4):328–348
87. Zarei O, Fesanghary M, Farshi B, Saffar RJ, Razfar MR (2009) Optimization of multipass face-milling via harmony search algorithm. J Mater Process Technol 209:2386–2392

Chapter 2
Modeling and Optimization of Machining Processes

2.1 Introduction

Machining operations have been the core of the manufacturing industry since the industrial revolution. Machining is a process of material removal using cutting tools and machine tools to accurately obtain the required product dimensions with good surface finish. The manufacturing industries strive to achieve either a minimum cost of production or a maximum production rate, or an optimum combination of both, along with better product quality in machining.

The machining process is influenced by a number of input and output variables. Machining process input variables are the process-independent variables and include the following:

- Machine tool (rigidity, capacity, accuracy, etc.);
- Cutting tool (material, coating, geometry, nature of engagement with the work material, tool rigidity, etc.);
- Cutting conditions (speed, feed, and depth of cut);
- Work material properties (hardness, tensile strength, chemical composition, microstructure, method of production, thermal conductivity, ductility, shape and dimensions of the job, work piece rigidity, etc.);
- Cutting fluid properties and characteristics.

Machining process output variables are the process-dependent variables and include the following:

- Cutting tool life/tool wear/tool wear rate,
- Cutting forces/specific cutting forces,
- Power consumption/specific power consumption;
- Processed surface finish;
- Processed dimensional accuracy;
- Material removal rate (MRR);

R. V. Rao, *Advanced Modeling and Optimization of Manufacturing Processes*, Springer Series in Advanced Manufacturing, DOI: 10.1007/978-0-85729-015-1_2,

- Noise;
- Vibrations;
- Cutting temperature;
- Chip characteristics.

The technology of metal cutting has grown substantially over time owing to the contribution from many branches of engineering with a common goal of achieving higher machining process efficiency. Selection of optimal machining conditions is a key factor in achieving this goal. In any multi-stage metal cutting operation, the manufacturer seeks to set the process-related controllable input variables at their optimal operating conditions with minimum effect of uncontrollable or noise variables on the levels and variability in the outputs. To design and implement an effective process control for machining operation by parameter optimization, a manufacturer seeks to balance between quality and cost at each stage of operation resulting in improved delivery and reduced warranty or field failure of a product under consideration [196, 285].

Machining processes include traditional processes (such as turning, milling, grinding, drilling, finishing, etc.) and advanced processes (such as electrical discharge machining, electrochemical machining, ultrasonic machining, abrasive jet machining, laser beam machining, etc.). Due to complexity and uncertainty of the machining processes, soft computing techniques (such as neural networks, fuzzy sets, genetic algorithms, simulated annealing, particle swarm optimization (PSO), artificial bee colony (ABC) algorithm, etc.) are being preferred to physics-based models for predicting the performance of the machining processes and optimizing them. The modeling and optimization aspects of some of the important machining processes are described in the next sections.

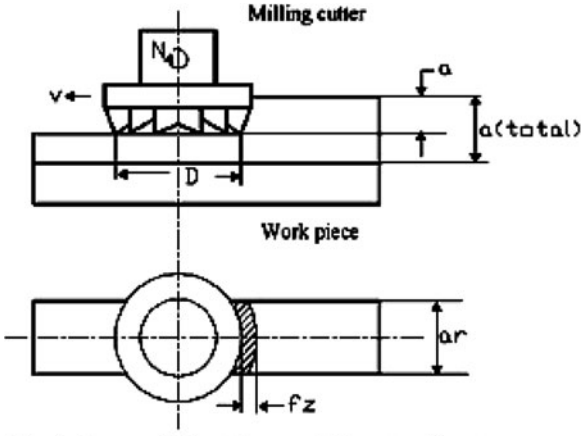

N: spindle speed; V: cutting speed; D: cutter diameter;
a: depth of cut; a_r: width of cut; f_z: feed per tooth

Fig. 2.1 Milling operation (from [237]; reprinted with permission from Elsevier)

2.2 Milling Process

Milling is the machining process in which the metal is removed by a rotating multiple tooth cutter. As the cutter rotates, each tooth removes a small amount of material from the advancing work for each spindle revolution. The relative motion between cutter and the work piece can be in any direction and hence surfaces having any orientation can be machined in milling. Figure 2.1 shows a milling operation. Milling operation can be performed in a single pass or in multiple passes. Multi-pass operations are often preferred to single pass operations for economic reasons and are generally used to machine stocks that cannot be removed in a single pass. Milling processes are employed for machining flat surfaces, contoured surfaces, surfaces of revolution, and helical surfaces of various cross-sections.

Various investigators had presented techniques, both traditional and non-traditional, for modeling and optimization of milling processes. Wang [305] presented a neural network-based approach to multiple objective optimization of milling process parameters. First, the problem of determining the optimum machining parameters was formulated as a multiple-objective optimization problem. Then, neural networks were proposed to represent manufacturers' preference structures. However, optimization by using neural networks may often ends in local minima or fails to converge on a result.

Armarego et al. [16] discussed development of computer-aided constrained optimization analyses and strategies for multi-pass peripheral- and end-milling operations. The constrained optimization was based on criteria typified by the maximum production rate and included a range of practical constraints of relevance to rough milling such as the machine tool-limiting power, torque, feed force and feed-speed boundaries. The authors opined that a combination of mathematical optimization analyses and limited use of numerical search techniques provides clearly defined computer-aided strategies which guarantee the final global optimum solutions. Simulation studies had verified the software and demonstrated the superiority of multi-pass over single pass.

Tolouei-Rad and Bidhendi [288] described development and utilization of an optimization system which determines optimum machining parameters for milling operations. The method of feasible direction was used for optimization. The optimized parameters were intended for use by the NC machines. The authors had considered maximization of profit rate as an objective function in milling operation. The feasible solution denotes the local minimum of the problem. However, this local minimum need not be the global one unless the problem is convex programming problem. Optimization model developed in their work was non-convex. Wang [306] outlined and discussed optimization analysis, strategy and CAM software for single pass end-milling on computer numerical control (CNC) machine tools based on criteria typified by the maximum production rate and allowing for a range of machine tool and component surface roughness constraints. It was shown that the deterministic optimization approach involving mathematical

analyses of constrained economic trends and their graphical representation on the feed-speed domain provides a deeper understanding of the influences of constraints and a clearly defined strategy which guarantees the global optimum solutions. Numerical simulation studies had demonstrated the economic benefits of using this strategy over handbook recommendations as well as in assessing, selecting and improving machine-tool design specifications.

Zheng et al. [328] presented a new approach to theoretical modeling and simulation of cutting forces in face milling. Based on a predictive machining theory, the action of a milling cutter was modeled as the simultaneous actions of a number of single-point cutting tools. The milling forces were predicted from the workpiece material properties, cutter parameters, tooth geometry, cutting conditions and types of milling. The properties of the workpiece material were considered as functions of strain, strain-rate and temperature in the cutting region. It took into account the effect of the intermittent contact between each milling tooth and the workpiece on the temperature in the cutting region. It also took into account the effect of cutter runout on the undeformed chip thickness.

Sonmez et al. [278] studied multi-pass milling operation based on the maximum production rate criterion and used an algorithm adopted from the study of Agapiou [4] which was presented for the multi-pass turning operations. Although the results showed significant improvement over handbook recommendations, the optimization techniques used in their work (dynamic programming and using geometric programming) either tend to result in local minima or take a long time to converge on a reasonable result. Choi and Yang [60] suggested an algorithm for estimating the cutting depth based on the pattern of cutting force. The cutting force pattern, rather than its magnitude, better reflects the change of the cutting depth, because while the magnitude is influenced by several cutting parameters, the pattern is affected mainly by the cutting depth. The proposed algorithm can be applied to extensive cutting circumstances, such as presence of tool wear, change of work material hardness, etc.

Shunmugam et al. [272] considered a face-milling operation. The machining parameters such as number of passes, depth of cut in each pass, speed and feed were obtained using a genetic algorithm (GA), to yield minimum total production cost while considering technological constraints such as allowable speed and feed, dimensional accuracy, surface finish, tool wear and machine-tool capabilities. Although GA has advantages over the traditional techniques, the successful application of GA depends on the population size or the diversity of individual solutions in the search space. If GA cannot hold its diversity well before the global optimum is reached, it may prematurely converge to a local optimum. Although maintaining diversity is the predominant concern of GA, it also reduces the performance of GA. Baek et al. [23] analyzed the effects of the insert run-out errors and the variation of the feed rate on the surface roughness and the dimensional accuracy in a face-milling operation using a surface roughness model. The validity of the developed model was proved through cutting experiments, and the model was used to predict the machined surface roughness from the information of the insert run-outs and the cutting parameters. From the estimated surface roughness

value, the optimal feed rate that gave a maximum MRR under the given surface roughness constraint could be selected by a bisection method.

Chen and Savage [54] used fuzzy net-based model to predict surface roughness under different tool and work piece combination for end-milling process. Speed, feed and depth of cut, vibration, tool diameter, tool material, and work piece material were used as input variables for fuzzy system. The authors found that the predicted surface roughness was within an error of 10%. Li et al. [173] modeled the cutting forces in helical end-milling based on a predictive machining theory, in which the machining characteristic factors were predicted from input data of fundamental workpiece material properties, tool geometry and cutting conditions. In the model, each tooth of a helical end-milling cutter was discretized into a number of slices along the cutter axis to account for the helix angle effect on the cutting forces. The cutting action of each of the slices was modeled as an oblique cutting process. For the first slice of each tooth, it was modeled as oblique cutting with end cutting edge effect and tool nose radius effect, whereas the cutting actions of other slices were modeled as oblique cutting without end cutting edge effect and tool nose radius effect. The cutting forces in the oblique cutting processes were predicted using a predictive machining theory. The total cutting forces acting on the cutter was obtained as the sum of the forces at all the cutting slices of all the teeth. A Windows-based simulation system for the cutting forces in helical end milling was developed using the model.

Benardos and Vosniakos [35] presented a neural network modeling approach for the prediction of surface roughness (R_a) in CNC face milling. The data used for the training and checking of the networks' performance was derived from the experiments conducted on a CNC milling machine according to the principles of Taguchi's design of experiments (DoE) method. The factors considered in the experiment were the depth of cut, the feed rate per tooth, the cutting speed, the engagement and wear of the cutting tool, the use of cutting fluid and the three components of the cutting force. Using feed-forward artificial neural networks (ANNs) trained with the Levenberg–Marquardt algorithm, the most influential of the factors were determined, again using DoE principles, and a $5 \times 3 \times 1$ ANN based on them was able to predict the surface roughness with a mean squared error equal to 1.86%.

Tandon et al. [286] proposed and implemented PSO technique to optimize multiple machining parameters simultaneously for the case of milling. An ANN predictive model for critical process parameters was used to predict the cutting forces which in turn were used by the PSO algorithm to optimize the cutting conditions subject to a comprehensive set of constraints. Next, the algorithm was used to optimize both feed and speed for a typical case found in industry, namely, pocket-milling. Machining time reductions of up to 35% were observed. Lo [182] used an adaptive network-based fuzzy inference system (ANFIS) to predict the work piece surface roughness after the end-milling process. Three milling parameters that have a major impact on the surface roughness, including spindle speed, feed rate and depth of cut, were analyzed. Two different membership functions, triangular and trapezoidal, were adopted during the training process of

ANFIS in order to compare the prediction accuracy of surface roughness by the two membership functions. The predicted surface roughness values derived from ANFIS were compared with experimental data. The comparison indicated that the adoption of both triangular and trapezoidal membership functions in ANFIS achieved very satisfactory accuracy. When a triangular membership function was adopted, the prediction accuracy of ANFIS reached was as high as 96%.

Ghani et al. [103] applied Taguchi optimization method to optimize cutting parameters in end milling when machining hardened steel AISI H13 with TiN-coated P10 carbide insert tool under semi-finishing and finishing conditions of high-speed cutting. The milling parameters evaluated were cutting speed, feed rate and depth of cut. An orthogonal array, signal-to-noise (S/N) ratio and Pareto analysis of variance (ANOVA) were employed to analyze the effect of these milling parameters. The analysis of the result showed that the optimal combination for low resultant cutting force and good surface finish were high cutting speed, low feed rate and low depth of cut. Using Taguchi method for DOE, other significant effects such as the interaction among milling parameters were also investigated. The study showed that the Taguchi method is suitable to solve the stated problem with minimum number of trials as compared with a full factorial design.

Li and Li [172] developed theoretical cutting force model for helical end milling with cutter runout using a predictive machining theory, which predicts cutting forces from the input data of workpiece material properties, tool geometry and cutting conditions. In the model, a helical end-milling cutter was discretized into a number of slices along the cutter axis to account for the helix angle effect. The cutting action for a tooth segment in the first slice was modeled as oblique cutting with end cutting edge effect and tool nose radius effect, whereas the cutting actions of other slices were modeled as oblique cutting without end cutting edge effect and tool nose radius effect. The influence of cutter runout on chip load was considered based on the true tooth trajectories. The total cutting force was the sum of the forces at all the cutting slices of the cutter. The model was verified with experimental milling tests.

Kovacic et al. [159] proposed modeling of cutting forces with genetic programming, which imitates principles of living beings. Measurements were made for two materials (aluminum alloy $AlMgSi_1$ and steel 1.2343) and two different types of milling (conventional milling and STEP milling). For each material and type of milling parameters, tensile strength and hardness of work piece, tool diameter, cutting depth, spindle speed, feeding and type of milling were monitored, and cutting forces were measured for each combination of milling parameters. On the basis of the experimental data, different models for cutting forces prediction were obtained by genetic programming. Wang et al. [311] presented an approach to select the optimal machining parameters for multi-pass milling. It was based on two recent approaches, genetic algorithm (GA) and simulated annealing (SA), which have been applied to many difficult combinatorial optimization problems with certain strengths and weaknesses. A hybrid of GA and SA (GSA) was presented to use the strengths of GA and SA and overcome their weaknesses. In order to improve, the performance of GSA further, the parallel genetic

simulated annealing (PGSA) was developed and used to optimize the cutting parameters for multi-pass milling process. For comparison, conventional parallel GA (PGA) was also chosen as another optimization method. An application example that was solved previously using the geometric programming (GP) and dynamic programming (DP) method was presented. From the given results, PGSA was shown to be more suitable and efficient for optimizing the cutting parameters for milling operation than GP + DP and PGA.

El-Mounayri et al. [82] presented an integrated product development system for optimized CNC ball-end milling. First, the developed model was extended from flat end milling to ball-end milling. Second, the optimization was extended from 2D (speed and feed) to 3 (1/2) D (speed, feed, radial and axial depths of cut). Third, the modeling and simulation of the flat end milling was extended to include more input variables. Finally, a feed-forward three layer fully interconnected radial basis function neural network was introduced to and was successfully implemented for the case of ball-end milling. The work was verified and validated using typical machining scenarios.

Baro et al. [29] proposed a model to deal with the modeling of cutting forces in a face-milling operation performed using self-propelling inserts. The proposed model incorporates differences in the machining mechanics of self-propelling inserts due to the difference in their geometry and rotation in a static force prediction model in a face-milling operation with stationary inserts. The predicted values of cutting forces evaluated by the proposed model were in excellent agreement with the experimental value than those predicted using the static force model. Radhakrishnan and Nandan [234] predicted cutting force model using regression and neural networks. A regression model was used to filter out abnormal data points and the filtered data were used in neural network for better prediction.

Liu and Cheng [178] presented a new approach modeling and predicting the machining dynamics for peripheral milling. First, a machining dynamics model was developed based on the regenerative vibrations of the cutter and workpiece excited by the dynamic cutting forces, which were mathematically modeled and experimentally verified by the authors. Then, the mechanism of surface generation was analyzed and formulated based on the geometry and kinematics of the cutter. Thereafter a simulation model of the machining dynamics is implemented using Simulink. In order to verify the effectiveness of the approach, the transfer functions of a typical cutting system in a vertical CNC machine center were measured in both normal and feed directions by an instrumented hammer and accelerometers. Then a set of well-designed cutting trials was carried out to record and analyze the dynamic cutting forces, the vibrations of the spindle head and workpiece, and the surface roughness and waviness. Corresponding simulations of the machining processes of these cutting trials based on the machining dynamics model were investigated and the simulation results are analyzed and compared to the measurements. It was shown that the proposed machining dynamics model could well predict the dynamic cutting forces, the vibrations of the cutter and workpiece.

Ozcelik et al. [220] determined optimum cutting parameters of Inconel 718 to enable minimum surface roughness under the constraints of roughness and MRR. In doing this, advantages of statistical experimental design technique, experimental measurements, ANN and genetic optimization method were exploited in an integrated manner. Cutting experiments were designed based on statistical three-level full factorial experimental design technique. A predictive model for surface roughness was created using a feed-forward ANN exploiting experimental data. Neural network model and analytical definition of MRR were employed in the construction of optimization problem. The optimization problem was solved by an effective genetic algorithm for variety of constraint limits. Additional experiments were conducted to compare optimum values and their corresponding roughness and MRR values predicted from the genetic algorithm. The authors opined that the neural network model coupled with genetic algorithm can be effectively utilized to find the best or optimum cutting-parameter values for a specific cutting condition in end milling of Inconel 718. Budak and Tekeli [44] had shown that, for the maximization of chatter free MRR, radial depth of cut is of equal importance. The authors had proposed a method to determine the optimal combination of depths of cut, so that chatter free MRR is maximized. The application of the method was demonstrated on a pocketing example where significant reduction in the machining time was obtained using the optimal depths. The procedure can easily be integrated to a CAD/CAM system or a virtual machining environment in order to identify the optimal milling conditions.

Reddy and Rao [242] conducted experimental studies to see the effect of tool geometry (radial rake angle and nose radius) and cutting conditions (cutting speed and feed rate) on the machining performance during end milling of medium carbon steel. The first and second order mathematical models, in terms of machining parameters, were developed for surface roughness prediction using response surface methodology (RSM) on the basis of experimental results. The model selected for optimization was validated with the Chi-square test. The significance of these parameters on surface roughness was established with ANOVA. An attempt was also been made to optimize the surface roughness prediction model using genetic algorithms (GA). The GA program gave minimum values of surface roughness and their respective optimal conditions. In another work, Reddy and Rao [243] presented an experimental investigation of the influence of tool geometry (radial rake angle and nose radius) and cutting conditions (cutting speed and feed rate) on machining performance in dry milling with four fluted solid TiAlN-coated carbide end mill cutters based on Taguchi's experimental design method. The mathematical model, in terms of machining parameters, was developed for surface roughness prediction using RSM. The optimization was then carried out with genetic algorithms using the surface roughness model developed. This methodology helps to determine the best possible tool geometry and cutting conditions for dry milling.

Dutta et al. [78] predicted the wear of the tungsten carbide inserts using neural network during face milling of steel. They proposed a new approach called modified back-propagation neural network with delta bar delta (MBPNND)

learning to enhance the convergence speed and prediction accuracy of the network. The authors found that MBPNND was efficient compared to three other approaches, viz., back-propagation neural network, fuzzy back-propagation neural network, and modified back-propagation neural network.

Öktem et al. [210] developed a Taguchi optimization method for low surface roughness in terms of process parameters when milling the mold surfaces of 7075-T6 aluminum material. Considering the process parameters of feed, cutting speed, axial-radial depth of cut, and machining tolerance, a series of milling experiments were performed to measure the roughness data. A regression analysis was applied to determine the fitness of data used in the Taguchi optimization method using milling experiments based on a full factorial design. Taguchi orthogonal arrays, S/N ratio, and ANOVA were used to find the optimal levels and the effect of the process parameters on surface roughness. Sreeram et al. [280] investigated the process parameter optimization aspects of the micro-end milling. The influence of depth of cut on tool life was illustrated and depth of cut was also considered as one of the decision variables in the optimization problem. Genetic algorithms (GA) was used to optimize the cutting parameters.

Baskar et al. [33] outlined the development of an optimization strategy to determine the optimum cutting parameters for multi-tool milling operations like face milling, corner milling, pocket milling and slot milling. The developed strategy was based on the maximum profit rate criterion and incorporated five technological constraints. Optimization procedures based on the genetic algorithm, hill climbing algorithm and memetic algorithm were demonstrated for the optimization of machining parameters for milling operation. An objective function based on maximum profit in milling operation was developed and the results obtained were used in NC machine. The results were compared and analyzed with method of feasible directions and handbook recommendations. Onwubolu [211, 212] proposed a new optimization technique based on Tribes for determination of the cutting parameters in multi-pass milling operations such as plain milling and face milling by simultaneously considering multi-pass rough machining and finish machining. The optimum milling parameters were determined by minimizing the maximum production rate criterion subject to several practical technological constraints. The cutting model formulated was a nonlinear, constrained programming problem. Although the results obtained in his work using tribes showed significant improvement over other traditional and non-traditional algorithms, but the results are not valid as some of the constraints in the solution obtained are violated.

Cus et al. [65] presented an intelligent system for on-line monitoring and optimization of the cutting process on the model of the ball-end milling. An intelligent system for monitoring and optimization in ball-end milling was developed both in hardware and software. It was based on a PC, which was connected to the CNC main processor module through a serial-port so that control and communication could be realized. The monitoring system was based on LabVIEW software, the data acquisition system and the measuring devices (sensors) for the cutting force measuring. The measured values were delivered to

the computer program through the data acquisition system for data processing and analysis. The optimization technique was based on genetic algorithms for the determination of the cutting conditions in machining operations. Experimental results showed that the proposed genetic algorithm-based procedure for solving the optimization problem can be integrated into a real-time intelligent manufacturing system for solving complex machining optimization problems. Tang [287] studied an optimization strategy for high-speed machining of hardened die/mold steel based on machining feature analysis. An objective function concerning machining cost and associated optimization algorithm based on machining time and cutting length calculation was proposed. Constraints to satisfy specific machining strategies when high-speed machining the hardened die/mold steel, trochoid tool path pattern in slot end milling to avoid over-heat and feed rate adaptation to avoid over-load, were also discussed. As a case study, the tool selection problem when machining a die part with multiple machining features was investigated.

Aykut et al. [22] used ANNs for modeling the effects of machinability on chip removal cutting parameters for face-milling of satellite 6 in asymmetric milling processes. Cutting forces with three axes were predicted by changing cutting speed, feed rate and depth of cut under dry conditions. Experimental studies were carried out to obtain training and test data and scaled conjugate gradient (SCG) feed-forward back-propagation algorithm was used in the networks. Main parameters for the experiments were the cutting speed, feed rate, depth of cut and cutting forces. These results showed that the ANNs can be used for predicting the effects of machinability on chip removal cutting parameters for face-milling of satellite 6 in asymmetric milling processes. Fontaine et al. [92, 93] studied the influence of tool-work piece inclination on cutting forces in ball-end milling. Cutting forces calculated from a thermomechanical modeling were discussed in detail and compared to experimental results. The proposed modeling of ball-end milling was applied to machining operations with straight tool paths and various tool-surface inclinations. Both ramping and contouring configurations were studied. The experimental results were obtained from ball-end milling tests performed on a three-axis CNC equipped with a Kistler dynamometer. The evolution of the maximum values of cutting forces acting on the tool was investigated in order to identify the optimum inclination angle. Influences of cutting conditions, radial run-out and plowing on cutting forces and cutting stability were discussed.

Ghosh et al. [104] developed a neural network-based sensor fusion model to estimate tool wear during CNC milling process. Signals in the form of cutting forces, spindle motor current, and sound pressure level were used as inputs for neural network. The authors had proposed newer methods such as feature space filtering, prediction space filtering, etc., to improve prediction accuracy and found that the prediction is satisfactory in a real-time error prone environment. Palanisamy et al. [224] developed a mathematical model based on both the material behavior and the machine dynamics to determine cutting force for milling operations. The system used for optimization was based genetic algorithms.

The machining time was considered as the objective function and constraints were tool life, limits of feed rate, depth of cut, cutting speed, surface roughness, cutting force and amplitude of vibrations while maintaining a constant MRR. Experimental end-milling tests were performed on mild steel to measure surface roughness, cutting force using milling tool dynamometer and vibration using a fast Fourier transform (FFT) analyzer for the optimized cutting parameters in a universal milling machine using an HSS cutter.

Ching-Kao and Lu [59] presented an optimal cutting-parameter design of heavy cutting in side milling for SUS304 stainless steel. The orthogonal array with grey-fuzzy logic was applied to optimize the side milling process with multiple performance characteristics. A grey-fuzzy reasoning grade obtained from the grey-fuzzy logics analysis was used as a performance index to determine the optimal cutting parameters. The selected cutting parameters were spindle speed, feed per tooth, axial depth of cut and radial depth of cut, while the considered performance characteristics were tool life and metal removal rate (MRR). The results of confirmation experiments revealed that grey-fuzzy logic could effectively acquire an optimal combination of the cutting parameters.

Kadirgama et al. [139] developed the surface roughness prediction models, with the aid of statistical methods, for hastelloy C-22HS when machined by physical vapor deposition (PVD)- and chemical vapor deposition (CVD)-coated carbide cutting tools under various cutting conditions. These prediction models were then compared with the results obtained experimentally. By using RSM, first order models were developed with 95% confidence level. The surface roughness models were developed in terms of cutting speed, feed rate and axial depth using RSM as a tool of DoE. In general, the results obtained from the mathematical models were in good agreement with those obtained from the machining experiments. It was found that the feed rate, cutting speed and axial depth played a major role in determining the surface roughness. PVD-coated cutting tool performed better than CVD when machining hastelloy C-22HS. It was observed that most of the chips from the PVD-cutting tool were in the form of discontinuous chip while CVD-cutting tool produced continuous chips.

SSavas and Ozay [262] presented an approach for optimization of cutting parameters leading to minimum surface roughness by using genetic algorithm in the tangential turn-milling process. During testing, the effects of the cutting parameters on the surface roughness were investigated. Additionally, by using genetic algorithms for each of the cutting parameters (depth of cut, work piece speed, tool speed and feed rate) minimum surface roughness for the process of tangential turn-milling was determined according to the cutting parameters.

Onwubolu et al. [218] presented an enhanced approach to predictive modeling for determining tool-wear in end-milling operations based on enhanced-group method of data handling (e-GMDH). Using milling input parameters (speed, feed, and depth of cut) and response (tool wear), the data for the model was partitioned into training and testing datasets, and the training dataset was used to realize a predictive model that was a function of the input parameters and the coefficients

determined. The results realized using e-GMDH method were promising, and the comparative study presented showed that the e-GMDH outperforms polynomial neural network (PNN). The extended PSO technique was applied to obtain the optimal parameters.

Chakraborty et al. [48] focused on end-milling of AISI 4340 steel with multi-layer PVD-coated carbide inserts under semi-dry and dry cutting conditions and proposes a mixed effects model for the analysis of the longitudinal data obtained from a designed experiment. This modeling approach considered unobserved heterogeneity during machining and proposed a tool wear progression model that has a higher power of detecting effects of significant factors than traditional regression models. One such source of variation is work piece hardness that was observed within and across test blocks. From the wear progression model developed, the lowest initial flank wear values were obtained at a cutting speed of 183 m/min, a feed rate of 0.10 mm/rev under semi-dry cutting conditions. A higher rate of wear progression and lower tool life was observed at the higher cutting speed level of 229 m/min. Cutting speed had the most significant effect on flank wear progression in this study. Depth of cut on the other hand did not show any significant effect on tool wear when compared to cutting speed, feed and cutting conditions. From this analysis, diffusion wear was confirmed under both semi-dry and dry machining conditions. It was expected that the proposed model could reduce the number of repetitions in tool wear modeling experiment for tool manufacturers leading to substantial cost savings.

Rai and Xirouchakis [235] presented an overview of a comprehensive finite element method (FEM)-based milling process plan verification model and associated tools, which by considering the effects of fixturing, operation sequence, tool path and cutting parameters simulates the milling process in a transient 3D virtual environment and predicts the part thin wall deflections and elastic–plastic deformations during machining. The prediction accuracy of the model was validated experimentally and the obtained numerical and experimental results were found in good agreement.

Wan et al. [304] developed a systematic procedure to simulate the peripheral milling process of thin-walled workpiece. The procedure integrates the cutting force module consisting of calculating the instantaneous uncut chip thickness, calibrating the instantaneous cutting force coefficients and the cutting process module consisting of calculating the cutting configuration and static form errors. It can be used to check the process reasonability and to optimize the process parameters for high precision milling. The regeneration mechanism in flexible static end milling was investigated both theoretically and numerically. Comparisons of the cutting forces and form errors obtained numerically and experimentally confirmed the validity of the simulation procedure.

Merdol and Altintas [191] presented generalized process simulation and optimization strategies to predict and improve the performance of three-axis milling operations. Cutter-part engagement conditions were extracted from a solid modeling system. The cutting force distribution along the engaged cutting edge-part surface was evaluated based on the laws of mechanics of milling. By integrating

the distributed force along the cutting edge, total forces, torque and power were either predicted analytically using closed-form solutions, or numerically if the cutting tool shape was discontinuous. Simulation results were then used in a constraint-based optimization scheme to maximize the MRR by calculating acceptable feed rate levels. The proposed virtual milling system was demonstrated experimentally in milling a stamping die with free form surfaces.

Iqbal et al. [132] developed a fuzzy expert system for parameter optimization that includes prediction of tool life and surface finish in hard-milling (high-speed milling of steel having 45 HRC hardness) process. Lu et al. [185] investigated optimum design of the cutting parameters for rough cutting processes in high-speed end milling on SKD61 tool steel. The major performance characteristics selected to evaluate the processes were tool life and MRR, and the corresponding cutting parameters were milling type, spindle speed, feed per tooth, radial depth of cut, and axial depth of cut. Grey relational analysis that uses grey relational grade as performance index was specially adopted to determine the optimal combination of cutting parameters. Moreover, the principal component analysis was applied to evaluate the weighting values corresponding to various performance characteristics so that their relative importance could be properly and objectively described. The results of confirmation experiments revealed that grey relational analysis coupled with principal component analysis can effectively acquire the optimal combination of cutting parameters.

Budak et al. [45] presented models for 5-axis milling process geometry, cutting force and stability. The application of the models in selection of important parameters was also demonstrated. A practical method, developed for the extraction of cutting geometry, was used in simulation of a complete 5-axis cycle. Totis [290] presented a new probabilistic algorithm for a robust analysis of stability in milling, which performs the stability analysis on an uncertain dynamic milling model. In this approach, model parameters were considered as random variables, and robust analysis of stability was carried out in order to estimate system's probability of instability for a given combination of cutting parameters. By doing so, probabilistic instead of deterministic stability lobes were obtained, and a new criterion for system stability based on level curves and gradient of the probabilistic lobes could be applied to identify optimal robust stable cutting conditions. Experimental validation consisted of different phases: firstly, machining system dynamics were estimated by means of pulse tests. Secondly, cutting force coefficients were determined by performing cutting tests. Eventually, chatter tests were performed and the experimental stability lobes were compared with the predicted robust stable regions.

Ho et al. [125] used ANFIS with the genetic learning algorithm to predict the work piece surface roughness for the end-milling process. The hybrid Taguchi-genetic learning algorithm (HTGLA) was applied in the ANFIS to determine the most suitable membership functions and to simultaneously find the optimal premise and consequent parameters by directly minimizing the root-mean-squared-error performance criterion. Experimental results showed that the HTGLA-based ANFIS approach outperforms the ANFIS methods given in the Matlab toolbox.

Yang et al. [319] applied the DoE approach to optimize parameters of a CNC end-milling process for high-purity graphite under dry machining. The groove difference (i.e., dimensional accuracy of groove width) and the roughness average at the bottom plane of the inside groove (i.e., the plane of end milling) were studied. Planning of experiment was based on a Taguchi orthogonal array table. The ANOVA was adapted to identify the most influential factors on the CNC end-milling process. Simultaneously, a mathematical predictive model for predictions of the groove difference and the roughness average was developed by applying regression analysis in terms of cutting speed, feed rate, and depth of cut. The feed rate was found to be the most significant factor affecting the groove difference and the roughness average in end-milling process for high-purity graphite.

Kersting and Zabel [144] developed an optimization approach based on the multi-objective evolutionary algorithm S-metric selection evolutionary multi-objective optimization algorithm (SMS-EMOA) combined with a multi-population approach for NC tool path optimization in a five-axis milling process. It was shown that the idea of taking one evolutionary run in every restriction-free area increases the diversity of the NC-path designs and could also improve the corresponding Pareto fronts. Experiments on different NC-paths structures—such as circular, linear, and angled segments—showed promising results for characteristic elements.

Onwubolu [213] introduced a combined hybrid group method for data handling and optimization approach to predict burr types formed during face milling. The hybrid group method for data handling (hybrid GMDH) network was constructed for realizing predictive models for the machining of aluminum alloy, and differential evolution was selected for the optimization of burr formation problem resulting in finding optimal parameter for minimizing burr formation. Burr type was included as a parameter resulting in a classification scheme in which the burr type becomes the group label and it is therefore possible in the future to classify a machining process into any of these burr types. The resulting hybrid GMDH output was in agreement with experimental results.

Patel et al. [227] presented an experimental study to optimize the surface quality of an end-milled surface on a Vertical Machining Center using Taguchi's nested experimental design. The effect of various machining parameters on surface roughness was investigated on two different work piece materials, Aluminum alloy and Plain Carbon Steel. Other control factors, namely, feed rate and spindle speed, depth of cut and radial engagement of tool were varied in the experiment to measure surface roughness at four different positions on the work piece. Position was taken as an uncontrollable noise factor. Depth of cut was observed to be the most significant factor that affecting the surface roughness. Also, better surface finish was obtained while machining aluminum alloy as compared to plain carbon steel. Spindle speed and feed rate were the other two significant factors while machining aluminum alloy parts, although these factors did not significantly affect the finish for steel. Radial engagement of tool had no impact on the surface finish for aluminum alloy, while it had a significant impact for plain carbon steel.

Routara et al. [245] conducted experiments for three different work piece materials to see the effect of work piece material variation in this respect. Five roughness parameters, viz., center line average roughness, root mean square roughness, skewness, kurtosis and mean line peak spacing were considered. The second-order mathematical models, in terms of the machining parameters, were developed for each of these five roughness parameters prediction using RSM on the basis of experimental results. The roughness models as well as the significance of the machining parameters were validated with ANOVA. It was found that the response surface models for different roughness parameters were specific to work piece materials. An attempt was also made to obtain optimum cutting conditions with respect to each of the five roughness parameters using a response optimization technique.

Prakasvudhisarn et al. [231] proposed an approach to determine optimal cutting condition for desired surface roughness in end milling. The approach consists of two parts: machine learning technique called support vector machine to predict surface roughness and PSO technique for parameters optimization. The authors found that PSO showed consistent near-optimal solution with little effort. Uros et al. [298] developed a reliable method to predict flank wear during end-milling process. A neural-fuzzy scheme was applied to perform the prediction of flank wear from cutting force signals. The construction of an ANFIS system that seeks to provide a linguistic model for the estimation of tool wear from the knowledge embedded in the neural network was presented. Machining experiments conducted indicated that using an appropriate maximum force signals, the flank wear could be predicted within 4% of the actual wear for various end-milling conditions.

Yildiz [321] presented a new hybrid optimization approach based on immune algorithm and hill climbing local search algorithm. The purpose was to develop a new optimization approach for solving design and manufacturing optimization problems. In order to evaluate the proposed optimization approach, single objective test problem, multi-objective I-beam and machine-tool optimization problems taken from the literature were solved. Finally, the hybrid approach was applied to a case study for milling operations to show its effectiveness in machining operations. The results of the hybrid approach for the case study were compared with those of genetic algorithm, the feasible direction method and handbook recommendations.

Zarei et al. [324] presented a harmony search (HS) algorithm to determine the optimum cutting parameters for multi-pass face milling. The optimum value of machining parameters including number of passes, depth of cut in each pass, speed and feed was obtained to minimize total production cost while considering technological constraints such as allowable speed, feed, surface finish, tool life and machine-tool capabilities. An illustrative example was used to demonstrate the ability of the HS algorithm and for validation purpose, the genetic algorithm (GA) was used to solve the same problem. Comparison of the results revealed that the HS algorithm converges to optimum solution with higher accuracy in comparison with GA. Wei et al. [313] presented an approach for modeling of the

process geometry in peripheral milling of curved surfaces. The modeled process geometry involves feed direction, equivalent feedrate and cutter entry/exit angle. The equivalent feedrate, which was defined at the centroid of cutting cross-section, was proposed to measure the actual machining feedrate. The milling process of curved surface was discretized at intervals of feed per tooth for describing the variation of process geometry. The mathematical models for calculating the process geometry of each segmented cutting process were presented. Two same curved surfaces were machined. The tool paths were carried out with NURBS interpolation and traditional consecutive small line segments interpolation, respectively.

Rao and Pawar [237] presented optimization aspects of a multi-pass milling operation. The objective considered was minimization of production time (i.e. maximization of production rate) subjected to various constraints of arbor strength, arbor deflection, and cutting power. Various cutting strategies were considered to determine the optimal process parameters like the number of passes, depth of cut for each pass, cutting speed, and feed. The upper and lower bounds of the process parameters were also considered. The optimization was carried out using three non-traditional optimization algorithms namely, ABC, PSO, and simulated annealing (SA). An application example was presented and solved to illustrate the effectiveness of the presented algorithms. The results of the presented algorithms were compared with the previously published results obtained by using other optimization techniques. The authors had reported that the convergence rate of ABC and PSO algorithms was very high and these algorithms required only little iteration for convergence to the optimal solution, whereas SA algorithm required comparatively more iterations for convergence. The accuracy of solution obtained by using ABC and PSO algorithms was better as compared to the results obtained by using SA algorithm.

Now an example is presented to demonstrate the process parameter optimization of multi-pass milling operations.

2.2.1 *Example 1: Process Parameter Optimization of Multi-pass Milling for Maximization of Production rate*

This example is focused on optimization of process parameters of multi-pass milling operations considering minimization of total production time as the objective function (i.e. maximization of production rate) with constraints of arbor strength, arbor deflection and cutting power. Feed per tooth, speed and depth of cut are considered as process parameters.

The optimization model of milling process is formulated based on the analysis given by Sonmez et al. [278]. The decision variables (i.e. process parameters) considered for this model are feed per tooth (f_z), cutting speed (V) and depth of cut (a). The objective function and the constraints are formulated as discussed below.

For a milling operation, the total production time (T_{pr}) is composed of the following items:

1. Machine preparation time (T_p), which is as given by Eq. 2.1

$$T_p = T_s/N_b \tag{2.1}$$

where T_s = setup time, and N_b = total number of components in batch.

2. Loading unloading time (T_L)
3. Process adjusting and quick return time (T_a)
4. Machining time (T_m)
5. Tool changing time per component (T_c), which is as given by Eq. 2.2

$$T_c = T_d T_m/T \tag{2.2}$$

where T_d = time for changing a dull cutting edge or tool and T = tool life

For a single pass milling operation, the total production time (T_{pr}) is the sum of the above time elements and can be written as:

$$T_{pr} = T_p + T_L + T_a + T_m + T_c \tag{2.3}$$

or

$$T_{pr} = (T_s/N_b) + T_L + T_a + T_m + T_d(T_m/T) \tag{2.4}$$

For a multi-pass operation, Eq. 2.4 becomes

$$T_{pr} = (T_s/N_b) + T_L + \sum_{i=1}^{Np} T_{ai} + T_{mi} + T_d(T_{mi}/T) \tag{2.5}$$

where N_p = total number of passes and subscript '*i*' denotes *i*th pass.

For a particular milling operation, the machining time is given as:

$$T_m = L/f \tag{2.6}$$

where L = length of cut, f = feed rate = $f_z \times z \times N$; where f_z = feed per tooth, z = number of teeth on milling cutter, and N = spindle speed (rpm).

N is given by equation:

$$N = 1,000V/\pi D \tag{2.7}$$

where D = cutter diameter, V = cutting speed.

Tool life can be determined by using the formula given by Eq. 2.8.

$$T = \left(\left(C_v^{1/m} D^{(bv/m)}\right)\left(B_m B_h B_p B_t\right)^{1/m}\right) \Big/ \left(V^{1/m} a^{ev/m} f_{zi}^{uv/m} a_r^{rv/m} z^{nv/m} \lambda_s^{qv/m}\right) \tag{2.8}$$

where a = depth of cut, a_r = width of the cut, B_m, B_k, B_p, B_t are the correction coefficients, m, ev, uv, rv, nv, qv, and bv are the exponents, C_v = process constant, and λ_s = cutting inclination angle.

On substituting Eqs. 2.6, 2.7, and 2.8 in Eq. 2.5, the objective function for multi-pass milling operation is expressed as given by Eq. 2.9.

$$T_{pr} = (T_s/N_b) + T_L + N_p T_a + \sum_{i=1}^{Np} \pi DL/f_{zi} z 1{,}000 V_i + W \tag{2.9}$$

where $W = [(T_d \pi L V_i^{(1/m\ -\ 1)} a_i^{ev/m} f_{zi}^{(uv/m\ -\ 1)} a_r^{rv/m} z^{(nv/m\ -\ 1)} \lambda_s^{qv/m})/(1{,}000 C_v^{1/m} D^{(bv/m\ -\ 1)})] \times (B_m B_h B_p B_t)^{1/m}$.

Following three constraints are considered in this optimization model:

1. Arbor strength: The arbor is subjected to torsion from the action of resistance to cutting. Therefore, the selected values of process parameters should ensure that the arbor is safe from strength point of view.

$$F_s - F_c \geq 0 \tag{2.10}$$

where

$$\text{mean peripheral cutting force} = F_c = C_{zp} a_r z D^{bz} a^{ez} f_z^{uz} \tag{2.11}$$

C_{zp} = process constant; bz, ez, and uz are exponents.
Permissible force for arbor strength (kg) = F_s

$$F_s = 0.1 k_b d_a^3 \Big/ \left(\left(0.08 L_a + 0.65 \left((0.25 L_a)^2 + (0.5 \alpha D)^2 \right)^{1/2} \right) \right) \tag{2.12}$$

where k_b = permissible bending strength of arbor; d_a = arbor diameter; L_a = arbor length between supports; $\alpha = k_b/(1.3\ k_t)$; k_t = permissible torsional strength of arbor.

2. Arbor deflection: The selected values of process parameters should be checked for arbor deflection as given by Eq. 2.13.

$$F_d - F_c \geq 0 \tag{2.13}$$

where F_d is the permissible force for arbor deflection (kg)

$$F_d = 4 E e d_a^4 / L_a^3 \tag{2.14}$$

where E = modulus of elasticity of arbor material; e = permissible value of arbor deflection.
For roughing operation $e = 0.2$ mm and for finishing operation $e = 0.05$ mm.

3. Power: Power required for the cutting operation should not exceed the effective power transmitted to cutting point by the machine tool. This is ensured by Equation 2.15.

$$P_c - (F_c V/6, 120) \geq 0 \tag{2.15}$$

where P_c = cutting power (kW) = P_m*η, P_m = nominal motor power, η = overall efficiency.
The three process parameters and their bounds considered are as given below.

i. Feed per tooth: The optimum feed must be in the range determined by maximum and minimum values of the feed rates of the machine.

$$f_{z\min} \leq f_z \leq f_{z\max} \tag{2.16}$$

where

$$f_{z\min} = f_{\min}/zN_{\max} \tag{2.17}$$

$$f_{z\max} = f_{\max}/zN_{\min} \tag{2.18}$$

f_{max} = maximum spindle feed rate (mm/min) and f_{min} = minimum spindle feed rate (mm/min), N_{max} = maximum spindle speed, N_{min} = minimum spindle speed.

ii. Cutting speed: The optimum cutting speed must be in the range determined by maximum spindle speed ($N_{max)}$ and minimum spindle speed ($N_{min)}$ of the machine.

$$V_{\min} \leq V \leq V_{\max} \tag{2.19}$$

where

$$V_{\max} = \pi DN_{\max}/1,000 \tag{2.20}$$

$$V_{\min} = \pi DN_{\min}/1,000 \tag{2.21}$$

iii. Depth of cut: For a milling operation, the upper and lower bounds for depth of cut are as specified by Eq. 2.22.

$$a_{\min} \leq a \leq a_{\max}(\text{mm}) \tag{2.22}$$

where a_{min} is the minimum depth of cut and a_{max} is the maximum depth of cut.

Specifications of the required parameters and values of the constants considered by Sonmez et al. [278] and used in the present work are given below:

- Type of machining: plain milling
- Motor power (P_m) = 5.5 kW, efficiency, η = 0.7
- Arbor diameter d_a = 27 mm, arbor length between supports L_a = 210 mm
- Permissible bending stress of arbor k_b: 140 MPa
- Permissible torsional stress of arbor k_t: 120 MPa
- Modulus of elasticity of arbor material E = 200 GPa
- Spindle speed range: 31.5–2,000 rpm, feed rate range 14–900 mm/min
- Tool material HSS, tool diameter D = 63 mm, number of teeth z = 8

- Material: structural carbon steel (C # 0.6%)
- Tensile strength 750 MPa, Brinell hardness number = 150
- Length of cut $L_a = 160$ mm, width of cut $a_r = 50$ mm, depth of cut $a = 5$ mm
- Loading and unloading time of one work piece $T_L = 1.5$ min
- Set-up time of fixtures and machine tool $T_s = 10$ min
- Tool change time $T_c = 5$ min
- Process adjusting and quick return time $T_a = 0.1$ (min/part)
- Lot size (number of parts in the batch) $N_b = 100$
- Cutting inclination = 30°
- Constants: $B_m = 1$, $B_k = 1$, $B_p = 0.8$, $B_t = 0.8$, $m = 0.33$, $ev = 0.3$, $uv = 0.4$, $rv = 0.1$, $nv = 0.1$, $qv = 0$, $Cv = 35.4$, $bv = 0.45$, $C_{zp} = 68.2$, $bz = -0.86$, $ez = 0.86$, and $uz = 0.72$.

Bounds for variables:

$$0.000875 \leq f_z \leq 3.571 \tag{2.23}$$

$$6.234 \leq V \leq 395.84(\text{m/min}) \tag{2.24}$$

$$0.5 \leq a \leq 4(\text{mm}) \tag{2.25}$$

In the present work, various feasible cutting strategies are adopted to determine the optimum number of passes required and depth of cut for each pass. The results of optimization for these strategies using ABC algorithm are shown in Table 2.1. It is observed from Table 2.1 that among various cutting strategies for multi-pass milling with total depth of cut of 5 mm, the strategy 2 with three rough cuts each

Table 2.1 Results of optimization using ABC for various cutting strategies in milling operation (from [237]; reprinted with permission from Elsevier)

Sr No.	Cutting strategy	f_z (mm/tooth)	V (m/min)	T_2 (per pass) (min)	T_2 (min)	T_1 (min)	$T_{pr} = (T_1 + T_2)$ min
1	$a_{rough} = 2$	0.231	48.117	0.475	1.378	1.9	3.278
	$a_{rough} = 2$	0.231	48.117	0.475			
	$a_{finish} = 1$	0.189	74.090	0.428			
2	$a_{rough} = 1.5$	0.337	46.982	0.343	1.240	2.0	3.240
	$a_{rough} = 1.5$	0.337	46.982	0.343			
	$a_{rough} = 1.5$	0.337	46.982	0.343			
	$a_{finish} = 0.5$	0.432	64.41	0.211			
3	$a_{rough} = 2$	0.231	48.117	0.475	1.355	2.0	3.355
	$a_{rough} = 1$	0.552	47.519	0.226			
	$a_{rough} = 1$	0.552	47.519	0.226			
	$a_{finish} = 1$	0.189	74.090	0.428			
4	$a_{rough} = 1$	0.552	47.519	0.226	1.332	2.1	3.432
	$a_{rough} = 1$	0.552	47.519	0.226			
	$a_{rough} = 1$	0.552	47.519	0.226			
	$a_{rough} =$	0.552	47.519	0.226			
	$a_{finish} = 1$	0.189	74.090	0.428			

of 1.5 mm and a finish cut of 0.5 mm is optimum as indicated by minimum production time of 3.24 min. The value of feed per tooth for finishing cut provided by strategy 2 is also much less than that provided by other strategies. In milling operation as the feed per tooth decreases, surface finish increases. Hence strategy 2 also ensures better surface finish as compare to other strategies.

The optimum process parameter values obtained by ABC algorithm for a given multi pass milling operation are given below:

- Number of passes required = 4.
- Number of rough cutting passes = 3 with depth of cut in each roughing pass = 1.5 mm
- Number of finish passes = 1 with depth of cut in finishing pass = 0.5 mm.
- For roughing pass: feed per tooth = 0.337 mm/tooth and cutting speed = 46.982 m/min
- For finishing pass: feed per tooth = 0.432 mm/tooth and cutting speed = 64.41 m/min
- Total production time (T_{pr}) = 3.240 min.

Optimality of the above-mentioned solution could be confirmed from the Figs. 2.2, 2.3, 2.4, 2.5, and 2.6. Figure 2.2 shows variation of production time and various constraints with feed per tooth for rough milling operation. As feed per tooth increases, production time reduces; hence higher value of feed rate is desired. However, the strength constraint is violated after feed per tooth attains a value of 0.337 mm. This confirms the optimum value of feed per tooth selected using ABC algorithm for rough milling operation.

Figure 2.3 shows variation of production time and constraints with cutting speed for rough milling operation. Since the deflection constraint is having a constant positive value in this figure, Fig. 2.4 is plotted neglecting the deflection

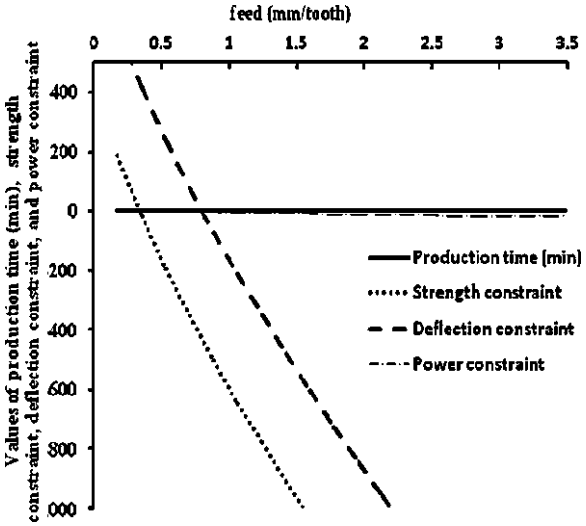

Fig. 2.2 Variation of production time and constraints with feed per tooth for rough milling (from [237]; reprinted with permission from Elsevier)

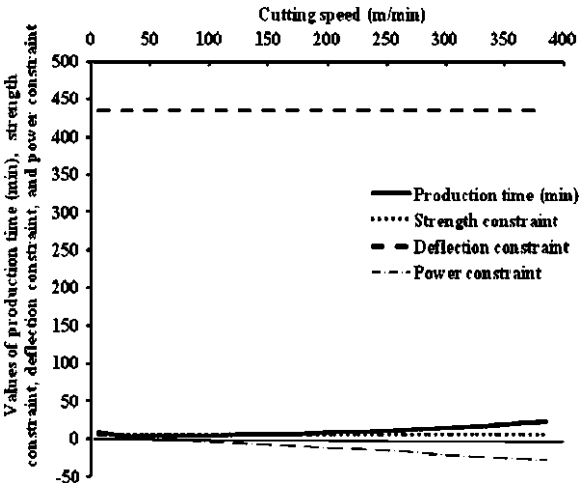

Fig. 2.3 Variation of production time and constraints with cutting speed for rough milling (from [237]; reprinted with permission from Elsevier)

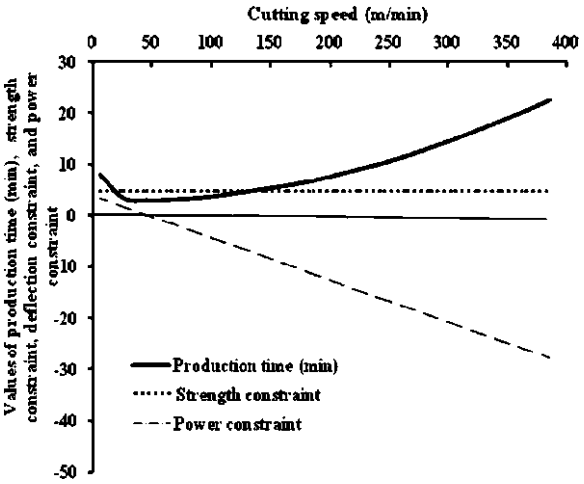

Fig. 2.4 Variation of production time and constraints with cutting speed for rough milling neglecting the deflection constraint (from [237]; reprinted with permission from Elsevier)

constraint to indicate more clearly the variation of production time and other two constraints with cutting speed. As shown in Fig. 2.4, production time initially decreases with increase in cutting speed, till cutting speed attains a value of 47 m/min, after which the production time increases with increase in cutting speed. Thus, a cutting speed of 47 m/min is considered as optimum and the production time is minimum at this cutting speed value without violating any constraint.

Figure 2.5 shows variation of production time and constraints with feed per tooth for finish milling operation. Although higher value of feed per tooth is desired to achieve minimum value of production time, the deflection constraint is violated for any value of feed per tooth higher than 0.432 mm. This confirms the optimum value of feed per tooth selected using ABC algorithm.

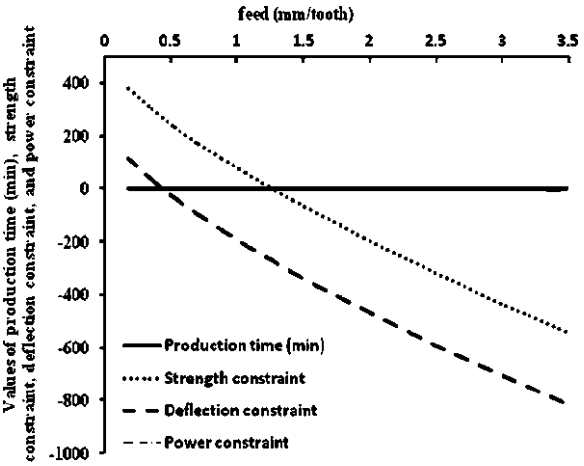

Fig. 2.5 Variation of production time and constraints with feed per tooth for finish milling (from [237]; reprinted with permission from Elsevier)

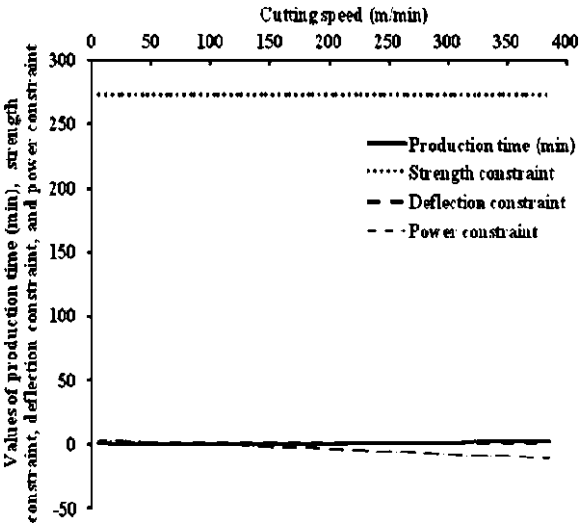

Fig. 2.6 Variation of production time and constraints with cutting speed for finish milling (from [237]; reprinted with permission from Elsevier)

Figure 2.6 shows variation of production time and constraints with cutting speed for finish milling operation. Since the strength constraint is having a constant positive value in this figure, Fig. 2.7 is plotted neglecting the strength constraint to indicate more clearly the variation of production time and other two constraints with cutting speed. As shown in Fig. 2.7, production time initially decreases with increase in cutting speed, till cutting speed attains a value of 64.41 m/min, after which the production time increases with increase in cutting speed. Thus for finish milling operation, a cutting speed of 64.41 m/min is considered as optimum and the time is minimum at this cutting speed value without violating any constraint. The results of optimization using ABC, PSO, and SA

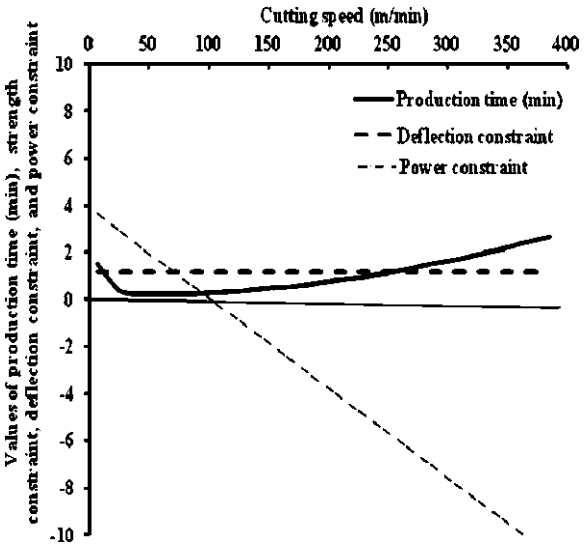

Fig. 2.7 Variation of production time and constraints with cutting speed for finish milling neglecting the strength constraint (from [237]; reprinted with permission from Elsevier)

algorithms along with those obtained by previous researchers are presented in Table 2.2.

The convergence of ABC, PSO and SA algorithms for rough milling and finish milling for maximum production rate is shown in Figs. 2.8 and 2.9 respectively.

Table 2.2 shows the comparative performance of various proposed techniques, i.e. ABC, PSO and SA along with those reported in literature by using various other optimization techniques. It is observed that for the optimum solution obtained by using optimization methods like GP, GA, PGSA, and Tribes violate most of the constraints (indicated by negative values in Table 2.2). This is due to the fact that previous researchers [211, 212, 278, 311] considered the unit of cutting force specified by Equation 2.11 in 'Newtons' whereas it must be in 'kg'. The unit of cutting force in 'kg' as considered in the present work is supported by the following two facts:

1. By considering the unit of cutting force in 'Newtons', the optimum solutions obtained by using GP, GA, PGSA and Tribes [211, 212, 278, 311] are not at all influenced by the any of the constraints. This is indicated by a very large difference between permissible value of the constraining parameter and its corresponding value provided by the optimum solution. This clearly indicates that the consideration of unit of cutting force in 'Newtons' by the previous researchers is wrong.
2. The values of feed per tooth obtained by using GP, GA, PGSA are much higher (>0.55 mm) than practically achievable value of feed per tooth (<0.45 mm) in case of plain milling operation.

Due to the above-mentioned reasons, the optimum solutions obtained by previous researchers [211, 212, 278, 311] are not valid. For the optimum solution

Table 2.2 Results of optimization for maximization of production rate in milling operation by using various optimization algorithms (from [237]; reprinted with permission from Elsevier)

Method	Cutting strategy	f_z	V	SC	DC	PC	T_2	T_{pr}
GP Sonmez et al. [278]	a_{rough} = 3	0.338	26.40	−405	24.92	−0.08	0.813	2.614
	a_{finish} = 2	0.570	25.16	−430	−702	0		
GA Wang et al. [311]	a_{rough} = 3	0.366	24.69	−459	−28.81	−0.04	0.810	2.610
	a_{finish} = 2	0.5667	25.16	−427	698	0		
PGSA Wang et al. [311]	a_{rough} = 3	0.3693	24.25	−465	−35	0.2	0.800	2.600
	a_{finish} = 2	0.5886	24.58	−452	−74	0		
Tribes Onwubolu [211]	a_{rough} = 3	0.587	36.27	−8.5	−420	−4.18	0.512	2.212
	a_{rough} = 2	0.902	30.16	−797	−1,069	−2.57		
ABC	a_{rough} = 1.5	0.337	46.982	4.708	435.02	0.004	1.240	3.240
	a_{rough} = 1.5	0.337	46.982	4.708	435.02	0.004		
	a_{rough} = 1.5	0.337	46.982	4.708	435.02	0.004		
	a_{finish} = 0.5	0.432	64.41	271.97	1.131	1.400		
PSO	a_{rough} = 1.5	0.34	46.61	1.5	431.9	0.01	1.240	3.240
	a_{rough} = 1.5	0.34	46.61	1.5	431.9	0.01		
	a_{rough} = 1.5	0.34	46.61	1.5	431.9	0.01		
	a_{finish} = 0.5	0.434	63.58	271.9	0.35	1.422		
SA	a_{rough} = 1.5	0.336	44.633	5.779	436.1	0.204	1.263	3.263
	a_{rough} = 1.5	0.336	44.633	5.779	436.1	0.204		
	a_{rough} = 1.5	0.336	44.633	5.779	436.1	0.204		
	a_{finish} = 0.5	0.429	57.23	273.91	2.296	1.683		

SC arbor strength constraint, *DC* arbor deflection constraint, *PC* power constraint

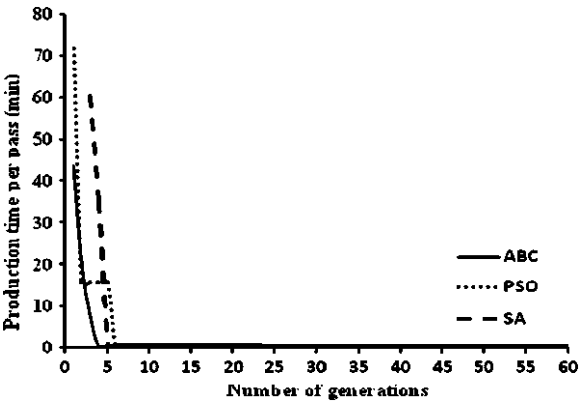

Fig. 2.8 Convergence of ABC, PSO and SA algorithms for rough milling for maximization of production rate (from [237]; reprinted with permission from Elsevier)

obtained by using ABC, PSO, and SA algorithms, the difference between permissible value of the constraining parameter and its corresponding value provided by optimum solution is very less, which proves the validity and accuracy of the solution. It also reveals the fact that the unit of cutting force considered (in 'kg') in

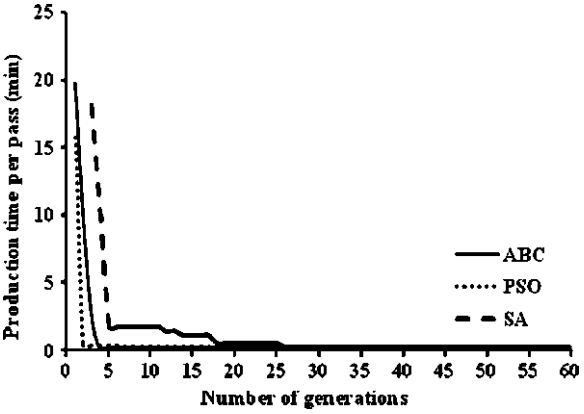

Fig. 2.9 Convergence of ABC, PSO, and SA algorithms for finish milling for maximization of production rate (from [237]; reprinted with permission from Elsevier)

this work is appropriate. Also, the value of feed per tooth provided by the optimum solution using ABC, PSO and SA is more appropriate from practical point of view. Thus, although the optimum solutions obtained by using methodologies like GP, GA, PGSA and Tribes seem to be better than that obtained by using, ABC, PSO, and SA algorithms, the optimum solution obtained by using the proposed algorithms in this work is only valid and appropriate.

2.2.2 *Example 2: Process Parameter Optimization of Multi-pass Milling for Minimization of Cost*

The optimization model for milling process formulated in the present work is based on the analysis given by Shunmugam et al. [272]. The decision variables considered are feed per tooth (s), cutting speed (V) and depth of cut (a).

The objective function in this model is to minimize the total cost (U_t) as given by the Eq. 2.26.

$$U_t = U_f + \sum_{i=1}^{n} U_{ri} + k_0 t_p \tag{2.26}$$

where U_f and U_r is the cost per pass (U) for finish and roughing operation, respectively, as given by Eq. 2.27.

$$U = k_0 t_m + (k_t z)(t_m/T_R) + k_0 t_m (z t_e/T_R) + k_0 (L h_1 + h_2) \tag{2.27}$$

where t_m is the machining time $= L_t/zsN$; $L_t = L + a_p$ (for roughing operation); $L =$ length of workpiece; a_p is approach distance; $L_t = L + D$ (for finishing operation); D is cutter diameter; z is number of teeth; k_t is cost of cutting edge; T_R is the tool replacement life; t_e is the tool-exchange time $= 1.5$ min/cut edge;

h_1 is the tool return time; h_2 is the rapid tool advance/return time; k_o is the overhead cost; t_p is the tool preparation time; and N is the spindle speed $= V/0.16\pi$.

The four practical constraints are considered in this optimization model are given below.

1. Cutting force constraint (FC):

$$S^{yF}A^{xF} \leq F_{max}D^{qF}\eta^{wF}/C_F B^{tF}z^{pF}k_F \tag{2.28}$$

2. Cutting power constraint (PC):

$$VC_p a^{xp}S^{yp}\left(B^{tp}z^{Pp}/D^{qp}\right)k_p \leq P_{max} \tag{2.29}$$

3. Surface roughness constraint (RC):

$$0.0321s^2/r_e \leq 25 \times 10^{-3}(\text{for roughing}) \tag{2.30}$$

$$0.0321s^2/r_e \leq 2.5 \times 10^{-3}(\text{for finishing}) \tag{2.31}$$

4. Tool life constraint:

$$\left(C_v K_v/T_R^m V_{max}\right)\left(D^{qv}/B^{tv}z^{pv}\right) \leq s^{yv}a^{xv} \leq \left(C_v K_v/T_R^m V_{min}\right) \tag{2.32}$$

In the above equations, F_{max} is maximum cutting force; η is the effect of rotational frequency of the spindle; B is the width of the workpiece $= 100$ mm. C_F and K_F are constants with regard to the tool and work piece material. xF, yF, tF, wF, qF, pF, C_v, m, xv, yv, pv, qv, tv, k_v, C_P, xp, yp, tp, P_P, q_P, k_P and k_F are exponents. P_{max} is the maximum cutting power; and r_e is the nose radius.Variable bounds are:

$$1 \leq a \leq 4; 0.1 \leq s \leq 0.6; 50 \leq V \leq 300.$$

As the milling operation is having multiple passes, various feasible cutting strategies are adopted to determine the optimum number of passes required and depth of cut for each pass. The results of optimization for these strategies using ABC algorithm are shown in Table 2.3. It is observed from Table 2.3 that among various cutting strategies for multi-pass milling with a total depth of cut of 8 mm, the strategy 2 with following optimum parameters is the best strategy.

- Number of passes required = 3.
- Number of rough cutting passes = 2 with depth of cut in first and second pass 4 and 3 mm, respectively.
- Number of finish passes = 1 with depth of cut in finishing pass = 1 mm.
- Feed per tooth for roughing pass 1 = 0.319 mm/tooth
- Feed per tooth for roughing pass 2 = 0.434 mm/tooth
- Feed per tooth for finishing pass = 0.275 mm/tooth

Table 2.3 Results of optimization using ABC algorithm for various strategies

Strategy number	Cutting strategy	s (mm/tooth)	V (m/min)	R_a (μm)	P (KW)	F (N)	Cost (US$)
1	$a_{rough} = 2$	0.523	77.083	8.79	7.924	6,175.14	0.377
	$a_{rough} = 2$	0.523	77.083	8.79	7.924	6,175.14	0.377
	$a_{rough} = 2$	0.523	77.083	8.79	7.924	6,175.14	0.377
	$a_{finish} = 2$	0.274	125	2.41	7.96	3,827	0.495
	Total cost						1.626
2	$a_{rough} = 3$	0.434	60.41	6.164	7.95	7,800	0.447
	$a_{rough} = 2$	0.523	77.083	8.79	7.924	6,175.14	0.377
	$a_{rough} = 2$	0.523	77.083	8.79	7.924	6,175.14	0.377
	$a_{finish} = 1$	0.275	232.08	2.44	7.96	2,061	0.374
	Total cost						1.575
3	$a_{rough} = 3$	0.434	60.41	6.164	7.95	7,800	0.447
	$a_{rough} = 3$	0.434	60.41	6.164	7.95	7,800	0.447
	$a_{rough} = 1$	0.586	133.333	11.05	8	3,602.78	0.308
	$a_{finish} = 1$	0.275	232.08	2.44	7.96	2,061	0.374
	Total cost						1.576
4	$a_{rough} = 4$	0.319	58.75	3.269	7.83	7,992.6	0.54
	$a_{rough} = 2$	0.523	77.083	8.79	7.924	6,175.14	0.377
	$a_{finish} = 2$	0.274	125	2.41	7.96	3,827	0.495
	Total cost						1.412
5	$a_{rough} = 4$	0.319	58.75	3.269	7.83	7,992.6	0.54
	$a_{rough} = 3$	0.434	60.41	6.164	7.95	7,800	0.447
	$a_{finish} = 1$	0.275	232.08	2.44	7.96	2,061	0.374
	Total cost						1.361
6	$a_{rough} = 3$	0.434	60.41	6.164	7.95	7,800	0.447
	$a_{rough} = 3$	0.434	60.41	6.164	7.95	7,800	0.447
	$a_{finish} = 2$	0.274	125	2.41	7.96	3,827	0.495
	Total cost						1.389

R_a surface roughness, P cutting power, F cutting force

- Cutting speed for roughing pass 1 = 58.75 m/min
- Cutting speed for roughing pass 2 = 60.41 m/min
- Cutting speed for finishing pass = 232.08 m/min
- Total production cost = 1.361 US$.

The performance of various algorithms namely SA, PSO, ABC, harmony search (HS) used by Zarei et al. [324], modified HS (HS_M), shuffled frog leaping (SFL), GA used by Shunmugam et al. [272] is studied in terms of accuracy of the solution and convergence rate. Table 2.4 shows the results of optimization obtained by using SA, PSO, ABC, HS_M, SFL, HS, and GA algorithms.

Figure 2.10 shows the convergence rate of SA, PSO, ABC, modified HS, and SFL algorithms. It is observed that for the present example, the PSO, ABC and SFL algorithms perform better than the other algorithms, i.e. HS [324], and GA [272]. As shown in Table 2.4, results of optimization using ABC algorithm show significant improvement of 13.45% in objective function over that of GA [272].

Table 2.4 Results of optimization by using various optimization algorithms

Method	Cutting strategy	s (mm/tooth)	V (m/min)	R_a (μm)	P (KW)	F (N)	Cost (US$)
SA	a_{rough} = 4	0.305	60.833	2.98	7.83	7,731.52	0.546
	a_{rough} = 3	0.45	59.583	6.50	7.89	7,958.20	0.450
	a_{finish} = 1	0.2725	234.166	2.38	7.96	2,042.68	0.375
	Total cost						1.371
PSO	a_{rough} = 4	0.318	60.034	3.24	7.97	7,974.05	0.536
	a_{rough} = 3	0.449	60.467	6.47	7.99	7,945.11	0.447
	a_{finish} = 1	0.2788	230.81	2.49	7.98	2,077.52	0.373
	Total cost						1.356
ABC	a_{rough} = 4	0.319	58.75	3.26	7.81	7,792.60	0.540
	a_{rough} = 3	0.444	60.41	6.33	7.98	7,879.55	0.447
	a_{finish} = 1	0.275	232.91	2.43	7.97	2,056.53	0.374
	Total cost						1.361
HS_M	a_{rough} = 4	0.261	69.58	2.18	7.98	6,889.64	0.550
	a_{rough} = 3	0.361	68.333	4.18	7.69	6,760.72	0.462
	a_{finish} = 1	0.2667	238.75	2.28	7.99	2,010.41	0.374
	Total cost						1.386
SFL	a_{rough} = 4	0.304	61.666	2.97	7.91	7,712.75	0.540
	a_{rough} = 3	0.429	61.799	5.91	7.90	7,681.68	0.450
	a_{finish} = 1	0.2783	229.58	2.49	7.93	2,024.76	0.374
	Total cost						1.364
HS Zarei et al. [324]	a_{rough} = 3	0.453	60.75	6.59	8	8,000	0.4446
	a_{rough} = 3	0.453	60.75	6.59	8	8,000	0.4446
	a_{finish} = 2	0.279	119.2	2.50	8	3,879	0.5047
	Total cost						1.3939
GA Shunmugam et al. [272, 273]	a_{rough} = 4	0.100	141.7	0.321	7.99	3,387.5	0.6589
	a_{rough} = 2	0.307	115.3	3.021	7.99	4,163.3	0.4089
	a_{finish} = 2	0.279	119.2	2.5	7.69	3,878.8	0.5047
	Total cost						1.5725

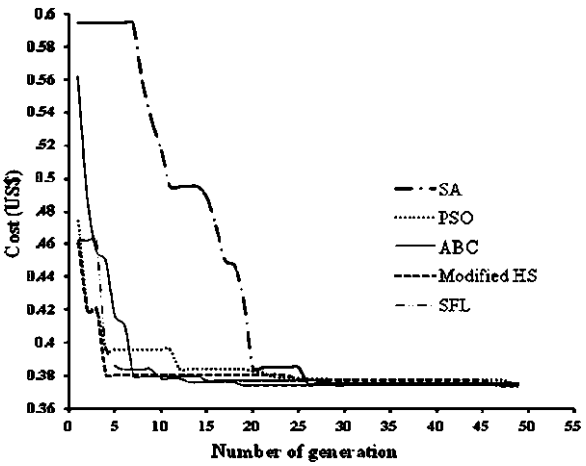

Fig. 2.10 Convergence of various algorithms for multi-pass milling optimization for cost

Although the results obtained by using the modified harmony search algorithm are almost same as that of ABC algorithm, the ABC algorithm provides better accuracy of solution than HS algorithm.

2.3 Grinding Process

Grinding is one of the important and widely used manufacturing processes in engineering industries. Grinding practice is a large and diverse area of manufacturing and tool making. It can produce very fine finishes and very accurate dimensions; yet in mass production contexts it can also rough out large volumes of metal quite rapidly. It is usually better suited to the machining of very hard materials. Compared to regular machining, it is usually better suited to taking very shallow cuts. The kind of surface to be generated, the kinematics of the machining operation as well as the shape or the profile of the grinding wheel are characteristic properties of the grinding process. As a result, there are different grinding processes: surface grinding, cylindrical grinding and shape grinding. Another factor for subdividing different grinding processes is the position of the contact area on the workpiece itself. This criterion is used to distinguish between external and internal grinding. Furthermore, it is possible to differentiate according to the active grinding wheel surface, the feed direction and the control method used. The chucking of the workpiece also has to be taken into account.

The success of any grinding process in terms of cost and quality depends on proper selection of various operating conditions in grinding process such as wheel speed, workpiece speed, depth of dressing and lead of dressing, area of contact, grinding fluid, etc. A significant improvement in the process efficiency may be obtained by appropriate modeling and optimization of these process parameters that identifies and determines the regions of critical process control factors leading to desired outputs with acceptable variations ensuring lowest cost of manufacturing. Amitay [14] reported the technique of optimizing both grinding and dressing conditions for the maximum workpiece removal rate subjected to constraints on workpiece burn and surface finish in an adaptive control system. Venk et al. [301] presented an approach to develop and use an expert system to accomplish problem formulation and aid optimization of the centerless grinding process. A detailed case study was presented to illustrate the actual working of the approach. In one case, a productivity improvement of 173% was observed over 40 optimization cycles and in another case an improvement of 540% in the parts variable cost over 42 optimization cycles was realized.

Inasaki [131] proposed in-process monitoring methods using power and acoustics emission sensors to detect malfunctions in the internal grinding process. In addition, a new internal grinding cycle featuring rapid indeed was proposed to minimize the grinding cycle time. Tönshoff et al. [289] described the state-of-the-art in the modeling and simulation of grinding processes. The kinematics of the

grinding process were characterized by a series of statistically irregular and separate engagements. Topography models were used to describe the structure of the grinding wheel, taking the quantities of motion and the geometric parameters into account. Chip formation was represented in chip thickness models. During the process of chip formation, energy was transformed. Additionally, forces were generated. The kinematic and energetic processes were taken into consideration for temperature and surface integrity models as well as for models for describing the surface roughness of the workpiece. Different approaches to modeling were compared. Furthermore, the benefits as well as the limits of model application and simulation were discussed. Trmal et al. [291] described the development of an expert system based on a grinding database and a knowledge base, which included the results and conclusions of academic research as well as industrial expertise. For a given grinding situation, the system uses a model which takes into account a number of factors dependent on the input conditions. The value of these factors was determined by the inference engine. Thus, it relates the grinding conditions (e.g., wheel type, grinding machine, workpiece material, operating parameters) to the output parameters, such as grinding force and specific energy; it also provides data on more practical industrial parameters, such as surface roughness and probability of surface burns. Sathyanarayanan et al. [260] utilized neural network approach to model the creep-feed grinding (CFG) of superalloys, Ti-6Al-4V and Inconel 718. A back-propagation learning algorithm was adopted to capture the system behavior. The neural network learns to associate the inputs (feed rate, depth of cut and wheel bond type) with the outputs (surface finish, force and power) and predicts the systems outputs within the working conditions. Mathematical formulation of a multi-objective optimization problem was then carried out by utilizing the network models. The optimization study results were presented in the form of decision tables and value path diagrams to assist the decision-making process.

Wen et al. [315] applied successive quadratic programming (QP) approach using a multi-objective function model with a weighted approach for optimization of surface grinding process parameters. However, by this approach the convergence to an optimal solution depends on the chosen initial solution. Also the algorithm tends to get stuck to the local optimal solution. Zhu et al. [330] introduced a dynamic modeling approach which was proposed as a computerized methodology to generalize grinding research findings and production expertise as far as possible and to make them available for the production grinding environment. A number of objective functions were developed to dynamically describe relationships between input and output parameters for the cylindrical plunge grinding process, such as grinding forces, specific energy, grinding temperature, surface roughness, grinding ratio, etc. The authors described a comprehensive computer-aided system developed for optimum selection of grinding parameters with consideration of multiple criteria and constraints. The system consisted of multiple dynamic models, modifier databases, knowledge bases and a user interface. The process of optimum specification of grinding parameters was divided strategically into two layers. Layer I was for determination of grinding conditions

and Layer II for optimum selection of equivalent chip thickness and operating parameters.

Rowe et al. [246] provided an extensive review on various approaches based on artificial intelligence to the grinding process. Liao and Chen [176] showed how back-propagation (BP) neural networks can be used to model and optimize grinding processes, using CFG of alumina with diamond wheels as an example. First, a generalized back-propagation neural network with two-hidden layers was used to establish the process model. Then the back-propagation algorithm with Boltzmann factor was used to find the global optimal settings for the grinding process. From the simulation results obtained, it was found that the implemented neural network approach yielded a more accurate process model than the regression method. It was also shown that, unlike the conventional back-propagation network, proper use of the Boltzmann factor with BP can effectively avoid local minima and generate the global optimal solution.

Rowe et al. [247] reviewed research into the use of intelligent control and optimization techniques in grinding and proposed the incorporation of intelligent techniques into CNCs. Two main trends were evidenced in the development of AI technologies in grinding: desktop systems to assist tool and parameter selection and self-optimizing systems integrated within the machine controller. It was predicted that future developments would favor increasing incorporation of intelligence into CNC. Xiao and Malkin [316] developed an on-line optimization system for cylindrical plunge grinding to minimize production time while ensuring part quality requirements. The system was capable of optimizing the grinding and dressing parameters in response to in-process and post-process measurements which characterize the process and update the process model. The system encompasses a complete set of realistic constraints, considers time dependent behavior, and also optimizes the dressing interval. The system was implemented on an instrumented internal grinder in the laboratory and in actual production.

Vinolas et al. [303] presented, step-by-step, the capabilities that a general-purpose simulation environment, such as Simulink/Matlab, provides for an intuitive and efficient modeling of grinding processes. Starting from a revision of the different approaches which can be found in the technical literature, the author begins with the well-known block-diagram first presented by Snoeys. Next, the author had shown how this block-diagram was incorporated into the Simulink environment and how the different parameters for the simulation were introduced in the model (machine, grinding wheel and process parameters). Hundt et al. [128] developed a kinematic model of single edge cutting action in grinding. The model described the force pulse created by chip formation at the cutting edge. This pulse was assumed to excite acoustic emission (AE) signals. The typical values of its features (risetime, width, amplitude) determine the requirements for the measurement equipment. AE was measured on the workpiece during grinding and was analyzed in the frequency range between 70 kHz and 3.5 MHz. A suitable signal analysis strategy was developed to extract meaningful information from the AE signal using frequency domain feature extraction. The comparison of model and measurement output allows the identification of model parameters.

The parameter values give a description of the grinding wheel state and the process state.

Rowe et al. [248] presented the advantages of a multi-agent approach for the selection of grinding conditions. The agents consist of case-based reasoning, neural network reasoning and rule-based reasoning. Case-based reasoning was employed as the main problem-solving agent to select combinations of the grinding wheel and values of control parameters. Rule-based reasoning was employed where relevant data were not available in the case base. A neural network was employed to select a grinding wheel if required. The operator makes the final decision about the wheel or the values of control parameters. The multi-agent approach combines the strengths of the different agents employed, to generate hybrid solutions and overcomes the limitations of any single approach. A blackboard method was used as the means of integrating the multi-agent system. The system demonstrates the potential of using artificial intelligence for selection of grinding conditions, as well as the capability to develop a powerful database by learning from experience.

Brinksmeier et al. [41] proposed NN and fuzzy set-based model to optimize the grinding processes. They evaluated the grinding process in terms of geometric quantities (such as dimension, shape, waviness, and surface integrity and product quality, i.e., surface roughness. Hekman and Liang [124] presented a method for optimizing the horizontal feed rate when using depth of cut manipulation to improve part parallelism in grinding. In vertical spindle surface grinding, achievable single pass tolerances are often limited by the grinding wheel and machine compliance. Previous work consisted of precisely adjusting the depth of cut during grinding to enhance the dimensional tolerance without the need of additional spark-out passes. The authors had optimized the horizontal feed rate for cost functions based on a weighting of processing time and a term related to the dimensional error in the part. In the optimization, a force model predicts the grinding force. Experimental results for six optimization weightings were given which demonstrated the effectiveness of the feed rate optimization as compared to a constant feed rate with the same processing time in the context of the parallelism of the ground part.

Lee and Shin [168] proposed fuzzy basis function neural networks for modeling of grinding processes to find optimal process conditions. The model was applied for two grinding optimization problems, viz., CFG and surface grinding process, and it was found that the NN-based algorithm outperforms traditional optimization techniques in surface grinding process. Saravanan and Sachithanandam [254] proposed GA-based optimization procedure to optimize cutting conditions, viz., wheel speed, work speed, lead of dressing, and depth of dressing in multi-objective surface grinding problem. They found that GA performs better than traditional quadratic programming.

Gupta et al. [115] developed a technique that generates a number of solution sets for each of the input parameters. The user can then select a set with values comparable to the desired output and satisfying the process constraints and the objective. Input variables which can be considered for obtaining optimal

conditions include wheel and machine parameters with in-feed being the most promising one. For critical components, conditions for "burn-free" workpiece can also be determined. Li et al. [174] presented an optimum strategy permitting burn to appear in the rough grinding stage. On the basis of the basic grinding models, the objective function and constraint functions for the multi-parameter optimum grinding process were developed. The non-linear optimum grinding control parameters were obtained through computer simulation, and the actual grinding process was controlled by these parameters. The results of the experiments confirmed the exactitude of the optimum models and the feasibility of the optimum strategy. This work had created the pre-condition for grinding automation, virtual grinding and intelligent grinding systems.

Saravanan et al. [256] developed a genetic algorithm (GA)-based optimization procedure to optimize grinding conditions, viz. wheel speed, workpiece speed, depth of dressing and lead of dressing, using multi-objective function model with a weighted approach for surface grinding process. The procedure evaluates the production cost and production rate for the optimum grinding condition, subjected to constraints such as thermal damage, wheel wear parameters, machine tool stiffness and surface finish. The GA procedure was illustrated with an example and optimum results such as production cost, surface finish, MRR were compared with the results of application of quadratic programming technique. However, the genetic algorithm has its own limitations such as risk of replacement of a good parent string with the deteriorated child, less convergence speed and difficulty in selecting the controlling parameters such as population size, crossover rate and mutation rate. Also the results of genetic algorithm presented by the authors are erroneous.

Dhavalikar et al. [72] applied combined Taguchi and dual response methodology to determine the robust condition for minimization of out of roundness error of workpiece for centerless grinding operation. Optimization was then carried out by using Monte Carlo simulation procedure. Guo et al. [112] carried out optimization of continuous-dress creep-feed (CDCF) grinding processes to reduce cycle time and wheel consumption by adaptively adjusting work speed and dress in-feed based on grinding models and in-process power monitoring. Heat flux was kept below the fluid burnout limits to avoid thermal damage to the ground surface. Grinding forces were controlled below the allowable values to avoid coating cracks caused by excessive strain on the blade. By implementing this approach, 40% cycle time reduction was demonstrated while maintaining the heat flux and grinding forces below their allowable critical values.

Shaji and Radhakrishnan [264] investigated the possibility of using graphite as a lubricating medium to reduce the heat generated at the grinding zone in surface grinding. Their work deals with the analysis of the process parameters such as speed, feed, in-feed and mode of dressing as influential factors, on the force components and surface finish developed based on Taguchi's experimental design methods. Taguchi's tools such as orthogonal array, S/N ratio, factor effect analysis, ANOVA, etc., were used for this purpose and an optimal condition was found out. The results were compared with the results obtained in the conventional

coolant grinding. Gopal and Rao [106] conducted experiments to study the effect of wheel parameters; grain size and grain density and grinding parameters; depth of cut and feed on the surface roughness and surface damage. The significance of the grinding parameters on the selected responses was evaluated using ANOVA. Mathematical models were developed using the experimental data considering only the significant parameters. A genetic algorithm (GA) code was developed to optimize the grinding conditions for maximum material removal, using a multi-objective function model, by imposing surface roughness and surface damage constraints. The choice of including manufacturer's constraints on the basis of functional requirements of the component for maximizing the production rate was also embedded in the GA code.

Hashimoto and Lahoti [119] described the effect of set-up conditions on three stability criteria of the centerless grinding system. It also presented guidelines for determining proper set-up conditions to avoid spinners, chatter vibration and roundness problems. Finally, an algorithm for providing the optimum set-up condition based on process aims was proposed and the simulation results were discussed. Guo et al. [113] investigated the process monitoring and control of CDCF form grinding using model-based simulation and in-process power measurement and its application to grinding of turbine blade root serrations. For blade root serration grinding, it is essential that the grinding force be maintained below a critical limit to avoid cracking of the thermal environmental barrier coating (TEBC) at the blade airfoils, and that the heat flux at the grinding zone be kept below the fluid burnout limit to avoid thermal damage to the part. A blade root form grinding process was first simulated and optimized by utilizing the variable-feed approach developed previously, whereby both the dress in-feed and part feed rate were adaptively varied to minimize cycle time while maintaining the force and heat flux below specified limits. Both the grinding forces and heat flux were obtained from the measured power. Maintaining the monitored power signature from production processes within the acceptable power limits established in this way ensures a normal grinding process. Deviations from the normal process signature profile indicate possible process issues.

Nandi and Pratihar [203] developed a method for automatic design of fuzzy logic controller (FLC) using a genetic algorithm (GA). The performance of an FLC depends on its knowledge base (KB), which consists of membership function distributions (also known as data base) and rule base. To design a proper KB of the FLC, the designer should have a thorough knowledge of the process to be controlled. Sometimes, it becomes difficult to gather knowledge of the process beforehand Thus, designing the proper KB of an FLC is not an easy task. The authors had proposed a new approach for designing the KB of an FLC (using a GA) and its effectiveness was compared to a previous approach based on GA-fuzzy combination for making predictions of power requirement and surface finish in grinding.

Ali and Zhang [12] presented a practical and consistent fuzzy rule-based model for estimating the grinding conditions at which burn limits occur. The model consists of 37 absolute and eight relative rules. It has a wide range of applications

over many types of steels, Alundum wheels, and grinding conditions. It is also simple to implement, from a rule-chart mode to an intelligent on-line adaptive control mode. Kim [149] developed a neurofuzzy model to optimize cycle time in plunge grinding process. The grinding power, peak value of power spectrum, and time constant were used as inputs for neural network to estimate workpiece surface roughness. From the results obtained, it was found that the model was more reliable than regression model. Samhouri and Surgenor [251] proposed an ANFIS to predict surface roughness in grinding process. The power spectral density parameters of piezoelectric accelerometer were used as inputs to ANFIS and the authors found prediction accuracy as 91%.

Nandi and Banerjee [201] used fuzzy basis function neural network to predict surface roughness and corresponding power requirement in cylindrical plunge grinding process. Wheel speed, work speed, and feed rate were considered as input variables and, power requirement and surface roughness as output variables of the network architecture. The fuzzy rule base was designed automatically using a genetic algorithm and from the results, it was concluded that the model predicts better than mathematical models. Jayakumar et al. [135] reviewed and discussed the application of acoustic emission technique (AET) for on-line monitoring of various forming processes such as punch stretching, drawing, blanking, forging, machining and grinding. Kwak [163] presented an application of Taguchi and RSM for the geometric error. The effect of grinding parameters on the geometric error was evaluated and optimum grinding conditions for minimizing the geometric error were determined. A second-order response model for the geometric error was developed and the utilization of the response surface model was evaluated with constraints of the surface roughness and the MRR. Confirmation experiments were conducted at an optimal condition and selected two conditions for observing accuracy of the developed response surface model. Lizarralde et al. [181] described a software tool which was developed for setting up and optimization of centerless plunge grinding processes to avoid geometric instabilities. The software generates stability maps showing the stable and non-stable geometric configurations and the number of lobes generated in non-stable conditions. Complementary time domain models quantitatively predict the evolution of the profile error for each geometric configuration.

Govindhasamy et al. [108] described the development of neural model-based control strategies for the optimization of an industrial aluminum substrate disk grinding process. Using historical grindstone performance data, a NARX-based neural network model was developed. This model was then used to implement a direct inverse controller and an internal model controller based on the process settings and previous removal rates. Preliminary plant investigations showed that thickness defects could be reduced by 50% or more, compared to other schemes employed. Asokan et al. [20] applied PSO technique to optimize the grinding process parameters such as wheel speed, workpiece speed, depth of dressing, and lead of dressing, simultaneously subjected to a comprehensive set of process constraints, with an objective of minimizing the production cost and maximizing the production rate per workpiece, besides obtaining the finest possible surface

finish. Optimal values of the machining conditions obtained by PSO were compared with the results of genetic algorithm and quadratic programming techniques.

Bhattacharyya and Mukherjee [36] attempted a dynamic analysis of the process of modification of surface topography of a ball bearing during the grinding process using bond graph techniques. Such modification results from material removal by abrasion. The position of any point of the surface profile, with respect to a nominal subcutaneous surface, was expressed as a bivariate, orthogonal series of spherical harmonics. The angular coordinates of the aforesaid point in a spherical coordinate system were taken as the two variables. The net MRR was expressed as a sum of the rate of change of the individual harmonic coefficients. While the net rate of deformation was obtained from an elastoplastic analysis of the contact forces, the wear rate was obtained as an empirical function of the contact forces, velocities and material properties of the surfaces in contact. The effect of various process parameters, such as grinding speed, preload, and entry point orientation were studied.

Brinksmeier et al. [42] presented an overview of the current state of the art in modeling and simulation of grinding processes: Physical process models (analytical and numerical models) and empirical process models (regression analysis, artificial neural net models) as well as heuristic process models (rule-based models) were taken into account, and outlined with respect to their achievements. The models were characterized by the process parameters such as grinding force, grinding temperature, etc., as well as work results including surface topography and surface integrity. Furthermore, the capabilities and the limitations of the presented model types and simulation approaches were exemplified. The authors had made the following important observations (from [42]; reprinted with permission from Elsevier).

1. Basically fundamental analytical approaches (FA) provide a good way to illustrate insights of the grinding processes. It has to be considered that the models developed so far are limited to the ranges of the different parameters. Furthermore, the quality of a fundamental analytical model depends on the accuracy of the experimentally determined input parameters. For example, measuring the process temperatures and heat transfer coefficients is limited by the current measuring techniques and these data are sensitive to errors and change with the variation of the process parameters.
2. Different approaches have been developed concerning kinematic models. Due to the high level of detail, the modeling results are of high convergence to real grinding processes. The modeling of a realistic grinding wheel topography needs a comparatively high effort. Today, evaluating the grinding process using a complex kinematic model for a few milliseconds of grinding process time requires several hours of calculation time. The strong dependence of the abrasive process on the cutting edge geometry of the single grits can only be considered in approximation. Therefore, absolute values of grinding forces or surface roughnesses can not be calculated, but their trends can be identified.

3. The aim of finite element analysis (FEA) is the physical simulation of a total process. Due to the complexity of the grinding process the computational effort is quite high. The grinding experiments and material tests needed for the verification of simulations are limited by current measuring techniques as current material tests do not allow for deriving the material laws for all ranges of parameters, in particular for the determination of flow curves at high machining speeds. Furthermore, the computational power is not sufficient for the modeling of a complete grinding wheel with microscopic finite elements at the surface. Experiments are necessary for the verification of simulated surface topographies and grinding forces today and for the verification of the subsurface properties in future.
4. The aim of molecular dynamics (MD) modeling is the detailed description of the material microstructure regarding the dynamics and interactions of atomic arrangements. Using MD, it is possible to accomplish a three dimensional simulation of the dynamics and local interactions of a single or a few grits with a small workpiece model. For this simulation an enormous CPU-power is needed. Even for rather small models in absolute size, the calculation time easily exceeds 100 CPU hours. This results from the detailed 3D modeling of the material structure with its anisotropic crystal properties and the time consuming determination of the atom–atom interactions. Another shortcoming in MD simulation is related to the number and quality of available material specific potential functions. All possible interactions between atoms and molecules need to be described by a suitable function and individual material parameters. Still often suitable potential functions and parameters are only known for pure materials or a few binary systems.
5. Basically regression analysis models (RA) are able to sufficiently map relationships between input and output variables and are therefore state of the art. The low computational power needed for the calculation makes the use of this type of model quite comfortable. The achievable quality of simulation is dependent on the effort and number of experiments. In consequence, the scope of applications for the developed model is very limited in most cases. Operating the developed model for a different application usually results in a significantly worse quality of simulation results. First attempts to broaden the scope of applications by combining basic models with additional model types are promising. However, the experimental effort and the extensive coefficient calculations still remain important factors for the choice of this model type.
6. The performance of ANNs relies heavily on the quality and amount of data sets (input and output data) for training and testing. The advantage of ANN is its ability to handle so-called soft input parameters, parameters without a numerical value, such as coolant type, nozzle type, etc., and to inter- and extrapolate in a certain range. The model can easily be adapted to different manufacturing problems and is able to handle slightly incomplete data bases. The development of the design of an adequate network structure is rather complex. The lack of transparency of the knowledge stored inside the ANN and the effort for developing an adequate network design leads to a poor acceptance

in industry. Promising research projects concentrate on hybrid models. The combination of several models can significantly improve the modeling quality.

7. Rule-based models (RB) can help modeling the human reasoning process, especially when it comes to ill-defined or difficult problems. Fuzzy set theory has the capability to take the knowledge into account which is based on human experience, even if the available information is incomplete or fuzzy. Furthermore rule-based models are able to process several input parameters. For a realistic modeling, a sophisticated knowledge base is important to achieve good predictions for the quality of the output parameters. Regarding the simulation results the quality depends on the number of linguistic variables. The simulation quality is high for specific applications, but difficult to transfer to other grinding processes. Furthermore, rule-based models are well suited for combinations with other model approaches for improving the effectiveness. The effort for the start up of modeling is comparatively low for empirical models in comparison to other approaches like FEM, RB and MD, where a deeper process and model understanding and programming skills are necessary.

Alagumurthi et al. [9] compared and contrasted factorial design with Taguchi's DOE used in the determination of optimum grinding conditions. Optimum grinding conditions and grinding cycle time were estimated for each DOE and results were compared and analyzed. ANOVA analysis was carried out for the interpretation and for obtaining insight into the process as a whole. The factorial method was reported as more efficient, when interactions between process variables were present. It also helps in developing either a mathematical or regression model of the process for future use.

Weinert et al. [314] developed a simulation tool to improve the flexible production process and in order to ensure a suitable process strategy. The simulation comprises a geometric-kinematic process simulation and a finite elements simulation. The authors had presented basic parts of the investigation, modeling and simulation of the NC-shape grinding process with toroid grinding wheels. Krishna [160] applied differential evolution (DE) algorithm for optimization of process parameters of grinding operation. However, the solution obtained using differential algorithm are erroneous for rough grinding operation whereas, for finish grinding operation the optimum values suggested by the author lies outside their respective bounds and hence the solution is not valid.

Mukherjee and Ray [197] attempted to provide a systematic methodology to develop a multivariate linear regression model, hypothesis testing for the influence of nonlinear terms to linear model, and accordingly selection of a suitable ANN-based inferential model with improved prediction accuracy and control of grinding behavior. The methodology suggests the use of various statistical techniques, such as Q–Q (quantile–quantile) plotting, data transformation, data standardization, outlier detection test, model adequacy test, model cross-validation and generalization. The suitability of the recommended methodology was illustrated with the help of an engine cylinder liner grinding (honing) case example, in a leading automotive manufacturing unit in India. In another work,

Mukherjee and Ray [198] applied an empirical modeling technique based on direct observations, for prediction of a two-stage grinding process behavior having multiple response characteristics of continuous variables, and to determine overall optimal process design to meet the specific customer requirements. In order to achieve the above goal, the authors had proposed an integrated approach using multivariate regression, desirability function, and metaheuristic search technique. Three different metaheuristic search techniques, viz. real-coded genetic algorithm, simulated annealing, and a modified Tabu search based on novel Mahalanobis multivariate distance approach to identify Tabu moves, were employed to determine near optimal path conditions for an industrial case study of two-stage CNC grinding (honing) optimization problem, having various process and variable constraints. Computational study results based on different metaheuristics, and applied on the same two-stage optimization problem, showed that the modified Tabu search performs better and also offer opportunities to be extended for other multi-stage metal-cutting process optimization problems.

Park and Liang [226] developed a predictive model for the micro-grinding process by combined consideration of mechanical and thermal effects within a single grit interaction model at the micro-scale level of material removal while the size effect of micro-machining was incorporated. To assess the thermal effects, a heat transfer model based on the moving heat source analysis was integrated into the developed model. This model quantitatively predicts micro-grinding forces based on micro-grinding wheel topography and material properties including crystallographic effects. Experimental testing in a micro-grinding configuration was pursued to validate the predictive model by comparing measurements to analytical calculations in the context of orthogonal micro-grinding forces. The analytical model is seen to capture the main trend of the experimental results, while smaller deviations were found over larger depths of cut range. Liu et al. [180] built a model of the grinding force for aerospace alloys using an empirical approach. A robust DoE that included orthogonal arrays and the S/N ratio were tightly integrated to acquire reliable force data. In order to obtain clear and correct force signals, an optimized matching method to select parameters and filters was put forward based on a correlation function. The results verified that a wavelet filter gives much better accuracy. A set of empirical models of the grinding force for superalloy CMSX4 were build up using multivariate analysis and these models were characterized by the process parameters such as depth of cut, feed rate, wheel speed as well as wheel diameter.

Bigerelle et al. [37] introduced an engineering attempt to rigorously model a synchronizing functional surface (cone surface of idler gear) according to its finish specifications. The virtual input surface was generated by an original fractal function, which reproduces the surface signature due to the wheel grinding process. To model the subsequent super-finishing operation by belt finishing process, which uses a soft-coated belt as a tool, an algorithm simulating the abrasive polishing conditions was especially developed and applied to rework the initial fractal surface. The basic idea of this model was that the higher the height of a peak of the profile, the lower its probability of resistance during an abrasion cycle.

The belt finishing process was modeled by five parameters: two parameters that characterize the initial surface (fractal dimension and range amplitude) and three parameters describing the abrasion polishing process (probability of resistance, wear volume and the number of abrasion cycles). A functional model with an optimization scheme was created. This simulation provides the morphology of the initial surface and how to cope with the super-finishing process to obtain the functionality of the surface. Finally, it was shown that automotive designers impose morphological specifications obtained by the belt grinding process to prevent scuffing of the motor parts.

Ahearne and Byrne [8] developed an upper-bound simulation of the meso-scale engagement kinematics with analysis algorithms that provide estimates of local kinematical parameters. These were correlated with local measurements for typical brittle-mode micro-grinding parameters including measurements of the local normal force. The results generally correlated for surface roughness but not for local normal force where equilibration was attributed to system local and bending stiffness components.

Choi et al. [61] presented generalized grinding process models developed for cylindrical grinding processes based on the systematic analysis and experiments. The generalized model forms were established to maintain the same model structures with a minimal number of parameters so that the model coefficients could be determined through a small number of experiments when applied to different grinding workpiece materials and wheels. The relationships for power, surface roughness, G-ratio and surface burning were established for various steel alloys and alumina grinding wheels. It was shown that the established models provide good predictive capabilities while maintaining simple structures. Stępień [282] presented an advanced probabilistic model of the grinding process considering the random arrangement of the grain vertices at the wheel active surface. The general model was developed based on well-founded assumptions. The process of shaping the ground surface roughness, the probability of contact between the grains and the work-material as well as the undeformed chip thickness were described along the grinding zone. Eight special models obtained by substituting general relationships with special functions were also presented. The calculations performed for the special models lead to interesting conclusions relating to the real length of the grinding zone, which is considerably longer than the nominal (geometric) contact length, taken by default in most known approaches.

Fernandes et al. [91] presented a process to simulate an active vibration control system in a centerless grinding machine. Based on the updated finite element (FE) model of the machine, the structural modifications performed to incorporate active elements were detailed, as well as the subsequent reduction procedure to obtain a low-order state space model. This reduced structural model was integrated in the cutting process model giving a tool adapted for the purpose of simulating different control laws. Using the developed model, a control algorithm was checked. The simulation results were in agreement with the experimentally obtained ones. This model constitutes a powerful tool to evaluate the effectiveness of different approaches, making it possible to tackle an optimization process of the control

system by means of simulations and, thus, avoiding the costs that would involve the practical implementation of each one.

Doman et al. [73] presented a review of two-dimensional (2D) and three-dimensional (3D) finite element grinding models and categorized them by the scale of the modeling approach—either macro- or micro-scale. Macro-scale models consider the overall wheel–workpiece interaction while micro-scale models focus on the individual grain–workpiece interactions. Each model was discussed and the relevant boundary conditions, material constitutive treatments, and load inputs were compared. Future directions for finite element grinding modeling were then recommended and, based on the results of this review, synthesized current state-of-the-art macro- and micro-scale modeling approaches were presented.

Sedighi and Afshari [263] aimed to optimize CFG process by an approach using integrated Genetic Algorithm-Neural Network (GA-NN) system. The aim was to obtain the maximal MRR and the minimum of the surface roughness. For optimization, MRR was calculated with a mathematic formula and a Back-Propagation (BP) artificial neural-network were used to prediction of surface roughness. The parameters used in the optimization process were reduced to three grinding conditions which consisted of wheel speed, workpiece speed and depth of cut. All of other parameters such as workpiece length, workpiece material, wheel diameter, wheel material and width of grinding were taken as constant. The BP neural network was trained using the scaled conjugate gradient algorithm (SCGA). The results of the neural network were compared with experimental values. It was observed that the BP model could predict the surface roughness satisfactorily. For optimization of CFG process, an M-file program was written in Matlab software to integrate GA and NN. After generation of each population by GA, firstly, the BP network predicted surface roughness and the MRR was calculated with mathematic formula. By using this integrated GA-NN system, optimal parameters of CFG process were obtained. The obtained results showed that the integrated GA-NN system was successful in determining the optimal process parameters.

Mani and Patvardhan [187] formulated the ceramic grinding optimization problem as a non-linear constrained optimization problem. The authors had proposed a real coded Adaptive Quantum inspired Evolutionary Algorithm to solve the optimization problem. The algorithm is free from user selectable parameters in evolutionary operators as the same is determined adaptively. The algorithm does not require mutation for maintaining diversity. The results also showed that the proposed algorithm is fast and robust. Xu et al. [317] proposed a compact centerless grinding unit composed mainly of an ultrasonic elliptic-vibration shoe and installed onto the worktable of a multipurpose surface grinder to perform tangential-feed centerless grinding operations. However, for the complete establishment of the new method, it is crucial to clarify the workpiece rounding process and the effects of process parameters such as the worktable feed rate, the stock removal and the workpiece rotational speed on the machining accuracy, i.e., workpiece roundness, so that the optimum grinding conditions can be determined. The

authors had investigated the effects of the process parameters on workpiece roundness by simulation and experiments. For the simulation analysis, a grinding model taking into account the elastic deformation of the machine was created. Then, a practical way to determine the machining-elasticity parameter was developed. Further, simulation analysis was carried out to predict the variation of workpiece roundness during grinding and to discover how the process parameters affect the roundness. Finally, actual grinding operations were performed to confirm the simulation results. The obtained results indicated that: (1) a slower worktable feed rate and higher workpiece rotational speed give better roundness; (2) better roundness can be also obtained when the stock removal is set at a larger value; (3) the workpiece roundness was improved from an initial value of 23.9 μm to a final value of 0.84 μm after grinding.

Drazumeric et al. [74] discussed the simulation of a through-feed centerless grinding process in a virtual environment (VE). The developed simulations were based on an analytical grinding gap model describing the grinding gap macro geometry and workpiece kinematics. First of all, the model was embedded in a desktop application (Cegris), which facilitated regulating wheel truing and the determination of set-up variables, both of which yielded an optimal grinding gap macro geometry in a reduced set-up time. Finally, the Cegris was ported to a CAVE (CAVE Automatic Virtual Environment) for an interactive visualization of the process, an application used to train machine tool operators. Siddiquee et al. [275] investigated optimum design of an in-feed centerless cylindrical grinding process performed on EN52 austenitic valve steel (DIN: X45CrSi93). The major performance characteristics selected to evaluate the process were surface roughness, out of cylindricity of the valve stem and diametral tolerance, and the corresponding centerless cylindrical grinding process parameters were dressing feed, grinding feed, dwell time and cycle time. Grey relational analysis that uses grey relational grade as performance index was specially adopted to determine the optimal combination of centerless cylindrical grinding process parameters. Moreover, the principal component analysis was applied to evaluate the weighting values corresponding to various performance characteristics so that their relative importance could be properly and objectively described. The results of confirmation experiments revealed that grey relational analysis coupled with principal component analysis can effectively be used to obtain the optimal combination of centerless cylindrical grinding process parameters.

Rao and Pawar [238] presented the multi-objective optimization of process parameters of grinding process using various non-traditional optimization techniques such as ABC, harmony search, and simulated annealing algorithms. The objectives considered were production cost, production rate, and surface finish subjected to the constraints of thermal damage, wheel wear, and machine tool stiffness. The process variables considered for optimization were wheel speed, work piece speed, depth of dressing, and lead of dressing. The results of the algorithms were compared with the previously published results obtained by using other optimization techniques.

2.3.1 Example 1: Modeling and Optimization of Rough Grinding Process

As numerous process parameters are involved in grinding process, it is difficult and complex to optimize each and every parameter. Various process parameters such as wheel speed, workpiece speed, cutting depth, in-feed, traverse feed, area of contact, dressing, etc. affect significantly the performance measures such as production cost, production rate and surface finish. However, to compare the performance of the proposed algorithms in this work with that of quadratic programming, genetic algorithm, and differential evolution, the same process parameters, i.e. wheel speed 'V_s' (m/min), workpiece speed 'V_w' (m/min), depth of dressing 'doc' (mm) and lead of dressing 'L' (mm/rev) as considered by Wen et al. [315], Saravanan et al. [256] and Krishna [160] are considered.

The three objectives considered in this work are:

- Minimization of production cost 'C_T' ($/pc).
- Maximize the production rate in terms of workpiece removal parameter 'WRP' (mm^3/min N).
- Minimization of surface roughness 'R_a' (μm).

However, keeping in view of the specific requirement of finish grinding and rough grinding operation, these three objective functions are divided into two groups as follows:

For rough grinding operation following two objective functions are considered with the condition that the surface roughness value should not exceed 1.8 μm.

1. Minimization of production cost (C_T) in $/piece
2. Maximize the production rate in terms of workpiece removal parameter 'WRP' (mm^3/min N).Whereas, for finish grinding operation following two objective functions are considered with the condition that the workpiece removal parameter should not be less than 20 mm^3/min N.
3. Minimization of production cost 'C_T' ($/pc).
4. Minimization of surface roughness 'R_a' (μm).

These three objective functions 'C_T', 'WRP', 'R_a' can be expressed in terms of the process variables [315].

$$\begin{aligned} C_T = {} & (M_c/60p)((L_w + L_e)/1,000V_w)((b_w + b_e)/f_b)\left(\left(a_w/a_p\right) + S_p\right. \\ & \left. + \left(a_w b_w L_w/\pi D_e b_s a_p G\right)\right) + (M_c/60p)((S_d/V_r) + t_1) + (M_c t_{ch}/60N_t) \\ & + (M_c \pi b_s D_e/60pN_d LV_s 1,000) + C_s((a_w b_w L_w/pG) + (\pi(\text{doc}) b_s D_e/pN_d)) \\ & + (C_d/pN_{td}) \end{aligned} \tag{2.33}$$

where M_c is cost per hour of labor and administration, L_w is length of workpiece, L_e is empty length of grinding, b_w is width of workpiece, b_e is empty width of grinding, f_b is cross feed rate, a_w is total thickness of cut, a_p is down feed of grinding, S_p is number of spark out grinding, D_e is diameter of wheel, b_s is width of

wheel, G is grinding ratio, S_d is distance of wheel idling, p is number of workpieces loaded on the table, V_r is speed of wheel idling, t_1 is time of loading and unlading workpieces, t_{ch} is time of adjusting machine tool, N_t is batch size of the workpieces, N_d is total number of workpieces to be ground between two dressing, N_{td} is total number of workpieces to be ground during the life of dresser, C_s is cost of wheel per mm^3 and C_d is cost of dressing.

$$\mathrm{WRP}=94.4\left[\left((1+(2(\mathrm{doc})/3L)\right)L^{11/19}(V_w/V_s)^{3/19}V_s\right]\Big/\left[D_e^{43/304}\mathrm{VOL}^{0.47}d_g^{5/38}R_c^{27/19}\right] \tag{2.34}$$

where VOL = wheel bond percentage, d_g = grind size, R_c = workpiece hardness.

$$\begin{aligned} R_a &= 0.4587\,T_{ave}^{0.3} \quad \text{for } 0<T_{ave}<0.254, \text{ else,} \\ R_a &= 0.78667\,T_{ave}^{0.72} \quad \text{for } 0.254<T_{ave}<2.54 \end{aligned} \tag{2.35}$$

where

$$T_{ave} = 12.5\times 10^3\left(d_g^{16/27}a_p^{19/27}\Big/D_e^{8/27}\right)(1+\mathrm{doc}/L)L^{16/27}(V_w/V_s)^{16/27} \tag{2.36}$$

Various constraints considered in the optimization model are discussed below.

1. Thermal damage constraint: The grinding process requires very high energy per unit volume of material removed. Whatever the energy that is concentrated within the grinding zone, it is converted into heat. The high thermal energy causes damage to the workpiece, and it leads to the reduced production rate. The specific energy U is calculated by Eq. 2.37.

$$\begin{aligned} U= 13.8 &+ \left(9.64\times 10^{-4}V_s/a_pV_w\right) + \left(6.9\times 10^{-3}(2,102.4V_w/D_eV_s)\right) \\ &\times\left(A_0+K_uV_sL_wa_w\Big/V_wD_e^{1/2}a_p^{1/2}\right)\left(V_sD_e^{1/2}\Big/V_wa_p^{1/2}\right) \end{aligned} \tag{2.37}$$

where K_u = wear constant.

The critical specific energy U^* at which burning starts is expressed in terms of the operating parameters as

$$U^* = 6.2+1.76\left(D_e^{0.25}\Big/a_p^{0.75}V_w^{0.5}\right) \tag{2.38}$$

The thermal damage constraint is then specified as,

$$U^*-U\geq 0 \tag{2.39}$$

2. Wheel wear parameter constraint: Wheel wear parameter WWP (mm^3/min N) is related directly to the grinding conditions. For single-point diamond dressing, it is given by Eq. 2.40.

$$\begin{aligned}\mathrm{WWP} = &\left[\left(k_p a_p d_g^{5/38} R_c^{27/29}\right) \Big/ \left(D_e^{1.2/\mathrm{VOL}-43/304}\mathrm{VOL}^{0.38}\right)\right] \\ &\times\left[(1+(\mathrm{doc}/L))L^{27/19}(V_s/V_w)^{3/19}V_w/((1+(2\mathrm{doc}/3L)))\right]\end{aligned} \tag{2.40}$$

The wheel wear constraint is obtained as,

$$(\mathrm{WRP}/\mathrm{WWP}) - G \geq 0 \tag{2.41}$$

3. Machine tool stiffness constraint: Chatter results in poorer surface quality and lowers machining production rate. Chatter avoidance is therefore a significant constraint in selection of machining parameters. The relationship between grinding stiffness K_c (*N*/mm), wheel wear stiffness K_s (*N*/mm), and operating parameters during grinding is given below.

$$K_c = 1,000 V_w f_b/\mathrm{WRP} \tag{2.42}$$

$$K_s = 1,000 V_s f_b/\mathrm{WWP} \tag{2.43}$$

To avoid chatter, the constraint given by Eq. 2.44 has to be fulfilled.

$$\mathrm{MSC} - |R_{em}|/K_m \geq 0 \tag{2.44}$$

where

$$\mathrm{MSC} = (1/2K_c)(1 + V_w/V_s G) + (1/K_s) \tag{2.45}$$

R_{em} = dynamic machine characteristics, K_m = Static machine stiffness.

The combined objective function (to be minimized) formulated for rough grinding operation (Z_R) is given in Eq. 2.45.

Minimize

$$Z_R = W_1\left(C_t/C_t^*\right) - W_2(\mathrm{WRP}/\mathrm{WRP}^*) \tag{2.46}$$

where W_1 and W_2 are the weighing factors with value 0.5 each.

C_T^* = 10 ($/pc); WRP* = 20 mm^3/min N.

Subjected to the constraints specified by Eqs. 2.39, 2.41, and 2.44.

Parameters bounds for the four process variables are as follows:

$$1,000 \leq V_s \leq 2,023\ \mathrm{m/min} \tag{2.47}$$

$$10 \leq V_w \leq 22.70\ \mathrm{m/min} \tag{2.48}$$

$$0.01 \leq \mathrm{doc} \leq 0.1370\ \mathrm{mm} \tag{2.49}$$

$$0.01 \leq L \leq 0.1370\ \mathrm{mm/rev} \tag{2.50}$$

The parameter setting for the various algorithms to solve the optimization problem of rough grinding process is below:

Controlling parameters for ABC:

- Number of employed bees = 5
- Number of onlookers bees = 11
- Number of scout bees = 1
- Maximum number of iterations = 150

Controlling parameters for PSO:

- Number of particles in swarm = 5
- Inertia weight = 0.65
- Acceleration coefficient (c_1) = 1.65
- Acceleration coefficient (c_2) = 1.55
- Number of iterations = 50

Controlling parameters for SA:

- Initial temperature = 200
- Decrement factor = 0.1
- Number of iterations = 100

Controlling parameters for HS_M:

- Harmony memory size = 5
- Harmony memory consideration rate = 0.8
- Pitch adjusting rate = 0.4
- Number of improvisations = 150

Controlling Parameters for SFL:

- Total number of frogs = 20
- Number of memeflexes = 5
- Number of frogs in each memeflex = 4

Table 2.5 provides the values of constants and parameters used in optimization of grinding process. The results of optimization are shown in Table 2.6.

From Table 2.6, it can be understood that various algorithms are competing with each other. Particularly, ABC, PSO, SFL, HS_M, and SA are good competitors. Optimality of the solutions obtained by using these algorithms can be confirmed. For example, optimality of the solution obtained by using ABC algorithm could be confirmed from the Figs. 2.11 and 2.12. Figure 2.11 shows Variation of wheel wear parameter constraint, surface roughness constraint, and combined objective function with wheel speed. Since the thermal damage constraint and machine tool stiffness constraint are having almost constant positive values for all values of wheel speed, Fig. 2.11 is plotted neglecting thermal damage constraint and machine tool stiffness constraint to indicate more clearly the variation of other two constraints with wheel speed. As shown in Fig. 2.11, the combined objective function value reduces with increase in

Table 2.5 Values of the constants and parameters used in parameter optimization of grinding process (from [238]; reprinted with permission from the Council of the Institution of Mechanical Engineers, UK)

Notation	Description	Unit	Value
M_c	Cost per hour labor and administration	\$/h	30
L_w	Length of workpiece	mm	300
L_e	Empty length of grinding	mm	150
b_w	Width of workpiece	mm	60
b_e	Empty width of grinding	mm	25
f_b	Cross-feed rate	mm/pass	2
a_w	Total thickness of cut	mm	0.1
a_p	Down feed of grinding	mm/pass	0.0505
S_p	Number of spark out grinding		2
D_e	Diameter of wheel	mm	355
b_s	Width of wheel	mm	25
G	Grinding ratio		60
S_d	Distance of wheel idling	mm	100
p	Number of workpieces loaded on the table		1
V_r	Speed of wheel idling	mm/min	254
t_l	Time of loading and unlading workpieces	min	5
t_{ch}	Time of adjusting machine tool	min	30
N_t	Batch size of the workpieces		12
N_d	Total number of workpieces to be ground between two dressings		20
N_{td}	Total number of workpieces to be ground during the life of dresser		2,000
C_s	Cost of wheel per mm^3	\$	0.003
C_d	Cost of dressing	\$	25
VOL	Wheel bond percentage		6.99
d_g	Grind size	mm	0.3
R_c	Workpiece hardness	HRC	58
K_u	Wear constant	mm^{-1}	3.937×10^{-7}
R_{em}	Dynamic machine characteristics		1
K_m	Static machine stiffness	N/mm	100,000
K_a	Constant dependent on coolant and grain type		0.0869

wheel speed. This is due to the fact that with increase in wheel speed, the workpiece removal parameter increases without affecting cost. The constraints are also well satisfied at higher values of wheel speed. Hence the optimum value of wheel speed selected at its upper bound value of 2,023 m/min is appropriate. If the wheel speed is increased the size of the chips removed by a single abrasive grain is reduced which in turn reduces the wear of the wheel.

Figure 2.12 shows the variation of thermal damage constraint, wheel wear parameter constraint, surface roughness constraint, and combined objective function with workpiece speed. Figure 2.12 is plotted neglecting the machine tool

Table 2.6 Results of multi-objective optimization of rough grinding using various algorithms

Method	V_s	V_w	doc	L	C_T	WRP	R_a	COF
QP[A]	2,000	19.96	0.055	0.044	6.2	17.47	1.74	−0.127
GA[B]	1,998	11.30	0.101	0.065	7.1	21.68	1.79	−0.187
DE[C]	2,023	10.00	0.130	0.109	7.9	26.57	1.80[a]	−0.249
DE[C]	2,023	10.00	0.130	0.109	7.9	26.57	1.87[b]	−0.249
ABC	2,023	10.973	0.097	0.137	7.942	25.00	1.80	−0.226
PSO	2,023	10.00	0.110	0.137	8.33	25.63	1.798	−0.224
SFL	2,023	12.878	0.0762	0.1359	7.34	23.76	1.799	−0.226
HS	2,023	10.783	0.100	0.134	8.0167	24.983	1.798	−0.224
SA	2,023	11.48	0.089	0.137	7.755	24.45	1.789	−0.223

[a] Values wrongly calculated by Krishna [160]
[b] Corrected values; [A] Wen et al. [315]; [B] Saravanan et al. [256]; [C] Krishna [160]

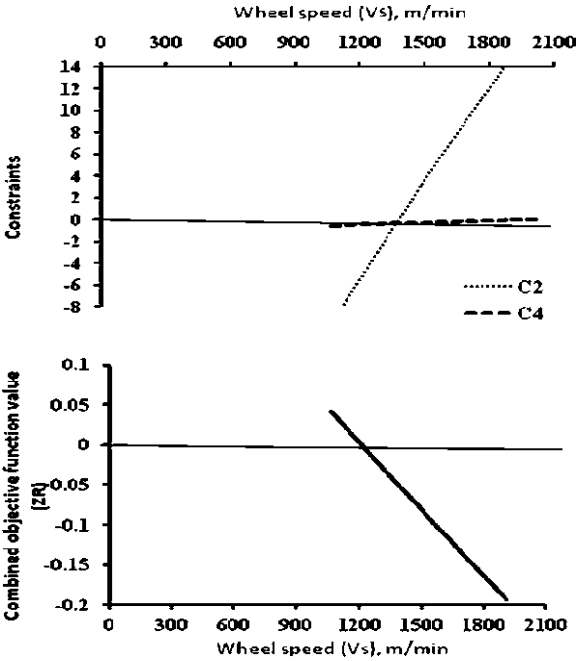

Fig. 2.11 Variation of wheel wear parameter constraint (C2), surface roughness constraint (C4), and combined objective function (Z_R) with wheel speed (V_s) (from [238]; reprinted with permission from the Council of the Institution of Mechanical Engineers, UK)

stiffness constraint as it has almost constant positive values for all values of workpiece speed. As shown in Fig. 2.12, the combined objective function value reduces (as workpiece removal parameter increases and cost reduces) with increase in workpiece speed. Thus, higher value of workpiece speed is desirable. However, at any value of workpiece speed higher than 10 m/min (i.e. lower bound value), the surface roughness constraint is violated. This is due to increase of wheel wear with the increase in workpiece speed.

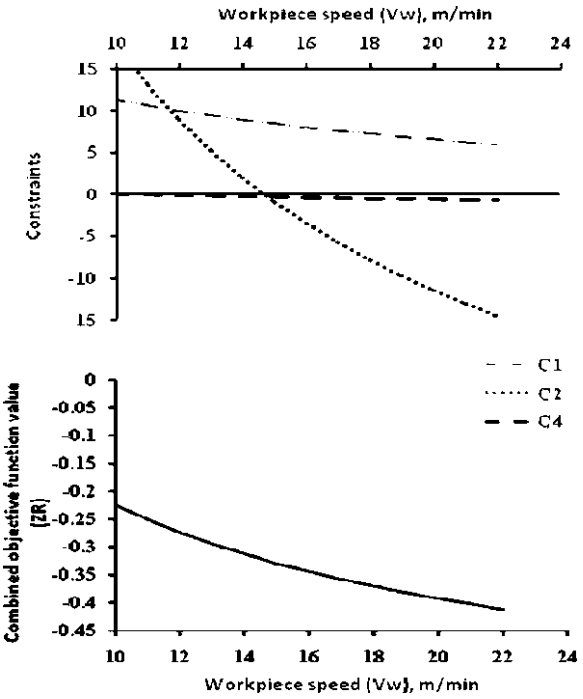

Fig. 2.12 Variation of thermal damage constraint (C1), wheel wear parameter constraint (C2), surface roughness constraint (C4), and combined objective function (Z_R) with workpiece speed (V_w) (from [238]; reprinted with permission from the Council of the Institution of Mechanical Engineers, UK)

Figure 2.13 shows the Variation of wheel wear parameter constraint, surface roughness constraint, and combined objective function with depth of dressing. Since the thermal damage constraint and machine tool stiffness constraint are having almost constant positive values for all values of wheel speed, Fig. 2.13 is plotted neglecting thermal damage constraint and machine tool stiffness constraint. As shown in Fig. 2.13, the combined objective function value decreases with the increase in depth of dressing. Thus, the higher value of depth of dressing is desirable. However, for any value of depth of dressing higher than 0.11 mm, the surface roughness constraint is violated. This confirms the optimum value depth of dressing selected using PSO algorithm for rough grinding operation.

Figure 2.14 shows variation of wheel wear parameter constraint, surface roughness constraint, and combined objective function with lead of dressing. Since the thermal damage constraint and machine tool stiffness constraint are having almost constant positive values for all values of wheel speed, Fig. 2.14 is plotted neglecting thermal damage constraint and machine tool stiffness constraint. As shown in Fig. 2.14, the combined objective function value initially increases up to a certain value and thereafter decreases with increase in lead of dressing. Thus, the minimum value of combined objective function occurred at both, lower bound and upper bound values of lead of dressing. However, the upper bound value of lead of dressing should be selected, as at lower bound value of lead of dressing, surface roughness constraint is violated.

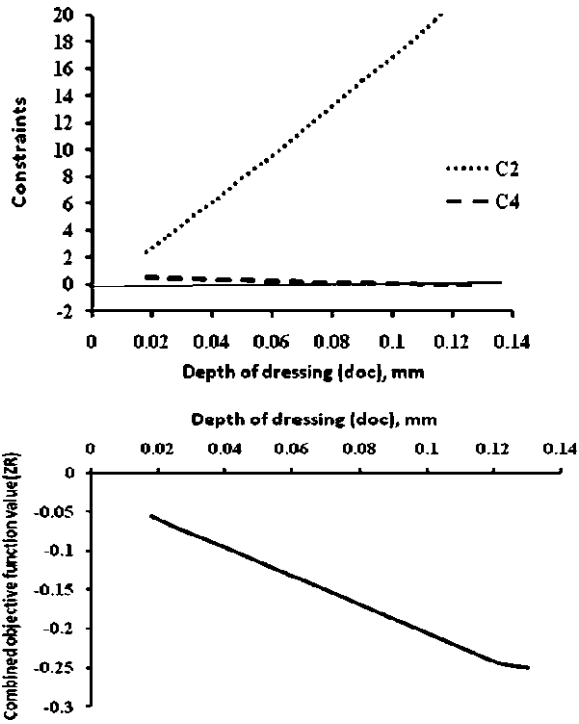

Fig. 2.13 Variation of wheel wear parameter constraint (C2), surface roughness constraint (C4), and combined objective function (Z_R) with depth of dressing (from [238]; reprinted with permission from the Council of the Institution of Mechanical Engineers, UK)

Table 2.6 shows the optimum process parameter data for the considered example along with the previously published results using other methods. Although the result of optimization using differential evolution algorithm seems to be better than that using ABC, it is erroneous and the corrected result is not valid as the surface roughness value (1.87 μm) exceeds than the specified value (1.8 μm). The improvement in combined objective function for rough grinding over that of quadratic programming is 78% each in case of application of ABC and SFL algorithms, 77% in the case of HS, 75.6% in the case of SA, and 47% in the case of GA. It is found that that the convergence rate of ABC and SFL algorithms is better than the other algorithms.

2.3.2 Example 2: Modeling and Optimization of Finish Grinding Process

This example presents the multi-objective optimization of finish grinding process. The combined objective function formulated for finish grinding operation (Z_F) is given in Eq. 2.51.

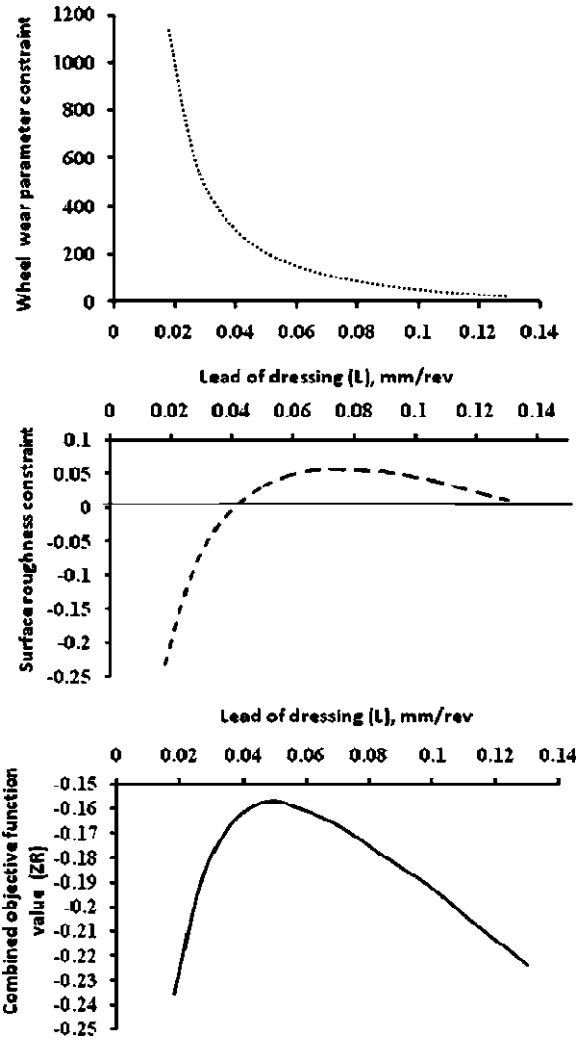

Fig. 2.14 Variation of wheel wear parameter constraint, surface roughness constraint, and combined objective function (Z_R) with lead of dressing (L) (from [238]; reprinted with permission from the Council of the Institution of Mechanical Engineers, UK)

Minimize

$$Z_F = W_1 * (C_T/C_T*) + W_3 * (R_a/R_a*) \tag{2.51}$$

where W_1 and W_3 are the weighting factors. For demonstration, these values are assumed as 0.3 and 0.7, respectively. The constraints are same as specified by Eqs. 2.39, 2.41, and 2.44. Parameters bounds for the four process variables are same as given in example 1. Table 2.7 shows the optimum process parameter data for above example, along with the previously published results using other methods. As shown in Table 2.7, although the result of optimization using differential evolution algorithm [160] seems to be better than that using SA, HS_M,

Table 2.7 Results of multi-objective optimization for finish grinding operation

Method	V_s	V_w	doc	L	C_T	WRP	R_a	Z_F
QP[A]	2,000	19.99	0.052	0.091	7.7	20.00	0.83	0.554
GA[B]	1,986	21.40	0.024	0.136	6.6[a]	20.08	0.83	0.521[a]
GA	1,986	21.40	0.024	0.136	7.36[b]	20.08	0.83	0.542[b]
DE[C]	2,170	17.49	0.008	0.137	7.48	20.33	0.65	0.497
SA	2,023	22.7	0.01	0.137	7.11	20.01	0.79	0.520
HS_M	2,023	22.7	0.01	0.137	7.11	20.01	0.79	0.520
ABC	2,023	22.7	0.01	0.137	7.11	20.01	0.79	0.520

[a] Values wrongly calculated by Saravanan et al. [256]
[b] Corrected values; [A] Wen et al. [315]; [B] Saravanan et al. [256]; [C] Krishna [160]

and ABC algorithms, is not valid as the values of some process parameters like wheel speed (V_s) and depth of dressing (doc) lies outside their respective bounds ($V_s = 2{,}170 > 2{,}023$ and $\text{doc} = 0.008 < 0.01$). The result obtained by using genetic algorithm [256] is erroneous.

2.4 Turning Process

Turning is one of the most basic machining processes. The part is rotated while a single point cutting tool is moved parallel to the axis of rotation. Turning can be done on the external surface of the part as well as internally (boring). The starting material is generally a work piece generated by other processes such as casting, forging, extrusion, or drawing. Turning can be done manually, in a traditional form of lathe, which frequently requires continuous supervision by the operator, or by using a computer-controlled and automated lathe which does not. This type of machine tool is referred to as having computer numerical control, better known as CNC and is commonly used with many other types of machine tools besides the lathe.

The turning process can be of different types such as straight turning, taper turning, profiling or external grooving. Turning process can produce various shapes of materials such as straight, conical, curved, or grooved work pieces. In general, turning uses simple single-point cutting tools. Each group of work piece materials has an optimum set of tools angles which have been developed through the years.

In turning process, parameters such as cutting tool geometry and materials, number of passes, depth of cut for each pass, the depth of cut, feed rates, cutting speeds as well as the use of cutting fluids will impact the production costs, MRRs, tool lives, cutting forces, and the machining qualities like the surface roughness, the roundness of circular and dimensional deviations of the product. Basically, tool life, cutting force, and surface roughness are strongly correlated with cutting parameters such as cutting speed, feed rate, and depth of cut. Proper selection of

the cutting parameters can obtain a minimum cost, maximum MRRs, longer tool life, a lower cutting force, and better surface roughness.

In machining processes, the most commonly used optimization criterion is specific cost, which has been used by many authors [13, 64, 175, 258, 302, 310]. Sometimes, other criteria like machining time [63], MRR [58] or tool life [195] were used too. However, these single-objective approaches have a limited value to fix the optimal cutting conditions, due to the complex nature of the machining processes, where several different and contradictory objectives must be simultaneously optimized.

Some multi-objective approaches were reported in cutting-parameters optimization [64, 169, 332], but mainly they use a priori techniques, where the decision maker combines the different objectives into a scalar cost function. This actually makes the multi-objective problem, single-objective prior to optimization. On the other hand, in the a posteriori techniques, the decision maker is presented with a set of non-dominated optimal candidate solutions and chooses from that set. These solutions are optimal in the wide sense that no other solution in the search space are superior to them when all optimization objectives are simultaneously considered. They are also known as Pareto-optimal solutions.

In dealing with multi-objective optimization problems, classical optimization methods (weighted sum methods, goal programming, min–max methods, etc.) are not efficient, because they cannot find multiple solutions in a single run, thereby requiring them to be applied as many times as the number of desired Pareto-optimal solutions. On the contrary, studies on evolutionary algorithms have shown that these methods can be efficiently used to eliminate most of the above-mentioned difficulties of classical methods [279].

Optimization of multi-pass turning operations plays an important role in process planning for machining, since multi-pass machining operations are more widely used than single-pass machining operations in manufacturing industry. In order to achieve overall optimal results in multi-pass turning operations, trade-offs are usually established not only among the various conflicting machining performance measures, but also among all passes in a given turning operation. The optimization objective of multi-pass turning operations differs from that of single-pass operations. In rough turning operations, the highest possible MRR is aimed at, within the constraints of other appropriate machining performance measures. However, the surface roughness is the most important measure in comparison with all other measures in finish turning operations. To implement the importance of one or more of the machining performance measures in optimization, various weighting factors are applied to these measures in the objective function. Major machining performance measures, which directly depend on the cutting parameters, including surface roughness, cutting force, chip form/chip breakability, tool-life and MRR, are predicted using a hybrid model in terms of cutting conditions: cutting speed, feed and depth of cut. The early work for single-pass turning, which includes the effect of progressive tool-wear, and the subsequent work involving the establishment of a performance-based criterion for the selection of optimum cutting conditions and cutting tool selection, have more recently been extended to cover multi-pass turning using genetic algorithms.

Many iterative mathematical search algorithms with their applications were reported in the literature. Chua et al. [63] presented the numerical optimization of minimizing total production time per component for multi-pass turning operations subjected to practical constraints such as force, power, machining speed and feed using sequential quadratic programming technique. Gopalakrishnan and Al-Khayyal [107] used a geometric programming technique for parameter selection in turning process considering a few constraints.

The problem of determining the optimum machining conditions for single-pass and multi-pass operations was investigated by Agapiou [5]. An objective function incorporating a combination of the minimum production cost and minimum production time requirements was considered for optimization. The two criteria of production cost and production time were prioritized through their weight coefficients. A constant multiplier was used to normalize the objective function. The optimum machining conditions were then determined by the Nelder–Mead simplex method. Physical constraints regarding the cutting parameters were also considered. The superiority of the combined objective function over the earlier proposed single criterion objective functions, using the production cost, or production time, or maximum rate of profit, was illustrated. In another work, Agapiou [6] investigated the problem of determining the optimum machining conditions for multi-pass operations. The optimum number of machining passes was obtained through the dynamic programming technique and the optimum machining conditions for each pass were then determined based on the objective function discussed in Agapiou [5].

Kiliç et al. [146] described a computer-aided graphical technique that is capable of mapping all of the relevant constraints and a number of objective function contours in the cutting speed versus feed rate plane. The software developed first generates all data points necessary to draw the constraints and the contours and then loads the data to a graphics package, which draws and displays the contours together with the constraints on the same graph. All of the graphical points were obtained analytically. The optimum point can readily be identified by inspecting the graph displayed on the screen. Tan and Creese [285] used a sequential method based on linear programming to attain optimal machine parameter settings in multi-pass turning operation. Gupta et al. [114] proposed a methodology for selection of depth of cut for rough and finished passes in multi-pass turning operation to minimize total manufacturing cost by integer linear programming.

Wang et al. [308] used genetic algorithms for optimal selection of cutting conditions and cutting tools in multi-pass turning operations. Chen and Tsai [55] developed an optimization algorithm based on the simulated annealing (SA) algorithm and the Hooke–Jeeves pattern search (PS) for optimization of multi-pass turning operations. The cutting process was divided into multi-pass rough machining and finish machining. Machining parameters were determined to optimize the cutting conditions in the sense of the minimum unit production cost under a set of practical machining constraints.

Kee [143] discussed constrained optimization analyses and strategies for selecting the optimum cutting conditions for multi-pass rough turning operations

on CNC and conventional lathes. The analysis was based on the criterion typified by the maximum production rate and incorporated various relevant technological constraints. The approach adopted in arriving at the final solution involved a combination of theoretical economic trends and numerical search methods. Popular multi-pass solution strategies such as using all equal passes or all equal passes except one past were shown to be useful approximations but the final computer-aided optimal solutions yielded unequal cutting conditions per pass. Numerical case studies supported the importance of using developed optimization strategies rather than handbook recommendations, and demonstrated the effects of major variables as well as the superiority of multi-pass over single pass production rates.

Prasad et al. [232] combined linear programming and geometric programming to optimize the values of process parameters for a multi-pass turning operation. Chen et al. [56] proposed an integer programming and dynamic programming-based two-tier approach for reduction of machining time in NC machining by cutter selection and machining plane. Yang and Tarng [318] employed Taguchi method to investigate the cutting characteristics of S45C steel bars using tungsten carbide cutting tools. The optimal cutting parameters of the cutting speed, the feed rate and the depth of cut for turning operations with regard to performance indexes such as tool life and surface roughness were considered.

Cakir and Gurarda [46] described a procedure to calculate the machining conditions, such as the cutting speed, feed rate and depth of cut for turning operations with minimum production cost or the maximum production rate as the objective function. The optimum number of machining passes and the depth of cut for each pass was obtained through the dynamic programming technique and optimum values of machining conditions for each pass were determined based on the objective function criteria by search method application to the feasible region. Production cost and production time values were determined for different work piece and tool materials for the same input data. In the optimization procedure, the objective functions were subjected to the constraints of maximum and minimum feed rates and speeds available, cutting power, tool life, deflection of work piece, axial pre-load and surface roughness. By graphical representation of the objective function and the constraints in the developed software, the effects of constraints on the objective function were evaluated.

Reddy et al. [244] presented a genetic algorithm for the optimal sub-division of the depth of cut. The total production cost minimization was achieved by adding the minimum costs of the individual rough passes and the finish pass. The resulting sub-division of the depth of cut offered lower cost as compared to that given by the enumerative search techniques based on integer programming and dynamic programming.

Nian et al. [207] proposed the optimization of turning operations based on the Taguchi method with multiple performance characteristics. The orthogonal array, multi-response S/N ratio, and ANOVA were employed to study the performance characteristics in turning operations. Three cutting parameters namely, cutting speed, feed rate, and depth of cut, were optimized with considerations of multiple performance characteristics including tool life, cutting force, and surface finish. Experimental results were provided to illustrate the effectiveness of the approach.

Cakir and Gurarda [47] described a procedure to calculate the machining conditions for milling operations with minimum production cost as the objective function. Optimum values of machining conditions for each pass were determined by circular direction search method which was specifically developed for this purpose. The effects of constraints on the objective function were evaluated by graphical representation of the objective function and the constraints in the developed software.

Liang et al. [175] extended the study of Wang et al. [308] on determination of optimal process parameter settings for multi-pass turning operation. Hui et al. [127] showed how the choice of machining conditions for turning significantly impact on quality cost, by solving a nonlinear continuous constrained optimization problem using a nonlinear optimization search algorithm, based on quasi-Newton method and a finite difference gradient

Saravanan et al. [255] described various optimization procedures for solving the CNC turning problem to find the optimum operating parameters such as cutting speed and feed rate. The mathematical model proposed by Agapiou [5] was used for finding the optimum parameters. Total production time was considered as the objective function, subject to constraints such as cutting force, power, tool–chip interface temperature and surface roughness of the product. Conventional optimization techniques such as the Nelder–Mead simplex method and the boundary search procedure, and non-conventional techniques such as genetic algorithms and simulated annealing were employed and an example was given to illustrate the working procedures for determining the optimum operating parameters.

Onwubolu and Kumalo [215] proposed an optimization technique based on genetic algorithms for determination of the cutting parameters in multi-pass machining operations by simultaneously considering multi-pass rough machining and finish machining. The optimum machining parameters were determined by minimizing the unit production cost subject to twenty practical machining constraints. The cutting model formulated was a non-linear, constrained programming problem. Vijayakumar et al. [302] used the mathematical model which originally was developed by Shin and Joo [267] and extended by Chen and Tsai [55]. The minimum unit production cost criterion was adopted as the objective of the proposed model. The production cost for machining one unit piece was represented by the sum of the following four terms (from [302]; reprinted with permission from Elsevier):

Minimize

$$\mathrm{UC} = C_\mathrm{M} + C_\mathrm{I} + C_\mathrm{R} + C_\mathrm{T} \tag{2.52}$$

$$C_\mathrm{M} = K_0[(\pi DL/1,000V_\mathrm{t}f_\mathrm{r})\,((d_\mathrm{t} - d_\mathrm{s})/d_\mathrm{r}) + (\pi DL/1,000V_\mathrm{s}f_\mathrm{s})] \tag{2.53}$$

$$C_\mathrm{I} = K_0[t_\mathrm{c} + (h_1 L + h_2)\,((d_\mathrm{t} - d_\mathrm{s})/d_\mathrm{r} + 1)] \tag{2.54}$$

$$C_\mathrm{R} = K_0 t_\mathrm{e}/T_\mathrm{p}[(\pi DL/1,000V_\mathrm{t}f_\mathrm{r})\,((d_\mathrm{t} - d_\mathrm{s})/d_\mathrm{r}) + (\pi DL/1,000V_\mathrm{s}f_\mathrm{s})] \tag{2.55}$$

$$C_\mathrm{T} = K_\mathrm{t}/T_\mathrm{p}\,[(\pi DL/1,000V_\mathrm{t}f_\mathrm{r})\,((d_\mathrm{t} - d_\mathrm{s})/d_\mathrm{r}) + (\pi DL/1,000V_\mathrm{s}f_\mathrm{s})] \tag{2.56}$$

Eight constraints were considered for the rough cutting operation including the stable cutting region constraint and chip-tool interface temperature constraint.

$$V_{\mathrm{rL}} \le V_{\mathrm{r}} \le V_{\mathrm{rU}} \tag{2.57}$$

$$f_{\mathrm{rL}} \le f_{\mathrm{r}} \le f_{\mathrm{rU}} \tag{2.58}$$

$$d_{\mathrm{rL}} \le d_{\mathrm{r}} \le d_{\mathrm{rU}} \tag{2.59}$$

$$T_{\mathrm{L}} \le T_{\mathrm{r}} \le T_{\mathrm{U}} \tag{2.60}$$

$$F_{\mathrm{r}} = k_1 (f_{\mathrm{r}})^{\mu} (d_{\mathrm{r}})^{\nu} \le F_{\mathrm{u}} \tag{2.61}$$

$$P_{\mathrm{r}} = (F_{\mathrm{r}} V_{\mathrm{r}} / 6,120\eta) \le P_{\mathrm{U}} \tag{2.62}$$

$$Q_{\mathrm{r}} = k_2 (V_{\mathrm{r}})^{\tau} (f_{\mathrm{r}})^{\varphi} (d_{\mathrm{r}})^{\delta} \le Q_{\mathrm{U}} \tag{2.63}$$

$$V_{\mathrm{r}}^{\lambda} f_{\mathrm{r}} (d_{\mathrm{r}})^{\nu} \ge \mathrm{SC} \tag{2.64}$$

In addition, the following constraints were considered for the finish cutting operation and these included the constraints on stable cutting region, chip-tool interface temperature, and the surface roughness.

$$V_{\mathrm{sL}} \le V_{\mathrm{s}} \le V_{\mathrm{sU}} \tag{2.65}$$

$$f_{\mathrm{sL}} \le f_{\mathrm{s}} \le f_{\mathrm{sU}} \tag{2.66}$$

$$d_{\mathrm{sL}} \le d_{\mathrm{s}} \le d_{\mathrm{sU}} \tag{2.67}$$

$$T_{\mathrm{L}} \le T_{\mathrm{s}} \le T_{\mathrm{U}} \tag{2.68}$$

$$F_{\mathrm{s}} = k_1 (f_{\mathrm{s}})^{\mu} (d_{\mathrm{s}})^{\nu} \le F_{\mathrm{u}} \tag{2.69}$$

$$P_{\mathrm{s}} = (F_{\mathrm{s}} V_{\mathrm{s}} / 6,120\eta) \le P_{\mathrm{U}} \tag{2.70}$$

$$Q_{\mathrm{s}} = k_2 (V_{\mathrm{s}})^{\tau} (f_{\mathrm{s}})^{\varphi} (d_{\mathrm{s}})^{\delta} \le Q_{\mathrm{U}} \tag{2.71}$$

$$V_{\mathrm{s}}^{\lambda} f_{\mathrm{s}} (d_{\mathrm{s}})^{\nu} \ge \mathrm{SC} \tag{2.72}$$

$$f_{\mathrm{s}}^2 / 8R \le \mathrm{S}R_{\mathrm{U}} \tag{2.73}$$

The constraints for roughing and finishing parameter relations were given by the following equations.

$$V_{\mathrm{s}} \ge k_3 V_{\mathrm{r}} \tag{2.74}$$

$$f_{\mathrm{r}} \ge k_4 f_{\mathrm{s}} \tag{2.75}$$

$$d_{\mathrm{r}} \ge k_5 d_{\mathrm{s}} \tag{2.76}$$

where UC is the unit production cost except material cost; C_I is the machine idle cost due to loading and unloading operations and tool idle motion time ($/piece); C_M is the cutting cost by actual time in cut ($/piece); C_R is the tool replacement cost ($/piece); C_T is the tool cost ($/piece); d_r and d_s are the depths of cut for each pass of rough and finish machining; d_{rL} and d_{rU} are the lower and upper bound S of depth of cut in rough machining (mm); d_{sL} and d_{sU} are the lower and upper bounds of depth of cut in finish machining (mm); d_t is the depth of material to be removed (mm); D and L are the diameter and length of work piece (mm); f_r and f_s are the feed rates in rough and finish machining (mm/rev); f_{rL} and f_{rU} are the lower and upper bounds of feed rate in rough machining (mm/rev); f_{sL} and f_{sU} are the lower and upper bounds of feed rate in finish machining (mm/rev); F_r and F_s are the cutting forces during rough and finish machining (kgf); F_u is the maximum allowable cutting force (kgf); h_1 and h_2 are constants relating to cutting tool travel and approach/departure time (min); k_o is the direct labor cost + overhead ($/min); k_t is the cutting edge cost ($/edge); k_1 is the coefficient pertaining to specific tool–work piece combination; k_2 is the coefficient pertaining to equation of chip–tool interface temperature; k_3, k_4 and k_5 are the constants for roughing and finishing parameter relations; n is the number of rough passes; P_r and P_s are cutting powers during roughing and finishing (kW); P_U is the maximum allowable cutting power (kW); Q_r and Q_s are the temperatures during roughing and finishing (°C); Q_U is the maximum allowable temperature (°C); SC is the limit of stable cutting region; SR_U is the maximum allowable surface roughness (mm); R is the nose radius of cutting tool (mm); T is the tool life (min); t_c is the constant term of machine idling time (min); t_e is the tool exchange time (min); T_L and T_U are the lower and upper bounds of tool life; T_r and T_s are the tool life, expected tool life for rough machining and expected tool life for finish machining; T_p is the tool life of weighted combination of T_r and T_s (min); V_r and V_s are the cutting speeds in rough and finish machining (m/min); V_{rL} and V_{rU} are the lower and upper bounds of cutting speed in rough machining (m/min); V_{sL} and V_{sU} are the lower and upper bounds of cutting speed in finish machining (m/min); η is the power efficiency (= 0.85), λ and v are the constants pertaining to expression of stable cutting region; μ and v are constants of cutting force equation; and τ, φ and δ are the constants pertaining to expression of chip–tool interface temperature.

Shin and Joo [267] provided an example with certain data for the above optimization model and decomposed the optimization problem into two separate sub-problems. They dealt with these two sub-problems separately using an approach combining the Fobonacci search and dynamic programming. The minimum production cost found was $ 2.385/unit. Chen and Tsai [55] proposed an approach that combined the simulated annealing algorithm and Hooke–Jeeves pattern search technique and found the minimum production cost as $2.2974/unit. Chen and Tsai [55] extended the multi-pass turning operation model of Shin and Joo [267] by adding seven more constraints including stable cutting region constraints, chip–tool interface temperature constraints, and roughing and finishing parameter relations. Based on the same machining data of the problem

used by Shin and Joo [267], the minimum production cost obtained by Chen and Tsai [55] was $2.2959/unit.

Onwubolu and Kumalo [215, 216] proposed a technique based on a genetic algorithm to determine the optimal machining parameters for the extended model of Chen and Tsai [55] and calculated the production cost as $1.761/unit, which was substantially lower than that of Chen and Tsai [55]. However, the optimal value obtained by Onwubolu and Kumalo [215, 216] was proved to be impractical by Chen and Chen [53]. They pointed out that Onwubolu and Kumalo incorrectly handled the machining model since the number of rough cuts in their method was not limited to an integer value. Baykasoglu and Dereli [34] used simulated annealing approach to optimize cutting conditions in their heuristic model. However, they did not take surface finish into consideration. Vijayakumar et al. [302] proposed an ant colony optimization method to solve the same problem and claimed that the ant colony-based approach found an even better solution at $1.6262/unit. However, Wang [307] proved that for the given cutting speeds and feeds for the rough cut and the finishing cut as determined by Vijayakumar et al. [302], without considering violating any constraint, the lowest value of production cost was actually $1.968/unit.

Lee and Tarng [169] investigated optimal cutting parameters for maximizing production rate or minimizing production cost in multistage turning operations. A machining model was constructed based on a polynomial network. The polynomial network can learn the relationships between cutting parameters (cutting speed, feed rate, and depth of cut) and cutting performance (surface roughness, cutting force, and tool life) through a self-organizing adaptive modeling technique. Once the geometric model for machined parts and various time and cost components of the turning operation are given, an optimization algorithm using a sequential quadratic programming method can then be applied to the polynomial network for determining optimal cutting parameters.

Davim [66] presented a study of the influence of cutting conditions on the surface finish obtained by turning. A plan of experiments, based on the techniques of Taguchi, was designed and executed on controlled machining. Davim [67] investigated the influence of cutting conditions (cutting velocity and feed) and cutting time on turning metal matrix composites. An orthogonal array and the ANOVA were employed to investigate the cutting characteristics of flank wear, power required, and surface roughness.

Wang et al. [310] presented an optimization analysis for the selection of economic cutting conditions in single pass turning operations using a deterministic approach. The optimization was based on criteria typified by the maximum production rate and included a number of practical constraints. It was shown that the deterministic optimization approach involving mathematical analyses of constrained economic trends and graphical representation on the feed-speed domain provides a clearly defined strategy that not only provides a unique global optimum solution, but also the software that is suitable for on-line CAM applications.

Kwon et al. [164] used a fuzzy adaptive modeling technique, which adapts the membership functions in accordance with the magnitude of the process variations,

to predict surface roughness. Test results showed good agreement between the actual process output and the predicted surface roughness. António and Davim [15] presented the results of an experimental study concerned with the evolution of cutting forces, tool wear and surface roughness, as functions of time when turning the particulate metal matrix composite A356/20/SiCp-T6. Inserts with polycrystalline diamond (PCD) were tested. Cutting forces were measured using a piezoelectric dynamometer. The wear type was identified and its evolution with cutting time was measured. To model the phenomena, a hybrid technique based on an evolutionary search over the design space defined by the experimental results was considered. Optimal cutting conditions were searched using a genetic algorithm based on an elitist strategy.

Suresh et al. [284] developed a surface roughness prediction model for machining mild steel, using RSM. The experimentation was carried out with TiN-coated tungsten carbide (CNMG) cutting tools, for machining mild steel work-pieces covering a wide range of machining conditions. A second order mathematical model, in terms of machining parameters, was developed for surface roughness prediction using RSM. This model gives the factor effects of the individual process parameters. An attempt was also made to optimize the surface roughness prediction model using genetic algorithms (GA) to optimize the objective function. A number of tool wear monitoring schemes have been proposed that employ vibrations, ultrasonic, torque, power, velocity, and temperature sensors and sensor fusion. Sick [274] reviewed a number of research papers dealing with online and indirect tool wear monitoring in turning using ANNs. Mainly, vibrations, acoustic emission (AE), torque, power, velocity, and temperature sensors were employed for obtaining the feedback for indirect estimation of tool wear.

Feng and Wang [87] found multiple regression analysis and neural networks equally effective in predicting surface roughness for a finish turning process. Zuperl and Cus [332]proposed a neural network-based approach to complex optimization of cutting parameters. The authors had described the multi-objective technique of optimization of cutting conditions by means of the neural networks taking into consideration the technological, economic and organizational limitations. To reach higher precision of the predicted results, a neural optimization algorithm was developed and presented to ensure simple, fast and efficient optimization of all important turning parameters. The approach is suitable for fast determination of optimum cutting parameters during machining, where there is not enough time for deep analysis.

Cus and Balic [64] proposed a new optimization technique based on genetic algorithms (GA) for the determination of the cutting parameters in machining operations. Bouzid [40] described a method for calculating the optimum cutting conditions, in turning for objective criterion such as maximum production rate. The method used empirical models for tool life, roughness and cutting forces. Coefficients of these models were determined based on turning experiments in high-speed machining. Four types of commercially available inserts were used to turn an AISI 4340 steel. Three CVD-coated inserts and one ceramic tool were

studied. The machine power and the maximum spindle speed were considered as the process constraints.

Manna and Bhattacharyya [188] took the significant cutting parameters into consideration and used multiple linear regression mathematical models relating the surface roughness height to the cutting parameters for turning process of Al/SiC-MMC. Nandi and Pratihar [204] developed an expert system based on the fuzzy basis function network (FBFN) to predict surface finish in ultra-precision turning. An approach for automatic design of rule base and the weight factors (WFs) for different rules was developed using a genetic algorithm, based on error reduction measures.

Jiao et al. [137] used a fuzzy adaptive network (FAN) to model surface roughness in turning operations. FANs are five-layered network representation of the corresponding fuzzy inference rules. Each node performs a particular function on the incoming signals, which is characterized by a set of parameters. In order to represent different adaptive capabilities, the nodes can be classified into adaptive nodes with parameters that can be tuned by the learning procedure, and fixed nodes. The nodes in the first layer, divided into subgroups, store the membership functions associated with the input variables in the premise section of the fuzzy IF–THEN rules. Each subgroup in this layer can be interpreted as the linguistic terms of a particular input linguistic variable. Nodes in subsequent second layer perform the fuzzy aggregation of the premise section of the fuzzy IF–THEN rules. Nodes in successive layers represent the operations in the consequence section of the fuzzy IF–THEN rules. The FAN network has both the learning ability of neural network and linguistic representation of complex, not well-understood, vague phenomenon. Furthermore, it can continuously improve the initially obtained rough model based on the daily operating data. To illustrate this approach, a model representing the influences of machining parameters on surface roughness was established and then the model was verified by the use of the results of pilot experiments. Finally, a comparison with the results based on statistical regression was provided.

Pal and Chakraborty [223] predicted surface roughness by taking main cutting force, feed force, cutting speed, feed, and depth of cut as input parameters of the network. Sonar et al. [277] studied the performance of RBF network for predicting lower, most likely, and upper estimates of surface roughness in turning process. They observed that the performance of RBF neural network was slightly inferior to MLP neural networks.

Tzeng [295] proposed a set of optimal turning parameters for producing high dimensional precision and accuracy in the CNC turning process. Taguchi dynamic approach coupled with a proposed ideal function model was applied to optimize eight control factors for common tool steels SKD-11 and SKD-61. The control factors were coolant, cutting speed, feed, depth of cut, coating type, chip-breaker geometry, nose radius and shape of the insert, which were designed in a $L18$ orthogonal array and carried out in the experiments. The results showed that the factors associated with the cutting tool and feed had the most significant effects on the dimensional variation of the test piece. The combined optimized process

factors not only produced optimized dimensional precision and accuracy but also resulted in improved surface roughness.

Roy [249] made an attempt to design an expert system using two soft computing tools, namely fuzzy logic and genetic algorithm, so that the surface finish in ultra-precision diamond turning of metal matrix composite could be modeled for a set of given cutting parameters, namely spindle speed, feed rate and depth of cut. An optimized knowledge base of the fuzzy expert system was obtained using a binary-coded genetic algorithm. The GA-based training was done off-line. The GA-trained fuzzy expert system (GAFES) was able to predict surface finish in ultra-precision diamond turning of Al6061/SiC_p metal matrix composite before conducting actual experiments.

By analyzing and modeling the forming process of work piece and the error sources contributing to machining precision of work piece in turning operation, Yao et al. [320] presented the cutter trajectory and attitude representation to characterize the geometric errors of machined work piece in virtual manufacturing (VM). A surface topography simulation model was established to simulate the surface finish profile generated after a turning operation. This representation was implemented in the Virtual Machining and Measuring Cell (VMMC) developed by the authors to represent and predict the geometric errors of work piece.

Aslan et al. [19] used an orthogonal array and the ANOVA to optimization of cutting parameters in turning hardened AISI 4140 steel (63 HRC) with Al_2O_3 + TiCN mixed ceramic tool. The flank wear (VB) and surface roughness (Ra) were investigated to determine optimal values of cutting parameters, such as cutting speed, feed rate and depth of cut. Nalbant et al. [200] used Taguchi method to find the optimal cutting parameters for surface roughness in turning operations of AISI 1030 steel bars using TiN-coated tools. Three cutting parameters, namely, insert radius, feed rate, and depth of cut, were optimized with considerations of surface roughness, and so on. The effect of water-soluble cutting fluids under different ratios was also considered in this study.

Sardiñas et al. [258] proposed a multi-objective optimization method, based on a posteriori technique and using genetic algorithms to obtain the optimal parameters of cutting depth, feed and speed in turning process. Application example of turning a steel bar by means of a P20 carbide tool on a CNC lathe was presented and empirical models were experimentally obtained for tool life and cutting force. Two different, mutually conflicting objectives were optimized in this model. The first objective was the production rate, τ, measured as the entire time required to carry out the process (from [258]; reprinted with permission from Elsevier):

$$\tau = \tau_S + (V/M)(1 + \tau_{TC}/T) + \tau_0 \tag{2.77}$$

Where τ_S, τ_{TC} and τ_0 are the set-up time, the tool change time, and the time during which the tool does not cut respectively; V is the volume of the removed metal; T the tool life, and M the MRR. The tool life (T) is related with the cutting parameters (i.e. cutting speed (v), feed (f), and depth of cut (a)) by the Taylor's extended law,

$$T = C_T v^{\alpha} f^{\beta} a^{\gamma} \tag{2.78}$$

α, β and γ are the coefficients experimentally obtained.

MRR was computed by the expression,

$$M = 1000vfa \tag{2.79}$$

The second objective was the used tool life, ξ, considered as the part of the whole tool life which is consumed in the process.

$$\xi = (V/MT)^{*}100\% \tag{2.80}$$

Usually, for a particular cutting process, τ_S, τ_{TC}, τ_0 and V can be considered constant values, so that the objectives are functions of T and M, and, consequently, they depend upon the decision variables, v, f, and a.

The constraints which affect the selection of the optimal cutting conditions are the allowed values for the cutting parameters given by the following equations.

$$a_{\min} \leq a \leq a_{\max} \tag{2.81}$$

$$f_{\min} \leq f \leq f_{\max} \tag{2.82}$$

$$v_{\min} \leq v \leq v_{\max} \tag{2.83}$$

Also there are some constraints related to the machine features. The cutting force, F_C, must not be greater than a certain maximum value, $F_{C-\max}$, given by the strength and stability of the machine and the cutting tool. The cutting force is computed from empirical expressions in the form:

$$F_c = C_F v^{\alpha'} f^{\beta'} a^{\gamma'} \tag{2.84}$$

Where C_F, α', β' and γ' are coefficients experimentally obtained.

Another machine-related constraint is the maximum allowable value for cutting power, P, which must not surpass the machine motor power, P_{MOT} (considering the friction losses in the transmission):

$$P = \left(vF_c/6 \times 10^4\right) \leq (P_{MOT}\eta/100) \tag{2.85}$$

η is the motor efficiency.

In the finishing operations, the obtained surface roughness, R, must be smaller than the specified value, $R_{\max}$, given by technological criteria, so that the following equation is satisfied.

$$R = 124f^2/r_e \leq R_{\max} \tag{2.86}$$

Where r_e is the tool nose radius.

The results were analyzed for several different production conditions. The advantages of multi-objective optimization approach over the single-objective one were explained.

Abburi and Dixit [1] developed a knowledge-based system for the prediction of surface roughness in turning process. Neural networks and fuzzy set theory were used for this purpose. Knowledge acquired from the shop floor was used to train the neural network. The trained network provided a number of data sets, which were fed to a fuzzy set-based rule generation module. A large number of IF–THEN rules were generated, which were reduced to a smaller set of rules by using Boolean operations. The performance of the developed knowledge-based system was studied with the experimental data of dry and wet turning of mild steel with HSS and carbide tools. The developed rule base can be used for predicting surface roughness for given process variables as well as for the prediction of process variables for a given surface roughness. The concise set of rules helps the user in understanding the behavior of the cutting process and to assess the effectiveness of the model.

Ee et al. [80] presented an overview of research at the University of Kentucky on extensions to the conventional tool wear and tool life methodologies when machining with grooved tool inserts resulting from the more complex wear features observed and the more subtle failure criteria applied. The influence of cutting conditions including the cutting speed, feed and depth of cut on the tool life was studied experimentally using tools with chip-groove geometries and different tool coatings. It was shown that the slope and intercept of the log–log plot of tool life versus feed, for example, change considerably for different chip-groove geometries or different tool coatings. An empirical tool-life equation to consider the effects of these parameters was proposed.

Balaji et al. [26] presented developments in chip control research and provided major applications in turning operations involving the use of complex grooved tool inserts. The authors concluded with details of an attempt to develop a computer-aided process planning system incorporating a predictive capability for chip breakability in turning operations.

Al-Aomar and Al-Okaily [11] presented a Parameter Design (PD) approach that provides near-optimal settings to the process parameters of a single lathe machine with high-volume production. Optimized process parameters included both machining parameters (cutting speed, feed rate, and depth of cut) and production parameters (material order size and inventory safety stock and reorder point). The authors had extended the conventional per-part machining cost model into a per-order production cost model by consolidating the production economics of both machining parameters and production controls. Discrete Event Simulation (DES) was utilized to capture the stochastic and dynamic production attributes and to transfer the static machine PD model into a dynamic PD-DES production model. The model was also utilized to accumulate the per-order running cost over production time while incorporating the impacts of process variability in tool life, labor efficiency, machining conditions, order lead time, and demand rate. Using the PD-DES model as a dynamic fitness function, a Simple Genetic Algorithm (SGA) was developed and applied to a CNC lathe machine to determine near-optimal settings to both machining and production process parameters so that the overall per-order production cost was minimized. Results showed effective SGA

convergence profile with relatively low number of search generations. The benefits of the per-order cost model were illustrated by repeating the SGA solution using machine productivity as a fitness criterion. The new SGA solution resulted in a better productivity but at a higher per-order cost. The effectiveness of SGA search was illustrated by outperforming the solutions obtained from two-level and three-level full factorial designs.

Yildiz and Ozturk [323] developed a hybrid robust genetic algorithm (HRGA) based on Taguchi's method and genetic algorithm. After the approach was validated by single and multi-objective benchmark problems, it was applied to the optimization of machining economic problems in multi-pass turning operation. They showed that convergence speed and accuracy of HRGA to global optimal results was better than better than those of Chen and Tsai [55], Chen and Chen [53] and Chen [52]. Mukherjee and Ray [196] critically appraised the application potential of several modeling and optimization techniques in metal cutting processes, classified under several criteria, and a generic framework for parameter optimization in metal cutting processes was suggested for the benefits of selection of an appropriate approach.

Saravanan et al. [257] optimized the machining parameters for turning cylindrical stocks into continuous finished profiles. The machining parameters considered in multi-pass turning were depth of cut, cutting speed and feed. The machining performance was measured by the production cost. The constraints considered in this problem were cutting force, power, tool tip temperature, etc. Due to high complexity of this machining optimization problem, six non-traditional algorithms, the genetic algorithm (GA), simulated annealing algorithm (SA), Tabu search algorithm (TS), memetic algorithm (MA), ant colony algorithm (ACO) and the PSO were employed to resolve this problem. The results obtained from GA, SA,TS, ACO, MA and PSO were compared for various profiles. Also, a comprehensive user-friendly software package was developed to input the profile interactively and to obtain the optimal parameters using all six algorithms.

Satishkumar et al. [261] discussed the use of non-traditional optimization techniques such as genetic algorithms, simulated Annealing and ant colony optimization for optimizing the depth of cut in multi-pass turning. Karpat and Özel [141] proposed a dynamic-neighborhood particle swarm optimization DN-PSO) methodology to handle multi-objective optimization problems existing in turning process planning. The objective was to obtain a group of optimal process parameters for each of three different case studies presented in their work. The case studies considered in the work were: minimizing surface roughness values and maximizing the productivity, maximizing tool life and MRR, and minimizing machining-induced stresses on the surface and minimizing surface roughness. The optimum cutting conditions for each case study can be selected from calculated Pareto-optimal fronts by the user according to production planning requirements. The results indicated that the proposed methodology for solving the multi-objective optimization problems with conflicting objectives was effective.

Paiva et al. [222] presented a hybrid approach, combining RSM and principal component analysis (PCA) to optimize multiple correlated responses in a turning

process. Since a great number of manufacturing processes present sets of correlated responses, this approach could be extended to many applications. As a case study, the turning process of the AISI 52100 hardened steel was examined considering three input factors: cutting speed, feed rate, and depth of cut. The outputs considered were: the mixed ceramic tool life, processing cost per piece, cutting time, the total turning cycle time, surface roughness and the material removing rate. The aggregation of these targets into a single objective function was conducted using the score of the first principal component of the responses' correlation matrix and the experimental region was used as the main constraint of the problem. Considering that the first principal component was not enough to represent the original data set, a complementary constraint defined in terms of the second principal component score was added. The original responses have the same weights and the multivariate optimization led to the maximization of MRR while minimizing the other outputs. The kind of optimization assumed by the multivariate objective function was established by examining the eigenvectors of the correlation matrix formed with the original outputs. The results indicated that the multi-response optimization was achieved at a cutting speed of 238 m/min, with a feed rate of 0.08 mm/rev and at a depth of cut of 0.32 mm.

Al-Ahmari [10] developed empirical models for tool life, surface roughness and cutting force for turning operations. Process parameters (cutting speed, feed rate, depth of cut and tool nose radius) were used as inputs to the developed machinability models. Two important data mining techniques were used: RSM and neural networks. Data of 28 experiments when turning austenitic AISI 302 were used to generate, compare and evaluate the proposed models of tool life, cutting force and surface roughness for the considered material. Gurel and Akturk [116] gave an effective model for the problem of minimizing total manufacturing cost subject to a given total weighted completion time level. The authors deduced some optimality properties for this problem. Based on these properties, a heuristic algorithm was proposed to generate an approximate set of efficient solutions. The computational results indicated that the proposed algorithm performed better than the GAMS/MINOS commercial solver both in terms of solution quality and computational requirements such that the average CPU time was only 8% of the time required by the GAMS/MINOS.

Jawahir and Wang [134] presented a summary of developments in modeling and optimization of machining processes, focusing on turning and milling operations. With a brief analysis of past research on predictive modeling, the authors presented the analytical, numerical and empirical modeling efforts for 2D and 3D chip formation covering the development of a universal slip-line model, a comprehensive finite element model, and integrated hybrid models. This included a newly developed equivalent tool face (ET) model and new tool-life relationships developed for machining with complex grooved tools. A performance-based machining optimization method developed for predicting optimum cutting conditions and cutting tool selection was also presented.

Basak et al. [31] used RBF models to predict surface roughness in finish hard turning process of AISI D2 cold rolled steel with mixed ceramic tools. For better

modeling of an RBF network, assistance of multiple-linear regression was taken. The authors had observed that in RBF neural network training, the spread parameter, which is essentially the zone of influence of a neuron, plays a significant role.

Nalbant et al. [200] used Taguchi method to find the optimal cutting parameters for surface roughness in turning. The orthogonal array, the S/N ratio, and ANOVA were employed to study the performance characteristics in turning operations of AISI 1030 steel bars using TiN-coated tools. Three cutting parameters namely, insert radius, feed rate, and depth of cut, were optimized with considerations of surface roughness.

Wang et al. [312] presented a summary of recent developments in developing performance-based machining optimization methodologies for turning operations. Four major machining performance measures (cutting force, tool wear/tool life, chip form/chip breakability, and surface roughness) were considered for the development and integration of hybrid models for single and multi-pass turning operations with and without the effects of progressive tool wear. Non-linear programming techniques were used for single-pass operations, and a genetic algorithm approach was adopted for multi-pass operations. The methodology offers the selection of optimum cutting conditions and cutting tools for turning with complex grooved tools.

Quiza et al. [233] carried out an experimental investigation on tool wear prediction on ceramic cutting tools used for turning hardened cold rolled tool steel. They predicted tool wear with the help of neural network and regression models. The neural network model was found superior to the regression model.

Soft computing optimization techniques, viz., genetic algorithm, PSO, and simulated annealing, were used for optimizing neural network model parameters. Natarajan et al. [205] employed a neural network model For tool life estimation that was optimized by PSO. The use of PSO resulted in reduction of training time by 50%.

Kim et al. [155] explored the applicability of real coded genetic algorithm (RGA) in machining optimization. In their work, RGA was compared to SA, continuous SA, GA, and generalized reduced gradient method. Ojha et al. [209] used neural network, fuzzy set, and genetic algorithm-based soft computing methodology to optimize process parameters in multi-pass turning operation. Neural network was used for prediction of surface finish and tool life. In view of uncertainty, surface roughness was quantified by using fuzzy number. An equal depth of cut for roughing passes along with a single finish pass strategy, was considered in the optimization model. The optimization model was applied for determining the optimum cutting parameters for two cases, viz., minimization of production cost and maximization of production rate.

Sharma et al. [265] measured machining variables such as cutting forces and surface roughness during turning at different cutting parameters such as approaching angle, speed, feed and depth of cut. The data obtained by experimentation was analyzed and used to construct model using neural networks. The model obtained was then tested with the experimental data.

Manna and Salodkar [189] described a procedure to obtain the machining conditions for turning operation considering unit cost of production as an objective function. The optimality conditions for single point cutting operations were determined based on the objective function using dynamic programming technique. The optimal policy of machining conditions were determined for evolution of minimum cost considering the important cost related machining criteria such as actual machining time, tool reuse time, set up time, tool life, and tool changing time. The mathematical models were also developed. The effects of different constraints on the objective functions were analyzed through various graphical representations. Taguchi method was also used to optimize the cutting parameters to achieve better surface finish and to identify the most effective parameter for cost evolution during turning. Taking significant cutting parameters into consideration and using multiple linear regressions, mathematical model relating to the surface roughness height R_a was established to investigate the influence of cutting parameters during turning.

Davim et al. [70] developed surface roughness prediction models using ANN to investigate the effects of cutting conditions free-machining steel, 9SMnPb28 k(DIN). The ANN model of surface roughness parameters was developed with the cutting conditions such as feed rate, cutting speed and depth of cut as the affecting process parameters. The experiments were planned as per L_{27} orthogonal array with three levels defined for each of the factors in order to develop the knowledge base for ANN training using error back-propagation training algorithm (EBPTA). 3D surface plots were generated using ANN model to study the interaction effects of cutting conditions on surface roughness parameters. The analysis revealed that cutting speed and feed rate have significant effects in reducing the surface roughness, while the depth of cut has the least effect.

Aggarwal et al. [7] optimized multiple characteristics (tool life, cutting force, surface roughness and power consumption) in CNC turning of AISI P-20 tool steel using liquid nitrogen as a coolant. Four controllable factors of the turning process, viz. cutting speed, feed, depth of cut and nose radius were studied. Face centered central composite design was used for experimentation. RSM was used for modeling the responses. Desirability function was used for single and multiple response optimization.

Horng and Chiang [126] developed an algorithm to determine the optimum manufacturing conditions for turning Hadfield steel with Al_2O_3/TiC mixed ceramic tool by coupling the grey relational analysis with the fuzzy logic. The flank wear and surface roughness were adopted to evaluate the machiniablity performances. Various cutting parameters, such as cutting speed, feed rate, depth of cut and nose radius of tool were explored by experiment. An orthogonal array was employed for the experimental design. This proposed algorithm obtains a grey–fuzzy reasoning grade to evaluate the multiple performance characteristics through the grey relational coefficient of each performance characteristic. The response table, response graph and ANOVA were used to find the optimal levels and the effect of cutting parameters on the flank wear and surface roughness.

A confirmation test within the optimal machining parameters was conducted to indicate the effectiveness of this proposed algorithm.

Umbrello et al. [297] presented a predictive hybrid model based on the ANNs and FEM that can be used for both forward and inverse prediction. The former was able to determine a residual stresses profile corresponding to a given tool, material and process conditions, the latter was able to determine these conditions when a constraint on the residual stresses distribution was given. Three layer neural networks were trained basing on selected data from numerical investigations on hard machining of 52100 bearing steel, and then validated with data obtained by the experiments.

Tzeng et al. [296] investigated the optimization of CNC turning operation parameters for SKD11 (JIS) using the Grey relational analysis method. Nine experimental runs based on an orthogonal array of Taguchi method were performed. The surface properties of roughness average and roughness maximum as well as the roundness were selected as the quality targets. An optimal parameter combination of the turning operation was obtained via Grey relational analysis. By analyzing the Grey relational grade matrix, the degree of influence of each controllable process factor on individual quality targets was found. Through ANOVA, the depth of cut was reported as the most significant controlled factor for the turning operation when the minimization of the roughness average, the roughness maximum and the roundness are simultaneously considered.

Yildiz [322] proposed a hybrid method combining immune algorithm with a hill climbing local search algorithm for solving complex real-world optimization problems. The objective was to contribute to the development of more efficient optimization approaches with the help of immune algorithm and hill climbing algorithm. The hybrid algorithm combined the exploration speed of immune algorithm with the powerful ability to avoid being trapped in local minimum of hill climbing. The hybrid algorithm was applied to the optimization of machining parameters in a multi-pass turning operation problem which was previously considered by Shin and Joo [267], Chen and Tsai [55], Chen and Chen [53], Chen [52], and Yildiz and Ozturk [323].

Muthukrishnan and Davim [199] studied the surface roughness of Al–SiC (20 p) by turning the composite bars using coarse grade PCD insert under different cutting conditions. Experimental data collected were tested with ANOVA and ANN techniques. Multilayer perceptron model was constructed with back-propagation algorithm using the input parameters of depth of cut, cutting speed and feed. Output parameter was surface finish of the machined component. On completion of the experimental test, ANOVA and an ANN were used to validate the results obtained and also to predict the behavior of the system under any condition within the operating range.

Gaitonde et al. [100] presented the application of Taguchi method and the utility concept for optimizing the machining parameters in turning of free-machining steel using a cemented carbide tool. A set of optimal process parameters, such as feed rate, cutting speed, and depth of cut on two multiple performance characteristics, namely, surface roughness and MRR was developed. The

experiments were planned as per L_9 orthogonal array. The optimal level of the process parameters was determined through the analysis of means (ANOM). The relative importance among the process parameters was identified through the ANOVA. The ANOVA results indicated that the most significant process parameter was cutting speed followed by depth of cut. The optimization results revealed that a combination of higher levels of cutting speed and depth of cut along with feed rate is essential in order to simultaneously minimize the surface roughness and to maximize the MRR.

Srinivas et al. [281] proposed a methodology for selecting optimum machining parameters in multi-pass turning using particle swarm intelligence to minimize unit production cost subjected to practical constraints. Chandrasekaran et al. [49] reviewed the application of soft computing tools such as neural networks, fuzzy sets, genetic algorithms, simulated annealing, ant colony optimization, and PSO to four machining processes—turning, milling, drilling, and grinding. The authors highlighted the progress made in this area and discussed the issues that need to be addressed.

Rajemi et al. [236] developed a new model and methodology for optimizing the energy footprint for a machined product. The total energy of machining a component by the turning process was modeled and optimized to derive an economic tool-life that satisfies the minimum energy footprint requirement. The work clearly identified the critical parameters in minimizing energy use and hence reducing the energy cost and environmental footprint. Additionally, the paper explored and discussed the conflict and synergy between economical and environmental considerations as well as the effect of system boundaries in determining optimum machining conditions.

Bouacha et al. [39] conducted an experimental study of hard turning with CBN tool of AISI 52100 bearing steel, hardened at 64 HRC. The main objectives were focused on delimiting the hard turning domain and to develop the relationship between cutting parameters (cutting speed, feed rate, and depth of cut) and machining output variables (surface roughness and cutting forces) through the RSM. The combined effects of the cutting parameters on machining output variables were investigated while employing the ANOVA. The quadratic model of RSM associated with response optimization technique and composite desirability was used to find optimum values of machining parameters with respect to the objectives (surface roughness and cutting force values). Results showed the degree of influence of feed rate and cutting speed on surface roughness. The depth of cut exhibited maximum influence on cutting forces as compared to the feed rate and cutting speed.

2.5 Drilling Process

Drilling is the operation of producing circular holes in the workpiece by using a rotating cutter called ‘drill’. The machine used for drilling is called drilling

machine. The drilling operation can also be accomplished in lathe, in which the drill is held in tailstock and the work is held by the chuck. The most common drill used is the twist drill. The peripheral speed of the drill called cutting speed, movement of the drill along the axis of the hole for one revolution called feed, and radius of the drill called as depth of cut are the process parameters. The special feature of drilling is that the cutting speed varies along the cutting edge, from almost zero near the center of the drill to the circumferential speed of the drill at its outer radius. These parameters may be optimized for obtaining the minimum cost of machining and minimum production time.

Various investigators had presented techniques, both traditional and non-traditional, for modeling and optimization of drilling processes. Mauch and Lauderbaugh [190] introduced an analytical model that predicts thrust and torque levels for drilling. These predictions were based on drill geometry, yield shear stress, and chip thickness. This model was presented in contrast to previous empirical models which required large amounts of experimental data and are of questionable use outside of the experimental range. The model was developed by dividing the drill tip into three regions with each region having a separate metal cutting model. The chisel edge comprised two of the three regions. The inner chisel edge region was modeled as an indentation process: while the outer chisel edge region was modeled using orthogonal cutting theory. A new analytical expression was developed to define the transition point between these two regions. This expression was found to be in excellent agreement with empirical results of other researchers. Finally, the lip region of the drill was modeled by dividing the region into N cutting elements and modeling each element with oblique cutting theory. The total force and torque were then computed by summing the contributions from each of the three regions. The model can be used for both conventional and split-point high-speed steel drill tip geometries. However, the model can be easily extended to include other geometries. Thrust and torque predictions from the analytical model were compared with experimental results that were generated by using conventional and split-point drills to drill 2024-T351 aluminum.

Khajavi and Komanduri [145] used back-propagation neural network (BPNN) model to predict drill wear employing multiple sensors. The signals from four sensors, viz., thrust, torque, and strain in two directions, were used. It was found that the change in area under power spectral density plots shows good correlation with corner drill wear. The authors concluded that one sensor signal would be adequate for drill wear estimation. Biglari and Fang [38] used real-time fuzzy logic control for maximizing drill life in a small-hole drilling (3 mm diameter) process. Experiments were conducted under five different drill wear conditions—initial, normal wear, acceptable wear, severe wear, and drill failure to record thrust force, torque, and radial force, which developed 53 fuzzy rules. The methodology based on online monitoring of drill wear was used for controlling drill feed rate for maximum tool life. Stone and Krishnamurthy [283] used neural network to model the relationship between feed rate and the thrust force during drilling of fiber-reinforced composite materials using diamond-tipped drill. They developed a neural network-based controller that minimizes the problem of

delamination or crack growth during the drilling process. The authors compared the proposed method with experimental results and found that thrust force controlled drilling process is advantageous over conventional constant feed drilling process.

Kolahan and Liang [156] reported a tabu-search approach to minimize the cost in hole-making processes. Four issues, namely, tool travel scheduling, tool switch scheduling, tool selection, and machining speed specification were simultaneously addressed. The problem has a structure similar to the traveling salesman problem (TSP) and hence is NP-complete. The performance of the proposed approach was tested using an example problem.

Lee et al. [171] described the use of an abductive network for modeling drilling processes. A number of drilling experiments were carried out on a CNC machining center (first MCV-641) using HSS twist drills for the machining of S45C steel plates. The drilling process parameters were selected by varying the drill diameter in the range of 8–12 mm, the cutting speed in the range of 10–30 m/min and the feedrate in the range of 0.06–0.24 mm/rev. Each of these process parameters was set at three levels. Therefore, 27 ($3 \times 3 \times 3$) drilling experiments were designed based on the process parameter combinations. However, only 25 drilling experiments were performed due to the limited power of the machine. The drill-life was defined as the period of drilling time until the average flank wear land was equal to 0.3 mm or the maximum flank wear land equal to 0.6 mm. In the experiments, the flank wear land was measured on both cutting edges of the drill using a tool microscope. The mean flank wear land was calculated by averaging six places of the flank wear land on the cutting edges. The MRR is calculated by using the following equation:

$$\text{MRR} = 0.25\pi D^2 fN \tag{2.87}$$

where D is the drill diameter (mm), f is the feedrate (mm/rev) and N is the rotational speed of the drill (rpm), which can be calculated from Equation 2.88.

$$N = 1000V/\pi D \tag{2.88}$$

where V is the cutting speed in m/min.

The thrust force and torque signals were measured and used as the inputs to the network. The drilling performance (tool life, MRR, thrust force and torque) with the corresponding process parameters (drill diameter, cutting speed and feedrate) was developed as training data base, a three-layer abductive network for predicting tool life was synthesized automatically. The abductive network was composed of a number of functional nodes and these nodes were self-organized to form an optimal network architecture by using a predicted squared error (PSE) criterion. Once the process parameters (drill diameter, cutting speed and feedrate) are given, the drilling performance (tool life, MRR, thrust force and torque) can be predicted by this developed network. Since the tool life and the MRR are the two different objectives, a normalization of tool life and MRR between zero and unity was required. A weighting method was then adopted to transform the normalized tool

life T_L and normalized MRR M_R into a single objective format. The objective function was formulated as follows:

$$\text{Objective function} = -w_1 T_L - w_2 M_R \tag{2.89}$$

Where, w_1 and w_2 were the weights of the normalized tool life T_L and normalized MRR M_R in optimization. The inequality constraints on the thrust force F_T and torque T_Q were given as follows:

$$0 < F_T < \text{UF}_T \tag{2.90}$$

$$0 < T_Q < \text{UT}_Q \tag{2.91}$$

Where, UF_T and UT_Q are the upper bounds of the thrust force F_T and of the torque T_Q, respectively.

Several cases were presented by Lee et al. [171] to illustrate the optimization of the process parameters in drilling operations. Through the simulated annealing searching, the optimal process parameters with several weighting combinations were obtained. Experimental results were provided to confirm the effectiveness of this approach.

Lin and Ting [177] predicted drill wear using neural network and regression models. Average thrust force and torque, spindle speed, feed rate, and drill diameter were used as input parameters and average flank wear was the only output parameter of the neural network. The authors found that the neural networks with two hidden layers learn faster and can more accurately estimate tool wear than the networks with one hidden layer. Elhachimi et al. [81] presented a new theoretical model to predict thrust and torque in high-speed drilling. The method involved determining the continuous distributions of thrust and torque along the lip and the chisel edge of a twist drill. The calculation used the oblique cutting model for the lip and the orthogonal cutting model for the chisel edge. Thrust and torque were obtained in terms of the geometric features of the drill, the cutting conditions and the properties of the machined material.

Liu et al. [179] used polynomial network for in-process prediction of corner wear on the drill. The polynomial network was composed of a number of functional nodes having self-organizing feature with an ability to construct the relationship between input and output variables. Thrust force or torque, cutting speed, feed rate, and drill diameter were used as input parameters. The authors found that the use of thrust force in the model provides predictions within an error of 10%. Shunmugam et al. [273] presented a model based on production cost and the optimal conditions were obtained considering technological and machine tool constraints. This approach is quite useful in arriving at the cutting parameters automatically in a computer-assisted process planning system.

Hashmi et al. [120] developed fuzzy logic model for selection of cutting speed to drill three different work materials, viz., medium carbon steel, low carbon alloy steel, and medium carbon-free-machining steel. The predicted drilling speeds for

different work material hardness showed good corelation with Machining Data Handbook.

Mahdy [186] attempted to find out the best combination of drilling and enlarging as well as chamfering prior to enlarging, which minimizes the obtained burr size. A flowchart was developed for the determination of the optimum conditions of drilling with minimum manufacturing cost from the point of view of burr formation. It enabled also the evaluation of the electrochemical deburring (ECD) time to obtain the required deburring radius with minimum cost for drilling followed by ECD, especially in case of drilling intersecting holes. Zhang et al. [326] presented a theoretical analysis for predicting mean values of thrust and torque in vibration drilling fiber-reinforced composite materials. The model was based on mechanics of vibration cutting analysis and the continuous distributions of thrust and torque along the lip and the chisel edge of a twist drill. The result of a simulation study had shown a very good agreement between the theoretical predictions and the experimental evidence. On the same cutting conditions, the thrust and the torque by the vibration drilling method were reduced by 20–30 percent, compared with conventional drilling.

Ertunc et al. [86] proposed two techniques for the on-line identification of tool wear based on the measurement of cutting forces and power signals. These techniques use hidden Markov models (HMMs), commonly used in speech recognition. In the first method, bargraph monitoring of the HMM probabilities was used to track the progress of tool wear during the drilling operation. In the second method, sensor signals that correspond to various types of wear status, e.g., sharp, workable and dull, were classified using a multiple modeling method. Experimental results demonstrated the effectiveness of the proposed methods. Although this work focused on on-line tool wear condition monitoring for drilling operations, the HMM monitoring techniques can be applied to other cutting processes.

Kim et al. [154] developed control charts for drilling burr formation for stainless, AISI 304L, and low alloy steel, AISI 4118. Split point twist drills were used for the experiments of this work. A drilling burr control chart, based on experimental data, is a tool for prediction and control of drilling burrs. Burr classification was carried out based on the geometric characteristics, burr formation mechanisms and sizes of the burrs. New parameters consisting of cutting condition variables and drill diameter were developed, and used to show unique distributions of the burr types. Burr types and the resultant burr size showed great dependence on the new parameters regardless of the drill diameters. Through the chart, burr type can be predicted with given cutting conditions. Also cutting conditions that are believed to create preferred burr types can be selected.

Davim and António [68] presented experimental and numerical study of the cutting forces, tool wear and surface finish, measured when drilling the particulate metal matrix composite A356/20/SiCp-T6. The experimental work was developed through the continuous measurement of the cutting forces with an appropriate piezoelectric dynamometer. The wear type was identified and its evolution with cutting time was measured. Drills with PCD were tested. The surface finish of the holes was evaluated with a profilometer. Using the experimental results,

a numerical search of optimal drilling conditions was performed. Since there were contradictory objectives, such as maximization of tool life and minimization of tool wear, the concept of the Pareto optimum solution was considered in the optimization procedure. An evolution strategy was adopted to obtain the optimal solution for cutting speed, feed rate and tool life prediction with industrial interest. In another work, Davim and António [69] proposed a methodology aiming at the selection of the optimized values for cutting conditions in turning and drilling operations of aluminum matrix composites. A hybrid technique based on an evolutionary search over a design space obtained by experimental way was considered. The machining forces, the surface finish and the tool wear were experimentally measured considering the feed and the cutting velocity as predefined parameters.

Karthikeyan et al. [142] attempted to optimize the drilling characteristics for Al/SiC_p composites using fuzzy logic and genetic algorithms (GA). The drilling characteristics studied were drill wear, specific energy and surface roughness. The parameters considered for the study included volume fraction of SiC in the aluminum matrix, cutting speed and feed rate. The experimental data was trained and simulated using fuzzy logic and optimization of cutting conditions were performed using genetic algorithms. The optimized cutting conditions were validated using confirmation experiments. Kim and Ahn [150] proposed a monitoring method, based on neural network and spindle motor power sensing, to detect the state of chip disposal in drilling. If chip flow is bad during drilling, both the static component and the fluctuation of the dynamic component of drilling torque increase highly. Therefore, both of these components could be helpful in monitoring the chip disposal state during drilling. Drilling torque was indirectly measured by sensing the spindle motor power through an AC spindle motor drive system. From the spindle motor power measurements, variance/mean, mean absolute deviation, gradient, and event count were calculated as feature vectors and then presented to the neural network to make a decision on the state of chip disposal. The selected features were sensitive to changes in the state of chip disposal but comparatively insensitive to changes in drilling conditions. A three-layered neural network with an error-back-propagation algorithm was used. Experimental results showed that the monitoring system could successfully recognize the state of chip disposal over a wide range of drilling conditions.

Abu-Mahfouz [3] compared several architectures of feed-forward BPNN for tool condition monitoring of twist drill wear. The network was trained using vibration data and five drill wear conditions, viz., chisel wear, crater wear, flank wear, edge fracture, and corner wear, which were artificially introduced in the network for prediction of drill wear. Fully connected networks were found to be better than grouped network and the vibration signals are promising data for tool condition monitoring.

Balykov [27] presented the results of experimental studies in selecting optimum characteristics for diamond drills and optimum treatment procedures for drilling holes of 1–70 mm in diameter in hard brittle nonmetallic materials such as quartz, ceramics, glass, and glass ceramics. To obtain experimental-

mathematical models, a randomized experimental design was used at the screening stage, i.e., a half-replica of the full factorial experiment 2^3, and an orthogonal compositional design of the second order of type 3^5 was used at the main stage. The diamond drilling process was optimized using simplex methods. The correlation of the estimated values with experimental data showed the adequacy of the results obtained.

Kim and Ramulu [153] optimized the drilling process of graphite/bismaleimide-titanium alloy (Gr/Bi–Ti) stacks in terms of machined hole quality and machining cost. The drilling experiments were conducted by using two different cutter materials, HSS-Co and carbide. Drilled hole quality parameters included surface texture, titanium burrs, hole diameter, cylindricity, and roundness deviation. Machining cost was estimated through drill wear experimentations. A multiple objective linear program was used to optimize drilling feed and speed not only to maximize each hole quality parameter to the greatest extent possible but also to minimize machining cost. Optimum process conditions for achieving desired hole quality and process cost were found to be a combination of low feed and low speed when using carbide drills, and high feed and low speed in drilling with HSS-Co drills.

Tsao and Hocheng [293] presented a prediction and evaluation of delamination factor while using a twist drill, a candle stick drill and a saw drill. The approach was based on Taguchi's method and the ANOVA. An ultrasonic C-Scan to examine the delamination of carbon fiber-reinforced plastic (CFRP) laminate was used. The experiments were conducted to study the delamination factor under various cutting conditions. The experimental results indicated that the feed rate and the drill diameter were recognized to make the most significant contribution to the overall performance. The objective was to establish a correlation between feed rate, spindle speed and drill diameter with the induced delamination in a CFRP laminate. The correlation was obtained by multi-variable linear regression and was compared with the experimental results.

A new approach based on PSO was developed by Onwubolu and Clerc [214] for solving the drilling path optimization problem. The problem was modeled as a TSP with appropriate weights and cost functions. Pedersen [229] studied the optimization of a hole of given area which was placed in the interior of a plate with an arbitrary external boundary. To avoid stress concentrations the shape of the hole must be smooth (continuous curvature). The optimization was performed in relation to maximizing the first eigen frequency or maximizing the gap between the first and second eigen frequency. An inverse solution was also shown, i.e. finding the shape and position of a hole in the plate that result in a specified eigen frequency. A rather general parameterization with only seven design parameters was applied, including the possibility of going from an ellipse to a rectangle or even to a triangle. Optimal designs were obtained iteratively using mathematical programming, where each of the redesigns were based on finite element (FE) analysis and sensitivity analysis. Mindlin plate theory was the basis for the FE analysis and the semi-analytical sensitivity analysis included only the elements on the boundary of the hole.

Sanjay et al. [253] proposed BPNN to detect drill wear on 8 mm HSS drill while machining mild steel. The network was trained using spindle speed, feed, drill size, machining time, torque, and thrust force as input parameters. The authors found that the three layered network with the hidden layer having two and ten neurons was the best layered network and predicted values were accurate compared to regression analysis for all the combinations of cutting speed and feed.

Nouari et al. [208] discussed the change in wear mechanisms as a function of cutting speed and coating material. The cutting tests were performed on a rigid instrumented drilling bench without the use of cutting fluids. AA2024 aluminum alloy was used to investigate the wear mechanisms of cemented tungsten carbide and HSS tools. Three cutting speeds (25, 65 and 165 m/min) and a constant feed rate of 0.04 mm/rev were selected for the experiments. The best results in terms of maximum and minimum hole diameter deviations and surface roughness were obtained for the uncoated and coated tungsten carbide drills. The results also showed that HSS tool is not suitable for dry machining of AA2024 aluminum alloy.

Bandyopadhyay et al. [28] reported the use of Taguchi DoE technique to study the effects of the pulse energy, pulse repetition rate, pulse duration, focal position, nozzle standoff, type of gas and gas pressure of the assist gas on the quality of the laser-drilled holes and ascertain optimum processing conditions. Minimum taper in the drilled hole was considered as the desired target response. The entire study was conducted in three phases:(a) screening experiments to identify process variables that critically influence taper in laser-drilled holes, (b) optimization experiments to ascertain the set of parameters that would yield minimum taper and (c) validation trials to assess the validity of the experimental procedures and results. Results indicated that laser drilling with focal position on the surface of the material being drilled and employing low level values of pulse duration and pulse energy represents the ideal conditions to achieve minimum taper in laser-drilled holes.

Langella et al. [165] presented a mechanistic model for use in predicting thrust and torque during composite materials drilling. They specified the number of coefficients to be experimentally determined and provided a detailed analysis of the problems associated with the action of the chisel edge. Their theoretical approach was suggested by the observation that during a drilling process the prerequisites for orthogonal fiber cutting are met for an infinitesimal instant. Hence their decision to simulate a conventional drilling process by developing a model with only two semi-empirical coefficients. The method proposed is comparatively user-friendly since the semi-empirical coefficients concerned can be determined without difficulty by means of simple linear relations. The results obtained were satisfactorily validated by comparing the test findings with the corresponding theoretical data and it is possible to conclude that the model affords a focused approach to the definition of the most appropriate drill geometry and cutting parameters in composite materials drilling.

Paul et al. [228] investigated the optimization of twist drill point geometries in order to minimize thrust and torque in drilling. A point geometry parameterization based on the drill grinding parameters was used to ensure manufacturability of the

optimized geometry. Three commonly used drill point geometries, namely, conical, RaCon® and helical, were optimized for drilling forces while maintaining the inherent characteristics of each of the profiles. A significant reduction was shown in the drilling forces for the optimized drills. Drills with the optimized conical point profile were produced and tests were conducted to validate the reduction in thrust and torque.

Heisel et al. [123] presented a method for the determination of the burr dimensions to be expected in short-hole drilling, simultaneously taking the parameters into consideration which influence the burr formation. These parameters were yield stress, forces and the geometry of the inserts. The method was based on empirical cutting examinations and took account of the correlation between different burr parameters and the machining conditions such as cutting speed, feed and tool geometry. Using Schaefer's burr value, it was possible to make a quantitative evaluation of the burr dimensions. The method was verified for the materials 16 MnCr 5 and Ck 45 in case of dry machining.

Bağci and Ozcelik [24] investigated the effects of drilling parameters (drilling depth, feed rate, and spindle speed) on the twist drill bit temperature and thrust force in the dry drilling of Al 7075-T651 material. During dry drilling experiments, drill bit temperature and thrust forces were measured. Drill temperatures were measured by inserting standard thermocouples through the coolant (oil) hole of TiN/TiAlN- coated carbide drills. The settings of drilling parameters were determined by using the Taguchi experimental design method. An orthogonal array, the S/N ratio, and the ANOVA were employed to analyze the effect of drilling parameters. The objective was to establish a model using multiple regression analysis between spindle speed, drilling depth, feed rate, and drilling method with the drill bit temperature and thrust force in a Al 7075-T651 alloy material. The study showed that the Taguchi method is suitable to solve the problems with a minimum number of trials as compared with a full factorial design.

Sanjay and Jyothi [252] aimed to identify suitable parameters for the prediction of surface roughness. Back-propagation neural networks were used for the detection of surface roughness. Drill diameter, cutting speed, feed and machining time were given as inputs to the neural network structure and surface roughness was estimated. Drilling experiments with 12 mm drills are performed at three cutting speeds and feeds. The number of neurons are selected from 1,2,3,…, 20. The learning rate was selected as 0.01, and no smoothing factor was used. The best structure of neural network was selected based on a criteria including the minimum of sum of squares with the actual value of surface roughness. For mathematical analysis, an inverse coefficient matrix method was used for calculating the estimated values of surface roughness. Comparative analysis was performed between actual values and estimated values obtained by mathematical analysis and neural network structures.

Bağci and Ozcelik [25] investigated the effects of drilling depth, spindle speed and feed rate on the drill bit temperature in step-by-step and continuous dry drilling. Drill temperatures were measured by inserting standard thermocouples

through the coolant (oil) hole of TiN/TiAlN-coated carbide drills. Experimental studies were conducted by using two different workpiece materials, AISI 1040 steel and Al 7075-T651. Fernandes and Cook [90] described the development of an empirical model of the maximum thrust force and torque produced during drilling of carbon fiber with a 'one shot' drill bit. Shaw's simplified equations were adapted in order to accommodate for tool wear and used to predict maximum thrust force and torque in the drilling of carbon composite with a 'one shot' drill bit. The mathematical model was dependent on the number of holes drilled previously, the geometry of the drill bit, the feed used and the thickness of the workpiece. Ozcelik and Bağci [219] investigated the influences of the spindle speed and feed rate on the drill temperature responses. A new experimental approach was developed to measure drill temperature in drilling process. Drill temperatures were measured by inserting standard thermocouples through the coolant (oil) hole of TiAlN-coated carbide drills. Experimental parameters used in the study were based on Taguchi's method. Experimental study was conducted by using two different workpiece materials, AISI 1040 steel and Al 7075-T651. The drill bit temperature was predicted using a numerical calculation with Third Wave AdvantEdge^{TM} Lagrangian based on explicit FEA software. The results obtained from experimental study and finite element analyses (FEA) were compared. Good agreement between the measured and analyzed temperature results was found in dry drilling process.

Sardiñas et al. [259] proposed a multi-objective optimization of the drilling process of a laminate composite material. The composite material tested was a CFRP material, epoxy matrix reinforced with 55% of carbon fibers. The experiments were carried out in a laminated plate (CFRP) with 4 mm of thickness, using a 5-mm diameter drill (helical flute K10 drill). The depth of the holes was 4 mm. The tests were repeated once. A piezoelectric dynamometer with a load amplifier was used to acquire the torque and feed force. The damage around the holes (entry and exit) was measured with a shop microscope. The damage of hole was quantified by the delamination factor (D_F), accordingly the following equation (from [259]; reprinted with permission from Elsevier)

$$D_F = D_{max}/D_{hole} \tag{2.92}$$

D_{max} is the maximum diameter of the damage hole and D_{hole} the diameter of the hole in μm.

An experimental design of two factors (cutting speed and feed rate) and three levels was used. Cutting speed 'V' was varied from 30 to 50 m/min and feed rate 'f' was varied from 0.05 to 0.20 mm/rev. In order to obtain the models from experimental data, some regression analyses were carried out. Six models were developed for each dependent variable.

$$M_T = 0.1272 f^{0.3061} \tag{2.93}$$

$$M_{T-MAX} = 0.4611 f^{0.5551} \tag{2.94}$$

$$F_{\mathrm{F}} = 133.6 f^{0.6561} \tag{2.95}$$

$$F_{\mathrm{F-MAX}} = 252.8 f^{0.6620} \tag{2.96}$$

$$D_{\mathrm{F0}} = 1.193 f^{0.1429} V^{0.1022} \tag{2.97}$$

$$D_{\mathrm{F1}} = 0.9104 f^{0.01402} V^{0.04123} \tag{2.98}$$

M_{T} and $M_{\mathrm{T\text{-}MAX}}$ are the average cutting torque and maximum cutting torque, respectively. F_{F} and $F_{\mathrm{F\text{-}MAX}}$ are the average cutting force and maximum cutting force, respectively. D_{F0} and D_{F1} are the delamination factors at the entrance and exit, respectively.

The cutting parameters (cutting speed V, and the feed rate f) were used as decision variables in the optimization problem. Two different and mutually conflicting objectives were selected to be optimized. The first objective was the MRR, which can be computed by the following expression:

$$\mathrm{MRR} = 250\, VfD \tag{2.99}$$

MRR represents the productivity of the drilling process and is inversely proportional to the machining time.

The second optimization objective was the delamination factor, D_{F}.

$$D_{\mathrm{F}} = \max(D_{\mathrm{F0}}, D_{\mathrm{F1}}) \tag{2.100}$$

This objective describes the surface quality of the produced hole.

It is possible to note that the first objective must be maximized while the second one must be minimized. In order to homogenize all objectives, the MRR must be multiplied by -1. After this change, there were only minimization objectives in the problem.

There are some constraints that limit the search space in the considered optimization problem.

$$V_{\min} \leq V \leq V_{\max} \tag{2.101}$$

$$f_{\min} \leq f \leq f_{\max} \tag{2.102}$$

$$M_{\mathrm{T-MAX}} \leq [M_{\mathrm{T}}] \tag{2.103}$$

$$F_{\mathrm{F-MAX}} \leq [F_F] \tag{2.104}$$

$$P = 2\pi M_{\mathrm{T}} N/6 \times 10^4 \leq P_{\mathrm{MOT}} \eta \tag{2.105}$$

Where, $\mathrm{V_{max}}$ and $\mathrm{V_{min}}$ are the maximum and minimum allowed values of the cutting speed respectively, $\mathrm{f_{max}}$ and $\mathrm{f_{min}}$ are the maximum and minimum allowed values of the feed rate respectively, $[\mathrm{M_T}]$ and $[\mathrm{F_F}]$ are the allowed values of the cutting torque and cutting force respectively given by the technical features of the machine tool, P is the cutting power, $\mathrm{P_{MOT}}$ is the machine tool motor power, η is the efficiency of the transmission, and N is the spindle speed in rpm.

A micro-genetic algorithm was implemented to carry out the optimization of the process parameters. An a posteriori approach was used to obtain a set of optimal solutions. Finally, the obtained outcomes were arranged in graphical form (Pareto's front) and analyzed to make the proper decision for different process preferences.

Onwubolu and Kumar [217] presented a mathematical model for correlating the interactions of some drilling control parameters such as speed, feed rate and drill diameter and their effects on some responses such as axial force and torque acting on the cutting tool during drilling by means of RSM. For this exercise, a three-level full factorial design was chosen for experimentation using a PC-based computer numerically controlled drilling machine built in-house. The significance of the mathematical model developed was ascertained using Microsoft Excel® regression analysis module. The results obtained showed that the mathematical model was useful not only for predicting optimum process parameters for achieving the desired quality but for process optimization. Using the optimal combination of these parameters is useful in minimizing the axial force and torque of drilling operations; by extension, other drilling parameters such as cutting pressure, MRR, and power could be optimized since they depend on the combination of drilling parameters which affect the axial force and torque.

Kuar et al. [161] carried out experimental investigations into CNC pulsed Nd:YAG laser micro-drilling of zirconium oxide (ZrO_2). Influence of laser machining parameters on the heat affected zone (HAZ) thickness and phenomena of tapering of the machined micro-holes was experimentally investigated. RSM-based optimal parametric analysis was performed to determine the optimal setting of process parameters such as pulse frequency and pulse width, lamp current, assist air pressure for achieving minimum HAZ thickness and taper of the micro-hole machined by pulsed Nd:YAG laser. Minimum HAZ thickness was obtained as 0.0675 mm when the lamp current, pulse frequency, assisted air pressure and pulse width were set at optimal parametric setting i.e. 17 amp, 2.0 kHz, 2.0 kg/cm^2 and 2% of the duty cycle, respectively. Minimum taper was achieved as 0.0319 at optimal parametric setting i.e. the lamp current of 17 amp, pulse frequency of 2.0 kHz, assisted air pressure of 0.6 kg/cm^2 and pulse width of 2% of the duty cycle. Analysis was also carried out for multi-optimization of both the responses i.e. HAZ thickness and taper during pulsed Nd:YAG laser micro-drilling on ZrO_2.

Arul et al. [17] performed drilling experiments on a $(0/\pm 45/90)_{2s}$ 3-mm-thick glass fiber-reinforced laminate using 4-, 6- and 8-mm-diameter HSS drills. The machining response of the quasi-isotropic laminate was studied by monitoring the thrust and torque. The performance of the HSS drills for different cutting conditions was studied by measuring the tool wear. Delamination due to drilling is a major concern in machining a composite laminate and was analyzed by using linear elastic fracture mechanics, classical plate bending theory, and the mechanics of composites. A mechanical model for evaluating the critical thrust at which delamination was initiated at different ply locations was used, and the critical thrust force at the onset of delamination was found to be 70 N. The work analyzed data on the thrust force, torque, and tool life by using a group method data

handling (GMDH) algorithm. An optimization algorithm using simulated annealing with a performance index was then applied to search for the optimal process parameters for delaminatien constrained drilling.

Onwubolu [211, 212] presented a mathematical model for correlating the interactions of some drilling control parameters such as speed, feed rate and drill diameter, and their effects on some responses such as axial force and torque acting on the cutting tool during drilling by means of RSM. For this exercise, a three-level full factorial design was chosen for experimentation using a computer-based computer numerically controlled drilling machine built in-house. Second, since finding the optimum set of experimental factors that produces maximum or minimum value of response(s), is a major step in RSM, the author had described a new approach which was the optimization of the mathematical model realized from the RSM using one of the recent optimization techniques, Tribes. Comparing the optimization results for another published response problem between Gauss-Jordan algorithm and Tribes approaches, it was found that Tribes clocked a better result. Consequently, the author had reported the use of RSM for analyzing the cause and effect of process parameters on responses, but also on optimization of the process parameters themselves in order to realize optimal responses.

Sheng and Tomizuka [266] developed an intelligent control system using neural network and fuzzy logic to control thrust force in drilling process. Drill head position information is included in neural network model and fuzzy logic was used to deal with gain variation due to drill wear. The proposed model was compared with simulation and experimental results. It was found that the method worked well over a wide operating range.

Ghaiebi and Solimanpur [102] dealt with the optimization of hole-making operations in conditions where a hole may need several tools to get completed. The objective was to minimize the summation of tool airtime and tool switch time. This objective was affected by the sequence through which each operation of each hole was done. The problem was formulated as a 0–1 non-linear mathematical model. An ant algorithm was developed to solve the proposed mathematical model. An illustrative example showed the application of the algorithm to optimize the sequence of hole-making operations in a typical industrial part. The performance of the proposed algorithm was tested through solving six benchmark problems. The author's assumption was that a hole is made in multiple passes each of which need a particular tool and the machining process can be started from any point.

Mohan et al. [194] conducted a series of experiments using TRIAC VMC CNC machining center to machine the composite laminate specimens at various cutting parameters and material parameters. The measured results of delamination at the entry and exit side of the specimen were measured and analyzed using commercial statistical software MINITAB 14. The experimental results indicated that the specimen thickness, feed rate and cutting speed are reckoned to be the most significant factors contributing to the delamination. A S/N ratio was employed to analyze the influence of various parameters on peel up and push down delamination factor in drilling of glass fiber-reinforced plastic (GFRP) composite

laminates. The main objective of the study was to determine factors and combination of factors that influence the delamination using Taguchi and RSM and to achieve the optimization machining conditions that would result in minimum delamination. From the analysis it was evident that among the all significant parameters, specimen thickness and cutting speed had significant influence on peel up delamination and the specimen thickness and feed had more significant influence on push down delamination. Confirmation experiments were conducted to verify the predicted optimal parameters with the experimental results, good agreement between the predicted and experimental results obtained to be of the order of 99%. Garg et al. [101] compared BPNN with RBFN for prediction of flank wear in drilling process. Chip thickness was used as additional parameter to train the networks. From the results, the authors found that RBFN requires large number of training patterns and large network architecture to achieve same level of desired accuracy as the BPNN in machining copper and mild steel work piece with HSS drill bits.

Ghaiebi and Solimanpur [102] used an ant algorithm to minimize tool air-time and tool switching time in a multiple hole-making process employing several tools. The authors found that the proposed method is effective and efficient compared to traditional dynamic programming. Dvivedi and Kumar [79] investigated ultrasonic drilling of commercially pure titanium and titanium alloy (Ti-6Al-4v). During the experiments, process parameters such as work piece, grit size, slurry concentration, power rating and tools were changed to explore their effect on the surface roughness. Taguchi's technique was applied to obtain an optimal setting of ultrasonic drilling process parameters. Average surface roughness (Ra) was measured by using the Optical Profiling System. Two-dimensional and three-dimensional contour plots were obtained from the profiling system to quantify and visualize the surface roughness. From the experimental results and further analysis, it was concluded that the effect of slurry concentration and grit size had a significant effect on surface roughness more than other parameters.

Kurt et al. [162] reported application of Taguchi methods to optimize surface finish and hole diameter accuracy in the dry drilling of Al 2024 alloy. The parameters of hole quality were analyzed under varying cutting speeds (30, 45, and 60 m/min), feed rates (0.15, 0.20, and 0.25 mm/rev), depths of drilling (15 and 25 mm), and different drilling tools (uncoated and TiN- and TiAlN-coated) with a 118° point angle. This study included dry drilling with HSS twist drills. The settings of the drilling parameters were determined by using Taguchi's experimental design method. Orthogonal arrays of Taguchi, the S/N ratio, the ANOVA, and regression analyses were employed to find the optimal levels and to analyze the effect of the drilling parameters on surface finish and hole diameter accuracy values.

Arul et al. [18] employed acoustic emission (AE) sensing for on-line detection of workpiece status and to improve the process stability and workpiece quality by minimizing associated defects. Drilling trials were conducted on woven glass fabric/epoxy with high-speed steel (HSS) drills to determine the relationship between AE rms and cutting parameters. The variation of AE rms and power were

in close correlation to the flank wear and hole shrinkage. The experimental results showed that AE was very sensitive to the response of the drilling environment. Gaitonde et al. [94] presented the application of the Taguchi optimization method for simultaneous minimization of burr height and burr thickness influenced by cutting conditions and drill geometry. The Taguchi design approach to the multi-objective optimization problem was based on the introduction of a new concept of fitness function for each trial of orthogonal array. The fitness function was derived through mapping the objective functions of the drill optimization problem. Optimal values of cutting speed, feed, point angle and lip clearance angle were determined for selected drill diameter values to minimize burr height and burr thickness during drilling of AISI 316L stainless steel workpieces.

Chang et al. [50] considered a scheduling problem for drilling operation in a real-world printed circuit board factory. Two derivatives of multi-objective genetic algorithms were proposed under two objectives, i.e. makespan and total tardiness time. The algorithms possessed a rare characteristic from traditional multi-objective genetic algorithms. The crossover and mutation rates of the proposed algorithms can be variables or adjusted according to the searching performance while the rates of traditional algorithm are fixed. Production data retrieved from the shop floor were used as the test instances. The numerical results indicated that both the proposed multi-objective genetic algorithms performed satisfactorily and the adaptive multi-objective genetic algorithm performs better. Abrão et al. [2] presented a literature survey on the machining of composite materials, more specifically on drilling of GFRP and CFRP. Aspects such as tool materials and geometry, machining parameters and their influence on the thrust force and torque were investigated. Additionally, the quality of the holes produced was also assessed, with special attention paid to the delamination damage. The results indicated that despite the fact that some aspects, such as the effect of cutting parameters and tool geometry on the quality of the hole had been extensively studied over the last years, the phenomena associated to shearing of polymeric composite materials require additional studies in order to allow a better understanding of the behavior of this category of materials when subjected to cutting.

Tsao [292] investigated the thrust force and surface roughness of core drill with drill parameters (grit size of diamond, thickness, feed rate and spindle speed) in drilling CFRP laminates. A L_{27} (3^{13}) orthogonal array and S/N were employed to analyze the effect of drill parameters. Using Taguchi method for design of a robust experiment, the interactions among factors were also investigated. The experimental results indicated that thickness and feed rate were recognized to make the most significant contribution to the overall performance. The correlation was obtained by multi-variable non-linear regression and compared with the experimental results. The confirmation tests demonstrated a feasible and an effective method for the evaluation of drilling-induced thrust force and surface roughness (errors within 10%) in drilling of composite material.

Choi et al. [62] used neural network to predict incipient stage of drill failure so as to prevent any damage in the drilling process. Time and frequency domains of feed motor current were taken as input parameters and drill wear state, viz.,

0.1 mm for normal state and 0.9 mm for drill failure state, as output parameters of the neural network. The authors found that the proposed algorithm predicted the drill breakage accurately for different cutting conditions and machine tool types. Basavarajappa et al. [32] discussed the influence of cutting parameters on drilling characteristics of hybrid metal matrix composites (MMCs)—Al2219/15SiCp and Al2219/15SiCp–3Gr. The composites were fabricated using stir casting method. The Taguchi DoE and ANOVA were employed to analyze the drilling characteristics of these composites. The experiments were conducted to study the effect of spindle speed and feed rate on feed force, surface finish and burr height using solid carbide multifacet drills of 5 mm diameter. The results revealed that the dependent variables were greatly influenced by the feed rate rather than the speed for both the composites. The ceramic–graphite reinforced composite has better machinibility than those reinforced with SiCp composites.

Tsao and Hocheng [294] presented the prediction and evaluation of thrust force and surface roughness in drilling of composite material using candle stick drill. The approach was based on Taguchi method and the ANN. The experimental results indicated that the feed rate and the drill diameter are the most significant factors affecting the thrust force, while the feed rate and spindle speed contributing most to the surface roughness. In this study, the objective was to establish a correlation between the feed rate, spindle speed and drill diameter with the induced thrust force and surface roughness in drilling composite laminate. The correlations were obtained by multi-variable regression analysis and radial basis function network (RBFN) and compared with the experimental results. The results indicated that the RBFN is more effective than multi-variable regression analysis.

Zhu and Zhang [329] presented a new approach to solve the drilling path optimization problem belonging to discrete space, based on the PSO algorithm. Since the standard PSO algorithm is not guaranteed to be global convergent or local convergent, based on the mathematical model, the algorithm was improved by adopting the method to generate the stop evolution particle once again to obtain the ability of convergence on the global optimization solution. Also, the operators were proposed by establishing the Order Exchange Unit (OEU) and the Order Exchange List (OEL) to satisfy the need of integer coding in drilling path optimization. The experimentations indicated that the improved algorithm has the characteristics of easy realization, fast convergence speed, and better global convergence capability. The new PSO can play a role in solving the problem of drilling path optimization.

Among the scientific problems in drilling, determining thrust forces for any drill geometry and any work material remains an issue. This question is especially critical in the context of the self-vibratory drilling (SVD) technology, since thrust force governs the trajectory of cutting lips. In order to predict the dynamical behavior of the self-vibratory drilling head (SVDH), Guibert et al. [110] developed a numerical simulator to predict the relevant behavior of the SVD operations. The authors had proposed to divide cutting edges into several parts in order to define the local contribution of this part to the macroscopic thrust force. Local models were identified during the penetration of the drill.

Nandi and Davim [202] studied drilling performances with minimum quantity lubricant (MQL). Fuzzy logic rules were used to develop fuzzy rule-based model (FRBM). The performance of FRBM depends on two different aspects: structures of fuzzy rules and the associated fuzzy sets (membership function distributions, MFDs). The authors had investigated the performances of FRBMs based on Mamdani and TSK-types of fuzzy logic rules with different shapes of MFDs for prediction and performance analysis of machining with MQL in drilling of aluminum alloy. A comparison of the model predictions with experimental results and those published in the literature showed that FRBM with TSK-type fuzzy rules describes excellent trade-off with experimental measurements.

Lauderbaugh [167] presented a methodology to combine experimental, simulation, and statistical tools to reduce the time and cost of parameter studies. The statistical analysis was based on an experimentally verified simulation that predicts burr height, force, heat flux, and temperature at breakthrough. The analysis was based on parameters typical of 2024-T351 aluminum and 7075-T6 aluminum. Parameter interactions were also considered. The results were compared well to the experimental studies presented in the literature. Haber et al. [117] presented a strategy for the optimal tuning of a fuzzy controller in a networked control system using an off-line simulated annealing approach. The optimal tuning of the fuzzy controller using a maximum known delay was based on the integral time absolute error (ITAE) performance index. The goal was to obtain the optimal tuning parameters for the input scaling factors where the ITAE performance index was minimized. In this study, a step change in the force reference signal was considered as a disturbance, and the goal was to assess how well the system follows set-point changes using the ITAE criterion. In order to improve the efficiency of high-performance drilling processes while preserving tool life, the study focused on the design and implementation of an optimal fuzzy-control system for drilling force. Experimental tests of the drilling of two materials (GGG40 and 17-4 PH) corroborated the excellent transient response and the minimum overshoot predicted by the simulation results. The optimal fuzzy-control system reduced the influence of the increase in cutting force, eliminating the risk of rapid drill wear and catastrophic drill breakage.

Rawat and Attia [241] presented an experimental investigation of the wear mechanisms of tungsten carbide (WC) drills during dry high-speed drilling of quasi-isotropic woven graphite fiber epoxy composites. Tool wear was evaluated at spindle speeds of up to 15,000 rpm using a standard two flute drill. The authors had examined the non-linear behavior of this tribo-system and the interdependence of the wear process and cutting forces in relation to surface damage of the system components. It was found that chipping and abrasion were the main mechanisms controlling the deterioration of WC drill. The two friction regimes, the lightly and heavily loaded, were found to dictate the increase in forces, delamination of composite and surface roughness. The aggressive rubbing by fractured graphite fibers and WC grains against the soft epoxy matrix caused high temperature rise and consequently enhanced flank wear. During the primary and secondary wear stages, wear on the flank face of main cutting edges was found to be dominant,

while adhesion of carbon was found to occur along with abrasion in the tertiary zone. Tool life results revealed the increase in the delamination and surface roughness with transition from the primary to tertiary wear regime. The correlation between tool wear, delamination damage and surface roughness was established. Finally it was concluded that a tool replacement strategy could be devised by monitoring the cutting forces.

Audy [21] presented the results of a systematic computer-assisted study focused on determining, and describing, from a mathematical point of view, the relationship between the drill point geometrical features and the performance measures as assessed by the cutting forces and power in drilling. This was followed by a study of predicted influences of drilling variables on the generated thrust, torque and power. The results were presented for different types of modern commercial tool surface coatings and work-piece materials. It was suggested that this sort of information may be used, by both tool manufacturers and users, to assist in the optimization, and selection, of the drill point geometrical features for 'best' performance. Panda et al. [225] used two different types of ANN architectures viz. back-propagation neural network (BPNN) and radial basis function network (RBFN) in an attempt to predict flank wear in drills. Flank wear in drill depends upon speed, feed rate, drill diameter and hence these parameters along with other derived parameters such as thrust force, torque and vibration were used to predict flank wear using ANN. Effect of using increasing number of sensors in the efficacy of predicting drill wear by using ANN was studied. It was observed that inclusion of vibration signal along with thrust force and torque leads to better prediction of drill wear. The results obtained from the two different ANN architectures were compared and some useful conclusions were derived.

Karnik et al. [140] focused on the analysis of delamination behavior as a function of drilling process parameters at the entrance of the CFRP plates. The delamination analysis in high-speed drilling was performed by developing an ANN model with spindle speed, feed rate and point angle as the affecting parameters. A multilayer feed-forward ANN architecture, trained using error back-propagation training algorithm (EBPTA) was employed for this purpose. Drilling experiments were conducted as per full factorial design using cemented carbide (grade K20) twist drills. The ANN model so developed was validated by presenting training and new testing input patterns. The validated ANN model was then used to generate the direct and interaction effect plots to analyze the delamination behavior. The simulation results illustrated the effectiveness of the ANN models to analyze the effects of drilling process parameters on delamination factor. The analysis also demonstrated the advantage of employing higher speed in controlling the delamination during drilling.

Zolgharni et al. [331] demonstrated enhancements of performance and energy efficiency of cutting tools by deposition of diamond-like carbon (DLC) coatings on machine parts. DLC was deposited on steel drill bits, using plasma-enhanced chemical vapor deposition (PECVD) with the acetylene precursor diluted with argon, to produce a surface with low friction and low wear rate. Drill bit performance in dry drilling of aluminum was quantified by analysis of power

consumption and swarf flow. Optimized deposition conditions produced drill bits with greatly enhanced performance over uncoated drill bits, showing a 25% reduction in swarf clogging, a 36% reduction in power consumption and a greater than five-fold increase in lifetime. Surface analysis with scanning electron microscopy showed that DLC-coated drills exhibit much lower aluminum build up on the trailing shank of the drill, enhancing the anti-adhering properties of the drill and reducing heat generation during operation, resulting in the observed improvements in efficiency.

Gaitonde et al. [95] presented the methodology of Taguchi optimization method for simultaneous minimization of delamination factor at entry and exit of the holes in drilling of SUPERPAN DÉCOR (melamine coating layer) medium density fiberboard (MDF) panel. The delamination in drilling of MDF affects the aesthetical aspect of the final product and hence it is essential to select the best combination values of the drilling process parameters to minimize it. The utility concept was employed for the multi-performance characteristics optimization using Taguchi design. The experiments were carried out as per L_9 orthogonal array with each experiment performed under different conditions of feed rate and cutting speed. The ANOM was performed to determine the optimal levels of the parameters and the ANOVA was employed to identify the level of importance of the machining parameters on delamination factor. The investigations revealed that the delamination can be effectively reduced in drilling of MDF materials by employing the higher cutting speed and lower feed rate values.

In their another work, Gaitonde et al. [96] presented the application of Taguchi optimization method for simultaneous minimization of burr height and burr thickness influenced by cutting conditions and drill geometry. Optimal values of cutting speed, feed, point angle and lip clearance angle were determined for selected drill diameter values to minimize burr height and burr thickness during drilling of AISI 316L stainless steel workpieces. The effectiveness of the proposed approach was demonstrated through simulation results and experimental verifications. In another work, Gaitonde et al. [97] investigated the application of genetic algorithm (GA) for burr size minimization in drilling of AISI 316L stainless steel using HSS twist drills. Experiments were planned as per central composite rotatable DoE. The second order mathematical models for burr height and burr thickness were developed using RSM with cutting speed, feed, drill diameter, point angle and lip clearance angle as affecting parameters. The developed RSM models were then employed with GA to determine the optimal process parameters for a given drill diameter that results in minimum burr height and thickness. The simulation results revealed that point angle and cutting speed have significant effects in minimizing burr size.

Gaitonde et al. [98] presented the effects of process parameters on delamination during high-speed drilling of CFRP composites. The drilling experiments using cemented carbide (K20) twist drills were performed based on full factorial DoE with three levels defined for each of the process parameters. The computed values of delamination factor were empirically related to process parameters by developing a second order non-linear regression model based on RSM. The effects of

cutting speed, feed rate and point angle on delamination factor were analyzed using the models by generating response surface plots. The investigations revealed that the delamination tendency decreases with increase in cutting speed. The study also suggested low values of feed rate and point angle combination for reducing the damage. The details of model development and model adequacy test by ANOVA were presented by the authors.

Gaitonde et al. [99] attempted to predict and minimize the delamination in drilling of MDF. The experiments were carried out on LAMIPAN PB panel based on orthogonal array with feed rate and cutting speed as process parameters. The second order delamination factor models at entry and exit of the holes were developed using RSM. The parametric analysis was carried out to study the interaction effects of the machining parameters. Taguchi's quality loss function approach was employed to simultaneously minimize the delamination factor at entry and exit of the holes. From the ANOM and ANOVA, the optimal combination level and the significant parameters on delamination factor were obtained. The optimization results showed that the combination of low feed rate with high cutting speed was necessary to minimize delamination in drilling of MDF.

Haq et al. [118] presented a new approach for the optimization of drilling parameters on drilling Al/SiC metal matrix composite with multiple responses based on orthogonal array with grey relational analysis. Experiments were conducted on LM25-based aluminum alloy reinforced with green-bonded silicon carbide of size 25 μm (10% volume fraction). Drilling tests were carried out using TiN-coated HSS twist drills of 10 mm diameter under dry condition. In this study, drilling parameters namely cutting speed, feed and point angle were optimized with the considerations of multi responses such as surface roughness, cutting force and torque. A grey relational grade was obtained from the grey analysis. Based on the grey relational grade, optimum levels of parameters were identified and significant contribution of parameters was determined by ANOVA. Experimental results had shown that the responses in drilling process can be improved effectively through the new approach.

Singh et al. [276] made an attempt to investigate statistically the relative significance of the drilling parameters on the thrust force and torque. The results of ANOVA were then used to make assumptions for developing a Finite Element model for predicting drilling-induced damage. The FE results were found in good agreement with the experimental results.

Messaoud and Weihs [192] used non-linear time series modeling to setup an on-line modeling approach of the time varying dynamics of the process. An on-line monitoring strategy, based on control charts, was formed to detect chatter vibration. The results showed that the modeling approach provides an on-line procedure that can answer questions about the time varying dynamics of the process. The on-line monitoring strategy can detect the start of the transition from stable drilling to chatter vibration and some alarm signals are related to changing physical conditions of the process. Zhang and Chen [325] presented a study where the Taguchi Design was applied to optimize the surface quality in a CNC drilling operation. The control factors included feed rate, spindle speed, peck rate, and tool type while

the noise factors simulated were shop vibration and the presence or absence of magnetism in the workpiece material. Through statistical analysis of response variables and S/N ratios, the determined significant factors were the spindle speed, tool type, and peck rate, and the optimal combination of cutting parameters were selected. Confirmation tests verified that the selected optimal combination through Taguchi Design were able to achieve desired surface roughness.

Jadoun et al. [133] presented a study of the effect of process parameters on production accuracy obtained through ultrasonic drilling of holes in alumina-based ceramics using silicon carbide abrasive. Production accuracy in ultrasonic drilling involves both dimensional accuracy (hole oversize) and form accuracy (out-of-roundness and conicity). The parameters considered were workpiece material, tool material, grit size of the abrasive, power rating and slurry concentration. Taguchi's optimization approach was used to obtain the optimal parameters. The significant parameters were also identified and their effect on oversize, out-of-roundness and conicity were studied. Johansen and Lund [138] studied the problem of maximizing the safety against failure of a fully three dimensional laminated composite structure. The geometrically linear formulation of an eight node equivalent single layer solid shell finite element which utilizes fully three dimensional linear elastic orthotropic material properties was presented. Sensitivity analysis with respect to localized failure criteria functions was performed through use of semi-analytically calculated design sensitivities derived by the direct differentiation approach. Models were hierarchically refined in a two stage procedure, where a coarse mesh model was refined through the laminate thickness to obtain fully three dimensional descriptions of the detailed stress–strain state in localized zones of interest, making it possible to take into account in-plane and transverse delamination failure effects.

Prakash et al. [230] presented the systematic experimental investigation, analysis and optimization of delamination factor in drilling of medium-density fiberboards (MDF). Experiments were conducted on CNC drilling machine at various cutting conditions. The parameters considered for the experiments were cutting speed, feed rate and drill diameter. An empirical model was developed for predicting the delamination factor at entry and exit of the holes in drilling of MDF boards. Desirability function-based approach was employed for the optimization of drilling parameters for minimizing the delamination factor at entry and exit in drilling of MDF boards. The influences of different parameters and their interactions are studied in detail and presented.

Kilickap [147] investigated the influence of the cutting parameters, such as cutting speed and feed rate, and point angle on delamination produced when drilling a GFRP composite. The damage generated associated with drilling GFRP composites was observed, both at the entrance and the exit during the drilling. Hence it was essential to obtain optimum cutting parameters minimizing delamination during drilling of GFRP composites. The author had presented the application of Taguchi method and ANOVA for minimization of delamination influenced by drilling parameters and drill point angle. The optimum drilling parameter combination was obtained by using the analysis of S/N ratio. The conclusion revealed that feed rate and cutting speed were the most influential

factors on the delamination. The best results of the delamination were obtained at lower cutting speeds and feed rates. In another work, Kilickap [148] presented the use of Taguchi and RSM for minimizing the burr height and the surface roughness in drilling Al-7075. The Taguchi method was used to find optimal cutting parameters. The author had investigated the influence of cutting parameters, such as cutting speed and feed rate, and point angle on burr height and surface roughness produced when drilling Al-7075. A plan of experiments, based on L_{27} Taguchi design method, was performed drilling with cutting parameters in Al-7075. All tests were conducted without coolant at cutting speeds of 4, 12, and 20 m/min and feed rates of 0.1, 0.2, and 0.3 mm/rev and point angle of 90°, 118°, and 135°. The orthogonal array, S/N ratio, and ANOVA were employed to investigate the optimal drilling parameters of Al-7075. From the ANOM and ANOVA, the optimal combination levels and the significant drilling parameters on burr height and surface roughness were obtained. The optimization results showed that the combination of low cutting speed, low feed rate, and high point angle is necessary to minimize burr height. The best results of the surface roughness were obtained at lower cutting speed and feed rates while at higher point angle.

Chandrasekaran et al. [49] reviewed the application of soft computing tools to four machining processes—turning, milling, drilling and grinding. The authors had highlighted the progress made and discussed the issues that need to be addressed. Iliescu et al. [130] presented the prediction and evaluation of thrust force in drilling of carbon composite material. In order to extend tool life and improve quality of hole drilling, a better understanding of uncoated and coated tool behaviors is required. The authors had described the development of a phenomenological model between the thrust force, the drilling parameters and the tool wear. The experimental results indicated that the feed rate, the cutting speed and the tool wear were the most significant factors affecting the thrust force. The model can be used for tool-wear monitoring.

Gómez et al. [105] studied a drilling process with different degrees of wear in the drill bit to find relationships between acoustic emission (AE) and torque measured during the drilling process, and also with the degree of wear of the tool. SAE 1040 steel samples were drilled, making holes with 5 mm diameter twist drill bits in continuous feed. The drill bits were modified with "artificial" (produced by spark-erosion) and "real" (obtained by regular mechanical use) failures such as different degrees of wear in the cutting edge and the outer corner. For every drilled hole, torque and AE were simultaneously measured and acquired. The correlation between the AE parameters and torque measured during the drilling process was studied. Torque was measured as a control parameter to follow the dynamic behavior of the drill bit. An alternative AE feature, called Mean Power (MP) showed a good correlation with torque when the moving average (MA) was computed. The AE mean power (MP) was related to different degrees of wear in drill bits. Clusters for the different levels of wear in a 2-D plot were obtained. In that plot the moving variance of the MP versus the moving average of the MP, for each case of wear, were represented. This application was aimed at repetitive

manufacturing operations, where many signals per second may be obtained with fixed parameters as shape, drill bit diameter, spindle speed, and feed.

2.6 Finishing Processes

Interest in the precision machining of engineering materials has increased greatly. To ensure reliable performance and prolonged service life of modern machinery, its components require to be manufactured not only with high dimensional and geometrical accuracy but also with high surface finish. The surface finish has a vital role in influencing functional characteristics like wear resistance, fatigue strength, corrosion resistance and power loss due to friction. Unfortunately, normal machining methods like turning, milling or even classical grinding can not meet this stringent requirement. Therefore, finishing processes like lapping, honing, polishing, and superfinishing are being employed to achieve and improve the functional properties in the machine component.

2.6.1 Lapping Process

Lapping is regarded as the oldest method of obtaining a fine finish. Lapping is basically an abrasive process in which loose abrasives function as cutting points finding momentary support from the laps. Material removal in lapping usually ranges from 0.003 to 0.03 mm but many reach 0.08–0.1 mm in certain cases. Cast iron is the mostly used lap material. However, soft steel, copper, brass, hardwood as well as hardened steel and glass are also used. The abrasives of lapping include Al_2O_3 and SiC (grain size 5–100 μm), Cr_2O_3 (grain size 1–2 μm), B_4C_3 (grain size 5–60 μm), and diamond (grain size 0.5–5 μm). Vehicle materials for lapping include machine oil, rape oil, and grease. Technical parameters affecting lapping processes are unit pressure, the grain size of abrasive, concentration of abrasive in the vehicle, and lapping speed. Lapping is performed either manually or by machine. Hand lapping is done with abrasive powder as lapping medium, whereas machine lapping is done either with abrasive powder or with bonded abrasive wheel. Figure 2.15 shows the scheme of lapping process.

Lapping, a typical finishing method, is generally used for the purpose of obtaining a high quality of surface, but, because it is a very slow process, it needs to be characterized and optimized. However, it is quite difficult to characterize and optimize the process by means of a theoretical model because it is a very complicated and random process, affected by numerous variables and factors of the process as well as those of the environment. Thus, experimental approaches are needed to analyze the process. The statistical design method makes the experimental analysis efficient, systematic and logical. Chen et al. [57] carried out a series of lapping experiments with a specially designed lapping machine.

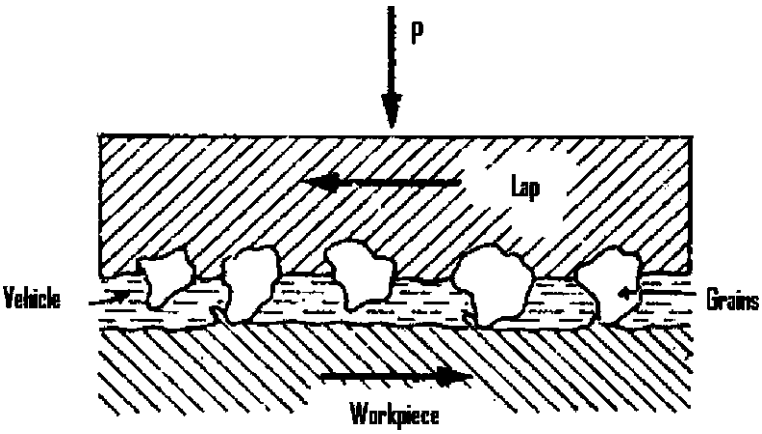

Fig. 2.15 Lapping process

Workpiece materials used in the experiments were representatives of advanced ceramics such as Si_3N_4, SiC, ZrO_2 and Al_2O_3. Influences of the lapping pressure as well as the relative speed on the material removal process were investigated. The role of the hardness of the lapping plate on the lapping process was studied. The results obtained through the study provided some useful information for improving the efficiency of ceramics lapping.

Kim and Choi [151] used the experimental design method to analyze the characteristics of the cylindrical lapping of fine-ceramics, Al_2O_3. An experimental apparatus was manufactured by the authors in the laboratory. The lapping wheel makes line-contact with the workpiece and has a traverse motion as well as a vibrational motion in the axial direction. The lapping pressure was applied to the workpiece by means of an air cylinder and was maintained at a constant value. Cylindrical fine-ceramic workpieces, Al_2O_3, of length 120 mm and diameter 70 mm were used. The initial surface roughnesses had somewhat different values, ranging from 1.5 to 1.6 μm according to the workpiece. Lapping compound was made by mixing diamond abrasive and kerosine. In this experiment, the aim was to obtain the effect of each variable on the response quantitatively and for this purpose only two levels for each variable being selected. Lapping pressure, A (0.5 and 1 kgf/cm^2); circumferential speed, B (11 and 22 m/min); vibrational frequency, C (5 and 10 Hz); grain size, D (5–10 μm and 20–30 μm); lapping time, E (10 and 20 min); and traverse speed, F (12.5 and 25 mm/min). High and low levels were represented as +1, and −1, respectively. The optimal variable combination for the improvement of surface roughness was found to be $A^+B^-C^+D^+E^+F^+$ which represents the simplest form of characterization for the process.

The amount of surface roughness improvement was chosen as a response variable, and surface roughnesses of ten points were measured for each experiment and averaged for use in the calculations. The process of the cylindrical lapping of fine-ceramics was characterized by computing the effects of each variable on the

response quantitatively in a screening experiment, the calculated effects determining which variables were significant or not. It appeared that three variables, i.e. lapping pressure, abrasive grain size and lapping time, had significant effects on the response. Each of these variables could be selected as a variable for RSM, but the authors had selected only two variables, lapping pressure and lapping time. Abrasive grain size was excluded because it did not have a continuous value. RSM was then applied for the significant variables to determine the critical point (or the) stationary point of lapping. The second order model for the surface roughness (Y) fitted by the least-squares method is as follows:

$$Y = 1.274 + 0.0043X_1 + 0.0124X_2 - 0.0245X_1^2 - 0.0021X_2^2 \qquad (2.106)$$

where X_1 and X_2 represent coded variables of lapping pressure and lapping time, respectively. As a result, the time for the maximum improvement of surface roughness under given lapping conditions as well as maximum improvement value were predicted by the fitted model.

In another work, Kim and Choi [152] performed the cylindrical lapping experiment using Taguchi's L_8 orthogonal array and analyzed by ANOVA table. As a result, effective variables and interaction effects were identified and discussed. Also the optimal variable combination to obtain the largest percentage improvement of surface roughness was selected and confirmatory experiments were performed. Wang et al. [309] developed a computer-controlled system for ultra-precision lapping of granite surface plates. The system can easily achieve a high lapping efficiency and high flatness accuracy due to its capability of on-line measurement of flatness, optimization of the lapping process, and automation of the lapping operation. The system was successfully applied to a number of granite surface plates, and the results showed that a flatness error of less than 2 μm over a 1 m × 2 m area was obtained. The authors also presented the principle of on-line measurement of flatness and experimental results based on the computer-controlled lapping system.

Guevarra et al. [109] presented a new approach in lapping process in making appropriate condition to improve the manufacturing operations for ball screw. After grinding, high precision ball screw was lapped by highly skilled operators. These operators have the ability to control and maintain the lapping conditions by sensing the lapping torque manually. Prior to lapping process, the effective diameter must be measured to find out the effective threaded profile along the screw shaft. The section which has a large effective diameter will be primarily lapped wherein the lapping torque is high. The authors had established a control scheme on the automatic lapping machine for high precision ball screw in both measuring and finishing process. A prototyped horizontal lapping machine with in-process torque monitoring system was designed, built, and tested. This was to determine the relationship among lapping torque, effective diameter, and error on travel to establish the measurement system to control the finishing operations efficiently and eventually improve and eliminate the various sorts of error components in a ball screw. The experimental results showed that the new lapping

method could adequately predict the effective diameter and error on travel by observing the lapping torque.

Micro-ultrasonic assisted lapping shows a high feasibility of generating microstructures with aspect ratios up to even larger than five in brittle materials. Through introducing several innovative strategies such as rotated tool, on-machine tool preparation, and vibration-applied workpiece, holes as small as 5 μm in diameter have been machined in quartz glass and silicon. Complex structures like spiral trenches have also been claimed true by use of the path-controlled scanning mode. But, the currently available knowledge on micro ultrasonic assisted lapping is still insufficient especially on tool wear, subsurface damage control, and relatively coarse surface roughness in the scanning mode. Further investigations in these aspects include the introduction of AE-based sensing and monitoring. Zhang et al. [327] reviewed some new advances in micro ultrasonic assisted lapping. The authors had opined that a success in this area of research would open up promising prospects for cost-effective manufacture of micro fluidics and their wear-resistant molds.

In general, to maximize the MRR in lapping operation, an optimum lapping pressure and abrasive concentration in the vehicle, and lapping time have to be chosen. With the increase in lapping pressure and MRR increases. However, MRR increases only up to certain value of lapping pressure and then decreases. Both MRR and surface roughness increase with the increase in abrasive grain size. The grain size corresponding to permissible surface roughness and maximum MRR may be different. Primary consideration is made on the permissible surface roughness in selecting abrasive grain size. Both MRR and surface roughness decrease with the increase in lapping time.

2.6.2 Honing Process

Honing is a finishing process, in which a tool called hone carries out a combined rotary and reciprocating motion while the workpiece does not perform any working motion. Most honing is done on internal cylindrical surface, such as automobile cylindrical walls. The honing stones are held against the workpiece with controlled light pressure. The honing head is not guided externally but, instead, floats in the hole, being guided by the work surface. In honing rotary and oscillatory motions are combined to produce a cross hatched lay pattern. The honing stones are given a complex motion so as to prevent every single grit from repeating its path over the work surface. The critical process parameters are, (1) rotation speed, (2) oscillation speed, (3) length and position of the stroke, and (4) honing stick pressure. With conventional abrasive honing stick, several strokes are necessary to obtain the desired finish on the work piece. However, with introduction of high-performance diamond and CBN grits it is now possible to perform the honing operation in just one complete stroke. Advent of precisely engineered microcrystalline CBN grit has enhanced the capability further. Honing

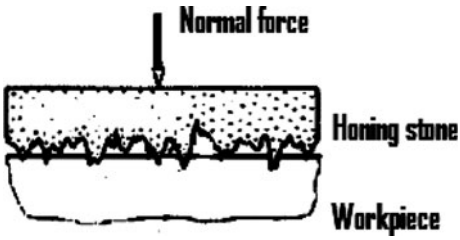

Fig. 2.16 Honing Process

stick with microcrystalline CBN grit can maintain sharp cutting condition with consistent results over long duration. Figure 2.16 shows the honing process.

The important parameters that affect MRR and surface roughness (R) are, (1) unit pressure, (2) peripheral honing speed, and (3) honing time. The unit pressure should be selected so as to get minimum surface roughness with highest possible MRR. An increase of peripheral honing speed leads to enhancement of MRR and decrease in surface roughness. With increase in honing time, MRR decreases. On the other hand, surface roughness decreases and after attaining a minimum value again rises. The selection of honing time depends very much on the permissible surface roughness.

Saljé and See [250] investigated the influence of honing stone topography on honing process. By variation of sharpening conditions, honing stone topography was adapted to the honing process so that a constant workpiece roughness was produced immediately after sharpening. Also correlations between normal force, tangential force, MRR and workplace roughness were investigated and different strategies for supervising and controlling the honing process were given. Another possibility for optimization was given by increasing the cutting speed.

Guo et al. [111] reported the optimization of the structure parameters by calculating the machining accuracy coefficient and wear coefficient of inside-triangle and outside-triangle radial structure honing wheels. With a design circulation program and analyzing the results data, it was obvious that suitable radial structure honing wheels were obtained to improve the machining accuracy in ultra-precision plane honing. Furthermore, the results were used for the derivation of the best pattern structure of the wheel with lesser honing wheel wear and high machining accuracy.

Providing an analytical model for an abrasive process such as honing is extremely difficult, if not impossible. The fact that using IS0 13565 will have to deal with five surface roughness parameters further complicates the modeling task. For decades, the arithmetic average (AA or R_a) and root sum of squares (RSS or R_q) have been the two major surface roughness measures to define a broad range of surfaces for a mechanical product. A number of drawbacks have been identified in recent years with the above measures. To map more scientifically and closely the surface roughness to the product functions and performances, ISO 13565 has defined a different set of measures, including R_k, R_{pk}, R_{vk}, M_{r1}, and M_{r2}. This has not only made process planning different and much more difficult, but also made

modeling of the relationship between these roughness measures and the machining parameters a multiple-input and multiple-output problem. While some companies are trying the traditional trial-and-error method to implement the ISO 13565 standard, Feng et al. [88] applied ANNs to develop an empirical model for the honing process of engine cylinder liners in order to help reduce emissions, improve oil efficiency, and prolong engine life. Threefold cross-validation was applied to develop the models. Hypothesis testing and the prediction error statistics were employed to select the best model. Data from industrial experiments based on fractional factorial design illustrated the goodness of the modeling approach and the models.

Feng et al. [89] proposed a rigorous procedure for evaluating the validation and data splitting methods in predictive regression modeling. Experimental data from a honing surface roughness study was used to illustrate the methodology. In particular, the individual versus average data splitting methods as well as the fivefold versus threefold cross-validation methods were compared. The authors had showed that statistical tests and prediction errors evaluation are important in subset selection and cross-validation of predictive regression models. No statistical differences were found between the fivefold and the threefold cross-validation methods, and between use of the individual and average data splitting methods in predictive regression modeling.

Electro chemical honing (ECH) is a hybrid electrolytic precision microfinishing technology that integrates physicochemical actions of the and conventional honing processes to provide controlled functional surface-generation and fast material removal capabilities in a single operation. Dubey [75] presented a Taguchi loss function-based hybrid strategy for the multi-performance optimization of electrochemical honing process. The proposed strategy utilizes a radial basis function neural network (RBFNN) for the process parametric mapping with the loss functions of ECH multi-performance characteristics determined through a Taguchi matrix robust experimental design. The network outputs were then unified using desirability function (DF) approach to provide an objective function to genetic algorithm (GA). Finally, GA predicts the optimal process parametric settings for multi-performance optimization of ECH. Simulated results confirmed the feasibility of the strategy and showed good close agreement with actual experimental results over a wide range of machining conditions employed in the process. In another work, Dubey [76] made a critical evaluation of Taguchi-RBFNN-DF-GA strategy and GA-tuned fuzzy Taguchi inference application, their prospective features, strengths and weaknesses for benefit of the user and research fraternity. The methodologies were demonstrated using a case study of multi-performance modeling and optimization control ECH, involving three performance criteria. Results indicated that all three techniques are well suited to the complex manufacturing processes that involve several correlated variables with vaguely defined parametric relationships like in ECH. It was also found that the predicted optimal results are sensitive to the way the factorial interactions are treated. The actual experimental results at the optimal parametric conditions predicted using the three approaches were quite close.

Dubey [77] presented a utility-based Taguchi loss function strategy for the multi-response optimization of ECH process. The approach utilized a composite utility function using the Taguchi loss functions of multiple ECH responses in selecting the optimal parametric settings such that the overall functional utility of the product was maximized. The use of the Taguchi loss functions ensured the process was robust against the random variations. Actual experiments confirmed the feasibility of the strategy over a wide range of machining conditions employed in ECH.

2.6.3 Superfinishing Process

Superfinishing is widely used as a subsequent operation after grinding to reduce surface roughness and increase bearing load capacity. During superfinishing of cylindrical surfaces, an axially oscillating abrasive stone is pressed against a rotating workpiece. The ratio of axial oscillation frequency to workpiece rotational frequency should be selected so as to avoid integer values, which result in low stock removal, and half values, which can lead to lobe formation. Finer grit stones provide smoother surface finishes but less stock removal; therefore, the grit size selected should be only fine enough to generate the required surface roughness. Varghese and Malkin [299] explored methods for enhancing superfinishing performance. Experiments conducted on hardened bearing steel indicated the existence of an optimal applied contact pressure where both the stock removal and the finishing ratio were maximum and the specific energy was minimum. Above the critical pressure, the stock removal was adversely affected by loading of debris on the stone surface. Applying ultrasonic vibrations normal to the surface was found to reduce loading by promoting stone wear. Further enhancement in superfinishing performance was achieved by providing axial grooves on the stone surface. The use of ultrasonic vibrations together with axially grooved stones increased the stock removal by as much as 65% while providing comparable surface roughness. In another work, Varghese and Malkin [300] presented the details of selection of optimal superfinishing conditions. Experimental results were presented that show the effect of contact pressure, process kinematics, and grit size on superfinishing behavior. An optimal contact pressure was found at which the removal rate was maximized.

Simulation of wear evolution during abrasive processes is a very difficult task compared to that of machining processes because of the degree of randomness of geometry and disposition of cutting teeth. Superfinishing is a specific case of abrasive process, where the temperature is not consistently involved. A wear model and a numerical method of simulating the process, involving data collected in a testing experiment that resulted in determining an abrasive function, were presented by Neagu-Ventzel et al. [206] for the specific case of the superfinishing the ball track of an inner bearing ring. Four types of stones were tested while abrading a cylindrical sample of M50 steel, using a high fluidity oil as a lubricant.

The abrasive function characteristic to the materials involved in the process was determined. The wear volume of stone, that resulted in simulation and superfinishing experiments, was compared for three of the stones, and a good agreement between them was obtained, endorsing the viability of the simulation. The stability of the results with mesh refinement was analyzed. Three other output parameters of the simulated process and their dependency on the stone type were discussed. This model of superfinishing wear and simulation of superfinishing process can be used in conjunction with a database resulted from a standardized testing wear experiment, for predicting the wear volume and distribution of tool and workpiece in superfinishing.

Chang et al. [51] described a systematic investigation of the effect of process parameters on evolution of superfinished surface texture. For a given stone, the surface roughness reaches a steady state value as the process proceeds, regardless of test conditions, in the rough finishing regime. An analysis of experimental surface roughness data indicated that this process characteristic can be well described by an exponential form of time dependence and the contact pressure has no effect on this time dependence. Optimal performance associated with higher MRR, fairly fine surface finish and less production time in rough superfinishing can be achieved using higher workpiece rotational speed and contact pressure.

Bigerelle et al. [37] introduced an engineering attempt to rigorously model a synchronizing functional surface (cone surface of idler gear) according to its finish specifications. The virtual input surface was generated by an original fractal function, which reproduces the surface "signature" due to the wheel grinding process. To model the subsequent superfinishing operation by belt finishing process, which uses a soft-coated belt as a tool, an algorithm simulating the abrasive polishing conditions was developed and applied to rework the initial fractal surface. The basic idea of this model was that the higher the height of a peak of the profile, the lower its probability of resistance during an abrasion cycle. The belt finishing process was modeled by five parameters: two parameters that characterize the initial surface (fractal dimension and range amplitude) and three parameters describing the abrasion polishing process (probability of resistance, wear volume and the number of abrasion cycles). A functional model with an optimization scheme was created. This simulation provides the morphology of the initial surface and how to cope with the superfinishing process to obtain the functionality of the surface. An elevated initial roughness was required from which slow erosion was proceeded to erode peaks and conserve some valleys of the initial profile (lubricant tanks). Finally, it was shown that automotive designers impose morphological specifications obtained by the belt grinding process to prevent scuffing of the motor parts. However, this methodology possesses some limitations: characterizing a functionality of surfaces with roughness parameters reduces irreversibly the information on surface and it is ambiguous to state that if a surface is characterized by these parameters then its functionality is reached. A way to minimize these artifacts is to characterize the surface with multi-scale measures, so the surface will possess the same characteristic at all the scales. Even in this case, it does not assume that other surfaces will not possess the same functionality: the

multi-scale characterization must be proceeded by taking into account the pertinent scale on which the morphology plays a major role on the functionality of the surface.

Jiang and Ge [136] described through centerless superfinishing as a final process in roller bearing manufacturing to the better performance of bearings. Applied loads, rotational speeds, reciprocating frequencies and amplitude of superfinishing stones are crucial parameters, which mainly influence the surface topography, and are difficult to be adjusted to achieve optimal superfinishing effect. A superfinishing model was established, which included cutting and motion models and then a simulation method was presented to form the topography on the condition of various combinations of the above three parameters. This work provides a useful means to select reasonable combination of superfinishing parameters for roller bearing buildings.

Brinksmeier et al. [43] presented a new grinding strategy for a surface superfinishing and a grind-strengthening of the surface layer of steels in a single grinding step. Grinding with the new process strategy leads to benefits because a grind-strengthened surface layer eliminates initial wear and abrasion within the system, reduces surface finish roughness, extends fatigue strength, and reduces risk of part failure during operation.

2.6.4 Ball-Burnishing Process

Ball burnishing, a plastic deformation process, is becoming more popular as a finishing process. The ball-burnishing process consists of pressing hardened steel rolls or balls into the surface of the workpiece and imparting a feed motion to the same. Ball burnishing of a cylindrical surface is illustrated in Fig. 2.17. Burnishing process has an influence on microstructure of the burnished components. The parameters affecting the surface finish are: burnishing force, feed, ball or roller material, number of passes, workpiece material, and lubrication.

Loh et al. [183] reported that, ball-burnishing parameters have an influence on surface hardness of the burnished component. These parameters also influence burnished surface wear resistance. Experimental work based on 3^4 factorial design was carried out on a vertical machining center to establish the effects of ball-burnishing parameters on the surface roughness of AISI 1045 specimens. Analyses of the results by the ANOVA technique and the F test showed that the ball material, the lubricant, the feed and the depth of penetration, have significant effects on the surface roughness. A pre-machined surface roughness of 4 μm could be finished to about 0.772 μm. In another work, Loh et al. [184] reported on the optimization of the surface finish produced by the ball-burnishing process, using the RSM technique. A second-order mathematical model correlating two predominant process parameters, viz, depth of penetration and feed, with the surface roughness parameter R_{tm} was obtained. The model can be used in selecting the optimum process parameters for obtaining a desired controlled surface finish. The

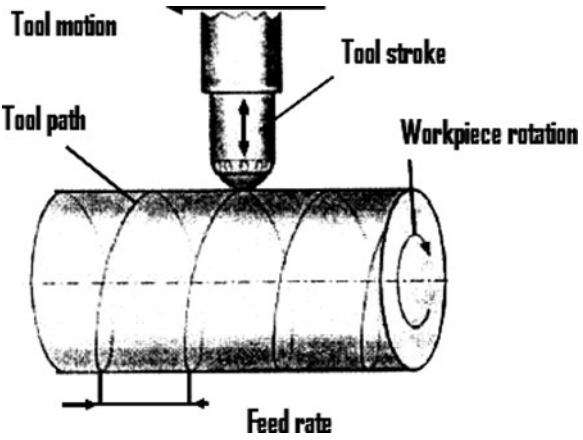

Fig. 2.17 Ball-burnishing process

optimum surface roughness predicted by the model was found to agree well with the results of experiment.

The effect of the process on specimens of different materials was studied by many authors. Lee et al. [170] reported that, the surface of 316L stainless steel was improved by ball-burnishing process. The surface finish of brass components also was improved by optimizing the number of ball passes with the burnishing force [122]. The process also increased the adhesive wear resistance of an electrically conductive polyester–carbon film [193]. Wear resistance and adhesive wear resistance of the brass components were also increased by burnishing processes [121].

El-Wahab and Abdelhay [85] developed a new algorithm for burnishing complex profiles on CNC machine centers using a newly designed burnishing tool. The selection of tool parameters was established to determine the burnishing ball size, spring stiffness and retaining rim height to satisfy an optimum performance. Experimental work and theoretical analysis were utilized for this purpose. A burnishing algorithm was developed to compute the geometrical path of the tool along a hemispherical contour shape, in order to ensure a uniform predetermined burnishing force and to prevent any geometrical interference. The developed algorithm introduced a new G-code function and new parameters to the tool data memory. A case study was presented to illustrate and support the usage of both the proposed tool design and new CNC algorithm.

To study the effect of burnishing process on the specimen's characteristics as well as to optimize the process parameters, models for the process are effective tools. Shiou and Chen [268] introduced the possible ball-burnishing surface finish process of a freeform surface plastic injection mold on a machining center. The design and manufacture of a burnishing tool was first accomplished in this study. The optimal plane ball-burnishing parameters were determined by utilizing the Taguchi's orthogonal array method for plastic injection molding steel PDS5 on a machining center. Four burnishing parameters, namely the ball material, burnishing speed, burnishing force, and feed, were selected as the experimental

factors of Taguchi's DoE to determine the optimal burnishing parameters, which have the dominant influence on surface roughness. The optimal burnishing parameters were found out after conducting the experiments of the Taguchi's L_{18} orthogonal table, ANOVA, and the full factorial experiment. The optimal plane burnishing parameters for the plastic injection mold steel PDS5 were the combination of the tungsten carbide ball, the burnishing speed of 200 mm/min, the burnishing force of 300 N, and the feed of 40 μm. The surface roughness R_a of the specimen could be improved from about 1–0.07 μm by using the optimal burnishing parameters for plane burnishing. Applying the optimal burnishing parameters for plane burnishing to freeform surface plastic injection mold, the surface roughness R_a of freeform surface region on the tested plastic injection part could be improved from about 0.842–0.187 μm, through a comparison between using the fine milled and using the ball-burnished mold cavity. de Lacalle et al. [71] studied the use of the ball-burnishing process to improve the final quality of Inconel 718 surfaces. This process changes the roughness and residual stresses of the previously end-milled surfaces, achieving the finishing requirements for engine components. Both the burnishing system and main parameters were taken into account, considering their influence on finishing. Workpiece surface integrity was ensured due to the compression effect of this surface enhancement process and its associated cold working. Results of different tested pieces were discussed in relation to the maximum and mean surface roughness achieved microstructure and surface hardness. Results of heat-treated low carbon mold steel P20 (32 HRC) were compared with those for the nickel alloy Inconel 718 (solution treated and age hardening, 40 HRC). The main conclusions were that using a large radial width of cut in the previous end-milling operation, together with a small radial width of cut during burnishing can produce acceptable final roughness and compression cold working is higher and deeper in the Inconel 718 than in the steel case.

Korzynski [157] proposed a model of burnishing using a spherical tool and studied the force–surface roughness relation. Shiou and Ciou [270] developed a vibration-assisted spherical polishing system driven by a piezoelectric actuator on a machining center to improve the burnished surface roughness of hardened STAVAX plastic mold stainless steel and to reduce the volumetric wear of the polishing ball. The optimal plane surface ball-burnishing and vibration-assisted spherical polishing parameters of the specimens were determined after conducting the Taguchi's L_9 and L_{18} matrix experiments, respectively. The surface roughness $R_a = 0.10$ μm, on average, of the burnished specimens could be improved to $R_a = 0.036$ μm ($R_{max} = 0.380$ μm) using the optimal plane surface vibration-assisted spherical polishing process. The improvement of volumetric wear of the polishing ball was about 72% using the vibration-assisted polishing process compared with the non-vibrated polishing process. A simplified kinetic model of the vibration-assisted spherical polishing system for the burnished surface profile was also derived by the authors. Applying the optimal plane surface ball-burnishing and vibrated spherical polishing parameters sequentially to a fine-milled freeform surface carrier of an F-theta scan lens, the surface roughness of

$R_a = 0.045$ μm, on average, within the measuring range of 149 μm × 112 μm on the freeform surface, was obtainable.

Rao et al. [239] carried out experimental work based on 3^4 factorial design to establish the effects of ball-burnishing parameters on the surface hardness of high-strength low alloy steels (HSLA) dual-phase (DP) steel specimens. Statistical analysis of the results showed that the speed, feed, lubricant and ball diameter have significant effect on surface hardness. In another work, Rao et al. [240] carried out experimentation to establish the effect of burnishing parameters viz., feed rate, speed, force, ball diameter and lubricant on surface hardness, and wear resistance of HSLA dual-phase steel specimens. The result indicated that burnishing parameters have significant effect on the surface hardness and wear resistance.

El-Tayeb et al. [84] designed and fabricated simple and inexpensive burnishing tools, with interchangeable adapter for ball and roller. Then, ball-burnishing processes were carried out on aluminum 6061 under different parameters and different burnishing orientations to investigate the role of burnishing speed, burnishing force and burnishing tool dimension on the surface qualities and tribological properties. The results showed that burnishing speed of 330 rpm and burnishing force of 160 N produce optimum results. Meanwhile, a decrease in the burnishing ball diameter led to a considerable improvement in the surface roughness up to 75%. On the other hand, parallel burnishing orientation exhibited lower friction coefficient compared to cross-burnishing orientation. Furthermore, ball-burnishing process was capable of improving friction coefficient by 48% reduction and weight loss by 60-80% reduction of burnished surface of Aluminum 6061.

Shiou and Hsu [271] aimed to improve surface roughness of the hardened and tempered STAVAX plastic mold stainless steel using the ball grinding, ball-burnishing and ball-polishing surface finish processes on a machining center. The flat surface optimal ball-burnishing and spherical polishing parameters were determined after conducting the Taguchi's L_9 and L_{18} matrix experiments, ANOVA, and the full factorial experiment, respectively. The surface roughness of the ground test specimens could be improved from about $R_a = 0.5167$–0.123 μm on average by using the optimal flat surface ball-burnishing parameters. The surface roughness of the burnished specimens could be further improved to $R_a = 20$ nm (nm) by using the spherical polishing process with determined optimal parameters. By using the finest available commercial grain size of the abrasive material aluminum oxide (Al_2O_3, WA) as 1 μm in diameter (grid no. 10,000), the mean surface roughness value of $R_a = 16.7$ nm on average was possible. The determined flat surface optimal burnishing and polishing parameters were then applied sequentially to the freeform surface test object of a F-theta scan lens, to improve the surface roughness. The surface roughness value R_a of freeform surface region on the STAVAX tested part, which was hardened and tempered (HRC = 50), could be improved sequentially from about 1.83 to 0.035 μm on average.

Shiou and Cheng [269] applied the sequential ball-burnishing and ball-polishing processes successfully to the ultra-precision surface finish of the NAK80 mold tool steel on a CNC machining center. The optimal flat surface polishing

parameters of the developed system for the NAK80 mold tool steel were determined by conducting the experiments of the Taguchi's L_{18} orthogonal table, ANOVA, and the full factorial experiments. The burnished surface roughness of the test specimens could be improved from about R_a 0.06 μm to 0.016 μm in average using the determined optimal polishing parameters. Applying the optimal flat surface ball-burnishing and ball-polishing parameters sequentially to a fine-milled spherical lens mold cavity of NAK80 mold tool steel, the surface roughness R_a of the surface on the tested parts could be improved sequentially from about 1.0 μm in average to 0.020 μm in average.

Laouar et al. [166] focused on the application of burnishing treatment (ball burnishing) on XC48 steel and parameters optimization of treatment regime. Three important parameters were considered: burnishing force, burnishing feed, and ball radius. An empirical model was developed to illustrate the relationship between these parameters and superficial layer characteristics defined by surface roughness and superficial hardness. A program was developed in order to determine the optimum treatment regimes for each characteristic. Ibrahim et al. [129] dealt with the control of ball-burnishing parameters of steel components via fuzzy logic. The burnishing tool using three balls was designed and constructed in such a way as to replace the three original adjustable jaws of the center rest. The center rest and the lathe saddle were clamped together to operate as one piece. Experimental work was conducted on a lathe to study the effect of burnishing parameters (feed, speed, force, and number of balls used in single pass) on surface characteristics (surface roundness error). Experimental results from the work were used as a knowledge base to prepare a fuzzy logic model to control burnishing parameters. The results obtained from the experimental work and fuzzy model showed that good surface characteristics can be achieved by using this center rest ball-burnishing tool. Burnishing force, burnishing feed and number of balls in single pass are the most important parameters that play an important role in controlling the values of all surface characteristics. The results obtained from the fuzzy model were highly consistent with experimental results.

Basak and Goktas [30] burnished an Aluminum alloy (Al 7075 T6) using different burnishing parameters (number of revolution, feed, number of passes, and pressure force) with burnishing apparatus. Burnishing parameters which affect to surface roughness and surface hardness on Al 7075 T6 materials were discussed. Using the experimental results a fuzzy logic model was used to achieve the best parameters for the burnishing process. The fuzzy model predictions suggested that the most suitable values for surface roughness were the pressure force of 200 N, and a feed of 0.1 mm/rev with two tool passes. These results, which obtained from the fuzzy model, were highly consistent with the experiments.

Pa [221] discussed the performance assessment of the continuous burnishing processes following electrochemical finishing using a design, which incorporates a finish-tool that includes an electrode and a nonconductive burnishing tool. It was expected to spread a freeform surface finish instead of the conventional hand or machine polishing. In the experiment, a model toy missile was taken as a work-piece. The electrode was used with the continuous and pulsed direct current

application. The burnishing tool used ceramic material and was connected with the electrode and axial feed. It was found that the finished effect of the finish-tool with convex features was better than mat of the concave features. Pulsing direct current could slightly improve the effect of electrochemical finishing. This presents an effective and low-cost finishing process that includes the design of a finish-tool, which uses burnishing assistance, and follows electrochemical finishing after traditional machining makes the freeform surface of a workpiece smooth and bright.

El-Taweel and El-Axir [83] studied the analysis and optimization of the ball-burnishing process. The Taguchi technique was employed to identify the effect of burnishing parameters, i.e., burnishing speed burnishing feed, burnishing force and number of passes, on surface roughness, surface micro-hardness, improvement ratio of surface roughness, and improvement ratio of surface micro-hardness. Taguchi tools such as ANOVA, S/N ratio and additive model were used to analyze, obtain the significant parameters and evaluate the optimum combination levels of ball-burnishing process parameters. The analysis of results showed that the burnishing force with a contribution percent of 39.87% for surface roughness and 42.85% for surface micro-hardness had the dominant effect on both surface roughness and micro-hardness followed by burnishing feed, burnishing speed and then by the number of passes.

Korzynski and Pacana [158] presented the results of examining the centerless roller burnishing technology worked out by them. The structure and the construction details of a prototype device for the centerless burnishing of shafts were presented. The experiments were carried on using 41Cr4 steel workpieces. The effects of the workpiece hardness, the surface roughness before burnishing, the deformation multiplicity and the tool interference on the roughness and the geometric structure after burnishing were investigated. The significant influence of the above parameters was confirmed and described as a mathematical power model. It also showed a beneficial effect of centerless burnishing parameters on roughness and geometric structure of the surface.

References

1. Abburi NR, Dixit US (2006) A knowledge-based system for the prediction of surface roughness in turning process. Robot Comput Integr Manuf 22(4):363–372
2. Abrão AM, Faria PE, Rubio JC, Reis P, Davim JP (2007) Drilling of fiber reinforced plastics: a review. J Mater Process Technol 186(1–3):1–7
3. Abu-Mahfouz I (2003) Drilling wear detection and classification using vibration signals and artificial neural network. Int J Mach Tools Manuf 43:707–720
4. Agapiou JS (1992a) The optimization of machining operations based on a combined criterion-Part 2 Multi-pass operations. J Eng Ind 114:508–513
5. Agapiou JS (1992b) An optimization of multi-stage machining system, part I: Mathematical solution part 2: The algorithm and application. J Eng Ind 114:524–538
6. Agapiou JS (1992c) The optimization of machining operation based on a combined criterion, part I: The use of combined objectives in single-pass operations. J Eng Ind 114:500–507

7. Aggarwal A, Singh H, Kumar P, Singh M (2008) Optimization of multiple quality characteristics for CNC turning under cryogenic cutting environment using desirability function. J Mater Process Technol 205(1–3):42–50
8. Ahearne E, Byrne G (2008) Simulation of the local kinematics in rotational grinding. CIRP Ann Manuf Technol 57(1):333–336
9. Alagumurthi N, Palaniradja K, Soundararajan V (2006) Optimization of grinding process through design of experiment (DOE): a comparative study. Mater Manuf Process 21(1):19–21
10. Al-Ahmari AMA (2007) Predictive machinability models for a selected hard material in turning operations. J Mater Process Technol 190(1–3):305–311
11. Al-Aomar R, Al-Okaily A (2006) A GA-based parameter design for single machine turning process with high-volume production. Comput Ind Eng 50(3):317–337
12. Ali YM, Zhang LC (2004) A fuzzy model for predicting burns in surface grinding of steel. Int J Mach Tools Manuf 44(5):563–571
13. Amiolemhen E, Ibhadode AOA (2004) Application of genetic algorithms—determination of the optimal machining parameters in the conversion of a cylindrical bar stock into a continuous finished profile. Int J Mach Tools Manuf 44(12–13):1403–1412
14. Amitay G (1981) Adaptive control optimization of grinding. J Eng Ind 103(1):103–108
15. António CAC, Davim JP (2002) Optimal cutting conditions in turning of particulate metal matrix composites based on experiment and a genetic search model. Compos Part A Appl Sci Manuf 33(2):213–219
16. Armarego EJA, Smith AJR, Wang J (1994) Computer-aided constrained optimization analyses and strategies for multipass helical tooth milling operations. CIRP Ann Manuf Technol 43(1):437–442
17. Arul S, Raj DS, Vijayaraghavan L, Malhotra SK, Krishnamurthy R (2006) Modeling and optimization of process parameters for defect toleranced drilling of GFRP composites. Mater Manuf Process 21(4):357–365
18. Arul S, Vijayaraghavan L, Malhotra SK (2007) Online monitoring of acoustic emission for quality control in drilling of polymeric composites. J Mater Process Technol 185(1–3):184–190
19. Aslan E, Camuscu N, Birgoren B (2007) Design optimization of cutting parameters when turning hardened AISI 4140 steel (63 HRC) with Al_2O_3 + TiCN mixed ceramic tool. Mater Des 28:1618–1622
20. Asokan P, Baskar N, Babu K (2005) Optimization of surface grinding operations using particle swarm optimization technique. J Manuf Sci Eng 127(4):885–892
21. Audy J (2008) A study of computer-assisted analysis of effects of drill geometry and surface coating on forces and power in drilling. J Mater Process Technol 204(1–3):130–138
22. Aykut Ş, Gölcü M, Semiz S, Ergür HS (2007) Modeling of cutting forces as function of cutting parameters for face milling of satellite 6 using an artificial neural network. J Mater Process Technol 190(1–3):199–203
23. Baek DK, Ko TJ, Kim HS (2001) Optimization of feedrate in a face milling operation using a surface roughness model. Int J Mach Tools Manuf 41(3):451–462
24. Bağci E, Ozcelik B (2006a) Analysis of temperature changes on the twist drill under different drilling conditions based on Taguchi method during dry drilling of Al 7075–T651. Int J Adv Manuf Technol 29(7–8):629–636
25. Bağci E, Ozcelik B (2006b) Investigation of the effect of drilling conditions on the twist drill temperature during step-by-step and continuous dry drilling. Mater Des 27(6):446–454
26. Balaji AK, Ghosh R, Fang XD, Stevenson R, Jawahir IS (2006) Performance-based predictive models and optimization methods for turning operations and applications: part 2-Assessment of chip forms/chip breakability. J Manuf Process 8(2):144–158
27. Balykov AV (2003) Optimization of diamond drilling using an extreme experimental design. Glass Ceram 60(7–8):213–216

28. Bandyopadhyay S, Gokhale H, Sundar JKS, Sundararajan G, Joshi SV (2005) A statistical approach to determine process parameter impact in Nd:YAG laser drilling of IN718 and Ti-6Al-4V sheets. Opt Lasers Eng 43(2):163–182
29. Baro PK, Joshi SS, Kapoor SG (2005) Modeling of cutting forces in a face-milling operation with self-propelled round insert milling cutter. Int J Mach Tools Manuf 45(7–8):831–839
30. Basak H, Goktas HH (2009) Burnishing process on al-alloy and optimization of surface roughness and surface hardness by fuzzy logic. Mater Des 30(4):1275–1281
31. Basak S, Dixit US, Davim JP (2007) Application of radial basis function neural networks in optimization of hard turning of AISI D2 cold-worked steel with a ceramic tool. Proc Inst Mech Eng Part B J Eng Manuf 221:987–998
32. Basavarajappa S, Chandramohan G, Davim JP (2008) Some studies on drilling of hybrid metal matrix composites based on Taguchi techniques. J Mater Process Technol 196(1–3):332–338
33. Baskar N, Asokan P, Saravanan R, Prabhaharan G (2006) Selection of optimal machining parameters for multi-tool milling operations using a memetic algorithm. J Mater Process Technol 174:239–249
34. Baykasoglu A, Dereli T (2002) Novel algorithm approach to generate the 'number of passes' and 'depth of cuts' for the optimization routines of multi pass machining. Int J Prod Res 40:1549–1565
35. Benardos PG, Vosniakos GC (2002) Prediction of surface roughness in CNC face milling using neural networks and Taguchi's design of experiments. Robot Comput Integr Manuf 18(5–6):343–354
36. Bhattacharyya K, Mukherjee A (2006) Modeling and simulation of centerless grinding of ball bearings. Simul Modell Pract Theory 14(7):971–988
37. Bigerelle M, Hagege B, El-Mansori M (2008) Mechanical modeling of micro-scale abrasion in superfinish belt grinding. Tribol Int 41(11):992–1001
38. Biglari FR, Fang XD (1995) Real-time fuzzy logic control for maximizing the tool life of small-diameter drills. Fuzzy Sets Syst 72:91–101
39. Bouacha K, Yallese MA, Mabrouki T, Rigal JF (2010) Statistical analysis of surface roughness and cutting forces using response surface methodology in hard turning of AISI 52100 bearing steel with CBN tool. Int J Refra Met Hard Mater 28(3):349–361
40. Bouzid W (2005) Cutting parameter optimization to minimize production time in high speed turning. J Mater Process Technol 161(3):388–395
41. Brinksmeier E, Tonshoff HK, Czenkusch C, Heinzel C (1998) Modeling and optimization of grinding processes. J Intell Manuf 9:303–314
42. Brinksmeier E, Aurich JC, Govekar E, Heinzel C, Hoffmeister HW, Klocke F, Peters J, Rentsch R, Stephenson DJ, Uhlmann E, Weinert K, Wittmann M (2006) Advances in modeling and simulation of grinding processes. CIRP Ann Manuf Technol 55(2):667–696
43. Brinksmeier E, Heinzel C, Bleil N (2009) Superfinishing and grind-strengthening with elastic bonding system. J Mater Process Technol 209(20):6117–6123
44. Budak E, Tekeli A (2005) Maximizing chatter free material removal rate in milling through optimal selection of axial and radial depth of cut pairs. CIRP Ann Manuf Technol 54(1):353–356
45. Budak E, Ozturk E, Tunc LT (2009) Modeling and simulation of 5-axis milling processes. CIRP Ann Manuf Technol 58(1):347–350
46. Cakir MC, Gurarda A (1998) Optimization and graphical representation of machining conditions in multi-pass turning operations. Comput Integr Manuf Syst 11(3):157–170
47. Cakir MC, Gurarda A (2000) Optimization of machining conditions for multi-tool milling operations. Int J Prod Res 38(15):3537–3552
48. Chakraborty P, Asfour S, Cho S, Onar A, Lynn M (2008) Modeling tool wear progression by using mixed effects modeling technique when end-milling AISI 4340 steel. J Mater Process Technol 205(1–3):190–202

49. Chandrasekaran M, Muralidhar M, Krishna CM, Dixit US (2010) Application of soft computing techniques in machining performance prediction and optimization: a literature review. Int J Adv Manuf Technol 46(5–8):445–464
50. Chang PC, Hsieh JC, Wang CY (2007) Adaptive multi-objective genetic algorithms for scheduling of drilling operation in printed circuit board industry. Appl Soft Comput 7(3):800–806
51. Chang SH, Farris TN, Chandrasekar S (2008) Experimental analysis on evolution of superfinished surface texture. J Mater Process Technol 203(1–3):365–371
52. Chen MC (2004) Optimizing machining economics models of turning operations using the scatter search approach. Int J Prod Res 42:2611–2625
53. Chen MC , Chen KY (2003) Optimization of multipass turning operations with genetic algorithms: a note. Int J Prod Res 41(14):3385–3388
54. Chen JC, Savage M (2001) A fuzzy-net-based multilevel in-process surface roughness recognition system in milling operations. Int J Adv Manuf Technol 17(9):670–676
55. Chen MC, Tsai DM (1996) A simulated annealing approach for optimization of multi-pass turning operations. Int J Prod Res 34(10):2803–2825
56. Chen YH, Lee YS, Fang SC (1998) Optimal cutter selection and machining plane determination for process planning and NC machining of complex surfaces. J Manuf Syst 17(5):371–388
57. Chen C, Sakai S, Inasaki I (1991) Lapping of advanced ceramics. Mater Manuf Process 6(2):211–226
58. Chien WT, Tsai CS (2003) The investigation on the prediction of tool wear and determination of optimum cutting conditions in machining 17-4PH stainless steel. J Mater Process Technol 140(1–3):340–345
59. Ching-Kao C, Lu HS (2007) The optimal cutting-parameter selection of heavy cutting process in side milling for SUS304 stainless steel. Int J Adv Manuf Technol 34(5–6):440–447
60. Choi JG, Yang MY (1999) In-process prediction of cutting depths in end milling. Int J Mach Tools Manuf 39(5):705–721
61. Choi TJ, Subrahmanya N, Li H, Shin YC (2008a) Generalized practical models of cylindrical plunge grinding processes. Int J Mach Tools Manuf 48(1):61–72
62. Choi YJ, Park MS, Chu CN (2008b) Prediction of drill failure using features extraction in time and frequency domains of feed motor current. Int J Mach Tools Manuf 48:29–39
63. Chua MS, Loh HT, Wong YS, Rahman M (1991) Optimization of cutting conditions for multi-pass turning operations using sequential quadratic programming. J Mater Process Technol 28(1–2):253–262
64. Cus F, Balic J (2003) Optimization of cutting process by GA approach. Robot Comput Integr Manuf 19:113–121
65. Cus F, Milfelner M, Balic J (2006) An intelligent system for monitoring and optimization of ball-end milling process. J Mater Process Technol 175(1–3):90–97
66. Davim JP (2001) A note on the determination of optimal cutting conditions for surface finish obtained in turning using design of experiments. J Mater Process Technol 116(2–3):305–308
67. Davim JP (2003) Design of optimization of cutting parameters for turning metal matrix composites based on the orthogonal arrays. J Mater Process Technol 132:340–344
68. Davim JP, António CAC (2001a) Optimal drilling of particulate metal matrix composites based on experimental and numerical procedures. Int J Mach Tools Manuf 41(1):21–31
69. Davim JP, António CAC (2001b) Optimization of cutting conditions in machining of aluminium matrix composites using a numerical and experimental model. J Mater Process Technol 112(1):78–82
70. Davim JP, Gaitonde VN, Karnik SR (2008) Investigations into the effect of cutting conditions on surface roughness in turning of free machining steel by ANN models. J Mater Process Technol 205(1–3):16–23

71. de Lacalle LNL, Lamikiz A, Sánchez JA, Arana JL (2007) The effect of ball burnishing on heat-treated steel and Inconel 718 milled surfaces. Int J Adv Manuf Technol 32(9–10):958–968
72. Dhavalikar MN, Kulkarni MS, Mariappan V (2003) Combined Taguchi and dual response method for optimization of a centerless grinding operation. J Mater Process Technol 132:90–94
73. Doman DA, Warkentin A, Bauer R (2009) Finite element modeling approaches in grinding. Int J Mach Tools Manuf 49(2):109–116
74. Drazumeric R, Krajnik P, Vrabic R, Meyer B, Butala P, Kosel F, Kopac J (2010) Modeling of grinding gap macro geometry and workpiece kinematics in throughfeed centreless grinding. J Mater Process Technol 210(1):104–109
75. Dubey AK (2008a) A hybrid approach for multi-performance optimization of the electro chemical honing process. Int J Adv Manuf Technol. doi:10.1007/s00170-008-1422-8
76. Dubey AK (2008b) Multi-performance modeling and optimization control strategies for electro chemical honing: a critical evaluation. Int J Adv Manuf Technol. doi: 10.1007/s00170-008-1477-6
77. Dubey AK (2009) Multi-response optimization of electro chemical honing using utility-based Taguchi approach. Int J Adv Manuf Technol 41(7–8):749–759
78. Dutta RK, Paul S, Chattopadhyay AB (2006) The efficacy of back propagation neural network with delta bar delta learning in predicting the wear of carbide inserts in face milling. Int J Adv Manuf Technol 31(5–6):434–442
79. Dvivedi A, Kumar P (2007) Surface quality evaluation in ultrasonic drilling through the Taguchi technique. Int J Adv Manuf Technol 34(1–2):131–140
80. Ee KC, Li PX, Balaji AK, Jawahir IS, Stevenson R (2006) Performance-based predictive models and optimization methods for turning operations and applications: part 1. Tool wear/tool life in turning with coated grooved tools. J Manuf Process 8(1):54–66
81. Elhachimi M, Torbaty S, Joyot P (1999) Mechanical modeling of high speed drilling. 1: predicting torque and thrust. Int J Mach Tools Manuf 39(4):553–568
82. El-Mounayri H, Kishawy H, Briceno J (2005) Optimization of CNC ball end milling: a neural network-based model. J Mater Process Technol 166(1):50–62
83. El-Taweel TA, El-Axir MH (2009) Analysis and optimization of the ball burnishing process through the Taguchi technique. Int J Adv Manuf Technol 41(3–4):301–310
84. El-Tayeb NSM, Low KO, Brevern PV (2008) Enhancement of surface quality and tribological properties using ball burnishing process. Mach Sci Tech 12(2):234–248
85. El-Wahab AI, Abdelhay AM (1998) A new algorithm and tool design for CNC profile burnishing. Int J Prod Res 36(7):1977–1985
86. Ertunc HM, Loparo KA, Ocak H (2001) Tool wear condition monitoring in drilling operations using hidden Markov models (HMMs). Int J Mach Tools Manuf 41(9):1363–1384
87. Feng CX, Wang X (2002) Development of empirical models for surface roughness prediction in finish turning. Int J Adv Manuf Technol 20:348–356
88. Feng CX, Wang X, Yu Z (2002) Neural networks modeling of honing surface roughness parameters defined by ISO 13565. J Manuf Syst 21(5):395–408
89. Feng CXJ, Yu ZGS, Wang JHJ (2005) Validation and data splitting in predictive regression modeling of honing surface roughness data. Int J Prod Res 43(8):1555–1571
90. Fernandes M, Cook C (2006) Drilling of carbon composites using a one shot drill bit. Part II: empirical modeling of maximum thrust force. Int J Mach Tools Manuf 46(1):76–79
91. Fernandes MH, Garitaonandia I, Albizuri J, Hernández JM, Barrenetxea D (2009) Simulation of an active vibration control system in a centerless grinding machine using a reduced updated FE model. Int J Mach Tools Manuf 49(3–4):239–245
92. Fontaine M, Moufki A, Devillez A, Dudzinski D (2007a) Modeling of cutting forces in ball-end milling with tool–surface inclination: Part I. Predictive force model and experimental validation. J Mater Process Technol 189:73–84

93. Fontaine M, Devillez A, Moufki A, Dudzinski D (2007b) Modeling of cutting forces in ball-end milling with tool–surface inclination: Part II. Influence of cutting conditions, run-out, ploughing and inclination angle. J Mater Process Technol 189(1–3):85–96
94. Gaitonde VN, Karnik SR, Achyutha BT, Siddeswarappa B (2007) Methodology of Taguchi optimization for multi-objective drilling problem to minimize burr size. Int J Adv Manuf Technol 34(1–2):1–8
95. Gaitonde VN, Karnik SR, Achyutha BT, Siddeswarappa B (2008a) Taguchi optimization in drilling of AISI 316L stainless steel to minimize burr size using multi-performance objective based on membership function. J Mater Process Technol 202(1–3):374–379
96. Gaitonde VN, Karnik SR, Achyutha BT, Siddeswarappa B (2008b) Genetic algorithm-based burr size minimization in drilling of AISI 316L stainless steel. J Mater Process Technol 197(1–3):225–236
97. Gaitonde VN, Karnik SR, Davim JP (2008c) Taguchi multiple-performance characteristics optimization in drilling of medium density fibreboard (MDF) to minimize delamination using utility concept. J Mater Process Technol 196(1–3):73–78
98. Gaitonde VN, Karnik SR, Davim JP (2008d) Prediction and minimization of delamination in drilling of medium-density fiberboard (MDF) using response surface methodology and taguchi design. Mater Manuf Processes 23(4):377–384
99. Gaitonde VN, Karnik SR, Rubio JC, Correia AE, Abrão AM, Davim JP (2008e) Analysis of parametric influence on delamination in high-speed drilling of carbon fiber reinforced plastic composites. J Mater Process Technol 203(1–3):431–438
100. Gaitonde VN, Karnik SR, Davim JP (2009) Multiperformance optimization in turning of free-machining steel using taguchi method and utility concept. J Mater Eng Perform 18(3):231–236
101. Garg S, Pal SK, Chakraborty D (2007) Evaluation of the performance of back propagation and radial basis function neural networks in predicting the drill flank wear. Neural Comput Appl 16:407–417
102. Ghaiebi H, Solimanpur M (2007) An ant algorithm for optimization of hole-making operations. Comput Ind Eng 52:308–319
103. Ghani JA, Choudhury IA, Hassan HH (2004) Application of Taguchi method in the optimization of end milling parameters. J Mater Process Technol 145(1):84–92
104. Ghosh N, Ravi YB, Mukhopadyay S, Paul S, Mohanty AR, Chattopadyay AB (2007) Estimation of tool wear during CNC milling using neural network-based sensor fusion. Mech Syst Signal Process 21:466–479
105. Gómez MP, Hey AM, Ruzzante JE, D'Attellis CE (2010) Tool wear evaluation in drilling by acoustic emission. Phys Procedia 3(1):819–825
106. Gopal AV, Rao PV (2003) Selection of optimum conditions for maximum material removal rate with surface finish and damage as constraints in SiC grinding. Int J Mach Tools Manuf 43(13):1327–1336
107. Gopalakrishnan B, Al-Khayyal F (1991) Machine parameter selection for turning with constraints: an analytical approach based on geometric programming. Int J Prod Res 29(9):1897–1908
108. Govindhasamy JJ, McLoone SF, Irwin GW, French JJ, Doyle RP (2005) Neural modeling, control and optimization of an industrial grinding process. Control Eng Pract 13(10):1243–1258
109. Guevarra DS, Kyusojin A, Isobe H, Kaneko Y (2002) Development of a new lapping method for high precision ball screw (2nd report): design and experimental study of an automatic lapping machine with in-process torque monitoring system. Precis Eng 26(4):389–395
110. Guibert N, Paris H, Rech J, Claudin C (2009) Identification of thrust force models for vibratory drilling. Int J Mach Tools Manuf 49(9):730–738
111. Guo YB, Zhang Y, Zhong JA, Syoji K (2002) Optimization of honing wheel structure parameters in ultra-precision plane honing. J Mater Process Technol 129(1–3):96–100

112. Guo C, Campomanes M, Mcintosh D, Becze C, Gree S, Malkin S (2003) Optimization of continuous dress creep-feed form grinding process. CIRP Ann Manuf Technol 52(1): 259–262
113. Guo C, Campomanes M, Mcintosh D, Becze C, Malkin S (2004) Model-based monitoring and control of continuous dress creep-feed form grinding. CIRP Ann Manuf Technol 53(1):263–266
114. Gupta R, Batra JL, Lal GK (1995) Determination of optimal subdivision of depth of cut in multi-pass turning with constraints. Int J Prod Res 33(9):2555–2565
115. Gupta R, Shishodia KS, Sekhon GS (2001) Optimization of grinding process parameters using enumeration method. J Mater Process Technol 112(1):63–67
116. Gurel S, Akturk MS (2007) Considering manufacturing cost and scheduling performance on a CNC turning machine. Eur J Oper Res 177(1):325–343
117. Haber RE, Haber-Haber R, Jiménez A, Galán R (2009) An optimal fuzzy control system in a network environment based on simulated annealing-an application to a drilling process. Appl Soft Comput 9(3):889–895
118. Haq AN, Marimuthu P, Jeyapaul R (2008) Multi response optimization of machining parameters of drilling Al/SiC metal matrix composite using grey relational analysis in the Taguchi method. Int J Adv Manuf Technol 37(3–4):250–255
119. Hashimoto F, Lahoti GD (2004) Optimization of set-up conditions for stability of the centerless grinding process. CIRP Ann Manuf Technol 53(1):271–274
120. Hashmi K, Graham ID, Mills B (2000) Fuzzy logic based data selection for the drilling process. J Mater Process Technol 108:55–61
121. Hassan AM, Sulieman AD (1999) Improvement in the wear resistance of brass components by the ball burnishing process. J Mater Process Technol 96(1–3):73–80
122. Hassan AM, Al-Jalil HF, Ebied AA (1998) Burnishing force and number of ball passes for the optimum surface finish of brass components. J Mater Process Technol 83:176–179
123. Heisel U, Luik M, Eisseler R, Schaal M (2005) Prediction of parameters for the burr dimensions in short-hole drilling. CIRP Ann Manuf Technol 54(1):79–82
124. Hekman KA, Liang SY (1999) Feed rate optimization and depth of cut control for productivity and part parallelism in grinding. Mechatronics 9(5):447–462
125. Ho WH, Tsai JT, Lin BT, Chou JH (2009) Adaptive network-based fuzzy inference system for prediction of surface roughness in end milling process using hybrid Taguchi-genetic learning algorithm. Expert Syst Appl 36(2):3216–3222
126. Horng JT, Chiang KT (2008) A grey and fuzzy algorithms integrated approach to the optimization of turning Hadfield steel with Al_2O_3/TiC mixed ceramic tool. J Mater Process Technol 207(1–3):89–97
127. Hui YV, Leung LC, Linn R (2001) Optimal machining conditions with cost of quality and tool maintenance for turning. Int J Prod Res 39(4):647–665
128. Hundt W, Kuster F, Rehsteiner F (1997) Model-based AE monitoring of the grinding process. CIRP Ann Manuf Technol 46(1):243–247
129. Ibrahim AA, Rabbo SMA, El-Axir MH, Ebied AA (2009) Center rest balls burnishing parameters adaptation of steel components using fuzzy logic. J Mater Process Technol 209(5):2428–2435
130. Iliescu D, Gehin D, Gutierrez ME, Girot F (2010) Modeling and tool wear in drilling of CFRP. Int J Mach Tools Manuf 50(2):204–213
131. Inasaki I (1991) Monitoring and optimization of internal grinding process. CIRP Ann Manuf Technol 40(1):359–362
132. Iqbal A, Dar NU, He N, Hammouda MMI, Li L (2009) Self-developing fuzzy expert system: a novel learning approach, fitting for manufacturing domain. J Intell Manuf 31(5–6):434–442. doi:10.1007/s10845-009-0252-31
133. Jadoun RS, Kumar P, Mishra BK (2009) Taguchi's optimization of process parameters for production accuracy in ultrasonic drilling of engineering ceramics. Prod Eng 3(3):243–253
134. Jawahir IS, Wang X (2007) Development of hybrid predictive models and optimization techniques for machining operations. J Mater Process Technol 185(1–3):46–59

135. Jayakumar T, Mukhopadhyay CK, Venugopal S, Mannan SL, Raj B (2005) A review of the application of acoustic emission techniques for monitoring forming and grinding processes. J Mater Process Technol 159(1):48–61
136. Jiang Q, Ge Z (2002) Simulation on topography of superfinished roller surfaces. Sci China B: Chem 45(2):122–126
137. Jiao Y, Lei S, Pei ZJ, Lee ES (2004) Fuzzy adaptive networks in machining process modeling: surface roughness prediction for turning operations. Int J Mach Tools Manuf 44(15):1643–1651
138. Johansen L, Lund E (2009) Optimization of laminated composite structures using delamination criteria and hierarchical models. Struct Multidiscip Optim 38(4):357–375
139. Kadirgama K, Abou-El-Hossein KA, Mohammad B, Habeeb H (2007) Statistical model to determine surface roughness when milling hastelloy C-22HS. J Mech Sci Technol 21(10): 1651–1655
140. Karnik SR, Gaitonde VN, Rubio JC, Correia AE, Abrão AM, Davim JP (2008) Delamination analysis in high speed drilling of carbon fiber reinforced plastics (CFRP) using artificial neural network model. Mater Des 29(9):1768–1776
141. Karpat Y, Özel T (2007) Multi-objective optimization for turning processes using neural network modeling and dynamic-neighborhood particle swarm optimization. Int J Adv Manuf Technol 35(3–4):234–247
142. Karthikeyan R, Jaiganesh S, Pai BC (2002) Optimization of drilling characteristics for Al/SiCp composites using fuzzy/GA. Metals Mater Int 8(2):163–168
143. Kee PK (1996) Development of constrained optimization analyses and strategies for multi-pass rough turning operations. Int J Mach Tools Manuf 36(1):115–127
144. Kersting P, Zabel A (2009) Optimizing NC-tool paths for simultaneous five-axis milling based on multi-population multi-objective evolutionary algorithms. Adv Eng Softw 40(6):452–463
145. Khajavi AN, Komanduri R (1993) On multisensor approach in drill wear monitoring. CIRP Ann Manuf Technol 42:71–74
146. Kiliç SE, Cogun C, Şen DT (1993) A computer-aided graphical technique for the optimization of machining conditions. Comput Ind 22(3):319–326
147. Kilickap E (2010a) Optimization of cutting parameters on delamination based on Taguchi method during drilling of GFRP composite. Expert Syst Appl 37(8):6116–6122
148. Kilickap E (2010b) Modeling and optimization of burr height in drilling of Al-7075 using Taguchi method and response surface methodology. Int J Adv Manuf Technol. doi: 10.1007/s00170-009-2469-x
149. Kim GH (2002) Evaluation of pre-estimation model to the in process surface roughness for grinding operations. Int J Korean Soc Precis Eng 3:24–30
150. Kim HY, Ahn JH (2002) Chip disposal state monitoring in drilling using neural network based spindle motor power sensing. Int J Mach Tools Manuf 42(10):1113–1119
151. Kim JD, Choi MS (1995a) A study on the optimization of the cylindrical lapping process for engineering fine-ceramics (Al_2O_3) by the statistical design method. J Mater Process Technol 52(2–4):368–385
152. Kim JD, Choi MS (1995b) Stochastic approach to experimental analysis of cylindrical lapping process. Int J Mach Tools Manuf 35(1):51–59
153. Kim D, Ramulu M (2004) Drilling process optimization for graphite/bismaleimide–titanium alloy stacks. Compos Struct 63(1):101–114
154. Kim J, Min S, Dornfeld DA (2001) Optimization and control of drilling burr formation of AISI 304L and AISI 4118 based on drilling burr control charts. Int J Mach Tools Manuf 41(7):923–936
155. Kim SS, Kim IH, Mani V, Kim HJ (2008) Real-coded genetic algorithm for machining condition optimization. Int J Adv Manuf Technol 38:884–895
156. Kolahan F, Liang M (1996) A tabu search approach to optimization of drilling operations. Comput Ind Eng 31(1–2):371–374

157. Korzynski M (2007) Modeling and experimental validation of the force–surface roughness relation for smoothing burnishing with a spherical tool. J Mach Tools Manuf 47:1956–1964
158. Korzynski M, Pacana A (2010) Centreless burnishing and influence of its parameters on machining effects. J Mater Process Technol 210(9):1217–1223
159. Kovacic M, Balic J, Brezocnik M (2004) Evolutionary approach for cutting forces prediction in milling. J Mater Process Technol 155–156:1647–1652
160. Krishna AG (2007) Optimization of surface grinding operations using a differential evolution approach. J Mater Process Technol 183:202–209
161. Kuar AS, Doloi B, Bhattacharya B (2006) Modeling and analysis of pulsed Nd:YAG laser machining characteristics during micro-drilling of zirconia (ZrO_2). Int J Mach Tools Manuf 46(12–13):1301–1310
162. Kurt M, Bağci E, Kaynak Y (2009) Application of Taguchi methods in the optimization of cutting parameters for surface finish and hole diameter accuracy in dry drilling processes. Int J Adv Manuf Technol 40(5–6):458–469
163. Kwak JS (2005) Application of Taguchi and response surface methodologies for geometric error in surface grinding process. Int J Mach Tools Manuf 45(3):327–334
164. Kwon Y, Fischer GW, Tseng TL (2002) Fuzzy neuron adaptive modeling to predict surface roughness under process variations in CNC turning. J Manuf Syst 21(6):440–450
165. Langella A, Nele L, Maio A (2005) A torque and thrust prediction model for drilling of composite materials. Compos Part A Appl Sci Manuf 36(1):83–93
166. Laouar L, Hamadache H, Saad S, Bouchelaghem A, Mekhilef S (2009) Mechanical surface treatment of steel-Optimization parameters of regime. Phys Procedia 2(3):1213–1221
167. Lauderbaugh LK (2009) Analysis of the effects of process parameters on exit burrs in drilling using a combined simulation and experimental approach. J Mater Process Technol 209(4):1909–1919
168. Lee CW, Shin YC (2000) Evolutionary modeling and optimization of grinding process. Int J Prod Res 38(12):2787–2813
169. Lee BY, Tarng YS (2000) Cutting-parameter selection for maximizing production rate or minimizing production cost in multistage turning operations. J Mater Process Technol 105(1–2):61–66
170. Lee SG, Tam SC, Loh NH (1993) Ball burnishing of 316 l stainless steel. J Mater Process Technol 37:241–251
171. Lee BY, Liu HS, Tarng YS (1998) Modeling and optimization of drilling process. J Mater Process Technol 74(1–3):149–157
172. Li XP, Li HZ (2004) Theoretical modeling of cutting forces in helical end milling with cutter runout. Int J Mech Sci 46(9):1399–1414
173. Li HZ, Zhang WB, Li XP (2001) Modeling of cutting forces in helical end milling using a predictive machining theory. Int J Mech Sci 43(8):1711–1730
174. Li GF, Wang LS, Yang LB (2002) Multi-parameter optimization and control of the cylindrical grinding process. J Mater Process Technol 129(1–3):232–236
175. Liang M, Mgwatu M, Zuo M (2001) Integration of cutting parameter selection and tool adjustment decision for multi-pass turning. Int J Adv Manuf Technol 17:861–869
176. Liao TW, Chen LJ (1994) A neural network approach for grinding processes: Modeling and optimization. Int J Mach Tools Manuf 34(7):919–937
177. Lin SC, Ting CJ (1999) Drill wear monitoring using neural networks. Int J Adv Manuf Technol 36:465–475
178. Liu X, Cheng K (2005) Modeling the machining dynamics of peripheral milling. Int J Mach Tools Manuf 45(11):1301–1320
179. Liu HS, Lee BY, Tarang YS (2000) In-process prediction of corner wear in drilling operations. Int J Adv Manuf Technol 101:152–158
180. Liu Q, Chen X, Wang Y, Gindy N (2008) Empirical modeling of grinding force based on multivariate analysis. J Mater Process Technol 203(1–3):420–430

181. Lizarralde R, Barrenetxea D, Gallego I, Marquinez JI, Bueno R (2005) Practical application of new simulation methods for the elimination of geometric instabilities in centerless grinding. CIRP Ann Manuf Technol 54(1):273–276
182. Lo SP (2003) An adaptive-network based fuzzy inference system for prediction of workpiece surface roughness in end milling. J Mater Process Technol 142(3):665–675
183. Loh NH, Tam SC, Miyazawa S (1989a) A study of the effects of ball-burnishing parameters on surface roughness using factorial design. J Mech Work Technol 18:53–61
184. Loh NH, Tam SC, Miyazawa S (1989b) Optimization of the surface finish produced by ball burnishing. J Mech Work Technol 19(1):101–107
185. Lu HS, Chang CK, Hwang NC, Chung CT (2009) Grey relational analysis coupled with principal component analysis for optimization design of the cutting parameters in high-speed end milling. J Mater Process Technol 209(8):3808–3817
186. Mahdy MAM (2001) Economic drilling conditions for a given deburring radius. J Mater Process Technol 110(2):197–205
187. Mani A, Patvardhan C (2010) Solving ceramic grinding optimization problem by adaptive quantum evolutionary algorithm. In: Proceedings of international conference intelligence system, model simulation, Liverpool, pp 43–48
188. Manna A, Bhattacharyya B (2004) Investigation for optimal parametric combination for achieving better surface finish during turning of Al/SiC-MMC. Int J Adv Manuf Technol 23:658–665
189. Manna A, Salodkar S (2008) Optimization of machining conditions for effective turning of E0300 alloy steel. J Mater Process Technol 203(1–3):147–153
190. Mauch CA, Lauderbaugh LK (1991) Modeling the drilling process—an analytical model to predict thrust force and torque. Precis Eng 13(3):233
191. Merdol SD, Altintas Y (2008) Virtual cutting and optimization of three-axis milling processes. Int J Mach Tools Manuf 48(10):1063–1071
192. Messaoud A, Weihs C (2009) Monitoring a deep hole drilling process by nonlinear time series modeling. J Sound Vib 321(3–5):620–630
193. Michael PC, Saka N, Rabinowicz E (1998) Burnishing and adhesive wear of an electrically conductive polyester-carbon film. Wear 132:265–285
194. Mohan NS, Kulkarni SM, Ramachandra A (2007) Delamination analysis in drilling process of glass fibre reinforced plastic (GFRP) composite materials. J Mater Process Technol 186(1–3):265–271
195. Molinari A, Nouari M (2002) Modeling of tool wear by diffusion in metal cutting. Wear 252(1–2):135–149
196. Mukherjee I, Ray PK (2006) A review of optimization techniques in metal cutting processes. Comput Ind Eng 50(1–2):15–34
197. Mukherjee I, Ray PK (2008a) A systematic solution methodology for inferential multivariate modeling of industrial grinding process. J Mater Process Technol 196(1–3): 379–392
198. Mukherjee I, Ray PK (2008b) Optimal process design of two-stage multiple responses grinding processes using desirability functions and metaheuristic technique. Appl Soft Comput 8(1):402–421
199. Muthukrishnan N, Davim JP (2009) Optimization of machining parameters of Al/SiC-MMC with ANOVA and ANN analysis. J Mater Process Technol 209(1):225–232
200. Nalbant M, Gökkaya H, Sur G (2007) Application of Taguchi method in the optimization of cutting parameters for surface roughness in turning. Mater Des 28(4):1379–1385
201. Nandi AK, Banerjee MK (2005) FBF-NN-based modeling of cylindrical plunge grinding process using a GA. J Mater Process Technol 162–163:655–664
202. Nandi AK, Davim JP (2009) A study of drilling performances with minimum quantity of lubricant using fuzzy logic rules. Mechatronics 19:218–232
203. Nandi AK, Pratihar DK (2004a) Automatic design of fuzzy logic controller using a genetic algorithm—to predict power requirement and surface finish in grinding. J Mater Process Technol 148(3):288–300

204. Nandi AK, Pratihar DK (2004b) An expert system based on FBFN using a GA to predict surface finish in ultra-precision turning. J Mater Process Technol 155–156:1150–1156
205. Natarajan U, Saravanan R, Periasamy VM (2006) Application of particle swarm optimization in artificial neural network for prediction of tool life. Int J Adv Manuf Technol 28:1084–1088
206. Neagu-Ventzel S, Cioc S, Marinescu I (2006) A wear model and simulation of superfinishing process: analysis for the superfinishing of bearing rings. Wear 260(9–10): 1061–1069
207. Nian CY, Yang WH, Tarng YS (1999) Optimization of turning operations with multiple performance characteristics. J Mater Process Technol 95(1–3):90–96
208. Nouari M, List G, Girot F, Gehin D (2005) Effect of machining parameters and coating on wear mechanisms in dry drilling of aluminium alloys. Int J Mach Tools Manuf 45(12–13):1436–1442
209. Ojha DK, Dixit US, Davim JP (2009) A soft computing based optimization of multi-pass turning processes. Int J Mater Prod Technol 35:145–166
210. Öktem H, Erzurumlu T, Çöl M (2006) A study of the Taguchi optimization method for surface roughness in finish milling of mold surfaces. Int J Adv Manuf Technol 28(7–8):694–700
211. Onwubolu GC (2006a) Selection of drilling operations parameters for optimal tool loading using integrated response surface methodology: a Tribes approach. Int J Prod Res 44(5): 959–980
212. Onwubolu GC (2006b) Performance-based optimization of multi-pass face milling operations using tribes. Int J Mach Tools Manuf 46:717–727
213. Onwubolu GC (2009) Prediction of burr formation during face milling using a hybrid GMDH network model with optimized cutting conditions. Int J Adv Manuf Technol 44(11–12):1083–1093
214. Onwubolu GC, Clerc M (2004) Optimal path for automated drilling operations by a new heuristic approach using particle swarm optimization. Int J Prod Res 42(3):473–491
215. Onwubolu GC, Kumalo T (2001a) Optimization of multipass turning operations with genetic algorithms. Int J Prod Res 39(16):3727–3745
216. Onwubolu GC, Kumalo T (2001b) Multi-pass turning operations optimization based on genetic algorithms. Proc Inst Mech Eng Part B J Eng Manuf 215:117–124
217. Onwubolu GC, Kumar S (2006) Response surface methodology-based approach to CNC drilling operations. J Mater Process Technol 171(1):41–47
218. Onwubolu GC, Buryan P, Lemke F (2008) Modeling tool wear in end-milling using enhanced GMDH learning networks. Int J Adv Manuf Technol 39(11–12):1080–1092
219. Ozcelik B, Bağci E (2006) Experimental and numerical studies on the determination of twist drill temperature in dry drilling: a new approach. Mater Des 27(10):920–927
220. Ozcelik B, Oktem H, Kurtaran H (2005) Optimum surface roughness in end milling Inconel 718 by coupling neural network model and genetic algorithm. Int J Adv Manuf Technol 27(3–4):234–241
221. Pa PS (2007) Design of freeform surface finish using burnishing assistance following electrochemical finishing. J Mech Sci Technol 21(10):1630–1636
222. Paiva AP, Ferreira JR, Balestrassi PP (2007) A multivariate hybrid approach applied to AISI 52100 hardened steel turning optimization. J Mater Process Technol 189(1–3):26–35
223. Pal SK, Chakraborty D (2005) Surface roughness prediction in turning using artificial neural network. Neural Comput Appl 14:319–324
224. Palanisamy P, Rajendran I, Shanmugasundaram S (2007) Optimization of machining parameters using genetic algorithm and experimental validation for end-milling operations. Int J Adv Manuf Technol 32(7–8):644–655
225. Panda SS, Chakraborty D, Pal SK (2008) Flank wear prediction in drilling using back propagation neural network and radial basis function network. App Soft Comput 8(2):858–871

226. Park HW, Liang SY (2008) Force modeling of micro-grinding incorporating crystallographic effects. Int J Mach Tools Manuf 48(15):1658–1667
227. Patel K, Batish A, Bhattacharya A (2009) Optimization of surface roughness in an end-milling operation using nested experimental design. Prod Eng 3(4–5):361–373
228. Paul A, Kapoor SG, DeVor RE (2005) Chisel edge and cutting lip shape optimization for improved twist drill point design. Int J Mach Tools Manuf 45(4–5):421–431
229. Pedersen NL (2004) Optimization of holes in plates for control of eigenfrequencies. Struct Multi Optim 28(1):1–10
230. Prakash S, Palanikumar K, Manoharan N (2009) Optimization of delamination factor in drilling medium-density fiberboards (MDF) using desirability-based approach. Int J Adv Manuf Technol 45(3–4):370–381
231. Prakasvudhisarn C, Kunnapapdeelert S, Yenradee P (2009) Optimal cutting condition determination for desired surface roughness in end milling. Int J Adv Manuf Technol 41(5–6):440–451
232. Prasad AVS, Rao RK, Rao VKS (1997) Optimal selection of process parameter for turning operation in CAPP system. Int J Prod Res 35(6):1495–1522
233. Quiza R, Figueira L, Davim JP (2008) Comparing statistical models and artificial neural networks on predicting the tool wear in hard machining D2 AISI steel. Int J Adv Manuf Technol 37:641–648
234. Radhakrishnan T, Nandan U (2005) Milling force prediction using regression and neural networks. J Intell Manuf 16(1):93–102
235. Rai JK, Xirouchakis P (2008) Finite element method based machining simulation environment for analyzing part errors induced during milling of thin-walled components. Int J Mach Tools Manuf 48(6):629–643
236. Rajemi MF, Mativenga PT, Aramcharoen A (2010) Sustainable machining: selection of optimum turning conditions based on minimum energy considerations. J Cleaner Prod 18(10–11):1059–1065
237. Rao RV, Pawar PJ (2010a) Parameter optimization of a multi-pass milling process using non-traditional optimization algorithms. Appl Soft Comp 10(2):445–456
238. Rao RV, Pawar PJ (2010b) Grinding process parameter optimization using non-traditional optimization algorithms. Proc Inst Mech Eng Part B J Eng Manuf. doi:10.1243/09544054JEM1782
239. Rao DS, Hebbar HS, Komaraiah M (2007) Surface hardening of high-strength low alloy steels (hsla) dual-phase steels by ball burnishing using factorial design. Mater Manuf Process 22(7):825–829
240. Rao DS, Hebbar HS, Komaraiah M, Kempaiah UN (2008) Investigations on the effect of ball burnishing parameters on surface hardness and wear resistance of HSLA dual-phase steels. Mater Manuf Process 23(3):295–302
241. Rawat S, Attia H (2009) Wear mechanisms and tool life management of WC–Co drills during dry high speed drilling of woven carbon fibre composites. Wear 267(5–8): 1022–1030
242. Reddy NSK, Rao PV (2005) Selection of optimum tool geometry and cutting conditions using a surface roughness prediction model for end milling. Int J Adv Manuf Technol 26(11–12):1202–1210
243. Reddy NSK, Rao PV (2006) Selection of an optimal parametric combination for achieving a better surface finish in dry milling using genetic algorithms. Int J Adv Manuf Technol 28(5–6):463–473
244. Reddy SVB, Shunmugam MS, Narendran TT (1998) Optimal sub-division of the depth of cut to achieve minimum production cost in multi-pass turning using a genetic algorithm. J Mater Process Technol 79(1–3):101–108
245. Routara BC, Bandyopadhyay A, Sahoo P (2009) Roughness modeling and optimization in CNC end milling using response surface method: effect of workpiece material variation. Int J Adv Manuf Technol 40(11–12):1166–1180

246. Rowe WB, Yan L, Inasaki I, Malkin S (1994) Application of artificial intelligence in grinding. CIRP Ann Manuf Technol 43(2):521–531
247. Rowe WB, Li Y, Mills B, Allanson DR (1996) Application of intelligent CNC in grinding. Comput Ind 31(1):45–60
248. Rowe WB, Li Y, Chen X, Mills B (1997) An intelligent multiagent approach for selection of grinding conditions. CIRP Ann Manuf Technol 46(1):233–238
249. Roy SS (2006) Design of genetic-fuzzy expert system for predicting surface finish in ultra-precision diamond turning of metal matrix composite. J Mater Process Technol 173(3):337–344
250. Saljé E, See MV (1987) Process-Optimization in Honing. CIRP Ann Manuf Technol 36(1):235–239
251. Samhouri MS, Surgenor BW (2005) Surface roughness in grinding: on-line prediction with adaptive neuro-fuzzy inference system. Trans NAMRI/SME 33:57–64
252. Sanjay C, Jyothi C (2006) A study of surface roughness in drilling using mathematical analysis and neural networks. Int J Adv Manuf Technol 29(9–10):846–852
253. Sanjay C, Neema ML, Chin CW (2005) Modeling of tool wear in drilling by statistical analysis and neural network. J Mater Process Technol 170:494–500
254. Saravanan R, Sachithanandam M (2001) Genetic algorithm (GA) for multivariable surface grinding process optimization using a multi-objective function model. Int J Adv Manuf Technol 17:330–338
255. Saravanan R, Ashokan P, Sachithanandam M (2001) Comparative analysis of conventional and non-conventional optimization technique for CNC-turning process. Int J Adv Manuf Technol 17:471–476
256. Saravanan R, Asokan P, Sachidanandam M (2002) A multi-objective genetic algorithm (GA) approach for optimization of surface grinding operations. Int J Mach Tools Manuf 42(12):1327–1334
257. Saravanan R, Sankar RS, Asokan P, Vijayakumar K, Prabhaharan G (2005) Optimization of cutting conditions during continuous finished profile machining using non-traditional techniques. Int J Adv Manuf Technol 26(1–2):30–40
258. Sardiñas RQ, Reis P, Davim JP (2006a) Multi-objective optimization of cutting parameters for drilling laminate composite materials by using genetic algorithms. Compos Sci Technol 66(15):3083–3088
259. Sardiñas RQ, Santana MR, Brindis EAA (2006b) Genetic algorithm-based multi-objective optimization of cutting parameters in turning processes. Eng Appl Artif Intell 19(2):127–133
260. Sathyanarayanan G, Lin IJ, Chen MK (1992) Neural network modeling and multiobjective optimization of creep feed grinding of superalloys. Int J Prod Res 30(10):2421–2438
261. Satishkumar S, Asokan P, Kumanan S (2006) Optimization of depth of cut in multi-pass turning using nontraditional optimization techniques. Int J Adv Manuf Technol 29(3–4):230–238
262. Savas V, Ozay C (2008) The optimization of the surface roughness in the process of tangential turn-milling using genetic algorithm. Int J Adv Manuf Technol 37(3–4):335–340
263. Sedighi M, Afshari D (2009) Creep feed grinding optimization by an integrated GA-NN system. J Intell Manuf. doi:10.1007/s10845-009-0243-4
264. Shaji S, Radhakrishnan V (2003) Analysis of process parameters in surface grinding with graphite as lubricant based on the Taguchi method. J Mater Process Technol 141(1):51–59
265. Sharma VS, Dhiman S, Sehgal R, Sharma SK (2008) Estimation of cutting forces and surface roughness for hard turning using neural networks. Int J Adv Manuf Technol 19(4):473–483
266. Sheng Y, Tomizuka M (2006) Intelligent modeling of thrust force in drilling process. J Dyn Syst Meas Control 128(4):846–856
267. Shin YC, Joo YS (1992) Optimization of machining conditions with practical constraints. Int J Prod Res 30(12):2907–2919

268. Shiou FJ, Chen CH (2003) Freeform surface finish of plastic injection mold by using ball-burnishing process. J Mater Process Technol 140(1–3):248–254
269. Shiou FJ, Cheng CH (2008) Ultra-precision surface finish of NAK80 mould tool steel using sequential ball burnishing and ball polishing processes. J Mater Process Technol 201(1–3):554–559
270. Shiou FJ, Ciou HS (2008) Ultra-precision surface finish of the hardened stainless mold steel using vibration-assisted ball polishing process. Int J Mach Tools Manuf 48(7–8):721–732
271. Shiou FJ, Hsu CC (2008) Surface finishing of hardened and tempered stainless tool steel using sequential ball grinding, ball burnishing and ball polishing processes on a machining centre. J Mater Process Technol 205(1–3):249–258
272. Shunmugam MS, Reddy SVB, Narendran AA (2000a) Selection of optimal conditions in multi-pass face-milling using a genetic algorithm. Int J Mach Tools Manuf 40:401–414
273. Shunmugam MS, Reddy SVB, Narendran TT (2000b) Optimal selection of parameters in multi-tool drilling. J Mater Process Technol 103(2):318–323
274. Sick B (2002) On-line and indirect tool wear monitoring in turning with artificial neural net works: a review of more than a decade of research. Mech Syst Signal Process 16(4):487–546
275. Siddiquee AN, Khan ZA, Mallick Z (2010) Grey relational analysis coupled with principal component analysis for optimization design of the process parameters in in-feed centreless cylindrical grinding. Int J Adv Manuf Technol 46(9–12):983–992
276. Singh I, Bhatnagar N, Viswanath P (2008) Drilling of uni-directional glass fiber reinforced plastics: experimental and finite element study. Mater Des 29(2):546–553
277. Sonar DK, Dixit US, Ojha DK (2006) The application of radial basis function neural network for predicting the surface roughness in a turning process. Int J Adv Manuf Technol 27(7–8):661–666
278. Sonmez AI, Baykasoglu A, Dereli T, Filiz IH (1999) Dynamic optimization of multipass milling operations via geometric programming. Int J Mach Tools Manuf 39:297–332
279. Soodamani R, Liu ZQ (2000) GA-based learning for a model-based object recognition system. Int J Approx Reas 23(2):85–109
280. Sreeram S, Kumar AS, Rahman M, Zaman MT (2006) Optimization of cutting parameters in micro end milling operations in dry cutting condition using genetic algorithms. Int J Adv Manuf Technol 30(11–12):1030–1039
281. Srinivas J, Giri R, Yang SH (2009) Optimization of multi-pass turning using particle swarm intelligence. Int J Adv Manuf Technol 40(1–2):56–66
282. Stępień P (2009) A probabilistic model of the grinding process. Appl Math Modell 33(10):3863–3884
283. Stone R, Krishnamurthy K (1996) A neural network thrust force controller to minimize delaminating during drilling of graphite—epoxy laminates. Int J Mach Tools Manuf 36:985–1003
284. Suresh PVS, Rao PV, Deshmukh SG (2002) A genetic algorithmic approach for optimization of surface roughness prediction model. Int J Mach Tools Manuf 42(6):675–680
285. Tan FP, Creese RC (1995) A generalized multi-pass machining model for machining parameter selection in turning. Int J Prod Res 33(5):1467–1487
286. Tandon V, El-Mounayri H, Kishawy H (2002) NC end milling optimization using evolutionary computation. Int J Mach Tools Manuf 42(5):595–605
287. Tang Y (2006) Optimization strategy in end milling process for high speed machining of hardened die/mold steel. J Univ Sci Technol Beijing Miner Metall Mater 13(3):240–243
288. Tolouei-Rad M, Bidhendi IM (1997) On the optimization of machining parameters for milling operations. Int J Mach Tools Manuf 37:1–16
289. Tönshoff HK, Peters J, Inasaki I, Paul T (1992) Modeling and simulation of grinding processes. CIRP Ann Manuf Technol 41(2):677–688
290. Totis G (2009) RCPM: a new method for robust chatter prediction in milling. Int J Mach Tools Manuf 49(3–4):273–284

291. Trmal GJ, Zhu CB, Midha PS (1992) An expert system for grinding process optimization. J Mater Process Technol 33(4):507–517
292. Tsao CC (2007) Taguchi analysis of drilling quality associated with core drill in drilling of composite material. Int J Adv Manuf Technol 32(9–10):877–884
293. Tsao CC, Hocheng H (2004) Taguchi analysis of delamination associated with various drill bits in drilling of composite material. Int J Mach Tools Manuf 44(10):1085–1090
294. Tsao CC, Hocheng H (2008) Evaluation of thrust force and surface roughness in drilling composite material using Taguchi analysis and neural network. J Mater Process Technol 203(1–3):342–348
295. Tzeng YF (2006) Parameter design optimization of computerised numerical control turning tool steels for high dimensional precision and accuracy. Mater Des 27(8):665–675
296. Tzeng CJ, Lin YH, Yang YK, Jeng MC (2009) Optimization of turning operations with multiple performance characteristics using the Taguchi method and Grey relational analysis. J Mater Process Technol 209(6):2753–2759
297. Umbrello D, Ambrogio G, Filice L, Shivpuri R (2008) A hybrid finite element method: artificial neural network approach for predicting residual stresses and the optimal cutting conditions during hard turning of AISI 52100 bearing steel. Mater Des 29(4):873–883
298. Uros Z, Franc C, Edi K (2009) Adaptive network based inference system for estimation of flank wear in end-milling. J Mater Process Technol 209(3):1504–1511
299. Varghese B, Malkin S (1998) Experimental investigation of methods to enhance stock removal for superfinishing. CIRP Ann Manuf Technol 47(1):231–234
300. Varghese B, Malkin S (2000) Selection of optimal superfinishing parameters. J Manuf Process 2(2):124–130
301. Venk S, Govind R, Merchant ME (1990) An expert system approach to optimization of the centerless grinding process. CIRP Ann Manuf Technol 39(1):489–492
302. Vijayakumar K, Prabhaharan G, Asokan P, Saravanan R (2003) Optimization of multi-pass turning operations using ant colony system. Int J Mach Tools Manuf 43(15):1633–1639
303. Vinolas J, Biera J, Nieto J, Llorente JI, Vigneau J (1997) the use of an efficient and intuitive tool for the dynamic modeling of grinding processes. CIRP Ann Manuf Technol 46(1):239–242
304. Wan M, Zhang WH, Tan G, Qin GH (2008) Systematic simulation procedure of peripheral milling process of thin-walled workpiece. J Mater Process Technol 197(1–3):122–131
305. Wang J (1993) Multiple objective optimization of machining operations based on neural networks. Int J Adv Manuf Technol 8:235–243
306. Wang J (1998) Computer-aided economic optimization of end-milling operations. Int J Prod Econ 54(3):307–320
307. Wang YC (2007) A note on 'optimization of multi-pass turning operations using ant colony system'. Int J Mach Tools Manuf 47(12–13):2057–2059
308. Wang DX, Zuo MJ, Qi KZ, Liang M (1996) Online tool adjustment with adaptive tool wear function identification. Int J Prod Res 34(9):2499–2515
309. Wang J, Zhang B, Xue B (2000) Computer-controlled lapping system for granite surface plates. J Manuf Syst 19(3):149–155
310. Wang X, Da ZJ, Balaji AK, Jawahir IS (2002) Performance-based optimal selection of cutting conditions and cutting tools in multi-pass turning operations using genetic algorithms. Int J Prod Res 40(9):2053–2065
311. Wang ZG, Rahman M, Wong YS, Sun J (2005) Optimization of multi-pass milling using parallel genetic algorithm and parallel genetic simulated annealing. Int J Mach Tools Manuf 45:1726–1734
312. Wang X, Da ZJ, Balaji AK, Jawahir IS (2007) Performance-based predictive models and optimization methods for turning operations and applications: part 3-optimum cutting conditions and selection of cutting tools. J Manuf Processes 9(1):61–74
313. Wei ZC, Wang MJ, Ma RG, Wang L (2010) Modeling of process geometry in peripheral milling of curved surfaces. J Mater Process Technol 210(5):799–806

314. Weinert K, Blum H, Jansen T, Rademacher A (2007) Simulation based optimization of the NC-shape grinding process with toroid grinding wheels. Prod Eng 1(3):245–252
315. Wen XM, Tay AAO, Nee AYC (1992) Micro-computer-based optimization of the surface grinding process. J Mater Process Technol 29(1–3):75–90
316. Xiao G, Malkin S (1996) On-line optimization for internal plunge grinding. CIRP Ann Manuf Technol 45(1):287–292
317. Xu W, Wu Y, Sato T, Lin W (2010) Effects of process parameters on workpiece roundness in tangential-feed centerless grinding using a surface grinder. J Mater Process Technol 210(5):759–766
318. Yang WH, Tarng YS (1998) Design optimization of cutting parameters for turning operations based on the Taguchi method. J Mater Process Technol 84:122–129
319. Yang YK, Chuang MT, Lin SS (2009) Optimization of dry machining parameters for high-purity graphite in end milling process via design of experiments methods. J Mater Process Technol 209(9):4395–4400
320. Yao Y, Zhao H, Li J, Yuan Z (2006) Modeling of virtual workpiece with machining errors representation in turning. J Mater Process Technol 172(3):437–444
321. Yildiz AR (2009a) An effective hybrid immune-hill climbing optimization approach for solving design and manufacturing optimization problems in industry. J Mater Process Technol 209(6):2773–2780
322. Yildiz AR (2009b) A novel hybrid immune algorithm for optimization of machining parameters in milling operations. Robot Comput Integr Manuf 25(2):261–270
323. Yildiz AR, Ozturk F (2006) Hybrid enhanced genetic algorithm to select optimal machining parameters in turning operation. Proc Inst Mech Eng Part B J Eng Manuf 220(12): 2041–2053
324. Zarei O, Fesanghary M, Farshi B, Saffar RJ, Razfar MR (2009) Optimization of multipass face-milling via harmony search algorithm. J Mater Process Technol 209:2386–2392
325. Zhang JZ, Chen JC (2009) Surface roughness optimization in a drilling operation using the taguchi design method. Mater Manuf Processes 24(4):459–467
326. Zhang LB, Wang LJ, Liu XY, Zhao HW, Wang X, Luo HY (2001) Mechanical model for predicting thrust and torque in vibration drilling fibre-reinforced composite materials. Int J Mach Tools Manuf 41(5):641–657
327. Zhang C, Rentsch R, Brinksmeier E (2005) Advances in micro ultrasonic assisted lapping of microstructures in hard–brittle materials: a brief review and outlook. Int J Mach Tools Manuf 45(7–8):881–890
328. Zheng HQ, Li XP, Wong YS, Nee AYC (1999) Theoretical modeling and simulation of cutting forces in face milling with cutter runout. Int J Mach Tools Manuf 39(12):2003–2018
329. Zhu GY, Zhang WB (2008) Drilling path optimization by the particle swarm optimization algorithm with global convergence characteristics. Int J Prod Res 46:2299–2311
330. Zhu CB, Midha PS, Trmal GJ (1993) A dynamic modeling approach to computer aided optimum selection of grinding parameters. J Mater Process Technol 38(1–2):227–245
331. Zolgharni M, Jones BJ, Bulpett R, Anson AW, Fanks J (2008) Energy efficiency improvements in dry drilling with optimised diamond-like carbon coatings. Diam Rel Mater 17(7–10):1733–1737
332. Zuperl U, Cus F (2003) Optimization of cutting conditions during cutting by using neural networks. Robot Comput Integr Manuf 19(1–2):189–199

Chapter 3
Modeling and Optimization of Modern Machining Processes

3.1 Modern Machining Processes

Traditional machining processes, such as turning, grinding, drilling, milling, etc., remove material by chip formation, abrasion, or micro-chipping. There are situations, however, where these processes are not satisfactory, economical, or even possible, for the following reasons [114]:

1. The hardness and strength of the material is very high (typically above 400 HB) or the material is too brittle.
2. The work piece is too flexible, slender, or delicate to withstand the cutting or grinding forces, or the parts are too difficult to fix.
3. The shape of the part is complex.
4. Surface finish and dimensional tolerance requirements are more rigorous than those obtained by other processes.
5. Temperature rise and residual stresses in the work piece are not desirable or acceptable.

These requirements have led to the development of modern machining processes. Beginning in the 1940s, these advanced methods are called non-traditional or modern or unconventional machining processes. Over the last four decades, there has been a large increase in the number of non-traditional machining processes (NTMPs). Today, NTMPs with vastly different capabilities and specifications are available for a wide range of applications. According to nature of energy employed in machining, NTMPs are further classified into the following groups:

1. Mechanical processes such as ultrasonic machining, abrasive jet machining (AJM), water jet machining (WJM), abrasive water jet machining (AWJM), etc.
2. Chemical and electrochemical processes such as electro-chemical machining (ECM), electro-chemical grinding, electro-chemical honing, etc.

R. V. Rao, *Advanced Modeling and Optimization of Manufacturing Processes*, Springer Series in Advanced Manufacturing, DOI: 10.1007/978-0-85729-015-1_3,

3. Thermal and electro thermal processes such as electric discharge machining, laser beam machining (LBM), plasma arc machining, ion beam machining, etc.
4. Finishing processes such as abrasive flow machining, magnetic abrasive finishing, etc.

The modeling and optimization aspects of some of the above modern machining processes are described in this chapter.

3.2 AWJM Process

AWJM process uses a high velocity water jet in combination with abrasive particles for cutting different types of materials using a setup as shown in Fig. 3.1. A stream of small abrasive particles is introduced and entrained in the water jet in such a manner that water jet's momentum is partly transferred to the abrasive particles. The process thus combines the benefit of the two other advanced

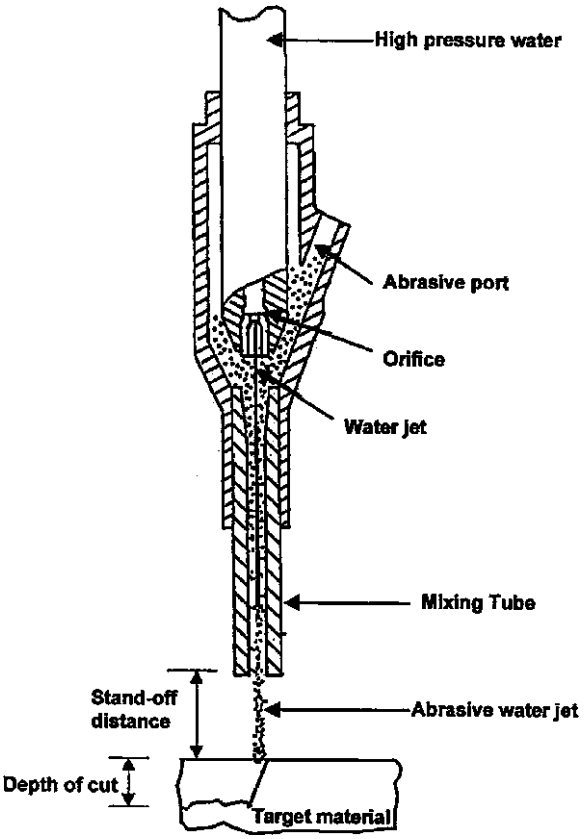

Fig. 3.1 General scheme of abrasive water jet machining (AWJM) process (from [100]; reprinted with permission from Elsevier)

machining processes namely, WJM and AJM. This process relies on erosive action of an abrasive laden water jet for applications of cutting, drilling, and general cleaning and descaling of thick sections of very soft to very hard materials at high rates. Visual examination of the cutting process in AWJM suggests two dominant modes of material removal. First is erosion by cutting wear due to particle impact at shallow angles on the top surface of the kerf. Second is deformation wear due to excessive plastic deformation caused by particle impact at large angles, deeper into the kerf.

A variety of materials can be machined by AWJM including copper and its alloys, aluminum, lead, steel, tungsten carbide, titanium, ceramics, composites, acrylic, concrete, rocks, graphite, silica glass, etc. Its most promising application includes machining of sandwiched honeycomb structural materials frequently used in the aerospace industries. The main advantages of the process include omni-directional cutting, minimal thermal damage, no burrs, high cutting speed and efficiency, suitability for automation, and cutting without delamination.

Comprehensive qualitative and quantitative analyses of the material removal mechanism and subsequently the development of analytical models of material removal are necessary for a better understanding and to achieve the optimum process performance. Several attempts were made to study the influence of different process parameters on the important performance measures of AWJM process. Hashish [82] used erosion model of Finnie [70] to develop a model to predict combined depth of cut due to deformation wear and cutting wear. However, the use of this model is limited to brittle materials only and it does not include the effect of particle size and shape. To overcome these limitations, Hashish [81] developed an improved erosion model.

Hocheng and Chang [89] discussed the kerf formation of a ceramic plate cut by an abrasive water jet (AWJ). The mechanism and the effectiveness of material removal were studied and different materials were found to possess different removal rates in machining and there also existed a critical combination of hydraulic pressure, abrasive flow rate and traverse speed, below which through-cut for a certain thickness could not be achieved. The wall finish achieved was determined by the mesh size of the abrasives.

Kovacevic and Fang [123] showed that the selection of the AWJ cutting parameters for a required depth of cut in the given material can be effectively done by applying the principles of the fuzzy set theory. This approach eliminates the need for extensive experimental work in order to select the magnitudes of the most influential AWJ parameters on the depth of cut. A number of case studies were performed to verify the validity of the proposed methodology for selecting the AWJ cutting parameters in order to achieve the predetermined depth of cut.

Chen et al. [43] developed experimental techniques based on statistical experimental design principles and theoretical investigations were conducted to study AWJM cutting of alumina-based ceramics. Semi-empirical cutting depth equations were determined for the prediction and optimization of the AWJM cutting performance. Kovacevic et al. [124] reviewed the state of the art of research and development in AWJM. Hoogstrate et al. [91] described the

developments in equipment and process models which make it possible to exploit the advantages of AWJ technology completely, thereby eliminating or minimizing the disadvantages.

Arola and Ramulu [9] conducted an experimental study to determine the influence of material properties on the surface integrity and texture that result from AWJ machining of metals. A microstructure analysis, micro-hardness measurements, and profilometry were used in determining the depth of plastic deformation and surface texture that result from material removal. Models available for dry abrasive erosion were adopted and found useful in understanding the influence of material properties on the hydrodynamic erosion process. It was found that the depth of subsurface plastic deformation is inversely proportional to a metals strength coefficient and extends the greatest depth near jet entry in the initial damage region. Choi and Choi [48] developed an analytical model to predict volume of material removed by single abrasive particle and thickness of the fracture developed backside of the target material.

Based on Hashish's [81] improved erosion model, Paul et al. [180] developed analytical model of generalized kerf shape for ductile materials considering variation in kerf width along its depth. A mathematical model for total depth of cut for polycrystalline materials accounting for the effects of abrasive particle size and shape was further developed by Paul et al. [180]. However, this model is for brittle materials only and it can cause an error of up to 20% in predicting the depth of cut. Chen et al. [41] conducted experiments based on statistical design principles to study AWJ machining of ceramics. The research work, involving multi-directional cutting, was conducted to examine the effect of jet impact angles on cutting quality. Furthermore, new cutting head oscillation techniques were applied for better cutting.

Hassan and Kosmol [83] presented a model of AWJM using the finite element method (FEM) in order to explain the abrasive particle–workpiece interaction process. Also, the model predicts the depth of deformation as a result of abrasive particle impact. The main objective was to develop an FE model which would enable the prediction of the depth of cut without any cutting experiments. The new model takes into account the precise representation of the constitutive behavior of the workpiece material under AWJ dynamic loading conditions. Forces acting on the abrasive particle were automatically calculated at each time step. The results showed that plastic deformation was highly localized.

Vikram and Babu [240] proposed a new approach for modeling the three-dimensional (3D) topography produced on AWJ machined surface. It makes use of the trajectory of jet, predicted from the theory of ballistics and Bitter's theory of erosion for material removal, for numerically simulating the cutting front. The 2D topography at different depths of the cut surface was generated by considering the trajectories on the cutting front and the abrasive particles impacting the walls of cut surface randomly. For realistic generation of topography on cut surfaces, several instantaneous profiles generated in each region of cut were superimposed to obtain an effective profile. The nature of effective profiles thus predicted was analyzed and validated using power spectral density analysis. The effective

profiles predicted at different depths were, in turn, used to generate the 3D topography of AWJ machined surface. Results obtained with the proposed model were validated with the experimental results.

Hoogstrate et al. [90] described the development of a 'coherent set of models' for a category of these processes, namely those which use high velocity of the particles to obtain the necessary energy to machine a workpiece surface. The usability of this 'coherent set of models' was explained with its application in the field of high-pressure AWJ cutting. A forecast to the application of this modeling technique to other loose abrasive machining processes as micro-abrasive air jet machining was given. Wang and Guo [243] developed a semi-empirical model for predicting the depth of jet penetration in AWJ machining of polymer matrix composites. The plausibility of the model was then assessed by analyzing the predicted trends of this performance measure and by comparing with the experimental results. It is shown that the model gives adequate predictions and can be used for process planning.

Deam et al. [54] developed a model for predicting the shape of the cut profile in industrial cutting processes and applied to AWJM. The well-known physics of abrasive wear was used in the process model, which was cast in intrinsic coordinates. This choice of coordinates enabled a formulation of the problem that led to simple solutions and also a good understanding of the process. Akkurt et al. [3] explained the effects of feed rate and thickness of workpiece on the roughness. Considering experimental data, effects of the composition of the material on surface roughness were assessed. The authors had evaluated the deformation effect of AWJ on workpieces that have the same composition but different thickness. In the study pure aluminum, Al-6061 aluminum alloy, brass-353 ($\alpha + \beta$ brass), AISI 1030 and AISI 304 steel materials were cut with AWJ at different feed rates. Improvement in surface roughness of pure aluminum remains in narrow limited range when compared with the ratio of decrease in feed rate. Brass and AISI 1030 materials that have higher strength than aluminum resulted in higher surface roughness for thinner workpieces. Reducing feed rate from 25 to 20 mm/min deteriorated the surface properties of 20 mm thickness workpiece of AISI 304, in contrast to all of the other studied 20 mm thickness materials.

Liu et al. [148] developed computational fluid dynamics (CFD) models for ultrahigh velocity water jets and AWJs using the Fluent6 flow solver. Jet dynamic characteristics for the flow downstream from a very fine nozzle were then simulated under steady state, turbulent, two-phase and three-phase flow conditions. Water and particle velocities in a jet were obtained under different input and boundary conditions to provide an insight into the jet characteristics and a fundamental understanding of the kerf formation process in AWJ cutting. For the range of downstream distances considered, the results indicate that a jet is characterized by an initial rapid decay of the axial velocity at the jet centre while the cross-sectional flow evolves toward a top-hat profile downstream.

Eltobgy et al. [68] developed a modified form of Finnie's model for erosion for application to AWJM. This modified form was able to deal with curved

surfaces rather than flat surfaces only. Furthermore, the new modeling approach was capable of simulating multiple particle erosion. This approach used standard material properties and required no calibration constants. The modelled results agreed well with both experimental and analytical data. Shanmugam and Masood [216] presented an investigation on the kerf taper angle, an important cutting performance measure, generated by AWJM to machine two types of composites: epoxy pre-impregnated graphite woven fabric and glass epoxy. Comprehensive factorial DOE was carried out in varying the traverse speed, abrasive flow rate, standoff distance and water pressure. Using the dimensional technique and adopting the energy conservation approach, the kerf taper angle was related to the operating parameters in the form of a predictive model.

Ma and Deam [152] measured the kerf geometry using an optical microscope. Using these measurements, a simple empirical correlation for the kerf profile shape under different traverse speed was developed that fits the kerf shape well. The mechanisms underlying the formation the kerf profile were discussed and the optimum speed for achieving the straightest cutting edge was presented. Junkar et al. [107] presented an explicit finite element analysis (FEA) of a single abrasive particle impact on stainless steel 1.4301 (AISI 304) in AWJ machining. In the experimental verification, the shapes of craters on the workpiece material were observed and compared with FEA simulation results by means of crater sphericity. The influences of the impact angle and particle velocity were observed. Especially the impact angle emerged as a very suitable process parameter for experimental verification of FEA simulation, where crater sphericity was observed. Results of the FEA simulation were in good agreement with those obtained from the experimental verification.

Jegaraj and Babu [106] reported the experimental studies carried out to investigate the influence of orifice and focusing tube bore variation on the performance of AWJs in cutting 6063-T6 aluminum alloy. The performance was assessed in terms of different parameters such as depth of cut, kerf width and surface roughness. This study made use of Taguchi's DOE and analysis of variance (ANOVA) to analyze the performance of AWJM. These experimental data were used to build empirical models. An hybrid strategy combining the response equations of the empirical model with fuzzy model was proposed to arrive at suitable set of process parameters for achieving desired cutting performance considering the variation in orifice and focusing tube bore.

Wang [242] presented a study of the depth of jet penetration (or depth of cut) in AWJ machining of alumina ceramics with controlled nozzle oscillation. An experimental investigation was carried out first to study the effects of nozzle oscillation at small angles on the depth of cut under different combinations of process parameters. Based on the test conditions, it was found that nozzle oscillation at small angles can improve the depth of cut by as much as 82% if the cutting parameters are correctly selected. Depending on the other cutting parameters, it was found that a high oscillation frequency (10–14 Hz) with a low oscillation angle (4°–6°) can maximize the depth of cut. Using a dimensional analysis technique, predictive models for jet penetration when cutting alumina

ceramics with and without nozzle oscillation were developed and verified. Khan and Haque [116] presented a comparative analysis of the performance of garnet, aluminum oxide and silicon oxide during AWJM of glass. The study showed that width of cut increases as the stand-off distance of the nozzle from the work is increased which is due to divergence shape of the AWJ.

Srinivasu and Babu [230] presented a neuro-genetic approach to suggest the process parameters for maintaining the desired depth of cut in AWJ machining by considering the change in diameter of focusing nozzle, i.e., for adaptive control of AWJ machining process. An artificial neural network (ANN)-based model was developed for prediction of depth of cut by considering the diameter of focusing nozzle along with the controllable process parameters such as water pressure, abrasive flow rate and jet traverse rate. ANN model combined with genetic algorithm (GA), i.e., neuro-genetic approach, was proposed to suggest the process parameters. Further, the merits of the proposed approach were shown by comparing the results obtained with the proposed approach to the results obtained with fuzzy-genetic approach [37]. Finally, the effectiveness of the proposed approach was assessed by conducting the experiments with the suggested process parameters and comparing them with the desired results.

Zaki et al. [260] provided a careful validation for the simulation of an impinging abrasive liquid jet, taking progressively into account the necessary features: impingement, free-surface, and particles. Orbanic and Junkar [175] studied the macro-mechanism of AWJM from the point of cutting front and striation formation analysis. The striation on the surface cut with AWJM is a characteristic phenomenon which is strongly present when cutting with high traverse velocities for particular material type and thickness of workpiece. The connection between the cutting front step formation and striation formation was explained through series of experiments, which included visual observations of cutting transparent material and through analogies, which deal with river meandering and wear of pneumatic conveyor bends.

Azmir and Ahsan [13] conducted experimental investigations to assess the influence of AWJM process parameters on surface roughness (R_a) of glass fiber reinforced epoxy composites. The approach was based on Taguchi's method and analysis of variance (ANOVA) to optimize the AWJM process parameters for effective machining. It was found that the type of abrasive materials, hydraulic pressure, standoff distance and traverse rate were the significant control factors and the cutting orientation was the insignificant control factor in controlling the R_a. For noise factors effect, the forms of glass fibers and thickness of composite laminate showed the greatest influence on R_a. A mathematical model was developed using piecewise linear regression analysis to predict the performance of R_a in terms of the cutting parameters of AWJM. The models successfully predicted the R_a of an AWJ machined glass/epoxy laminate within the limit of this study. It was confirmed that the determined optimum combination of AWJM parameters satisfy the real need for machining of glass fiber reinforced epoxy composites in practice. In another work, Azmir and Ahsan [12] studied surface roughness (R_a) and kerf taper ratio (T_R) characteristics of an AWJ machined surfaces of glass/epoxy

composite laminate. Taguchi's DOE and analysis of variance were used to determine the effect of machining parameters on R_a and T_R. Hydraulic pressure and type of abrasive materials were considered as the most significant control factor in influencing R_a and T_R, respectively. Due to hardness of aluminum oxide type of abrasive materials, it performed better than garnet in terms of both machining characteristics. Increasing the hydraulic pressure and abrasive mass flow rate resulted in a better machining performance for both criteria. Meanwhile, decreasing the standoff distance and traverse rate improved both criteria of machining performance. Cutting orientation did not influence the machining performance in both cases. So, it was confirmed that increasing the kinetic energy of AWJM process may produce better quality of cuts.

Manu and Babu [159] presented a model of the AWJ turning process considering material removal from the circumference of a rotating cylindrical specimen. The methodology involved the use of Finnie's theory of erosion to estimate the volume of material removed by the impacting abrasive particles. The model considered the impact of jet at an angle to the workpiece surface to account for the curvature of the workpiece. Unlike earlier works, this model considered the continuous change in local impact angle caused by the change in workpiece diameter. The flow stress of the workpiece material was determined using a novel experiment involving the same abrasive and workpiece materials. The adequacy of the proposed model was examined through AWJ turning tests under various process parameter combinations. The final diameters predicted by the model were found to be in good agreement with the experimental results.

Hlaváč [87] performed both the theoretical and the experimental works to verify and specify the physical relationships among parameters of AWJs used for cutting, the properties of cut materials and the output parameters of cutting, usually the depth of the cut. The new part of the model was designed to enable the calculation of the angle of the cutting head tilt so that the jet penetrating the material might exit it approximately along the normal to the material surface created at the point of jet axis entry. This model was experimentally verified and its high reliability and applicability were confirmed on quasi-homogeneous materials.

Srinivasu et al. [229] proposed AWJM as the ideal processing technique for structural ceramics. 3D shapes can be generated by enveloping them with successions of jet footprints (kerf geometries) generated by varying the process operating parameters. To enable this, the authors had investigated the influence of key kinematic operating parameters (i.e., jet impingement angle and jet feed rate) on the kerf geometry and its dimensional characteristics. Furthermore, the kerf generation mechanism under multi-pass jet erosion was analyzed to get control over erosion depth in multi-pass machining. It was found that by varying jet impingement angle (90°–40°), the symmetric/asymmetric kerf geometry was intimately dependent on the variation of standoff distance (SOD), abrasive particle velocity distributions and their local impact angles accounted across the jet footprint. Variation in jet feed rate influenced the exposure time of material to jet and enhanced the erosion capability of abrasives impacting at shallow angles.

Furthermore, at lower jet feed rates, the depth of erosion increased and the low energy abrasive particles along trailing edge of jet plume got enough time to erode the material that resulted in variation of slope of kerf walls and hence, overall geometry. Based on these observations, the multi-pass trials showed that the successive passes have to account for both the local impact angles of abrasive particles as well as the actual SOD (SOD + initial kerf depth). By understanding the influence of key kinematic operating parameters on the kerf geometry and its dimensional characteristics, the authors had established a good basis for developing strategies for controlled 3D AWJ machining of complex shapes.

Although AWJM has been employed in different setups (e.g., through cutting, milling, turning and cleaning) to generate surfaces in various workpiece materials (e.g., metallic alloys, ceramics and composites), up to now there is scarce information on the use of this technology in cutting super-hard materials such as diamond-based materials. Axinte et al. [11] reported on a preliminary study of the capability of AWJ cutting of polycrystalline diamond (PCD) using abrasive media with different hardness, i.e., aluminum oxide (Al_2O_3), silicon carbide (SiC) and diamond. While keeping some operating parameters constant (pump pressure, stand-off distance and size of abrasives), the feed was adjusted to enable full jet penetration for each type of abrasives. It was found that not only the material removal rates (MRR) vary significantly with the employment of different types of abrasives but also the nozzle wear ratios, with further implications on the kerf quality (width, taper angle) of diamond cut surfaces. Furthermore, in-depth studies of the cut surfaces helped to reveal the material removal mechanism when different types of abrasives were employed: Al_2O_3—low intensity erosion; SiC—medium erosion with undesired cracking; diamond—high intensity erosion. The experimental results showed that while Al_2O_3 and SiC abrasive media yield modest MRR (comparable with those obtained by electro-discharge machining-EDM), the use of diamond abrasives can greatly increase (>200 times) the productivity of AWJ through cutting of PCD test pieces at acceptable roughness ($R_a < 1.6$ μm) and integrity (i.e., crack-free) of the cut surfaces.

Wang and Wang [245] conducted a theoretical analysis to develop a flow model for the AWJ. The main concern was whether the abrasive particles could be treated as a pseudo-fluid phase. A two-fluid model was developed based on the fundamental laws of conservation. A control volume method was used to discretize the equations, and a phase-coupled SIMPLE algorithm was adopted to solve the pressure–velocity coupling equations. The quasi 2D flow field outside a conventional nozzle used in AWJ was analyzed and computed to validate the model.

Mostofa et al. [170] presented CFD and theoretical analyses to optimize the mixing of components by the multi-phase approach. Water, air, and abrasives were mixed in a mixing chamber. This modeling was used to predict the influence of air and abrasives on the mixing at different distances within the mixing tube. At the same time, particle tracking was conducted to monitor the erosion rate density at the nozzle wall. Results showed that nozzle length has

an effect on the mixing of water, air, and the abrasives, and that the velocity of the water jet influences the erosion rate at the nozzle wall. The $k - \varepsilon$ turbulence model was used for simulation of the abrasive coupled with air. This investigation revealed that the erosion in the nozzle body is higher at the initial zone and that as the length of the nozzle length increases, the volume fraction of air increases accordingly.

Very few efforts were made for optimization of process parameters of AWJM process parameters. Chakravarthy and Babu [38] considered three decision variables namely, water jet pressure, jet traverse feed, and abrasive flow rate to achieve two conflicting objectives, i.e., maximization of production rate and minimization of abrasive consumption. These two objectives were combined in a single objective as a total of machining cost by assigning suitable weightages to each of the objective. Genetic algorithm was used as a tool for optimization. However, the authors had not considered any constraint and no bounds for variables were specified. To overcome above limitations, Jain et al. [102] used genetic algorithm as a tool for optimization of five process parameters of AWJM process namely, water jet pressure at the nozzle exit (P_w), diameter of AWJ nozzle (d_{awn}), feed rate of nozzle (f_n), mass flow rate of water (M_w), and mass flow rate of abrasives (M_a). The authors obtained optimum values of process parameters for maximum MRR with power consumption as a constraint. However, although GA has advantages over the traditional optimization techniques, the successful application of GA depends on the population size or the diversity of individual solutions in the search space. If GA cannot hold its diversity well before the global optimum is reached, it may prematurely converge to a local optimum. Hence, in this chapter an effort is made to verify if any improvement in the solution is possible by employing some other recent optimization techniques such as PSO and ABC algorithms to the same optimization model.

The optimization model for AWJM process is formulated in the present work based on the analysis given by Hashish [81]. The five decision variables considered for this model are: water jet pressure at the nozzle exit (P_w), diameter of AWJ nozzle (d_{awn}), feed rate of nozzle (f_n), mass flow rate of water (M_w) and mass flow rate of abrasives (M_a).

The objective is to maximize the MRR (Z_1), given by Eq. 3.1

$$\text{Maximize} \quad Z_1 = d_{awn} f_n (h_c + h_d), \tag{3.1}$$

where h_c is the indentation depth due to cutting wear as given by Eq. 3.2

$$\begin{aligned} h_c = &\left[1.028 \times 10^{4.5} \xi / C_k^{1/3} f_r^{0.4}\right] \left[d_{awn}^{0.2} M_a^{0.4} / f_n^{0.4}\right] \left[M_w P_w^{0.5} / (M_a + M_w)\right] \\ &- \left[18.48 K_a^{2/3} \xi^{1/3} / C_k^{1/3} f_r^{0.4}\right] \left[M_w P_w^{0.5} / (M_a + M_w)\right]; \quad \text{if } \alpha_t \le \alpha_0 \end{aligned} \tag{3.2}$$

$$h_c = 0, \quad \text{if } \alpha_t \le \alpha_0 \tag{3.3}$$

'h_d' is the indentation depth due to deformation wear as given by Eq. 3.4.

$$h_d = \left[\eta_a d_{awn} M_a \left(K_1 M_w P_w^{0.5} - (M_a + M_w) v_{ac}\right)^2\right] \Big/ \left\{\left[1,570.8 \sigma_{fw} d_{awn}^2 f_n (M_a + M_w)^2\right] + (K_1 C_{fw} \eta_a)\left(K_1 M_w P_w^{0.5} - (M_a + M_w) v_{ac}\right) M_a M_w P_w^{0.5}\right\} \quad (3.4)$$

$$\alpha_0 \sim \left[0.02164 C_k^{1/3} f_r^{0.4} / K_a^{2/3} \xi^{1/3}\right] \left[(M_a + M_w)/M_w P_w^{0.5}\right]^{1/3} (\text{degrees}) \quad (3.5)$$

$$\alpha_t \sim \left[0.389 \times 10^{-4.5} C_k \rho_a^{0.4} / \xi\right] \left[d_{awn}^{0.8} f_n^{0.4} (M_a + M_w)/M_a^{0.4} M_w P_w^{0.5}\right] (\text{degrees}) \quad (3.6)$$

$$v_{ac} = \left[5\pi^2 \sigma_{cw}^{2.5} / \rho_a^{0.5} \left((1 - V_a^2)\right)/E_{Ya} + \left((1 - V_w^2)/E_{Yw}\right)\right]^2 (\text{mm/s}) \quad (3.7)$$

$$K_1 = 1.414 \times 10^{4.5} \xi \quad (3.8)$$

$$C_k = \left[3,000 \sigma_{fw} f_r^{0.6} / \rho_a\right]^{1/2} (\text{mm/s}). \quad (3.9)$$

Values of the constants and parameters are given in Table 3.1.
The constraint on permissible value of surface roughness is given by Eq. 3.10.

$$1 - P_w M_w / P_{max} \geq 0. \quad (3.10)$$

The bounds for the five variables are given in Eqs. 3.11–3.15.

$$50 \leq P_w \leq 400 \, (\text{MPa}) \quad (3.11)$$

$$0.5 \leq d_{awn} \leq 5 \, (\text{mm}) \quad (3.12)$$

Table 3.1 Values of the constants and parameters (from [102]; reprinted with permission from Elsevier)

Notation	Description	Value (unit)
ρ_a	Density of abrasive particles	3.95×10^{-6} (kg/mm^3)
v_a	Poisson ratio of abrasive particles	0.25
E_{Ya}	Modulus of elasticity of abrasive particles	350,000 (MPa)
f_r	Roundness factor of abrasive particles	0.35
f_s	Sphericity factor of abrasive particles	0.78
η_a	Proportion of abrasive grains effectively participating in machining	0.70
v_w	Poisson ratio of work material	0.20
E_{Yw}	Modulus of elasticity of work material	114,000 (MPa)
σ_{ew}	Elastic limit of work material	883 (MPa)
σ_{fw}	Flow stress of work material	8,142 (MPa)
C_{fw}	Drag friction coefficient of work material	0.002
ξ	Mixing efficiency between abrasive and water	0.8
P_{max}	Allowable power consumption value	56 (kW)
K_a	Constant	3

$$0.2 \leq f_n \leq 25 \text{ (mm/s)} \tag{3.13}$$

$$0.02 \leq M_w \leq 0.2 \text{ (kg/s)} \tag{3.14}$$

$$0.0003 \leq M_w \leq 0.08 \text{ (kg/s)}. \tag{3.15}$$

An example is considered to demonstrate and validate the PSO and ABC algorithms for the optimization of process parameters of the AWJM process. The example is based on the model proposed by Hashish [81]. Specifications of the required parameters and values of the constants considered by Jain et al. [102], given in Table 3.1, are used in the present work.

Controlling parameters for ABC:

- Number of employed bees = 5.
- Number of onlookers bees = 11.
- Number of scout bees = 1.
- Maximum The number of iterations = 150.

Controlling parameters for PSO:

- Number of particles in swarm = 5.
- Inertia weight = 0.65.
- Acceleration coefficient (C_1) = 1.65.
- Acceleration coefficient (C_2) = 1.75.
- Number of iterations = 50.

The optimum selection of operating parameters of PSO algorithm like acceleration constants 'c_1' and 'c_2' as well as inertia coefficient 'w' is very essential for convergence of the algorithm. This can be achieved only when the condition given by Eq. 3.16 is satisfied [25].

$$w > 0.5(\phi_1 + \phi_2) - 1, \tag{3.16}$$

where

$$\phi_1 = c_1 r_1;\ \phi_2 = c_2 r_2.$$

As the feasible range for w is 0–1 and for c_1 and c_2 is 0–2, the selected values of w, c_1 and c_2 should be such that the Eq. 3.16 is satisfied for all possible values of random numbers r_1 and r_2 in the range 0–1. Keeping in view of this, considerable number of trials is conduced and the values of w, c_1 and c_2 are finally selected as 0.65, 1.65 and 1.75, respectively. Hence, the selected values of w, c_1 and c_2 in the present work are appropriate for convergence of the algorithm.

For the above parameter settings, the results of optimization are shown in Table 3.2.

It can be observed from Table 3.2 that PSO has given better results (i.e., maximum MRR) compared to GA and ABC algorithms. Optimality of the solution could be confirmed from the Figs. 3.2, 3.3, 3.4, 3.5, and 3.6. Figures 3.2 and 3.3 show the variation of MRR with diameter of AWJ nozzle and feed rate

Table 3.2 Results of optimization using various algorithms

Method	d_{awn} (mm)	f_n (mm/s)	M_w (kg/s)	P_w (MPa)	M_a (kg/s)	α_0 (deg)	α_t (deg)	h_c (deg)	h_d (mm)	MRR (mm^3/S)	Power (kW)
GA [102]	3.726	23.17	0.141	398.3	0.079	0.384	0.572	0.00	1.04	90.257	56
PSO	3.242	13.08	0.140	400	0.080	0.385	0.384	3.31	2.12	230.50	56
ABC	3.062	9.158	0.143	386	0.08	0.386	0.310	3.881	3.11	218.49	56

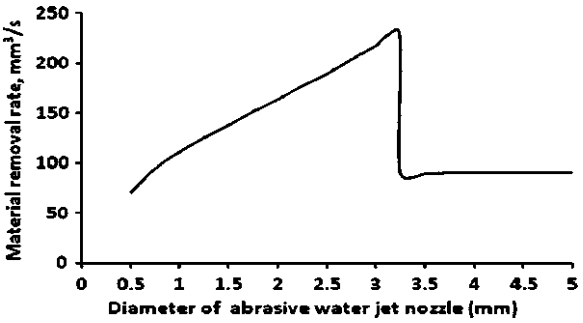

Fig. 3.2 Variation of material removal rate with diameter of abrasive water jet nozzle

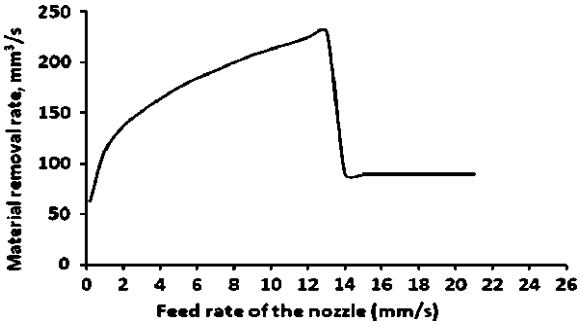

Fig. 3.3 Variation of material removal rate with feed rate of nozzle

of nozzle, respectively. Power consumption constraint is not shown in Fig. 3.2 as well as in Fig. 3.3, as it attains almost constant positive value for all values of 'd_{awn}' and 'f_n'. As shown in Figs. 3.2 and 3.3, the MRR increases with increase in diameter of AWJ nozzle and feed rate of nozzle up to a certain critical values of 3.242 mm and 13.084 mm/s, respectively. However, MRR drastically decreases after these critical values. This is due to fact that for any value higher than 3.242 mm and 13.084 mm/s for 'd_{awn}' and 'f_n', respectively, the angle of impingement at the top of the machined surface 'α_t' exceeds the critical impact angle 'α_0', thereby making the cutting wear 'h_c' = 0 as specified by condition given in Eq. 3.3. From this point of view, the selection of diameter of AWJ nozzle equal to 3.242 mm and feed rate of nozzle equal to 13.084 mm/s is appropriate.

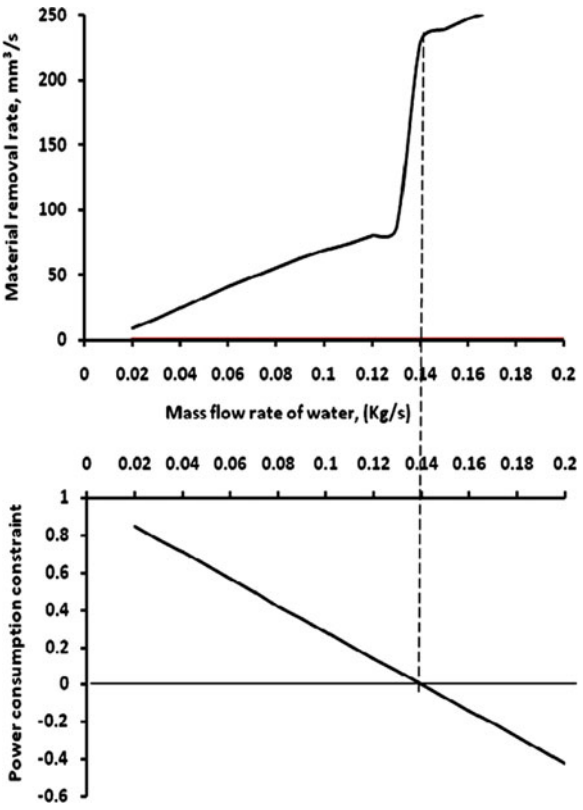

Fig. 3.4 Variation of material removal rate and power consumption constraint with M_w

Figure 3.4 shows the variation of MRR and power consumption constraint with mass flow rate of water. As shown in Fig. 3.4, the MRR initially increases gradually with increase in mass flow rate of water up to a critical value of 0.14 kg/s and thereafter the MRR suddenly increases as the condition specified by Eq. 3.2 is satisfied at this value. After this critical point, the MRR again increases gradually. From this point of view, higher value of mass flow rate of water is desired. However, as shown in Fig. 3.4, the constraint on power consumption is violated for any value of mass flow rate of water more than 0.14 kg/s. Hence, the optimum value of mass flow rate of water equal to 0.14 kg/s is appropriate.

Figures 3.5 and 3.6 show variation of MRR with water jet pressure at nozzle exit and mass flow rate of abrasives, respectively. As shown in Figs. 3.5 and 3.6, MRR increases with increase in both these variables. It is also observed that the critical point at which the condition specified by Eq. 3.2 is satisfied resulting into highest MRR occurs at upper bound values of both water jet pressure at nozzle exit and mass flow rate of abrasives. Therefore, selection of upper bound values equal to 400 MPa and 0.080 kg/s, respectively, of water jet pressure at nozzle exit and mass flow rate of abrasives are appropriate. Figure 3.7 shows the convergence of PSO algorithm.

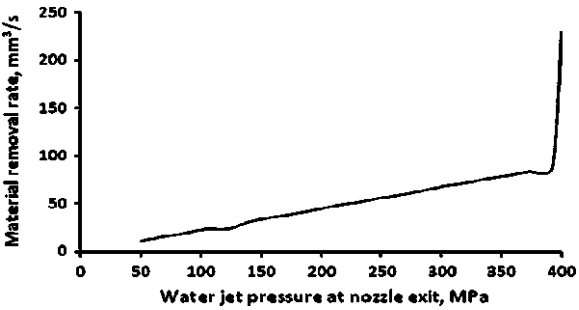

Fig. 3.5 Variation of material removal rate with water jet pressure at nozzle exit

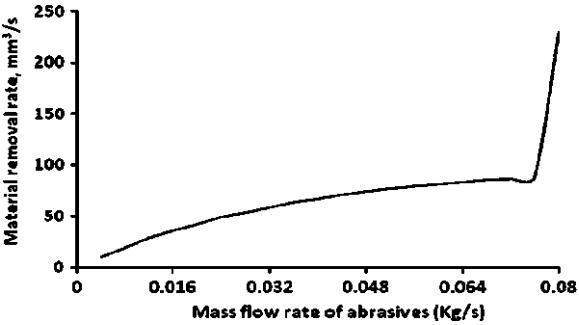

Fig. 3.6 Variation of material removal rate with mass flow rate of abrasives

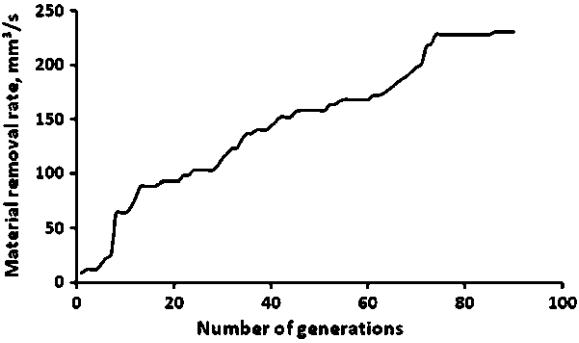

Fig. 3.7 Convergence of PSO algorithm

For AWJM, if angle of impingement at the top of the machined surface 'α_t' exceeds the critical impact angle 'α_0' then no material removal is assumed to occur by cutting wear ($h_c = 0$) and the material removal takes place only due to the deformation wear, resulting into relatively less MRR [180]. As shown in Table 3.2, for the solution obtained using genetic algorithm, as 'α_t' exceeds 'α_0', indentation depth of cutting wear (h_c) becomes zero and hence results in less MRR as compared to the solution obtained using particle swarm optimization (PSO) algorithm for which 'α_t' $<$ 'α_0'. The optimum values of process variables obtained using PSO algorithm also results in higher value of depth of deformation wear (h_d) than that obtained using genetic algorithm, which further increases the MRR. The combined effect thus leads to the improvement in objective function by about 155%.

3.3 Ultrasonic Machining Process

The use of new materials such as carbides, ceramics, nimonics, diamonds, etc., is increasing in industries such as aerospace, nuclear engineering, manufacturing and many others owing to their high strength to weight ratio, hardness and heat resistant qualities. In spite of recent technological advancements, the conventional machining processes such as turning, grinding, drilling, milling, etc., are inadequate to machine these materials from standpoint of economic production. Besides, machining of these materials into complex shapes is difficult, time consuming and sometimes impossible. Advanced machining processes have emerged to overcome these difficulties. Today, modern machining processes with vastly different capabilities and specifications are available for a wide range of applications.

Ultrasonic machining (USM) process is one of the modern machining processes. The term ultrasonic is used to describe the vibratory wave of frequency above that of upper frequency limit of the human ear. Ultrasonic machining is a process in which material is removed due to action of abrasive grains [113]. The abrasive particles are driven into the work surface by a tool oscillating normal to the work surface at a high frequency. The tool is shaped as the approximate mirror image of the configuration of cavity desired in workpiece. Figure 3.8 shows the general arrangement of ultrasonic machining process [100].

USM process can handle large variety of materials as it is not limited by the electrical or chemical characteristics of work material. The process has the

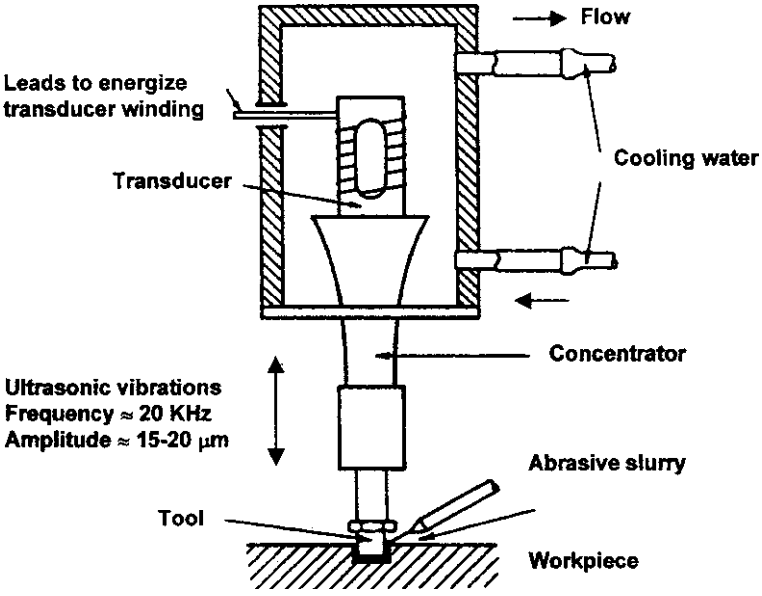

Fig. 3.8 Ultrasonic machining process (from [100]; reprinted with permission from Elsevier)

advantage of machining hard and brittle materials into complex shapes with good accuracy and reasonable surface finish. Considerable economy results from the ultrasonic machining of hard alloy tools and dies on account of their high resistance. The process is particularly suitable to make holes with a curved axis of any shape that can be made on tool. However, the major limitation of the ultrasonic machining process is its low MRR characteristic. It is therefore very essential to improve the metal cutting rates for this process without affecting surface finish of the work piece. This can be achieved through optimum selection of various machining process parameters influencing the MRR and surface finish in ultrasonic machining process.

USM is characterized by low MRR and very little surface damage to the work material. It can be used for machining both electrically conductive and non-conductive materials preferably with low ductility and high hardness (above 40 HRC). Its potential is not limited by electrical or chemical characteristics of the work material. Mechanisms of material removal in USM include: (1) mechanical abrasion by direct hammering of abrasive particles, (2) micro-chipping due to impacting action of freely moving abrasive particles, (3) cavitation effect of abrasive slurry and (4) chemical action associated with the carrier fluid.

Various analytical MRR models for USM were suggested by researchers. Shaw [218] was the first researcher to propose a static and simple analytical model giving the relationship between MRR and vibration amplitude, frequency, abrasive grit size and concentration, and feed force. But, its predictions do not agree well with experimental observations. Miller [165] developed an MRR model based on plastic deformation restricting its application to ductile materials only, while Rosenberg et al. [201] included the statistical distribution of abrasive particle size in their computationally intensive model. Cook [53] proposed the simplest model to predict linear machining rate. Kainth et al. [109] proposed a model in which the machining rate can be evaluated quantitatively using material properties of the tool and workpiece which was not possible with earlier theories. This model, however, predicts linear relation of MRR with static force that is not practically true. Nair and Ghosh [171] also proposed another computationally intensive model simulating the principles of elastic wave propagation. Wang and Rajurkar [244] suggested a more realistic model taking into account the stochastic and dynamic nature of the process. But, this is applicable to perfectly brittle materials only. Lee and Chan [137] developed an analytical model to predict the effects of amplitude of the tool tip, the static load applied and the size of the abrasive on the MRR and the surface roughness. They concluded that increase the amplitude of the tool vibration, the static load applied, and the grit size of the abrasive would result in an increase in the MRR and roughening of the machined surfaces.

Komaraiah et al. [120] conducted experiments on the ultrasonic machining of different workpiece materials—glass, porcelain, ferrite and alumina—using various tool materials. The effects of mechanical properties of the workpiece and tool materials on surface roughness and accuracy were analyzed. The influences of the type and size of the abrasive grains used and the amplitude of ultrasonic oscillations were studied. An attempt was made to study the influence of the rotation of

the workpiece, in addition to an ultrasonically oscillated tool, on the MRR and surface roughness of the workpieces produced. The rotary mode of ultrasonic machining was found to be superior to conventional ultrasonic machining.

Benkirane et al. [24] studied contour machining using a three-axis numerical control machine. In order to understand its principles and to be able to predict the MRR for modeling and simulation of the process, an experimental and analytical work was carried out. The effects of the main parameters were studied using two statistical methods. They showed an advantage for the neural network one, which gave a more precise prediction of the removal rate compared with the Taguchi method. Wiercigroch [247] postulated that the main mechanism of the enhancement of MRR in ultrasonic machining is associated with high amplitudes forces generated by impacts, which act on the workpiece and help to develop microcracking in the cutting zone. The inherent non-linearity of the discontinuous impact process was modelled to generate the pattern of the impact forces. A novel procedure for calculating the MRR was proposed, which explained the experimentally observed fall in MRR at higher static forces.

Rotary ultrasonic machining (RUM) is a hybrid process which combines mechanisms of USM and grinding process. RUM has potential for higher MRR and clean cuts while maintaining low cutting pressures and giving little surface damage and strength reduction. Therefore, it is especially suitable for ceramic machining. Also, the rotary motion of the tool in RUM enhances MRR, accuracy, and tool life, and reduces cutting forces. Prabhakar et al. [186] proposed a theoretical MRR model based on brittle fracture whose predictions do not agree with the experimental observations. Pei et al. [182] reported a mechanistic model to predict MRR. Pei and Ferreira [181] also reported the modeling of material removal in RUM by ductile mode. Jain and Jain [100] presented various analytical models developed by the researchers for mechanical type modern machining processes including the RUM process.

Ya et al. [250] analyzed the movement of the abrasive particles in the tool tip of RUM. The impact and grinding of the abrasive in the tool tip on the machined surface were considered as the main factors in the MRR. The crack propagation in rotary USM was investigated using the theory of fracture mechanics. A mathematical model for the MRR was proposed in order to provide a theoretical basis for the analyzing of the process of rotary USM.

Hu et al. [96] proposed an approach to model the MRR during RUM of ceramics and applied to predict the MRR for the case of magnesia stabilized zirconia. A five factor two-level factorial design was used to study the relationships between MRR and the controllable machining parameters. The results shed more light on the material removal mechanism in RUM.

Ma et al. [153] proposed a theoretical model of the thrust cutting force in ultrasonic elliptical vibration cutting and the reason for the machining accuracy improvement by applying ultrasonic elliptical vibration was clarified theoretically. Finally, the effect of ultrasonic elliptical vibration cutting on machining accuracy was verified experimentally by utilizing an ultrasonic elliptical vibration cutting system. Mitrofanov et al. [168] dealt with finite element (FE) modeling of

ultrasonically assisted turning (UAT). In this processing technology, high frequency vibration (frequency of 20 kHz and amplitude of 10 μm) was superimposed on the movement of the cutting tool. The developed FE model allows transient, coupled thermomechanical modeling of both ultrasonic and conventional turning of elasto-plastic materials. The Johnson–Cook material model was adopted for Inconel 718 in simulations. Comparative analyses of temperature distribution in the cutting region and cutting tool were carried out for both turning schemes. Plastic strains during cutting and residual strains in the machined layer were analyzed and compared with the results of nano-indentation tests of Inconel 718 specimens processed with and without application of ultrasonic vibration. Overall reduction in cutting forces and temperatures for ultrasonic turning in comparison to conventional turning was explained.

Li et al. [143] performed RUM to drill holes on CMC panels. The feasibility to machine CMC using RUM was investigated. Cutting forces and MRR were compared for machining of CMC with and without ultrasonic vibration and for two types of CMC materials and one typical advanced ceramic material (alumina). Furthermore, the authors had presented the results of a designed experimental investigation into RUM of CMC. A three-variable two-level full factorial design was employed to reveal main effects as well as interaction effects of three RUM process parameters (spindle speed, feed rate, and ultrasonic power). The process outputs studied included cutting force, MRR, and hole quality (in terms of chipping dimensions).

Li et al. [139] developed a 3D FEA model to study the effects of three parameters (cutting depth, support length, and pre-tightening load) on the maximum normal stress and von Mises stress in the region where the edge chipping initiates. Two failure criteria (the maximum normal stress criterion and von Mises stress criterion) were used to predict the relation between the edge chipping thickness and the support length. Furthermore, a solution to reduce the edge chipping was proposed based upon the FEA simulations and verified by experiments.

Singh and Khamba [224] reviewed the fundamental principles of stationary ultrasonic machining, the material removal mechanisms involved and the effect of operating parameters on MRR, tool wear rate, and work piece surface finish of titanium and its alloys for applications in manufacturing industries. Dvivedi and Kumar [61] investigated ultrasonic drilling of Ti-6Al-4V. Process parameters such as work piece, grit size, slurry concentration, power rating and tools were changed to explore their effect on the surface roughness. Taguchi's technique was applied to obtain an optimal setting of parameters.

Singh and Khamba [222] used Taguchi approach to model the MRR during ultrasonic machining of titanium and its alloys. Relationships between MRR and other controllable machining parameters (power rating, tool type, slurry concentration, slurry type, slurry temperature, and slurry size) have been deduced using Taguchi technique. In another work, Singh and Khamba [223] modeled MRR, tool wear rate, and surface roughness during ultrasonic machining of titanium and its alloys using Taguchi's L18 orthogonal arrays. In another work,

Singh and Khamba [220] modeled surface roughness in ultrasonic machining of titanium using Buckingham-Π approach.

Amini et al. [6] studied machining of IN738 with a tool vibrating at ultrasonic frequency. The machining forces and stresses acting on the workpiece during the process, and the effect of process parameters such as cutting speed, tool geometry and vibration amplitude were investigated. The authors also worked out the material and the optimum configuration of the vibratory tool able to operate at an ultrasonic frequency within acceptable range. The results indicated that the forces and the stresses acting on the workpiece followed periodic changes during ultrasonic assisted turning and were augmented with an increase in the ultrasonic vibration amplitude or the cutting speed.

Hsu et al. [94] discussed the machining characteristics of Inconel 718 by combining ultrasonic vibration with high-temperature-aided cutting. Taguchi experimental design was used to clarify the influence of various machining parameters on the machining characteristics. The authors had discussed six machining parameters, including cutting tool made of different materials, depth of cut, cutting speed, feed rate, working temperature and ultrasonic power. The machining characteristics studied included surface roughness and cutting force to the experimental results, as Inconel 718 is heated for high-temperature.

Pujana et al. [189] applied ultrasonic vibration on the drilling of Ti6Al4V workpiece samples. Several parameters of ultrasonic assisted drilling were monitored, including feed force, chip formation by means of high-speed imaging, and temperature measurement on the drill tip by means of infrared radiation thermometry. Ultrasonic assistance offered lower feed force and higher process temperatures as compared to conventional drilling.

Nath and Rahman [173] found that the ultrasonic cutting mechanism is influenced by three important parameters: tool vibration frequency, tool vibration amplitude and workpiece cutting speed that determine the cutting force. However, the relation between the cutting force and these three parameters was not clearly established. Jadoun et al. [99] presented a study of the effect of process parameters on production accuracy obtained through ultrasonic drilling of holes in alumina-based ceramics using silicon carbide abrasive. Production accuracy in ultrasonic drilling involves both dimensional accuracy (hole oversize) and form accuracy (out-of-roundness and conicity). The parameters considered were workpiece material, tool material, grit size of the abrasive, power rating and slurry concentration. Taguchi's optimization approach was used to obtain the optimal parameters.

Kumar and Khamba [132] applied the Taguchi multi-objective optimization technique for determining the optimum combination of various input factors as type of abrasive slurry, their size and concentration, nature of tool material and power rating of the machine for the ductile chip formation in the machining of satellite. In another work, Kumar and Khamba [133] applied Taguchi approach for statistical analysis of experimental parameters in ultrasonic machining of tungsten carbide. Singh and Gill [219] carried out fuzzy modeling and simulation of ultrasonic drilling of porcelain ceramic with hollow stainless steel tools.

Singh and Khamba [221] used outcome of the Taguchi model for developing a mathematical model for tool wear rate; using Buckingham's π-theorem for stationary ultrasonic machining of titanium and its alloys. Six input parameters, namely, tool material, power rating, slurry type, slurry temperature, slurry concentration, and slurry grit size were selected to give output in form of tool wear rate. The authors had described the main effects of these variables on tool wear rate.

Kumar and Khamba [134] explored the use of USM for commercial machining of pure titanium and evaluation of MRR under controlled experimental conditions. The optimal settings of parameters were determined through experiments planned, conducted, and analyzed using Taguchi method. An attempt was made to construct a micro-model for prediction of MRR in USM of titanium using dimensional analysis. The predictions from this model were validated by conducting experiments. A relation was established between the mode of material removal and the energy input rate corresponding to the different process conditions.

The main effort made for optimization of process parameters of ultrasonic machining process parameters by non-traditional optimization algorithms is by Jain et al. [102]. The authors used genetic algorithm as a tool for optimization of five process parameters of ultrasonic machining process namely, amplitude of vibration, frequency of vibration, mean diameter of abrasive grain, volumetric concentration of abrasive particles in slurry, and static feed force. However, although genetic algorithm (GA) has advantages over the traditional optimization techniques, the successful application of GA depends on the population size or the diversity of individual solutions in the search space. If GA cannot hold its diversity well before the global optimum is reached, it may prematurely converge to a local optimum. Rao et al. [198] presented optimization aspects of ultrasonic machining process. The objective considered was maximization of MRR subjected to the constraint of surface roughness. The process variables considered for optimization were amplitude of ultrasonic vibration, frequency of ultrasonic vibration, mean diameter of abrasive particles, volumetric concentration of abrasive particles, and static feed force. The optimization was carried out using three non-traditional optimization algorithms namely, artificial bee colony (ABC), modified harmony search (HS_M), and PSO. An application example was presented and solved to illustrate the effectiveness of the presented algorithms. The results of the presented algorithms were compared with the previously published results obtained using genetic algorithm. Hence, efforts are extended to use other optimization algorithms such as SA and SFL algorithms to provide solutions. The optimization model of the USM process is given below.

The objective is to maximize the MRR (Z_1) [102],

$$Z_1 = 4.963 A_t^{0.25} K_u^{0.75} F_s^{0.75} A_v^{0.75} C_{av}^{0.25} d_m f_v \Big/ \left(\sigma_{fw}\,(1+\lambda)\right)^{0.75}, \tag{3.17}$$

where the decision variables are A_v, amplitude of vibration (mm); f_v frequency of vibration (Hz); d_m mean diameter of abrasive grain (mm); C_{av}, columetric

concentration of abrasive particles in slurry, and F_s, static feed force (N). K_u is a constant of proportionality (mm^{-1}) relating mean diameter of abrasive grains, and diameter of projections on an abrasive grain ($=K_u\, d_m^2$).

The constraint on permissible surface roughness Z_2 is given below.

$$Z_2 = \left[1, 154.7(F_s A_v d_m)^{0.5}\right] \Big/ \left[(A_t \sigma_{fw}\,(1+\lambda))^{0.5} (R_a)_{max} C_{av}\right] \geq 0. \tag{3.18}$$

The bounds for the five variables are as given by Eqs. 3.19–3.23.

$$0.005 \leq A_v \leq 0.1\ (\text{mm}) \tag{3.19}$$

$$10,000 \leq f_v \leq 40,000\ (\text{Hz}) \tag{3.20}$$

$$0.007 \leq d_m \leq 0.15\ (\text{mm}) \tag{3.21}$$

$$0.05 \leq C_{av} \leq 0.5 \tag{3.22}$$

$$4.5 \leq F_s \leq 45\ (\text{N}). \tag{3.23}$$

The combined objective function (Z) considering the objective (Z_1) and constraint (Z_2) is then formulated as:

$$\text{Minimize}\, Z = -Z_1 - \text{penalty} \times Z_2. \tag{3.24}$$

An adaptive penalty scheme [183] is used to accommodate the inclusion of constraint. Using this approach, the fitness value (f') is calculated as,

$$f' = f + \sum_{i=1}^{m} k_i g_{i-\text{avg}} \text{ if the constraint is violated; else } f' = f. \tag{3.25}$$

The penalty parameter is defined at each iteration as,

$$k_i = \left(\left|f_{\text{avg}}\right| g_{i-\text{avg}}\right) \Big/ \sum_{i=1}^{m} \left(g_{l-\text{avg}}\right)^2, \tag{3.26}$$

where f is the objective function value, m the number of constraints, g the specific constraint value with violated constraint, f_{avg} the average of objective function value in the current population, and $g_{l-\text{avg}}$ is the violation of lth constraint averaged over the current population.

The parameter settings for the various techniques to solve the optimization problem of USM process are given below:

Controlling parameters for PSO:

- Number of particles in swarm = 5.
- Inertia weight = 0.65.
- Acceleration coefficient (c_1) = 1.65.
- Acceleration coefficient (c_2) = 1.75.
- Number of iterations = 50.

Controlling parameters for SA:

- Initial temperature = 200.
- Decrement factor = 0.01.
- Number of iterations = 100.

Controlling parameters for HS_M:

- Harmony memory size = 5.
- Harmony memory consideration rate = 0.8.
- Pitch adjusting rate = 0.32.
- Number of improvisations = 150.

Controlling parameters for ABC:

- Number of employed bees = 5.
- Number of onlookers bees = 11.
- Number of scout bees = 1.
- Maximum number of iterations = 150.

Controlling parameters for SFL:

- Total number of frogs = 20.
- Number of memeflexes = 5.
- Number of frogs in each memeflex = 4.
- Number of improvisations = 50.

For the above parameter settings, the results of optimization are shown in Table 3.3.

From Table 3.3, it can be understood that the PSO and ABC algorithms give better results compared to other optimization algorithms. As shown in Table 3.5, the result obtained using the presented algorithms, i.e., ABC and PSO algorithms show significant improvement ($\cong 11\%$) and HS algorithm shows improvement of about 9% over the result obtained using GA. It is interesting to note that although the value of MRR obtained using ABC, PSO, and HS_M is almost same, the optimal combination of parameters provided by these algorithms is markedly different. This indicates that the model is highly multi-modal. The model therefore has number of local optimum solutions also. As an illustration, one of

Table 3.3 Results of optimization of USM process using various algorithms

Method	A_v (mm)	F_v (Hz)	d_m (mm)	C_{av}	F_s (N)	MRR (mm^3/s)	Constraint value
GA [102]	0.0263	39333.9	0.1336	0.479	10.8	3.553	0.0214
ABC	0.0167	40000	0.15	0.5	16.4	3.941	0.0124
HS_M	0.0582	40000	0.15	0.5	4.5	3.870	0.0244
PSO	0.06	40000	0.15	0.5	4.5	3.95	0.0095
SA	0.077	40000	0.114	0.5	4.53	3.660	0.0185
SFL	0.02271	40000	0.14	0.5	12.78	3.894	0.0079

the local optimum solutions obtained is $A_v = 0.0111$ mm, $f_v = 25{,}000$ Hz, $d_m = 0.15$ mm, $C_{av} = 0.5$, and $F_s = 24.75$ N, for which MRR = 2.5 mm^3/s with constraint value 0.000873. For this local optimum solution there is no further scope of improvement as constraint value is almost equal to zero. However, the global optimum solution obtained using PSO algorithm provides MRR = 3.950 mm^3/s, showing about 57% improvement over this local optimum solution which is generally obtained using traditional methods of optimization. This improvement using PSO algorithm is due to the collaborative population-based search which the PSO algorithm follows. PSO system combines local search methods through self experience with the global search methods through neighboring experience, thus attempting to perfectly balance the exploration and exploitation process. The improvement using ABC is mainly due to the fact that the ABC algorithm combines both, the stochastic selection scheme based on the fitness values carried out by onlooker bees, and greedy selection scheme used by onlookers and employed bees to update the source position. Also, the neighbor source production mechanism in ABC is similar to the mutation process, which is self-adapting. The selection of operating parameters, i.e., number of employed bees, number of onlooker bees and number of scouts, in ABC algorithm is relatively easy as compared to GA, PSO and SA algorithms. HS algorithm shows improvement over the genetic algorithm as it overcomes the drawback of GA's building block theory which works well only when the relationship among variables in the chromosome is carefully considered. HS explicitly considers the relationship using ensemble operation. This clearly justifies the use of advanced optimization algorithms like ABC, HS, and PSO, as in present study, to solve such multi-modal problem.

Optimality of the solution obtained by ABC algorithm could be confirmed from the Figs. 3.9, 3.10, 3.11, 3.12, and 3.13. Figure 3.9 shows the variation of MRR and constraint value with amplitude of ultrasonic vibrations. As shown in Fig. 3.9,

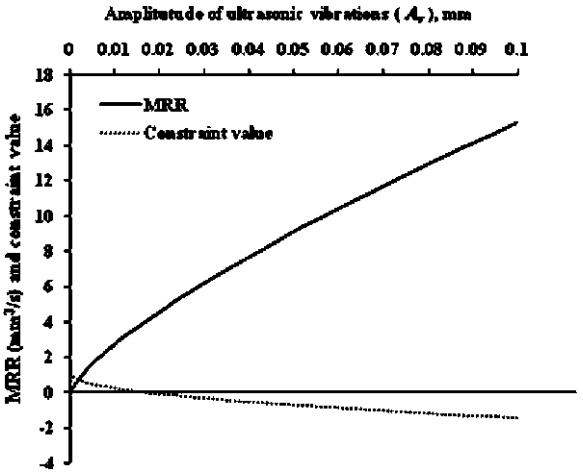

Fig. 3.9 Variation of material removal rate and constraint value with amplitude of ultrasonic vibrations

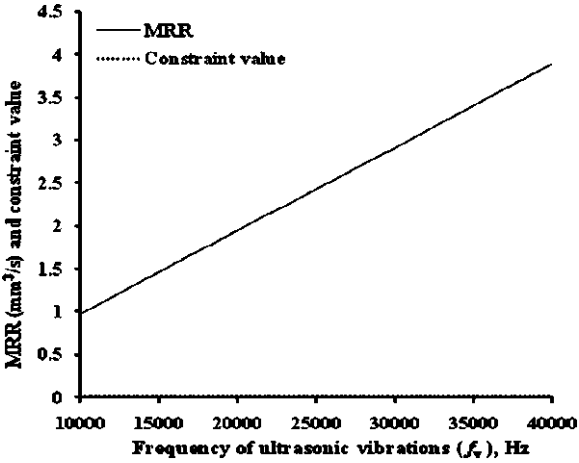

Fig. 3.10 Variation of material removal rate and constraint value with frequency of ultrasonic vibrations

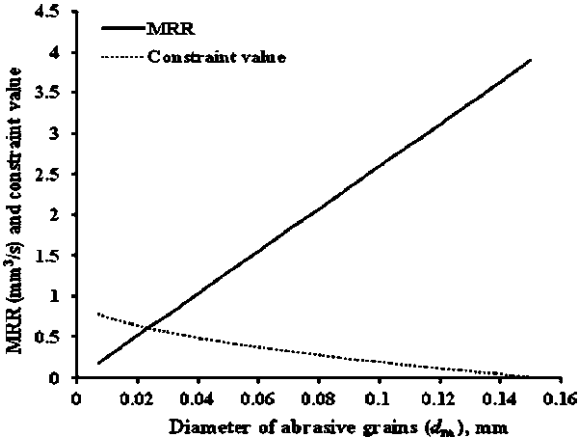

Fig. 3.11 Variation of material removal rate and constraint value with diameter of abrasive grains

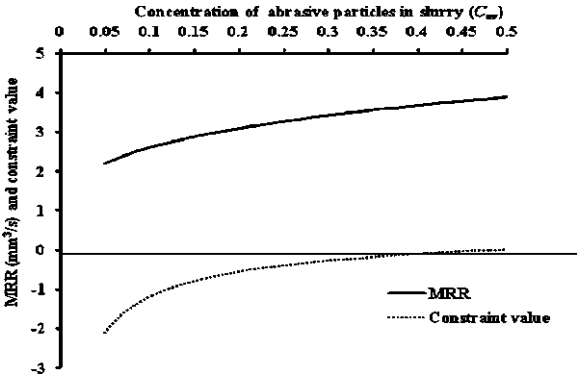

Fig. 3.12 Variation of material removal rate and constraint value with concentration of abrasive particles in slurry

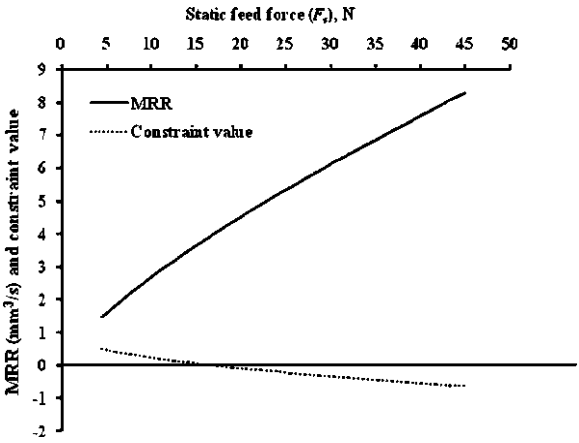

Fig. 3.13 Variation of material removal rate and constraint value with static feed force

the MRR increases with increase in amplitude of ultrasonic vibration. From this point of view higher value of amplitude should be selected. However, as shown in Fig. 3.9, the constraint on surface roughness is violated for any value of amplitude of ultrasonic vibration more than 0.01614. Hence, the optimum value of amplitude of ultrasonic vibration equal to 0.01614 mm obtained using ABC algorithm is appropriate. Figure 3.10 shows the variation of MRR and constraint value with frequency of ultrasonic vibrations.

As shown in Fig. 3.10, the MRR increases with increase in frequency of ultrasonic vibration, higher value of frequency of ultrasonic vibration is desired. Also, as the surface roughness constraint is having a constant positive value, the selection of upper bound value of frequency of ultrasonic vibration, i.e., 40,000 Hz is appropriate.

Figures 3.11 and 3.12 show variation of MRR and constraint value with diameter of abrasive grains and concentration of abrasive particles in slurry, respectively.

MRR increases with increase in both the diameter of abrasive grains as well as concentration of abrasive particles in slurry. Therefore, selection of higher values of diameter of abrasive grains and concentration of abrasive particles in slurry are desired. As the constraint on surface roughness is also satisfied at upper bound value of these both variables, values of diameter of abrasive grains and concentration of abrasive particles in slurry equal to 0.15 mm and 0.5, respectively, provided by ABC algorithm are appropriate.

Figure 3.13 shows variation of MRR and constraint value with static feed force. As shown in Fig. 3.13, the MRR increases with increase in static feed force also. From this point of view, higher value of static feed force is desired. However, as shown in Fig. 3.13, the constraint on surface roughness is violated for any value of static feed force more than 16.407. Hence, the optimum value of static feed force equal to 16.407 N is appropriate.

3.4 Wire Electric Discharge Machining (WEDM) Process

WEDM is one of the widely accepted advanced machining processes used to machine components with intricate shapes and profiles. It is considered as a unique adaptation of the conventional EDM process which uses an electrode to initialize the sparking process. As shown in Fig. 3.14, WEDM utilizes a continuously traveling wire electrode made of thin copper, brass or tungsten. On application of a proper voltage, discharge occurs between the wire electrode and the workpiece in the presence of a flood of deionized water of high insulation resistance. The material is eroded ahead of the wire through a series of repetitive sparks between electrodes, i.e., workpiece and the wire.

WEDM has been gaining wide acceptance in modern tooling applications, machining of advanced ceramic materials and modern composite materials due to following reasons [88]:

- As the wire diameter is small (0.05–0.3 mm), the process is capable of achieving very small corner radii.
- The wire is kept in tension using a mechanical tensioning device reducing the tendency of producing inaccurate parts.

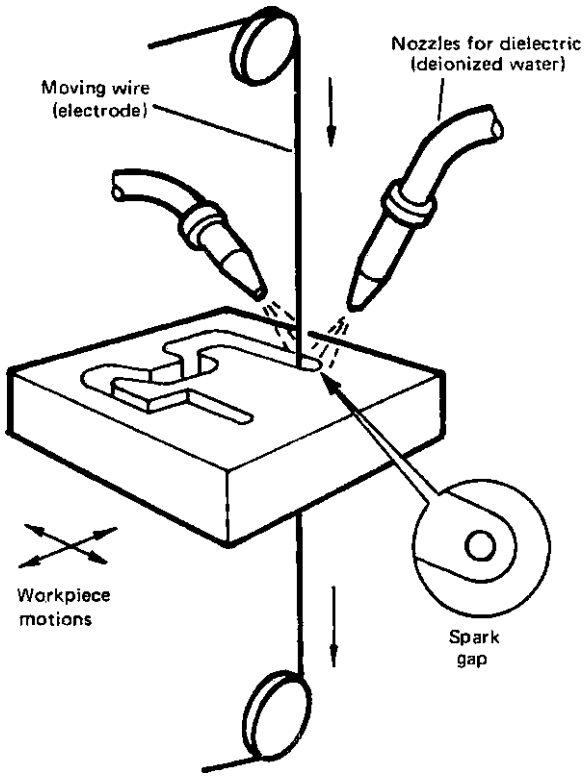

Fig. 3.14 Basic sheme of wire EDM process (from [197]; reprinted with permission from the Council of the Institution of Mechanical Engineers, UK)

- During the WEDM process there is no direct contact between the workpiece and the wire, eliminating the mechanical stresses during machining.
- WEDM process is able to machine exotic and high strength and temperature resistive (HSTR) materials and eliminate the geometrical changes occurring in the machining of heat-treated steels.

While the material removal mechanisms of EDM and WEDM are similar, their functional characteristics are not identical. WEDM uses a thin wire continuously feeding through the workpiece by a microprocessor, which enable parts of complex shapes to be machined with exceptional high accuracy. A varying degree of taper ranging from 15° for a 100 mm thick to 30° for a 400 mm thick workpiece can also be obtained on the cut surface. The microprocessor also constantly maintains the gap between the wire and the workpiece, which varies from 0.025 to 0.05 mm. WEDM eliminates the need for elaborate pre-shaped electrodes, which are commonly required in EDM to perform the roughing and finishing operations. In the case of WEDM, the wire has to make several machining passes along the profile to be machined to attain the required dimensional accuracy and surface finish. WEDM uses deionized water instead of hydrocarbon oil as the dielectric fluid and contains it within the sparking zone. The deionized water is not suitable for conventional EDM as it causes rapid electrode wear, but its low viscosity and rapid cooling rate make it ideal for WEDM.

Wire EDM manufacturers and users always want to achieve higher machining productivity with a desired accuracy and surface finish. Performance of the WEDM process, however, is affected by many factors such as servo feed setting, peak current, pulse on-time, pulse off-time, wire tension, etc., and a single parameter change will influence the process in a complex way. Because of many variables and the complex and stochastic nature of the process, achieving the optimal performance, even for a highly skilled operator with a state-of-the-art wire EDM machine is rarely possible. An effective way to solve this problem is to discover the relationship between the performance of the process and its controllable input parameters by modeling the process through suitable mathematical techniques and optimization using suitable optimization algorithm.

Several attempts were made to study the influence of different process parameters on the important performance measures of WEDM process such as cutting rate, surface finish and MRR using various problem-solving tools. Quite a few researchers had tried to optimize the cutting performance by adopting various traditional and non-traditional optimization techniques. Metal removal rate (MRR) and surface finish were optimized by Scott et al. [212] by explicit enumeration based on signal-to-noise ratio. Further, they split the problem into optimization of MRR with surface finish constraint and optimization of surface finish with MRR as constraint and applied dynamic programming method. Wang and Rajurkar [246] analyzed theoretically and experimentally an existing electrical discharge machine servo mechanism and described modeling of the process. Spur and Schönbeck [227] designed a theoretical model studying the influence of the workpiece material and the pulse-type properties on the WEDM of a workpiece with an

anodic polarity. Tarng et al. [233] used a simple weighting method to transform the cutting velocity and surface roughness into a single objective and arrived at the optimal parameters by employing simulated annealing technique. They considered pulse on/off duration, peak current, open circuit voltage, servo reference voltage; electrical capacitance and table speed are the critical parameters for the estimation of the cutting rate and surface finish.

Anand [7] used a fractional factorial experiment with an orthogonal array layout to obtain the most desirable process specification for improving the WEDM dimensional accuracy and surface roughness. Liu and Esterling [147] proposed a solid modeling method, which can precisely represent the geometry cut by the WEDM process. Liao et al. [144] applied method of feasible direction for optimization of the process parameters such as table feed rate and pulse on-time with an objective as to maximize the MRR with surface roughness and spark gap as constraints. In another work, Liao et al. [144] proposed an approach of determining the parameter settings based on the Taguchi quality design method and the analysis of variance. The results showed that the MRR and surface finish are easily influenced by the table feed rate and pulse on-time, which can also be used to control the discharging frequency for the prevention of wire breakage.

Spedding and Wang [226] optimized the process parameter settings using ANN modeling to characterize the WEDM workpiece surfaces. They obtained the optimum combination of the parameters namely pulse width, time between two pulses, wire mechanical tension, and wire feed space for maximum cutting speed, keeping the surface roughness and waviness within the required limits. Hsue et al. [95] developed a model to estimate the MRR during geometrical cutting by considering wire deflection with transformed exponential trajectory of the wire centre. Konda et al. [121] classified the various potential factors affecting the WEDM performance measures into five major categories namely the different properties of the workpiece material and dielectric fluid, machine characteristics, adjustable machining parameters, and component geometry. In addition, they applied the DOE technique to study and optimize the possible effects of variables during process design and development, and validated the experimental results using noise-to-signal (S/N) ratio analysis. Gokler and Ozanozgu [75] studied the selection of the most suitable cutting and offset parameter combination to get a desired surface roughness for a constant wire speed and dielectric flushing pressure. Han et al. [77] developed a simulation system, which accurately reproduces the discharge phenomena of WEDM. The system also applies an adaptive control, which automatically generates an optimal machining condition for high precision WEDM.

Liao et al. [145] used a feed-forward neural network to estimate the workpiece height and distinguish the machining condition in WEDM. Some experiments were carried out to verify the effectiveness of this approach. Based on the on-line estimated workpiece height, a rule-based strategy was proposed to maintain optimal and stable machining. According to the rule-based strategy, servo voltage and power settings can be adjusted correctly to suit the workpiece profile. Experimental results demonstrated that high machining efficiency and stable machining can be achieved by means of the rule-based control strategy.

Huang and Liao [97] used grey relational and S/N ratio analysis to demonstrate the influence of table feed and pulse on-time on the MRR. Tosun et al. [235] investigated the effect of the pulse duration, open circuit voltage, wire speed and dielectric flushing pressure on workpiece surface roughness. It was found that the increasing pulse duration, open circuit voltage and wire speed increase with the surface roughness, whereas increasing dielectric fluid pressure decreases the surface roughness.

Puri and Bhattacharyya [190] carried out an extensive study of the wire lag phenomenon in WEDM. All the machine control parameters were considered simultaneously for the machining operation which comprised a rough cut followed by a trim cut. The objective of the study was to carry out an experimental investigation based on the Taguchi method involving 13 control factors with three levels for an orthogonal array L_{27} (3^3). The main influencing factors were determined for given machining criteria, such as: average cutting speed, surface finish characteristic and geometrical inaccuracy caused due to wire lag. Also, the optimum parametric settings for different machining situations were found out and reported.

Tosun et al. [235] experimentally investigated the variation of workpiece surface roughness with varying pulse duration, open circuit voltage, wire speed and dielectric fluid pressure in WEDM process. Brass wire with 0.25 mm diameter and SAE 4140 steel with 10 mm thickness were used as tool and workpiece materials in the experiments, respectively. It was found experimentally that the increasing pulse duration, open circuit voltage and wire speed, increase the surface roughness whereas the increasing dielectric fluid pressure decreases the surface roughness. The variation of workpiece surface roughness with machining parameters was modelled using a power function. The level of importance of the machining parameters on the workpiece surface roughness was determined using analysis of variance.

Saha et al. [203] developed a simple finite element model and a new approach to predict the thermal distribution in the wire fairly accurately. The model can be used to optimize the different parameters of the system to prevent wire breakage. At any instant of time, the spatial heat distribution profile of the wire can be mapped on the transient analysis of any point on the wire traversing through all the heat zones from the top spool to the bottom end. Based on this principle, the finite element model and optimization algorithm were used to determine that the heat generated was the critical variable responsible for wire breakage. The model successfully predicts the thermal distribution profile accurately for various wire materials, for increased wire velocity and for reduction in heat transfer coefficient. This simple model is a precursor for the development of 3D finite element models that can describe the cross-sectional wire erosion as the workpiece cutting progresses. The modeling can lead to the development of a smart electro-discharge machining system with a sensor and feedback control to increase the cutting speed and minimize breakage.

Sanchez et al. [206] described a hybrid computer-integrated system for the improvement of the accuracy of corner cutting that combines experimental knowledge of the process and numerical simulation. Based on a technological database and a user-friendly interface, the system allows the user to select the

optimum cutting strategy, either by wire path modification (when productivity is the main concern) or by cutting regime modification (when high accuracy is required). Simulation supported the decision-taking process by reducing the cost and time-consuming experimental trials. The validity of the system was tested through a series of case studies, which showed the improvements in accuracy and productivity with respect to the commonly used strategies.

Hascalyk and Caydas [80] through experimental investigations showed that intensity of the process energy affects significantly the amount of recast, surface roughness, and microcracking. Tosun et al. [236] presented an investigation on the optimization and the effect of machining parameters on kerf and the MRR in WEDM operations. The simulated annealing algorithm was then applied to select optimal values of machining parameters for multi-objective problem considering minimization of kerf and maximization of MRR. Hewidy et al. [84] developed a mathematical model based on response surface methodology (RSM) for correlating the inter-relationships of various WEDM machining parameters of Inconel 601 material such as peak current, duty factor, wire tension and water pressure on the MRR, wear ratio and surface roughness.

Kuriakose and Shunmugam [135] presented a multiple regression model to represent relationship between input variables and two conflicting objectives, i.e., cutting velocity and surface finish. A multi-objective optimization method based on a Non-Dominated Sorting Genetic Algorithm (NSGA) was then used to optimize Wire EDM process. The process engineer can select optimal combination of parameters from the pareto-optimal solution set, depending on the requirements. Sarkar et al. [210] obtained pareto-optimal combinations of process variables namely pulse on-time, pulse off-time, peak current, servo reference voltage, wire tension and dielectric flow rate for maximization of cutting speed with constraint on surface roughness and dimensional deviation. However, the method of optimization is not specified. Chiang and Chang [47] presented an effective approach for the optimization of the WEDM process of Al_2O_3 particle-reinforced material (6061 alloy) with multiple-performance characteristics based on the grey relational analysis (GRA). The response table and response graph for each level of the machining parameters were obtained form the grey relational grade. In this study, the machining parameters namely the cutting radius of working piece, on-time of discharging, off-time of discharging, arc on-time of discharging, arc off-time of discharging, servo voltage, wire feed and water flow were optimized with considerations of multiple-performance characteristics, such as the surface removal rate and the maximum surface roughness.

Manna and Bhattacharyya [156] presented a reliable set of parameters that demonstrate versatility, and numerous and diverse range based on experience and technology. The authors had investigated the parameters setting during the machining of aluminum-reinforced silicon carbide metal matrix composite (Al/SiC-MMC). The Taguchi method was used to optimize the CNC-wire cut-EDM parameters. According to the Taguchi quality design Concept, a L_{18} ($2^1 \times 3^7$) mixed orthogonal array was used to determine the S/N ratio, and an analysis of variance (ANOVA) and the *F* test values were used to indicate the significant

machining parameters affecting the machining performance. From experimental results and through ANOVA and F test values, the significant factors were determined for each machining performance criteria, such as the MRR, surface roughness, gap current and spark gap (gap width). Considering these significant CNC-wire cut-EDM parameters, verification of the improvement in the quality characteristics for machining Al/SiC-MMC was made with a confirmation test with respect to the chosen initial or reference parameter setting. Mathematical models relating to the machining performance were established using the Gauss elimination method for the effective machining of Al/SiC-MMC. The determined optimal combination of CNC-wire cut-EDM parameters obtained from the study satisfied the real requirement of quality machining of Al/SiC-MMC in practice.

Sarkar et al. [207] studied WEDM process of γ titanium aluminide and attempted to develop an appropriate machining strategy for a maximum process criteria yield. A feed-forward back-propagation neural network (BPNN) was developed to model the machining process. The three most important parameters—cutting speed, surface roughness and wire offset—were considered as measures of the process performance. The model is capable of predicting the response parameters as a function of six different control parameters, i.e., pulse on-time, pulse off-time, peak current, wire tension, dielectric flow rate and servo reference voltage. Experimental results demonstrated that the machining model is suitable and the optimization strategy satisfies practical requirements.

Kanlayasiri and Boonmung [110] developed a mathematical model using multiple regression method to formulate the pulse on-time and pulse-peak current to the surface roughness. Mahapatra and Patnaik [155] used Taguchi's parameter design, significant machining parameters affecting the performance measures were identified as discharge current, pulse duration, pulse frequency, wire speed, wire tension, and dielectric flow. It was observed that a combination of factors for optimization of each performance measure was different. The relationship between control factors and responses like MRR, SF and kerf were established by means of non-linear regression analysis, resulting in a valid mathematical model. Finally, genetic algorithm was employed to optimize the WEDM process with multiple objectives. The study demonstrated that the WEDM process parameters can be adjusted to achieve better MRR, surface finish and cutting width simultaneously.

Lee and Liao [138] presented a control system to improve the efficiency of machining a workpiece with varying thickness in the WEDM process. The abnormal ratio R_{ab} defined by the proportion of abnormal sparks in a sampling period was taken as the controlled variable. A gain self-tuning fuzzy control algorithm was used so that the transient situation can be suppressed immediately and a stable performance can be achieved. In addition, the grey predictor was adopted to compensate the time-delayed R_{ab} caused by the low-pass filter data processing.

Hargrove and Ding [79] developed a FEM program to model temperature distribution in the workpiece under the conditions of different cutting parameters. The thermal parameters of low carbon steel (AISI4340) were selected to conduct this simulation. The thickness of the temperature affected layers for different cutting parameters was computed based on a critical temperature value. Through

minimizing the thickness of the temperature affected layers and satisfying a certain cutting speed, a set of the cutting process parameters were determined for workpiece manufacture. On the other hand, the experimental investigation of the effects of cutting parameters on the thickness of the AISI4340 workpiece surface layers in WEDM was used to validate the simulation results. This study is helpful for developing advanced control strategies to enhance the complex contouring capabilities and machining rate while avoiding harmful surface damage.

Han et al. [76] described the influence of the machining parameters (including pulse duration, discharge current, sustained pulse time, pulse interval time, polarity effect, material and dielectric) on surface roughness in the finish cut of WEDM. Experiments proved that the surface roughness can be improved by decreasing both pulse duration and discharge current. When the pulse energy per discharge is constant, short pulses and long pulses will result in the same surface roughness but dissimilar surface morphology and different MRR. The removal rate when a short pulse duration is used is much higher than when the pulse duration is long. Moreover, from the single discharge experiments, it was found that a long pulse duration combined with a low peak value could not produce craters on the workpiece surface any more when the pulse energy was reduced to a certain value. However, the condition of short pulse duration with high peak value still could produce clear craters on the workpiece surface. This indicated that a short pulse duration combined with a high peak value can generate better surface roughness, which cannot be achieved with long pulses. It was also found that reversed polarity machining with the appropriate pulse energy can improve the machined surface roughness somewhat better compared with normal polarity in finish machining.

Yuan et al. [259] discussed the development of reliable multi-objective optimization based on Gaussian process regression (GPR) to optimize the high-speed wire-cut electrical discharge machining (WEDM-HS) process, considering mean current, on-time and off-time as input features and material remove rate (MRR) and Surface Roughness (SR) as output responses. Experiments were conducted to evaluate the proposed intelligent approach in terms of optimization process accuracy and reliability. The experimental results showed that GPR models have the advantage over other regressive models in terms of model accuracy and feature scaling and probabilistic variance.

Saha et al. [202] developed a second-order multi-variable regression model and a feed-forward BPNN model to correlate the input process parameters, such as pulse on-time, pulse off-time, peak current, and capacitance with the performance measures namely, cutting speed and surface roughness while machining tungsten carbide–cobalt (WC–Co) composite material. From a large number of neural network architectures, 4-11-2 was found to be the optimal one to predict cutting speed and surface roughness with 3.29% overall mean prediction error. The multivariable regression model yielded an overall mean prediction error of 6.02%. Both the models were used to study the effect of input parameters on the cutting speed and surface roughness, and finally to corroborate them with those of the experimental results. Scanning electron micrographs revealed that at higher energy

level the machined surface was characterized by several microcracks and loosely bound solidified WC grains.

Ramakrishnan and Karunamoorthy [193] described the development of ANN models and multi-response optimization technique to predict and select the best cutting parameters of WEDM process. To predict the performance characteristics namely MRR and surface roughness, ANN models were developed using back-propagation algorithms. Inconel 718 was selected as work material to conduct experiments. A brass wire of 0.25 mm diameter was applied as tool electrode to cut the specimen. Experiments were planned as per Taguchi's L9 orthogonal array. Experiments were performed under different cutting conditions of pulse on-time, delay time, wire feed speed, and ignition current. The responses were optimized concurrently using multi-response signal-to-noise (MRSN) ratio in addition to Taguchi's parametric design approach. Analysis of variance (ANOVA) was employed to identify the level of importance of the machining parameters on the multiple-performance characteristics. Finally, experimental confirmations were carried out to identify the effectiveness of this proposed method.

Plaza et al. [185] presented two original models for the prediction of angular error in WEDM taper-cutting to reduce the experimental load and to contribute a more general approach to the problem. Results showed that part thickness and taper angle are the most influencing variables in the problem.

Çaydaş et al. [33] developed an adaptive neuro-fuzzy inference system (ANFIS) model for the prediction of the white layer thickness (WLT) and the average surface roughness achieved as a function of the process parameters. Pulse duration, open circuit voltage, dielectric flushing pressure and wire feed rate were taken as model's input features. The model combined modeling function of fuzzy inference with the learning ability of ANN; and a set of rules was generated directly from the experimental data. The model's predictions were compared with experimental results for verifying the approach.

Rao and Pawar [197] highlighted the development of mathematical models using response surface modeling (RSM) for correlating the inter-relationships of various WEDM parameters such as pulse on-time, pulse off-time, peak current, and servo feed setting on the machining speed and surface roughness. ABC algorithm was then applied to find the optimal combination of process parameters with an objective of achieving maximum machining speed for a desired value of surface finish.

Rao et al. [194] optimized the surface roughness of die sinking electric discharge machining by considering the simultaneous affect of various input parameters. The experiments were carried out on Ti6Al4V, HE15, 15CDV6 and M-250. Experiments were conducted by varying the peak current and voltage and the corresponding values of surface roughness were measured. Multiperceptron neural network models were developed using Neuro Solutions package. Genetic algorithm concept was used to optimize the weighting factors of the network. It was observed that the error when the network was optimized by genetic algorithm came down to less than 2% from more than 5%.

Chen et al. [42] analyzed variation of cutting velocity and workpiece surface finish depending on WEDM process parameters during manufacture of pure

tungsten profiles. A method integrating BPNN and simulated annealing (SA) algorithm was proposed to determine an optimal parameter setting of the WEDM process. The specimens were prepared under different WEDM process conditions based on a Taguchi orthogonal array table. The results of 18 experimental runs were utilized to train the BPNN predicting the cutting velocity, roughness average (R_a), and roughness maximum (R_t) properties at various WEDM process conditions and then the SAA approaches was applied to search for an optimal setting. In addition, the analysis of variance (ANOVA) was implemented to identify significant factors for the WEDM process and the proposed algorithm was also compared with respect to the confirmation experiments. The results showed that the BPNN/SA method is an effective tool for the optimization of WEDM process parameters.

Although various researchers have considered the effect of different process variables on various performance measures, these efforts need to be further extended by considering more performance measures and more input variables. Machining speed and surface finish are considered to be very crucial and important performance measures for WEDM, hence the same are considered in the present work. A mathematical model relating these performance measures with four important process parameters, namely pulse on-time (T_{on}), pulse off-time (T_{off}), peak current (I_p) and servo feed setting (F), is developed using a second-order RSM technique, as first-order models often give lack-of-fit [169].

Furthermore, it is revealed from the literature that mathematical programming techniques like method of feasible direction, Taguchi methods, etc., had been used to solve optimization problems in WEDM process. However, these traditional methods of optimization do not fare well over a broad spectrum of problem domains. Moreover, traditional techniques may not be robust and they tend to obtain a local optimal solution. Considering the drawbacks of traditional optimization techniques, attempts are being made to optimize the machining problem using evolutionary optimization techniques. These methods use the fitness information instead of the functional derivatives making them more robust and effective. These methods thus avoid the problem of getting trapped in local optima and enable to obtain a global (or nearly global) optimum solution. Efforts are continuing to use more recent optimization algorithms, which are more powerful, robust and able to provide accurate solution.

Now an example is presented to demonstrate the process parameter optimization of WEDM process using recently developed optimization algorithms.

3.4.1 Example: Parameter Optimization of WEDM Process

Rao and Pawar [197] highlighted the development of mathematical models using RSM for correlating the inter-relationships of various WEDM parameters such as pulse on-time, pulse off-time, peak current, and servo feed setting on the machining speed and surface roughness. A mathematical model relating these performance measures with four important process parameters namely, pulse on-time (T_{on}), pulse off-time (T_{off}), peak current (I_p) and servo feed setting (F), on

cutting speed (V) and surface roughness (R_a) is developed using a second-order RSM technique.

RSM is a collection of statistical and mathematical methods that are useful for modeling and optimization of the engineering science problems. RSM quantifies the relationship between the controllable input parameters and the obtained responses. In modeling of manufacturing processes using RSM, sufficient data is collected through designed experimentation. An experiment is designed with 2^k (where k = number of variables, in this study $k = 4$) factorial with central composite-second-order ratable design is used. This consists of number of corner points = 16, number of axial points = 8, and a centre point at zero level = 4. The axial points are located in a coded test condition space through parameter 'α'. For the design to remain rotatable, 'α' is determined as $(2^k)^{1/4} = 2$. Thus, the coded level for the axial points is at 2. The center point is repeated four times to estimate the pure error. The coded value corresponding to actual value for each process variable is derived using following formula:

$$\text{Coded test condition} = (\text{ATC} - \text{MTC})/0.5 \times \text{RTC}, \tag{3.27}$$

where ATC is actual test condition, MTC mean test condition and RTC is range of test condition.

As an illustration, if actual test condition of 'pulse on-time (T_{on})' is 5 then, the corresponding coded value is $[5 - ((4 + 8)/2)]/[(8 - 4)/2] = -0.5$.

The coded numbers are thus obtained from following transformation equations:

$$x_1 = (T_{on} - T_{on0})/\Delta T_{on} \tag{3.28}$$

$$x_2 = (T_{off} - T_{off0})/\Delta T_{off} \tag{3.29}$$

$$x_3 = \left(I_p - I_{p0}\right)/\Delta I_p \tag{3.30}$$

$$x_4 = (F - F_0)/\Delta F \tag{3.31}$$

where x_1, x_2, x_3 and x_4 are the coded values of the variables T_{on}, T_{off},I_p, and F, respectively. T_{on0}, T_{off0}, I_{p0}, and F_0 are the values of pulse on-time, pulse off-time, peak current, and servo feed setting at zero level. ΔT_{on}, ΔT_{off}, ΔI_p and ΔF are the intervals of variation in T_{on}, T_{off}, I_p, and F, respectively. Table 3.4 shows coded values of process variables. The details of experimental set-up used for data collection are given below:

Table 3.4 Coded values of process variables (from [197]; reprinted with permission from the Council of the Institution of Mechanical Engineers, UK)

Factors	Coded levels				
	−2	−1	0	+1	+2
Pulse on-time	2	4	6	8	10
Pulse off-time	6	10	20	30	40
Peak current	65	90	115	140	165
Servo feed setting	20	30	40	50	60

The details of the experiments are as below:

- Machine type/make: CNC-WEDM, Elektra ELPULSE-30.
- Workpiece specification: Rectangular cavity of size: 60 × 110 × 12 mm.
- Material: OHNS.
- Surface roughness measuring device: Hommel tester T-500.
- Wire material: Brass.
- Wire diameter: 0.25 mm.
- Wire tension: 8 N.
- Dielectric fluid: Deionized water.

The coded levels of the process variables are as shown in Table 3.4.

To study the effect of process parameters, i.e., T_{on}, T_{off}, I_p, and F, on performance measures, i.e., machining speed (V_m) and surface roughness (R_a), a second-order polynomial response is fitted to the data shown in Table 3.5 into the following equations.

Table 3.5 The data collected through actual experiments (from [197]; reprinted with permission from the Council of the Institution of Mechanical Engineers, UK)

S.no.	T_{on} (μs)	T_{off} (μs)	I_p (Amp)	F	V_m (mm/min)	R_a (μm)
1	−1	−1	−1	−1	1.15	1.6
2	1	−1	−1	−1	1.50	2.5
3	−1	1	−1	−1	0.93	1.5
4	1	1	−1	−1	1.16	1.8
5	−1	−1	1	−1	1.54	2.2
6	1	−1	1	−1	1.58	2.3
7	−1	1	1	−1	1.13	1.7
8	1	1	1	−1	1.30	2.0
9	−1	−1	−1	1	1.58	2.3
10	1	−1	−1	1	1.90	3.7
11	−1	1	−1	1	1.05	1.5
12	1	1	−1	1	1.48	2.4
13	−1	−1	1	1	1.90	3.1
14	1	−1	1	1	1.57	2.4
15	−1	1	1	1	1.10	1.5
16	1	1	1	1	1.28	2.1
17	0	0	0	0	1.55	3.4
18	0	0	0	0	1.55	4.0
19	0	0	0	0	1.56	3.5
20	0	0	0	0	1.56	3.5
21	2	0	0	0	1.75	3.3
22	−2	0	0	0	1.13	1.6
23	0	2	0	0	1.35	1.8
24	0	−2	0	0	1.95	2.6
25	0	0	2	0	1.60	1.2
26	0	0	−2	0	0.81	3.0
27	0	0	0	2	1.70	1.6
28	0	0	0	−2	0.95	3.7

$$y = b_0 + \sum_{i=1}^{k} b_i x_i + \sum_{i=1}^{k} b_{ii} x_i^2 + \sum_{j>1}^{k} b_{ii} x_i x_j, \tag{3.32}$$

where 'y' is the response and the x_i (1, 2, …, k) are coded levels of k quantitative variables. The coefficient b_0 is the free term, the coefficients b_i are the linear terms, the coefficients b_{ii} are the quadratic terms, and the coefficients b_{ij} are the interaction terms. Equations 3.33 and 3.34 are then derived by determining the values of the coefficients using the least square technique for the observations collected for machining speed (V_m) and surface roughness (R_a), respectively.

$$\begin{aligned} V_m = {} & 1.555 + 0.109x_1 - 0.187x_2 + 0.0929x_3 + 0.1279x_4 + 0.0393x_1x_2 \\ & - 0.0793x_1x_3 - 0.01188x_1x_4 - 0.01688x_2x_3 - 0.0493x_2x_4 - 0.0606x_3x_4 \\ & - 0.03219x_1^2 + 0.02031x_2^2 0.0909x_3^2 - 0.06094x_4^2 \end{aligned} \tag{3.33}$$

$$\begin{aligned} R_a = {} & 3.6 + 0.2979x_1 - 0.2979x_2 - 0.1479x_3 - 0.03542x_4 + 0.021875x_1x_2 \\ & - 0.2031x_1x_3 + 0.04062x_1x_4 + 0.01562x_2x_3 - 0.1531x_2x_4 \\ & - 0.1031x_3x_4 - 0.3182x_1^2 - 0.3807x_2^2 - 0.4057x_3^2 - 0.2682x_4^2 \end{aligned} \tag{3.34}$$

To test whether the data are well fitted in model or not, the values of standard error of estimates (S) of the regression analysis for machining speed and surface roughness are obtained as 0.148 and 0.644, respectively, whereas the values of standard deviation (S_y) for machining speed and surface roughness are obtained as 0.443 and 1.186, respectively. As $S < S_y$ for regression analysis of both machining speed and surface roughness, it indicates that both regression models have merit.

The actual extent of improvement, using regression analysis rather than describing data as an average value, is quantified by the coefficient of determination (R^2), which varies from 0 to 1. Value of $R^2 = 1$ indicates perfect fit, whereas $R^2 = 0$ indicates no improvement. For machining speed and surface roughness, R^2 values are calculated as 0.89 and 0.71, respectively. The R^2 value is moderately high for machining speed and is moderate for surface roughness. Hence, the models developed for machining speed and surface roughness fits the data well. F statistics can be used whether these results with such high values of R^2, occurred by chance. Probability that these high values occurred by chance are calculated as 0.000459 and 0.00805 for machining speed and surface roughness, respectively. As these values are very small, it can be concluded that the regression analysis is useful in predicting the response. Based on the analysis discussed, the optimization model is as then formulated as below.

Objective function: Maximize V_m (given by Eq. 3.31)

The constraint is to ensure that the surface roughness value (R_a) should not exceed permissible surface roughness (R_{per}) as specified by Eq. 3.35 below

$$R_{\text{per}} - R_{\text{a}} \geq 0, \tag{3.35}$$

where R_{a} is the surface roughness value as specified by Eq. 3.36. The upper and lower bound values for these variables are as given below.

$$4 \leq T_{\text{on}} \leq 8\ \mu\text{s} \tag{3.36}$$

$$10 \leq T_{\text{off}} \leq 30\ \mu\text{s} \tag{3.37}$$

$$90 \leq I_{\text{P}} \leq 140\ \text{amp} \tag{3.38}$$

$$30 \leq F \leq 50 \tag{3.39}$$

3.4.1.1 Optimization Using ABC Algorithm

Following steps are used for Optimization using ABC algorithm to solve the above optimization problem.

Step 1 Parameter selection

Food source represents a possible solution to the problem of minimization of production-time in the present work. Number of initial solutions (i.e., the number of food sources) considered in this work are five. The value of each food source depends on the fitness value of the objective function. For every food source there is only one employed bee (employed forager). In other words, the number of employed bees is equal to number of food sources. Hence, in the present work number of employed bees is considered to be four. The unemployed forager can be scout or an onlooker bee. The number of onlooker bees must be greater than the number of employed bees. When the algorithm is tried for parameters of optimization values of number of employed bees = 10 and colony size = 25, it is observed that as the number of onlooker bees and hence the population size increases, the algorithm performs better in terms of convergence rate. However, after a sufficient value of number of onlooker bees, any increment in the value does not improve the performance of the algorithm. For the problem considered in this work, number of onlooker bees is considered to be 11, which can provide an acceptable convergence speed for search. The colony size is the sum of number of employed bees and number of onlooker bees. Hence, the colony size is 15. Number of scout bees is usually 5–30% of the colony size. In the present work, the number of scout bee is taken as 5% of the colony size, i.e., one. The parameters of optimization thus selected in this example are summarized as below:

- Number of employed bees = 4.
- Number of onlookers bees = 11.

- Number of scout bees = 1.
- Maximum number of iterations = 150.

Step 2 Calculate the nectar amount of each food source
The employed bees are moved to the food sources and the nectar amount of these food sources is evaluated based on their fitness value as defined by the objective function given by Eq. 3.33 subjected to constraint given by Eq. 3.34.

Step 3 Determine the probabilities using the nectar amount
If the nectar amount of a food source "θ_i" is F_i, then the probability (P_i) of choosing this food source by an onlooker bee is expressed as:

$$P_i = f_i \Big/ \sum_{k=1}^{S} (1/f_k), \tag{3.40}$$

where "S" is the number of food sources.

Step 4 Calculate the number of onlooker bees, which will be sent to food sources
Based on the probabilities calculated in step 3, the number (N) of onlookers bees sent to food source "θ_i" is calculated as:

$$N = P_i \times m \tag{3.41}$$

where 'm' is the total number of onlooker bees.

Step 5 Calculate the fitness value of each onlooker bee
After watching the dances of employed bees, an onlooker bee goes to the region of food source "θ_i" by the probability given by Eq. 3.42.

$$\theta_i(c+1) = \theta_i(c) \pm \phi_i(c) \tag{3.42}$$

where "c" is number of generation. ϕ_i (c) is a randomly produced step to find a food source with a more nectar around 'θ_i'. ϕ_i (c) is calculated by taking the difference of the same parts of $\theta_i(c)$ and $\theta_k(c)$ ("k" is a randomly produced index) food positions. If the nectar amount $F_i(c + 1)$ at $\theta_i(c + 1)$ is higher than at $\theta_i(c)$, then the bees go to the hive and share information with others and the position $\theta_i(c)$ of the food source is changed to $\theta_i(c + 1)$ otherwise $\theta_i(c)$ is kept as it is. If the position 'θ_i' of the food source "i" cannot be improved through the predetermined number of trials, then that food source 'θ_i' is abandoned by its employed bee and then the bee becomes a scout. The scout starts searching new food source, and after finding the new source, the new position is accepted as 'θ_i'.

Step 6 Evaluate the best solution
Position of the best onlooker bee is identified for each food source. The global best of the honeybee swarm in each generation is obtained and it may replace the global best at previous generation if it has better fitness value.

Step 7 Update the scout bee

The worst employed bees, as many as the number of scout bees in the population, are, respectively, compared with the scout solutions. If the scout solution is better than employed solution, employed solution is replaced with scout solution. Else employed solution is transferred to the next generation without any change. The results of optimization by applying the above steps of ABC algorithm are shown in Table 3.6.

3.4.1.2 Optimization Using PSO Algorithm

Determination of the optimum selection of operating parameters of PSO algorithm like acceleration constants 'c_1' and 'c_2' as well as inertia coefficient 'w' is very essential for convergence of the algorithm. Considering the velocity and positions of a particle at discrete time steps, the following non-homogeneous recurrence relation is obtained:

$$X_{i+1} = (1 + w - \phi_1 - \phi_2)X_i - wX_{i-1} + \phi_1 * p\text{Best}_i + \phi_2 * g\text{Best}_i, \tag{3.43}$$

where $\phi_1 = c_1 \times r_1$ and $\phi_2 = c_2 \times r_2$.

This recurrence relation can be written in matrix–vector notation as the product

$$\begin{bmatrix} X_{i+1} \\ X_i \\ 1 \end{bmatrix} = \begin{bmatrix} 1 + w - \phi_1 - \phi_2 & -w & \phi_1 * p\text{Best}_i + \phi_2 * gBest_i \\ 1 & 0 & 0 \\ 0 & 0 & 1 \end{bmatrix} \begin{bmatrix} X_i \\ X_{i+1} \\ 1 \end{bmatrix}. \tag{3.44}$$

Characteristic polynomial of the matrix in Eq. 3.44 is

$$(1 - \lambda)\left(w - \lambda(1 + w - \phi_1 - \phi_2) + \lambda^2\right). \tag{3.45}$$

The solution to this polynomial gives the following eigen values,

$$\lambda_1 = (1 + w - \phi_1 - \phi_2 + r)/2 \tag{3.46}$$

$$\lambda_2 = (1 + w - \phi_1 - \phi_2 - r)/2 \tag{3.47}$$

Table 3.6 The results of optimization for $R_a = 2$ μm using various algorithms

Method	T_{on} (μs)	T_{off} (μs)	I_p (Amp)	F	V_m (mm/min)
ABC	8	30	132.57	50	1.422
PSO	4	23.23	140	50	1.420
HS_M	8	29.66	134.15	50	1.420
SA	8	29.66	134.15	50	1.414
SFL	7.972	29.8	133.375	50	1.419

$$r = \left((1 + w - \phi_1 - \phi_2)^2 - 4w\right)^2. \tag{3.48}$$

Now, to ensure the convergence of algorithm, the values of λ_1 and λ_2 should be such that

$$\max(|\lambda_1|, |\lambda_2|) < 1. \tag{3.49}$$

This can be achieved only when the condition given by Eq. 3.48 is satisfied.

$$w > 0.5\,(\phi_1 + \phi_2) - 1. \tag{3.50}$$

As the feasible range for w is 0–1 and for c_1 and c_2 is 0–2, the selected values of w, c_1 and c_2 should be such that the above equations are satisfied for all possible values of random numbers r_1 and r_2 in the range 0–1. Keeping in view of this, considerable number of trials are conduced and the values of w, c_1 and c_2 are finally selected as 0.65, 1.65 and 1.75, respectively. Thus, the controlling parameters of PSO algorithm for the present case are:

- Number of particles in swarm = 5.
- Inertia weight = 0.65.
- Acceleration coefficient (C_1) = 1.65.
- Acceleration coefficient (C_2) = 1.75.
- Number of iterations = 50.

The results of optimization using the above parameter setting for PSO algorithm are shown in Table 3.6.

3.4.1.3 Optimization Using SA Algorithm

Using the simulated annealing technique, the objective function to minimize the machining speed is written as:

$$\text{Min.}\, Z = -w \times Z_1 - (P_1 \times Z_2), \tag{3.51}$$

where Z is the combined objective function, Z_1 the objective function given by Eq. 3.33, Z_2 the constraint value given by Eq. 3.34, w the weight of the objective function, and P_1 is the penalties assigned for violation of constraints Z_2. In present case, $P_1 = 35$ if a particular constraint is violated, else penalty = 0. However, one may use any other penalty function method.

Penalty is defined in the objective function in such a way that a point having higher value of 'Z_1' but with small negative value of 'Z_2' should be accepted at higher temperature to search another point in the vicinity. However, it should be ensured that such a point should never appear in the final solution. The initial temperature is obtained by calculating the average of the function values at a boundary points as given below:

$$\text{Initial temperature} \quad T_0 = \sum Z_{\text{Nb}} = /n, \tag{3.52}$$

where Z_{Nb} is the value of objective function at each boundary point and n is the number of boundary points. The initial temperature is calculated as 1.40 and the decrement factor is considered as 0.01. At any current point $X(t)$, the new value of the parameters for the successive iterations is calculated using the formula,

$$x(t+1) = x(t) + \sigma\left(\sum^{N} R_i - 0.5N\right) \tag{3.53}$$

where $\sigma = (X_{\max} - X_{\min})/6$; R is the random number; and N is the number of random numbers used. In the present work, six random numbers are used. While starting the process, the initial values for the parameters are taken as the average of the respective parameter limits. The algorithm is terminated when a sufficiently small temperature is obtained or a small enough change in function value is found.

Therefore the parameter setting for SA algorithm is:

- Initial temperature = 1.40.
- Decrement factor = 0.01.
- Number of iterations = 100.

The results of optimization using the above parameter setting for SA algorithm are shown in Table 3.6.

3.4.1.4 Optimization Using HS_M Algorithm

Controlling parameters of HS algorithm are the harmony memory size (HMS), or the number of solution vectors in the harmony memory; harmony memory considering rate (HMCR); pitch adjusting rate (PAR); number of decision variables (N) and the number of improvisations (NI), or stopping criterion. The harmony memory (HM) is a memory location where all the solution vectors (sets of decision variables) are stored. This HM is similar to the genetic pool in the GA. The HMCR and PAR are parameters that are used to improve the solution vector. After several trial runs following values of controlling parameter of HS algorithm are obtained;

- Harmony memory size = 5.
- Harmony memory consideration rate = 0.7.
- Pitch adjusting rate = 0.7.
- Number of improvisations = 150.

The results of optimization using the above parameter setting for HS_M algorithm are shown in Table 3.6.

3.4.1.5 Optimization Using SFL Algorithm

Following parameters of optimization of SFL are considered after several trial runs.

- Total number of frogs = 20.
- Number of memeflexes = 5.
- Number of frogs in each memeflex = 4.
- Number of improvisations = 50.

The results of optimization using the above parameter setting for SFL algorithm are shown in Table 3.6.

Now, using the parameter settings for various algorithms, results of optimization of WEDM process are given in Table 3.6

The Optimality of the solution obtained using ABC algorithm could be confirmed from Figs. 3.15, 3.16, 3.17, and 3.18. Figure 3.15 shows the variation of machining speed and constraint with pulse on-time.

As shown in Fig. 3.15, the machining speed increases with increase in pulse on-time; hence higher value of pulse on-time is desired. Thus, the selection of upper bound value of pulse on-time $T_{on} = 8$ μs is appropriate. It is also observed that the surface roughness initially increases and then decreases with pulse on-time. Hence, the constraint is initially violated beyond value of $T_{on} \cong 5.3$ μs, however, it is satisfied again at $T_{on} = 8$ μs. Variation of machining speed and constraint with pulse off-time is shown in Fig. 3.16.

As shown in Fig. 3.16, machining speed decreases but surface finish increases with the increase in pulse off-time. Thus, from machining speed point of view, lower value of pulse off-time is desired. However, upper bound value (30 μs) of pulse off-time is selected as for any value below 30 μs, surface roughness constraint is violated. Figure 3.17 shows variation of machining speed and constraint value with peak current.

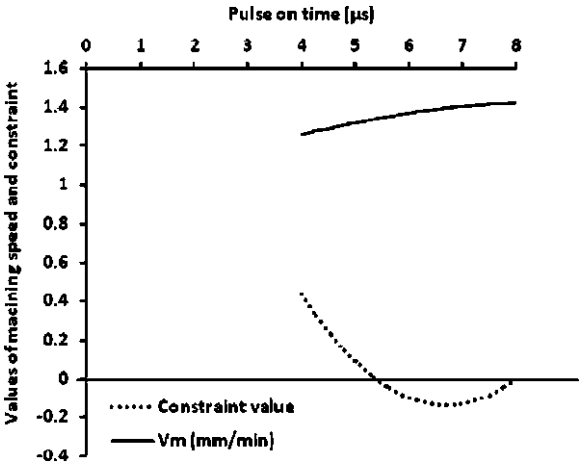

Fig. 3.15 Variation of machining speed and constraint value with pulse on-time (from [197]; reprinted with permission from the Council of the Institution of Mechanical Engineers, UK)

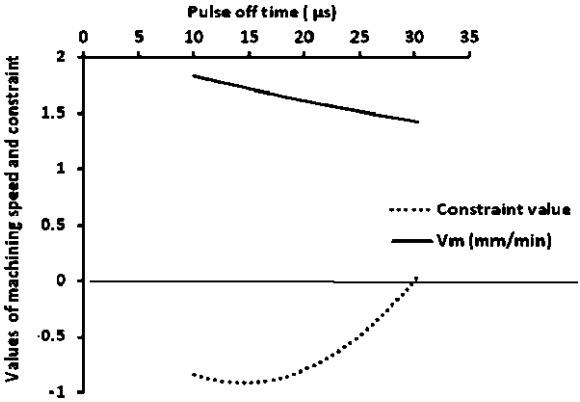

Fig. 3.16 Variation of machining speed and constraint value with pulse off-time (from [197]; reprinted with permission from the Council of the Institution of Mechanical Engineers, UK)

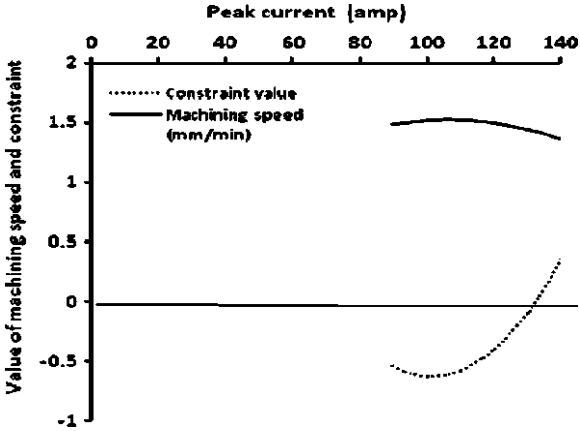

Fig. 3.17 Variation of machining speed and constraint value with peak current (from [197]; reprinted with permission from the Council of the Institution of Mechanical Engineers, UK)

As shown in Fig. 3.17, the machining speed initially increases slightly with peak current up to certain value ($\cong 107$ amps) and then decreases with increases in peak current. Values of peak current up to 107 amp cannot be selected as for these values the constraint is violated. From this point of view lower value of peak current should be selected. As the value selected for peak current of 132.52 amp is the lowest value at which the constraint is satisfied, is appropriate. Figure 3.18 shows variation of machining speed and constraint value with servo feed setting.

It is observed from Fig. 3.18 that servo feed setting has less effect on machining speed but affects the surface roughness significantly. Better surface finish can be achieved for higher value of servo feed setting. From this view point, selection of upper bound value of servo feed setting (=50) is appropriate. Figure 3.19 shows the convergence of ABC algorithm.

It is observed from the Table 3.6, that ABC algorithm outperforms other algorithm in terms of accuracy of the solution for the present application. This is due to the fact that ABC algorithm combines both, the stochastic selection scheme carried out by onlooker bees, and greedy selection scheme used by onlookers and employed bees to update the source position. The model formulated in this work is

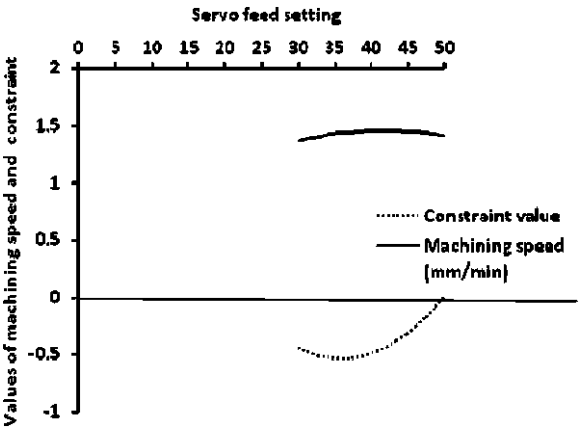

Fig. 3.18 Variation of machining speed and constraint value with servo feed setting (from [197]; reprinted with permission from the Council of the Institution of Mechanical Engineers, UK)

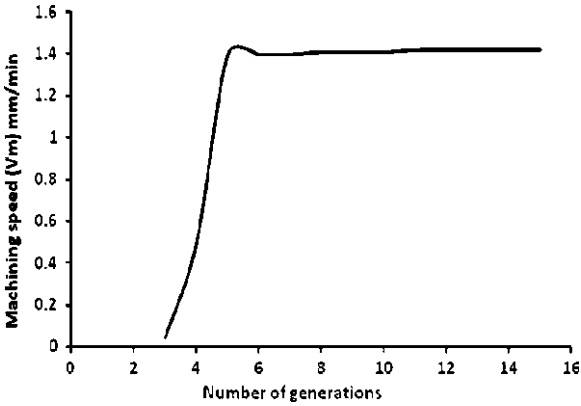

Fig. 3.19 Convergence of ABC algortihm (from [197]; reprinted with permission from the Council of the Institution of Mechanical Engineers, UK)

of multi-modal nature as it has a number of local optima. As an illustration, for desired value of $R_a = 2.1$ μm, one of the local optimum solution is: $T_{on} = 4$, $T_{off} = 10$, $I_p = 90$, and $F = 31$ with corresponding value of $V_m = 1.106$ mm/min and constraint value zero thus showing no scope for further improvement. However, the global optimum solution obtained using ABC provides $V_m = 1.465$ mm/min, showing about 32% improvement over the local optimum solution which is generally obtained using traditional methods of optimization. This clearly justifies the use of advanced optimization algorithms.

3.5 ECM Process

ECM is one of the NTMPs used to machine extremely hard materials that are difficult to cut cleanly using traditional methods of machining. The first process resembling ECM was patented by Gusseff in 1929. Significant advances during the

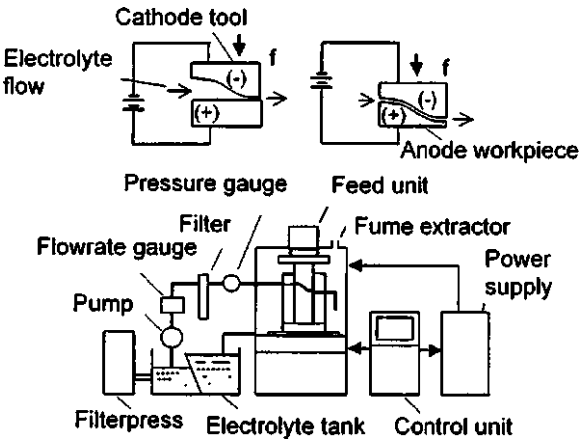

Fig. 3.20 ECM principle and equipment (from [200]; reprinted with permission from the Council of the Institution of Mechanical Engineers, UK)

1950s and 1960s developed ECM into a major technology in the aircraft and aerospace industries to machine high-strength alloys. As of now, ECM is employed in many ways by automotive, aerospace, nuclear, defense, tool and die making, offshore petroleum, medical, and electronic industries (e.g., turbine blades, engine castings, bearing cages, gears, dies and molds, artillery projectiles, surgical implants, diagnostic devices, etc.).

The basis of ECM is the phenomenon of electrolysis, whose laws were established by Faraday in 1833. Faraday proved that if two conductive poles are placed in a conductive electrolyte bath and energized by a current, metal may be depleted from the positive pole (anode) and plated onto the negative pole (cathode). Thus, ECM can be used to remove an electrically conductive work piece material through anodic dissolution. The principle and equipment used in ECM process is illustrated in Fig. 3.20 [192].

The work piece and the tool are the anode and cathode, respectively, of an electrolytic cell, and a constant potential difference (usually about 5–30 V) is applied across them producing a high current density of 10–200 A/cm^2. A suitable electrolyte (NaCl or $NaNO_3$ aqueous solution) is chosen so that the cathode shape remains unchanged during electrolysis. The electrolyte is pumped at a rate 3–60 m/s, through the gap between the electrodes to remove the machining waste (i.e., dissolved material, usually metal hydroxide) and to diminish unwanted effects such as those that arise with cathodic gas generation and electrical heating. The rate at which metal is then removed from the anode is approximately in inverse proportion to the distance between the electrodes. As machining proceeds, and with the simultaneous movement of the cathode at a typical rate, for example, 0.02 mm/s toward the anode, the gap width along the electrode length will gradually tend to reach a steady-state value. Under these conditions, a shape, approximately negative mirror image of the cathode, will be reproduced on the anode as the cathode does not alter during the ECM process. A typical gap width then can be about 0.4 mm.

No mechanical or thermal energy is involved in ECM process. Hard metals can be shaped electrolytically using ECM and the rate of machining does not depend on their hardness. The tool electrode used in the process does not wear, and therefore soft metals can be used as tools to form shapes on harder work pieces, unlike conventional machining methods. The process is used to smooth surfaces, drill holes, form complex shapes, and remove fatigue cracks in steel structures. Its combination with other techniques yields fresh applications in diverse industries.

The characteristics of ECM can be summarized as given below:

- Mechanics of material removal: electrolysis.
- Medium: conducting electrolyte.
- Tool material: copper, brass and steel.
- Tool wear: infinite.
- Gap: 50–800 μm.
- MRR: 0.1–10 mm/min.
- Surface finish: very high order of 0.6 μm.
- Critical parameters: voltage, current, feed rate, electrolyte flow velocity, and electrolyte conductivity.
- Materials application: all conducting metals and alloys.
- Shape application: blind complex cavities, curved surfaces, through cutting, and large through cavities.

The advantages of ECM process can be stated as:

- No tool wear.
- Components are not subject to either thermal or mechanical stresses.
- Non-rigid and open work pieces can be machined easily as there is no contact between the tool and work piece.
- Complex dimensional shapes can be machined repeatedly and accurately on hard and high-strength metals.
- Deep holes can be drilled or several holes at once.
- Fragile parts which cannot take more loads and also brittle materials which tend to develop cracks during machining can be machined easily.
- Smooth and bright surface finishes of 0.6 μm can be achieved.
- ECM is a time saving process when compared with conventional machining.

With recent advances in machining accuracy and precision, the electronics industry has begun to use ECM for micromachining components. ECM with pulsed DC voltage offers an enhanced accuracy control. The combination of ECM with other machining processes has been shown to yield performance superior to that achieved by individual processes. ECM and its pulse system are finding new applications in finishing molds and dies for many industrial components. Through its integration with many other enabling technologies, ECM is finding wider applications and increasing acceptance in a variety of other industries.

Despite the advances, ECM process has certain limitations. Some of the limitations can be stated as:

- Higher initial investment.
- High specific energy consumption (about 150 times that required for conventional processes) leading to high operating cost.
- High tooling cost.
- High maintenance cost.
- Unsuitable for electrically non-conducting materials and jobs with very small dimensions.
- Problems of corrosion, toxicity, and safety.
- Problems of process monitoring and control, tool design, disposal of waste, electrolyte processing, etc.

Due to these limitations, a very careful decision making during process planning is necessary before using ECM for the practical purposes. ECM process parameters optimization is an important component of this activity because use of optimum process parameters can significantly improve the process performance and process economics by reducing various costs. Generally, ECM process parameters are selected either based on the experience, expertise, and knowledge of the operator or from the propriety machining handbooks. Selection of process parameters based on the operator experience does not completely satisfy the requirements of high efficiency and good quality. While machining tables can be a better choice in a factory environment for one or two applications but cannot be used for a wide range of applications and operating conditions. In most of the cases, selected process parameters are conservative and far from the optimum. This hinders optimum utilization of the process capabilities. Selecting optimum values of process parameters without optimization requires elaborate experimentation which is costly, time consuming, and tedious. Therefore, most cost-effective, efficient, and economic utilization of ECM necessitates selecting the optimum values of important ECM process parameters so as to optimize the measures of process performance. These performance measures generally include maximizing MRR and tool life, and minimizing dimensional inaccuracy and machining cost. Minimizing dimensional inaccuracy is an important aspect in those critical applications where tight tolerances are desired.

Bhattacharyya and Sorkhel [22] highlighted features of the development of a comprehensive mathematical model for correlating the interactive and higher-order influences of various machining parameters on the dominant machining criteria, i.e., the MRR and the overcut phenomena, through RSM, utilizing relevant experimental data as obtained through experimentation. The authors highlighted the various test results that also confirmed the validity and correctiveness of the developed mathematical models for analyzing the effects of various process parameters on the machining rate and overcut phenomena. Optimal combination of these parameters can be used in order to achieve maximization of the MRR and the minimum overcut effects for optimal accuracy of shape features.

Adam and Maria [2] presented the primary investigations of machining with a flat rectangular universal electrode. The authors had developed a simple

mathematical model for MRR and stated that in the case of sculptured surfaces machining with flat ended electrode it was possible to reach higher MRR and smaller surface waviness than with a ball ended electrode. However, further investigations are required to prove these statements. Kozak [126] and Kozak et al. [127] presented the concept and prototype of a computer-aided engineering (CAE) system that can be used to solve different task of ECM, such as: tool-electrode design, selection of optimal machining variant and input machining parameters optimization. The system uses computer simulation software that was developed for various kinds of ECM operations like: electrochemical (EC) sinking, EC milling, EC smoothing, ECM-CNC with a universal electrode and numerically controlled electrode movement, etc. The results of computer simulation of different ECM processes and results of experimental verifications were also presented. The CAE-ECM system was designed to solve the following technological problems:

- Simulation of the work piece shape change during machining with a fixed tool-electrode profile including accuracy analysis.
- Tool-electrode design for a required work piece shape.
- Simulation of ECM smoothing process.
- Determination of basic characteristics of different variants of the ECM process (ECM with rotating electrode, pulse ECM, ECM with vibrating electrode, etc.).

Bhattacharyya and Munda [20] made an attempt to develop an experimental set-up for carrying out in-depth research for achieving a satisfactory control of the process parameters to meet the micromachining requirements. Keeping in view these requirements, sets of experiments were carried out to investigate the influence of some of the predominant ECM process parameters such as machining voltage, electrolyte concentration, pulse on-time and frequency of pulsed power supply on the MRR and accuracy to fulfil the effective utilization of ECM system for micromachining.

Purcar et al. [188] proposed a general applicable numerical method for the simulation of 3D electrode shape changes obtained during ECM processes based on the "marker" method. The electrode shape change was found by displacing each node proportional with, and in the direction of the local current density according to Faraday's law. The local growth rate was obtained by numerically solving the potential model using the boundary element method. Results related to 3D ECM of the letter "E" were presented. Hewidy et al. [85] presented an analytical approach to establish mathematical model in an endeavor to asses the mechanism of metal removal for this novel and hybrid technique. The effect of input parameters and machining conditions on the effectiveness of tool vibration during ECM was fully investigated. The analytical model reveals that there could be a great complexity in the relationship between the tool amplitude and the equilibrium gap size, which could lead to tool damage, if the problem has not been carefully considered.

Asokan et al. [10] conducted experiments on ECM setup and developed two multiple regression models and an ANN model to determine the optimal

machining parameters. In their work, current (C), voltage (V), flow rate (U), and (inter-electrode) gap (G) were considered as machining process parameters, and MRR and surface roughness were considered as objectives. The ranges of process parameters considered by the authors are given below:

- Voltage, V (volts) = 20–32.
- Electrolyte flow velocity, U (m/s) = 6–9.
- Current, C (Amp) = 200–280.
- Inter-electrode gap, G (mm) = 0.1–0.5.

The authors had developed two models of multiple regressions and a model of ANN to map the relationship between process parameters and the objectives in terms of grey relational grade. The models were checked for their suitability as best predictive models. Instead of using experimental values directly in multiple regression models and ANN model, grey relational grades were used to study about multi-response characteristics. GRA was used to convert the multi-response optimization model into a single response grey relational grade.

Asokan et al. [10] developed the following multiple regression models to analyze the process parameters in ECM process:

Model I Linear model excluding interaction terms

$$\text{Grade} = 0.702 - 0.00010C - 0.00688V + 0.0128U + 0.062G \tag{3.54}$$

Model II Transformation of exponential model excluding interaction terms

$$\text{Grade} = T \times C^a V^b U^c G^d, \tag{3.55}$$

where T, a, b, c, and d are constants.
A logarithmic transformation was applied to convert the non-linear form of equation into the following linear form.

$$\ln\text{Grade} = \ln T + a\ln C + b\ln V + c\ln U + d\ln G. \tag{3.56}$$

This model assumes that there is a normal distribution of the dependent parameter for every combination of the values of the independent parameters. The regression equation developed using MINITAB software based on this model is shown below.

$$\text{GradeL} = 0.64 - 0.083CL - 0.321VL + 0.191FL + 0.018GL. \tag{3.57}$$

The predicted values were calculated using the regression Eqs. 3.54–3.57. The percentage deviation was computed between the experimental grade and predicted grade of both training data and test data. ANOVA was used to identify the significance of multiple regression models and the authors had

reported that there was no significant difference between the training data and test data.

In addition to developing the multiple regression models, Asokan et al. (2007) developed an ANN model to check which prediction model was best. In ANN model, the experimental data was normalized in the range of −1 to +1 using the following equation:

$$A_o = 2(a - a_{min})/(a_{max} - a_{min}) - 1, \tag{3.58}$$

where A_n is the normalized input data, a_{max} the maximum value of the input data, a_{min} the minimum value of the input data, and a is the input data to be normalized.

The process parameters and the output responses were organized into the input layer and the output layer, respectively, to train the network. The input variables were current, voltage, electrolyte flow rate, and gap. The total number of inputs nodes was four. The network was built to relate the process parameters and output responses. The output layer was considered as grey relational grade. The network was trained using the training data sets with experimental grade. The training parameters were set as follows:

- Learning rate = 0.01.
- Maximum allowed system error = 1e–10.
- Number of iterations = 10,000.

The network was tested, and ANOVA was performed and it was reported that there was no significant difference between training data and test data.

The average percentage deviations for the training data of the linear regression model, logarithmic transformation model, excluding interaction terms and ANN model were 12.7, 25.6 and 3.03, respectively. The average percentage deviations for the testing data of the three models were 9.83, 26.8 and 2.67. While examining the average percentage deviations of three models, ANN was having less percentage deviation. Hence ANN was considered as the best prediction model as compared to the regression models. Based on the testing results of the ANN, the operating parameters were optimized. Finally, the optimal conditions obtained were current at 200 A, voltage at 20 V, gap at 0.3 mm and flow rate at 9 m/s for maximizing MRR and surface roughness simultaneously among the 32 experimental data.

However, Asokan et al. [10] had not considered the effect of feed rate on the objectives of maximizing MRR and minimizing surface roughness. Feed rate, f, is an important process parameter that should be considered in the optimization process. Also, the operating ranges selected for process parameters particularly for the electrolyte flow rate, U, was low. Other important objectives such as maximizing dimensional accuracy and tool life were not considered. The alphabet 'L' was not explained. The authors had not considered any interaction effects of the process parameters in multiple regression modeling. Furthermore, it is observed that the authors had made many wrong calculations in determining the normalized values of C, V, F, and G. These wrong calculations had resulted in wrong grey

relational grades for ANN modeling. Hence, the subsequently drawn conclusion that ANN model was the best predictive model is doubtful. As a result, the optimization results obtained by Asokan et al. (2007) using ANN model are questionable.

Munda and Bhattacharyya [21] attempted to establish a comprehensive mathematical model for correlating the interactive and higher-order influences of various machining parameters, i.e., machining voltage pulse on/off ratio, machining voltage, electrolyte concentration, voltage frequency and tool vibration frequency on the predominant micromachining criteria, i.e., the MRR and the radial overcut (ROC) through RSM, utilizing relevant experimental data as obtained through experimentation. Validity and correctiveness of the developed mathematical models were also tested through analysis of variance. Optimal combination of these predominant micromachining process parameters was obtained from these mathematical models for higher machining rate with accuracy. Considering MRR and ROC simultaneously optimum values of predominant process parameters were obtained as: pulse on/off ratio 1.0, machining voltage 3 V, electrolyte concentration 15 g/l, voltage frequency of 42.118 Hz and tool vibration frequency as 300 Hz. The effects of various process parameters on the machining rate and radial overcut were also highlighted through different response surface graphs.

Senthilkumar et al. [215] investigated the influence of some predominant ECM process parameters such as applied voltage, electrolyte concentration, electrolyte flow rate and tool feed rate on the MRR, and surface roughness to fulfill the effective utilization of ECM of LM25 Al/10%SiC composites produced through stir casting. The contour plots were generated to study the effect of process parameters as well as their interactions. The process parameters were optimized based on RSM approach.

The next section describes the input–output process parameter relationship modeling and optimization of ECM process parameters.

3.5.1 Modeling and Optimization of ECM Process Parameters

ECM is a complex process and it is difficult to predict the changes that may occur in the gap between cathode and anode, known as inter-electrode gap (IEG). The electrolyte properties vary due to the emission of a considerable amount of heat and gas bubbles. In addition, hydrodynamic parameters, such as pressure, also vary along the electrolyte flow direction and make the analysis quite complicated. Bhattacharyya et al. [19] proposed a 2D inter-electrode gap model in which maximization of the MRR was considered as the objective function with tool feed rate (f) and electrolyte flow velocity (U) as the design parameters. The three constraints considered were temperature, passivity, and chocking. The temperature constraint is to avoid boiling of electrolyte, the choking constraint is to avoid electrolyte flow choking due to H_2 gas, and the passivity constraint is to avoid

formation of passive oxide film on the work surface due to O_2 gas. The objective function and the constraints are given below:

$$\text{Objective function : maximize MRR} = A_a f \left(\text{mm}^3/\text{s}\right) \tag{3.59}$$

where A_a is the projected area of work piece (mm^2). Since A_a is constant, the objective function is equivalent to: maximize MRR $= f_{\max}$.

The objective of the model proposed by Bhattacharyya et al. [19] was to maximize the feed rate satisfying the following three constraints:

1. The highest temperature attained by the electrolyte must be less that its boiling point.
2. Choking of the electrolyte flow due to H_2 gas should be avoided.
3. Passivation of the work surface due to O_2 gas must not occur.

The model was based on many simplified assumptions. The temperature constraint line was found to run significantly below the optimal point, and so was not considered. Thus, the optimization problem was reduced to:

$$\text{Choking constraint:} U \geq 2.60 f^2 \tag{3.60}$$

$$\text{Passivity constraint:} U \leq 3.38 f. \tag{3.61}$$

This problem was non-linear in nature and was solved by Bhattacharyya et al. [19] using a graphical technique which, in itself, was less accurate. In the above model, maximization of MRR was the only objective. Void fraction (i.e., volumetric gas concentration) was assumed to remain constant and a high value for the void fraction (0.7) was used, and the electrolyte conductivity was assumed to be a function of void fraction alone. However, it was shown by Hopenfeld and Cole [92] that temperature also has a significant effect on the electrolyte conductivity and hence, should be taken into account. Void fraction and pressure also vary significantly and therefore, should not be assumed constant during the process. Furthermore, parameter bounds for f and U should be specified.

Kozak [125] developed a 2D optimization model for ECM under steady state operating conditions, the objective was to maximize dimensional accuracy, i.e., the difference in inter-electrode gap (lEG) at inlet and outlet. The variation in lEG with respect to IEG at inlet is dependent upon the variation in electrolyte conductivity along the electrolyte flow path. Electrolyte conductivity is a function of the temperature and void fraction and is given by:

$$K_x/K_i = \left(1 - \alpha'_x\right)^k (1 + \alpha(T_x - T_i)), \tag{3.62}$$

where K_x is the electrical conductivity of electrolyte at a distance 'x' from the electrolyte entrance, K_i the electrical conductivity of electrolyte at the inlet, α'_x the void fraction at a distance 'x' from the electrolyte entrance, k the exponent,

α the temperature coefficient of electrolyte conductivity, and T_x and T_i are the temperatures at a distance of 'x' from the inlet and at the inlet, respectively.

Since K_x/K_i is always greater than one, the minimization of the difference in lEG at inlet and outlet is achieved by minimizing K_x/K_i. However, from a practical point of view, expressing the dimensional accuracy in terms of an absolute value (mm or μm) would be better than in terms of K_x/K_i.

El-Dardy [67] proposed a cost model of the ECM process considering various costs involved in the process. The costs considered were, machining cost, electrolyte cost, electrolyte changing cost, filter cost, filter cleaning cost, tool changing cost, and non-productive cost. The cost equation was arranged in terms of decision parameters namely, feed rate (f), electrolyte flow rate (U), and voltage (V).

$$N = a + bW + cf/V, \tag{3.63}$$

where n is the number of sparks per mm, and W is the metal removed in gm/liter of electrolyte flow.

$$W = 1,000\, A_a \rho_{\mathrm{w}} / Y_{\mathrm{i}} BU, \tag{3.64}$$

where ρ_{w} is the density of work piece, Y_{i} the inter-electrode gap at inlet, B the width of work piece, and a, b, and c are constants.

El-Dardy [67] obtained the optimum values of the decision parameters by partial differentiation of cost equation with respect to the decision parameters. However, the values of decision parameters obtained were not practical, as no constraints were considered in this model, Furthermore, some costs considered in the analysis (e.g., filter cost, electrolyte changing cost, etc.) contribute little to the objective function and can be neglected.

Hewidy et al. [86] analyzed the components of ECM cost such as costs of power consumption, machining, electrolyte, and labor with the objective to set out the basic principles for selecting a suitable electrochemical machine to meet the local production requirements of a company. The authors mentioned about the impossibility of having a generalized model for this purpose.

The models detailed above deal with single-objective optimization in ECM process. However, from a practical point of view, it is desirable to analyze a multi-objective problem. Acharya et al. [1] proposed a model, with three objective functions [maximization of MRR, minimization of difference in inter-electrode gap from inlet to outlet (or maximization of dimensional accuracy), and maximization of tool life]. Some of the assumptions made in earlier models had been relaxed to bring the problem nearer to the real situation and all three design parameters (feed rate, electrolyte flow velocity, and applied voltage) were taken into account. The optimum values of these design parameters were determined by satisfying constraints such as the boiling of the electrolyte, choking, passivity, and range of design parameters. The authors had formulated a multi-objective problem producing highly non-linearized equations. These were then linearized by regression analysis and converted into a goal-programming format, as the goal-programming solution technique requires the objective function and constraint

equations in a linear form. The objective functions and the constraints are explained below (from [1]; reprinted with permission from Elsevier):

Objective 1 Maximization of MRR

This is the product of projected area and tool feed rate and same as Eq. 3.57 proposed by Bhattacharyya et al. [19]. Thus, $\mathrm{MRR}_{\max} = f_{\max}$

Objective 2 Maximization of dimensional accuracy

ECM, perhaps, is the only machining process which does not allow checking the work piece dimensions in the course of machining. Although few techniques such as ultrasonic measurement of inter-electrode gap can be used [51], it is necessary to predetermine the control parameters to ensure the desired dimensional accuracy. Dimensional accuracy depends upon the difference in inter-electrode gap from inlet Y_{i} to outlet Y_{o}, which was given by:

$$Y_{\mathrm{o}} - Y_{\mathrm{i}} = [(K_o/K_i) - 1]K_i M_{\mathrm{w}} \eta_i V/\rho_{\mathrm{w}} Z_{\mathrm{w}} F f, \tag{3.65}$$

where M_{w} is the atomic weight of work piece, η_i the current efficiency, Z_{w} the valency of work piece, F the Faraday's constant, and K_x/K_i is same as given by Eq. 3.62. $K_x = K_o$ at outlet.

The objective of maximizing the dimensional accuracy (i.e., minimizing the dimensional inaccuracy) was attained by minimizing $(Y_{\mathrm{o}} - Y_{\mathrm{i}})$.

Objective 3 Maximization of tool life

Ideally, there is no tool wear in ECM but in actual practice and high feed rates, the tool eventually touches the work and results in sparking and wearing out of the tool. Maximization of tool life is ensured by minimizing the number of sparks per mm as given by the equation:

$$\eta_{\min} = a + bE_i f^2/VU + cf/V \tag{3.66}$$

$$E_i = 1,000 \times (A_a/B)\left[\left(\rho_{\mathrm{w}}^2 Z_{\mathrm{w}} F\right)/(K_i M_{\mathrm{w}} \eta_i)\right]. \tag{3.67}$$

Temperature constraint. To avoid boiling of electrolyte, the electrolyte temperature at the outlet should be less than the electrolyte boiling temperature. Mathematically this can be expressed as,

$$T_i - (1/\alpha)\left[1 - \left(\left(1 + S_{\mathrm{k}} f^2\right)/U\left(1 - \alpha'_{\max}\right)^n\right)^{0.5}\right] \le T_b, \tag{3.68}$$

$$\text{where} \quad S_{\mathrm{k}} = \left(2\alpha\gamma^2 L\right)/(K_i \rho_{\mathrm{e}} C_{\mathrm{e}} J_{\mathrm{cn}}) \tag{3.69}$$

$$\gamma = Z_{\mathrm{w}} F \rho_{\mathrm{w}}/M_{\mathrm{w}} \eta_i \tag{3.70}$$

T_{b} is the permitted outlet temperature for electrolyte, L the length of work piece, ρ_{e} the density of electrolyte, C_{e} the specific heat of electrolyte, $\alpha'_{\max}$ the maximum void fraction, and J_{cn} is the Joule's constant.

Passivity constraint. Oxygen evolved during ECM forms an oxide film, which is the root cause of passivity. To avoid passivity, the thickness of the oxygen gas bubble layer must be greater than the passive layer thickness. Mathematically this can be expressed as,

$$G_{\mathrm{t}}(T_0 + 273)f/\mathrm{U}\alpha'_{\max} \geq 1 \tag{3.71}$$

$$G_{\mathrm{t}} = \left(R\rho_{\mathrm{f}}R_{\mathrm{f}}L\gamma/P_{\mathrm{o}}t_{\mathrm{p}}i\right), \tag{3.72}$$

where R is the gas constant, ρ_{f} the passive film density, R_{f} the roughness factor, P_{o} the pressure at outlet, t_{p} the time taken for film formation, and i is the ionic current density.

Chocking constraint. Hydrogen evolved at the cathode during ECM process can choke the electrolyte flow. To avoid chocking of the electrolyte flow, maximum thickness of the hydrogen bubble layer should be less than the equilibrium inter-electrode gap. Mathematically, it can be expressed as,

$$\left[H_{\mathrm{t}}f^2(T_{\mathrm{o}} + 273)\right] / \left[VU\alpha'_{\max}\left(1 - \alpha'_{\max}\right)^n(1 + \alpha(T_{\mathrm{o}} - T_i))\right] \leq 1 \tag{3.73}$$

$$H_{\mathrm{t}} = M_{\mathrm{h}}RL\gamma^2/Z_{\mathrm{h}}P_{\mathrm{o}}FK_i, \tag{3.74}$$

where M_{h} is the atomic weight of hydrogen, and Z_{h} is the valency of hydrogen.

Acharya et al. [1] used the following input data for developing the multiple regression models:$M_{\mathrm{w}} = 56$ g, $\rho_{\mathrm{w}} = 7.86$ g/cm^3, $Z_{\mathrm{w}} = 2$, $L = 3$ cm, $\eta_i = 0.95$, $K_i = 0.3333$ S/cm, $\rho_{\mathrm{e}} = 1$ g/cm^3, $C_{\mathrm{e}} = 0.997$ cal/g°C, $\alpha = 0.02$/°C, $M_{\mathrm{h}} = 1$ g, $Z_{\mathrm{h}} = 1$, $\rho_{\mathrm{h}} = 0.003965$ g/cm^3, $R_{\mathrm{f}} = 1.25$, $\rho_{\mathrm{f}} = 0.042$ g/cm^3, $t_{\mathrm{p}} = 60$ s, $i = 1.25$ A/cm^2, $T_i = 27$°C, $R = 42{,}030$ g cm/g k, $J = 4.186$ J/cal, $P_{\mathrm{o}} = 6{,}000$ gf/cm^2, $T_{\mathrm{b}} = 65$°C, $\alpha'_{\max} = 0.7$, $Y_{\mathrm{i}} = 0.02$ cm, $a = -2.05$, $b = -0.325$, and $c = 26.78$.

Using multiple regression analysis, the equations for the objectives and the constraints were reduced to the following forms:

The first objective, Z_1, is to maximize the MRR and it is same as given by Eq. 3.59 The second objective, Z_2, is to maximize the dimensional accuracy (i.e., minimizing the dimensional inaccuracy) as given by following expression.

$$Z_2 = f^{0.381067} \times U^{-0.372623} \times V^{3.155414} \times e^{-3.128926}, \tag{3.75}$$

where Z_2 is the dimensional inaccuracy (μm).

The third objective, Z_3, is to maximize the tool life by minimizing the number of sparks per millimeter, which is given by the following expression:

$$Z_3 = f^{3.528345} \times U^{0.000742} \times V^{-2.52255} \times e^{0.391436}, \tag{3.76}$$

where Z_3 is the number of sparks per millimeter.

$$\text{Temperature constraint:} 1 - \left(f^{2.133007} \times \mathrm{U}^{-1.088937} \times \mathrm{V}^{-0.351436} \times \mathrm{e}^{0.321968}\right) \geq 0. \tag{3.77}$$

Passivity constraint:

$$\left(f^{-0.844369} \times U^{-2.526076} \times V^{1.546257} \times e^{12.57697}\right) - 1 \geq 0. \tag{3.78}$$

Choking constraint:

$$1 - \left(f^{0.075213} \times U^{-2.488362} \times V^{0.240542} \times e^{11.75651}\right) \geq 0. \tag{3.79}$$

Parameter bounds:

$$27 \leq T \leq 65(^{\circ}\mathrm{C}) \tag{3.80}$$

$$300 \leq U \leq 1,000(\mathrm{cm/s}) \tag{3.81}$$

$$3 \leq V \leq 21(\mathrm{Volts}). \tag{3.82}$$

The goodness of fit for the relationships given in Eqs. 3.75–3.79 was tested with F and t tests and found to be satisfactory. The goals for tool life and dimensional accuracy were kept at 4,000 sparks/m and 100 μm, respectively.

The model proposed by Acharya et al. [1] overcame the limitations of model proposed by Bhattacharyya et al. [19]. However, this model did not include the parameter bounds for feed rate and difference in inter-electrode gap. The optimization model was based on approximated objective functions and constraints. Furthermore, the rationale behind the selection of goals for dimensional accuracy and tool life was not explained.

The drawbacks of the model proposed by Acharya et al. [1] were overcome by Choobineh and Jain [49]. The authors had considered only two objective functions, i.e., maximization of MRR and maximization of dimensional accuracy. The third objective to maximize the tool life was eliminated as tool life is overachieved in most of the practical cases. The authors had used fuzzy set approach for assigning the degree of membership to each parameter within its boundary interval, and vertex method to find appropriate distribution of the objective functions. The modified goal-programming problem was then solved in the same manner as in Acharya et al. [1]. The parameter bounds for f and $(Y_o - Y_i)$ were included and the goals for f and $(Y_o - Y_i)$ were set as 0.02 mm/s and 525 μm, respectively. The authors had obtained optimum dimensional accuracy value of 181.07 μm for the optimum values of $f = 0.01275$ mm/s, $U = 400$ cm/s, and $V = 21$ Volts.

Jain and Jain [101] formulated the optimization model based on the analysis given in Acharya et al. [1] with certain modifications, i.e., expanding the parameter bound ranges for the tool feed rate (f) and electrolyte flow velocity (U) but without linearizing the objective functions and constraints. Based on the survey of feasible operating ranges for the decision parameters of the ECM process, the authors had presented information as given in Table 3.7. The optimization problem was then solved using real-coded genetic algorithms (GA). The details of GA employed by Jain and Jain [101] are given below:

Table 3.7 Feasible operating ranges of ECM process parameters (from [200]; reprinted with permission from the Council of the Institution of Mechanical Engineers, UK)

References	Tool feed rate (mm/s)	Electrolyte flow velocity (mm/s)	Applied voltage (*V*)
Acharya et al. [1]	–	3,000–10,000	3–21
Choobineh and Jain [49]	0.0100–0.025	4,000–20,000	3–21
Ghosh and Mallik [74]	0.0125–0.033	–	8–20
Benedict [23]	0.0080–0.320	15,000–60,000	4–30
McGeough [162]	Up to 0.02	3,000–30,000	10–20
Mishra [167]	0.0085–0.217	25,000–50,000	2–30
Jain [103]	–	20,000–30,000	5–25
Machinability Data Center [154]	0.0085–0.217	25,000–50,000	5–30
Jain and Jain [101]	0.0080–0.200	3,000–50,000	3–21

- Initial random number generation: Knuth's random number generator.
- Reproduction operator: binary tournament selection.
- Crossover operator: simulated binary crossover (SBX) with SBX distribution index $\eta_c = 2$ and 10.
- Crossover probability: 0.9.
- Mutation: polynomial probability distribution parameter $\eta_m = 10$ and 50.
- Mutation probability: reciprocal of number of decision parameters.
- Population size: 15, 20, and 25 times number of decision parameters.
- Number of generations: 100.

Reproduction, crossover, and mutation operators were directly applied to real parameter values in real-coded GA. Based on the results for different combinations of population size, SBX parameter, and polynomial mutation parameter, following overall optimum solution was obtained in the 100th generation of third run for a population size of 76, SBX parameter of 10, and polynomial mutation parameter of 50.

- Tool feed rate, f (mm/s) = 0.008.
- Electrolyte flow velocity, U (cm/s) = 2978.45.
- Applied voltage, V (Volts) = 16.5.

However, Jain and Jain [101] considered only single-objective optimization problem, i.e., to minimize the dimensional inaccuracy. It is also observed that the results obtained using genetic algorithm [101] violate the passivity constraint when applied to the model of Acharya et al. [1]. Jain and Jain [101] used the same model of Acharya et al. [1] for optimization of ECM process parameters. Even though Jain and Jain [101] mentioned that all constraints were satisfied, but when the values obtained by them are substituted in the constraint equations, the passivity constraint gets violated. Same is the case for the value of dimensional inaccuracy. Even though Jain and Jain [101] mentioned that the

optimum value of dimensional accuracy was obtained as 7.463 μm, but the value turns out to be 33.62 μm by putting the optimum values of genetic algorithm in the model proposed by Acharya et al. [1]. Furthermore, genetic algorithm has its own limitations such as risk of replacement of a good parent string with the deteriorated child, less convergence speed and difficulty in selecting the controlling parameters such as population size, crossover rate and mutation rate.

Rao et al. [200] proposed the application of a PSO algorithm to the same optimization model proposed by Acharya et al. [1] to find out if any improvement in the solution was possible. The authors had applied PSO algorithm by expanding the parameter bound ranges for the tool feed rate and electrolyte flow velocity. The objectives considered were dimensional accuracy, tool life, and MRR subjected to the constraints of temperature, choking, and passivity. Both single and multi-objective optimization aspects were considered. The results of PSO algorithm were compared with the results obtained by Acharya et al. [1], Choobineh and Jain [49], and Jain and Jain [101]. The results obtained using PSO algorithm were proved to be better and logical.

Now the same optimization problem is solved using ABC, SA, modified HS, and SFL algorithms. The parameters of optimization for various advanced optimization algorithms are selected as shown below.

Controlling parameters for ABC:

- Number of employed bees = 5.
- Number of onlookers bees = 11.
- Number of scout bees = 1.
- Maximum number of iterations = 150.

Controlling parameters for PSO:

- Number of particles in swarm = 5.
- Inertia weight = 0.65.
- Acceleration coefficient (C_1) = 1.65.
- Acceleration coefficient (C_2) = 1.75.
- Number of iterations = 50.

Controlling parameters for SA:

- Initial temperature = 200.
- Decrement factor = 0.01.
- Number of iterations = 100.

Controlling parameters for HS_M:

- Harmony memory size = 5.
- Harmony memory consideration rate = 0.8.
- Pitch adjusting rate = 0.3.
- Number of improvisations = 150.

Controlling parameters for SFL:

- Total number of frogs = 20.
- Number of memeflexes = 5.
- Number of frogs in each memeflex = 4.
- Number of improvisations = 50.

The results of single-objective optimization are given in Table 3.8. It is observed from the results that the solution obtained using shuffled frog leaping algorithm gives significantly smaller value of dimensional inaccuracy as compared to that of Acharya et al. [1], Choobineh and Jain [49], Jain and Jain [101], ABC, harmony search, and PSO algorithm [200] when applied to the model of Acharya et al. [1]. This improvement is mainly due to the use of better optimization technique which combines the benefits of the genetic-based Memetic Algorithm (MA) and the social behavior-based PSO algorithms.

Optimality of the above-mentioned solution could be confirmed from the Figs. 3.21, 3.22, and 3.23. As shown in Fig. 3.21, the dimensional inaccuracy increases with the tool feed rate. Therefore, the smallest possible value of the tool feed rate will minimize the dimensional inaccuracy. Also, the passivity constraint will be violated if higher value of tool feed rate is selected. Hence the tool feed rate at the lower bound ($f = 8$ μm/s) is selected.

The variation of electrolyte flow velocity is shown in Fig. 3.22. As the dimensional inaccuracy decreases with increase in the electrolyte flow velocity, selection of higher value of electrolyte flow velocity is desirable. However, the value of electrolyte flow velocity at lower bound ($U = 300$ cm/s) is obtained, as at any higher value than this, the passivity constraint is violated. This may be the reason for violation of passivity constraint for the solution obtained using genetic algorithm [101] when used in the optimization model of Acharya et al. [1].

Figure 3.23 shows that the dimensional inaccuracy increases with increase in voltage. Hence selection of lower value of applied voltage is desirable. However, to ensure the non-negativity of passivity constraint, the value of voltage (V) equal to 9.827 Volts is selected.

Table 3.8 Results of single-objective optimization

Method	f (μm/s)	U (cm/s)	V (Volts)	TC	PC	CC	Z
GP [1]	18.96	179	15	0.001	2.422	0.204	100
Fuzzy [49]	12.75	400	21	0.841	0.0559	0.886	181.07
GA [101]	8	2,978.45	16.5	0.992	**−0.993**	0.999	33.62
PSO	8	300	9.835	0.895	0.001	0.810	15.452
ABC	8	300	9.840	0.895	0.0025	0.813	15.470
SA	8	300	9.870	0.895	0.0072	0.813	15.620
HS_M	8	300	9.890	0.895	0.0104	0.813	15.720
SFL	8	300	9.827	0.895	0.0004	0.813	15.415

TC value of temperature constraint, *PC* value of passivity constraint, *CC* value of choking constraint

The bold value shows that the constraint 'PC' was violated by the GA approach

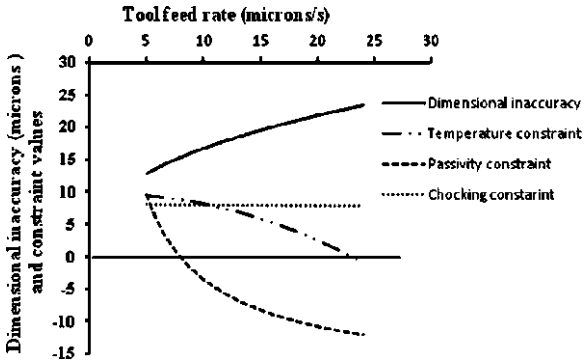

Fig. 3.21 Variation of the objective function and the constraints with tool feed rate (from [200]; reprinted with permission from the Council of the Institution of Mechanical Engineers, UK)

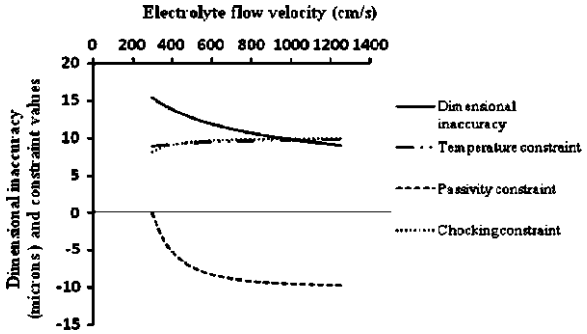

Fig. 3.22 Variation of the objective function and the constraints with electrolyte flow rate (from [200]; reprinted with permission from the Council of the Institution of Mechanical Engineers, UK)

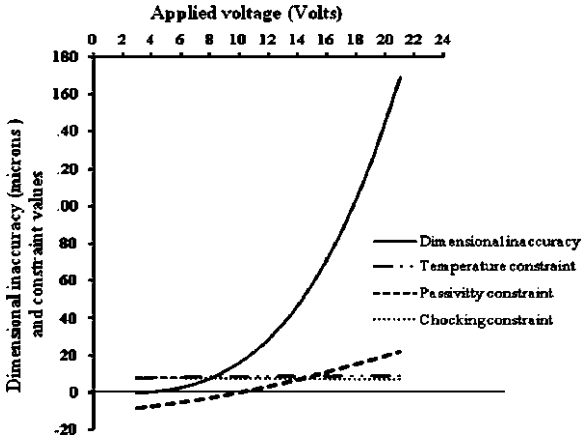

Fig. 3.23 Variation of the objective function and the constraints with applied voltage (from [200]; reprinted with permission from the Council of the Institution of Mechanical Engineers, UK)

For multi-objective optimization the three objectives considered are, MRR, dimensional inaccuracy, and tool life subjected to the constraints of temperature, passivity, and chocking. Decision variables, variable bounds and constraints are same as specified for single-objective optimization problem. The normalized

Table 3.9 Results of multi-objective optimization of ECM process

Method	f (μm/s)	U (cm/s)	V (Volts)	TC	PC	CC	Z
GP [1]	18.96	179	15	0.001	2.422	0.204	18.22
Fuzzy [49]	12.75	400	21	0.841	0.0559	0.886	5.47
GA [101]	8	2978.45	16.5	0.992	**−0.993**	0.999	1.23
PSO	8	300	13.225	0.905	0.583	0.799	1.811
ABC	8	339.166	13.33	0.918	0.215	0.851	1.767
SA	8	300	13.380	0.905	0.603	0.799	1.812
HS_M	8	300	13.14	0.905	0.567	0.800	1.802
SFL	8	300	13.33	0.905	0.603	0.799	1.801

TC value of temperature constraint, *PC* value of passivity constraint, *CC* value of choking constraint

The bold value shows that the constraint 'PC' was violated by the GA approach

combined objective function, Z, is formulated considering different weightages to all objectives and is given by the following equation:

$$Z = w_1(Z_1/Z_{1\min}) + w_2(Z_2/Z_{2\min}) - w_3(Z_3/Z_{3\max}), \tag{3.83}$$

where $Z_{1\min} = 15.452$ μm; $Z_{2\min} = 1.055$; and $Z_{3\max} = = 25$ μm/s. w_1, w_2, and w_3 are the weightages assigned to the objective functions Z_1, Z_2, and Z_3, respectively. The values of weightages can be calculated using the analytic hierarchy process [196]. The results of multi-objective optimization of ECM process are shown in Table 3.9.

It is observed from the results that the combined objective function, Z, obtained by ABC algorithm shows substantial improvement over Acharya et al. [1], Choobineh and Jain [49]. Although the results obtained by GA seem to be better but these are not valid as the passivity constraint gets violated. Results obtained by ABC, PSO, HS_M, and SA are equally good in terms of accuracy of solution. It should be noted that for the present case the results obtained using SFL algorithm are slightly better than even ABC, PSO, HS, and SA algorithms as SFL algorithm combines the benefits of the genetic-based Mimetic Algorithm (MA) and is the social behavior-based PSO algorithms.

It is observed from the review of past work that graphical solution technique and mathematical programming techniques such as goal programming, partial differentiation, multiple regression modeling, etc. had been used to solve the problem of optimization of process parameters of ECM. However, these traditional methods of optimization do not fare well over a broad spectrum of problem domains. Moreover, traditional techniques are not robust. Due to the complex nature of optimization problem, these techniques are not ideal for solving these problems, as they tend to obtain a local optimal solution. To overcome the drawbacks of traditional optimization techniques, researchers are now using evolutionary optimization techniques. Evolutionary computation consists of a variety of methods including optimization paradigms that are based on evolution mechanisms such as biological genetics and natural selection. These methods use the fitness information instead of the functional derivatives making them more

robust and effective. Most commonly used non-traditional optimization technique is the genetic algorithm. However, this method provides a near optimal solution for a complex problem having large number of parameters and constraints. This is mainly due to difficulty in determination of optimum controlling parameters. Therefore the efforts are continuing to use more recent optimization algorithms, which are more powerful, robust and able to provide accurate solution. It is also proposed to integrate the ANN models with meta heuristics for finding the optimal machining parameters.

3.6 LBM Process

LBM is accomplished by precisely manipulating a beam of coherent light to vaporize unwanted material. LBM is particularly suited to making accurately placed holes. It can be used to perform precision micromachining on all micro-electronic substrates such as ceramic, silicon, diamond, and graphite. Examples of microelectronic micromachining include cutting, scribing and drilling all sub-strates, trimming any hybrid resistors, patterning displays of glass or plastic and trace cutting on semiconductor wafers and chips.

Generation of the laser beam involves stimulating a lasing material by electrical discharges or lamps within a closed container. As the lasing material is stimulated, the beam is reflected internally by means of a partial mirror, until it achieves sufficient energy to escape as a stream of monochromatic coherent light. Mirrors or fiber optics are typically used to direct the coherent light to a lens, which focuses the light at the work zone. The narrowest part of the focused beam is generally less than 0.3 mm in diameter. Depending upon material thickness, kerf widths as small as 0.1 mm are possible. In order to be able to start cutting from somewhere else than the edge, a pierce is done before every cut. Piercing usually involves a high power pulsed laser beam which slowly makes a hole in the material.

There are three main types of lasers used in laser cutting. The CO_2 laser is suited for cutting, boring, and engraving. The neodymium (Nd) and neodymium yttrium–aluminum–garnet (Nd–YAG) lasers are identical in style and differ only in application. Nd is used for boring and where high energy but low repetition are required. The Nd–YAG laser is used where very high power is needed and for boring and engraving. Both CO_2 and Nd/Nd–YAG lasers can be used for welding. Common variants of CO_2 lasers include fast axial flow, slow axial flow, transverse flow, and slab.

CO_2 lasers are commonly pumped by passing a current through the gas mix (DC-excited) or using radio frequency energy (RF-excited). The RF method is newer and has become more popular. Since DC designs require electrodes inside the cavity, they can encounter electrode erosion and plating of electrode material on glassware and optics. Since RF resonators have external electrodes they are not prone to those problems.

In addition to the power source, the type of gas flow can affect performance as well. In a fast axial flow resonator, the mixture of carbon dioxide, helium and nitrogen is circulated at high velocity by a turbine or blower. Transverse flow lasers circulate the gas mix at a lower velocity, requiring a simpler blower. Slab or diffusion cooled resonators have a static gas field that requires no pressurization or glassware, leading to savings on replacement turbines and glassware.

The main strength of LBM process lies in its capability to machine almost all type materials in comparison to other widely used advanced machining methods such as EDM, ECM, and USM. In comparison to jet machining processes, it is quite suitable for cutting small and thin sheets with high cutting rates and can be applied to machine miniature objects unlike other jet machining processes such as water jet, and AWJM methods. Though it is non-contact type advanced machining method with high flexibility but thermal nature of the process requires careful control of the laser beam to avoid any undesired thermal effect. Among different variations, only laser drilling and cutting are being used most widely while 3-D LBM operations are not fully developed and a lot of research work is required before they can be put for industrial use. Unlike other, non-conventional energy sources laser beam source of energy can also be used as assistance during conventional machining of difficult-to-machine materials. The laser hybrid machining processes such as laser-assisted turning (LAT), laser-assisted shaping (LAS), laser-assisted grinding (LAG), laser-assisted EDM (LAEDM), laser-assisted ECM (LAECM), ultrasonic-assisted LBM (UALBM), laser-assisted etching (LAE) were found superior to a single machining technique in various machining applications.

The capability of LBM to cut complex shapes and drill micro-size holes with close tolerances in wide variety of materials has opened a new door to industries. Now-a-days, industries related to almost all manufacturing fields are adopting the LBM processes. Some unique applications of LBM involves cutting of stainless steel pipes with high cutting rates and at less cost than diamond saw cutting, cutting complex shapes in car doors, cutting QFN packages in electronic industries, producing cooling holes in turbine engines in aircraft industry, micro-fabrication of vias in PCB. The coronary stents used in medical field are micromachined by LBM. Unlike other thermal energy-based processes such as EDM and ECM it provides lesser heat-affected zone (HAZ) that makes it suitable for micromachining applications [62].

The literature related to modeling and optimization of LBM is mainly using statistical DOE such as Taguchi method and response surface method. Several analytical methods based on different solution methodologies, such as exact solution and numerical solution, have also been examined related to LBM. Few researchers concentrated on modeling and optimization of laser beam cutting through artificial intelligence-based techniques such as ANNs and fuzzy logic.

Tam et al. [231] proposed an overall figure-of-merit (FOM) function which integrates the weighted effects of the various quality characteristics of a laser-cut specimen and the cost components of a production environment. Taguchi methods and statistical techniques were used to formulate the experimental layout, to analyze the effect of each control factor on the results, and to predict the optimum

setting for each control factor. A set of confirmatory experiments was then conducted to verify the estimated response. A Trumpf 2000 laser machine which incorporated a Rofin Sinar RS500 laser was used to cut 4.5 mm thickness low-carbon steel sheets. Five control factors were used in a modified L_8 orthogonal array design. A high FOM was obtained using the treatment conditions of: beam power of 415 W, oxygen pressure of 0.12 MPa, focal position of 1/4, focal length of 63.5 mm, and cutting speed of 0.8 m/min.

Tam et al. [232] reported the use of the Taguchi technique of experimental design in optimizing the process parameters for drilling deep-holes in nickel-based superalloy, Inconel 718. The thickness of the material was 25.0 mm. Oxygen was the assist gas and the focal length of the focussing lens was 300 mm. The effects of five process parameters—pulse energy, pulse duration, pulse shape, focal position, and assist gas pressure—were explored. The various parameters were assigned to an L_{18} orthogonal array. The primary response under study was the drilling time. It was predicted that a minimum drilling time of 31.51 s was needed to drill a hole with a pulse energy of 30.0 J, a pulse duration of 1.8 ms, a "treble" pulse shape, and an oxygen pressure of 0.35 MPa.

Chen et al. [46] discussed the use of the Taguchi method of experimental design in optimizing process parameters for micro-engraving of iron oxide-coated glass using a Q-switched Nd:YAG laser. The effects of five key process parameters—beam expansion ratio, focal length, average laser power, pulse repetition rate and engraving speed—were explored. The primary response under study was the engraving line width. An L_{16} orthogonal array was used to accommodate the experiments. The study indicated that a minimum line width of 18 μm could be obtained with beam expansion ratio of 5×, focal length of 50 mm, laser average power of 0.4 W, pulse repetition rate of 5 kHz, and engraving speed of 5,000 mm/min.

Yilbas [255] examined the effect of the laser parameters and the material properties on the hole quality. A statistical approach, referred to as factorial design, was employed to test the significance level of the factors that affect the hole quality. Three materials, stainless steel, nickel and titanium, were considered. The experimental study yielded tables of significance of each factor on the aspects that determined the quality of the holes. The hole geometry was evaluated by assigning marks for each geometric feature, the marking scheme being conducted relevant to the importance of the hole feature.

Aloke et al. [5] formulated a physical model to estimate the dimensional accuracy of holes produced with laser cutting. The model included the assumption that the layer adjacent to the hole is plastically deformed and contains residual stresses up to the yield strength. The model was used to calculate the size of the hole and cut-out disk of varying radii in steel plates with thicknesses of 3.2 mm and 6.4 mm. The model-predicted data were verified with the experimental data obtained using a 1 kW continuous wave CO_2 laser. Results indicated that there was an excellent correlation between the model and the experimental data especially for smaller diameter holes.

Mathew et al. [161] conducted parametric studies on pulsed Nd:YAG laser cutting of carbon fiber reinforced plastic composites. Predictive models were developed based on important process parameters, viz. cutting speed, pulse energy, pulse duration, pulse repetition rate, and gas pressure. The responses considered were the HAZ and the taper of the cut surface. The optimization of process parameters was done using RSM. The thermal properties of the constituent material and the volume fraction of the fibers were understood as the principal factors that control the cutting performance.

Kaebernick et al. [108] presented a 3D analytical model of pulsed laser cutting, particularly aimed at predicting the quality of cut under various cutting conditions. The model was based on infinitesimal point heat sources, representing the effect of the laser beam on the surfaces inside the cutting zone, and it included the contribution of the oxygen reaction to the heating of the metal. Experiments with an Nd–YAG-Laser, cutting mild and stainless steel, were carried out to verify the predicted cutting results for various speeds, powers and pulse characteristics.

Cenna and Mathew [34] presented a theoretical model considering the spatial distribution of the laser beam, interaction time between the laser and the work material, absorption coefficient of the laser beam at the laser wavelength and the thermal properties of the material. It was assumed that the laser energy was absorbed through the entire thickness of the material. The developed model predicts the various parameters in laser cutting of composite materials such as kerf width at the entry and at the exit, MRR and energy transmitted through the cut kerf. The theoretical analysis also determines the position of the beam with respect to the cutting front. Experiments for different laser and material combinations to evaluate the effects of cutting parameters on the cut quality were carried out to compare with the predicted results. The results obtained showed very good agreement.

Yousef et al. [257] described how a multi-layered neural network can be used to model the non-linear laser micromachining process in an effort to predict the level of pulse energy needed to create a dent or crater with the desired depth and diameter. Laser pulses of different energy levels were impinged on the surface of several test materials in order to investigate the effect of pulse energy on the resulting crater geometry and the volume of material removed. The experimentally acquired data was used to train and test the neural network's performance. The key system inputs for the process model were mean depth and mean diameter of the crater, and the system outputs were pulse energy, variance of depth and variance of diameter. This study demonstrated that the proposed neural network approach can predict the behavior of the material removal process during laser machining to a high degree of accuracy.

Pajak et al. [176] presented a mathematical modeling of the laser-assisted jet-ECM (LAJECM). LAJECM process is a hybrid process, which combines a relatively low-power laser beam and an electrolyte jet. Compared to single jet-ECM, LAJECM yields better machining efficiency and precision, especially for small hole machining. The laser beam transfers additional heat onto a specific area of the work piece area resulting in changed machining conditions. This localization

effect of machining is the key to improving accuracy and efficiency of the LAJECM.

Yilbas [256] examined laser gas-assisted cutting process. Statistical method based on factorial analysis was introduced to identify the influence of cutting parameters on the resulting cut quality. International standards for thermal cutting were employed to identify the measurable variables when assessing the cut quality. Kerf width size was presented using scaling laws. Contribution of high temperature oxidation reaction in cutting due to assisting gas was accommodated in the analysis. First and second law efficiencies for laser cutting process were formulated. An experiment was conducted to assess the cutting quality and validate the Kerf width predictions. It was found that increasing laser beam scanning speed reduces the Kerf width while Kerf width increases with increasing laser output power. The main effects of all the parameters employed have significant influence on the resulting cutting quality.

Pan et al. [177] applied an Nd:YAG laser for thin plate magnesium alloy butt welding. The welding parameters governing the laser beam in thin plate butt welding were evaluated by measuring of the ultimate tensile stress. Kuar et al. (2006) conducted experimental investigations into CNC pulsed Nd:YAG laser micro-drilling of zirconium oxide (ZrO_2). Influence of laser machining parameters on the HAZ thickness and phenomena of tapering of the machined micro-holes was experimentally investigated. RSM-based optimal parametric analysis was performed to determine the optimal setting of process parameters such as pulse frequency and pulse width, lamp current, assist air pressure for achieving minimum HAZ thickness and taper of the micro-hole machined by pulsed Nd:YAG laser. Minimum HAZ thickness was obtained as 0.0675 mm when the lamp current, pulse frequency, assisted air pressure and pulse width were set at optimal parametric setting, i.e., 17 amp, 2.0 kHz, 2.0 kg/cm^2 and 2% of the duty cycle, respectively. Minimum taper was achieved as 0.0319 at optimal parametric setting, i.e., the lamp current of 17 amp, pulse frequency of 2.0 kHz, assisted air pressure of 0.6 kg/cm^2 and pulse width of 2% of the duty cycle. Lim et al. [146] studied on optimal cutting conditions of a high-speed feeding type laser cutting machine using Taguchi method.

Almeida et al. [4] investigated the effects of laser processing on the quality and formation of phases in the cut surface. The cutting process was performed on commercially pure titanium (grade 2) and alloy Ti-6Al-4V (grade 5) sheets. The obtained samples were analyzed through optical microscopy in order to determine the edge roughness formations. An increase on the superficial hardness on the cut region and the formation of nitrogen precipitates under a thin layer of a melted zone were verified. A factorial arrangement regarding the several combinations of different processing factors was built and the influence of these specific parameters, which were statistically significant for the process, was evaluated by the analysis of variance statistical test.

Li and Tsai [140] presented a novel effective method for optimizing laser cutting of specially shaped electronic printed circuit board (PCB) carrier substrates of advanced integrated circuit (IC) back-end packages that have multiple-

performance characteristics identified using GRA. Laser cutting parameters, including laser beam parameters (average laser power and *Q*-switch frequency), focusing parameters (laser beam focusing spot size), and machine parameters (laser cutting speed), were optimized based on multiple-performance characteristics. Some characteristics of the specially shaped flash memory module for IC packages, such as smart disk (SD) cards were verified. The characteristics of interest were the average surface roughness on a PCB substrate cross-section, and the maximum width of the HAZ. Eight experiments were conducted using GRA to optimize the settings for laser beam cutting parameters to generate various quality characteristics. Analysis of the grey relational grade indicated the parameter significance and the optimal parameter combinations for the laser cutting process.

Chang and Kuo [39] evaluated laser-assisted machining (LAM) as an economically viable process for manufacturing precision aluminum oxide ceramic parts. Experiments were conducted to obtain different measures of surface roughness for Al_2O_3 work pieces machined by laser assisted turning using a Nd:YAG laser.

The experimental results were analyzed using the Taguchi method, which facilitated identification of optimum machining conditions. The findings indicated that rotational speed, with a contribution percentage as high as 42.68%, had the most dominant effect on LAM system performance, followed by feed, depth of cut, and pulsed frequency. LAM's most important advantage was reported as its ability to produce much better work piece surface quality than does conventional machining, together with larger MRR and moderate tool wear.

Li et al. [141] reported the study of optimal laser parameters for cutting QFN (Quad Flat No-lead) packages using a diode pumped solid-state laser system. The QFN cutting path includes two different materials, which are the encapsulated epoxy and a copper lead frame substrate. The Taguchi's experimental method with orthogonal array of L_9 (3^4) was employed to obtain optimal combinatorial parameters. A quantified mechanism was proposed for examining the laser cutting quality of a QFN package. The influences of the various factors such as laser current, laser frequency, and cutting speed on the laser cutting quality was also examined. From the experimental results, the factors on the cutting quality in the order of decreasing significance were found to be (a) laser frequency, (b) cutting speed, and (c) laser driving current. The optimal parameters were obtained at the laser frequency of 2 kHz, the cutting speed of 2 mm/s, and the driving current of 29 A. Besides identifying this sequence of dominance, matrix experiment also determines the best level for each control factor. The verification experiment confirmed that the application of laser cutting technology to QFN was very successfully using the optimal laser parameters predicted from matrix experiments.

Masmiati and Philip [160] carried out experimental investigations to find the optimum ranges of parameters for drilling of polymers using a carbon dioxide (CO_2) laser cutting machine. An attempt was made to plan the experiment using Taguchi's method. Matrix experiment L_9 orthogonal array was used to conduct the experiments with four factors and three levels of each factor. Through experiments the effects of number of pulses, standoff distance, assist gas pressure and nozzle

diameter on the circularity of hole, spatter thickness, hole taper and MRR was assessed. The optimum conditions obtained from the analysis showed the combination of parameters that improves hole quality.

Ghoreishi and Nakhjavani [73] used neural networks for process modeling of laser cutting. Approximate experimental models of the process were developed by the neural network (Generalized Regression Neural Network—GRNN) according to the results of the experiments. Then the optimum input parameters (peak power, pulse time, pulse frequency, number of pulses, gas pressure and focal plane position) were specified using the genetic algorithm (GA) method, the results of which were the optimum output parameters. The output parameters included the hole entrance diameter, circularity of entrance and exit holes, hole exit diameter and taper angle of the hole. The tests were carried out on stainless steel 304 sheets with a thickness of 2.5 mm. A Nd:YAG laser machine was employed with a wavelength of 1.06 μm. Oxygen was used as an assist gas. Diameter of the central nucleus of laser beam was 600 μm. Considering the precision of the optimum numerical results and the high speed of the neural network in modeling, this method is reliable and economical and also confirms the qualitative results of the previous studies. Therefore, one can use this method to optimally adjust input parameters of the process in multipurpose and single purpose optimization modes, which indicates substitute application of the method for optimizing the laser percussion drilling process.

Dubey and Yadava [62] reviewed the research work carried out in the area of LBM of different materials and shapes. It reported about the experimental and theoretical studies of LBM to improve the process performance. Several modeling and optimization techniques for the determination of optimum laser beam cutting conditions were critically examined.

Analytical models are the mathematical models based on basic laws and principles, of a manufacturing process. These models can be divided into three categories, e.g., exact solution-based model, numerical solution-based model, and stochastic solution-based model. Exact solution based models are normally based on some hypothetical assumptions and sometimes they may not give the real solution. Numerical models are complex mathematical models widely used in engineering sciences but solution is based on numerical methods such as finite difference method (FDM), FEM, boundary element method (BEM), etc. Stochastic model is probabilistic in nature, i.e., for a range of inputs possibility of output falls in a range and most appropriate solution is very difficult. In LBM, there are so many analytical models which predict the system behavior in different operating conditions. The works of various researchers on analytical modeling of LBM process can be found in Dubey and Yadava [62].

Dubey and Yadava [63] presented a hybrid Taguchi method and response surface method (TMRSM) for the multi-response optimization of a laser beam cutting process. The approach first used the Taguchi quality loss function to find the optimum level of input cutting parameters such as gas pressure, pulse width, pulse frequency, and cutting speed. The optimum input parameter values were further used as the central values in the response surface method to develop and

optimize the second-order response model. The two quality characteristics Kerf width (KW), and MRR, that are of different nature (KW is of the smaller-the-better type, while MRR is of the higher the better type), were selected for simultaneous optimization. The results showed considerable improvement in both the quality characteristics when the hybrid approach was used, as compared the results of a single approach. The authored had performed experiments on a 200 W pulsed Nd:YAG LBM system with CNC work table. Oxygen was used as an assist gas. Focal length of lens used was 50 mm. Nozzle diameter (1.0 mm), nozzle tip distance (1.0 mm), and sheet material thickness (0.5 mm) were kept constant throughout the experimentation. The two quality characteristics analyzed were kerf width (KW) and MRR. The grain oriented high silicon-alloy steel sheet was used in the experiments as sheet material. The variable input process parameters (or control factors) considered were the gas pressure (1.5–3.5 kg/cm^2), pulse width or pulse duration (1.0–1.4 ms), pulse frequency (20–28 Hz), and cutting speed (25–75 mm/min).

The second-order response surface models for KW (mm) and MRR (mg/min) were developed from the experimental response values. The model developed using MINITAB software are as shown below.

$$\begin{aligned}\mathrm{KW} = {} & 0.1511 + 0.0746x_1 + 0.3736x_2 - 0.0191x_3 + 0.0021x_4 + 0.0013x_1^2 \\ & - 0.1274x_2^2 + 0.0008x_3^2 - 0.0126x_1x_2 - 0.0029x_1x_3 + 0.0010x_2x_3\end{aligned} \tag{3.84}$$

$$\begin{aligned}\mathrm{MRR} = {} & -97.6352 - 23.5623x_1 + 47.6419x_2 + 9.0159x_3 + 1.4135x_4 + 2.7470x_1^2 \\ & - 23.456x_2^2 - 0.1721x_3^2 - 0.0027x_4^2 + 11.2499x_1x_2 + 0.0417x_1x_3 \\ & - 0.1050x_1x_4 - 1.4063x_2x_3 + 0.2750x_2x_4 + 0.0175x_3x_4,\end{aligned} \tag{3.85}$$

where x_1 is the gas pressure (kg/cm^2), x_2 the pulse width (ms), x_3 the pulse frequency (Hz), and x_4 is the cutting speed (mm/min).

From the developed models, it was clear that the pulse width, cutting speed, square effect of pulse width, and interaction effect of pulse frequency and cutting speed are the significant factors for KW because of the reason that the absolute value of corresponding coefficients for these terms are quite high in comparison to other terms. Likewise, the MRR was significantly affected by cutting speed, pulse width, pulse frequency, and square effect of cutting speed.

The simultaneous optimization of weighted response for KW (weighting factor = 0.8) and MRR (weighting factor = 0.2) was obtained using MINITAB software. (1) The optimum value of KW and MRR obtained from multi-objective optimization using Taguchi method only were 0.3733 mm and 124.1095 mg/min, respectively, while using the hybrid approach these values were 0.3267 mm and 169.1667 mg/min, respectively. Hence a considerable improvement for both quality characteristics was found with hybrid approach of TMRSM.

Dubey and Yadava [64] applied a hybrid approach of Taguchi method and principal component analysis (PCA) for multi-objective optimization of pulsed Nd:YAG laser beam cutting of nickel-based superalloy (SUPERNI 718) sheet to achieve better cut qualities within existing resources. The three-quality characteristics kerf width, kerf deviation (along the length of cut), and kerf taper were considered for simultaneous optimization. The input parameters considered were assist gas pressure, pulse width, pulse frequency, and cutting speed. Initially, single-objective optimization was performed using Taguchi method and then the signal-to-noise (S/N) ratios obtained were further used in PCA for multi-objective optimization. The results included the prediction of optimum input parameter levels and their relative significance on multiple quality characteristics.

Samant and Dahotre [204] investigated machining of alumina using a JK 701 pulsed Nd:YAG laser. A hydrodynamic machining model was developed which incorporated the effect of multiple reflections on the amount of laser energy absorbed, the thermal effects for melting the material, vapor pressure effect for expelling out the molten material, material losses due to evaporation and the inverse effect of surface tension on the expelled depth. The model also incorporated the transient effect of laser beam de-focusing due to change in machined depth as a function of expelled material during machining for precise estimation of the melted depth during each pulse. It was observed that the material removal was a combination of melt expulsion and evaporation processes.

Çaydaş and Hasçalık [32] presented an effective approach for the optimization of laser cutting process of St-37 steel with multiple-performance characteristics based on the GRA. Sixteen experimental runs based on the Taguchi method of orthogonal arrays were performed to determine the best factor level condition. The response table and response graph for each level of the machining parameters were obtained from the grey relational grade. The laser cutting parameters such as laser power and cutting speed were optimized with consideration of multiple-performance characteristics, such as work piece surface roughness, top kerf width and width of HAZ. By analyzing the grey relational grade, it was observed that the laser power has more effect on responses rather than cutting speed.

Samant et al. [205] optimized the efficacy of pulsed Nd:YAG laser for the laser surface structuring (dressing) of porous alumina ceramic was optimized using the Taguchi analytical procedure. The laser processing parameters such as the pulse width, repetition rate and the scanning speed were evaluated and the factors essential to optimize the interdendritic porosity and grain size were predicted. The analysis of variance (ANOVA) helped to identify the processing parameters that contributed to minimize the porosity and maximize the grain size. The pulse repetition rate was the most significant factor in minimizing the interdendritic porosity while the scanning speed played a vital role in increasing the grain size. The Taguchi method could yield a combination of different process parameters that could be used to optimize the microstructural features.

Tsai et al. [238] employed a multiple regression analysis, and an ANN to build a predicting model for cutting Quad Flat Non-lead (QFN) packages using a Diode Pumped Solid State Laser (DPSSL) System. The predicting model included three

input variables of the current, the frequency and the cutting speed, and six cutting qualities of depths of the cutting line, widths of HAZ and cutting line for epoxy and for copper-compounded epoxy. After the training process from 27 sets of training data including input data and its output qualities, the average training error was 0.822% using a back-propagation (BP) neural network with Levenberg–Marquardt (LM) algorithm. The testing accuracy was then verified with extra 14 sets of experimental data and the average predicting error was 1.512%. The results showed that the ANN model has the predicting ability to estimate the laser cutting qualities of QFN packages. Finally, a genetic algorithm (GA) was applied to find the optimal cutting parameters that lead to least HAZ width and fast cutting speed with complete cutting. The optimal combination found was the current of 29 A, the frequency of 2.7 kHz and the cutting speed of 3.49 mm/s. The GA was helpful to determine the ideal laser cutting parameters in order to meet the desired cutting qualities and to avoid unnecessary adjustments in the subsequent cutting process.

Dhara et al. [57] investigated laser micromachining of tungsten-molybdenum general purpose high-speed steel (Rex M2). Selection of optimum machining parameter combinations for obtaining higher depth of groove and smaller height of recast layer is a challenging task due to the presence of a large number of process variables. There is no perfect combination of parameters which can simultaneously result in both the highest depth of groove and lowest height of recast layer. The authors had attempted to develop a strategy for predicting the optimum machining parameter setting for the generation of the maximum depth of groove with minimum height of recast layer. The experiments were performed on a CNC pulsed Nd:YAG laser machining system. Four parameters were chosen as inputs: lamp current (A), frequency (B), pulse Width (C), and air pressure (D). The levels of parameters selected were: 16, 17, and 18 amp for A; 4, 5, and 6 kHz for B; 4, 5, and 6% for C; and 1, 2, and 3 kg/cm^2 for D. There are other factors that can be expected to have an effect on the measure of performance. In order to minimize their effects, these parameters were held constant: the traverse speed (10 mm/s) and type of assisted gas (air). Four input parameters with three levels could have a total 3^4 combinations of experiments for full factorial design. A total of 33 experiments were conducted to get the responses. The responses considered were the depth of groove and height of recast layer. Levenberg Marquadt (LM) algorithm was used for training the feed-forward BPNN of type 4-25-2, one hidden layer with 25 neurons. Neural network toolbox of MATLAB software was used. After proper training of the network when the desired goal (the goal was set as the network output at least 10^{-6} decimal point close to the target value) was achieved, the network was simulated with other input parameters combinations and the network responses were compared with experimental responses. Thus, validation of the developed model was checked. Optimum parameter setting for the desired responses was then found out using the responses of the network model. The validation experiments for the developed model were conducted and it was found that prediction accuracy of the model is quite good. A graphical method was used to search out the optimal combinations of parameters from the set of all possible

combination of parameters setting, i.e., 625 predictions. Seven optimum parametric combinations were identified out of 625 combinations. Through this optimization strategy, one can obtain more optimal parametric combinations, which will lead to efficient utilization of LBM in practice.

Dhupal et al. [58] proposed a RSM-based mathematical modeling and analysis of machining characteristics of pulsed Nd:YAG laser during micro-grooving operation on a work piece of aluminum titanate. Lamp current, pulse frequency, pulse width, assist air pressure and cutting speed of laser beam were considered as machining process parameters during pulsed Nd:YAG laser micro-grooving operation. The response criteria selected for analysis were deviation of taper and deviation of depth characteristics of micro-groove produced on a work piece made of aluminum titanate (Al_2TiO_5). The analysis of variance test was also carried out to check the adequacy of the developed regression mathematical models. The optimal process parameter settings are assist air pressure of 1.3 kgf/cm^2, lamp current of 20.44 amp, pulse frequency of 1.0 kHz, pulse width of 10% of duty cycle, and cutting speed of 10 mm/s for achieving the predicted minimum deviation of taper and deviation of depth of laser micro-groove. From the analysis, it is evident that the deviation of taper angle and deviation of depth of the micro-groove can be reduced by a great extent by proper control of laser machining process parameters during micro-grooving on aluminum titanate (Al_2TiO_5).

Rao and Yadava [195] presented a hybrid optimization approach for the determination of the optimum laser cutting process parameters which minimize the kerf width, kerf taper, and kerf deviation together during pulsed Nd:YAG laser cutting of a thin sheet of nickel-based superalloy SUPERNI 718 (an equivalent grade to Inconel 718). A hybrid approach of Taguchi methodology and GRA was applied to achieve better cut qualities within existing resources. The input process parameters considered were oxygen pressure, pulse width, pulse frequency, and cutting speed. A higher resolution based L_{27} orthogonal array was used for conducting the experiments for both straight and curved cut profiles. The designed experimental results were used in GRA and the weights of the quality characteristics were determined by employing the entropy measurement method. The significant parameters were obtained by performing analysis of variance (ANOVA). The optimized parameters for straight and curved laser cut profiles were compared. On the basis of optimization results, it was found that the optimal parameter levels suggested for straight cut profiles were not valid for curved cut profiles. The results were verified by running confirmation tests.

Dhupal et al. [59] determined laser turning process parameters for producing square micro-grooves on cylindrical surface. The experiments were performed based on the statistical five level central composite design (CCD) techniques. The effects of laser turning process parameters, i.e., lamp current, pulse frequency, pulse width, cutting speed (revolution per minute, rpm) and assist gas pressure on the quality of the laser turned micro-grooves were studied. A predictive model for laser turning process parameters was created using a feed-forward ANN technique utilizing the experimental observation data based on RSM. The optimization problem was constructed based on RSM and was solved using multi-objective

genetic algorithm (GA). The neural network coupled with genetic algorithm was effectively utilized to find the optimum parameter value for a specific laser micro-turning condition in ceramic materials. The optimal process parameter settings were found as lamp current of 19 A, pulse frequency of 3.2 kHz, pulse width of 6% duty cycle, cutting speed as 22 rpm and assist air pressure of 0.13 N/mm^2 for achieving the predicted minimum deviation of upper width of −0.0101 mm, lower width 0.0098 mm and depth −0.0069 mm of laser turned micro-grooves.

Karazi and Brabazon (2009) presented four models developed for the prediction of the width and depth dimensions of CO_2 laser-formed micro-channels in glass. A 3^3 statistical DOE model was built and conducted with the power, pulse repetition frequency, and traverse speed of the laser machine as the selected parameters for investigation. Three feed-forward, back-propagation ANN models were also generated. These ANN models were varied to investigate the influence of variations in the number and the selection of training data. Model A was constructed with 24 data randomly selected from the experimental results, leaving three data points for model testing; Model B was constructed with the eight corner points of the experimental data space, and seven other randomly selected data, leaving 12 data points for testing; and Model C was constructed with 15 randomly selected data leaving 12 data points for testing. These models were developed separately for both micro-channel width and depth prediction. These ANN models were constructed in LabVIEW coding. The performance of these ANN models and the DOE model were compared. When compared with the actual results two of the ANN models showed greater average percentage error than the DOE model. The other ANN model showed an improved predictive capability that was approximately twice as good as that provided from the DOE model.

Ciurana et al. [50] focused on modeling and optimizing process parameters in pulsed laser micromachining. Use of continuous wave or pulsed lasers to perform micromachining of 3-D geometrical features on difficult-to-cut metals is a feasible option due the advantages offered such as tool-free and high precision material removal over conventional machining processes. Despite these advantages, pulsed laser micromachining is complex, highly dependent upon material absorption reflectivity, and ablation characteristics. Selection of process operational parameters is highly critical for successful laser micromachining. A set of designed experiments was carried out in a pulsed Nd:YAG laser system using AISI H13 hardened tool steel as work material. Several T-shaped deep features with straight and tapered walls were machined as representative mold cavities on the hardened tool steel. The relation between process parameters and quality characteristics was modeled with ANN. Predictions with ANNs were compared with experimental work. Multiobjective PSO of process parameters for minimum surface roughness and minimum volume error was carried out. This result showed that proposed models and swarm optimization approach are suitable to identify optimum process settings.

Biswas et al. [29] conducted Nd:YAG laser micro-drilling of gamma-titanium aluminide. The effect of different process parameters in the optimization of the process was investigated. The aspects considered were the hole circularity at exit

and the hole taper of the drilled hole. Lamp current, pulse frequency, air pressure and thickness of the job were selected as independent process variables. The CCD technique based on RSM was employed to plan the experiments to achieve optimum responses with a reduced number of experiments.

Bruneel et al. [30] investigated the processing times of ultrafast laser machining in the case of metals (copper and stainless steel). At a fluence of 2.5 J/cm^2, measurements of processing times were in good agreement with the calculations based on the ablation rates. The influence of laser repetition rates for 1, 5, 10 and 15 kHz was studied. A linear reduction of the processing time was expected with an increase of the repetition rate.

3.7 Electro Chemical Discharge Machining: A Hybrid Machining Process

Electro Chemical Discharge Machining (ECDM) is a hybrid technology that combines ECM and EDM. The ECM phase of this technology is responsible for the dressing, i.e., for the anodic dissolution of the layer, whereas the EDM phase is responsible for the trueing of the grinding wheel.

ECDM is a reproductive shaping process in which the form of the tool electrode is mirrored on the workpiece. It uses two electrodes: one is a cathode where the tool is connected, and the other is an anode or an auxiliary electrode. The workpiece is placed just below the tool, and along with the auxiliary electrode, is immersed in an electrolytic solution in a machining chamber. In the ECDM process the thermal erosive effects of electrical discharge (ED) action follows an electrochemical (EC) reaction. This electrochemical reaction helps in the generation of the positively charged ions and gas bubbles, e.g., hydrogen. These gas bubbles accumulate across the interface of the tool and the workpiece. The ED action takes place between the tool and the electrolyte across the gas bubble layers. If the applied DC power supply voltage is greater than the breakdown voltage of the insulating layer of the gas bubbles, a spark is initiated. Intensity and energy of the spark discharge increases with an increase in the applied voltage between two electrodes. A non-conducting ceramic workpiece is placed in the closed vicinity of the electrical discharge, and the material of the workpiece is melted, vapourized and eroded due to the transmission of a fraction of spark energy to the workpiece. This raises the temperature of the region dramatically, and a part of the molten portion of the workpiece is removed due to the mechanical shock resulting from the sudden phase change and the electrical spark discharge. Additional material removal also takes places due to thermal spalling. The thermal spalling of ceramics is usually defined as a mechanical failure of the material without melting due to a localized, thermally induced internal stress caused by a rapid temperature change that exceeds the bond strength of the materials. In ECDM, the material undergoes thermal cycling

under a spark discharge condition when pulsed DC voltage is applied and a complex temperature gradient is established. These results in internal thermal stresses and leads to thermal spall [16–18, 71, 104, 105, 130, 237].

The average grain protrusion of ECDM conditioned grinding wheels is much higher than the average grain protrusion of grinding wheels conditioned by means of conventional trueing and dressing. While in the case of ECDM conditioning grain protrusion is of approximately 75% of the average diameter of the grains, in the case of conventional conditioning this value is only of about 25%. Compared to conventional centerless grinding, ECDM centerless grinding produced much better results concerning both the surface roughness and the roundness of the ground workpieces.

Raghuram et al. [191] explored the influence of external circuit parameters on the discharge process. The experimental results of average voltage and current with NaOH and KOH electrolytes of 2, 5, 10 M concentrations with different circuit configurations were reported. The instantaneous voltage—current behavior during discharge at 60 V of NaOH, KOH and HCl electrolytes were reported also for concentrations of 2 and 5 M. The best circuit configuration for the machining of non-conducting material was discussed. The electrochemical discharge machining (ECDM) has been proved to be a potential process for the machining of high-strength non-conductive materials.

Schöpf et al. [211] illustrated the advantages of the ECDM trueing and dressing technology in comparison to conventional mechanical trueing and dressing methods concerning surface quality and roundness. The authors had presented experiments concerning "ECDM centerless grinding of cermet" and demonstrated that the ECDM technology is very suitable for the trueing and dressing of metal bonded diamond grinding wheels and hence for the high precision grinding of superhard cutting materials.

Peng and Liao (2004) developed a traveling wire electrochemical discharge machining (TW-ECDM) and used the process to slice the small size (10–30 mm diameter) optical glass and quartz bars. The electrical–thermal etching effect and its feasibility were investigated. The energy release intensities and their physical phenomena under different sizes of discharge wires, power source modulations and methods of electrolyte supply were discussed. The pulsed DC power proved better spark stability and more spark energy release proportion than constant DC power. The input power was modulated to obtain the appropriate frequencies and duty factors for machining glass and quartz materials. The ion translation rate, the electrolyte immersing depth and the concentration of the alkali were found to be the dominant factors of bubbles reaction. Based on the SEM photographs of the workpiece surface, it was noted that the more purple the sparks from the mixed gases of hydrogen and vapor, the better the etching effect was.

Wüthrich and Fascio [249] presented an overview of machining on non-conducting materials using ECDM process. Mediliyegedara [163] presented new developments in process control for the ECDM process. The design stages and the implementation issues of a personal computer-based real time controller for the ECDM process was discussed. A system identification experiment was carried out

to obtain the dynamics of the system and a process control algorithm was implemented in software form.

Sarkar et al. [207] described the development of a second-order, non-linear mathematical model for establishing the relationship among machining parameters, such as applied voltage, electrolyte concentration and inter-electrode gap, with the dominant machining process criteria, namely MRR, radial overcut (ROC) and thickness of HAZ, during an ECDM operation on silicon nitride. The model was developed based on RSM using the relevant experimental data, which were obtained during an ECDM micro-drilling operation on silicon nitride ceramics. The applied voltage (x_1), electrolyte concentration (x_2) and inter-electrode gap (x_3) were taken as controlling variables. During experimentation, the applied voltage was varied from 50 to 70 V, electrolyte concentration was varied from 10 to 30% by weight, and inter-electrode gap was varied from 20 to 40 mm. The mathematical relationship for correlating the MRR, ROC, and HAZ and the considered machining process parameters were expressed, using RSM, as given below:

$$\begin{aligned}\text{MRR} = {} & 0.60266 + 0.16049x_1 - 0.04044x_2 - 0.03481x_3 + 0.08781x_1^2 - 0.03060x_2^2 \\ & + 0.01358x_3^2 - 0.06500x_1x_2 - 0.037500x_1x_3 + 0.04500x_2x_3 \end{aligned} \tag{3.86}$$

$$\begin{aligned}\text{ROC} = {} & 0.16114 + 0.05333x_1 - 0.01017x_2 - 0.00716x_3 + 0.02454x_1^2 + 0.01727x_2^2 \\ & + 0.00598x_3^2 + 0.02603x_1x_2 - 0.00940x_1x_3 + 0.01493x_2x_3 \end{aligned} \tag{3.87}$$

$$\begin{aligned}\text{HAZ} = {} & 0.07835 + 0.01583x_1 - 0.00418x_2 - 0.00599x_3 + 0.00523x_1^2 + 0.00857x_2^2 \\ & + 0.00061x_3^2 + 0.00905x_1x_2 - 0.00060x_1x_3 + 0.00382x_2x_3. \end{aligned} \tag{3.88}$$

These developed mathematical models can be used to analyze the effects of the machining parameters on the MRR, ROC, and the thickness of the HAZ in the ECDM micro-drilling of silicon nitride. ANOVA and a confirmation test to verify the fit and adequacy of the developed mathematical models were performed. From the parametric analyses based on mathematical modeling, it was recommended that applied voltage has more significant effects on MRR, ROC and HAZ thickness during ECDM micro-drilling operation as compared to other machining parameters such as electrolyte concentration and inter-electrode gap.

Mediliyegedara et al. [164] presented the designing steps and simulation results of a pulse classification system for the ECDM process using ANN. An Electro-discharge machining (EDM) machine was modified by incorporating an electrolyte system and by modifying the control system. Gap voltage and working current waveforms were obtained. By observing the waveforms, pulses were classified into five groups. A feed-forward neural network was trained to classify pulses. Various neural network architectures were considered by changing the number of neurons in the hidden layer. The trained neural networks

were simulated. A quantitative analysis was performed to evaluate various neural network architectures.

Kim et al. [118] applied a series of rectangular voltage pulses to reduce the HAZ instead of the rectified or full-wave DC voltages. The effect of the frequency and duty ratio of the voltage pulse on the ECDM of Pyrex glass was experimentally investigated. The experimental results showed that the thermal damage of the microdrilled hole decreases as the frequency increases and as the duty ratio decreases. It was also found that the clearance increases as the tool diameter decreases.

Han et al. [78] used a partially side-insulated electrode that maintained a constant contact surface area with the electrolyte for the ECDM process to ensure that a uniform gas film was formed. Visual inspections indicated that the side-insulated tool provides new possibilities for describing the exact geometry of a gas film by inducing single bubble formations. Experiment results demonstrated that ECDM with a side-insulated electrode immersed in the electrolyte generated more stable spark discharges compared to non-insulated electrodes. Microchannels were fabricated to investigate the effects of the side insulation on the geometric accuracy and the surface integrity of the machined part.

The ECDM process has the potential to machine electrically non-conductive high-strength, high-temperature-resistant (HSHTR) ceramics, such as aluminum oxide (Al_2O_3). However, the conventional tool configurations and machining parameters show that the volume of material removed decreases with increasing machining depth and, finally, restricts the machining after a certain depth. To overcome this problem and to increase the volume of material removed during drilling operations on Al_2O_3, Chak and Rao [36] considered two different types of tool configurations, i.e., a spring-fed cylindrical hollow brass tool as a stationary electrode and a spring-fed cylindrical abrasive tool as a rotary electrode. The volume of material removed by each electrode was assessed under the influence of three parameters, namely, pulsed DC supply voltage, duty factor, and electrolyte conductivity, each at five different levels. The combined effect of the three parameters, i.e., pulsed DC supply voltage (x_1) varied from 60 to 120 V, duty factor (x_2) varied from 0.48 to 0.96, and electrolyte conductivity (x_3) varied from 275 to 375 mmho/cm, on the total volume of material removed (Y) from alumina by two types of tool electrode configurations for 20 sets of experiments was shown as Y_1 and Y_2.

$$Y_1 = 6.42 + 4.99x_1 + 3.20x_2 + 2.10x_3 + 0.941x_1^2 + 0.185x_2^2 - 0.101x_3^2 + 1.73x_1x_2 + 1.12x_1x_3 + 0.132x_2x_3 \tag{3.89}$$

$$Y_2 = 12.2 + 11.7x_1 + 5.47x_2 + 6.40x_3 + 3.61x_1^2 + 0.378x_2^2 - 0.678x_3^2 + 1.66x_1x_2 + 3.01x_1x_3 + 1.37x_2x_3 \tag{3.90}$$

Y_1 corresponds to the stationary electrode and Y_2 corresponds to the rotary electrode. The results revealed that the machining ability of the abrasive rotary electrode was better than the hollow stationary electrode, as it would enhance the cutting ability due to the presence of abrasive grains during machining.

Sarkar et al. [208] carried out experimental investigations to study the range of the parametric setting for micromachining operation as well as the effect of various process parameters such as applied voltage, electrolyte concentration and inter-electrode gap on MRR, Radial Over-Cut (ROC) and HAZ thickness during micro-drilling of non-conducting engineering ceramic materials such as aluminum oxide and zirconium oxide. The experiments were performed using electrolyte of KOH and NaOH salt solution. The investigation was made to find out the optimum value of ECDM process parametric conditions for higher MRR, lower overcut and also lower HAZ thickness during micro-drilling on ceramics. It was concluded that the quality of the hole during micro-drilling greatly depends on the applied voltage and electrolyte concentration.

Zheng et al. [262] designed and applied a novel pulse voltage configuration, called offset pulse voltage, in the ECDM process to improve gas film stability. The offset pulse voltage adds a constant voltage, called offset voltage, at T_{off} duration to enhance gas film stability and to further promote the discharge performance. The experimental results demonstrated that the increase in offset voltage at the pulse off duration generates more stable discharges when compared to those generated by the conventional pulse voltage. Results also showed that both the mean machining time and time deviation were decreased around 60% without sacrificing machining accuracy by an adequate offset voltage.

Sarkar et al. [209] investigated the influences of various power circuit configurations on the MRR, the tool wear rate (TWR), the radial overcut (ROC), and the HAZ using an NaOH salt solution as electrolyte. The individual effects of the inductance L, resistance R, and capacitance C of the power circuit on machining performance were studied experimentally in order to find their optimal values. Experiments were carried out to search for the pairwise effect of power circuit variables by considering their optimal values according to a Taguchi L_9 orthogonal array. Maximum MRR and minimum TWR were achieved at LC/60 V/20wt %/20 mm and RL/50 V/30 wt %/40 mm, respectively. Minimum ROC and minimum HAZ thickness were obtained at RC/50 V/10 wt %/40 mm. Thus, from the point of view of the accuracy and quality of the machined hole, an RC circuit was found to be most suitable for the micromachining of electrically non-conducting materials by the ECDM process.

Kulkarni [131] presented a systematic qualitative and quantitative analysis of ECDM process through experimental investigations. In situ, transient measurement of temperature (remotely sensed by pyrometer, at discharge striking zone) synchronized with online process current were performed. These synchronized measurements had led to qualitative formulation of the discharge formation and material removal mechanisms. Two varieties of K-type were used to sense the temperature at workpiece surface and temperature of electrolyte in the ECDM cell. With the online and post-process measurements, quantitative analysis of the

process was performed in terms of energy density striking the surface, geometry of discharge-affected (striking) region, MRR, energy associated with major process components and efficiency of the process. Energy density associated with a single discharge was experimentally determined and capability of single discharge was explained for utilization of ECDM process for micromachining.

Liu et al. [149] carried out an analysis of the discharge mechanism in electrochemical discharge machining (ECDM) of a particulate reinforced metal matrix composite and established a model to reveal the electric field acting on a hydrogen bubble in ECDM process. The model was found capable of predicting the position of the maximum field strength on the bubble surface as well as the critical breakdown voltage for spark initiation, for a given processing condition. A set of experiments was performed to verify the model and the experimental results agreed well with the predicted values. The experimental results also showed that an increase in current, duty cycle, pulse duration or electrolyte concentration would promote the occurrence of arcing action in ECDM. Compared to EDM, the volume of an arc eroded crater of ECDM was less than that of EDM. An XRD analysis of the phases of the EDM and ECDM specimens showed that the Al_4C_3 phase was detected on the former but not on the latter.

It has been observed from the above research works that the research has not yet been directed toward optimization of ECDM process parameters using advanced optimization techniques such as GA, PSO, ABC, etc.

3.8 Micro-Milling Process

Micro-milling, which is defined as the downscaling of the conventional milling process involving the use of end mill diameters in the sub-millimeter range [27], has become an established process for manufacturing of 3D meso and micro-components in metals and alloys. Micro-milling has its own characteristics, such as size effect, cutter edge radius and minimum chip thickness. Forces are exerted between the tool and the workpiece. Furthermore, tools used in micro-milling have diameters down to 100 mm and are characterized by long and smooth connections between the shaft and the cutting region. Micro-scale milling process is shown in Fig. 3.24. Figure 3.24a, b shows 3D and 2D representation of micro-milling process whereas, Fig. 3.24c, d shows deformation area in micro-milling. F_c and F_r are the force component, R is cutter edge radius, h is uncut chip thickness and f_t is feed per tooth.

One of the most significant characteristics of the micro-scale milling operation is the size effect. Some efforts have been carried out to explain it. Lucca et al. [151] investigated the size effect of cutting energy of micro-scale machining process through the experiments; they found non-linear increase in specific cutting energy or cutting forces as the uncut chip thickness was decreased. Kopalinsky and Oxley [122] studied the size effect with sharp tools by turning tests. They concluded that the cause was the decrease in the tool chip interface temperature.

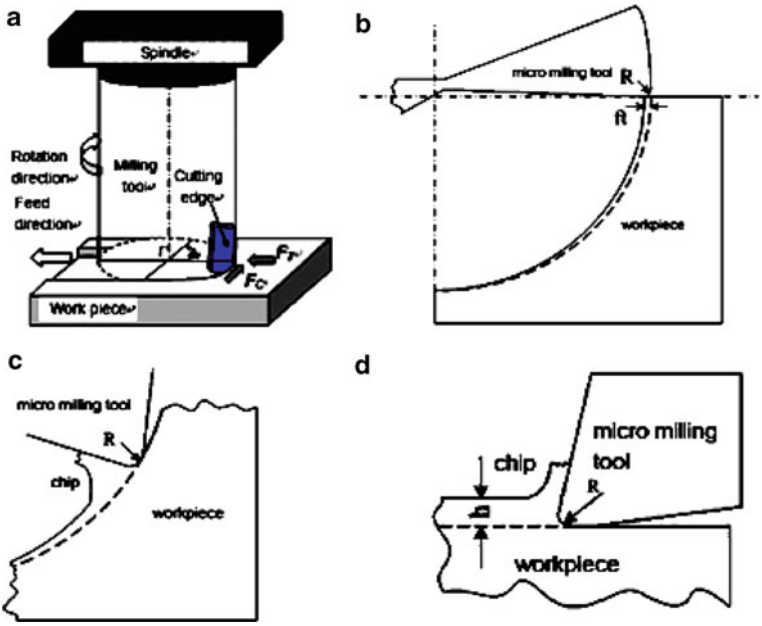

Fig. 3.24 Schematic representation of micro-milling process (from [136]; reprinted with permission from Elsevier)

Nakayama and Tamura [172] analyzed the size effect through experiments performed at a very low cutting speed to minimize the temperature and strain rate effects. They attributed this effect to plastic flow in the workpiece subsurface. The experiments of the previous researchers [122, 172] implied that there should be other underlying mechanisms for the size effect besides cutter edge radius, temperatures and strain rate. On the other hand, a similar size effect in micro-indentation tests was found in the mechanics studies, which was shown as remarkable material strengthening behaviors at the micron level.

Few efforts were carried out to study the chip formation characteristic of micro-milling processes. Shaw [217] studied the effect of round edges on the chip formation in micro-scale machining and stated that the plastic deformations would be prevented when the cutter edge radius is relatively larger than the uncut chip thickness. Kim et al. [117] investigated the effect of static tool deflection on the micro-milling and proposed a static chip model based on the attainable micro-scale machining force data. Liu et al. [150] investigated the chip formation using molecule dynamic (MD) simulations and presented an approach to calculate the minimum chip thickness by identifying a local maximum in the radial thrust forces in the micro-milling. Vogler et al. [241] determined the minimum chip thickness for steel using finite element (FE) simulations with regard of the microstructure properties of work material. Uhlmann and Schauer [239] developed innovative tool design of micro-end mills using the parameter technology in a FEM strain

simulation. The new tool design presented was successfully verified by micro-milling the tool steel PM × 190CrVMo 20 with a hardness of up to 62 HRC.

Micro-end milling (MEM) process promises to be an economical way to produce miniaturized components with excellent dimensional accuracy. However, to ensure economical production and quality of the products, it is important to select the most optimal cutting conditions required for the process. Many researchers had worked on the optimization of cutting speed and feed rates, but most of these works were restricted to turning of rotational parts although milling operations are commonly employed in today's manufacturing industry. While there are still quite a few attempts at optimization of milling operations, most of these works were on conventional end milling and peripheral milling operations [8]. In most of these studies depth of cut was not considered as an active decision variable, thus restricting them to single pass optimization strategies. Although optimization of multi-pass milling operations had been worked out, different strategies such as volume sectioning or optimal cut subdivision had been employed to find the optimal depth of cut separately [56, 251]. This method did not consider the effect of the depth of cut on the tool life and thus on the production cost. A machining economics or optimization problem involves the determination of the optimal set of cutting conditions viz. cutting speed, feed rate and depth of cut in order to satisfy a certain objective viz. minimum production cost, minimum production-time or maximum profit. The traditional methods often adopted for this process include graphical methods [234], dynamic programming [225], geometric programming [93] and numerical search methods [40] while modern intelligent methods include ANN [264], simulated annealing [44], fuzzy logic [52], etc.

In addition, several analytical cutting force models [15, 60, 69, 115, 261] had been developed to investigate the micro-scale machining process. Chae [35] surveyed the state of art of micro-scale machining and reported that current researches had made valuable attempts in this field though most of them were carried out by means of nano-level and macro-level approaches. From the discussions above, it is obvious that the processing system for micro-scale milling is far from established. Its characteristics need to be studied and the related mechanisms need to be revealed through experiments and theoretical modeling.

In any machining operation, the tool wear increases initially with machining time and then propagates gradually till a certain extent after which it increases drastically causing tool failure. Usually in conventional end milling operations with increase in depth of cut, the applied resultant cutting force for the material removal increases causing an increase in the rate of increase of tool wear, thereby causing tool failure. But in micro-end milling operations, unlike in conventional end milling operations, the tool life of the cutter was observed to increase with the increase in axial depth of cut up to a certain extent. This can be explained geometrically by considering the total tool engagement of the cutter in the cutting process. Total tool engagement is the angular length for which the cutting edge is in contact with the workpiece in one rotation of the cutter. In micro-end milling operations the depth of cut to the tool diameter ratio is much higher than that in conventional end milling operations as shown in Fig. 3.25.

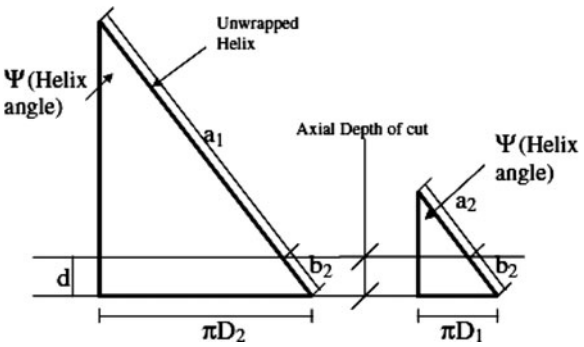

Fig. 3.25 Unwrapped helix faces of conventional tool (*right*) and micro-tool (*left*) (from [261]; reprinted with permission from Elsevier)

In Fig. 3.25 the unwrapped helix of a conventional tool and a micro-tool are shown and the amount of helix face involved in cutting for a certain depth of cut is compared in both cases.

In this figure, d is the axial depth of cut, $a_1 + b_2$ is the length of the unwrapped helix of the conventional tool (diameter D_2) and $a_2 + b_2$ is the length of the unwrapped helix of the micro-tool (diameter D_1). Therefore,

$$b_2/(a_1 + b_2) < b_2/(a_1 + b_2) \text{ as } a_1 > a_2. \tag{3.91}$$

This implies that the proportion of the helix face involved in the cutting action in the micro-tool is relatively higher than that in a conventional tool. This is because the range of diameters of cutters used in MEM operations (0.5– 2.00 mm) is not very high compared to the range of depths of cut (0.2–1.25 mm). This eventually results in a greater proportion of the helix face of the cutter participating in the cutting action. Because of this the total tool engagement is relatively higher in MEM operations than that in conventional end milling operations. This results in lesser amount of idle distance traversed by the cutting edge in one rotation of the tool, thereby reducing the intensity of the impact of the cutting edge against the workpiece.

The optimization model of the micro-end milling process is formulated based on the analysis given by Sreeram et al. [228]. The objective of this optimization model is to determine the optimal cutting conditions including the cutting speed (V), feed rate (f) and depth of cut (d) in order to minimize the unit production cost (UC) to manufacture a single component. In addition, this combination of the machining parameters should not violate the imposed set of constraints which govern the machining process. In micro-end milling operations the size of the product desired and the tool (end mill cutter) used are essentially small and hence there is no separate finishing operation being considered as a part of the complete machining operation. The unit production cost comprises raw material cost, actual machining cost, tool replacement cost, tool cost and set-up cost. The cutting constraints imposed on the machining process include the parameter bounds which are the minimum and maximum permissible values of the cutting parameters viz. the cutting speed, feed rate and depth of cut for MEM operations for the tool/workpiece combination considered, machining power constraint and the cutting

force constraint. While machining with slender end mills the surface roughness is usually very low offering a good surface quality except while machining with a broken tool. Tool breakage could easily be detected by drastic increase in the cutting force values and thus can be avoided by keeping the cutting force constraint within a certain limit. The objective function for this optimization model is described in the subsequent section.

In this model, the objective is to minimize the unit cost (UC) as given by the following expression:

$$\text{Minimize} \quad \text{UC} = K_1 V^{-1} f^{-1} d^{-1} + K_2 V^{\alpha-1} f^{\beta-1} d^{\gamma-1} \tag{3.92}$$

$$K_1 = C_0 \pi LWHb^{\delta-1}/1,000CD^{\omega-1}z \tag{3.93}$$

$$K_2 = (C_0 T_c + K_T)\pi LWHb^{\delta-1}/1,000CD^{\omega-1}z, \tag{3.94}$$

where α, β, γ, δ, ω are exponents in tool life equation, C_O is the direct labor cost + overhead (\$/min), L the length of the workpiece to be machined (mm), W the width of the workpiece to be machined (mm), H the depth of the workpiece to be machined (mm), b the width of cut, T_c the tool changing time (min), C the constant in tool life equation, D the diameter of the tool (mm), and z is the number of teeth on cutter.

Following two constraints were considered.

- Cutting force constraints:
  The cutting force as a single parameter is an optimal quantity for describing the net effect of all input variables. It is imperative that the cutting force is maintained below the limiting force in order to ensure good surface quality and to prevent breakage of cutting edges. In MEM, the diameter of cutters is very low and the stress variation on the tiny shaft of the micro-tool is much higher than that on a conventional tool. It is therefore very important to make sure that the cutting force does not increase drastically beyond a certain allowable limit. The cutting force constraint is expressed in terms of the cutting parameters as:

$$C_1 V^{\alpha 1} f^{\alpha 2} d^{\alpha 3} - 1 \leq 0, \tag{3.95}$$

  where α_1, α_2, α_3 are the exponents in cutting force equation and

$$C_1 = K/F_{\text{lim}} \tag{3.96}$$

  F_{lim} is the limiting cutting force (N).
- Cutting power constraint
  The power required during the machining operations should not exceed the maximum power available on the machine tool. For this case the expression for cutting power given by Tolouei-Rad [234] is used. This constraint is expressed as:

$$C_2 V d f^{0.8} - 1 \leq 0 \tag{3.97}$$

$$C_2 = 0.78 K_p bwz/60\pi D\eta P_{mt}, \tag{3.98}$$

where K_p is the power constant depending on work piece material, w is the tool wear factor, η the machine tool efficiency, and P_{mt} is the maximum allowable cutting force.

Now to illustrate the optimization aspects of micro-milling process, the following example which deals with the micro-end milling of a thin wall on a steel workpiece considered by Sreeram et al. [228] is considered. The workpiece is shown in Fig. 3.26.

The operations required to be performed on this workpiece are given in Table 3.10.

Sreeram et al. [228] used the following parameters of genetic algorithm for the optimization of micro-end milling process:

- Cross-over probability = 0.4.
- Mutation probability = 0.08.
- Number of chromosomes in the population, $N_p = 200$.

The results of optimization obtained using genetic algorithm had indicated a unit cost of $1.75 while the catalogue values suggested a unit cost of $4.281. It is clear that the obtained values of the unit cost by the genetic algorithm are much lower than the corresponding values of the unit cost obtained from the catalogue values of the parameters suggested by the tool manufacturer. The total cost of the component has been reduced by 59.12% (from $4.281 to $1.75) of the cost obtained by the parameter values suggested by the tool manufacturer. The efficiency of the algorithm can further be improved by increasing the number of iterations and widening the feed and cutting speed ranges a little more, as it can be observed that the optimal cutting speed and feed per tooth values for the step

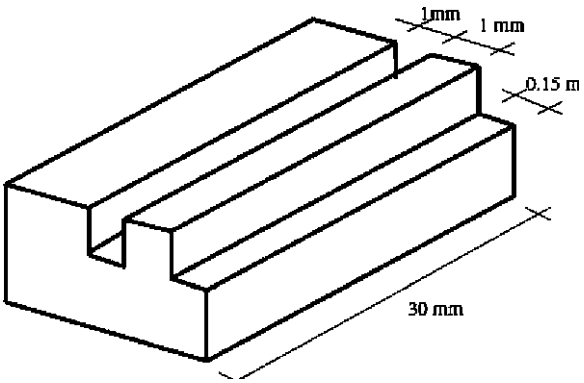

Fig. 3.26 Example workpiece for micro-end milling (from [228]; reprinted with permission from Springer Science + Business Media)

Table 3.10 Operations to be performed on the workpiece (from [228]; reprinted with permission from Springer Science + Business Media)

Operation no.	Operation type	Tool	Length (mm)	Width (mm)	Depth (mm)
1	Side milling	Micro	30 end mill	0.3	1
2	Slot milling	Micro	30 end mill	2	1

obtained are the maximum permitted values. However, the limited ranges of cutting parameters used are chosen carefully in order to avoid cutter breakage and excessive vibrations during the machining operation.

The optimization of micro end milling process can be carried out using various non-traditional techniques. Rao and Pawar [199] described the applications of non-traditional optimization techniques for the process parameter optimization of milling process and the same techniques can also be applied for the parameter optimization of micro end milling process.

Kang et al. [115] presented a cutting force model and predicted the cutting force in micro-end milling. The tool–workpiece contact at the flank face was considered in this model. The model took into account the tool edge radius effect, which is a characteristic of the micro-cutting mechanism. In this model, when the feed per tooth reached the tool edge radius level, predictions could be made for the characteristics of the feed and normal direction cutting forces that occur due to the tool edge radius effect which was not considered in the previous models. In fact, there was no difference between the cutting forces of the feed and normal directions when the feed per tooth was small and this was also clearly shown in the prediction results. Besides, the study clearly demonstrated that the predicted cutting forces were consistent with the experimental cutting forces.

Newby et al. [174] presented an empirical model for the analysis of cutting forces in micro-end milling operations. The approach used higher feed per tooth per radius of cutter ratios (compared to conventional end milling operations) and the true trochoidial nature of the tool edge path in the derivation of a chip thickness for micro-end milling operations. Cutting experiments were conducted in the micro-end milling regime and forces were recorded. These forces were then decomposed in order to present new empirical formulae for cutting pressure constants in micro-end milling operations. The model developed for cutting force constants can be used for better understanding of friction and forces in the micro-end milling process.

Lai et al. [136] presented mechanisms studies of micro-milling operation focusing on its characteristics, size effect, micro-cutter edge radius and minimum chip thickness. First, a modified Johnson–Cook constitutive equation was formulated to model the material strengthening behaviors at micron level using strain gradient plasticity. A finite element model for micro-scale orthogonal machining process was developed considering the material strengthening behaviors, micro-cutter edge radius and fracture behavior of the work material. Then, an analytical micro-scale milling force model was developed based on the FE simulations using the cutting principles and the slip-line theory. Extensive experiments of OFHC copper micro-milling using 0.1 mm diameter micro-tool were performed with miniaturized machine tool, and good agreements were achieved between the predicted and the experimental results. Finally, chip formation and size effect of micro-milling were investigated using the proposed model, and the effects of material strengthening behaviors and minimum chip thickness were discussed.

Demir [55] presented the application of micro-plasticity theory to predict the forces and the surface quality that stem from the anisotropy in the mechanical properties of single crystal fcc work-piece materials. The model predicts the

experimental differences in the height between entrance and exit burrs of copper single crystals observed in the studies of Min et al. [166]. The model is potentially applicable to calibration of milling force models.

Bissacco et al. [28] presented a theoretical model for cutting force prediction in micro-milling, taking into account the cutting edge radius size effect, the tool run out and the deviation of the chip flow angle from the inclination angle. A parameterization according to the uncut chip thickness to cutting edge radius ratio was used for the parameters involved in the force calculation. The model was verified by means of cutting force measurements in micro-milling. The results showed good agreement between predicted and measured forces. It was also demonstrated that the use of the Stabler's rule was a reasonable approximation and that micro-end mill run out was effectively compensated by the deflections induced by the cutting forces.

Malekian et al. [157] investigated the mechanistic modeling of micro-milling forces, with consideration of the effects of ploughing, elastic recovery, run-out, and dynamics. A ploughing force model that took the effect of elastic recovery into account was developed based on the interference volume between the tool and the workpiece. The elastic recovery was identified with experimental scratch tests using a conical indenter. The dynamics at the tool tip was indirectly identified by performing receptance coupling analysis through the mathematical coupling of the experimental dynamics with the analytical dynamics. The model was validated through micro-end milling experiments for a wide range of cutting conditions. In another work, Malekian et al. [158] examined factors affecting tool wear and a tool wear monitoring method using various sensors, such as accelerometers, force and acoustic emission sensors in micro-milling. The signals were fused through the neuro-fuzzy method, which then determined whether the tool was in good shape or was worn. An optical microscope was used to observe the actual tool condition, based upon the edge radius of the tool, during the experiment without disengaging the tool from the machine. The effectiveness of tool wear monitoring, based on a number of different sensors, was also investigated. Several cutting tests were performed to verify the monitoring scheme for the miniature micro-end mills.

Park and Malekian [178] examined the mechanistic modeling of shearing and ploughing domain cutting regimes to accurately predict micro-milling forces. The tool dynamics were indirectly identified by performing receptance coupling analysis. Furthermore, the Kalman filter compensation method was used to precisely measure the forces to obtain the cutting constants. In another work, Park and Rahnama [179] developed a robust chatter stability method based on the edge theorem and the automated zero exclusion principle for predicting the stability lobes, based on changing parameters between the minimum and maximum ranges in micro-milling operations. Experimental tests were performed to indirectly identify the tool tip dynamics through the receptance coupling method, to investigate process damping, and to identify changing dynamics. The stability lobes were simulated, and the experimental cutting tests were carried out to compare the results. The robust stability method with process damping results showed a good correlation with the experimental results.

Wissmiller and Pfefferkorn [248] characterized the heat transfer in micro-end mill tools during machining operations. Tool temperatures, above the unmachined workpiece surface, were measured using an infrared camera during slot milling of aluminum (6061-T6) and steel (1018) with 300 μm-diameter two-flute tungsten carbide end mills. The measured temperatures compared favorably with temperature distributions predicted by a 2D, transient, heat transfer model of the tool. The heat input was estimated by applying Loewen and Shaw's heat partitioning analysis.

Zhu et al. [263] proposed a multi-category classification approach for tool flank wear state identification in micro-milling. Continuous Hidden Markov models (HMMs) were adapted for modeling of the tool wear process in micro-milling, and estimation of the tool wear state given the cutting force features. For a noise-robust approach, the HMM outputs were connected via a medium filter to minimize the tool state before entry into the next state due to high noise level. A detailed study on the selection of HMM structures for tool condition monitoring was presented. Case studies on the tool state estimation in the micro-milling of pure copper and steel demonstrated the effectiveness and potential of these methods.

3.9 Micro-Drilling Process

Increasing demand for advanced difficult-to-process materials and the availability of high-power lasers have stimulated interest in research and development related to laser machining. The use of laser micro-drilling in manufacturing industry can be attributed to several advantages like high production rate, applicable to both conductive and non-conductive materials, no mechanical damage or tool wear due to non-contact processing, improved product quality, low material wastage, low production cost, small HAZ, and ecologically clean technology. The main issues related to Micro-drilling using laser are taper formation, production of non-circular holes, and thickness of HAZ. Yilbas and Yilbas [253] used a statistical method to investigate the effects of the variation of single-pulse laser drilling parameters on the hole geometry for Nimonic workpiece material using a full factorial design to identify the main and first-order interaction effects on the hole quality in single-pulse drilling including re-solidified material, taper, barreling, inlet cone, exit cone, surface debris and mean hole diameter. Yilbas [254] examined four materials nickel, tantalum, EN 58 B EN 58 B and titanium to obtain laser drilling speed using a statistical analysis. Yeo et al. [252] reviewed the mechanisms of some laser drilling processes, the types of laser used, the quality characteristics of a laser-drilled hole, the effects of drilling parameters, and the advantages and limitations of the laser hole-drilling operation.

Yilbas [255] conducted drilling experiments on three materials, stainless steel, nickel and titanium, using single-pulsed laser beam. In addition to statistical analysis of hole taper, some efforts have also been made to control hole taper via the development of drilling techniques. Ghoreishi et al. [72] employed a statistical

model to analyze and compare hole taper and circularity in laser percussion drilling on stainless steel and mild steel. Jackson and O'Neill [98] investigated the interaction phenomena of Q-switched, diode- pumped Nd:YAG laser using different wavelengths on tool steel. Bandhopadhayay et al. [14] investigated the influence of the process variables on hole diameter and taper angle of drilled holes produced on thick IN718 and Ti-6Al-4 V sheets by Nd:YAG laser.

Yu et al. [258] presented a new approach for effective self-flushing using planetary movement. Through micro-holes with an aspect ratio of 18 were drilled. This approach was also demonstrated by drilling blind non-circular micro-holes with sharp corners and edges. The process performance characteristics were analyzed under different machining conditions.

Pham et al. [184] presented some recent developments in micro-EDM in its various forms (wire, drilling, milling and die-sinking) and discussed the main research issues. The authors focused on the planning of the EDM process and the electrode wear problem. Special attention was paid to the factors and procedures influencing the accuracy achievable, including positioning approaches during EDM and electrode grinding.

Chen and Darling [45] investigated the use of a near ultraviolet Nd:YAG laser for rapid micromachining of sapphire and silicon. Cutting, marking and surface ablation of both materials were produced by direct writing using a high-speed x–y galvanomechanical beam positioner. Machining results such as ablation rate and efficiency were discussed. The results showed that the quality and efficiency of the laser machining depend on several factors, including focus length, beam feed rate (cutting speed) and the pulse repetition rate. The surface morphology and ablation rate indicated that the laser ablation process of sapphire could be a mixed photothermal and photochemical process, while that of silicon appeared dominated by a photothermal process when using a near UV nanosecond pulses.

Sen and Shan [213] highlighted the recent developments, new trends and the effect of key factors influencing the quality of the holes produced by jet-electrochemical drilling processes. The authors made a comparative study of electro jet drilling with another non-traditional hole-drilling process (laser percussion drilling). The laser percussion welding showed the potential and versatility of the electrochemical hole-drilling processes. In another work, Sen and Shan [214] reported experimental findings on the effects of important process parameters such as applied voltage, capillary outside diameter, feed rate, electrolyte concentration and inlet electrolyte pressure on the productivity and the quality of small holes (<800 μm dia) produced using the electrojet drilling process. Roundness error and surface roughness were used as the response parameters for evaluating the quality of hole whereas MRR was used as the response parameter for evaluating the process productivity. The experiments were performed on SUPERNI 263A material.

Li et al. [142] reported an investigation into a sequential laser and EDM micro-drilling technique for the manufacture of next generation fuel injection nozzles. A laser-drilled pilot hole was rimmed out by EDM drilling. It was found that this hybrid process eliminated the problems of recast and HAZ typically associated with the laser drilling process. The new process had enabled a 70% reduction in

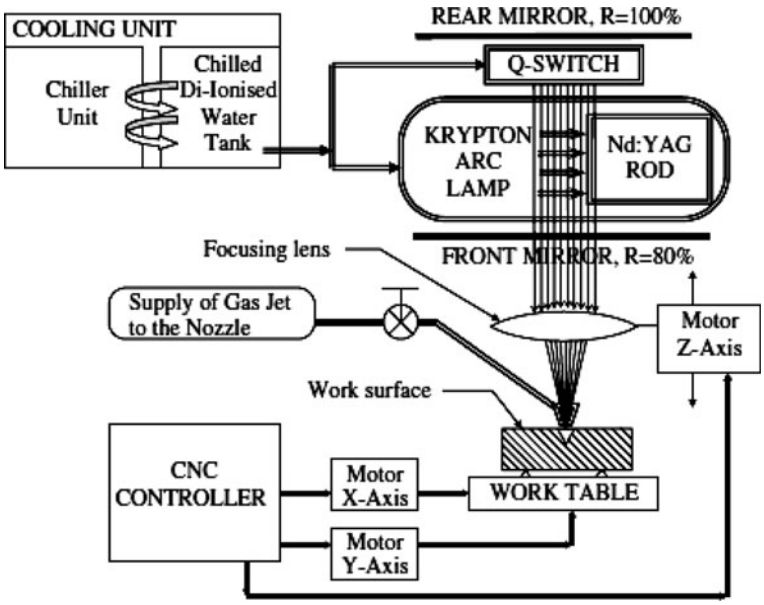

Fig. 3.27 Schematic representation of CNC Nd:YAG laser micro-drilling (from [128]; reprinted with permission from Elsevier)

total drilling time compared to standard EDM drilling. The quality of the holes was as good as direct EDM drilling, thus eliminating the need for re-certification of the drilling process. Various combinations of laser/EDM drilling conditions were examined. Optimum diameters for the pilot hole and the EDM electrode were identified for a particular diameter of fuel injection nozzle, giving the minimum total drilling time and the best quality holes. A special system was designed to enable the alignment of nozzles to be controlled to within $\pm$ 20 μm.

Kuar et al. [128] presented a CNC Nd:YAG laser system used for micro-drilling operation. Figure 3.27 shows the CNC Nd:YAG laser micro-drilling set up. For efficient micro-drilling operation the CNC Nd:YAG laser machining system consists of the various subsystems such as; laser source and beam delivery unit, power supply unit, radio frequency (RF) Q-switch driver unit, cooling unit and CNC controller for *X*, *Y*, and *Z* axes movement. Laser head consists of Nd:YAG rod and krypton arc lamp which are placed in two different focal point of an elliptical cavity.

Lasing medium in Nd:YAG lasers is neodymium atoms are embedded in yttrium aluminum garnet crystal host. Pump source is usually a krypton arc lamp. Nd:YAG crystal is excited by krypton arc lamp. For amplification of light, optical feedback is provided with 100% reflectivity rear mirror, and a front mirror of reflectivity 80%. The Q-switching is an excellent method to produce very short pulse width and very high peak power of laser light from a CW low-power laser. Main power supply unit controls the laser output by controlling intensity of light

emitted by krypton arc lamp. Cooling unit cools the system to avoid thermal damage of laser cavity, lamp, Nd:YAG rod and Q-switch.

The CNC controller consists of *X*–*Y*–*Z* axes and a controlling unit. Stepper motors are attached to each axis and connected to the controlling unit. This unit can control the axis through computer unit. Nd:YAG laser machining system. CNC *Z*-axis controller unit controls the *Z*-axis movement of lens. Over the table to hold work piece, the developed fixture is placed. It takes care of the job posture. CCD camera together with CCTV monitor is used for viewing the location of work piece and also for checking the proper focusing condition of surface of work piece before laser machining for achieving high quality laser micromachining characteristics. Figure 3.27 shows the schematic representation of CNC Nd:YAG laser micro-drilling system.

Kuar et al. [129] carried out experimental investigations into CNC pulsed Nd:YAG laser micro-drilling of zirconium oxide (ZrO_2). Influence of laser machining parameters on the HAZ thickness and phenomena of tapering of the machined micro-holes was experimentally investigated. RSM-based optimal parametric analysis was performed to determine the optimal setting of process parameters such as pulse frequency and pulse width, lamp current, assist air pressure for achieving minimum HAZ thickness and taper of the micro-hole machined by pulsed Nd:YAG laser. Minimum HAZ thickness was been obtained as 0.0675 mm when the lamp current, pulse frequency, assisted air pressure and pulse width were set at optimal parametric setting, i.e., 17 amp, 2.0 kHz, 2.0 kg/cm^2 and 2% of the duty cycle, respectively. Minimum taper was achieved as 0.0319 at optimal parametric setting, i.e., the lamp current of 17 amp, pulse frequency of 2.0 kHz, assisted air pressure of 0.6 kg/cm^2 and pulse width of 2% of the duty cycle. Analysis was also carried out for multi-optimization of both the responses, i.e., HAZ thickness and taper during pulsed Nd:YAG laser micro-drilling on ZrO_2.

Bigot et al. [26] investigated the optimization of machining parameters for rough and fine machining in micro-EDM. In one case, the parameters were selected to achieve the highest MRR. In the other case, the best surface roughness was targeted. Some of the main difficulties linked with micro-EDM were caused by the high wear occurring on the electrode. The study focused on a specific combination of electrode and workpiece material and proposed a typical method for micro-EDM process optimization. Kao and Shih [111] presented the design and tuning of a three-input fuzzy logic controller for electrical discharge machining (EDM) of diesel injector spray holes. The tuning process was based on the variable type and discretization level to balance the data precision and computational time for servo motion updates in the fuzzy logic controller and was performed to improve the micro-hole EDM drilling time. The type and number of input parameters were studied to select the gap voltage, spark ratio, and change of spark ratio as input parameters for the fuzzy logic controller. A gain scheduling controller was used as the baseline and showed excellent drilling time in drilling a 1.14 mm thick workpiece using a 150 μm diameter wire electrode. The tuned fuzzy logic controller was comparable with the gain scheduling controller in

drilling time and demonstrated its advantages on different EDM drilling configurations, including deep-hole and small-diameter micro-hole drilling.

Dubey and Yadava [62] reviewed the research work carried out in the area of LBM of different materials and shapes. The authors reported about the experimental and theoretical studies of LBM to improve the process performance. Several modeling and optimization techniques for the determination of optimum laser beam cutting conditions were critically examined. Dubey and Yadava [63] presented a hybrid Taguchi method and response surface method (TMRSM) for the multi-response optimization of a laser beam cutting process. The approach first used the Taguchi quality loss function to find the optimum level of input cutting parameters such as gas pressure, pulse width, pulse frequency and cutting speed. The optimum input parameter values were further used as the central values in the response surface method to develop and optimize the second-order response model. The two quality characteristics Kerf width (KW), and MRR, that are of different nature (KW is of the smaller-the-better type, while MRR is of the higher the better type), were selected for simultaneous optimization. The results showed considerable improvement in both the quality characteristics when the hybrid approach was used, as compared the results of a single approach. The authored had performed experiments on a 200 W pulsed Nd:YAG LBM system with CNC work table. Oxygen was used as an assist gas. Focal length of lens used was 50 mm. Nozzle diameter (1.0 mm), nozzle tip distance (1.0 mm), and sheet material thickness (0.5 mm) were kept constant throughout the experimentation. The two quality characteristics analyzed were kerf width (KW) and MRR. The grain oriented high silicon-alloy steel sheet was used in the experiments as sheet material. The variable input process parameters (or control factors) considered were the gas pressure (1.5–3.5 kg/cm^2), pulse width or pulse duration (1.0–1.4 ms), pulse frequency (20–28 Hz), and cutting speed (25–75 mm/min).

The second-order response surface models for KW (mm) and MRR (mg/min) were developed from the experimental response values. The model developed using MINITAB software are as shown below.

$$\begin{aligned}\mathrm{KW} = {} & 0.1511 + 0.0746x_1 + 0.3736x_2 - 0.0191x_3 + 0.0021x_4 + 0.0013x_1^2 \\ & - 0.1274x_2^2 + 0.0008x_3^2 - 0.0126x_1x_2 - 0.0029x_1x_3 + 0.0010x_2x_3\end{aligned} \tag{3.99}$$

$$\begin{aligned}\mathrm{MRR} = {} & -97.6352 - -23.5623x_1 + 47.6419x_2 + 9.0159x_3 + 1.4135x_4 + 2.7470x_1^2 \\ & - 23.456x_2^2 - 0.1721x_3^2 - \ 0.0027x_4^2 + \ 11.2499x_1x_2 + 0.0417x_1x_3 \\ & - 0.1050x_1x_4 - 1.4063x_2x_3 + \ 0.2750x_2x_4 + 0.0175x_3x_4\end{aligned} \tag{3.100}$$

where x_1 is the gas pressure (kg/cm^2), x_2 the pulse width (ms), x_3 the pulse frequency (Hz), and x_4 is the cutting speed (mm/min).

From the developed models, it was clear that the pulse width, cutting speed, square effect of pulse width, and interaction effect of pulse frequency and cutting speed are the significant factors for KW because of the reason that the absolute

value of corresponding coefficients for these terms are quite high in comparison to other terms. Likewise, the MRR was significantly affected by cutting speed, pulse width, pulse frequency, and square effect of cutting speed.

The simultaneous optimization of weighted response for KW (weighting factor = 0.8) and MRR (weighting factor = 0.2) was obtained using MINITAB software. (1) The optimum value of KW and MRR obtained from multi-objective optimization using Taguchi method only were 0.3733 mm and 124.1095 mg/min, respectively, while using the hybrid approach these values were 0.3267 mm and 169.1667 mg/min, respectively. Hence a considerable improvement for both quality characteristics was found with hybrid approach of TMRSM.

Dubey and Yadava [64] applied a hybrid approach of Taguchi method and principal component analysis (PCA) for multi-objective optimization of pulsed Nd:YAG laser beam cutting of nickel-based superalloy (SUPERNI 718) sheet to achieve better cut qualities within existing resources. The three-quality characteristics kerf width, kerf deviation (along the length of cut), and kerf taper were considered for simultaneous optimization. The input parameters considered were assist gas pressure, pulse width, pulse frequency, and cutting speed. Initially, single-objective optimization was performed using Taguchi method and then the signal-to-noise (S/N) ratios obtained were further used in PCA for multi-objective optimization. The results included the prediction of optimum input parameter levels and their relative significance on multiple quality characteristics.

Dubey and Yadava [65] optimized simultaneously two kerf qualities such as kerf deviation and kerf width using Taguchi quality loss function during pulsed Nd:YAG laser beam cutting of aluminum alloy sheet (0.9-mm thick). A considerable improvement in kerf quality was reported. In another work, Dubey and Yadava [66] reviewed the experimental investigations carried out to study the effect of various factors/process parameters on the performance of Nd:YAG LBM. The importance of different DOE methodologies used by various investigators for achieving the optimum value of different quality characteristics was discussed.

Karazi et al. [112] developed four models for the prediction of the width and depth dimensions of CO_2 laser-formed micro-channels in glass. A 3^3 statistical DOE model was built and conducted with the power (P), pulse repetition frequency (PRF), and traverse speed (U) of the laser machine as the selected parameters for investigation. Three feed-forward, back-propagation ANN models were also generated. These ANN models were varied to investigate the influence of variations in the number and the selection of training data. Model A was constructed with 24 data randomly selected from the experimental results, leaving three data points for model testing; Model B was constructed with the eight corner points of the experimental data space, and seven other randomly selected data, leaving 12 data points for testing; and Model C was constructed with 15 randomly selected data leaving 12 data points for testing. These models were developed separately for both micro-channel width and depth prediction. These ANN models were constructed in LabVIEW coding. The performance of these ANN models and the DOE model were compared. When compared with the actual results, two of the ANN models showed greater average percentage error than the DOE model.

The other ANN model showed an improved predictive capability that was approximately twice as good as that provided from the DOE model.

Pradhan et al. [187] attempted to optimize micro-EDM process parameters for machining Ti-6Al-4 V super alloy. To verify the optimal micro-EDM process parameters settings, MRR, tool wear rate (TWR), over cut (OC) and taper were chosen as observed performance criteria. In addition, four independent parameters such as peak current, pulse on-time, flushing pressure, and duty ratio were adopted for evaluation by the Taguchi method. From the ANOVA and S/N ratio graph, the significant process parameters and the optimal combination level of machining parameters were obtained. It was seen that machining performances were affected mostly by the peak current and pulse on-time during micro-EDM of titanium alloy. Mathematical models were developed to establish the relationship between various significant process parameters and micro-EDM performance criteria.

Klocke et al. [119] investigated size effects by downscaling the twist drilling process into the micro-range (diameter: $d = 50$ µm–1 mm). Therefore, experimental Micro-drilling tests in steel AISI 1045 (normalized and full-annealed) were performed with different cutting conditions (drill diameter, feed, cutting speed) and compared with data obtained from conventional drilling. Various size effects and its significant influence on the micro-cutting process were characterized with help of the experimental results. Additionally, the formula of Victor–Kienzle was adjusted to model the feed force in Micro-drilling operations.

Jadoun et al. [99] presented a study of the effect of process parameters on production accuracy obtained through ultrasonic drilling of holes in alumina-based ceramics using silicon carbide abrasive. Production accuracy in ultrasonic drilling involves both dimensional accuracy (hole oversize) and form accuracy (out-of-roundness and conicity). The parameters considered were workpiece material, tool material, grit size of the abrasive, power rating and slurry concentration. Taguchi's optimization approach was used to obtain the optimal parameters. The significant parameters were also identified and their effect on oversize, out-of-roundness and conicity were studied. The results obtained were validated by conducting the confirmation experiments.

Biswas et al. [29] studied Nd:YAG laser micro-drilling of gamma-titanium aluminide, a new material which performed well in laboratory tests as well as in different fields of engineering. The effect of different process parameters in the optimization of the process was investigated. The aspects considered were the hole circularity at exit and the hole taper of the drilled hole. Lamp current, pulse frequency, air pressure and thickness of the job were selected as independent process variables. The CCD technique based on RSM was employed to plan the experiments to achieve optimum responses with a reduced number of experiments. It was concluded that the various process parameters, i.e., lamp current, pulse frequency, air pressure and thickness can be optimally controlled for achieving desired responses like hole circularity at exit and hole taper using the developed mathematical model based on RSM. In CNC Nd:YAG laser micro-drilling of gamma-titanium aluminide, lamp current and sample thickness had shown a significant effect on both responses, i.e., hole circularity at exit and hole taper.

The pulse frequency and air pressure were dominant parameters for taper and for hole circularity, respectively. The optimum value of hole circularity at exit was calculated at lower values of lamp current, higher value of thickness and moderate values of air pressure and pulse frequency. The optimum value of hole taper was found out at lower value of lamp current, lower value of air pressure, higher value of pulse frequency and at higher thickness. Optimum values of both the responses were obtained at moderate values of lamp current, pulse frequency, air pressure and at higher values of job sample thickness.

3.9.1 Optimization of Laser Micro-Drilling Process

Very few efforts have been made for optimization of micro-drilling operation. Biswas et al. [29] developed a second-order response surface model to obtain the effect of the important process variable of laser Micro-drilling process such as lamp current (x_1), pulse frequency (x_2), air pressure (x_3), and thickness (x_4) on two main responses namely circularity at exit ($Y_{\text{circularity at exit}}$) and hole taper ($Y_{\text{hole taper}}$). The bounds for the four process variables are shown in Table 3.11.

A second-order model was developed by Biswas et al. [29] for the two responses, as given below:

$$\begin{aligned} Y_{\text{circularity at exit}} = {} & 0.93869 - 0.01052x_1 - 0.00268x_2 + 0.00372x_3 + 0.00059x_4 \\ & - 0.00079x_1^2 - 0.01529x_2^2 - 0.00934x_3^2 - 0.00304x_4^2 \\ & - 0.00379x_1x_2 + 0.00868x_1x_3 - 0.00685x_1x_4 - 0.00485x_2x_3 \\ & - 0.00383x_2x_4 + 0.00596x_3x_4 \end{aligned} \tag{3.101}$$

$$\begin{aligned} Y_{\text{hole taper}} = {} & 0.09453 + 0.00413x_1 + 0.000350268x_2 - 0.00187x_3 - 0.01955x_4 \\ & - 0.00036x_1^2 - 0.00036x_2^2 + 0.00174x_3^2 + 0.00283x_4^2 + 0.0009x_1x_2 \\ & - 0.0006x_1x_3 - 0.00274x_1x_4 - 0.00115x_2x_3 \\ & + 0.00278x_2x_4 + 0.00173x_3x_4. \end{aligned} \tag{3.102}$$

Based on the analysis discussed above, the optimization model was then formulated as: maximize $Y_{\text{circularity at exit}}$ (given by Eq. 3.101)

The constraint was related to the hole taper. The constraint was to ensure that the hole taper ($Y_{\text{holetaper}}$) should not exceed permissible value (Y_{per}) as specified by Eq. 3.103 given below.

Table 3.11 Bounds of process variables (from [29]; reprinted with permission from Elsevier)

Factors	Bounds		
	Symbol (unit)	Lower bound	Upper bound
Lamp current	x_1 (A)	20	22
Pulse frequency	x_2 (kHz)	0.8	1.6
Air pressure	x_3 (kg/cm^2)	1	2
Thickness	x_4 (mm)	0.48	0.68

Table 3.12 The results of optimization for $Y_{per} = 0.075$

Method	Lamp current (A)	Pulse frequency (kHz)	Air pressure (kg/cm^2)	Thickness	$Y_{\text{circularity at exit}}$
ABC	20	1.0266	1.4862	0.68	0.951
RSM [29]	21	1.2075	1.7247	0.6905	0.938

$$Y_{per} - Y_{\text{hole taper}} \geq 0. \tag{3.103}$$

Biswas et al. [29] applied RSM approach to solve the above optimization problem. RSM is intrinsic model-based technique when sequential experimentation is possible. It is also suitable when lower order polynomial regression equation exists to establish the relation between response and decision variables at the early stage of experimentation. However, RSM is unsuitable for solving highly non-linear, multi-modal functions and also in case of multiple objectives (Carlyle et al. [31]). Moreover, objective function needs to be continuously differentiable, which may not be the case in many complex physical processes. Hence this optimization problem is solved now using ABC to verify if any improvement is possible over the solution obtained by Biswas et al. [29]. The results of optimization using RSM method, and ABC algorithm are shown in Table 3.12.

It is observed from Table 3.12 that the results obtained using ABC algorithm are better than the results obtained using RSM method. This improvement is possible as the ABC algorithm combines both, the stochastic selection scheme carried out by onlooker bees, and greedy selection scheme used by onlookers and employed bees to update the source position. Also the neighbor source production mechanism in ABC is similar to the mutation process, which is self-adapting. The random selection process carried out by the scout bees maintains diversity in the solution. The ABC algorithm is thus flexible, simple to use and robust optimization algorithm, which can be used effectively in the optimization of multimodal and multi-variable problems.

References

1. Acharya BG, Jain VK, Batra JL (1986) Multi-objective optimization of ECM process. Precis Eng 8:88–96
2. Adam R, Maria ZS (2001) The mathematical modeling of electrochemical machining with flat ended universal electrodes. J Mater Process Technol 109:333–338
3. Akkurt A, Kulekci MK, Seker U, Ercan F (2004) Effect of feed rate on surface roughness in abrasive waterjet cutting applications. J Mater Process Technol 147(3):389–396
4. Almeida IA, De Rossi W, Lima MSF, Berretta JR, Nogueira GEC, Wetter NU, Vieira ND Jr (2006) Optimization of titanium cutting by factorial analysis of the pulsed Nd:YAG laser parameters. J Mater Process Technol 179(1–3):105–110
5. Aloke R, Girish V, Scrutton RF, Molian PA (1997) A model for prediction of dimensional tolerances of laser cut holes in mild steel thin plates. Int J Mach Tools Manuf 37:1069–1078
6. Amini S, Soleimanimehr H, Nategh MJ, Abudollah A, Sadeghi MH (2008) FEM analysis of ultrasonic-vibration-assisted turning and the vibratory tool. J Mater Process Technol 201(1–3):43–47

7. Anand KN (1996) Development of process technology in wire-cut operation for improving machining quality. Total Qual Manag 7(1):11–28
8. Armarego EA, Smith AJR, Wang J (1993) Constrained optimization strategies and CAM software for single-pass peripheral milling. Int J Prod Res 31:2139
9. Arola D, Ramulu M (1997) Material removal in abrasive waterjet machining of metals. Surface integrity and texture. Wear 210(1–2):50–58
10. Asokan P, Kumar PR, Jeyapaul R, Santhi M (2008) Development of multi-objective optimization models for electrochemical machining process. Int J Adv Manuf Technol 39(1–2):55–63
11. Axinte DA, Srinivasu DS, Kong MC, Butler-Smith PW (2009) Abrasive waterjet cutting of polycrystalline diamond: A preliminary investigation. Int J Mach Tools Manuf 49(10):797–803
12. Azmir MA, Ahsan AK (2009) A study of abrasive water jet machining process on glass/epoxy composite laminate. J Mater Process Technol 209(20):6168–6173
13. Azmir MA, Ahsan AK (2008) Investigation on glass/epoxy composite surfaces machined by abrasive water jet machining. J Mater Process Technol 198(1–3):122–128
14. Bandhopadhayay S, Sarin Sundar JK, Sunderajan G, Joshi SV (2002) Geometrical features and metallurgical characteristics of Nd:YAG laser drilled holes in thick IN718 and Ti-6Al-4V sheets. J Mater Process Technol 127:83–95
15. Tansel IN, Bao WY (2000) Modeling micro-end-milling operations-analytical cutting force model. Int J Mach Tools Manuf 40(15):2155–2173
16. Basak I, Ghosh A (1996) Mechanism of spark generation during electrochemical discharge machining; a theoretical model and experimental verification. J Mater Process Technol 62:46–53
17. Basak I, Ghosh A (1997) Mechanism of material removal in electrochemical discharge machining; a theoretical model and experimental verification. J Mater Process Technol 71:350–359
18. Bhattacharyya B, Doloi BN, Sorkhel SK (1999) Experimental investigations into electrochemical discharge machining (ECDM) for non-conducting ceramics materials. J Mater Process Technol 95:145–154
19. Bhattacharyya B, Sur B, Sorkhel SK (1973) Analysis for optimum parametric combination in electrochemical machining. CIRP Ann Manuf Technol 22:59–60
20. Bhattacharyya B, Munda J (2003) Experimental investigation on the influence of electrochemical machining parameters on machining rate and accuracy in micromachining domain. Int J Mach Tools Manuf 43(13):1301–1310
21. Bhattacharyya B, Munda J (2008) Investigation into electrochemical micromachining (EMM) through response surface methodology based approach. Int J Mach Tools Manuf 35(7-8)
22. Bhattacharyya B, Sorkhel SK (1998) Investigation for controlled electrochemical machining through response surface methodology-based approach. J Mater Process Technol 86(1–3): 200–207
23. Benedict GF (1987) Nontraditional manufacturing processes. Marcel Dekker, New York
24. Benkirane Y, Kremer D, Moisan A (1999) Ultrasonic machining: an analytical and experimental study on contour machining based on neural network. CIRP Ann Manuf Technol 48(1):135–138
25. Bergh F, Engelbrecht AP (2006) A study of particle swarm optimization particle trajectories. Inf Sci 176:937–971
26. Bigot S, Valentinčič J, Blatnik O, Junkar M (2006) Micro-EDM parameters optimization. In: Menz W, Dimov S, Fillon B (eds) 2nd international conference on multi-material micro manufacture. Elsevier, Oxford
27. Bissacco G, Hansen HN, De Chiffre L (2006) Size effects on surface generation in micro-milling of hardened tool steel. Ann CIRP 55(1):593–596
28. Bissacco G, Hansen HN, Slunsky J (2008) Modeling the cutting edge radius size effect for force prediction in micro-milling. CIRP Ann Manuf Technol 57(1):113–116

29. Biswas R, Kuar AS, Sarkar S, Mitra S (2010) A parametric study of pulsed Nd:YAG laser micro-drilling of gamma-titanium aluminide. Opt Laser Technol 42:23–31
30. Bruneel D, Matras G, Harzic RL, Huot N, König K, Audouard E (2010) Micromachining of metals with ultra-short Ti-Sapphire lasers: prediction and optimization of the processing time. Optics Lasers Eng 48(3):268–271
31. Carlyle WC, Montgomery DC, Runger GC (2000) Optimization problems and methods in quality control and improvement. J Qual Technol 31:1–17
32. Çaydaş U, Hasçalık A (2008) Use of the grey relational analysis to determine optimum laser cutting parameters with multi-performance characteristics. Opt Laser Technol 40(7):987–994
33. Çaydaş U, Ahmet H, Ekici S (2009) An adaptive neuro-fuzzy inference system (ANFIS) model for wire-EDM. Expert Syst Appl 36(3):6135–6139
34. Cenna AA, Mathew P (2002) Analysis and prediction of laser cutting parameters of fibre reinforced plastics (FRP) composite materials. Int J Mach Tools Manuf 42:105–113
35. Chae J, Park SS, Freiheit T (2006) Investigation of micro-cutting operations. Int J Mach Tools Manuf 46:313–332
36. Chak S, Rao PV (2008) The drilling of Al_2O_3 using a pulsed DC supply with a rotary abrasive electrode by the electrochemical discharge process. Int J Adv Manuf Technol 39:633–641
37. Chakravarthy PS, Babu NR (2000) A hybrid approach for selection of optimal process parameters in abrasive water jet cutting. Proc Inst Mech Eng Part B J Eng Manuf 214:781–791
38. Chakravarthy PS, Babu NR (1999) A new approach for selection of optimal process parameters in abrasive water jet cutting. Mater Manuf Process 14(4):581–600
39. Chang CW, Kuo CP (2007) Evaluation of surface roughness in laser-assisted machining of aluminum oxide ceramics with Taguchi method. Int J Mach Tools Manuf 47(1):141
40. Chang T, Wysk RA, Davis RP, Choi B (1982) Milling parameter optimization through a discrete variable transformation. Int J Prod Res 20:507
41. Chen L, Siores E, Wong WCK (1998) Optimising abrasive waterjet cutting of ceramic materials. J Mater Process Technol 74(1–3):251–254
42. Chen HC, Lin JC, Yang YK, Tsai CH (2010) Optimization of wire electrical discharge machining for pure tungsten using a neural network integrated simulated annealing approach. Expert Syst Appl. doi:10.1016/j.eswa.2010.04.020
43. Chen L, Siores E, Wong WCK (1996) Kerf characteristic in abrasive waterjet cutting of ceramic materials. Int J Mach Tools Manuf 36(11):1201–1206
44. Chen MC, Tsai DM (1996) A simulated annealing approach for optimization of multi-pass turning operations. Int J Prod Res 34:2803
45. Chen TC, Robert B, Darling RB (2005) Parametric studies on pulsed near ultraviolet frequency tripled Nd:YAG laser micromachining of sapphire and silicon. J Mater Process Technol 169:214–218
46. Chen YH, Tam SC, Chen WL, Zheng HY (1996) Application of Taguchi method in the optimization of laser micro-engraving of photomasks. Int J Mater Prod Technol 11(3–4):333–344
47. Chiang KT, Chang FP (2006) Optimization of the WEDM process of particle-reinforced material with multiple performance characteristics using grey relational analysis. J Mater Process Technol 180(1–3):96–101
48. Choi GS, Choi GH (1997) Process analysis and monitoring in abrasive water jet machining of alumina ceramics. Int J Mach Tools Manuf 37:295–307
49. Choobineh F, Jain VK (1993) A fuzzy sets approach for selecting optimum parameters of an ECM process. Process Adv Mater 3:225–232
50. Ciurana J, Arias G, Ozel T (2009) Neural network modeling and particle swarm optimization (PSO) of process parameters in pulsed laser micromachining of hardened AISI H13 steel. Mater Manuf Process 24(3):358–368

51. Clifton D, Mount AR, Alder GM, Jardine D (2002) Ultrasonic measurement of the inter-electrode gap in electro chemical machining. Int J Mach Tools Manuf 42:1259–1267
52. Clodeinir RP, Guerra REH, Haber RH, Alique A, Ros S (1999) Fuzzy model and hierarchical fuzzy control integration: an approach for milling process optimization. Comp Ind 39:199
53. Cook NH (1966) Manufacturing analysis. Addison-Wesley, London
54. Deam RT, Lemma E, Ahmed DH (2004) Modeling of the abrasive water jet cutting process. Wear 257(9–10):877–891
55. Demir E (2008) Taylor-based model for micro-machining of single crystal fcc materials including frictional effects-application to micro-milling process. Int J Mach Tools Manuf 48(1):1592–1598
56. Dereli T, Filiz IH, Baykasoglu A (2001) Optimizing cutting parameters in process planning of prismatic parts using genetic algorithms. Int J Prod Res 39:3303
57. Dhara SK, Kuar AS, Mitra S (2008) An artificial neural network approach on parametric optimization of laser micro-machining of die-steel. Int J Adv Manuf Technol 39(1–2):39–46
58. Dhupal D, Doloi B, Bhattacharyya B (2008) Parametric analysis and optimization of Nd:YAG laser micro-grooving of aluminum titanate (Al_2TiO_5) ceramics. Int J Adv Manuf Technol 36(9–10):883–893
59. Dhupal D, Doloi B, Bhattacharyya B (2009) Modeling and optimization on Nd:YAG laser turned micro-grooving of cylindrical ceramic material. Opt Lasers Eng 47(9):917–925
60. Dow TA, Miller EL, Garrard K (2004) Tool force and deflection compensation for small milling tools. Precis Eng 28:31–45
61. Dvivedi A, Kumar P (2007) Surface quality evaluation in ultrasonic drilling through the Taguchi technique. Int J Adv Manuf Technol 34(1–2):131–140
62. Dubey AK, Yadava V (2008) Laser beam machining—a review. Int J Mach Tools Manuf 48(6):609–628
63. Dubey AK, Yadava V (2008) Multi-objective optimization of laser beam cutting process. Opt Laser Technol 40(3):562–570
64. Dubey AK, Yadava V (2008) Multi-objective optimization of Nd:YAG laser cutting of nickel-based superalloy sheet using orthogonal array with principal component analysis. Opt Lasers Eng 46(2):124–132
65. Dubey AK, Yadava V (2008) Optimization of kerf quality during pulsed laser cutting of aluminum alloy sheet. J Mater Process Technol 204(1–3):412–418
66. Dubey AK, Yadava V (2008) Experimental study of Nd:YAG laser beam machining—an overview. J Mater Process Technol 195(1–3):15–26
67. El-Dardy MA (1982) Economic study of electro chemical machining. Int J Mach Tools Manuf 22:147–158
68. Eltobgy MS, Ng E, Elbestawi MA (2005) Finite element modeling of erosive wear. Int J Mach Tool Manuf 45:1337–1346
69. Fang N (2003) Slip-line modeling of machining with a rounded-edge tool—part I: new model and theory. J Mech Phys Solids 51:715–742
70. Finnie I (1960) Erosion of surfaces by solid particles. Wear 3:87–103
71. Gadalla AM, Bozkurt B, Faulk NM (1991) Modeling of thermal spalling during electrical discharge mechanism of TiB2. J Am Ceram Soc 74:801–806
72. Ghoreishi M, Low DKY, Li L (2002) Comparative statistical analysis of hole taper and circularity in laser percussion drilling. Int J Mach Tools Manuf 42:985–995
73. Ghoreishi M, Nakhjavani OB (2008) Optimization of effective factors in geometrical specifications of laser percussion drilled holes. J Mater Process Technol 196(1–3):303–310
74. Ghosh A, Mallik AK (1985) Manufacturing science. Affiliated East-West Press, New Delhi
75. Gokler MI, Ozanozgu AM (2000) Experimental investigation of effects of cutting parameters on surface roughness in the WEDM process. Int J Mach Tools Manuf 40(13):1831–1848
76. Han F, Jiang J, Yu D (2007) Finish cut of wire electrical discharge machining (WEDM). Int J Adv Manuf Technol 34(5–6)

77. Han F, Kunieda MT, Sendai T, Imai Y (2002) High precision simulation of WEDM using parametric programming. CIRP Ann Manuf Technol 51(1):165–168
78. Han MP, Min BK, Lee SJ (2008) Modeling gas film formation in electrochemical discharge machining process using a side-insulated electrode. J Micromech Microeng 18:50–58
79. Hargrove SK, Ding D (2007) Determining cutting parameters in wire EDM based on workpiece surface temperature distribution. Int J Adv Manuf Technol 34(3–4)
80. Hascalyk A, Caydas U (2004) Experimental study of wire electrical discharge machining of AISI D5 tool steel. J Mater Process Technol 148:362–367
81. Hashish M (1989) A model for abrasive water jet (AWJ) machining. J Eng Mater Technol 111:154–162
82. Hashish M (1984) A modeling study of metal cutting with abrasive water jets. J Eng Mater Technol 106:88–100
83. Hassan AI, Kosmol J (2001) Dynamic elastic–plastic analysis of 3D deformation in abrasive waterjet machining. J Mater Process Technol 113(1–3):337–341
84. Hewidy MS, El-Taweel TA, El-Safty MF (2005) Modeling the machining parameters of wire electrical discharge machining of Inconel 601 using RSM. J Mater Process Technol 169:328–336
85. Hewidy MS, Ebeid SJ, El-Taweel TA, Youssef AH (2007) Modeling the performance of ECM assisted by low frequency vibrations. J Mater Process Technol 189(1–3):466–472
86. Hewidy MS, Fattouh M, Elkhabeery M (1984) Some economical aspects of ECM processes. In: Proceedings of first AME conference, TT8. Military Technical College, Cairo, pp 87–94
87. Hlaváč LM (2009) Investigation of the abrasive water jet trajectory curvature inside the kerf. J Mater Process Technol 209(8):4154–4161
88. Ho KH, Newman ST, Rahimifard S, Allen RD (2004) State of the art in wire electrical discharge machining (WEDM). Int J Mach Tools Manuf 44:1247–1259
89. Hocheng H, Chang KR (1994) Material removal analysis in abrasive waterjet cutting of ceramic plates. J Mater Process Technol 40(3–4):287–304
90. Hoogstrate AM, Karpuschewski B, Luttervelt CAV, Kals HJJ (2002) Modeling of high velocity, loose abrasive machining processes. CIRP Ann Manuf Technol 51(1):263–266
91. Hoogstrate AM, Luttervelt CAV, Gosger P, Momber AW, Tönshoff HK, Louis H, Klocke F, Riviere D, Magnusson AC, Gardner J, Rajurkar KP, Kim TJ, Konacevic R, Ryd J, Henning A, Ojmertz C, Kruth JP, Meijer J, Leu MC (1997) Opportunities in abrasive water jet machining. CIRP Ann Manuf Technol 46(2):697–714
92. Hopenfeld J, Cole RR (1969) Prediction of the one dimensional equilibrium cutting gap in electro-chemical machining. ASME J Eng Indust 8:755–760
93. Hough CL, Goforth RE (1981) Optimization of the second order logarithmic machining economics problem by extended geometric programming—part II posynomial constraints. Am Inst Ind Eng Trans 13:234–238
94. Hsu CY, Lin YY, Lee WS, Lo SP (2008) Machining characteristics of Inconel 718 using ultrasonic and high temperature-aided cutting. J Mater Process Technol 198(1–3):359–365
95. Hsue WJ, Liao YS, Lu SS (1999) Fundamental geometry analysis of wire electrical discharge machining in corner cutting. Int J Mach Tools Manuf 39(4):651–667
96. Hu P, Zhang JM, Pei ZJ (2002) Clyde Treadwell Modeling of material removal rate in rotary ultrasonic machining: designed experiments. J Mater Process Technol 129(1–3):339–344
97. Huang JT, Liao YS (2003) Optimization of machining parameters of wire-EDM based on grey relational and statistical analyses. Int J Prod Res 41(8):1707–1720
98. Jackson MJ, O'Neill W (2003) Laser micro-drilling of tool steel using Nd:YAG lasers. J Mater Process Technol 142:517–525
99. Jadoun RS, Kumar P, Mishra BK (2009) Taguchi's optimization of process parameters for production accuracy in ultrasonic drilling of engineering ceramics. Prod Eng 3(3): 243–253
100. Jain NK, Jain VK (2001) Modeling of material removal in mechanical type advanced machining processes: state of the art review. Int J Mach Tools Manuf 41:1573–1635

101. Jain NK, Jain VK (2007) Optimization of electro chemical machining process parameters using genetic algorithm. Mach Sci Technol 11:235–258
102. Jain NK, Jain VK, Deb K (2007) Optimization of process parameters of mechanical type advanced machining processes using genetic algorithm. Int J Mach Tools Manuf 47:900–919
103. Jain VK (2002) Advanced machining processes. Allied Publishers, New Delhi
104. Jain VK, Dixit PM, Pandey PM (1999) On the analysis of electrochemical spark machining process. Int J Mach Tools Manuf 39:165–186
105. Jain VK, Srinivas P, Narayansamy K (1991) Experimental investigation into travelling wire electrochemical spark machining (TW-ECSM) of composites. J Eng Ind 27(1–2):75–84
106. Jegaraj JJR, Babu NR (2007) A soft computing approach for controlling the quality of cut with abrasive waterjet cutting system experiencing orifice and focusing tube wear. J Mater Process Technol 185(1–3):217–227
107. Junkar M, Jurisevic B, Fajdiga M, Grah M (2006) Finite element analysis of single-particle impact in abrasive water jet machining. Int J Impact Eng 32(7):1095–1112
108. Kaebernick H, Bicleanu D, Brandt M (1999) Theoretical and experimental investigation of pulsed laser cutting. CIRP Ann Manuf Technol 48(1):163–166
109. Kainth GS, Nandy A, Singh K (1979) On the mechanics of material removal in ultrasonic machining. Int J Mach Tool Des Res 19:33–41
110. Kanlayasiri K, Boonmung S (2007) Effects of wire-EDM machining variables on surface roughness of newly developed DC 53 die steel: Design of experiments and regression model. J Mater Process Technol 192–193:459–464
111. Kao CC, Shih AJ (2008) Design and tuning of a fuzzy logic controller for micro-hole electrical discharge machining. J Manuf Process 10(2):61–73
112. Karazi SM, Issa A, Brabazon D (2009) Comparison of ANN and DoE for the prediction of laser-machined micro-channel dimensions. Opt Laser Eng 47(9):956–964
113. Kaczmarek I (1976) Impact grinding (ultrasonic machining). In: Principles of machining by cutting abrasion and erosion, Peter Peregrinus Ltd, Stevenage
114. Kalpakjian S, Schmid S (2005) Manufacturing engineering and technology. Prentice Hall, New Jersey
115. Kang IS, Kim JS, Kim JH, Kang MC, Seo YW (2007) A mechanistic model of cutting force in the micro-end milling process. J Mater Process Technol 187–188:250–255
116. Khan AA, Haque MM (2007) Performance of different abrasive materials during abrasive water jet machining of glass. J Mater Process Technol 191:404–407
117. Kim CJ, Mayor JR, Ni J (2004) A static model of chip formation in micro-scale milling. J Manuf Sci Eng 126:710–718
118. Kim DJ, Ahn Y, Lee SH, Kim YK (2006) Voltage pulse frequency and duty ratio effects in an electrochemical discharge microdrilling process of Pyrex glass. Int J Mach Tools Manuf 46(10):1064–1067
119. Klocke F, Gerschwiler K, Abouridouane M (2009) Size effects of micro-drilling in steel. Prod Eng 3(1):69–72
120. Komaraiah M, Manan MA, Reddy PN, Victor S (1988) Investigation of surface roughness and accuracy in ultrasonic machining. Precis Eng 10(2):59–65
121. Konda R, Rajurkar KP, Bishu RR, Guha A, Parson M (1999) Design of experiments to study and optimize process performance. Int J Qual Reliab Manag 16(1):56–71
122. Kopalinsky EM, Oxley PLB (1984) Size effects in metal removal processes. Inst Phys Conf Ser 70:389–396
123. Kovacevic R, Fang M (1994) Modeling the influence of the abrasive waterjet cutting parameters on the depth of cut based on fuzzy rules. Int J Mach Tools Manuf 34(1):55–72
124. Kovacevic R, Hashish M, Mohan R, Ramulu M, Kim TJ, Geskin ES (1997) State of the art of research and development in abrasive waterjet machining. J Manuf Sci Eng 119(4):776–785
125. Kozak J (1975) Optimization of electro chemical machining (ECM) process from the point of view of geometrical accuracy. Archiwum Budowy Maszyn 22:387–398

126. Kozak J (2001) Computer simulation system for electrochemical shaping. J Mater Process Technol 109:354–359
127. Kozak J, Luczan D, Konrad L, Marek R, Robert S (2001) CAE-ECM system for electrochemical technology of parts and tools. J Mater Process Technol 107:293–299
128. Kuar AS, Doloi B, Bhattacharyya B (2006) Modeling and analysis of pulsed Nd:YAG laser machining characteristics during micro-drilling of zirconia(ZrO2). Int J Mach Tools Manuf 46:1301–1310
129. Kuar AS, Paul G, Mitra S (2006) Nd:YAG laser micromachining of alumina–aluminum interpenetrating phase composite using response surface methodology. Int J Mach Mach Mater 1(4):423–444
130. Kulkarni A, Sharan R, Lal GK (2002) An experimental study of discharge mechanism in electrochemical discharge machining. Int J Mach Tools Manuf 42:1121–1127
131. Kulkarni AV (2009) Systematic experimental analysis of electrochemical discharge machining process. Int J Mach Machinability Mater 6(3–4):194–212
132. Kumar V, Khamba JS (2009) Parametric optimization of ultrasonic machining of co-based super alloy using the Taguchi multi-objective approach. Prod Eng Res Dev 3:417–425
133. Kumar V, Khamba JS (2009) Statistical analysis of experimental parameters in ultrasonic machining of tungsten carbide using the Taguchi approach. J Am Ceram Soc 91:92–96
134. Kumar V, Khamba JS (2010) Modeling the material removal rate in ultrasonic machining using dimensional analysis. Int J Adv Manuf Technol 48(1–4):103–119
135. Kuriakose S, Shunmugam MS (2005) Multi-objective optimization of wire-electro discharge machining process by non-dominated sorting genetic algorithm. J Mater Process Technol 170:133–141
136. Lai X, Li H, Li C, Lin Z, Ni J (2008) Modeling and analysis of micro-scale milling considering size effect, micro-cutter edge radius and minimum chip thickness. Int J Mach Tools Manuf 48:1–14
137. Lee TC, Chan CW (1997) Mechanism of ultrasonic machining of ceramic composites. J Mater Process Technol 71:195–201
138. Lee WM, Liao YS (2007) Adaptive control of the WEDM process using a self-tuning fuzzy logic algorithm with grey prediction. Int J Adv Manuf Technol 34(5–6)
139. Li L, Diver C, Atkinson J, Giedl-Wagner R, Helml HJ (2006) Sequential laser and EDM micro-drilling for next generation fuel injection nozzle manufacture. CIRP Ann Manuf Technol 55(1):179–182
140. Li CH, Tsai MJ (2009) Multi-objective optimization of laser cutting for flash memory modules with special shapes using grey relational analysis. Opt Laser Technol 41(5):634–642
141. Li CH, Tsai MJ, Yang CD (2007) Study of optimal laser parameters for cutting QFN packages by Taguchi's matrix method. Opt Laser Technol 39:786–795
142. Li ZC, Cai LW, Pei ZJ, Treadwell C (2006) Edge-chipping reduction in rotary ultrasonic machining of ceramics: finite element analysis and experimental verification. Int J Mach Tools Manuf 46(12–13):1469–1477
143. Li ZC, Jiao Y, Deines TW, Pei ZJ, Treadwell C (2005) Rotary ultrasonic machining of ceramic matrix composites: feasibility study and designed experiments. Int J Mach Tools Manuf 45(12–13):1402–1411
144. Liao YS, Huang JT, Su HC (1997) A study on the machining parameters optimization of wire electrical discharge machining. J Mater Process Technol 71(3):487–493
145. Liao YS, Yan MT, Chang CC (2002) A neural network approaches for the on-line estimation of work piece height in WEDM. J Mater Process Technol 121(2–3):252–258
146. Lim SH, Lee CM, Chung WJ (2006) A study on optimal cutting condition of a high speed feeding type laser cutting machine by using Taguchi method. Int J Precis Eng Manuf 7(1):18–23
147. Liu CL, Esterling D (1997) Solid modeling of 4-axis wire EDM cut geometry. Comp Aided Des 29(12):803–810

148. Liu H, Wang J, Kelson N, Brown RJ (2004) A study of abrasive waterjet characteristics by CFD simulation. J Mater Process Technol 153–154:488–493
149. Liu JW, Yue TM, Guo ZN (2010) An analysis of the discharge mechanism in electrochemical discharge machining of particulate reinforced metal matrix composites. Int J Mach Tools Manuf 50(1):86–96
150. Liu X, Vogler MP, Kapoor SG, DeVor RE, Ehmann KF, Mayor R, Kim CJ, Ni J (2004) Micro-end milling with meso-machine-tool system. In: Proceedings of NSF Design, Service and Manufacturing Grantees and Research Conference, Dallas
151. Lucca DA, Rhorer RL, Komanduri R (1991) Energy dissipation in the ultra precision machining of copper. CIRP Ann Manuf Technol 40:69–72
152. Ma C, Deam RT (2006) A correlation for predicting the kerf profile from abrasive water jet cutting. Exp Therm Fluid Sci 30(4):337–343
153. Ma C, Shamoto E, Moriwaki T, Wang L (2004) Study of machining accuracy in ultrasonic elliptical vibration cutting. Int J Mach Tools Manuf 44(12–13):1305–1310
154. Machinability Data Center (1980) Machining data handbook. Metcut Research Associates, Ohio
155. Mahapatra SS, Patnaik A (2007) Optimization of wire electrical discharge machining (WEDM) process parameters using Taguchi method. Int J Adv Manuf Technol 34(9–10)
156. Manna A, Bhattacharyya B (2006) Taguchi and Gauss elimination method: A dual response approach for parametric optimization of CNC wire cut EDM of PRAlSiCMMC. Int J Adv Manuf Technol 28(1–2)
157. Malekian M, Park SS, Jun MBG (2009) Modeling of dynamic micro-milling cutting forces. Int J Mach Tools Manuf 49(7–8):586–598
158. Malekian M, Park SS, Jun MBG (2009) Tool wear monitoring of micro-milling operations. J Mater Process Technol 209(10):4903–4914
159. Manu R, Babu NR (2009) An erosion-based model for abrasive waterjet turning of ductile materials. Wear 266(11–12):1091–1097
160. Masmiati N, Philip PK (2007) Investigations on laser percussion drilling of some thermoplastic polymers. J Mater Process Technol 185:198–203
161. Mathew J, Goswami GL, Ramakrishnan N, Naik NK (1999) Parametric studies on pulsed Nd:YAG laser cutting of carbon fibre reinforced plastic composites. J Mater Process Technol 89–90:198–203
162. McGeough JA (1988) Advanced methods of machining. Chapman and Hall, New York
163. Mediliyegedara TKKR, De Silva AKM, Harrison DK, McGeough JA (2005) New developments in the process control of the hybrid electro chemical discharge machining (ECDM) process. J Mater Process Technol 167(2–3):338–343
164. Mediliyegedara TKKR, De Silva AKM, Harrison DK, McGeough JA, Hepburn D (2006) Designing steps and simulation results of a pulse classification system for the electro chemical discharge machining (ECDM) process-an artificial neural network approach. In: Advances in soft computing, applied soft computing technologies: the challenge of complexity. Springer, Hiedelberg
165. Miller GE (1957) Special theory of ultrasonic machining. J App Phys 28:149–156
166. Min S, Dornfeld D, Inasaki I, Ohmori H, Lee D, Deichmueller M, Yasuda T, Niwa K (2006) Variation in machinability of single crystal materials in micromachining. CIRP Ann Manuf Technol 55(1):105–110
167. Mishra PK (1997) Nonconventional machining. Narosa Publishing House, New Delhi
168. Mitrofanov AV, Babitsky VI, Silberschmidt VV (2004) Finite element analysis of ultrasonically assisted turning of Inconel 718. J Mater Process Technol 153–154:233–239
169. Montgomery DC (1997) Design and analysis of experiments. Wiley, New York
170. Mostofa MG, Kil KY, Hwan AJ (2010) Computational fluid analysis of abrasive waterjet cutting head. J Mech Sci Technol 24:249–252
171. Nair EV, Ghosh A (1985) A fundamental approach to the study of the mechanics of ultrasonic machining. Int J Prod Res 23:731–753
172. Nakayama K, Tamura K (1968) Size effect in metal-cutting force. J Eng Ind 90:119

173. Nath C, Rahman M (2008) Effect of machining parameters in ultrasonic vibration cutting. Int J Mach Tools Manuf 48(9):965–974
174. Newby G, Venkatachalam S, Liang SY (2007) Empirical analysis of cutting force constants in micro-end-milling operations. J Mater Process Technol 192–193(1):41–47
175. Orbanic H, Junkar M (2008) Analysis of striation formation mechanism in abrasive water jet cutting. Wear 265(5–6):821–830
176. Pajak PT, De Silva AKM, McGeough JA, Harrison DK (2004) Modeling the aspects of precision and efficiency in laser-assisted jet electrochemical machining (LAJECM). J Mater Process Technol 149(1–3):512–518
177. Pan LK, Wang CC, Hsiao YC, Ho KC (2005) Optimization of Nd:YAG laser welding onto magnesium alloy via Taguchi analysis. Opt Laser Technol 37(1):33–42
178. Park SS, Malekian M (2009) Mechanistic modeling and accurate measurement of micro-end milling forces. CIRP Ann Manuf Technol 58(1):49–52
179. Park SS, Rahnama R (2010) Robust chatter stability in micro-milling operations. CIRP Ann Manuf Technol 59(1):391–394
180. Paul S, Hoogstrate AM, Luttervelt VCA, Kals HJJ (1998) Analytical and experimental modeling of abrasive water jet cutting of ductile materials. J Mater Process Technol 73:189–199
181. Pei ZJ, Ferreira PM (1998) Modeling of ductile mode material removal in rotary ultrasonic machining. Int J Mach Tools Manuf 38:1399–1418
182. Pei ZJ, Prabhakar D, Ferreira PM, Haselkorn M (1995) A mechanistic approach to the prediction of material removal rates in rotary ultrasonic machining. J Eng Ind 117:142–151
183. Perez RE, Behdinan K (2007) Particle swarm approach for structural design optimization. Comput Struct 85:1579–1588
184. Pham DT, Dimov SS, Bigot S, Ivanov A, Popov K (2004) Micro-EDM—recent developments and research issues. J Mater Process Technol 149(1–3):50–57
185. Plaza S, Ortega N, Sanchez JA, Pombo I, Mendikute A (2009) Application of the wire electrical discharge machining (WEDM) process. Int J Adv Manuf Technol 44(5–6)
186. Prabhakar D, Pei ZJ, Ferreira PM, Haselkorn M (1993) A theoretical model for predicting material removal rates in rotary ultrasonic machining of ceramics. Trans NAMRI/SME XXI:167–172
187. Pradhan BB, Masanta M, Sarkar BR, Bhattacharyya B (2009) Investigation of electro-discharge micro-machining of titanium super alloy. Int J Adv Manuf Technol 41(11–12):1094–1106
188. Purcar M, Bortels L, Bossche BVD, Deconinck J (2004) 3D electrochemical machining computer simulations. J Mater Process Technol 149(1–3):472–478
189. Pujana J, Rivero A, Celaya A, de Lacalle LNL (2009) Analysis of ultrasonic-assisted drilling of Ti6Al4 V. Int J Mach Tools Manuf 49(6):500–508
190. Puri AB, Bhattacharyya B (2003) An analysis and optimization of the geometrical inaccuracy due to wire lag phenomenon in WEDM. Int J Mach Tools Manuf 43(2):151–159
191. Raghuram V, Pramila T, Srinivasa YG, Narayanasamy K (1995) Effect of the circuit parameters on the electrolytes in the electrochemical discharge phenomenon. J Mater Process Technol 52(2–4):301–318
192. Rajurkar KP, Zhu D, McGeough JA, Kozak J, De Silva A (1999) New developments in electro chemical machining. CIRP Ann Manuf Technol 48:567–579
193. Ramakrishnan R, Karunamoorthy L (2008) Modeling and multi-response optimization of Inconel 718 on machining of CNC WEDM process. J Mater Process Technol 7(1–3):343–349
194. Rao KM, Rangajanardhaa G, Hanumantha RD, Sreenivasa RM (2009) Development of hybrid model and optimization of surface roughness in electric discharge machining using artificial neural networks and genetic algorithm. J Mater Process Technol 3:1512–1520
195. Rao R, Yadava V (2009) Multi-objective optimization of Nd:YAG laser cutting of thin superalloy sheet using grey relational analysis with entropy measurement. Opt Laser Technol 41(8):922–930

196. Rao RV (2007) Decision making in the manufacturing environment using graph theory and fuzzy multiple attribute decision making methods. Springer, London
197. Rao RV, Pawar PJ (2009) Modeling and optimization of process parameters of wire electrical discharge machining. Proc Inst Mech Eng Part B J Eng Manuf 223(11):1431–1440
198. Rao RV, Pawar PJ, Davim JP (2010) Parameter optimization of ultrasonic machining process using non-traditional optimization algorithms. Mater Manuf Process (in press)
199. Rao RV, Pawar PJ (2010) Parameter optimization of a multi-pass milling process using non-traditional optimization algorithms. Appl Soft Comput 10:445–456
200. Rao RV, Pawar PJ, Shankar R (2008) Multi-objective optimization of electrochemical machining process parameters using a particle swarm optimization algorithm. Proc Inst Mech Eng Part B J Eng Manuf 222(8):949–958
201. Rosenberg LD, Kazantsev VF, Makarov LO, Yakhimovich DF (1964) Ultrasonic cutting. Consultant Bureau, New York
202. Saha P, Singha A, Pal SK, Saha P (2008) Soft computing models based prediction of cutting speed and surface roughness in wire electro-discharge machining of tungsten carbide cobalt composite. Int J Adv Manuf Technol 39(1–2)
203. Saha S, Pachon M, Ghoshal A, Schulz MJ (2004) Finite element modeling and optimization to prevent wire breakage in electro-discharge machining. Mech Res Commun 31(4):451–463
204. Samant AN, Dahotre NB (2008) Computational predictions in single-dimensional laser machining of alumina. Int J Mach Tools Manuf 48(12–13):1345–1353
205. Samant AN, Paital SR, Dahotre NB (2008) Process optimization in laser surface structuring of alumina. J Mater Process Technol 203(1–3):498–504
206. Sanchez JA, Lacalle LNL, Lamikiz A (2004) A computer-aided system for the optimization of the accuracy of the wire electro-discharge machining process. Int J Comp Integr Manuf 17(5):413–420
207. Sarkar BR, Doloi B, Bhattacharyya B (2006) Parametric analysis on electrochemical discharge machining of silicon nitride ceramics. Int J Adv Manuf Technol 28(9–10)
208. Sarkar BR, Doloi B, Bhattacharyya B (2008) Experimental investigation into electrochemical discharge microdrilling on advanced ceramics. Int J Manuf Technol Manag 13(204):214–225
209. Sarkar BR, Doloi B, Bhattacharyya B (2009) Investigation into the influences of the power circuit on the micro-electrochemical discharge machining process. Proc Inst Mech Eng Part B J Eng Manuf 223(2):133–144
210. Sarkar S, Mitra S, Bhattacharyya B (2005) Parametric analysis and optimization of wire electrical discharge machining of γ-titanium aluminide alloy. J Mater Process Technol 159:286–294
211. Schöpf M, Beltrami I, Boccadoro M, Kramer D, Schumacher B (2001) ECDM a new method for trueing and dressing of metal bonded diamond grinding tools. CIRP Ann Manuf Technol 50(1):125–128
212. Scott D, Boyina S, Rajurkar KP (1991) Analysis and optimization of parameter combination in wire electrical discharge machining. Int J Prod Res 29(11):2189–2207
213. Sen M, Shan HS (2005) A review of electrochemical macro- to micro-hole drilling processes. Int J Mach Tools Manuf 45(2):137–152
214. Sen M, Shan HS (2005) Analysis of hole quality characteristics in the electro jet drilling process. Int J Mach Tools Manuf 45(15):1706–1716
215. Senthilkumar C, Ganesan G, Karthikeyan R (2009) Study of electrochemical machining characteristics of Al/SiCp composites. Int J Adv Manuf Technol 43(3–4)
216. Shanmugam DK, Masood SH (2009) An investigation on kerf characteristics in abrasive waterjet cutting of layered composites. J Mater Process Technol 209(8):3887–3893
217. Shaw MC (1995) Precision finishing. CIRP Ann Manuf Technol 44(1):343–348
218. Shaw MC (1956) Ultrasonic grinding. Microtechnic 10:257–265
219. Singh J, Gill SS (2009) Fuzzy modeling and simulation of ultrasonic drilling of porcelain ceramic with hollow stainless steel tools. Mater Manuf Process 24:468–475

220. Singh R, Khamba JS (2009) Mathematical modeling of surface roughness in ultrasonic machining of titanium using Buckingham-Π approach: a review. Int J Abras Technol 2: 3–24
221. Singh R, Khamba JS (2009) Mathematical modeling of tool wear rate in ultrasonic machining of titanium. Int J Adv Manuf Technol 43(5–6):573–580
222. Singh R, Khamba JS (2007) Macromodel for ultrasonic machining of titanium and its alloys: designed experiments. Proc Inst Mech Eng Part B J Eng Manuf 221:221–229
223. Singh R, Khamba JS (2007) Taguchi technique for modeling material removal rate in ultrasonic machining of titanium. Mater Sci Eng A 460–461:365–369
224. Singh R, Khamba JS (2006) Ultrasonic machining of titanium and its alloys: a review. J Mater Process Technol 173(2):125–135
225. Sonmez AI, Baykasoglu A, Dereli T, Filiz IH (1999) Dynamic optimization of multi-pass milling operations via geometric programming. Int J Mach Tools Manuf 39(2):297
226. Spedding TA, Wang ZQ (1997) Parametric optimization and surface characterization of wire electrical discharge machining process. Precis Eng 20(1):5–15
227. Spur G, Schönbeck J (1993) Anode erosion in wire-EDM-a theoretical model. CIRP Ann Manuf Technol 42(1):253–256
228. Sreeram S, Kumar AS, Rahman M, Zaman MT (2006) Optimization of cutting parameters in micro-end milling operations under dry cutting conditions using genetic algorithms. Int J Adv Manuf Technol 30:1030–1039
229. Srinivasu DS, Axinte DA, Shipway PH, Folkes J (2009) Influence of kinematic operating parameters on kerf geometry in abrasive waterjet machining of silicon carbide ceramics. Int J Mach Tools Manuf 49(14):1077–1088
230. Srinivasu DS, Babu NR (2008) A neuro-genetic approach for selection of process parameters in abrasive waterjet cutting considering variation in diameter of focusing nozzle. Appl Soft Comput 8(1):809–819
231. Tam SC, Lim LEN, Quek KY (1992) Application of Taguchi method in the optimization of the laser-cutting process. J Mater Process Technol 29:63–74
232. Tam SC, Yeo CY, Jana S, Lau WS, Lim EN, Yang LJ (1993) Optimization of laser deep-hole drilling of Inconel 718 using the Taguchi method. J Mater Process Technol 37:741–757
233. Tarng YS, Ma SC, Chung LK (1995) Determination of optimal cutting parameters in wire electrical discharge machining. Int J Mach Tools Manuf 35(12):1693–1701
234. Tolouei-Rad M, Bidhendi IM (1996) On the optimization of machining parameters for milling operations. Int J Mach Tools Manuf 37:1–16
235. Tosun N, Cogun C, Inan A (2003) The effect of cutting parameters on work piece surface roughness in wire EDM. Mach Sci Technol 7(2):209–219
236. Tosun N, Cogun C, Tosun GA (2004) Study on kerf and material removal rate in wire electrical discharge machining based on Taguchi method. J Mater Process Technol 152:316–322
237. Trueman CS, Huddleston J (2000) Material removal by spalling during EDM of ceramics. J Eu Ceram Soc 20:1629–1635
238. Tsai MJ, Li CH, Chen CC (2008) Optimal laser-cutting parameters for QFN packages by utilizing artificial neural networks and genetic algorithm. J Mater Process Technol 208(1–3):270–283
239. Uhlmann E, Schauer K (2005) Dynamic load and strain analysis for the optimization of micro-end mills. CIRP Ann Manuf Technol 54(1):75–78
240. Vikram G, Babu NR (2002) Modeling and analysis of abrasive water jet cut surface topography. Int J Mach Tools Manuf 42(12):1345–1354
241. Vogler MP, Devor RE, Kapoor SG (2004) Microstructure-level force prediction model for micro-milling of multi- phase materials. J Manuf Sci Eng 125:202–209
242. Wang J (2007) Predictive depth of jet penetration models for abrasive waterjet cutting of alumina ceramics. Int J Mech Sci 49(3):306–316
243. Wang J, Guo DM (2002) A predictive depth of penetration model for abrasive waterjet cutting of polymer matrix composites. J Mater Process Technol 121(2–3):390–394

244. Wang ZY, Rajurkar KP (1996) Dynamic analysis of the ultrasonic machining process. J Manuf Sci Eng 118:376–381
245. Wang R, Wang M (2010) A two-fluid model of abrasive waterjet. J Mater Process Technol 210(1):190–196
246. Wang WM, Rajurkar KP (1992) Modeling and adaptive control of EDM systems. J Manuf Sys 11(5):334–335
247. Wiercigroch M, Neilson RD, Player MA (1999) Material removal rate prediction for ultrasonic drilling of hard materials using an impact oscillator approach. Phys Lett A 259(2):91–96
248. Wissmiller DL, Pfefferkorn FE (2009) Micro-end mill tool temperature measurement and prediction. J Manuf Process 11(1):45–53
249. Wüthrich R, Fascio V (2005) Machining of non-conducting materials using electrochemical discharge phenomenon—an overview. Int J Mach Tools Manuf 45(9):1095–1108
250. Ya G, Qin HW, Yang SC, Xu YW (2002) Analysis of the rotary ultrasonic machining mechanism. J Mater Process Technol 129(1–3):182–185
251. Yellowley I, Gunn EA (1989) The optimal subdivision of cut in multi-pass machining operations. Int J Prod Res 27:1573
252. Yeo CY, Tam SC, Jana S, Lau MWS (1994) A technical review of the laser drilling of aerospace materials. J Mater Process Technol 42(1):15–49
253. Yilbas BS, Yilbas Z (1987) Parameters affecting hole geometry in laser drilling of Nimonic 75. SPIE 744:87–91
254. Yilbas BS (1988) Investigation into drilling speed during laser drilling of metals. Opt Laser Technol 20(1):29–32
255. Yilbas BS (1997) Parametric study to improve laser hole drilling process. J Mater Process Technol 70:264–273
256. Yilbas BS (2004) Laser cutting quality assessment and thermal efficiency analysis. J Mater Process Technol 155–156:2106–2115
257. Yousef BF, Knopf GK, Bordatchev EV, Nikumb SK (2003) Neural network modeling and analysis of the material removal process during laser machining. Int J Adv Manuf Technol 22(1–2):41–53
258. Yu ZY, Rajurkar KP, Shen H (2002) High aspect ratio and complex shaped blind micro-holes by micro-EDM. CIRP Ann Manuf Technol 51(1):359–362
259. Yuan J, Wang K, Yu T, Fang M (2008) Reliable multi-objective optimization of high-speed WEDM process based on Gaussian process regression. Int J Mach Tools Manuf 48(1):47–60
260. Zaki M, Corre C, Kuszla P, Chinesta F (2008) Numerical simulation of the abrasive waterjet (AWJ) machining: multi-fluid solver validation and material removal model presentation. Int J Mater Forming 1(1):1403–1406
261. Zaman MT, Kumar AS, Rahman MS, Sreeram A (2006) Three dimensional analytical cutting force model for micro-end milling operation. Int J Mach Tools Manuf 46(3–4):353–366
262. Zheng ZP, Lin JK, Huang FY, Yan BW (2008) Improving the machining efficiency in electrochemical discharge machining (ECDM) microhole drilling by offset pulse voltage. J Micromech Microeng 18:24–36
263. Zhu K, Wong YS, Hong GS (2009) Multi-category micro-milling tool wear monitoring with continuous hidden Markov models. Mech Syts Signal Proc 23(2):547–560
264. Zuperl U, Cus F (2003) Optimization of cutting conditions during cutting by using neural networks. Rob Comput Integr Manuf 19:189

Chapter 4
Modeling and Optimization of Nano-finishing Processes

4.1 Introduction

Finishing operations represent a critical and expensive phase of overall production processes. The most labor intensive, uncontrollable area in the manufacturing of precision parts involves final finishing operations, which frequently demand as much as 15% of the total manufacturing cost. The dimensional and alignment accuracy and quality of surface finish are taken care of by finishing processes such as grinding, lapping, honing, and super-finishing (i.e. traditional methods of finishing). But, the applications of these traditional abrasive finishing processes are limited to the production of work pieces of basic forms such as flat, cylindrical, etc. These finishing processes are being pushed to their limits of performance especially in components of hard materials and complicated shapes. The need to develop finishing processes with wider bounds of application areas, better quality performance, higher productivity, and automatic operation has led to the development of nano-finishing processes.

Majority of the nano-finishing processes are loose flowing abrasive-based processes in which abrasive orientation and its geometry at the time of interaction with the work piece is not fixed. There are some nano-finishing processes, which do not come under the abrasive-based category, for example, laser beam machining, electron beam machining, ion beam machining, and proton beam machining. The abrasive-based nano-finishing processes include abrasive flow machining (AFM), magnetic abrasive finishing (MAF), magnetorheological finishing (MRF), magnetorheological abrasive flow finishing (MRAFF), elastic emission machining (EEM), magnetic float polishing (MFP), etc. EEM results in surface finish of the order of sub-nanometer level using the nanometer size abrasive particles with the precisely controlled forces. Except AFM and EEM, all other processes use a medium whose properties can be controlled externally with the help of magnetic field. This permits to control the forces acting on an abrasive particle; hence, the amount of material removed is also controlled. This class of processes is capable to

R. V. Rao, *Advanced Modeling and Optimization of Manufacturing Processes*, Springer Series in Advanced Manufacturing, DOI: 10.1007/978-0-85729-015-1_4,

produce surface roughness value of 8 nm or lower. Using better force control and still finer abrasive particles, some of these processes may result in the sub-nanometer surface roughness value on the finished part. This chapter presents AFM, MAF, MRAFF, and electrolytic in-process dressing (ELID) processes and their modeling and optimization aspects.

4.2 Abrasive Flow Machining Process

AFM, also called abrasive flow finishing (AFF), is an advanced finishing process that can be used to deburr, radius, polish, remove recast layer, and produce compressive residual stresses [22]. This process was developed by the Extrude Hone Corporation, USA in 1960s as a method to deburr and polish difficult-to-reach surfaces and edges by flowing abrasive laden polymer with special rheological properties. Figure 4.1 shows the schematic diagram of AFM process.

AFM process removes small quantity of material by flowing a semisolid abrasive-laden compound called 'media' (abrasive particles uniformly suspended in viscous chemical compound) through or across the surfaces of the work piece to be finished. Two vertically opposed cylinders extrude media back and forth through passages formed by the work piece and tooling. The machining action compares to a grinding or lapping operation as the media gently and uniformly abrades the surfaces and/or edges. The media acts as a 'self deformable stone' having

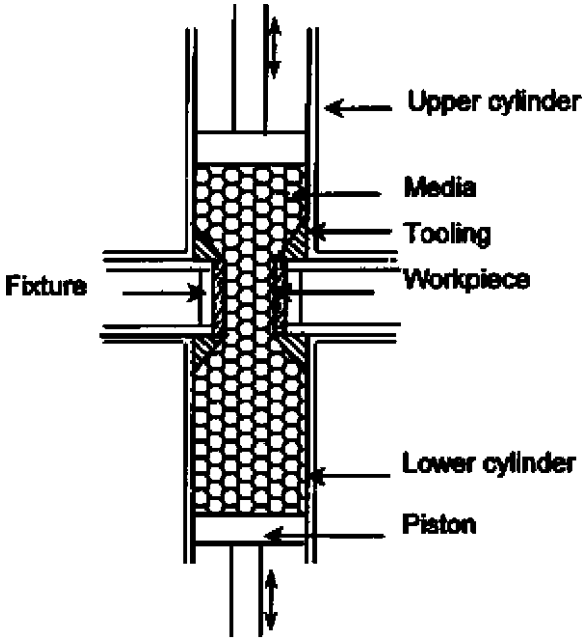

Fig. 4.1 Schematic diagram of AFM process (from [25]; reprinted with permission from Elsevier)

protruding abrasive particles acting as cutting tools. The media is composed of semisolid carrier (e.g. polyborosilixane) and abrasive grains. The abrasive action during AFM depends on the extrusion pressure, flow volume, and media flow speed determined by the machine setting in relation to media type, passage area and media formulation, which includes media viscosity, and abrasive type and size.

AFM process is gaining widespread attention due to its ability to produce consistent and predictable results. Removing stress raisers at sharp corners by producing controlled radii on edges can substantially improve thermal and mechanical fatigue strength of highly stressed components. Additional benefits over traditional finishing processes include substantial time saving and better control with regard to the accuracy and squareness of the bearing surfaces. The process can deburr holes as small as 0.2 mm and radius edges from 0.025–1.5 mm. Tolerances can be held to ±5 μm [59, 60].

The unique features of AFM such as versatility, efficiency, and economy make the process useful to perform a wide range of precision machining operations in the aerospace and automobile industries, manufacture of dies, and medical instruments. Some of the components machined by AFM include fuel injector nozzles, turbine blades, combustion liners, dies, etc. Materials from soft aluminum to tough nickel alloys, ceramics and carbides had been successfully micro-machined with this process. The process can simultaneously process multiple parts or many areas of a single work piece. Inaccessible areas and complex internal passages can be finished economically and effectively. Automatic AFM systems are capable of handling thousands of parts per day, greatly reducing labor costs by eliminating tedious handwork.

AFM process, however, is still in its early stages of development and extensive research efforts are continuing globally to fully understand its process mechanism and optimization. Much information is not available in the literature, which deals with modeling and optimization of the process. The relationship between process parameters and performance characteristics are not known completely. The abrasion ability of abrasive media is governed by many factors, especially by grain size, abrasive concentration, extrusion pressure, and hardness of work piece material. In order to analyze the influence of such parameters and other AFM conditions upon material removal and surface roughness of the machined surface, experimental investigations had been carried out by many researchers [23, 59, 76]. A stochastic modeling and analysis technique called data dependent system (DDS) was used by Williams and Rajurkar [76] to study the surface roughness profiles before and after AFM. Rajeshwar et al. [56] presented a simulation model to determine the characteristics of media flow during machining. The finite difference method was chosen for obtaining the solution. Williams [75] used acoustic emission signals to analyze the mechanism of surface generation in AFM and compared them to the acoustic emission signals of grinding process. Jain and Adsul [23] presented the effects of various parameters on material removal and surface roughness in terms of polynomial equations. Although these investigations are excellent, they seem to be rather lacking in theoretical treatment. Both

theoretical and empirical studies of abrasive flow machining are greatly hampered by the inherent random nature and multiplicity of parameters.

Jain et al. [29] used the experimental data and developed a back propagation neural network for modeling of AFM process. The three layer back propagation with four inputs, two outputs, and nine hidden nodes was employed for neural network. The network was trained using 35 samples that span the allowable ranges of input parameters. The inputs were media flow speed (v), percentage concentration of the abrasives (c), abrasive mesh size (d), and number of cycles (n), and outputs were material removal rate (MRR) and surface roughness (R_a). Random generator was used to initialize the values of the learning parameter. In order to decide the structure of neural network, the rate of error convergence was checked by changing the number of hidden layers and by adjusting the learning rate and momentum rate. As a result, a neural network with nine neurons in the hidden layer was adopted for storing knowledge in the form of weights between neurons. Simulation results showed a good agreement with experimental results for a wide range of machining conditions. Based on these results, the possibility of using the neural network model for surface quality and material removal rate prediction for AFM process was confirmed. This model could be used to study the AFM process by examining the effect of the input process parameters on the performance of AFM process.

In addition, [29] developed the following equations for the predictions of MRR and R_a using multiple regression analysis.

$$\text{MRR} = 5.285 \times 10^{-10} v^{1.6469} c^{3.0776} d^{-0.9371} n^{-0.1893} \tag{4.1}$$

$$R_a = 282,751.0\, v^{-1.8221} c^{-1.3222} d^{0.1368} n^{-0.2258} \tag{4.2}$$

Results of these empirical models agree with experimental results and neural network results of the authors. Unit of MRR used in regression analysis was grams per minute and derived empirical relation also gives MRR in same units. Use of volumetric units would have been more appropriate to as it eliminates dependence on material density.

Jain and Jain [24] described the analysis and simulation of the profile of finished surface and material removal by the interaction of abrasive grains with the work piece. Material removal in AFM process was simulated by successive abrasive grains grooving in the work piece. The height of the profile at that location was then modified to correspond to this interaction. The profile of the work surface as each active grain slides over it was modified by transforming the coordinates of the interfering profile of individual active grain to the work piece, based on geometrical considerations alone. The successive new heights of the work profile from the tip of the grain were then calculated, thus generating new work surface profiles. After each grooving event, the groove width and volume of material removal were calculated and stored. A simulated machined surface and volume of material removed were obtained after all the active grains present in the media participated during each AFM stroke. This process of simulation starting

from generation of random numbers to modification of work piece surface profile was continued until the required number of cycles of AFM process was completed. For studying the characteristics of the machined surface, a projected profile length of 12 mm was considered at a resolution of 1 μm. The numerical values of conditions used in the simulation are given below:

- Work piece material: mild steel (0.25%C)
- Hardness of work piece material: 2,177.80 N/mm^2
- Abrasive used: silicon carbide
- Mesh size of abrasives: 50–60
- Length of work piece: 38.5 mm
- Diameter of media cylinder: 87.5 mm
- Stroke length: 80 mm
- Density of sic abrasives: 3,220 kg/m$^{3.}$
- Initial surface roughness of work piece: 2.25 μm

To compare the results predicted from simulation, Jain and Jain [24] carried out the experiments and used response surface methodology (RSM) to develop multiple regression models for MRR and change in surface roughness ΔR_a. The effects of various parameters mainly, media pressure (x_1), number of cycles (x_2), reduction ratio (x_3), and percentage concentration of abrasives (x_4), on AFM performance were studied. The following second order response surface equations were obtained to predict MRR and change in surface roughness ΔR_a.

$$\begin{aligned}\text{MRR} = {} & 21.714 + 4.358x_1 + 5.350x_2 + 6.658x_3 + 4.025x_4 - 0.703\text{x}_1^2 \\ & - 0.928x_2^2 + 1.808x_3^2 + 0.158x_4^2 + 0.262\text{x}_1x_2 + 0.487x_1x_3 \\ & + 0.862x_1x_4 + 0.900x_2x_3 + 0.375x_2x_4 + 2.750x_3x_4 \end{aligned} \tag{4.3}$$

$$\begin{aligned}\Delta R_a = {} & 0.617 + 0.101x_1 + 0.119x_2 + 0.107x_3 + 0.067x_4 - 0.009x_1^2 \\ & - 0.006x_2^2 + 0.029x_3^2 + 0.006x_4^2 + 0.023x_1x_2 - 0.0006x_1x_3 \\ & + 0.0018x_1x_4 + 0.0068x_2x_3 + 0.0093x_2x_4 - 0.0118x_3x_4 \end{aligned} \tag{4.4}$$

The results of the simulation and RSM were in good agreement, which justified the use of this approach for simulating the surface obtainable in AFM. The simulation enabled the prediction of surface roughness and material removal with reference to percentage concentration and mesh size of abrasives, extrusion pressure, number of cycles, and reduction ratio. It was reported that MRR and ΔR_a increase with extrusion pressure, number of cycles, reduction ratio, and percentage concentration.

Jain et al. [30] developed a model for the flow of AFM media through cylindrical work piece and solved the same using finite element method (FEM). The model was shown to predict the radial stresses at the work piece surface with reasonable accuracy. The normal stress, so obtained from the flow model, was used for the estimation of MRR and surface roughness according to the following analytical models.

$$\text{Total volume removed in } N_c \text{ number of cycles} = n_s A_g \sum_{i=1}^{2N_c} L_i \tag{4.5}$$

$$\text{Surface roughness after } i^{\text{th}}\text{stroke } \left(R_a^i\right) = R_a^{i-1} - NL_s R_{pmc}^2 A_g / 7R_w^2 \tag{4.6}$$

where

$$n_s = 2\pi NL_s R_{pmc}^2 / R_w \tag{4.7}$$

$$L_i = \left[1 - \left(R_a^i / R_a^0\right)\right] L_w \tag{4.8}$$

$$A_g = \left[\left(d_m^2/4\right)\sin^{-1}(2a/d_m) - a(0.5d_m - h)\right] \tag{4.9}$$

$$a = (h(d_m - h))^{1/2} \tag{4.10}$$

A_g is the cross-sectional area of the groove generated by a spherical abrasive grain (mm^2), d_m the mean or average diameter of abrasive particles (mm), h is depth of indentation or penetration depth (mm), L_i the actual contact length between work piece and abrasive particles during ith stroke (mm), L_s the stroke length of piston in medium-containing cylinder in AFM process (mm), L_w the length of work piece (mm), N the number of abrasive grains acting per unit area of contact of AFM medium and cylinder, n_s total number of abrasive grains indenting the work piece surface per stroke, R_a^0 the initial surface roughness value (μm), R_a^i the surface roughness value after the ith stroke (μm), R_{pmc} radius of medium-containing cylinder in AFM process (mm), and R_w radius of work piece (mm).

However, the above Eqs. 4.5–4.10 are applicable only to axi-symmetric components as media flow was assumed to be axi-symmetric. The authors did not make a mention about the manner of computation of N. Furthermore, the analysis is computationally extensive, as radial stress has to be calculated using finite element method.

Jain and Adsul [23] studied the effects of different process parameters, such as number of cycles, concentration of abrasive, abrasive mesh size, and media flow speed, on material removal and surface finish. The dominant process parameter found was concentration of abrasive, followed by abrasive mesh size, number of cycles, and media flow speed. Experiments were performed with brass and aluminum as work materials. The experiments were planned with different number of cycles (0, 20, 40, 60, 80, and 100), concentration of abrasive in the media by weight (50, 60, 70, and 80%), mesh size (100, 150, 180, and 240), and media flow speed (406, 515, 652, and 812 mm/min).

The mathematical modeling of the AFM process was done using a multivariable curve fitting technique. The regression equations for MRR and change in surface roughness ΔR_a are given below.

For brass,

$$\text{MRR} = 0.0164 x_1^{0.7613} x_2^{2.0824} x_3^{-1.1028} x_4^{0.0372} \tag{4.11}$$

$$\Delta R_a = 9.98 \times 10^{-7} x_1^{0.6109} x_2^{1.6698} x_3^{-0.4987} x_4^{1.0080} \tag{4.12}$$

For aluminium,

$$\text{MRR} = 0.00032 x_1^{0.7886} x_2^{2.3122} x_3^{-1.0825} x_4^{0.5060} \tag{4.13}$$

$$\Delta R_a = 0.00116 x_1^{0.5570} x_2^{0.9509} x_3^{-0.5885} x_4^{0.4320} \tag{4.14}$$

For brass, the dominating process parameter was abrasive concentration (x_2), followed by abrasive mesh size (x_3), number of cycles (x_1), and media flow speed (x_4). The exponent for abrasive mesh size was negative which means that as the abrasive mesh size increases, MRR and ΔR_a decrease. However, for aluminum, the order of dominance of various parameters was different from that for brass. The reasons for this behavior could not be found. Also, the approach seems to be rather lacking in theoretical treatment.

Jain and Jain [25] presented the use of neural network for modeling and optimal selection of input parameters of AFM process. First, a generalized back-propagation neural network with four inputs, two outputs, and one hidden layer was used to establish the process model. The inputs were media flow speed (v) (cm/min), percentage concentration of the abrasives (c), abrasive mesh size (d), and number of cycles (n), and outputs were material removal rate (MRR), and surface roughness (R_a). A second network, which parallelizes the augmented Lagrange multiplier (ALM) algorithm, determined the corresponding optimal machining parameters by minimizing a performance index subjected to appropriate operating constraints. Simulation results confirmed the feasibility of this approach, and showed a good agreement with experimental results for a wide range of machining conditions. To validate the optimization results of the neural network approach, optimization of the AFM process was carried out using genetic algorithm. The equations used for optimization of MRR and R_a are shown below.

$$\text{MRR} = 5.285 \times 10^{-7} v^{1.6469} c^{3.0776} d^{-0.9371} n^{-0.1893} (\text{mg/min}) \tag{4.15}$$

$$R_a = 282,751.0\, v^{-1.8221} c^{-1.3222} d^{0.1368} n^{-0.2258} (\mu\text{m}) \tag{4.16}$$

In order to use genetic algorithm (GA), the constrained optimization problem was stated as follows,

$$\text{Maximize, MRR} \tag{4.17}$$

$$\text{subject to: } R_a \le R_{amax} \tag{4.18}$$

$$x_i^l \le x_i \le x_i^u \tag{4.19}$$

where x_i^l and x_i^u are the lower and upper bounds on process parameters x_i. Based on the experimental setup and work piece used, the limits on the input parameters were kept as $40 \le v \le 85$, $33 \le c \le 45$, $100 \le d \le 240$, $20 \le n \le 1{,}205$. The following parameters were chosen for GA: population size 50, maximum number

of generations 200, total string length 40, crossover probability 0.8, and mutation probability 0.01. The results obtained by neural network approach and GA were very close. It indicates that the neural network proposed by Jain and Jain [25] possessed sufficient knowledge to perform optimization.

Jain and Jain [26] proposed a model for the determination of specific energy and tangential forces in AFM process. It accounted for the process parameters of AFM, e.g. grain size, applied pressure, hardness of work piece material, number of cycles, and number of active grains. Heat transfer in AFM was also analyzed considering heat flow to the work piece and medium and theoretical results were compared with experimentally observed values of work piece temperatures. The dependence of the work piece temperature on the AFM parameters was also discussed. The model also predicts the fraction of heat entering into the work piece and medium. However, this model had not analyzed AFM process as a two-dimensional or three-dimensional unsteady state heat transfer problem to give more realistic temperature change in AFM process.

Singh and Shan [65] applied a magnetic field around the component being machined by AFM process to enhance the MRR. Gorana et al. [17] described a suitable two-component disc dynamometer for measuring axial and radial force components during AFM process. The influence of three controllable parameters (i.e. extrusion pressure, abrasive concentration, and grain size) on the responses (i.e. material removal, reduction in surface roughness, cutting forces, and active grain density) were studied. The preliminary experiments were conducted to select the ranges of parameters using single-factor experimental technique. Five levels for abrasive concentration (40, 45, 50, 55 and 60%) and for extrusion pressure (4, 5, 6, 7 and 8 MPa), and six levels for abrasive grain size (80, 120, 180, 220, 400, and 600 mesh) were used. A statistical 2^3 full factorial experimental technique was used to find out the main effect, interaction effect and contribution of each parameter to the machined work piece surface roughness. It was concluded that extrusion pressure, abrasive concentration, and grain size affect the cutting forces, active grain density, and finally reduction in surface roughness. The reduction in surface roughness was approximately linearly proportional to force ratio. Scanning electron microscopy showed that rubbing and ploughing were the possible mechanisms of material deformation.

Jain and Jain [27] developed a stochastic simulation model to determine the active grain density on the media surface, which was in contact with the work surface and correlated to experimental observations determined by a microscopic method. The simulation enabled prediction of the active grain density at any concentration and mesh size. The proposed stochastic simulation can be easily extended for simulation of surface generation in abrasive flow machining.

Gorana et al. [18] conducted scratching experiments to study the material removal mechanism in AFM process and developed theoretical expressions to calculate radial and axial forces acting on a single abrasive grain. They also measured these forces and active grain density experimentally. The conclusions arrived by the analysis about the presence of rubbing and ploughing was in agreement with the experimental AFM and scratching results. In another work [19],

the authors had proposed an analytical model to simulate and predict the surface roughness for different machining conditions in abrasive flow machining (AFM). The kinematic analysis was used to model the interaction between grain and work piece. Fundamental AFM parameters, such as the grain size, grain concentration, active grain density, grain spacing, forces on the grain, initial topography, and initial surface finish of the work piece were used to describe the grain–work piece interaction. The AFM process was studied under a systematic variation of grain size, grain concentration, and extrusion pressure with initial surface finish of the work piece. Simulation results showed consistency with the experimental results. It was concluded that active grain density during the AFM process increases with an increase in extrusion pressure and abrasive concentration in the medium, and this results in an increase in reduction in surface roughness value.

Centrifugal force assisted abrasive flow machining (CFAAFM) process was recently tried as a hybrid machining process with the aim towards the performance improvement of AFM process by applying centrifugal force on the abrasive laden media with a rotating centrifugal force generating rod introduced in the work piece passage. Walia et al. [71] explored the application of centrifugal force for the productivity enhancement of the process. The authors had reported that centrifugal force enhances the material removal rate and improves the scatter of surface roughness value in AFM. Cylindrical work pieces of brass were used for the experiment. During the experiments, parameters such as rotational speed of rectangular rod, extrusion pressure, and grit size were varied to explore their effects on material removal and scatter of surface roughness. Taguchi's parameter design strategy was applied to investigate the effect of process parameters on the material removal and scatter of surface roughness values. In another work [72], the authors had used an approach based on utility theory and Taguchi quality loss function for simultaneous optimization of more than one response characteristics. Three potential response parameters i.e. material removal, percent improvement of surface finish, and scatter of surface roughness over the fine-finished surface of a sleeve type work piece of brass were examined. Utility values based upon these response parameters were analyzed for optimization using Taguchi approach.

Ali-Tavoli et al. [1] proposed an approach using group method of data handling (GMDH)-type neural networks and genetic algorithms for modeling the effects of number of cycles and abrasive concentration on both material removal rate and surface roughness, using some experimentally obtained training and testing data for brass and aluminum in AFM process. Genetic algorithms were successfully used both for optimal design of generalized GMDH-type neural networks models of abrasive flow machining and for multi-objective Pareto based optimization of such processes. However, the approach had not considered other important process input parameters such as media flow speed, abrasive mesh size, etc. Furthermore, the approach is computationally more complex.

Wani et al. [74] proposed magnetic abrasive flow-finishing (MAFF) process combining the features of abrasive flow machining and magnetic abrasive finishing. MAFF provides a high level of surface finish and close tolerances for wide

range of industrial application. The authors focused on the modeling and simulation for the prediction of surface roughness on the work piece surface finished by MAFF process. A finite element model was developed to find the magnetic potential distribution in the magnetic abrasive brush formed during finishing action, and then it was used to evaluate machining pressure, surface finish, and material removal.

Jain et al. [28] derived the following equation to evaluate final surface roughness value after N_s number of strokes

$$(R_a)_{N_s} = R_a^0\left[1 - 226,814\left\{\left(K_{afm}/H_w R_a^0\right)(P_h/d)\left(\left(1+\eta_a(A_{pmc}L_s/A_w)cdN_s\right)^{1/2}-1\right)\right\}^2\right]^2 \tag{4.20}$$

where R_a^0 is initial surface roughness, H_w is Brinell hardness of work piece, P_h is extrusion pressure, A_{pmc} is cross-sectional area of piston of medium-containing cylinder, L_s is stroke length of piston, A_w is cross-sectional area of work piece, η_a is proportion of abrasives effectively participating in machining, c is volumetric concentration of abrasive particles, and d is mesh size. K_{afm} is a proportionality constant relating normal radial stress acting on the abrasive grain, $\sigma_r = K_{afm}P_h$. The following optimization model was formulated for AFM process based on the developed surface roughness model.

$$\text{Minimize, } (R_a)_{N_s} \tag{4.21}$$

Subject to: $1 - 226,814$

$$\times\left\{\left(K_{afm}/H_w R_a^0\right)(P_h/d)\left(\left(1+\eta_a(A_{pmc}L_s/A_w)cdN_s\right)^{1/2}-1\right)\right\}^2 \geq 0 \tag{4.22}$$

Equation 4.22 is a surface finish improvement constraint to ensure that the final surface roughness value after AFM process is smaller than the initial surface roughness value. Four decision parameters were considered by Jain et al. [28] in the optimization, and these were concentration of abrasives by volume (c), abrasive mesh size (d), number of strokes (N_s), and extrusion pressure (P_h). The parameter bounds for these four decision parameters were as shown below, $0.05 \leq c \leq 0.5$, $8 \leq d \leq 1,000$, $1 \leq N_s \leq 100$, and $0.7 \leq P_h \leq 25$.Values of the constants were taken as, $A_{pmc} = 5,026.5$ mm^2, $A_w = 484$ mm^2, $L_s = 80$ mm, $H_w = 2,000$ MPa, $\eta_a = 0.2$, $K_{afm} = 0.4$, and $R_a^0 = 3.0$ μm.

Jain et al. [28] used a real-coded GA with the following parameters to solve the optimization problem: population size = 15, 20, and 25 times the number of decision parameters, number of generations = 100, crossover probability = 0.9, mutation probability = 1/Number of decision parameters, simulated binary crossover (SBX) parameter 'η_c' = 2 and 10, and parameter for polynomial mutation 'η_m' = 10 and 50.

Following optimum solution was obtained in the 10th run for population size = 80, SBX parameter 'η_c' = 10, and polynomial mutation parameter 'η_m' = 10.

$c = 0.196$ (i.e. 19.6%), $d = 851$, $P_h = 0.81$ N/mm^2, $N_s = 23.3$ (≈ 23), optimum value of final surface roughness = 0.1041 μm, and value of surface finish improvement constraint (given by equation 5.22) = 0.18628.

However, even though Jain et al. [28] claimed that the optimal value of final surface roughness was 0.1041 μm, it can be found that the final surface roughness value was actually 2.996 μm by substituting the values of c, d, N_s, and P_h in the objective function given by Eq. 4.22. Since the initial value of surface roughness given was $R_a^0 = 3.0$ μm, the calculated value of 2.999 μm indicates that there was negligible improvement in the solution. Also, the value of surface finish improvement constraint (given by Eq. 4.22) was 0.999 (instead of 0.18628, as mentioned by Jain et al. [28]).

Rao et al. [58] proposed the application of PSO and SA algorithms to the optimization model proposed by Jain et al. [28] to find out if any improvement in the solution was possible. The following parameters were selected after various trials for PSO and SA algorithms:

- For PSO, maximum number of iterations = 40, inertia weight factor (w) = 0.65, and acceleration coefficients, $c_1 = 1.65$ and $c_2 = 1.75$, number of particles in swarm = 3
- For SA, maximum number of iterations = 250, initial temperature = 100, and temperature decrement factor = 0.1

Rao and Pawar [57] proposed the application of ABC algorithm and the following parameters were selected after various trials for ABC:

- Number of employed bees = 5, number of onlookers bees = 11, number of scout bees = 1, maximum number of iterations = 30.

The results obtained were proved to be better without violating the surface roughness constraint and only little iterations were required in ABC and PSO algorithms for convergence to the optimal solution. Table 4.1 shows comparison of the results of optimization using GA, PSO, SA, and ABC algorithms.

Table 4.1 Comparison of optimization results for AFM process

Reference	Technique	c	d	N_s	P_h	R_a	Constraint value
Jain et al. [28]	GA	0.196	851	23.3	0.81	0.1041[a]	0.18628[a]
	GA	0.196	851	23.3	0.81	2.996[b]	0.999[b]
Rao et al. [58]	PSO	0.32	1,000	73.10	15.96	0.000026	0.00293
Rao et al. [58]	SA	0.217	622.3	73.69	15.20	0.000105	0.00705
Rao and Pawar [57]	ABC	0.288	862.8	54.9	18.03	0.000013	0.002562

[a] Values wrongly calculated by Jain et al. [28]
[b] Corrected values

It is observed from the numerical results that very high surface finish of 0.000013 μm is achieved by selecting optimum parameters as provided by ABC without violating the surface roughness constraint. Although this value may not be practically attainable as we cannot machine the material below its atomic size, but it can be ensured that with the given set of parameters, maximum possible and attainable value of surface finish will be obtained, as the values of suggested optimum parameters lies within their specified bounds and also the set of optimum parameters satisfies the constraint on attainable of surface finish.

Mollah and Pratihar [49] determined the input–output relationships of AFM process using radial basis function networks (RBFNs). A batch mode of training was adopted to implement the principle of back-propagation (BP) algorithm (which works based on a steepest descent algorithm) and a genetic algorithm (GA), separately. The performances of RBFN tuned by a BP algorithm and that trained by a GA were compared on some test cases. The GA-optimized RBFN was found to perform slightly better than the BP-tuned RBFN. The back-propagation algorithm works on the principle of a steepest descent method, whose solutions have the chance of getting stuck at the local minima, whereas the probability of the GA solutions for being trapped at the local minima is less. However, their performances may depend on the nature of the deviation (error) function.

Abrasive particle movement pattern is an important factor in estimating the wear rate of materials, especially, as it is closely related to the burring, buffing, and polishing efficiency of the AFM process. There are generally two kinds of particle movement patterns in the AFM process, i.e. sliding–rubbing and rolling. In mechanism, AFM particle–work piece interaction is taking place in any one or a combination of the possible modes: elastic/plastic deformation by grooving particle movement; elastic/plastic deformation by rolling particle movement; chip formation (micro-cutting) by grooving particle movement, ridge formation by grooving and rolling particle movement, and low-cycle fatigue wear. Grooving particle movement pattern has a greater contribution to wear mass loss of work piece than rolling mode. Considering the machining efficiency of a machine part is predominantly dependent upon its wear mass loss speed, it can be concluded that particle movement patterns are key parameters to machining efficiency in AFM. Fang et al. [11] investigated ellipsoidal particles to understand particle movement patterns. An analytical model of ellipsoidal geometry to determine particle movement patterns in AFM was proposed with given particle ellipticity, normal load, particle size, and material hardness. From the analytical model and particle movement pattern criterion proposed by the authors, a statistic prediction of particle movement patterns was completed. It was found that a seat position of ellipsoid is an easy grooving position for a particle and a large ellipticity value predominantly increases grooving particle numbers. Kar et al. [36] attempted to develop a new media based on viscoelastic carrier and its characterization for fine finishing through AFM process. The silicone carbide of 80, 220, 400, 800, and 1,200 mesh size were used in the experimental work. The used rubbers (viscoelastic carriers) for this investigation were natural rubber grade RMA-4 and butyl rubber (IIR). The naphthenic oil was used as processing oil. The newly developed

media was again characterized through rheological properties. It was found that temperature, shear rate, creeping time, and frequency have impact on rheological properties, and the percentage ingredients of media govern trends of their relations.

Uhlmann et al. [69] modeled the AFM process of advanced ceramic materials using numerical simulation. A correlation between flow processes, surface formation, and edge rounding was developed. An insight into a process model was given, which was developed using modern simulation techniques. The objective of their approach was to predict results like surface quality and edge rounding on any user-defined geometry. Barletta [4] reviewed the use of abrasive fluidized bed equipment in a broad range of manufacturing processes. In particular, applications in deburring and finishing of complex-shaped metal components, super-finishing of dies for injection molding, cleaning and polishing of electronic devices, and surface preparation of tungsten carbide milling tools were reviewed. Attention was focused on the effects of the most important process parameters, such as machining time, abrasive type and mesh size, and flow or jet speed. The extent of material removal and the change in surface roughness as a function of the process parameters were addressed. Selected numerical and analytical models that are useful for automation and control purposes were discussed.

In order to enhance productivity of the AFM process, several modifications are being tried. Sankar et al. [61] introduced a concept of rotating the medium along its axis to achieve higher rate of finishing and material removal. This process was termed as drill bit-guided abrasive flow finishing (DBG-AFF) process. In order to provide random motion to the abrasives in the medium and cause frequent reshuffling of the medium, the medium was pushed through a helical fluted drill, which was placed in the finishing zone. The experiments were carried out to compare AFM and DBG-AFF processes with AISI 1040 and AISI 4340 as work piece materials. The performance of DBG-AFF compared to AFM is encouraging, specifically with reference to percentage change in average surface roughness ($\%\Delta R_a$) and amount of material removed. Modeling using non-linear multivariable regression analysis and artificial neural networks were carried out to conduct parametric analysis and understand, in depth, the DBG-AFF process. The simulation data of neural network showed good agreement with experimental results. In another work, Sankar et al. [62] studied the effects of different process parameters, such as extrusion pressure, number of cycles, viscosity of the medium on a change in average surface roughness (ΔR_a), and material removal, while machining a metal matrix composite (an aluminum alloy and its reinforcement with SiC). The work pieces were initially ground to a surface roughness value in the range of 0.6 ± 0.1 μm, and later were finished to the R_a value of 0.25 ± 0.05 μm using AFF process. The relationship between extrusion pressure and ΔR_a showed an optimum at about 6 MPa. In the same way, the relationship between weight percentage of processing oil (plasticizer) and ΔR_a also showed an optimum at 10 wt%. An increase in work piece hardness required more number of cycles to achieve the same level of improvement in ΔR_a. Material removal also increased with an increase in extrusion pressure and number of cycles, while it decreased with an increase in processing oil content in the medium. It was also

concluded that the mechanism of finishing and material removal in case of alloys is different from that in case of MMC.

Jain et al. [32] attempted to analyze the AFM process using finite element method (FEM) for finishing of external surfaces. Finite element model of forces acting on a single grain was developed to study the material removal mechanism of AFM. Response surface method (RSM) was used to carry out an experimental research to analyze the effect of extrusion pressure and number of cycles on material removal and surface finish. Results obtained from finite element analysis for material removal were compared with the experimental data obtained during AFM. It was concluded that the extrusion pressure affects the material removal significantly and the effect of number of cycles on material removal was higher in initial stage. For the same extrusion pressure and number of cycles, the increase in ΔR_a for conical surface was less compared to cylindrical surface.

Mali and Manna [47] used AFM to finish conventionally machined cylindrical surface of Al/15 wt% SiC_p–MMC work piece. The authors had presented the utilization of robust design-based Taguchi method for optimization of AFM parameters. The influences of AFM process parameters on surface finish and material removal were analyzed. Taguchi experimental design concept, L_{18} ($6^1 \times 3^7$) mixed orthogonal array was used to determine the *S*/*N* ratio and to optimize the AFM process parameters. The mathematical models for R_a, R_t, ΔR_a, and ΔR_t and MRR were established to investigate the influence of AFM parameters. Scanning electron micrographs testified the effectiveness of AFM process in fine finishing of Al/15 wt% SiC_p–MMC.

4.3 Magnetic Abrasive Finishing Process

Magnetic abrasive finishing (MAF) is one of the advanced finishing processes capable of producing excellent surface finish of the order of few nanometers on flat surfaces as well as internal and external surfaces of tube-type work pieces. The process can finish not only ferromagnetic materials such as steel but also the non-ferromagnetic materials such as stainless steel and brass. MAF process can be used for finishing, cleaning, deburring, and burnishing of metallic parts, as well as other advanced engineering material parts (e.g. parts made with silicon nitride, silicon carbide, aluminum oxide, etc.). The process is based on the electromagnetic behavior of the magnetic abrasive particles in the magnetic field. Figure 4.2 shows the schematic diagram of MAF process [33].

The work piece to be finished is located between two magnetic poles and gap between magnetic poles and work piece is filled with magnetic abrasive particles consisting of abrasive grains and ferromagnetic particles. Magnetic abrasive particles can be bonded type or unbonded type. Bonded magnetic abrasive particles are prepared by sintering of ferromagnetic particles and abrasives, whereas unbonded magnetic abrasive particles are a mechanical mixture of ferromagnetic particles and abrasives powder with a small amount of lubricant. The bonded type

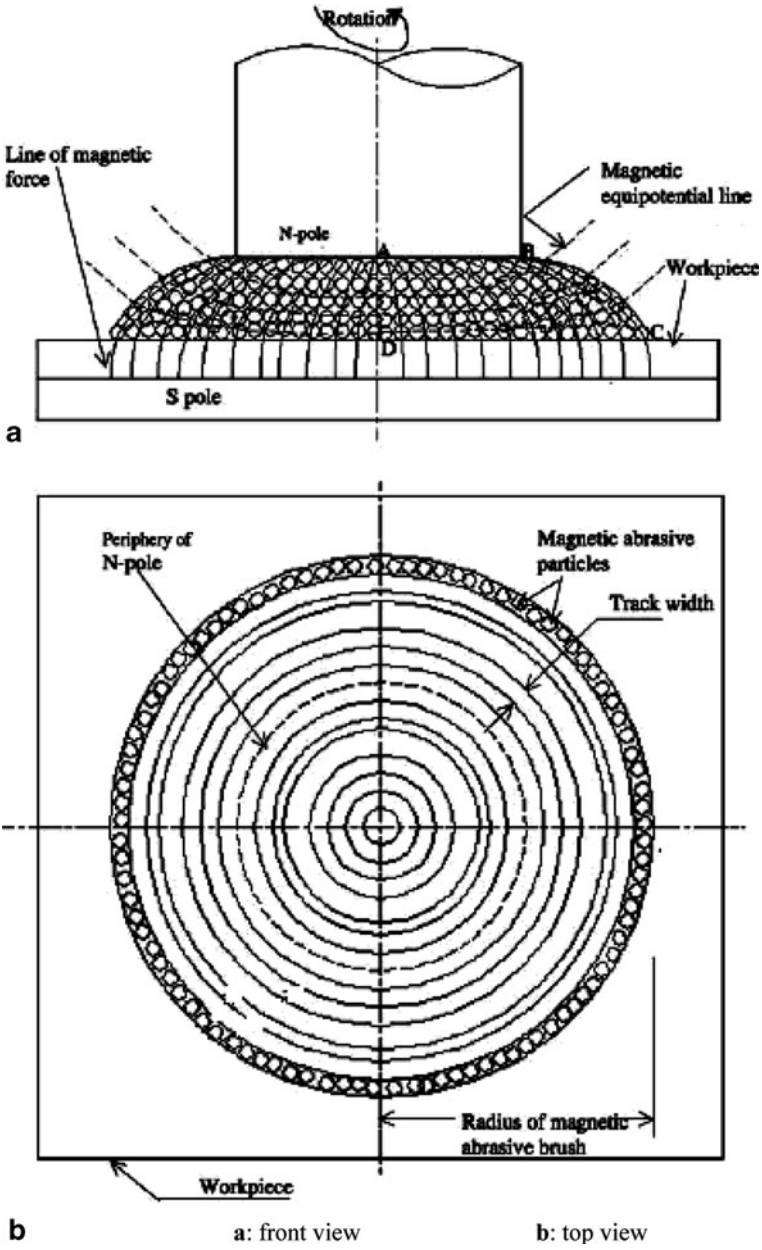

Fig. 4.2 Schematic of MAF process (from [33]; reprinted with permission from Springer Science + Business Media)

magnetic abrasive particles are mostly considered due to their excellent finishing effects. The magnetic abrasive particles join each other along the lines of magnetic force and form a magnetic abrasive flexible brush (MAFB) between the work piece and the magnetic pole. This brush behaves like a multi-point cutting tool for the finishing operation. When the magnetic N-pole is rotating, the MAFB also rotates like a flexible grinding wheel and finishing is done according to the forces acting on the abrasive particles [15, 33, 63, 77].

MAF process is gaining widespread attention due to its ability to produce consistent and predictable results. MAF process can be employed to produce optical, mechanical, and electronic components with micrometer or sub-micrometer form accuracy and surface roughness within nanometer range with hardly any surface defects. Finishing of bearings, precision automotive components, shafts, and artificial hip joints made of oxide ceramic and cobalt alloy are some of the example products for which this process can be applied. MAF process, however, is still in its early stages of development and extensive research efforts are continuing globally to fully understand its process mechanism and optimization. The following section describes the modeling and optimization aspects of the MAF process.

The main objectives of any finishing process are to (1) minimize the final surface roughness value and (2) minimize the size and shape inaccuracy. In MAF process, the important parameters influencing the surface quality are magnetic abrasive type and size, concentration of abrasives in ferromagnetic material, working gap between work piece and magnetic poles, magnetic flux density, relative motion between magnetic abrasive particles and work piece surface, amplitude and frequency of vibrations, axial movement or feed, finishing time, input current, and voltage applied to the electromagnet. To analyze the influence of these parameters on the surface roughness and material removal, many researchers carried out the experimental investigations.

Kremen et al. [42] developed a model to determine the time required to reduce the initial out-of-roundness by a specified amount. The hyperbolic relation between the normalized out-of-roundness error and finishing time was verified with this model. However, the proposed relation to estimate the finishing time was empirical. Kim and Choi [38] modeled and simulated the MAF process for finishing cylindrical work pieces. The surface roughness was predicted as a function of finishing time by a model that was derived from the removed volume of material. Kremen et al. [41] focused on the magnetic abrasive process as a sizing process and presented a theory, which explained the out-of-roundness error phenomenon based on force analysis of the material removal mechanism. Jain et al. [31] presented the effect of working gap (which is the space between the work piece and the electromagnets) and the circumferential speed on the performance of two important process parameters i.e. surface finish and MRR of the MAF process.

The effect of finishing time and the particle size on the MRR and surface finish in case of cylindrical magnetic abrasive finishing, using the unbonded magnetic abrasives, was presented by Chang et al. [8]. Experimental results indicated that steel grit is more suitable for MAF process because of its superior hardness and the polyhedron shape. Mori et al. [50] explained the formation of magnetic abrasive

brush from the viewpoint of brush forming energy. Polishing mechanism peculiar to this process was explained. Singh et al. [64] applied Taguchi's design of experiments to find out important parameters influencing the surface quality generated. Experimental results indicated that for a change in surface roughness, voltage and working gap were found to be the most significant parameters followed by grain mesh number and then rotational speed.

MAFF was tried as a hybrid machining process intended to provide high level of surface finish and close tolerance for wide range of industrial applications. Wani et al. [74] explored simulation method for prediction of surface roughness in MAFF process. Ko et al. [39] observed that the continuous flow of coolant and the Fe powder without abrasive was effective for deburring and surface quality.

Kim and Choi [38] developed a model for magnetic abrasive finishing of cylindrical surface using bonded magnetic abrasive particles. Predictions of the model developed by Kim and Choi [38] were in good agreement with the experimental results. Based on this model, Jain et al. [28] presented the details of parametric optimization of MAF process using a real coded genetic algorithm. The optimization model was formulated as shown below:

$$\text{Maximize } \Delta R_a = \left(9 \times 10^3 K_{maf} K_3^2 A_{air} l_M \mu_0 / 8\pi H_w L_w^2 \tan\theta\right)(V_t/d)(w_f I^2/(K_2 + w_f)) \tag{4.23}$$

where, ΔR_a is the difference between initial and final surface roughness value obtained by MAF, K_{maf} is the constant of proportionality and a function of a number of constants.

$$K_2 = 3(\mu_{rf} + 2)/\pi(\mu_{rf} - 1) \tag{4.24}$$

$$K_2 = n_c/(A_{air}(I_{air}/A_{air} + l_M/\mu_{em}A_M))(\text{per mm}) \tag{4.25}$$

n_c is the number of turns in magnetic coil, A_{air} the cross sectional area of air gap, l_{air} the length of air gap, μ_{em} the relative permeability of electromagnets, A_M the cross sectional area of magnet, l_M the length of the magnet, μ_{rf} the relative permeability of ferromagnetic material, θ the mean half asperity angle of abrasive cutting edges, H_w the Brinell hardness of work material, L_w the length of work piece to be machined, R_a^0 the initial surface roughness value, μ_0 the magnetic permeability in vacuum, d the mean diameter of the magnetic abrasive particles, v the relative velocity between magnetic abrasive particles and work piece, w_f the volume ratio of ferromagnetic material in the magnetic abrasive powder, I the input current, and t is the finishing time.

The constraint is on obtainable value of surface roughness, which is mathematically expressed as given below.

$$\begin{aligned} &1 - \left(358.1 K_{maf} K_3^2 A_{air} l_M \mu_0 / R_a^0 H_w L_w^2 \tan\theta\right)(V_t/d)\left(w_f I^2/(K_2 + w_f)\right) \\ &- \left(125/R_a^0 \tan\theta\right)\left(3K_3^2 \mu_0 / n_a H_w\right)^{1/2}\left(w_f I^2 d^2/(K_2 + w_f)\right)^{1/2} \geq 0.0 \end{aligned} \tag{4.26}$$

where n_a is the number of abrasives in magnetic abrasive particle.

This constraint conveys the meaning that for a given machining pressure, a critical value of surface roughness exists below which there is no further decrease in surface roughness (i.e. no further improvement in the surface finish). Smaller the positive fractional value of this constraint, smaller the value of the final surface roughness and higher the difference between the initial and final surface roughness values will be [28].

Five decision variables were considered by Jain et al. [28] in the optimization problem, and these include mean diameter of the magnetic abrasive particles (d), relative velocity between magnetic abrasive particles and work piece (v), volume ratio of ferromagnetic material in the magnetic abrasive powder (w), input current (I), and finishing time (t).

The parameter bounds for these five decision parameters were as shown as follows: $0.015 \leq d \leq 0.15$ (mm), $500 \leq v \leq 5{,}000$ (mm/s), $0.3 \leq w_f \leq 0.8$, $1 \leq I \leq 10$ (A), and $1 \leq t \leq 1{,}200$ (s).

Values of the constants were taken as $K_{maf} = 27.86 \times 10^{-6}$, $n_c = 2{,}000$, $A_{air} = 350$ mm^2, $l_{air} = 20$ mm, $\mu_{em} = 33$, $A_M = 1{,}225$ mm^2, $l_M = 665$ mm, $\mu_{rf} = 7{,}000$, $\theta = 70°$, $H_w = 5{,}500$ MPa, $L_w = 20$ mm, $R_a^0 = 0.27$ μm, $\mu_0 = 4\pi \times 10^{-7}$ H/m, and $n_a = 10$.

Jain et al. [28] used a real-coded genetic algorithm (GA) with the following parameters to solve the above optimization problem.

- Population size = 15, 20, and 25 times the number of decision parameters.
- Number of generations = 100.
- Crossover probability = 0.9.
- Mutation probability = 1/number of decision parameters.
- Simulated binary crossover (sbx) parameter 'η_c' = 2 and 10.
- Parameter for polynomial mutation 'η_m' = 10 and 50.

Following optimum solution was obtained in the tenth run for population size of 80, SBX parameter 'η_c'of 10, and polynomial mutation parameter 'η_m'of 10. $d = 0.015$ mm, $v = 852.6$ mm/s, $w_f = 0.446$ (44.6%), $I = 1.02$ A, $t = 5$ s, optimum value of the objective function i.e. difference between initial and final surface roughness values $\Delta R_a = 0.26873$ μm, final surface roughness value = 0.27−0.26873 = 0.00127 μm, and value of constraint on obtainable value of surface roughness = 0.0006 μm.

However, even though Jain et al. [28] claimed that the optimal values of ΔR_a and the constraint on obtainable surface finish were 0.26873 and 0.0006 μm, respectively, it can be found these values are actually 0.2739 and −0.0153 μm, respectively, by substituting the values of d, v, w_f, I, and t in the objective function given by Eqs. 5.23 and 5.26. Thus, the constraint was violated and the results presented by Jain et al. [28] are not valid.

Now, the PSO algorithm is applied to solve the above optimization problem. The optimum selection of operating parameters of the algorithm like acceleration constants 'c_1' and 'c_2' as well as inertia coefficient 'w' is very essential for convergence of the algorithm. To ensure the convergence of PSO algorithm,

the condition specified by Eq. 4.27 must be satisfied (Bergh and Engelbrecht [5]).

$$\max(|\lambda_1|, |\lambda_2|) < 1 \tag{4.27}$$

where λ_1 and λ_2 are the Eigen values given by Eqs. 5.28 and 5.29.

$$\lambda_1 = (1 + w - \phi_1 - \phi_2 + \gamma)/2 \tag{4.28}$$

$$\lambda_2 = (1 + w - \phi_1 - \phi_2 - \gamma)/2 \tag{4.29}$$

and

$$\gamma = \left[(1 + w - \phi_1 - \phi_2)^2 - 4w\right]^{1/2} \tag{4.30}$$

$\phi_1 = r_1 \times c_1$ and $\phi_2 = r_2 \times c_2$. Considering the feasible range for the value of '$\phi_1 + \phi_2$' as 0–4 and that for 'w' as 0–1, it can be observed that for convergent trajectories the relation given by Eq. 4.31 must be satisfied.

$$w > 0.5(\phi_1 + \phi_2) - 1 \tag{4.31}$$

Now, in the present study the values of $w = 0.65$, $c_1 = 1.65$, and $c_2 = 1.75$ are used. Considering the extreme possibility of random number as $r_1 = 0.95$ and $r_2 = 0.95$, the right hand term in Eq. 5.31 is $0.5 \times (0.95 \times 1.65 + 0.95 \times 1.75) - 1 = 0.61$, which is less than 0.65 thus satisfies the Eq. 4.31. Hence, the values of w, c_1, and c_2 selected in the present work are appropriate for convergence of the algorithm. Following optimum solution was obtained using the proposed PSO algorithm: $d = 0.015$ mm, $v = 2{,}458.7$ mm/s, $w_f = 0.3$ (30%), $I = 1.537$ A, $t = 1$ s, optimum value of the objective function $\Delta R_a = 0.2694$ μm, final surface roughness value $= 0.27 - 0.2694 = 0.0006$ μm, and value of constraint on obtainable value of surface roughness $= 0.00122$ μm. The results obtained showed that very high surface finish could be obtained using the set of optimum parameters suggested using PSO algorithm without violating the constraint on obtainable value of surface roughness. The initial surface finish of 0.27 μm is improved to 0.0006 μm in a very small finishing time.

The value of ΔR_a decreases with increase in the diameter of the magnetic abrasive particle, as it is a well-known fact that fine grains results into better surface finish. Therefore, the smallest possible value of diameter of magnetic abrasive particle will maximize 'ΔR_a' and hence the surfaces finish. Also, the constraint will be violated if higher value of diameter of magnetic abrasive particle is selected. Hence, the diameter of magnetic abrasive particle at the lower bound ($d = 0.015$ mm) is selected. As 'ΔR_a' and hence the surface finish increases with increase in the relative velocity 'v', selection of higher value of relative velocity 'v' is desirable. However, the value of relative velocity ($v = 2{,}458.7$ mm/s) is obtained, as at any value higher than this, the constraint on obtainable value of surface roughness is violated. ΔR_a increases with increase in the volume ratio of ferromagnetic material w_f. However, as the constraint on obtainable value of the

surface roughness is violated for any value of 'w_f' higher than 0.3, the value of 'w_f' at the lower bound ($w_f = 0.3$) is selected.

ΔR_a increases with increase in both the input current 'I' as well as finishing time 't'. However, selection of higher values of both these variables is restricted by the attainable value of surface roughness and hence the optimum value of input current (I) = 1.537 A and that of finishing time (t) = 1 s is selected.

Now, the same problem is attempted using the simulated annealing (SA) technique. The objective function considering maximization of the difference between the initial and final roughness value is written as:

$$\text{Min.}\, Z = -Z_1 - \text{Penalty} \times Z_2 \tag{4.32}$$

where, Z is the combined objective function, Z_1 the objective function given by Eq. 4.23, and Z_2 is the constraint given by Eq. 4.30.

In the objective function, penalty is defined in such a way that a point having higher value of 'Z_1' but with small negative value of 'Z_2' should be accepted at higher temperature to search another point in the vicinity. However, it should be ensured that such a point should never appear in the final solution. To take into account the constraint on obtainable value of surface roughness, the penalty is assigned as below.

$$\text{Penalty} = Z_{\min}/Z_{2\max} \tag{4.33}$$

where $Z_{\min}$ is the minimum value of combined objective function without considering penalty amd $Z_{2\max}$ is the maximum of negative values of power consumption constraint. In present case, penalty = 2, if $Z_2 < 0$; else penalty = 0.

The initial temperature is obtained by calculating the average of the function values at a boundary points as given by Eq. 4.34.

$$\text{Initial temperature } T_0 = \sum Z_{Nb}/n \tag{4.34}$$

where Z_{Nb} is the value of objective function at each boundary point and n is the number of boundary points. The initial temperature is calculated as 100 and the decrement factor is considered as 0.1. At any current point $X(t)$, the new value of the parameters for the successive iterations is calculated using the formula,

$$X(t+1) = X(t) + \sigma\left[\sum_{i=1}^{N} R_i - 0.5N\right] \tag{4.35}$$

where $\sigma = (X_{\max} - X_{\min})/6$; R is the random number, and N is the number of random numbers used. In the present work, six random numbers are used. While starting the process, the initial values for the parameters are taken as the average of the respective parameter limits. The algorithm is terminated when a sufficiently small temperature is obtained or a small enough change in function value is found.

Application of SA algorithm to solve the above optimization problem leads to the following optimum solution: $d = 0.0336$ mm, $v = 500$ mm/s, $w_f = 0.568$ (56.8%), $I = 4.07$ A, $t = 1$ s, optimum value of the objective function $\Delta R_a = 0.26758$ μm, final surface roughness value $= 0.27 - 0.26758 = 0.00242$ μm, and value of constraint on obtainable value of surface roughness $= 0.00154$ μm.

Table 4.2 presents the compiled results of optimization of MAF process parameters obtained using genetic algorithms [28], PSO, and SA algorithms. The results obtained using PSO algorithm are comparatively better and only few iterations are required in PSO algorithm for convergence to the optimal solution. The results of SA are better than the results of GA in this example.

El-Taweel [10] integrated the electrochemical turning (ECT) process and MAF to produce a combined process that improves the MRR and reduces surface roughness (SR). The study emphasized the features of the development of comprehensive mathematical models based on response surface methodology (RSM) for correlating the interactive and higher order influences of major machining parameters, i.e. magnetic flux density, applied voltage, tool feed rate, and work piece rotational speed on MRR and SR of 6061 Al/Al_2O_3 (10% wt) composite. The results demonstrated that assisting ECT with MAF leads to an increase machining efficiency and resultant surface quality significantly compared to that achieved with the traditional ECT.

Kumar and Yadav [40] developed a mathematical model for the prediction of magnetic potential using Maxwell's equations and finite element method to find the magnetic potential distribution within the gap between tool bottom surface and work piece top surface. From magnetic potential model, the magnetic pressure developed and corresponding heat flux generated on work piece surface were evaluated. Furthermore, a mathematical model was developed for heat transfer in the work piece and again finite element method was used for the prediction of temperature rise in the work piece. The effects of various operating input parameter on magnetic potential distribution in the gap and temperature rise in the work piece were studied.

Im et al. [20] experimented on a STS 304 cylindrical work piece using MAF process at 30,000 rpm, and the roughness, roundness, and changes in the micro-diameter were investigated. The study showed that it is possible to control the micro-diameter and weight of the STS 304 cylindrical work piece using a near

Table 4.2 Comparison of optimization results for MAF process

Technique	d	v	w_f	I	t	ΔR_a	Constraint value
GA[a]	0.015	852.6	0.446	1.02	5	0.26873[b]	0.0006[b]
GA	0.015	852.6	0.446	1.02	5	0.2739[c]	0.0153[c]
PSO	0.015	2,458.7	0.3	1.537	1	0.2694	0.00122
SA	0.0336	500	0.568	4.070	1	0.26758	0.00154

[a] Jain et al. [28]
[b] Values wrongly calculated by Jain et al. [28]
[c] Corrected values

linear approach. Surface roughness as fine as 0.06 μm and roundness as fine as 0.12 μm were achievable using a diamond paste with 1 μm particles. Vibrational motion applied to the work piece improved the surface roughness. The improvement of the surface roughness was achieved because the vibrational motion effectively removes unevenness in the rotational direction and the direction orthogonal to it.

Jain [21] gave a comprehensive overview of various flowing abrasive-based micro-/nano-finishing processes. The author had proposed a generalized mechanism of material removal for these processes and concluded that a single slot in the magnet during MAF gives higher finishing rate compared to the magnet without any slot. Yang et al. [78] used finite element method to analyze magnetic field characteristics for three different magnetic poles such as solid cylindrical pole, hollow cylindrical pole, and hollow cylindrical pole with grooves design. The results showed that the hollow cylindrical with grooves can generate the better surface roughness in MAF. The operations were demonstrated using a permanent magnetic polishing mechanism installed at a CNC machining center. The operations were performed using Taguchi experimental design, considering the effects of magnetic field, pole rotational speed, feed rate, working gap, abrasive, and lubrication. The optimal parameter conditions was obtained after experimental data analysis, the quality surface roughness ($R_{max} = 0.1$ mm), which is similar to a mirror surface, was obtained after confirmatory tests. The optimal parameter conditions for material removal weight were also obtained in MAF. The results showed that MAF technique can meet customer requirement and raise the value-added products simultaneously.

Kwak [43] attempted to improve the magnetic flux density in magnetic abrasive polishing process for non-ferrous materials, specially focused on magnesium. The magnetic flux density for ferrous and non-ferrous materials was simulated. To increase the magnetic flux density for non-ferrous materials, a practical method that installed a permanent magnet at the opposite side of the work piece to be machined was proposed and evaluated by computer simulation and experimental verification. For determining a dominant process factor and optimal conditions of the magnetic abrasive polishing for a thin magnesium plate as a case study, the design of experimental method was adopted. From the simulation and the experimentation, it was found that the location of the maximum magnetic flux density during the process was verified as a diameter/4 distance from the center of the inductor. When the working gap was 2 mm, the maximum magnitude of the magnetic flux density for non-ferrous material with a permanent magnet installed at the opposite side of the work piece surface to be machined was increased by about 35%. The rotational speed of the tool had a dominant effect on the improvement of surface roughness and the optimal conditions for the magnetic abrasive polishing of the magnesium alloy were an applied current of 2.0 A, working gap of 1 mm, rotational speed of 800 rpm and amount of powder of 0.7 g.

4.4 Magnetorheological Abrasive Flow Finishing Process

In magnetorheological abrasive flow finishing (MRAFF) process, magnetorheological polishing fluid (MRPF) is used as the medium. MRPF is a homogeneous mixture of carbonyl iron particles (CIPs) and abrasive particles in a base medium of grease and paraffin liquid. When an external magnetic field is applied, the CIPs in the fluid form a chain-like structure along the lines of magnetic field in between the two poles of an electromagnet. Surrounding CIPs chains give bonding strength to the embedded abrasive particles. When MRPF is extruded through the passage formed by the work piece and fixture, abrasive particles embedded into/between the chains of CIPs and in contact with the work piece surface do cutting action by shearing off peaks of surface undulations from the work piece surface. The basic mechanism of MRAFF process is shown in Fig. 4.3. The MRPF is extruded from the top MRPF cylinder to the bottom MRPF cylinder and vice versa, through the work piece (fixture) by a hydraulic pump. Using the electromagnet, magnetic field is applied selectively across the workpiece. Material removal from the work piece surface can be controlled externally by controlling extrusion pressure and magnetic field (or current supplied to the electromagnet coils).

Magnetorheological abrasive flow finishing (MRAFF) process is developed for super finishing of internal geometries of hard materials. This process relies for its performance on magnetorheological effect exhibited by carbonyl iron particles along with abrasive particles in non-magnetic viscoplastic base medium. The extent of finishing action depends on radial and tangential forces coming on abrasive particles due to carbonyl iron particles (CIPs) arranged in columnar structure in the presence of external magnetic field.

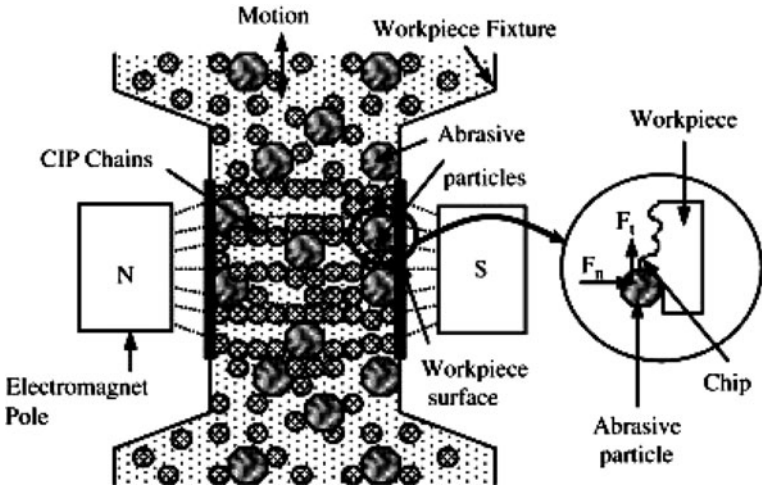

Fig. 4.3 Mechanism of magnetorheological abrasive flow finishing process (from [35]; reprinted with permission from Elsevier)

Jha and Jain [35] designed a hydraulically powered experimental setup to study the MRAFF process characteristics and performance. The setup consists of two MR-polishing fluid cylinders, two hydraulic actuators, electromagnet, fixture, and supporting frame. Experiments were conducted on stainless steel work pieces at different magnetic field strength to observe its effect on final surface finish. No measurable change in surface roughness was observed after finishing at zero magnetic field. However, for the same number of cycles the roughness reduced gradually with the increase of magnetic field. This validated the role of rheological behavior of magnetorheological polishing fluid in performing finishing action.

In another work, Jha and Jain [34] conducted experiments on stainless steel work pieces with different combinations of CIP and SiC particles in MRP fluid for same volume concentration. CIP chain structure and surface roughness evaluation model were proposed. Magnitudes of the forces on abrasive particles were then calculated and change in surface roughness was computed using the model developed to simulate final surface roughness. Based on the experimental work, the authors had made the following conclusions:

- For the same magnetic flux density, the finishing forces on abrasive particles are mainly dependent on number of CIPs in their vicinity, their micro-structural arrangement, and size. The magnetic force on a carbonyl iron particle is a function of particle volume, so size of CIP in comparison with abrasive size is an important factor affecting final surface roughness obtained in MRAFF process.
- Compared to the same size of CIP and abrasive particle, the surface finish improvement rate decreases with decrease in abrasive particles size (keeping CIP size constant) due to decrease in indenting force and sharing of the same force by more number of abrasive particles. This is also because of the decrease in interparticle magnetic force between CIPs which governs the holding force during shear and restrain breaking of chains in case of smaller particles.

Das et al. [9] developed a new precision finishing process called magnetorheological abrasive flow finishing (MRAFF), which is basically a combination of AFM and MRF, for nano-finishing of parts even with complicated geometry for a wide range of industrial applications. The authors had discussed the theoretical investigations into the mechanism of MRAFF process to study the effects of various process parameters. An attempt was made to analyze the medium flow through the fixture by finite difference method by assuming the medium as Bingham plastic to evaluate the stresses developed during the process. A capillary viscometer was designed and fabricated to study the effect of magnetic field on the rheological properties of the medium. Microstructure of the mixture of ferromagnetic and abrasive particles in magnetorheological polishing fluid (MRPF) was proposed, and normal force on the abrasive particles was calculated from the applied magnetic field. A model for the prediction of material removal and surface roughness was also presented. From the rheological experiments, it was concluded that the viscosity of the fluid increases in a third-order logarithmic function and also yield stress of the fluid increases with an increase in the magnetic field applied

across the fixture. It was observed from the numerical simulation that higher axial pressure gave rise to smaller plug flow region at a given magnetic field. From the fluid flow analysis, it was concluded that for the same applied pressure a larger plug flow region of the flowing fluid was obtained with higher magnetic field due to the formation of strong structure of CIP chains with increased magnetic field. Reduction in surface roughness value increased with an increase in current and number of finishing cycles. The BCC chain structure proposed for the modeling of a complex chain structure of MRPF seemed to be better represented and the comparison of theoretical and experimental results of surface roughness of work piece revealed that they were in good agreement.

4.5 Electrolytic In-process Dressing Process

The electrolytic in-process dressing (ELID) is a simple and efficient technique that can be easily adopted for any conventional machine. The basic ELID system consists of a metal-bonded diamond grinding wheel, an electrode, a power supply, and an electrolyte as illustrated in Fig. 4.4. The metal-bonded grinding wheel is made into a positive pole through the application of a brush smoothly contacting the wheel shaft. An electrode made of copper, covering 1/6 of the grinding wheel perimeter is connected to the negative pole. A straight type metal-bonded diamond grinding wheel is mounted on a vertical spindle and the gap between the grinding wheel and the electrode is adjusted to approximately 0.1–0.3 mm. In the small clearance between the positive and negative poles, electrolysis occurs through the

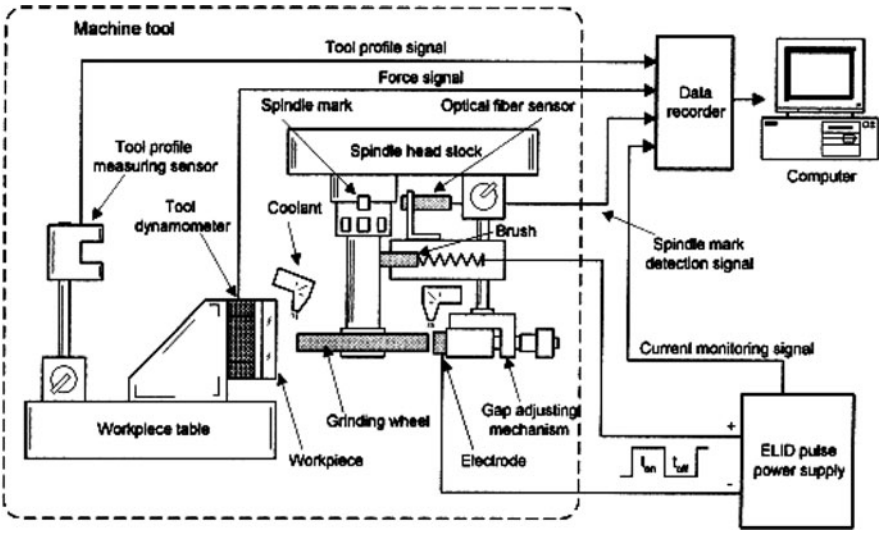

Fig. 4.4 ELID setup (from [12]; reprinted with permission from Elsevier)

supply of the grinding fluid and an electrical current. An electric current in the form of square pulse wave is supplied from the ELID power supply to the positive and negative poles. The peak current (I_p) and voltage can be varied within the ranges 1–10 A and 30–90 V, respectively. The T_{on} and T_{off} time can be varied from 1 to 10 μs using the timer switch provided on the ELID power supply. A standard grinding coolant is diluted in water and used as an electrolyte and coolant [12]. Metal-bonded super-abrasive diamond grinding wheels have superior qualities such as high bond strength, high stability, and high grindability.

Electrolytic in-process dressing (ELID) is an effective method to dress the grinding wheel during grinding. The wear mechanism of metal-bonded grinding wheels dressed using ELID is different from the conventional grinding methods, because the bond strength of the wheel-working surface is reduced by electrolysis. The reduction of bond strength reduces the grit-depth-of-cut and hence the surface finish is improved. The oxide layer formed on the surface of the grinding wheel experiences macro-fracture at the end of wheel life while machining hard and brittle work pieces. When the wheel wear is dominated by macro-fracture, the wheel-working surface is free from loaded chips and worn diamond grits. When the oxide layer is removed from the wheel surface, the electrical conductivity of the grinding wheel increases, and that stimulates electrolytic dressing. The conditions applied to the pulse current influence the amount of layer oxidizing from the grinding wheel surface. Longer pulse 'on' time increases the wheel wear. Shorter pulse 'on' time can be selected for a courser grit size wheel, since that type of wheel needs high grinding efficiency. Equal pulse 'on' and 'off' time is desired for finer grit size wheels to obtain stable and ultra-precision surface finish [12].

Various applications of ELID process include finishing of structural ceramic components [2, 3, 16, 79, 81], finishing of bearing steels [54], chemical vapor deposited silicon carbides [37, 80], precision internal grinding [51], mirror surface finish on optical mirrors [73, 79, 81], finishing of harder die materials such as SKDII and SKII51 ([45, 46], precision grinding of Ni–Cr–B–Si composite coating [66, 67], machining of micro-holes in hard and brittle materials [2], grinding of silicon wafers [52, 70], etc.

Rahman et al. [55] made attempt to understand the fundamental characteristics of ELID grinding and their influence on surface finish. The authors pointed out that even though ELID process is highly suitable for producing nano-surface finish, some non-linearities were found during in-process dressing due to the self-protecting oxide layer on the grinding wheel surface that resist the flow of current [53]. The thickness of the layer affects the ground surface finish and other parameters such as grinding force, grit protrusion, and wheel profile. Lee [44] studied the advantages of controlled ELID grinding by measuring the gap between the grinding wheel and the electrode. Controlled in-process dressing showed better results than uncontrolled dressing. The electrical parameters (such as voltage, current, current duty ratio), however, were considered to be the most influencing parameters during in-process dressing. Change in any of the electrical parameters affects the in-process dressing and the layer thickness.

The condition of defect free ductile surface was reported by Bifano et al. [6]. The critical depth-of-cut (d_c) to produce a defect free surface on hard and brittle material was expressed as shown by the following equation:

$$d_c \alpha (E/H)(K_c/H)^2 \tag{4.36}$$

where E is the Young's modulus, H is the hardness, and K_c is the fracture toughness. The critical depth-of-cut solely depends on the properties of material to be machined. For BK7 optical glass, the critical depth-of-cut is approximately equal to 45 nm. The maximum chip thickness or grit-depth-of-cut, h_{max}, is expressed as,

$$h_{max} = 2L_s(V_w/V_c)(a_e/d_s)^{1/2} \tag{4.37}$$

where L_s is the distance between the adjacent grits, V_w is the work speed (mm/min), V_c is wheel peripheral speed (rpm), a_e is the wheel depth of cut (μm), and d_s is the diameter of the wheel (mm). From the above expression, it is clear that the maximum chip thickness depends on both machining and wheel parameters [48, 68]. If the penetration depth of a single grit is less than the critical depth-of-cut, the chip deformation takes place plastically and that reduces the subsurface damages. The condition for ductile mode grinding can be expressed as shown below:

$$h_{max} < d_c. \tag{4.38}$$

The above condition can be obtained by controlling different machining parameters during grinding. For example, the increase of wheel speed or reduction of depth-of-cut reduces the chip thickness, but it needs special machines or special attachments. Recent studies show that ductile mode could be achieved using the conventional machine with the super-abrasive grinding wheels and the ELID. The superabrasive wheels reduce the distance between the adjacent grits (L_s) and minimize the chip thickness, but there is no explanation about the significance of bond strength and bonding mechanism during ELID grinding. The mode of material removal varies from fracture to plastic scratching based on the hardness of metal bond.

Fathima et al. [13] proposed a new grinding model for ultra-precision ELID grinding. The main focus was to develop a force model for the ultra-precision ELID grinding. When the material removal rate is very low, it is very important to estimate the real contact area between the wheel and work surfaces. The developed grinding model estimates the real contact area by considering the wheel and the work surface characterization and the effect of the electrolytic reaction at the grinding wheel edge. The effects of the microstructure changes on the wheel surface by the electrochemical reaction were implemented in the model in order to improve the efficiency of the developed model. The grinding model was simulated and the simulated results were substantiated by the experimental findings.

Though the ELID technique is simple, successful, and effective, several practical difficulties have been experienced and reported in the recent years. The

selection of good correlation between the grinding and the ELID parameters and the undefined wheel wear are some of the important factors to be considered. The above mentioned factors significantly influence the geometrical accuracy and the surface finish of the work piece, and hence it is very important to optimize the parameters for utilization and implementation of the ELID technique in an efficient way. The advancements in the simulation and virtual technologies in the recent years simplify several complicated manufacturing tasks.

Fathima et al. [14] developed a knowledge based feedback control system for optimizing and controlling the ELID process suitable for various materials and applications. The feedback system consists of a computer controlled pulsed power source (current and voltage in the form of pulse), the software necessary for the user interface and the knowledge database. In this system, it is possible for the user to describe the grinding job in terms of work material, wheel bond material and the machining parameters required for the job. The information inputs are used to select the optimized ELID parameters for the process, and to set the values for the process control from the knowledge database. The optimized parameter settings reduce the excessive wear rate of the wheel and improve the geometrical accuracy of the work. The feedback control system controls and maintains the optimized set values for ELID during grinding. However, it is difficult to eliminate the geometrical inaccuracies of the work piece in a single cycle. The main aim of the knowledge based feedback control system is to minimize the profile errors occurred during ELID grinding and the number of correction cycles necessary for obtaining the desired geometrical accuracy. It is expected that the number of correction cycles required to finish the work piece with the desired specifications using the feedback control system is expected to be less than the number of correction cycles required for finishing the work piece with the conventional controlled ELID process.

The optimization of the ELID grinding process was expressed as,

$$\mathrm{ELID}_{\mathrm{optimized}} = f(E_{\mathrm{p}}, G_{\mathrm{p}}, P_{\mathrm{w}}, P_{\mathrm{m}}) \text{ for conventional} \tag{4.39}$$

$$\mathrm{ELID}_{\mathrm{optimized}} = f(E_{\mathrm{p}}, G_{\mathrm{p}}, P_{\mathrm{w}}, P_{\mathrm{m}}, \mathrm{PID}_{\mathrm{p}}) \text{ for feedback control} \tag{4.40}$$

where E_{p} is the ELID parameters, G_{p} the grinding parameters, P_{w} the properties of the bond/layer, P_{m} the properties of the work material, and $\mathrm{PID}_{\mathrm{p}}$ is the PID controller parameters.From the feasibility studies conducted with the feedback control system developed for precision grinding of various optical and non-optical materials with different sizes, the authors had made the following observations:

- The response of the ELID process is different for different work materials and hence the process has to be optimized based on the work material to be ground.
- The application of the feedback control system reduces the geometrical inaccuracies and improves the surface finish especially on harder materials.
- The application of the feedback control system developed is very efficient for reducing the overall geometrical inaccuracies while grinding large work pieces.

- The application of the knowledge based feedback control system reduces the ambiguities experienced during ELID grinding.

ELID is gaining popularity for machining hard and brittle materials due to its excellent surface generation capabilities. However, no fundamental investigation on the formation and erosion of the oxide layer deposited on the wheel was satisfactorily conducted. Biswas et al. [7] conducted ELID grinding experiments and it was found that the electrolytic current attains a steady value. The dressing current is controlled by the oxide layer thickness, which in turn is determined by its formation during electrolytic dressing and erosion during grinding. When these formation and erosion rates reach equilibrium, a steady layer thickness is achieved, producing steady current. The phenomenon was theoretically investigated by formulating electrolytic dressing to find oxide formation per wheel rotation. The theoretical results showed that a constant current value was achieved due to equilibrium of oxide formation and erosion rates, and these were substantiated by experimental findings.

Study of ELID grinding shows that it is highly suitable for achieving nano-surface finishes on metals and non-metals. Different types of ELID process are highly suitable for machining and finishing micro shapes. Nano-surface finish can be achieved using ductile mode machining on hard and brittle materials. The results show that the ELID grinding can produce ductile surfaces without any sub-surface damage, which eliminates the lapping and polishing processes. Thus, surface finish can be improved with higher accuracy and tolerance since the component is produced using only one process. The major difficulties are the lack of feedback devices to control the in-process dressing, optimization of machining conditions, and modeling of ductile mode grinding. Efforts are being made in this direction.

References

1. Ali-Tavoli M, Zadeh NN, Khakhali A, Mehran M (2006) Multi-objective optimization of abrasive flow machining processes using polynomial neural networks and genetic algorithms. Mach Sci Technol 10:1–20
2. Bandyopadhyay BP, Ohmori H (1999) The effect of ELID grinding on the flexural strength of silicon nitride. Int J Mach Tools Manuf 39:839–853
3. Bandyopadhyay BP, Ohmori H, Takahashi I (1996) Ductile regime mirror finish grinding of ceramics with electrolytic in-process dressing (ELID) grinding. Mater Manuf Proc 11:789–801
4. Barletta M (2009) Progress in abrasive fluidized bed machining. J Mater Process Technol 209(20):6087–6102
5. Bergh F, Engelbrecht AP (2006) A study of particle swarm optimization particle trajectories. Inf Sci 176:937–971
6. Bifano TG, Dow TA, Scattergood RO (1991) Ductile-regime grinding: a new technology for machining brittle materials. J Eng Ind 113:184–189
7. Biswas I, Kumar AS, Rahman M (2010) A study on the equilibrium condition of the oxide layer in ELID grinding. Int J Abras Technol 3(1):7–12

8. Chang GW, Yan BH, Hsu RT (2002) Study on cylindrical magnetic abrasive finishing using unbonded magnetic abrasives. Int J Mach Tools Manuf 42:575–583
9. Das M, Jain VK, Ghoshdastidar PS (2008) Fluid flow analysis of magnetorheological abrasive flow finishing (MRAFF) process. Int J Mach Tools Manuf 48(3–4):415–426
10. El-Taweel TA (2008) Modeling and analysis of hybrid electrochemical turning-magnetic abrasive finishing of 6061 Al/Al_2O_3 composite. Int J Adv Manuf Technol 37(7–8):705–714
11. Fang L, Zhao J, Li B, Sun K (2009) Movement patterns of ellipsoidal particle in abrasive flow machining. J Mater Process Technol 209(20):6048–6056
12. Fathima K, Kumar AS, Rahman M, Lim HS (2003) A study on wear mechanism and wear reduction strategies in grinding wheels used for ELID grinding. Wear 254:1247–1255
13. Fathima K, Rahman M, Kumar AS, Lim HS (2007) Modeling of ultra-precision ELID grinding. J Manuf Sci Eng 129(2):296–302
14. Fathima K, Schinhaerl M, Geiss A, Rascher R, Sperber P (2010) A knowledge based feedback control system for precision ELID grinding. Precis Eng 34(10):124–132
15. Fox M, Agrawal K, Shinmura T, Komanduri R (1994) Magnetic abrasive finishing of rollers. CIRP Ann Manuf Technol 43(1):181–184
16. Fujihara K, Ohshiba K, Komatsu T, Ueno M, Ohmori H, Bandyopadhyay BP (1997) Precision surface grinding characteristics of ceramic matrix composites and structural ceramics with electrolytic inprocess dressing. Mach Sci Technol 1:81–94
17. Gorana VK, Jain VK, Lal GK (2004) Experimental investigations into cutting forces and active grain density during abrasive flow machining. Int J Mach Tools Manuf 44:201–211
18. Gorana VK, Jain VK, Lal GK (2006) Forces prediction during material deformation in abrasive flow machining. Wear 260:128–139
19. Gorana VK, Jain VK, Lal GK (2006) Prediction of surface roughness during abrasive flow machining. Int J Adv Manuf Technol 31:258–267
20. Im IT, Mun SD, Oh SM (2009) Micro machining of an STS 304 bar by magnetic abrasive finishing. J Mech Sci Technol 23(7):1982–1988
21. Jain VK (2009) Magnetic field assisted abrasive based micro-/nano-finishing. J Mater Process Technol 209(20):6022–6038
22. Jain VK (2000) Advanced machining processes. Allied Publishers, New Delhi
23. Jain VK, Adsul SG (2000) Experimental investigation into abrasive flow machining. Int J Mach Tools Manuf 40:1003–1021
24. Jain RK, Jain VK (1999) Simulation of surface generated in abrasive flow machining process. Robotics Comput Integr Manuf 15:403–412
25. Jain RK, Jain VK (2000) Optimum selection of machining conditions in abrasive flow machining using neural network. J Mater Process Technol 108:62–67
26. Jain RK, Jain VK (2001) Specific energy and temperature determination in abrasive flow machining process. Int J Mach Tools Manuf 41:1689–1704
27. Jain RK, Jain VK (2004) Stochastic simulation of active grain density in abrasive flow machining. J Mater Process Technol 152:17–22
28. Jain NK, Jain VK, Jha S (2007) Parametric optimization of advanced fine-finishing processes. Int J Adv Manuf Technol 34:1191–1213
29. Jain RK, Jain VK, Kalra PK (1999) Modeling of abrasive flow machining process: a neural network approach. Wear 231:242–248
30. Jain RK, Jain VK, Dixit PM (1999) Modeling of material removal and surface roughness in abrasive flow machining process. Int J Mach Tools Manuf 39:1903–1923
31. Jain VK, Kumar P, Behra PK, Jayswal SC (2001) Effect of working gap and cicumferential speed on the performance of magnetic abrasive finishing process. Wear 250:384–390
32. Jain VK, Kumar R, Dixit PM, Sidpara A (2009) Investigations into abrasive flow finishing of complex workpieces using FEM. Wear 267(1–4):71–80
33. Jayswal SC, Jain VK, Dixit PM (2005) Modeling and simulation of abrasive finishing process. Int J Adv Manuf Technol 26:477–490
34. Jha S, Jain VK (2006) Modeling and simulation of surface roughness in magnetorheological abrasive flow finishing (MRAFF) process. Wear 261(7–8):856–866

35. Jha S, Jain VK (2004) Design and development of the magnetorheological abrasive flow finishing process. Int J Mach Tools Manuf 44:1019–1029
36. Kar KK, Ravikumar NL, Tailor PB, Ramkumar J, Sathiyamoorthy D (2009) Performance evaluation and rheological characterization of newly developed butyl rubber based media for abrasive flow machining process. J Mater Process Technol 209(4):2212–2221
37. Kato T, Ohmori H, Zhang C, Yamazaki T, Akune Y, Hokkirigawa K (2001) Improvement of friction and wear properties of CVD-SiC films with new surface finishing method 'ELID-grinding. Key Eng Mater 196:91–101
38. Kim J, Choi M (1995) Simulation for the prediction of surface-accuracy in magnetic abrasive machining. J Mater Process Technol 53:630–642
39. Ko SL, Baron YM, Park JI (2007) Micro deburring for precision parts using magnetic abrasive finishing method. J Mater Process Technol 187–188:19–25
40. Kumar G, Yadav V (2009) Temperature distribution in the workpiece due to plane magnetic abrasive finishing using FEM. Int J Adv Manuf Technol 41(11–12):1051–1058
41. Kremen GZ, Elsayed EA, Rafalorich VI (1996) Mechanism of material removal in magnetic abrasive process and the accuracy of machining. Int J Prod Res 34(9):2629–2638
42. Kremen GZ, Elsayed EA, Ribeiro JL (1994) Machining time estimation for magnetic abrasive processes. Int J Prod Res 32(12):2817–2825
43. Kwak JS (2009) Enhanced magnetic abrasive polishing of non-ferrous metals utilizing a permanent magnet. Int J Mach Tools Manuf 49(7–8):613–618
44. Lee ES (2000) A study on the mirror-like grinding of die steel with optimum in-process electrolytic dressing. J Mater Process Technol 100(1–3):200–208
45. Lim HS, Ohmori H, Lin W, Qian J (2000) High productivity and high accuracy electrode-less ELID grinding on die material. J Mould Tehchnol 15:148–149
46. Lim HS, Ohmori H, Lin W, Qian J (2001) Electrode-less micro ELID grinding on die and mould material. Jpn Soc Grind Eng 45:298–303
47. Mali HS, Manna A (2010) Optimum selection of abrasive flow machining conditions during fine finishing of Al/15 wt% SiC-MMC using Taguchi method. Int J Adv Manuf Technol. doi:10.1007/s00170-010-2565-y
48. Mayer JE, Fang GP (1994) Effect of grit depth of cut on strength of ground ceramic. CIRP Ann Manuf Technol 43(1):299–312
49. Mollah AA, Pratihar DK (2008) Modeling of TIG welding and abrasive flow machining processes using radial basis function networks. Int J Adv Manuf Technol 37(9–10):937–952
50. Mori T, Hirota K, Kawashima Y (2003) Clarification of magnetic abrasive finishing mechanism. J Mater Process Technol 143–144:682–686
51. Ohmori H, Moriyasu S, Li W, Takahashi I, Park KY, Itoh N, Bandyopadhyay BP (1999) Highly efficient and precision fabrication of cylindrical parts from hard materials with the application of ELID (electrolytic in-process dressing). Mater Manuf Process 14:1–12
52. Ohmori H, Nakagawa T (1990) Mirror surface grinding of silicon wafers with electrolytic in-process dressing. CIRP Ann Manuf Technol 39(1):329–333
53. Ohmori H, Nakagawa T (1997) Utilization of nonlinear conditions in precision grinding with ELID (Electrolytic In-Process Dressing) for fabrication of hard material components. CIRP Ann Manuf Technol 46(1):261–264
54. Qian J, Wei L, Ohmori H (2000) Cylindrical grinding of bearing steel with electrolytic in-process dressing. Precis Eng 24:153–159
55. Rahman M, Kumar AS, Lim HS, Fatima K (2003) ELID grinding technique for nano finishing of brittle materials. SADHNA J Eng Sci Indian Acad Sci 28(5):1–18
56. Rajeshwar G, Kozak, Rajurkar KP (1994) Modeling and computer simulation of medium flow in abrasive flow machining process. In: Proceedings of International Mechanical Engineering Congress and Exposition. Chicago, PED 68:965–971
57. Rao RV, Pawar PJ (2010) Optimization of abrasive flow machining process parameters using artificial bee colony algorithm. In: Proceedings of International Conference on Advances in Mechanical Engineering. Surat, pp. 768–773

58. Rao RV, Pawar PJ, Davim JP (2009) Optimization of abrasive flow machining process parameters using particle swarm optimization and simulated annealing algorithms. In: Davim JP (ed) Artificial intelligence in manufacturing research. Nova Science Publications, New York
59. Rhoades LJ (1987) Abrasive flow machining with not-so-silly putty. Met Finish, 27–29 July
60. Rhoades LJ (1991) Abrasive flow machining: a case study. J Mater Process Technol 28:107–116
61. Sankar MR, Mondal S, Ramkumar J, Jain VK (2009) Experimental investigations and modeling of drill bit-guided abrasive flow finishing (DBG-AFF) process. Int J Adv Manuf Technol 42(7–8):678–688
62. Sankar MR, Ramkumar J, Jain VK (2009) Experimental investigation and mechanism of material removal in nano finishing of MMCs using abrasive flow finishing (AFF) process. Wear 266(7–8):688–698
63. Shinmura T, Takazawa K, Hatano E, Matsunaga T (1990) Study in magnetic abrasive finishing. CIRP Ann Manuf Technol 39(1):325–328
64. Singh DK, Jain VK, Raghuram V (2004) Parametric study of magnetic abrasive finishing process. J Mater Process Technol 149:22–29
65. Singh S, Shan HS (2002) Development of magneto abrasive flow machining process. Int J Mach Tools Manuf 42:953–959
66. Stephenson DJ, Hedge J, Corbett J (2002) Surface finishing of Ni–Cr–B–Si composite coatings by precision grinding. Int J Mach Tools Manuf 42:357–363
67. Stephenson DJ, Veselovac D, Manley S, Corbett C (2001) Ultra-precision grinding of hard steels. Precis Eng 25:336–345
68. Tonshoff HK, Peters I, Inasaki PT (1992) Modeling and simulation of grinding processes. CIRP Ann Manuf Technol 41(2):677–688
69. Uhlmann E, Mihotovic V, Coenen A (2009) Modeling the abrasive flow machining process on advanced ceramic materials. J Mater Process Technol 209(20):6062–6066
70. Venkatesh VC, Inasaki I, Toenshof HK, Nakagawa T, Marinescu ID (1995) Observations on polishing and ultraprecision machining of semiconductor substrate materials. CIRP Ann Manuf Technol 44:611–618
71. Walia RS, Shan HS, Kumar P (2006) Parametric optimization of centrifugal force- assisted abrasive flow machining (CFAAFM) by the Taguchi method. Mater Manuf Process 21:375–382
72. Walia RS, Shan HS, Kumar P (2006) Multi-response optimization of CFAAFM process through Taguchi method and utility concept. Mater Manuf Process 21:907–914
73. Wang P, Shi Z, Xin Q (2000) Optical surface grinding of optical glasses with ELID grinding technique. Proc SPIE Int Soc Opt Eng 4231:509–514
74. Wani AM, Yadava V, Khatri A (2007) Simulation for the prediction of surface roughness in magnetic abrasive flow finishing (MAFF). J Mater Process Technol 190(1–3):282–290
75. Williams RE (1998) Acoustic emission characteristics of abrasive flow machining. J Manuf Sci Eng 120:264–271
76. Williams RE, Rajurkar KP (1992) Stochastic modeling and analysis of abrasive flow machining. J Eng Ind 144:74–81
77. Yamaguchi H, Shinmura T (2004) Internal finishing process for alumina ceramic components by a magnetic field assisted finishing process. Precis Eng 28:135–142
78. Yang LD, Lin CT, Chow HM (2009) Optimization in MAF operations using Taguchi parameter design for AISI304 stainless steel. Int J Adv Manuf Technol 42(5–6):595–605
79. Zhang F, Li W, Qiu Z, Ohmori H (2000) Application of ELID grinding technique to precision machining of optics. Proc SPIE Int Soc Opt Eng 4231:218–223
80. Zhanga C, Ohmori H, Kato T, Morita N (2001) Evaluation of surface characteristics of ground CVDSiC using cast iron bond diamond wheels. Precis Eng 25:56–62
81. Zhang B, Yang F, Wang J, Zhu Z, Monahan R (2000) Stock removal rate and workpiece strength in multi-pass grinding of ceramics. J Mater Process Technol 104:178–184

Chapter 5
Modeling and Optimization of Rapid Prototyping Processes

5.1 Introduction

In a competitive market, the speed with which a product flows from concept to marketable product plays a crucial role. It is well known that products that are introduced before their competitors are generally more profitable and enjoy a larger share of the market. At the same time, there are important concerns regarding the production of high-quality products. For these reasons, there is a concerted effort to bring high-quality products to market quickly.

A new technology that considerably speeds the iterative product development process is the concept and practice of rapid prototyping (RP). The advantages of RP include

- Cost reduction up to 50%.
- Processing time reduction up to 75%. Physical models from CAD data files can be manufactured in a matter of hours to allow rapid evaluation of manufacturability and design effectiveness.
- Better visualization and concept verification.
- High design flexibility to enable short-term component modifications.
- Usage of prototype in subsequent manufacturing operations to obtain the final parts.
- Cost-effective component production for demonstration purposes, and functional test samples.
- Use of RP operations for production of rapid tooling for manufacturing operations.

Rapid prototyping processes can be classified into three major groups: subtractive, additive, and virtual. As the names imply, subtractive processes involve material removal from a work piece larger than the final part; additive processes build up a part by adding material incrementally; and virtual processes use advanced computer-based visualization technologies.

R. V. Rao, *Advanced Modeling and Optimization of Manufacturing Processes*, Springer Series in Advanced Manufacturing, DOI: 10.1007/978-0-85729-015-1_5,

There is a multitude of experimental RP methodologies either in development or used by small groups of individuals. The additive RP processes that are currently commercially available include stereolithography (SLA), selective laser sintering (SLS), laminated object manufacturing (LOM), fused deposition modeling (FDM), solid ground curing (SGC), 3D printing, and Ink Jet printing techniques.

Rapid prototyping systems have been used mainly in manufacturing industries such as automobiles, electric home appliances, and aerospace. Generally, RP processes begin with a stereolithography (STL) file that describes a model created by a CAD surface or a solid modeler. The RP models can be used to visualize or verify designs, to check for form, fit and function, or to produce a tooling (or master) pattern for casting or molding [39]. The basic methodology for all current RP techniques can be summarized as follows:

1. A CAD model is constructed and then converted to STL format. The resolution can be set to minimize stair stepping.
2. The RP machine processes the STL file by creating sliced layers of the model.
3. The first layer of the physical model is created. The model is then lowered by the thickness of the next layer, and the process is repeated until completion of the model.
4. The model and any supports are removed. The surface of the model is then finished and cleaned.

STL-based slicing is still the commonly used method in processing the problem of layered manufacturing. The advantage of slicing a STL file is that the problem is reduced to finding plane–intersections. Compared with STL-based slicing, direct slicing avoids some approximation that exists in STL format file. Some researchers propose a direct slicing method that can provide more exact laser beam paths by slicing a constructive solid geometry (CSG) representation of a part. However, a severe disadvantage of direct slicing is the capability among various CAD systems; in other words, it can only be used for a specific set of CAD software and machine, and is not applicable to any other CAD combinations.

5.2 Modeling and Optimization

Studies had been conducted to improve and optimize the RP process, so as to obtain high-quality parts produced on a wide range of commercial RP machines. Allen and Dutta [2] developed a method for automatically computing the support structure for the part in layer manufacturing and then deciding the best orientation from a candidate list of orientations. Sreeram and Dutta [36] developed a method to determine the optimal orientation based on variable slicing thickness in layered manufacturing for a polyhedral object.

Kim et al. [18] developed an optimization technique for optimal part orientation within the SLA process by considering an objective function related to the volume

of trapped liquid resin, the total height of the part in the build direction, and the area of surfaces with staircase protrusions. Frank and Fadel [10] proposed an expert system tool that considers the various parameters that affect the production of the prototype and recommends the best direction of building the part based on both the user's input as well as on a decision matrix implemented within the expert system. Cheng et al. [7] presented a multi-objective approach for determining the optimal part-building orientation. The authors had considered different objectives such as part accuracy and building time. Objective functions were developed based on known sources of errors affecting part accuracy and the requirements of good orientations during the building of a model. The objective functions employed weights assigned to various surface types affecting part accuracy. The primary objective was to attain the specified accuracy achievable with the process. The secondary objective was to minimize the building time. The authors gave examples to illustrate the algorithm for deriving the optimal orientation which can assure better part quality and higher building efficiency.

Nyaluke et al. [27] discussed component development in RP and part placement of models in the RP machine work space to optimize utilization of RP systems. The algorithm proposed fills the work space with parts by partitioning the work volume into layers and then filling these layers one after another.

Accurate build-time prediction for making stereolithography parts not only benefits the service industry with information necessary for correct pricing and effective job scheduling but also provides researchers with valuable information for various build parameter studies. Instead of the conventional methods of predicting build time based on the part's volume and surface, Chen and Sullivan [6] presented detailed scan and recoat information from the actual build files by incorporating the algorithms derived from a detailed study of the laser scan mechanism of the stereolithography machine. It was found that the scan velocity generated from the stereolithography machine depends primarily on the system's laser power, beam diameter, material properties, and the user's specification of cure depth. It was proved that this velocity is independent of the direction the laser travels and does not depend on the total number of segments of the scan path. In addition, the time required for the laser to jump from one spot to another without scan is linearly proportional to the total jump distance and can be calculated by a proposed constant velocity. It was concluded that the slower machine velocity results in an undesired amount of additional cure and proves to be the main cause of the Z dimensional inaccuracy.

Lan et al. [20] discussed the fabrication orientation problem from geometric and algorithmic points of view, and established decision criteria for the determination of good fabrication orientation for SLA. Hur and Lee [16] developed an algorithm to calculate the staircase area, quantifying the process errors by the volume supposed to be removed or added to the part, and the optimum layer thickness for the SLA system. They determined the optimum orientation based on the user's selection of primary criteria and the optimum thickness of the layers.

Solid ground curing (SGC) technology, one of the RP technologies, is suitable of building multiple parts with different geometry and dimensions in batch

production of rapid prototypes to minimize the cost of prototypes. However, the layout of CAD models in a graphic environment is time-consuming. Because of high cost of the resin, the layout of models in a batch is critical for the success of the SGC operations in any industrial environment.

Pham et al. [32] developed a decision support tool to help RP users determine a part orientation. Their tool considered many factors such as part cost, build time, problematic features (e.g., pipes, shells, critical surfaces, holes, and axes), optimally orientated features, overhanging area, and support volume for SLA. By multiplying position score for each candidate orientation by the weights assigned intuitively for each criterion, the total score for any candidate was obtained. The orientation with the highest score was selected as the desirable build-up direction.

Zhou et al. [43] conducted a detailed study of the most important five build parameters that affect the quality and accuracy of the final stereolithography parts, namely, the layer thickness, resultant overcure, hatch space, blade gap, and part location. To reduce the large amount of total number of experiments required, the study employed the Taguchi L27 orthogonal array for setting up the different combinations of the respective control factors, each at three different levels. A standard sample was developed which provides a benchmark for comparison of the total of 20 different dimensional, geometrical, and surface features. Using the RSM and ANOVA analysis techniques, together with the help of MINITAB software, the factors that are most significant in affecting the quality and accuracy of these 20 representative dimensional and form features, and surface roughness were identified. The analysis results also suggested the best setting of these control factors for each individual feature. For example, to build a square (or rectangular) hole vertically, a low value of resultant overcure (e.g., 0.001 inches) and medium layer thickness (e.g., 0.009 inches) must be used to effectively reduce the dimensional error caused by the extra overcure at the down facing layer and to provide adequate support so that the sagging problems can be eliminated. Aimed at producing the best overall quality parts, the authors had proposed an optimal setup of the build parameters for building a general part consisting of a mixture of the various features. Finally, the respective total laser scan time and the corresponding total recoating time were also examined separately for each of the 27 cases studied. It was concluded that the suggested optimal build condition corresponds to the least amount of laser scan time, although the total recoating time may increase due to the smaller layer thickness used.

Hardjadinata and Doumanidis [13] introduced a new solid freeform fabrication technology based on successive joining of thin metal foils by laser spot welding, followed by laser cutting of each layer contour. This technology was implemented in the laboratory using a robotic Nd:YAG laser station with optical fiber transfer, and the optimal bonding and cutting conditions were determined experimentally for steel prototypes. A flexible thermomechanical finite element model of the process was established, with its boundary conditions calibrated and its predictions verified by pyrometry and profilometry measurements. This numerical model was used to study the layer deformation due to thermal gradients and to develop weld

sequencing, cycle timing, and in-process heat treatment methods for minimization of warping distortions and residual stresses. This new rapid manufacturing technology can fabricate high-strength, high-density multi-metal parts and metal matrix composites as well as internal functional structures with encapsulated active components.

Grujicic et al. [11] developed a model for in-flight melting of feed-powder particles propelled through a laser beam in the Laser-Engineered Net Shaping (LENS) process. The model was next incorporated in an optimization analysis to determine optimum LENS process parameters (laser power, particle velocity, and the angle between the laser-beam axis and particle trajectory), which maximize the probability for in-flight particle melting while ensuring the absence of melting of the surface of the substrate. A simple model, based on solution of the thermal energy conservation equation, was also developed to determine the laser-power threshold for melting of the substrate surface. The optimization analysis was then applied to Inconel 625 Ni–Cr–Mo superalloy. The results showed that by maximizing the laser power and the residence time of the particles in the laser beam (increases with reductions in particle velocity and particle trajectory angle), the probability for in-flight particle melting can be greatly increased, i.e., relatively coarse (−30/+40 mesh size) particles can be melted by propelling them through the laser beam.

Choi and Samavedam [9] proposed a virtual reality (VR) system for modeling and optimization of RP processes. VR is an advanced human–computer interface that simulates a realistic environment and allows a designer to interact with it. The essence of VR is immersion and interactivity, which differentiates it from CAD systems. Immersion means to block out distractions and to focus on selective information with which the designer wants to work. Interactivity implies the ability that humans interact with events in the virtual world. Applications of VR have recently gained considerable momentum in industries. The system aimed to reduce the manufacturing risks of prototypes early in a product development cycle, and hence, reduce the number of costly design-build-test cycles. It involved modeling and simulation of RP in a virtual system, which facilitated visualization and testing the effects of process parameters on the part quality. Modeling of RP was based on quantifying the measures of part quality, which included accuracy, build-time and efficiency with orientation, layer thickness, and hatch distance. A mathematical model was developed to estimate the build-time of the SLS process which is described below (from Choi and Samavedam [9]; reprinted with permission from Elsevier):

The build-time estimator evaluates the time as a function of the laser velocity, scan distance, and layer thickness. For SLS, the laser velocity derived from Steen [37] is shown as Eq. 5.1.

$$\text{Velocity}\,(v) = (P_{\text{l}}(1-R))/\left(\rho d_{\text{b}} l_{\text{m}}\left[C_{\text{p}}(T_{\text{m}}-T_{\text{b}})+kL_{\text{h}}\right]\right) \tag{5.1}$$

where, P_{l} is the laser power (W), R is the reflectivity of the mirror, ρ is the material density (g mm^{-3}), d_{b} is the laser beam diameter (mm), l_{m} is the machine layer

thickness (mm), C_p is the specific heat (J g^{-1} K^{-1}), T_m is the melting temperature (K), T_b is the bed temperature (K), k is the sinter factor, and L_h is the latent heat (J g^{-1}).

The build-time of a part can be obtained by summing up the time taken for each layer. The time taken for building a layer can be divided into the scan time and the set-up time. The set-up time can be obtained from the machine manual, and it is normally constant for all layers. The time required for scanning a layer varies along the z-axis and can be obtained as a ratio of the scan distance to the scan velocity. The total scan distance within a layer can be obtained from the hatch file. The velocity can be estimated based on the process. For example, it can be estimated from Eq. 5.1 for the SLS process.

$$\text{Build time of a part} = \sum_{i=1}^{N_l} T_{li} + T_s N_l \tag{5.2}$$

$$\text{Scan time } (T_l) = L_d / L_v \tag{5.3}$$

where, T_l is the scan time of a layer (s), T_s is the set-up time of a layer (s), N_l is the total number of layers, L_d is the laser scan distance (mm), and L_v is the laser scan velocity (mm s^{-1}).

Setup time refers to the time that the SLS machine takes to spread a thin and even layer of powder to be sintered for the next slice. It refers to everything the machine does when it is not sintering.

$$\text{Setup time } (T_s) = t_{wd} + t_d + t_{wr} + t_h \tag{5.4}$$

where, t_{wd} is the time required for the work-bed to move down (s), t_d is the material deposition time (s), t_{wr} is the time required for the work-bed to rise up (s), and t_h is the time required to heat the material (s).

$$\text{Build time of a part} = (h/l_m)T_s + \sum_{i=1}^{N_l} d_{si}(l/l_m)/L_v \tag{5.5}$$

where, h is the total height of the part (mm) and l_m is the machine layer thickness (mm).

The algorithm presented by Choi and Samavedam [9] is a useful step in developing a build-time estimator for SLS machines. Unlike the previously available algorithms, their algorithm included the material properties, process parameters like layer thickness and hatch space and the machine parameters like work-bed temperature, power, and laser reflectivity. The model was integrated with the virtual simulation system to provide a test-bed to optimize the process parameters.

Zhang et al. [42] presented the layout optimization using simulated annealing (SA) technique. In model layout optimization, the model layout problem was identified to improve the productivity of the SGC process and to reduce the cost using SA technique. A move set to perturb new layout solutions was defined.

A new objective function was proposed and compared with the conventional linear-weighted objective function. The developed software tool kit can relieve Cubital machine operators from tedious and not necessarily effective work of packing part models on the DFE workstation. It can also receive the STL format from Pro/Engineer, generate the envelope automatically, and update the STL files of the models and the corresponding envelopes with the layout solution. The final layout can be transformed into VRML format and viewed with VRML viewer. The updated STL files can be directly loaded into the Cubital machine for manufacturing multiple parts in a batch.

To overcome the limitations of the layered manufacturing process, hybrid rapid-prototyping systems that allow material removal and deposition are being introduced. This approach should benefit from the advantages of conventional layered manufacturing and traditional CNC machining processes. To realize these advantages, however, an intelligent process plan must be generated. In the hybrid rapid-prototyping process, a part is decomposed into thick-layered 3D shapes, such that each layer can be machined and stacked easily. When each layer is generated from the part's shape, the build orientation is an important factor to be considered, because it greatly influences the lead-time, the machining accuracy, and the number of tool-accessible features in each setup. Hu et al. [15] described an algorithm to determine the build orientation. It considers the deposition process attributes and the machining process attributes simultaneously. The main criteria considered for determining the build direction were the tool accessibility of the machining features, the build time, the number of bridges, and the number of supports. In addition, a method was presented to secure a part with bridges instead of using specially designed fixtures.

Ahn et al. [1] characterized the properties of acrylonitrile butadiene styrene (ABS) parts fabricated by the FDM 1650. Using a design of experiment (DOE) approach, the process parameters of FDM, such as raster orientation, air gap, bead width, color, and model temperature were examined. Tensile strengths and compressive strengths of directionally fabricated specimens were measured and compared with injection-molded FDM ABS P400 material. For the FDM parts made with a 0.003 inch overlap between roads, the typical tensile strength ranged between 65 and 72% of the strength of injection-molded ABS P400. The compressive strength ranged from 80 to 90% of the injection-molded FDM ABS. Several build rules for designing FDM parts were formulated based on experimental results.

Harris et al. [14] conducted finite element analysis (FEA) on the ejection forces in injection-mold tooling (insert) made with a steriolithography process and concluded that smaller layer thickness and greater draft angle of the insert resulted in lower ejection forces. Besides this, it was pointed out that the adjustment of built layer thickness has a greater effect on ejection force than the adjustment of draft angle. However, the focus of the work of Harris et al. [14] was on minimization of the ejection force involved in the injection-molding process to avoid premature failure of tooling. Increasing the strength (tensile) of the die in addition to minimization of the ejection force would further increase the tool life.

Pandey et al. [30] presented a semi-empirical model for evaluation of surface roughness of a layered manufactured part by FDM. An attempt was made to address the problem of surface roughness resulting due to staircase effect in rapid prototyped parts using a simple material removal method, namely hot cutter machining (HCM). A fractional factorial DOEs, with two levels and four process parameters, was adopted to understand the effect of various process variables. ANOVA was used to find the significance index for process variables, and confidence level for the statistical model developed for the surface roughness of hot cutter machined surface. It was concluded that the proposed machining method was able to produce surface finish of the order of 0.3 μm with 87% confidence level. In another work, Pandey et al. [31] proposed a slicing procedure for FDM based on real-time edge profile of deposited layers. The procedure was implemented and examples were included to explain the adaptive slicing method.

Yang et al. [41] proposed a process planning approach based on a multi-orientational deposition (MOD) method to minimize the use of support structures, so as to improve the efficiency in layered manufacturing process and surface quality of a part built. An algorithm to determine the successive layer area difference for layer deposition and its application to overhang feature extraction and reduction using the MOD method was also introduced.

Masood et al. [25] presented a generic algorithm to determine the best part orientation for building a part in a layer-by-layer RP system. The algorithm works on the principle of computing the volumetric error (VE) in a part at different orientations and then determining the best orientation based on the minimum VE in the part. The algorithm was shown to work for a part of any shape and complexity, with any slice thickness, and for the orientation of a part about any selected axis. The part orientation system based on this algorithm graphically displays the VE at different part orientations and recommends the best part orientation. The system can help RP users in creating RP parts with a higher level of accuracy and surface finish.

Khan et al. [17] concluded that layer thickness, raster angle, and air gap influence the elastic performance of the compliant FDM ABS prototype. Lee et al. [22] performed experiments on cylindrical parts made from three RP processes such as FDM, 3D printer, and nano composite deposition (NCDS) to study the effect of build direction on the compressive strength. Experimental results showed that compressive strength is 11.6% higher for axial FDM specimen as compared to transverse FDM specimen. In 3D printing, diagonal specimen possessed maximum compressive strength in comparison to axial specimen. For NCDS, axial specimen showed compressive strength 23.6% higher than that of transverse specimen. Out of three RP technologies, parts built by NCDS were severely affected by the build direction.

Majumdar et al. [24] attempted laser-assisted fabrication of 316L stainless steel using a high-power (1.5 kW) continuous-wave diode laser. The main process variables for the present study were applied power density, scan speed, and powder feed rate. A detailed microstructural study of the surface and cross-section of the fabricated layer were carried out using optical and scanning electron microscopy

to understand the influence of laser parameters on microstructure of the surface and interface between the successive layers. The microstructure of the top layer was equiaxed and the near substrate region was fine dendritic; however, at the interface between two successive layers, it was coarsened. The morphology and degree of fineness of the microstructure was found to vary with laser parameters. The range of grain size (maximum grain size–minimum grain size) was taken as a measure of homogeneity. It was found that with increasing the scan speed, the range of grain size was minimized. Micro-porosities were present in the microstructure that reduced with increasing scan speed and found to be minimum at a medium powder feed rate. The optimum processing conditions were established by correlating the characteristics of the fabricated layer with process parameters.

Lee et al. [21] used the Taguchi method to find the optimal process parameters for FDM rapid prototyping machine that was used to produce ABS compliant prototype. An orthogonal array, main effect, the signal-to-noise (S/N) ratio, and analysis of variance (ANOVA) were employed to investigate the process parameters in order to achieve optimum elastic performance of a compliant ABS prototype so as to get maximum throwing distance from the prototype. Through this study, not only can the optimal process parameters for FDM process be obtained, but also the main process parameters that affect the performance of the prototype can be found.

The FDM3000 rapid prototyping machine with Insight 3.1 software was used in the study. Four parameters (air gap, raster angle, raster width, and layer thickness), each at three levels were taken into consideration in the study. Air gap was specified as solid fine, spare, and double wide. Raster angle was specified as 0°/90°, 45°/−45°, and 30°/60°. The 0°/90° angle means that FDM machine fabricates the alternate layers of the catapult on the horizontal plane by changing direction at 0° and 90° angles from the coordinate of the machine. Similarly, 45°/−45° and 30°/60° indicate the same deposition pattern followed by the machine.

Raster width was specified as 0.305, 0.655, and 0.98 mm. Layer thickness was varied from 0.178, 0.254, and 0.305 mm. The interactions between the parameters were not considered and other factors such as temperature and humidity were kept constant. The appropriate orthogonal array in this case was the standard L_9. The results were obtained by testing all the nine prototypes for different angles of displacement, i.e., 10°, 15°, and 20°. Each prototype represented each experiment of the orthogonal array. For 10° angle of displacement, air gap produced maximum contribution to the output performance of the product (throwing distance). For 15° angle of displacement, raster angle and layer thickness demonstrated almost equal maximum contribution to the output performance of the product (throwing distance), and for 20° angle of displacement, layer thickness gave the highest contribution to the output performance.

Byun and Lee [4] aimed to determine the optimal build-up direction of a part for different RP systems. The revised average weighted surface roughness, which considers stair-stepping effect, build time calculated by laser/knife/nozzle travel, and part cost calculated by build cost rate, labor cost rate, material cost, etc., were considered. Among the orientation candidates chosen from the convex hull of

a model, the best orientation was selected using the simple additive weighting method, a widely used multi-criterion method for decision making. The best orientation was also identified for each criterion. The algorithm can help RP users select the best build-up direction of the part and create optimal process planning.

Xiaomin et al. [40] proposed a new approach as a prototyping direction optimization of points data. Based on perspective theory, a curve surface was built up on the peak point of the produced point lattice of an entity. A lattice grid was used to represent the represent volume of the entity, which was employed in rapidly calculating the represent volume in real time. After analyzing the optimal object functions and strategy, authors adopted the genetic algorithm on selection of operators, cross breeding operators, mutation operators, iteration termination condition, and colony scales, etc. The optimization program was set up using Matlab and the optimization was obtained for prototyping direction. The simulation results showed that a three-dimensional reconstruction was not necessary based on this proposed points data prototyping direction optimization. On the basis of the proposed optimization approach, the best position of an entity can be located for RP, which can increase prototyping efficiency and reduce the time and money spending on prototyping.

Chockalingam et al. [8] attempted to study and optimize the Stereolithography process parameters of layer thickness, post-curing time, and orientation for maximum part strength. The experimental levels set for these three parameters to produce an SL part on an SLA 250/50 machine with CIBATOOL SL 5210 resin were: 0.1 mm, 0.125 mm, and 0.15 mm for layer thickness (L_t), 60, 90, and 120 min for post-curing time (P_c), and HX, VX, and HY for orientation (O). 18 experiments were conducted with the process parameters set at appropriate levels using L_{18} orthogonal array. The equation developed for part tensile strength is given below.

$$\begin{aligned} \mathrm{TS} = &- 89.878L_t^2 + 16.8L_t + 2.88 \times 10 - 4P_c^2 - 0.062P_c \\ &- 0.6345O^2 + (2.5655)O - 0.068L_tP_c + 7.667 \end{aligned} \tag{5.6}$$

The optimal combination of process parameters was 0.1 mm layer thickness, 60 min post-curing time, and vertical orientation (VX).

For low-volume production or for RP, sheet metal stamping tools can be made by an assemblage of steel sheets or layers and joined by several techniques (such as screws, bolts, brazing, and adhesive). However, an important problem in the design and the production of such tools is their mechanical behavior, in particular the strength of joining techniques which is crucial in the aim of achieving the highly required reliability of tools. If the mechanical behavior of tools can be mastered and accurately predicted, it can increase the life duration of tools and be more beneficial to the manufacturing community. In order to properly predict the mechanical behavior of tools, numerical simulation of stamping, taking into account elastic deformation of tools within a coupled FE analysis is needed. However, simulation results show that the effort and computational times required

for such a coupled simulation, in particular in a general three-dimensional (3D) case, could be prohibitive and unrealistic.

Oudjene et al. [28] proposed and developed a numerical procedure in two steps, which has the advantage of decoupling the simulation of the blank forming and the stress analysis of the elastic tools. Numerical application was presented for a layered stamping punch, based on the Stratoconception RP process, joined by screws in addition to an epoxy adhesive. The results were focused on the screw behavior, showing the potential interest of the developed procedure and numerical modeling technologies in designing layered tools joined by screws. In another work, Oudjene et al. [29] proposed and developed a simplified numerical procedure, based on two steps, for the 3D stress analysis of deformable tools (layered or not). In addition, an optimization procedure, based on DOEs and response surface method, was established in order to optimize the screw positions, which were crucial to the aim of achieving the required high strength and life duration of the assembly technique by screws. The results showed the feasibility of the developed procedure in the context of industrial applications.

In layer-based RP, a volumetric object is approximated as a pile of slices with vertical walls. Process parameter selection in layer-based prototyping is a multi-criteria multi-parameter optimization problem. A number of criteria may be used for assessing the quality of the prototype. Volumetric accuracy of shape approximation and building time are just two criteria taken in this work as an example. Criteria depend on process parameters, most commonly in a mutually contradictory manner. Model orientation and slice thickness constitute the minimum of process parameters to be considered, but others may also be added. For this reason, a neural network is used, trained by a number of input–output vectors, when analytical formulae representing the dependency of criteria on process parameters could not be developed and/or available numerical models take too long to execute. Vosniakos et al. [38] used neural network meta-models in the evaluation (cost) function of a genetic algorithm, each representing a particular criterion, and criteria were weighted according to the user's particular view. A case study was presented, referring to a wax model prototyping machine in which a particular tree for investment casting was built. A new criterion for assessing the quality of shape approximation was introduced, namely the local VE per slice.

Haipeng and Tianrui [12] presented a slicing algorithm based on the model geometrical continuity. In the strategy, the grouping matrix and the active triangle table were established by sorting for the triangular facets according to the minimum and maximum z-axis value of the triangular facets. By generating new intersecting facets table of each slicing plane and extracting only topology information of the current slicing plane, inner memory was remarkably saved, while the extracting time was also saved to some extent. The inefficient judgment about the location relations of triangle facets and slicing plane was avoided, thus advancing the slicing efficiency. Aiming at the inherence error in slicing operation brought by the approximation of the standard STL model, such as the non-closed cross-section contour and so on, an effective filtering and optimization algorithm based on feature analysis for the slicing profile was proposed by the authors. Case

study of a solid model was also presented to illustrate the feasibility and efficiency for the developed algorithms and the proposed strategy. The steps of the slicing algorithm proposed by Haipeng and Tianrui [12] are given below:

1. Input a STL file and get the maximum extent of this model.
2. Calculate the minimum and maximum z coordinates for each facet.
3. Construct the grouping matrix according to the minimum and maximum z coordinates.
4. Build topological structure and generate the active triangular facet table for the current layer.
5. Attach a sign to each edge in the active facet table. The sign has two values: unprocessed means that the intersection points on the edge must be calculated to obtain the slice contour and processed means that the edge has been calculated. Use the aforementioned method to calculate the intersection point until there is no edge signed unprocessed and put the intersections into the contour array.
6. Move to the next layer and determine whether the slicing position exceed the valid range. If no, return to Step 4. If yes, go to Step 7.
7. End procedure.

According to different RP methods, the processes and materials are quite different, and these RP materials should have special requirements to adapt to layer manufacturing method, which has complex composition and strict percentage requirements. To obtain desired dimensional tolerance and surface roughness with enough strength and appropriate construction time, experimental research should be performed for these different RP processes with specific material. Obviously, RP experiments have long process time, and are affected by multi factors, which include forming material composition and the process parameters. For optimal RP results, appropriate experimental proposal should be designed to find the relationship between material composition and RP product performance. As powder-based RP methods, three-dimensional printing (3DP), and selective laser sintering (SLS) are the most prominent RP methods for their flexibility in material selecting.

Rozman et al. [34] presented a model-based optimization of the process of printed circuit board laser structuring. For this purpose, a comprehensive theoretical model of the interaction between the traveling pulsed laser beam and conductive layer, as well as between the laser beam and the induced plasma plume was employed. The model was used to calculate process speed. Based on the process speed determined, the influence of pulse power, duration, and frequency on process speed was analyzed. In addition, an optimal range of process parameters with respect to process speed and quality was defined.

Nagahanumaiah et al. [26] presented a computer-aided rapid tooling process selection and manufacturability evaluation methodology for injection molding, supported by mold cost estimation models and RT process capability database. Rapid tooling process selection was based on process capability mapping in quality function deployment (QFD) against a set of tooling requirements that were prioritized through pairwise comparison using analytical hierarchal process

(AHP). The mold manufacturability for the selected RT process was carried out using fuzzy-analytic hierarchy process (fuzzy-AHP) to identify problem features, if any. This was followed by estimating the cost of RT mold and comparing it with a conventional mold, using cost models developed based on the concept of cost drivers and cost modifiers. The entire methodology was implemented in a software program using Visual C++ in Windows environment and demonstrated on an experimental mold as well as industrial cases. The proposed methodology enables selecting an appropriate rapid tooling process for a given injection mold requirement, and identifying critical features that could be modified to improve manufacturability, thereby achieving better quality and lower cost of molded parts along with shorter lead time.

Canellidis et al. [5] outlined the structure of a decision support system that automates the build orientation selection in the SLA process. The methodology employed a genetic algorithm, in order to search in an effective and quick way the solution space, in conjunction with a multi-criteria objective function which was employed for evaluating feasible solutions/orientations. For the formation of the multi-criteria function, the estimated fabrication time, comprising the estimated build time and post-processing time, and the average surface roughness of the part were considered. The importance of each criterion was defined via weighting factors. The associated software tool developed is fully customizable, allowing the consideration of different machine configurations. Four test cases concerning parts of different geometric complexity were examined. The computational results showed reasonably good solutions/orientations achieved within acceptable computational time limits. In order to improve the quality and optimality of the solutions computed by the methodology as well as its practical applicability, several issues for further research were identified. The authors concluded that a major issue was the detailed investigation of post-processing time in conjunction with surface quality. In this context, the assessment of accessibility of particular surfaces requiring finishing (both support removal and polishing) in a given orientation should be incorporated in the system. Furthermore, the surface roughness criterion assessment could be enhanced by incorporating into the problem the option of roughness tolerances and/or constraints for specific critical part surfaces. Quality assessment could also be enhanced through the incorporation of further criteria such as mechanical properties of the part and dimensional accuracy, which can also be associated with specific dimensional part tolerances.

Li [23] showed that much experimental work can be greatly decreased by the method of uniform design. The author's research was based on 3DP technique, and the research procedure can also be used for the development of SLS and other RP techniques and experiments. Plaster-based compound powder, which has the advantages of setting fast, with fine strength and surface finish and low cost, innoxious, and suitable for model making, was selected as an example for the experiments. The mean primary particle size of compound powder particle was 75 μm, without evident agglomeration. The plaster's original solidification time was less than 6 min, final solidification time was less than 30 min, and oven-dry compress strength was more than 20 MPa. Some additions such as polyvinyl

alcohol (PVA) and methyl cellulose (MC) powder as binder, a little anhydrite ($CaSO_4$) for setting speeder, and a little white carbon black for improving power's flowability were added. The bonder solution for the compound powder was aqueous solution (distilled water >95%), with small amount of polyvinyl pyrrolidone (PVP) and some other additions. Uniform design was adopted to decide the content of compound powder mixture for these multi-level, multi-factor 3DP experiments with only limited experiment times. 11 sets of experiments were conducted. For gross restriction of powder mixture, one component was removed from the regression analysis. Anhydrite's content (x_4) had the least effect for the experiments; thus the regression variables were plaster (x_1), PVA (x_2), MC (x_3), and white carbon black (x_5). The SPSS statistic software was used to analyze the 11 groups of experiments to set up the regression functions. The regression equations are as follows:

$$y_1 = 438.018 + 7.493x_1 - 0.278x_2x_3 - 13.14x_2x_5 - 2.859/x_5 \tag{5.7}$$

$$y_2 = 22.403 + 0.078x_3^2 - 0.032x_2x_3 - 0.583x_2x_5 - 1419.927/x_1 \tag{5.8}$$

$$y_3 = 14.839 - 0.134x_1 - 1.307x_3 + 0.229x_3^2 + 1.261x_2x_5 - -0.462/x_5 \tag{5.9}$$

$$y_4 = -22.947 + 0.297x_1 - 0.1x_2x_5 + 0.104/x_3 \tag{5.10}$$

$$y_5 = -12.641 + 0.196x_1 + 0.172x_3 - 0.012x_2x_3 + 2.461/x_2 - 0.32/x_2 \tag{5.11}$$

$$y_6 = -20.737 + 0.257x_1 + 1.124/x_2 - 0.1/x_5 \tag{5.12}$$

where, y_1, y_2, and y_3 denotes the density of products, Z direction compression strength, and surface evaluation respectively; y_4, y_5, and y_6 denote the dimensional difference percentage in the X, Y, Z directions.

To obtain the optimum powder mixture for 3DP process, a whole numerical objective function was proposed.

$$\min \mathrm{Y} = \alpha_1 \mathrm{y}_1 + \cdots + \alpha_n \mathrm{y}_n \tag{5.13}$$

where, Y denotes the evaluation function; $y_1,\ldots,y_n$ denote the sub-objective functions; and $\alpha_1,\ldots,\alpha_n$ denote the weights of the sub-objective functions. The weights present the relative importance of the different sub-objectives. The assistant parameter method was used to get the weights. The equality and inequality constraints of mixture considered were as given below.

$$x_1 + x_2 + x_3 + x_4 + x_5 = 100 \tag{5.14}$$

$$64 \le x_1 \le 100 \tag{5.15}$$

$$0.5 \le x_2 \le 25 \tag{5.16}$$

$$0.5 \le x_3 \le 5 \tag{5.17}$$

$$0.2 \leq x_5 \leq 1 \tag{5.18}$$

The above problem is a non-linear multi-objective optimization with equality and inequality constraints. The *f* min con function in optimization tool box of MATLAB software was used to solve the above problem. First, the weights were calculated and these were $\alpha_1 = 0.0331$, $\alpha_2 = -0.2138$, $\alpha_3 = 0.1768$, $\alpha_4 = 0.1044$, $\alpha_5 = 0.5959$, and $\alpha_6 = 0.3035$. The optimal mixture found was 82.3%, 12.3%, 0.6%, 4.6%, and 0.2%.

The Internet, incorporating computers and multimedia, has provided tremendous potential for remote integration and collaboration in business and manufacturing applications. Rapid prototyping and manufacturing (RPM) using the Internet can further enhance the design and manufacturing productivity, speed, and economy, as well as share the RP machines. Web-based RPM systems have been developed and employed to implement remote service and manufacturing for RP, enhance the availability of RPM facilities and improve the capability of rapid product development for a large number of small- and medium-sized enterprises. Lan [19] provided a comprehensive review of research on web-based RPM systems. Various architectures proposed for web-based RPM systems were presented. Furthermore, some key issues and enabling tools to implement the remote RPM systems, which involve (1) RPM process selection, (2) RP price quotation, (3) STL Viewer, (4) RP data pre-processing, (5) job planning and scheduling, (6) remote control and monitoring for RP machines, (7) security management, and (8) applying new technologies and concepts to the systems, were described in detail. The review gives an outlook on possible future development and research direction for web-based RPM systems.

The increasing rate of transplants due to damaged or affected tissues or organs by accidents or diseases and also by the aging of the population in many countries has motivated the research of some novel and alternative ways focused on restoring and replacing tissues. Biofabrication by means of RP techniques can help in the fashioning and final production of scaffolds devoted to support and stimulate the growth of new tissues. For soft tissues, a biomaterial known as Alginate has been studied and used as raw-material for scaffold fabrication. A scaffold must guarantee good strength and stiffness at the same time the material degrades gradually. Rezende et al. [33] described a single mathematical model that describes an interesting mechanical behavior of the degradation of alginated-scaffolds. The optimization process scheme using genetic algorithms to maximize the elastic modulus and therefore to aid the design of scaffolds in alginate was proposed.

In the case of prototype manufacturing, the criteria of interest are mechanical resistance, dimensional accuracy, surface quality, cost price, manufacturing time, etc. The prototype material selection depends mostly on the functional role of the prototype and its destination. The mechanical resistance depends on type of material and type of RP system. Features such as dimensional accuracy, surface quality, cost price, and manufacturing time depend essentially on the RP system. The surface quality or surface roughness is a function of the material type used by

RP system, layer thickness, and the existence or not of supports. The existence of supports influences the post-processing time and so on. The importance is a function of the prototype purpose. Each of the above criteria may become the objective of the optimization problem. If there are several optimization criteria, then the problem is that of a multi-objective optimization problem. Ancău and Caizar [3] proposed the multicriterial optimization of RP processes. The mathematical model of the optimization problem took into consideration surface quality of the prototype and the time of manufacturing as optimization criteria. The surface quality optimization criterion evaluation was done by the number of triangular facets from the 3D model surface in STL format, which are inclined with a specific angle, and the value of the area covered by these triangular facets.

Based on the mathematical model, a practical method to find the Pareto-optimal set was developed as a main goal. To solve the optimization problem, a computer program for RP processes simulation was designed. The program calculates the geometry of successive layers, as well as the necessary time for their materialization. Depending on the importance degree of each optimization criterion, the program offers the optimal solution. In addition, the program allows the user intervention in solving the problem optimization. The authors had reported that the manufacturing time is mostly influenced by height of the model along Oz axis, but also by the size and geometry of the cross sections and the step effect affects the surface quality. Theoretical concepts of multi-criterial optimization presented in this research are useful regardless of the number of optimization criteria simultaneously considered.

The manufacturing time on SLS and LOM systems includes different components. The general equation of the total manufacturing time T is (from Ancău and Caizar [3]; reprinted with permission from Elsevier)

$$T = T_{\text{pre}} + T_{\text{pr}} + T_{\text{post}} \tag{5.19}$$

where T_{pre} is the preprocessing time; T_{pr} the processing time; and T_{post} is the post-processing time.

Ancău and Caizar [3] developed the cost models for SLS and LOM systems. They assumed that the part material is plastic, with a constant layer thickness along Oz axis. The manufacturing cost equation, given by the authors for SLS, is

$$C = C_{\text{pre}} + C_{\text{pr}} + C_{\text{post}} \tag{5.20}$$

where C_{pre} is the preprocessing cost; C_{pr} the processing cost; and C_{post} is the post-processing cost.

The preprocessing cost C_{pre} may be calculated with

$$C_{\text{pre}} = \left(T_{\text{poz}} + T_{\text{param}}\right)\left(C_{\text{oper}} + C_{\text{comp}}\right) + T_{\text{setup}} \cdot C_{\text{oper}} \tag{5.21}$$

where T_{poz} is the necessary time to scale and adjust the part position; T_{param} is the time to input the system parameters; T_{setup} the setup time; C_{oper} the operator salary ($/min); and C_{comp} is the computational cost ($/min).

$$C_{\mathrm{pr}} = \left(T_{\mathrm{heat}} + T_{\mathrm{lp}} + T_{\mathrm{cool}}\right) C_{\mathrm{SLS}} + C_{\mathrm{mat}} \tag{5.22}$$

where, T_{heat} is the time to heat up the container; T_{lp} the time for layer processing; T_{cool} the time to cool down the container; C_{SLS} the cost of SLS system utilization ($/min); and C_{mat} is the material cost ($).

The time to heat up T_{heat} is

$$T_{\mathrm{heat}} = N_{\mathrm{lb}}\left(T_{\mathrm{1layer}} + T_{\mathrm{idle1}}\right) \tag{5.23}$$

where N_{lb} is the number of layers from the base; T_{1layer} the time to make one base layer; and T_{idle1} is the idle time per layer.

$$T_{\mathrm{lp}} = N_{\mathrm{p}}\left(T_{\mathrm{zp}} + T_{\mathrm{scan}} + T_{\mathrm{idle2}}\right) \tag{5.24}$$

where, N_{p} is the part layers number; T_{zp} the time for layer deposition during the build phase; T_{scan} the time for scanning the part cross-section by laser; and T_{idle2} is the idle time per layer in the build phase ($T_{\mathrm{idle}} \geq 0$).

$$T_{\mathrm{cool}} = N_2\left(T_{\mathrm{z2}} + T_{\mathrm{idle3}}\right) \tag{5.25}$$

where, N_2 is the number of layers in the canopy; T_{z2} the time for layer deposition during the cool down phase; and T_{idle3} is the idle time per layer in the cool down phase.

$$C_{\mathrm{post}} = \left(T_{\mathrm{rp}} + T_{\mathrm{pf}}\right) C_{\mathrm{oper}} + C_{\mathrm{aux}} \tag{5.26}$$

where T_{rp} is the time to remove the part from the container; T_{pf} the necessary time for prototype finishing; and C_{aux} is the cost of additional materials needed in the post-processing phase.

In the case of LOM, the manufacturing cost C_{pr} can be expressed by the equation

$$C_{\mathrm{pr}} = T_{\mathrm{base}}\left(C_{\mathrm{LOM}} + C_{\mathrm{oper}}\right) + N_{\mathrm{p}} T_{\mathrm{layer}} C_{\mathrm{LOM}} + C_{\mathrm{mat}} \tag{5.27}$$

where, T_{base} is the time to build the part base; C_{LOM} is the cost of LOM system utilization ($/min); C_{oper} is the operator salary ($/min); N_{p} is the theoretical number of layers; T_{layer} is the sum of times for one layer construction; and C_{mat} is the material cost.

$$T_{\mathrm{layer}} = T_{\mathrm{pgu}} + T_{\mathrm{madv}} + T_{\mathrm{heater}} + T_{\mathrm{cut}} + T_{\mathrm{pgd}} \tag{5.28}$$

where, T_{pgu} is the time needed by the system platform to rise up until the working plan; T_{madv} is the time for material advance with one step; T_{heater} is the time for heater motion forward and backward, so that the current layer is joined to precedent layer; T_{cut} is the time for laser to cut inner and outer contours, crosshatches, as well as the walls of the smallest box that enclose the prototype; and T_{pgd} is the time for platform retract to ease the material advance.

After the processing of the last layer, the prototype manufacturing is considered finished, and will start the post-processing phase. The prototype will be extracted from the box and the material in excess will be removed. After this, the prototype surface may be finished, painted etc. Even if the necessary time of this phase cannot be accurately calculated, it can be estimated by taking into account the part size, its geometric complexity, and the type of finishing operation required.

Sood et al. [35] considered five important process parameters of FDM such as layer thickness, orientation, raster angle, raster width, and air gap. Their influence on three responses such as tensile, flexural, and impact strength of test specimen was studied. Experiments were conducted based on central composite design (CCD) in order to reduce experimental runs. Empirical models relating response and process parameters were developed. The validity of the models was tested using analysis of variance (ANOVA). Response surface plots for each response were analyzed and optimal parameter setting for each response was determined. The major reason for weak strength was attributed to distortion within or between the layers. Finally, concept of desirability function was used for maximizing all responses simultaneously.

Part build orientation or orientation refers to the inclination of part in a build platform with respect to X, Y, and Z axes. X and Y-axes are considered parallel to build platform and Z-axis is along the direction of part build. It was specified at three levels as 0°, 15°, and 30°. Layer thickness is the thickness of layer deposited by nozzle and depends upon the type of nozzle used and it was specified at three levels as 0.127, 0.178, and 0.254 mm. Raster angle is a direction of raster relative to the X-axis of build table and it was specified at three levels as 0°, 30°, and 60°. Part raster width (raster width) is the width of raster pattern used to fill interior regions of part curves and it was specified at three levels as 0.4064, 0.4564, and 0. 5064 mm. Raster-to-raster gap (air gap) is the gap between two adjacent rasters on same layer; it was specified at three levels as 0, 0.004, and 0.008 mm.

In order to build empirical models for tensile strength, flexural strength, and impact strength, experiments were conducted based on CCD. Half factorial 2^5 unblocked design having 16 experimental runs, 10 (2K, where $K = 5$) axial runs and six center runs was employed.

Response surface equations for tensile strength (T_S), flexural strength (F_S), and impact strength (I_S) are given by the following equations in terms of un-coded units (from Sood et al. [35]; reprinted with permission from Elsevier):

$$\begin{aligned} T_S = {} & 13.5625 + 0.7156A - 1.3123B + 0.9760C + 0.5183E + 1.1671(A \times A) \\ & - 1.3014(B \times B) - 0.4363(A \times C) + 0.4364(A \times D) - 0.4364(A \times E) \\ & + 0.4364(B \times C) + 0.4898(B \times E) - 0.5389(C \times D) + 0.5389(C \times E) \\ & - 0.5389(D \times E) \end{aligned} \tag{5.29}$$

$$F_S = 29.9178 + 0.8719A - 4.8741B + 2.4251C - 0.9096D + 1.6626E - 1.7199(A \times C) + 1.7412(A \times D) - 1.1275(A \times E) + 1.0621(B \times E) + 1.0621(C \times E) - 1.0408(D \times E) \quad (5.30)$$

$$I_S = 0.401992 + 0.034198A + 0.008356B + 0.013673C + 0.021383(A \times A) + 0.008077(B \times D) \quad (5.31)$$

where, A is the layer thickness, B is the orientation, C is the raster angle, D is the raster width, and E is the air gap.

The response surface plots involving interaction terms were studied and the reasons behind the observed response were summarized as follows:

- Number of layers in a part depends upon the layer thickness and part orientation. If number of layers is more, it will result in high-temperature gradient towards the bottom of part. This will increase the diffusion between adjacent rasters and strength will improve. But high-temperature gradient is also responsible for distortion within the layers or between the layers. Moreover, increase in number of layers also increases the number of heating and cooling cycles and thus residual stress accumulation increases. This may result in distortion, interlayer cracking, and part de-lamination or fabrication failure. Hence, strength will reduce.
- Small raster angles are not preferable as they will result in long rasters which will increase the stress accumulation along the direction of deposition resulting in more distortion and hence weak bonding. But small raster angle also means that rasters are inclined along the direction of loading and will offer more resistance; thus strength will improve.
- Thick rasters result in stress accumulation along the width of part and have a same effect as the long rasters. But this stress accumulation results in high temperature near the boding surfaces which may improve the diffusion and may result in strong bond formation.
- Zero air gap will improve the diffusion between the adjacent rasters but may also decrease the heat dissipation as well as total bonding area.

To determine the optimal setting of process parameters that will maximize the tensile strength, flexural strength, and impact strength, respectively, desirability function (DF) was used.

$$\mathrm{DF} = \left(\prod_{i=1}^{n} d_i^{\mathrm{wi}} \right)^{1/p} \quad (5.32)$$

$$\text{where, } p = \left(\sum_{i=1}^{n} \text{wi} \right) \tag{5.33}$$

where, d_i is the desirability defined for the ith targeted output. For a goal to find a maximum, d_i is calculated as shown below.

$$d_i = 0, \quad \text{if } Y_i \leq \text{low}_i \tag{5.34}$$

$$d_i = ((Y_i - \text{low}_i)/(\text{High}_i - \text{low}_i)), \text{ if } \text{low}_i < Y_i < \text{High}_i \tag{5.35}$$

$$d_i = 1, \quad \text{if } Y_i \geq \text{High}_i \tag{5.36}$$

where, Y_i is the found value of the ith output during optimization process, and the low_i, High_i are the minimum and maximum values, respectively of the experimental data for the ith output. Since all the strengths were considered as equally important. Optimum factor levels that maximize the desirability function were calculated for respective strength together with its predicted value. The combined desirability function when all three responses were maximized simultaneously was also evaluated and the optimum factor levels were found.

Optimal factor setting for tensile and flexural strength was same, but it differed in factor levels of orientation and raster angle for impact strength. As far as simultaneous optimization of three strengths was considered, the factor levels were completely different from individual optimal factor setting. The study can be extended to reduce void formation and distortion and improve inter-laminar bonding. This study can also be extended in the direction of more complicated loading states, such as fatigue and vibration analysis.

RP is changing the way companies design and build products. Rapid prototyping has developed into three primary technological and application areas: concept modeling, rapid prototyping for fit, and function applications, and rapid manufacturing. It is believed that these three forms of free-form fabrication will grow exponentially over time. To achieve this growth, several technological developments related to materials, capacities of the RP machines, prototyping speed, and cost are needed.

References

1. Ahn SH, Montero M, Odell D, Roundy S, Wright PK (2002) Anisotropic material properties of fused deposition modeling ABS. Rapid Prototyp J 8(4):248–257
2. Allen S, Dutta D (1994) On the computation of part orientation using support structures in layered manufacturing. Technical report UM-MEAM-TR-94-15. Dept Mech Eng, Univ Michigan, Ann Arbour
3. Ancău M, Caizar C (2010) The computation of Pareto-optimal set in multicriterial optimization of rapid prototyping processes. Comput Ind Eng. doi:10.1016/j.cie.2010.01.015
4. Byun HS, Lee KH (2006) Determination of the optimal build direction for different rapid prototyping processes using multi-criterion decision making. Rob Comput Integr Manuf 22(1):69–80

5. Canellidis V, Giannatsis J, Dedoussis V (2009) Genetic-algorithm-based multi-objective optimization of the build orientation in stereolithography. Int J Adv Manuf Technol 45 (7–8):714–730
6. Chen CC, Sullivan PA (1996) Predicting total build-time and the resultant cure depth of the 3D stereolithography process. Rapid Prototyp J 2(4):27–40
7. Cheng W, Fuh JYH, Nee AYC, Wong YS, Loh HT, Miyazawa T (1995) Multi-objective optimization of part-building orientation in stereolithography. Rapid Prototyp J 1(4):12–23
8. Chockalingam K, Jawahar N, Ramanathan KN, Banerjee PS (2006) Optimization of stereolithography process parameters for part strength using design of experiments. Int J Adv Manuf Technol 29(1–2):79–88
9. Choi SH, Samavedam S (2002) Modeling and optimization of rapid prototyping. Comput Ind 47(1):39–53
10. Frank D, Fadel G (1995) Expert system-based selection of the preferred direction of build for rapid prototyping processes. J Intell Manuf 6(5):339–345
11. Grujicic M, Hu Y, Fadel GM, Keicher DM (2001) Optimization of the LENS rapid fabrication process for in-flight melting of feed powder. J Mater Synth Process 9(5):223–233
12. Haipeng P, Tianrui Z (2007) Generation and optimization of slice profile data in rapid prototyping and manufacturing. J Mater Process Technol 187(188):623–626
13. Hardjadinata G, Doumanidis CC (2001) Rapid prototyping by laser foil bonding and cutting: thermomechanical modeling and process optimization. J Manuf Process 3(2):108–119
14. Harris R, Hopkinso N, Newlyn H, Hague R, Dickens P (2002) Layer thickness and draft angle selection for stereolithography injection mould tooling. Int J Prod Res 40(3):719–729
15. Hu Z, Lee K, Hur J (2002) Determination of optimal build orientation for hybrid rapid-prototyping. J Mater Process Technol 130–131:378–383
16. Hur J, Lee K (1998) The development of a CAD environment to determine the preferred build-up direction for layered manufacturing. Int J Adv Manuf Technol 14:247–254
17. Khan ZA, Lee BH, Abdullah J (2005) Optimization of rapid prototyping parameters for production of flexible ABS object. J Mater Process Technol 169:54–61
18. Kim JY, Lee K, Park JC (1994) Determination of optimal part orientation in stereolithographic rapid prototyping. Technical report, Dept Mech Des Prod Eng, Seoul Nat Univ, Seoul
19. Lan H (2009) Web-based rapid prototyping and manufacturing systems: a review. Comput Ind 60(9):643–656
20. Lan PT, Chou SY, Chent LL, Gemmill D (1997) Determining fabrication orientations for rapid prototyping with stereolithography apparatus. Comput Aided Des 29(1):53–62
21. Lee BH, Abdullah J, Khan ZA (2005) Optimization of rapid prototyping parameters for production of flexible ABS object. J Mater Process Technol 169(1):54–61
22. Lee CS, Kim SG, Kim HJ, Ahn SH (2007) Measurement of anisotropic compressive strength of rapid prototyping parts. J Mater Process Technol 187–188:627–630
23. Li X (2009) Multi-object optimal design of rapid prototyping based on uniform experiment. Tsinghua Sci Technol 14(1):206–211
24. Majumdar JD, Pinkerton A, Liu Z, Manna I, Li L (2005) Microstructure characterisation and process optimization of laser assisted rapid fabrication of 316L stainless steel. Appl Surf Sci 247(1–4):320–327
25. Masood SH, Rattanawong W, Iovenitti P (2003) A generic algorithm for a best part orientation system for complex parts in rapid prototyping. J Mater Process Technol 139 (1–3):110–116
26. Nagahanumaiah, Subburaj K, Ravi B (2008) Computer aided rapid tooling process selection and manufacturability evaluation for injection mold development. Comput Ind 59(2–3): 262–276
27. Nyaluke A, Nasser B, Leep HR, Parsaei HR (1996) Rapid prototyping work space optimization. Comput Ind Eng 31(1–2):103–106
28. Oudjene M, Penazzi L, Batoz JL (2007) Towards the three-dimensional FE analysis of rapid prototyping tools for sheet metal stamping process. Finite Elem Anal Des 43(8):611–619

29. Oudjene M, Batoz JL, Penazzi L, Mercier F (2007) A methodology for the 3D stress analysis and the design of layered sheet metal forming tools joined by screws. J Mater Process Technol 189(1–3):334–343
30. Pandey PM, Reddy NV, Dhande SG (2003a) Real time adaptive slicing for fused deposition modelling. Int J Mach Tools Manuf 43(1):61–71
31. Pandey PM, Reddy NV, Dhande SG (2003b) Improvement of surface finish by staircase machining in fused deposition modeling. J Mater Process Technol 132(1–3):323–331
32. Pham DT, Dimov DT, Gault RS (1999) Part orientation in stereolithography. Int J Adv Manuf Technol 15:674–682
33. Rezende R, Rezende M, Bártolo P, Mendes A, Filho RM (2009) Optimization of scaffolds in alginate for biofabrication by genetic algorithms. Comput Aided Chem Eng 27:1935–1940
34. Rozman R, Kmetec B, Podobnik B, Kovačič D, Govekar E (2008) Optimization of direct laser structuring of printed circuit boards. Appl Surf Sci 254(17):5524–5529
35. Sood AK, Ohdar RK, Mahapatra SS (2010) Parametric appraisal of mechanical property of fused deposition modeling processed parts. Mater Des 31(1):287–295
36. Sreeram PN, Dutta D (1994) Determination of optimal orientation based on variable slicing thickness in layered manufacturing. Technical report UM-MEAM-TR-94-14. Dept Mech Eng, Univ Michigan, Ann Arbour
37. Steen WM (1998) Laser material processing. Springer-Verlag, Berlin
38. Vosniakos GC, Maroulis T, Pantelis D (2007) A method for optimizing process parameters in layer-based rapid prototyping. Proc Inst Mech Eng Part B J Eng Manuf 221(8):1329–1340
39. Williams RE, Komaragiri SN, Melton VL, Bishu RR (1996) Investigation of the effect of various build methods on the performance of rapid prototyping (stereolithography). J Mater Process Technol 61(1–2):173–178
40. Xiaomin C, Feng C, Wei Y (2006) Prototyping direction optimization of points data oriented rapid prototyping based on genetic algorithm. In: Wang ED (ed) Simulated evolution and learning. Springer-Verlag, Berlin
41. Yang Y, Fuh JYH, Loh HT, Wong YS (2003) Multi-orientational deposition to minimize support in the layered manufacturing process. J Manuf Syst 22(2):116–129
42. Zhang X, Zhou B, Zeng Y, Gu P (2002) Model layout optimization for solid ground curing rapid prototyping processes. Rob Comput Integr Manuf 18(1):41–51
43. Zhou JG, Herscovici D, Chen CC (2000) Parametric process optimization to improve the accuracy of rapid prototyped stereolithography parts. Int J Mach Tools Manuf 40(3):363–379

Chapter 6
Environmental Aspects of Manufacturing Processes

6.1 Environmentally Conscious Manufacturing

Nowadays, ever-increasing environmental problems are becoming a serious threat to the survival and development of society. After the publishing of ISO 9000 quality management standards, the ISO 14000 environmental management system standards, and the OHSAS 18001 occupational health and safety assessment series, one of our greatest strategic challenges is to apply the three series integrated into a management system in enterprises, not only from an engineering but also from a business and marketing perspective. The manufacturing industry is one of the main roots of environmental pollution. Therefore, minimizing the environmental impact of the manufacturing industry has become an important topic for all manufacturers. During these critical times, an advanced manufacturing mode, green manufacturing, suitable for a sustainable development strategy has been presented.

There is a growing interest in green manufacturing [also called environmentally conscious manufacturing (ECM)]. The current focus on green manufacturing is different from the traditional focus on pollution control. Here, the emphasis is on life cycle assessment (LCA). Products or processes are seen as interacting with the environment, and could have chain reaction effects on environmental pollution. Thus, rather than looking at any product or process in isolation, the manufacturer needs to adopt a cradle-to-grave approach for the product or process. For example, how much energy is expended in unit product manufacturing, how much resources are used, how much waste is created, and what are the product requirements for transportation and distribution? These are not issues that product designers are accustomed to considering. Their traditional role has been to look at the product on its own, and design products that meet specific guidelines and that may become environmental pollution laws. Today's focus is different. Manufacturers must take a product stewardship approach, and this will predict their survival in today's competitive environment [33].

R. V. Rao, *Advanced Modeling and Optimization of Manufacturing Processes*,
Springer Series in Advanced Manufacturing, DOI: 10.1007/978-0-85729-015-1_6,

Industrial economies have generated a tremendous amount of waste that is often not reused or properly disposed. Industrial societies are increasingly faced with the problems of hazardous waste management, locating new landfills, and the depletion of raw materials. Rather than continuing with this cycle of waste and extravagance, industrial economies should find better ways to convert wastes from one industry into input in another industry. This implies interdependence between industries, where one industry's output could become another's input. This cycle of dependence or reuse of material is generally referred to as recycling, and its goal is to eliminate or reduce waste.

The manufacturing industries must seek to minimize environmental impact and resource consumption during the entire product cycle. Industrial risk and the diversification of risk types have both increased with industrial development. At the same time, the risk acceptability threshold of the population has decreased. In response, industry has developed methodologies for risk prevention and protection [55]. Green manufacturing was first proposed about 15 years ago, so there are only few examples that can be used to evaluate risks, and many uncertain factors. Because of this incomplete and uncertain knowledge, decision-making methods based on probabilities to represent risk, which need many examples, cannot be used for green manufacturing projects [22]. In addition, green manufacturing involves a very wide range of topics, such as environmental consciousness, life cycle thinking, and sustainable development, which all increase the risk. Therefore, risk decision-making in green manufacturing projects must consider multiple indicators. Hua et al. [22] reported that industries are implementing green manufacturing projects for sustainable production for four types of risk categories: technological, organizational, financial and circumstantial. Each category is related to certain risk factors. These risks are described below:

- Technological risk—since the concept of green manufacturing is relatively new, its theories and technologies are still being developed. Only experience will show whether, or not, each technology can be used in green manufacturing projects to create extended benefits for industry, society, and in ecology. Therefore, there are many technological risk factors, including reliability, maintenance, and applicability.
- Organizational risk—green manufacturing is a new manufacturing mode with the product cycle extending to the entire product life (raw materials, production, use, recycling, and disposal), so traditional management methods are not suitable. Therefore, the management system must be reformed to successfully implement green manufacturing, which will lead to unpredictable risks. The main organizational risk factors are the integration of the management approach, the knowledge level of the lead group, and the knowledge level of the personnel.
- Financial risk—green manufacturing projects require a very long investment period due to the length of the entire product cycle, which increases the risk. Corporate income is gained by saving energy and materials, protecting the environment and workers, improving productivity and product quality, reducing costs, and by accurate market timing.

- Circumstantial risk—green manufacturing projects are constrained not only by internal resources, but also by external resources. Many uncertain circumstantial factors can cause critical risks and such external factors include laws, regulations, macro-economic changes, and industrial development.

Almost every function within organizations has been influenced by external and internal pressures to become environmentally sound. Issues, such as green consumerism and green product development have impacted marketing. Finance, information systems and technology, human resources and training, engineering and research, and development are all organizational functions that have been influenced by these environmental pressures. One of the functions that has been profoundly influenced by environmental pressures is the organizational operations and manufacturing function. The traditional reactive responses to these pressures are now being supplemented and replaced by more proactive, strategic, competitive responses. The research topics on ECM programs have focused on managerial practices, business processes, and technology. ECM programs include proactive measures, such as life cycle analysis of products, design for the environment, design for disassembly, total quality environmental management, remanufacturing, ISO14000 certification, and green supply chains. Each of these programs crosses inter- and intra-organizational boundaries. These programs work hand in hand with other environmental alternatives, such as development of environmental management systems, and green purchasing [40, 46]. Fei et al. (2005) presented the green manufacturing problem framework of machining systems. A series of investigations and practices on green manufacturing in machining system, performed by the authors for quite a long period, were introduced in brief, such as the optimizing system for raw material cutting, the matching system for energy saving in machining, the design of highly efficient dry hobbing machine tools, the multi-objective decision-making model for green manufacturing in machining systems, and the decision-making supporting system for green manufacturing in machining processes.

Pusavec et al. [38, 39] presented general issues, methods and a case study for achieving production sustainability on a machining technology level. To tackle these issues, the authors promoted the concept of sustainable production via the alternative machining technologies, namely cryogenic and high-pressure jet-assisted machining that have a high potential to cut costs and improve competitiveness by reducing resource consumption and thus creating less waste. The authors opined that the future of sustainable production is going to entail the use of alternative machining technologies to reduce consumption rates, environmental burdens and health risks simultaneously, while increasing performances and profitability. A case study of machining high-temperature Ni-alloy (Inconel 718) had shown that tooling costs represent the major contribution to the overall production cost, which contradicts previous analyses, and that sustainable machining alternatives offer a cost-effective route to improve economic, environmental, and social performance in comparison to conventional machining.

Achieving sustainability in manufacturing requires a holistic view spanning not just the product, and the manufacturing processes involved in its fabrication, but also the entire supply chain, including the manufacturing systems across multiple product life cycles. This requires improved models, metrics for sustainability evaluation, and optimization techniques at the product, process, and system levels. Jayal et al. [24] presented an overview of recent trends and new concepts in the development of sustainable products, processes and systems. Recent trends in developing improved sustainability scoring methods for products and processes, and predictive models and optimization techniques for sustainable manufacturing processes, focusing on dry, near-dry and cryogenic machining as examples, were described.

Now the concept of environmental conscious manufacturing is presented using environment-friendly machining as an example. Machining is one of the most important and major manufacturing processes, and it is estimated that machining processes contribute about 5% of the GDP in the developed world. The indirect impact of machining, due to its effect on surface integrity, and hence on product life, is even greater. Moreover, as economic factors induce shorter product cycles, and more flexible manufacturing systems, the importance of machining is expected to increase even further.

6.2 Environment-friendly Machining

The heat is generated in metal cutting operations due to plastic deformation of work materials, friction at the tool–chip interface, and friction between the clearance face of the tool and the work piece. The heat generation increases the temperature of both the work piece and the tool point, resulting in decrease in hardness, and hence tool life. The machined surface will also be less smooth, and the possibility of built-up edge increases. Therefore, the use of a cutting fluid during a machining operation is very essential. The major factors that govern the selection of cutting fluids are: (1) the machining process, (2) cutting tool material, and (3) work piece material. Other factors, such as compatibility with the machine tool, performance requirements, operator interaction, environment friendliness, and economy must also be looked into.

6.2.1 Dry Machining

Machining of materials without using any cutting fluids is called dry machining. However, in most of the cases, a machining operation without cutting fluid will be acceptable only if it is possible to guarantee that this equals or surpasses the part quality and machining times achieved in wet machining. The introduction of dry machining requires suitable measures to compensate for the primary functions of the cutting fluid. But this, in turn, calls for a very detailed analysis of the boundary

conditions and for thorough understanding of the complex interrelationships which link the process, tool, part and machine tool. Klocke and Eisenblatter [25] presented a wide range of examples of successful implementation of dry machining of cast iron, steel, aluminum and even super alloys and titanium. The introduction of dry cutting techniques may also include, MQL e.g. milling and drilling of aluminum alloys, to achieve part quality and machining times comparable with wet cutting. In practice, dry machining is only practical when all operations can be done dry. Very often, this is not the case under present conditions. Appropriate action, therefore, has to be taken to further improve the technology of dry cutting.

Sreejith and Ngoi [50] presented a state-of-art and the recent advancements in dry machining. Dry machining is only possible when all the operations can be done dry. Technology has to be further improved if dry cutting is to be fully employed in industries. Kirillov et al. [27] considered the basic aspects of dry cutting of hard-to-machine materials, with compensation of the physical functions of the lubricant and coolant fluids and such compensation measures include the use of a hard-alloy tool with a multifunctional multilayer nanostructural alloy; a system for ionizing the gas supplied to the cutting zone; and a device for generating tangential ultrasound waves applied to the cutting tool.

Dudzinski et al. [12] presented advances concerning dry and high-speed machining of Inconel 718. Some solutions to reduce the use of coolants were explored, and different coating techniques to enable a move towards dry machining were examined. In dry machining, the positive effects of coolants have to be obtained by another way. For the removal of chips from cutting zone, heat evacuation must be guaranteed. The process must preserve an acceptable surface integrity. Tools with high hot hardness, high refractivity, low adhesion and low friction properties are required. Oxide PVD-coatings combine a reduction of friction at elevated temperature with high wear resistance, and show excellent performance during drilling high strength materials. Solid lubricants, such as MoS_2/titanium composite coatings or WC/C coatings give useful results when machining Inconel 718 under dry conditions.

Experiments and machining simulation have to work together to find a way to the dry cutting of Inconel 718. The objective is to find the suitable tool and appropriate coating to define the better geometrical tool configuration and the optimal cutting conditions to obtain more acceptable surface integrity and the longer tool life.

Chiou et al. [8] investigated the performance of a cutting tool embedded with a heat pipe on reducing cutting temperature and wear in machining. An embedded heat pipe technology was developed to effectively remove the heat generated at the tool–chip interface in machining, thereby, reducing tool wear and prolonging tool life. In particular, the technique can effectively minimize pollution and contamination of the environment caused by cutting fluids, and the health problems of skin exposure and particulate inhalation in manufacturing. The ANSYS finite element analysis simulations showed that the temperature near the cutting edge drops significantly with an embedded heat pipe during machining. Experiments were carried out to characterize the temperature distributions when performing turning

experiments using a cutting tool installed with an embedded heat pipe. The performance of the heat pipe on reducing the cutting tool temperature was further supported by the observations of cutting tool material color, chip color, and the chip radius of curvature.

Marksberry and Jawahir [34] presented a new method to predict tool-wear/tool-life performance in near-dry machining (NDM) by extending a Taylor speed-based dry machining equation. Experimental work and validation of the model was performed in an automotive production environment in the machining of steel wheel rims. Tool wear measurements obtained during the validation of the model showed that NDM can improve tool-wear/tool-life over four times compared to dry machining.

6.2.2 Cryogenic Machining

Cryogenic cooling in metal cutting has been studied nearly for six decades, however, many of the studies and most remarkable of them particularly in terms of application methods have been done in last decade and striking results have been achieved. Cryogenic cooling is still attractive and has been examined in material cutting field. Almost all type of materials from ductile to hard and brittles have been machined in cryogenic cooling studies by many cutting tools. However, different kinds of steels were used widely in tests; non-ferrous metals, non-metallic and composite materials should be examined more. In addition, most of the studies have included turning operations. Other machining operations such as milling and drilling could be attempted more with cryogenic cooling. When compared with dry cutting and conventional cooling, the most considerable characteristics of the cryogenic cooling application in machining operations could be determined as enabling substantial improvement in tool life and surface finish-dimensional accuracy through reduction in tool wear through control of machining temperature desirably at the cutting zone.

Cryogenic machining imparts several improvements that can be categorized as: (1) environmentally friendly and safe: Nitrogen is a non-hazardous gas that constitutes 79% of atmospheric air; (2) increased productivity: both hardness and toughness of cutting tool materials have been shown to increase under cryogenic cooling, allowing increased material removal rates. Tool wear was also observed to be uniform and predictable, (3) improved surface quality: cryogenically machined powder metal and hardened steel parts showed reduced surface and subsurface damage, and improved fatigue resistance. Compressive residual stresses and white layer characteristics have also been shown to improve with cryogenic cooling, (4) step reduction and process change: cryogenic cooling results in more economical machining in the fully heat-treated condition for most PM parts, allowing intermediate heat-treating steps to be eliminated. For hard materials, cryogenic cooling may also enable a process change from slow grinding to a faster hard turning process.

Cryogenic cooling has been executed in cutting operations in different ways using liquid nitrogen for pre-cooling the workpiece, cooling the chip, cooling the cutting tool and cutting zone. Cutting tool and cutting zone have been cooled cryogenically by heat transmission, general repulsing of the coolant to the cutting zone and spraying in jets with nozzles too. Cold temperatures were also used for strengthening of the cutting tools by cryogenic treatment. Many studies have been done to explore the most efficient one. In these studies, comparisons have been made between conventional cutting strategies and cryogenic cooling methods, however, opposite outcomes have been proved by the researchers, such as producing of the LN2 jet application was the best results, providing of indirect cryogenic cooling better performance than LN2 sprays and being cooling of the tool more significant than the cooling of workpiece at high-cutting speeds in cryogenic machining and the opposite claim at low-cutting speeds regarding of tool life.

Hong et al. [21] reviewed how the temperature affects Ti-6Al-4V properties, and compared different cryogenic cooling strategies. Based on these findings, a new economical cryogenic cooling approach was proposed. Using a minimum amount of liquid nitrogen (LN2), this innovation featured a specially designed micro-nozzle. Formed between the chip breaker and the tool rake face, the nozzle lifts the chip and injects focused LN2 into the chip–tool interface at the point of highest temperature. As the nitrogen evaporates, a nitrogen cushion formed by evaporating nitrogen lowers the coefficient of friction between the chip and the tool. An auxiliary mini-nozzle that sprays LN2 onto the flank at the cutting edge further reduces the cutting temperature. The study found that the combination of these two micro-nozzles provides the most effective cooling while using the lowest LN2 flow rate. The cryogenic machining tests showed that tool life increases up to five times the state-of the-art emulsion cooling, outperforming other machining approaches.

Paul et al. [37] conducted experimental investigation in the role of cryogenic cooling by liquid nitrogen jet on tool wear and surface finish in plain turning of AISI 1060 steel at industrial speed-feed combination by two types of carbide inserts of different geometric configurations. The results were compared with dry machining and machining with soluble oil as coolant. The results indicated substantial benefit of cryogenic cooling on tool life and surface finish. This was attributed to mainly reduction in cutting zone temperature and favorable change in the chip–tool interaction. Further, it was evident that machining with soluble oil cooling failed to provide any significant improvement in tool life, rather surface finish was deteriorated. Dhar et al. [10] investigated the role of cryogenic cooling by liquid nitrogen jet on average chip–tool interface temperature, tool wear, dimensional accuracy and surface finish in turning AISI 4140 steel under industrial speed–feed conditions.

De Chiffre et al. [9] carried out experimental investigations in which the efficiency of cryogenic CO_2 was compared with that of a commercial water-based product with respect to tool life, cutting forces, chip disposal and workpiece surface finish. The experimental results showed that CO_2 applied at a rate of about

6 g/s is an efficient coolant for threading as well as for parting/grooving stainless steel. Threading can be carried out with gas alone but the best performance was obtained adding 6 ml/min unadditivated vegetable oil to the gas. In the case of parting/grooving, addition of oil (10 ml/min) to the gas is mandatory.

Dhar and Kamruzzman [11] dealt with experimental investigation in the role of cryogenic cooling by liquid nitrogen jet on cutting temperature, tool wear, surface finish and dimensional deviation in turning of AISI 4037 steel at industrial speed–feed combination by coated carbide insert. The results were compared with dry machining and machining with soluble oil as coolant. The results of the work indicated substantial benefit of cryogenic cooling on tool life, surface finish and dimensional deviation. This was attributed mainly to the reduction in cutting zone temperature and favorable change in the chip–tool interaction. Further, it was evident that machining with soluble oil cooling failed to provide any significant improvement in tool life, rather surface finish was deteriorated.

Kumar and Choudhury [28] conducted experimental study of the effect of cryogenic cooling on tool wear and high-frequency dynamic cutting forces generated during high-speed machining of stainless steel. Experiments were carried out both in dry and cryogenic conditions as per design of experiments to understand the relative advantage offered by cryogenic cooling. It was found from the experimental results that cryogenic cooling was effective in bringing down the cutting temperatures that attributed for the substantial reduction in the flank wear (37.39%) and such input parameters as speed, feed and depth of cut were correlated with output parameters, namely cutting force and flank wear through a regression equation. It was concluded that cryogenic cooling is a possible answer for high-speed environment-friendly machining.

Firouzdor et al. [14] studied the influence of deep cryogenic treatment on wear resistance and tool life of M2 HSS drills in high-speed dry drilling configuration of carbon steels. The experimental results indicated 77 and 126% improvement in cryogenic-treated and cryogenic- and temper-treated drill lives, respectively. The results of wear rate test were in agreement with drill life test. Chemical composition of chips were also reported to show the onset of seizure in drilling test and the consequence of seizure in promoting dissolution wear by diffusion mechanism. Wear resistance improvement was mainly attributed to the resistance of cryogenically treated drills against diffusion wear mechanism, due to the formation of fine and homogeneous carbide particles during cryogenic treatment. In addition, transformation of retained austenite to martensite played an effective role, i.e. improved hardness values.

Aggarwal et al. [2] optimized multiple characteristics (tool life, cutting force, surface roughness and power consumption) in CNC turning of AISI P-20 tool steel using liquid nitrogen as a coolant. Four controllable factors of the turning process viz. cutting speed (A), feed (B), depth of cut (C) and nose radius (D) were studied. The ranges of A, B, C and D were 120–200 m/min, 0.10–0.14 mm/rev, 0.2–0.5 mm, and 0.4–1.2 mm respectively. Face centered central composite design was used for experimentation. Response surface methodology was used for

modeling the responses. The responses were consequently expressed in the form of regression equations as follows:

$$\begin{aligned}\text{Cutting force} = {} & -220.74 - 5.16A + 9507.92B + 470.92C - 23.24D + 4.41AB \\ & + 0.51AC - 1483.54BC + 0.01A^2 - 34885.52B^2 - 172.63C^2 \\ & + 17.34D^2 \pm 8.26 \end{aligned} \tag{6.1}$$

$$\begin{aligned}\text{Tool life} = {} & 80.85 - 0.19A + 98.14B - 12.78C - 0.38D + 0.08AB - 1048.38B^2 \\ & - 14.69C^2 \pm 0.083 \end{aligned} \tag{6.2}$$

$$\begin{aligned}\text{Surface roughness} = {} & 6.97 - 4.41E - 003A - 101.62B - 1.08C - 0.21D + 7.29e \\ & - 003AC + 4.58BC - 2.03BD + 446.77B^2 + 0.05D^2 \\ & \pm 2.083e - 003 \end{aligned} \tag{6.3}$$

$$\begin{aligned}\text{Power consumption} = {} & 320.92 + 3.33A - 7888.88B - 51.85C + 161.11D \\ & - 6.25AB + 8.33AC + 54166.66B^2 \pm 533.33 \end{aligned} \tag{6.4}$$

The high value of coefficient of determination indicated that the model adequately explained the CNC turning process. The models were adequate, but it would become very cumbersome to determine the optimal value using this technique. Desirability function was thus used to overcome this problem. Desirability function was used for single and multiple response optimization.

Yildiz and Nalbant [58] investigated liquid nitrogen as a cryogenic coolant in terms of application methods in material removal operations and its effects on cutting tool and workpiece material properties, cutting temperature, tool wear/life, surface roughness and dimensional deviation, friction and cutting forces. As a result, cryogenic cooling has been determined as one of the most favorable method for material cutting operations due to being capable of considerable improvement in tool life and surface finish through reduction in tool wear through control of machining temperature desirably at the cutting zone.

Reddy et al. [44] conducted machining studies on C45 workpiece using both untreated and deep cryogenic-treated tungsten carbide cutting tool inserts. The machinability of the C45 steel workpiece was evaluated in terms of flank wear of the cutting tool inserts, main cutting force and surface finish of the machined workpieces. The flank wear of deep cryogenic-treated carbide tools was lower than that of untreated carbide tools on machining of C45 steel. The cutting force during machining of C45 steel was lower with the deep cryogenic-treated carbide tools when compared with the untreated carbide tools. The surface finish produced on machining the C45 steel workpiece was better with the deep cryogenic treated carbide tools than when compared with the untreated carbide tools.

El-Tayeb et al. [13] investigated the potential of cryogenic effect on frictional behavior of a newly developed titanium alloy Ti–5Al–4V–0.6Mo–0.4Fe (Ti54) sliding against tungsten carbide and compared with conventional titanium alloy

Ti6Al4V (Ti64). Four models were developed to describe the interrelationship between the friction coefficient (response) and independent variables such as speed, load, and sliding distance (time). These variables were investigated using the design of experiments and utilization of the response surface methodology (RSM). Using this method, it was possible to study the effect of main and mixed (interaction) independent variables on the friction coefficient (COF) of both titanium alloys. Under cryogenic condition, the friction coefficient of both Ti64 and Ti54 behaved differently, i.e. an increase in the case of Ti64 and decrease in the case of Ti54. For Ti64, at higher levels of load and speed, sliding in cryogenic conditions produced relatively higher friction coefficients when compared with those obtained in dry air conditions. In contrast, introduction of cryogenic fluid reduced the friction coefficients of Ti54 at all tested conditions of load, speed, and time.

By using the factorial design, a total of 17 experiments were conducted and regression coefficients were calculated. The full models for average friction coefficients of Ti64 and Ti54 for each sliding condition, i.e. dry and cryogenic, were obtained as shown below.

- For dry friction coefficient of Ti64D:

$$\mathrm{COF_{D64}} = 0.5694 + 0.0122\mathrm{S} + 0.0422\mathrm{L} + 0.0139\mathrm{T} - 0.0184\mathrm{L}^2 - 0.0074\mathrm{T}^2 - 0162\mathrm{S} \tag{6.5}$$

- For cryogenic friction coefficient of Ti64C

$$\mathrm{COF_{C64}} = 0.5069 + 0.0395\mathrm{S} + 0.0377\mathrm{L} + 0.015\mathrm{T} + 0.045\mathrm{LT} \tag{6.6}$$

- For dry friction coefficient of Ti54D

$$\mathrm{COF_{D54}} = 0.5841 + 0.037\mathrm{S} + 0.0451\mathrm{L} + 0.016\mathrm{T} - 0.0264\mathrm{L}^2 + 0.034\mathrm{SL} + 0.0446\mathrm{LT} \tag{6.7}$$

- For cryogenic friction coefficient of Ti54C

$$\mathrm{COF_{C54}} = 0.4581 + 0.0582\mathrm{S} + 0.0549\mathrm{L} - 0.0112\mathrm{T} - 0.0185\mathrm{L}^2 - 0.0235\mathrm{T}^2 \tag{6.8}$$

where S sliding speed (m/s), $L = 2 \times$ normal load (N), and $T = 3 \times$ sliding time (min).

It should be noted that the above equations are valid over the range of tested conditions $0.1295 <$ speed < 0.9705 m/s; $6.464 <$ load < 22.956 N; $2.636 <$ sliding time < 9.364 s for sliding the titanium alloys (Ti64D, Ti64C, Ti54D, and Ti54C) on counterface of tungsten carbide. The established models indicated that interaction of loads and speeds was more effective for both Ti-alloys, and have the most substantial influence on the friction. In addition, coefficient of friction (COF) for both alloys behaved linearly with the speed, but non-linearly with the load.

Abdulkareem et al. [1] studied the cooling effect of copper electrode on the die-sinking of electrical discharge machining of titanium alloy (Ti-6Al-4V). Investigation on the effect of cooling on electrode wear and surface roughness of the workpiece was carried out. Design of experiment plan for rotatable central composite design of second order with four variables at five levels each was employed to carry out the investigation. Current intensity (I), pulse on-time (t_{on}), pulse off-time (t_{off}), and gap voltage (v) were considered as the machining parameters, while electrode wear and surface roughness were the responses. The analysis of the influence of cooling on the responses was carried out and presented. It was possible to reduce electrode wear ratio up to 27% by electrode cooling. Surface roughness was also reduced while machining with electrode cooling. After the EDM of titanium alloy with and without liquid nitrogen using copper electrodes, it was observed that the liquid nitrogen reduces the temperature of copper electrode thereby minimizes its melting and vaporization and the cooling effect of liquid nitrogen improves the electrical and thermal conductivities of copper. It was also observed from the experimental results that irrespective of the values of the machining parameters used, there was a reduction in wear of electrode and surface roughness was smoother during the EDM of titanium alloy with liquid nitrogen.

Li et al. [31] studied the effect of deep cryogenic treatment (DCT) on the microstructure and properties (hardness, toughness and the content of retained austenite) of a new developed cold work die steel (Cr8Mo2SiV). The execution of the DCT in different processes showed a varying effect on materials. It was shown that the hardness of the DCT specimens was higher (+0.5HRC to +2HRC), whereas the toughness was lower when compared with the conventionally treated specimens (quenching and tempering).

Gill et al. [16] reviewed the cryoprocessing aspects of the cutting tools. Cryoprocessing, a supplementary process to conventional heat treatment process, is the process of deep-freezing materials at cryogenic temperatures to enhance the mechanical and physical properties of materials being treated. The execution of cryoprocessing on cutting tool materials increases wear resistance, hardness, and dimensional stability and reduces tool consumption and down time for the machine tool set up, thus leading to cost reductions. The three most significant parameters of cryoprocessing identified as primarily affecting the wear resistance/tool life were soaking temperature, soaking period, and cooling rate. However, these treatment parameters need to be optimized with respect to tool material and type of machining process. Determination of appropriate levels of the above parameters will result in maximum wear resistance as well as save time and energy involved in the process. The effects of cryoprocessing on tool steels and carbides, metallurgical aspects including reduced amount of retained austenite, precipitation of η-carbides, phase change in carbides, improvement in wear resistance, and applications were reviewed for manufacturing industry. The improvement in wear resistance and hardness by cryoprocessing was attributed to the combined effect of conversion of retained austenite to martensite and precipitation of η-carbides in case of tool steels. The phenomenon responsible for improved wear resistance in carbide cutting tools is the combined effect of increased number of η phase

particles and increase in bounding strength of binders used. Although it was confirmed that cryogenic processing can improve the service life of tools, the degree of improvement experienced and the underlying mechanism remains ambiguous. The steps involved in cryoprocessing are critical enough to account for the significant incongruity in post-treated performance.

Sharma et al. [48] presented an overview of major advances in techniques as minimum quantity lubrication (MQL)/near-dry machining (NDM), high-pressure coolant (HPC), cryogenic cooling, compressed air cooling and use of solid lubricants/coolants. A brief survey of modeling/FEA techniques was also performed and the following observations were made (from [48]; reprinted with permission from Elsevier).

- The application of cryogenic cooling for turning of difficult to cut materials has resulted in several fold increase in tool life without compromising on the environmental conditions. Tool life improves dramatically due to the fact that cryogenic fluid is able to penetrate the chip–tool interface and perform both lubrication and cooling functions satisfactorily, but cooling function in particular. Productivity is also high as cryogenic cooling shows better results at higher feed rates.
- With the MQL/NDM technique, there can be a remarkable reduction in machining cost, quantity of lubricant used and surface roughness by properly orienting the nozzle on flank face of the tool. Further performance of MQL can be enhanced using chip evacuation system. From viewpoint of cost, health, safety and environment, performance of MQL technique is better with the use of vegetable oils as compared to mineral oils.
- Turning with HPC technique results in formation of segmented chips, better penetration at interface and thus lower cutting force, better tool life and acceptable surface finish. It seems to be a potential solution for turning of hard-to-cut materials. Directing the nozzle at particular location plays a vital role in machining with HPC.
- Performance of solid lubricants is better at higher cutting speed, it means they offer opportunities for increasing the MRR. Higher the adhesion quality of solid lubricants, better will be their performance. Pollution-free environment and capacity to handle high-cutting temperature are encouraging the use of these lubricants.
- Air, water vapor and other environment-friendly gases mixtures are better solutions for green cutting. Air when mixed with oil gives better performance. The use of water vapor as coolant is encouraging due to their better lubrication qualities. Straight oils provide the best lubrication but poor cooling capacities. Water, on the other hand, is an effective cooling agent, removing heat 2.5 times more rapidly than the oil. The performance of water is encouraging when it is mixed with soluble oils.
- Researchers proposed the use of vegetable oils as coolants in cutting. The performance of coconut oil as coolant was encouraging at lower cutting speeds.

It indicates that other types of vegetable oil can also be checked for their suitability as coolant in turning process.
- The use of heat pipe arrangement in the tool holder is another alternative of low cost environment-friendly cooling in machining.
- All types of cooling techniques gave good results with almost all the tool materials in particular with carbide (coated/uncoated) and PCBN.
- Development of analytical models and application of FEA techniques helps in predicting the tool wear, surface characteristics, fluid aerosol generation, etc. under different cooling methods. These models and FEA techniques can serve as a basis for planning machining process with use of different cooling techniques.

6.2.3 Solid Lubricant-Assisted Machining

Solid lubricant-assisted machining is a novel concept to control the machining zone temperature without polluting the environment. Graphite and molybdenum disulfide (MoS_2) are the predominant materials used as solid lubricants [47]. In the form of dry powder, these materials are effective lubricant additives due to their lamellar structure. The lamellas orient parallel to the surface in the direction of motion. Even between highly loaded stationary surfaces, the lamellar structure is able to prevent contact. In the direction of motion, lamellas easily shear over each other resulting in a low friction. Large particles perform better on relatively rough surface at low speed, finer particle on relatively smooth surface and at higher speeds. Other components that are useful solid lubricants include boron nitride, polytetrafluoroethylene (PTFE), talc, calcium fluoride, cerium fluoride and tungsten disulfides.

Reddy and Rao [43] investigated the role of solid lubricant-assisted machining with graphite and molybdenum disulfide lubricants on surface quality, cutting forces and specific energy while machining AISI 1045 steel using cutting tools of different tool geometry (radial rake angle and nose radius). The performance of solid lubricant-assisted machining was studied in comparison with that of wet machining. The results indicated that there was a considerable improvement in the process performance with solid lubricant-assisted machining when compared with that of machining with cutting fluids.

Experiments were carried out to study the effect of solid lubricants on surface finish and chip thickness. It was observed that both the factors improved by the use of solid lubricants because of effective removal of heat from the cutting zone [35].

During the machining of thoroughly hardened AISI 52100 steel with ceramic inserts by using solid lubricants such as graphite and molybdenum disulfide, it was observed that at high-cutting speed range, the solid lubricants were more effective. Solid lubricant-assisted hard turning produced low value of surface roughness when compared with the dry hard turning. The decrease in surface roughness due to solid lubricants can be attributed to the inherent lubricating properties of the

solid lubricants even at extreme temperatures. This is due to the layered lattice structure of these lubricants [49].

Guleryuz et al. [18] reported the machining and wear performance of TiN-coated and patterned carbide inserts incorporating indium as a solid lubricant. Cutting tests were conducted by turning hardened 4340 steel in both lubricated and dry conditions. During turning, periodic flank wear measurements were made. The chips formed during cutting were examined by scanning electron microscopy, as the condition of the chip reflects the conditions obtained during machining. Inserts subject to dry machining were also examined using optical microscopy and X-ray photoelectron spectroscopy to determine the extent of damage on the rake surface as well as the degree of material transfer. The results showed indium to be effective in reducing flank wear during lubricated machining, but little additional benefit of patterning was observed. For dry machining, some degree of improvement was noted in the patterned sample, but the degree of lubricity brought about by the indium coating was not sufficient and the overall flank wear was higher than the lubricated tests. However, the wear and damage on the rake surface along the path of the chip was reduced by the presence of the in-containing micro-reservoirs. An additional test was conducted using an instrument that simulates temperature effects during machining, and it was found that the lubricity achieved by coatings is lost above 450°C. These results suggest that the use of indium is limited to below this temperature, and above this temperature transforms to a less lubricious indium oxide.

Low values of surface roughness while turning with solid lubricants is due to the inherent lubricating properties of these lubricants even at extreme temperatures. Value of surface roughness produced by molybdenum disulfide as lubricant is lower than that produced by graphite as lubricant due to its strong adhesion quality in comparison to graphite. The value of cutting forces is less with solid lubricants when compared with dry and wet machining due to the lattice layer structure of solid lubricants, which acts as an effective lubricant film. Above all, solid lubricants are environment-friendly and produce no harmful effect on the newly generated work surface.

The role of machining process modeling is recognized in industry, due to the relevant advantages that an effective and reliable model can supply [5]. Within this framework, the potentialities linked to the use of advanced numerical models and in particular finite-element techniques have been recognized by a large number of researchers all over the world [29]. For machining under wet cutting conditions, the research till now has been either experimental investigations or finite-element method simulations. It is important to characterize the thermal field in the cutting zone to design an efficient cryogenic cooling system for high-speed machining. Researchers used Jeager's model of moving heat sources and block partition principles to estimate average temperature at the shear plane and at the chip–tool interface. However, this model could not be taken into account variation in thermal properties of work and tool material with temperature, the elasto-plastic nature of chip–tool interaction, work–tool interaction at the wear land in flank, etc. [32].

Three-dimensional FEM models are marginally more accurate than two-dimensional models, but these are complex to develop and require more computational effort.

Considering the intricacies involved in the heat transfer of the cryogenic cutting process, the FE results can be a good reference for understanding the temperature distribution on tool [20]. Based on the finite difference method (FDM), a thermal analysis was performed to decide the ejection direction of the coolant. It was concluded that cooling fluid should be ejected towards the rake and clearance faces.

To address the issue of the environmental concerns of cutting fluids in near-dry machining, Bell et al. [4] developed an analytical model to predict the aerosol generation rate. The cutting fluid aerosol generation in turning process is due to spin-off, splash and evaporation mechanism separately or in combination. In the analytical model, two primary aerosol formation mechanisms were considered: aerosol runaway and evaporation, when air–fluid mixture is applied to the insert flank face. Both the analysis and experimental results showed that the aerosol runaway has a significantly higher effect on aerosol generation in near-dry turning. The analytical results showed a good agreement with the experimental results.

6.2.4 Minimal Quantity Lubrication Machining

Brinksmeier et al. [6] showed the effect of coolant type, coolant composition and coolant supply on grinding processes and process results. Investigations in the fields of fluid dynamic processes in supply nozzles and in the grinding zone are the key to optimization of cooling and lubrication during grinding, thus offering the chance to minimize the amount of coolant in circulation, leading to a reduction in adverse environmental effects and cost.

Hassan and Yao [19] optimized the process of face milling of ($\alpha + \beta$) titanium alloy while using MQL as the cooling technique using the Taguchi method. The cutting speed, feed rate and depth of cut were optimized with consideration of multiple performance characteristics including tool life, volume removed and surface roughness. The experimental results showed that the multiple performance characteristics can be simultaneously improved through this approach, and the feed rate is the most influential cutting parameter in the face milling of titanium alloys.

Li and Liang [30] developed the analytical understanding of mechanical and environmental effects of MQL in machining and profiles the MQL performance as functions of machining and fluid application parameters. Physics-based predictive models were formulated to quantitatively describe the resulting contact stress and temperature distributions under completely dry, MQL (under boundary lubrication) and flood cooling conditions in cylindrical turning. On that basis, the air quality effects in terms of cutting fluid aerosol emission rate and droplet size distribution were derived through the modeling of evaporation, runaway aerosol atomization, and dissipation processes. In addition, the abrasion, adhesion, and diffusion wear mechanisms under time-evolving cutter geometry were quantitatively evaluated for the development of a tool wear and tool life relationship with the fluid application condition. Experimental measurements of force, temperature,

aerosol concentration, and tool flank wear rate in dry, MQL, and fluid cooling cases were also pursued to calibrate and validate the predictive models. The MQL performance profile was assessed through the sensitive analysis of tool utilization, power consumption, and air quality with respect to MQL application parameters; and it serves as a basis to support the overall optimization of machining process by incorporating both mechanical and environmental considerations.

Bruni et al. [7] investigated the effect of lubrication-cooling condition on surface roughness in finish face milling operations. Different cutting speeds and lubrication-cooling conditions (dry, wet and MQL), in finish face milling of AISI 420 B stainless steel, were considered. Analytical and artificial neural network models, able to predict the surface roughness under different machining conditions, were proposed.

Iqbal et al. [23] studied the effects of four parameters, namely, hardened steel's microstructure, workpiece inclination angle, cutting speed, and radial depth of cut on tool life and surface roughness (in directions of feed and pick-feed). The milling was performed under environment of MQL, using coated carbide ball-nose end mills. The quantification of the effects was done using a new response surface methodology known as the D-optimal method. For tool life, workpiece material was found as the most influential parameter followed by the rotational speed of tool. High values of tool's rotational speed proved unfavorable for tool life but favorable for surface finish. In addition, the effects of workpiece inclination angle and radial depth of cut were analyzed upon effective cutting speed and cusp height and, subsequently, upon surface roughness. The major tool damage mechanisms detected were notch wear, adhesion, and chipping. The severity of chipping was relatively smaller when compared with that of adhesion and of notch wear because of reduced effective cutting speeds and feed rate employed.

In the MQL technique, a large volume of oil mist is discharged to the environment. Aoyama et al. [3] proposed a new lean lubrication system for a near-dry machining process called "direct oil drop supply system (DOS)". The performance of the DOS technique was evaluated by the milling processes. The DOS technique can supply a very small oil drop directly to the cutting edge without making oil mist, and the DOS showed almost same machining performances as compared to the MQL technique.

Gaitonde et al. [16] investigated MQL in machining as an established alternative to completely dry or flood lubricating system from the viewpoint of cost, ecology and human health issues. The work was aimed at determining the optimum amount of MQL and the most appropriate cutting speed and feed rate during turning of brass using K10 carbide tool. Taguchi technique with the utility concept, a multi-response optimization method, was proposed for simultaneous minimization of surface roughness and specific cutting force. The experiments were planned as per Taguchi's L_9 orthogonal array with each experiment performed under different conditions of MQL, cutting speed and feed rate. The analysis of means (ANOM) and ANOVA on multi-response signal-to-noise (S/N) ratio were employed for determining the optimal parameter levels and identifying the level of importance of the process parameters. The optimization results indicated that

MQL of 200 ml/h, cutting speed of 200 m/min and a feed rate of 0.05 mm/rev was essential to simultaneously minimize surface roughness and specific cutting force.

Sreejith [51] reported on the effect of different lubricant environments when 6061 aluminum alloy was machined with diamond-coated carbide tools. The effect of dry machining, MQL, and flooded coolant conditions was analyzed with respect to the cutting forces, surface roughness of the machined work piece and tool wear. The three types of coolant environments were compared. It was found that MQL condition would be a very good alternative to flooded coolant/lubricant conditions. Therefore, it appears that MQL, if properly employed, can replace the flooded coolant/lubricant environment which is presently employed in most of the cutting/machining applications, thereby not only the machining will be environmental-friendly but also will improve the machinability characteristics.

Tasdelen [52] dealt with the results obtained at cutting with MQL at different oil amounts, dry compressed air and emulsion. The results were discussed in terms of wear, chip contact, forces/torques and surface finish. The short hole drilling tests with indexable inserts showed that MQL and compressed air usage had resulted lower wear both on the center and periphery insert compared to drilling with emulsion. The surface finish values had shown that cutting with compressed air resulted in side flow and sticking of the work piece material on the walls of the hole that gave bad surface finish. The longer chips were evidenced for emulsion in comparison to MQL and air assisted drilling.

Nandi and Davim [36] directed high-pressure coolant jets into the tool–chip interface to sufficiently penetrate and change the thermal, frictional and mechanical conditions in the cutting zone. High-pressure cooling using neat oil and water-soluble oil was undertaken and its effects on machining evaluation parameters such as chip form, chip breakability, cutting forces, coefficient of friction, contact length, tool life and surface finish of the finished workpiece were evaluated in comparison with those from the conventional cooling method. The results showed that significant improvement in tool life and other evaluation parameters could be achieved utilizing moderate range of coolant pressure.

Fratila [15] presented an overview on some requirements to be considered for a successful MQL application into industrial practice. The evaluation of NDM effects on the gear milling process efficiency, with respect to hob wear, surface quality, cooling effect, and environment protection was carried out. Khan et al. [26] presented the effects of MQL by vegetable oil-based cutting fluid on the turning performance of low alloy steel AISI 9310 when compared with completely dry and wet machining in terms of chip–tool interface temperature, chip formation mode, tool wear and surface roughness. The MQL was provided with a spray of air and vegetable oil. MQL machining performed much superior as compared to the dry and wet machining due to substantial reduction in cutting zone temperature enabling favorable chip formation and chip–tool interaction. It was also seen from the results that the substantial reduction in tool wears resulted in enhanced the tool life and surface finish.

Wang et al. [57] investigated the effects of different coolant supply strategies (using flood coolant, dry cutting, and MQL) on cutting performance in continuous

and interrupted turning process of Ti6Al4V. Based on the observation of the cutting forces with the different coolant supply strategies, the mean friction coefficient in the sliding region at the tool–chip interface WAS obtained and used in a finite-element method (FEM) to simulate the deformation process of Ti6Al4V during turning. From the FEM simulation and Oxley's predictive machining theory, cutting forces were estimated under different coolant supply strategies.

Nandi and Davim [36] studied the drilling performances with minimum quantity lubricant (MQL). Fuzzy logic rules, which were derived based on fuzzy set theory, were used to develop fuzzy rule-based model (FRBM). The performance of FRBM depended on two different aspects: structures of fuzzy rules and the associated fuzzy sets [membership function distributions (MFDs)]. The aim of the study was to investigate the performances of FRBMs based on Mamdani and TSK-types of fuzzy logic rules with different shapes of MFDs for prediction and performance analysis of machining with MQL in drilling of aluminum alloy. A comparison of the model predictions with experimental results and those published in the literature showed that FRBM with TSK-type fuzzy rules described excellent trade-off with experimental measurements.

Tawakoli et al. [53, 54] studied the influences of workpiece hardness and grinding parameters including wheel speed, feed rate and depth of cut on the basis of the grinding forces and surface quality properties to develop optimum grinding performances, such as cooling, lubrication, high ecological and environmental safety.

Rao and Patel [41] presented a cylindrical grinding operation in which four short-listed grinding fluids were tested. Eight cutting fluid criteria were considered, of which four were the machining process output variables such as wheel wear (WW), tangential force (TF), grinding temperature (GT), and surface roughness (SR), and four were the cutting fluid properties and characteristics, such as recyclability (R), toxic harm rate (TH), environment pollution tendency (EP) and stability (S). The authors had proposed a multiple attribute decision-making (MADM) method known as PROMETHEE for selection of right cutting fluid. In another work, Rao and Patel [42] proposed a novel MADM method for cutting fluid selection considering the objective weights of the cutting fluid selection attributes and the preferences of the decision maker.

Tawakoli et al. [53] carried out investigations on the influence of different types of coolant lubricants and grinding wheels on the grinding process results. The tests were performed in presence of fluid, air jet and 11 types of coolant lubricants, as well as, in dry condition. The grinding wheels employed were vitrified bond corundum, resin bond corundum and vitrified bond SG wheels. The results indicated that SG wheels and MQL oils have potential in comparison to vitrified and resin bond corundums and water miscible oils. In addition, the lowest thermal damages, material side flow on the ground surface and wheel loading were generated by using the SG grinding wheel in MQL grinding process. In another work, Tawakoli et al. [54] showed that the setting location of the nozzle is an important factor regarding the effective application of MQL oil mist. It was shown that optimal grinding results can be obtained when the MQL nozzle is positioned

angularly toward the wheel (at approximately 10°–20° to the workpiece surface). In addition, it was found that the efficient transportation of oil droplets to the contact zone required higher mass flow rate of the oil mist towards the grains flat area and longer deposition distance of an oil droplet. Grinding forces and surface roughness has been achieved.

Sadeghi et al. [45] compared several grinding fluids, including mineral, vegetable and synthetic esters oil, on the basis of the grinding forces and surface quality properties that would be suitable for MQL grinding applications, to develop a multifunctional fluid having the MQL results such as cooling, lubrication and high ecological and environmental safety performances. The grinding performance of fluids was also evaluated in dry and conventional fluid grinding techniques.

Tosun and Pihtili [56] presented the optimization of the face milling process of 7075 aluminum alloy by using the gray relational analysis for both cooling techniques of conventional cooling and MQL, considering the performance characteristics such as surface roughness and material removal rate. Experiments were performed under different cutting conditions, such as spindle speed, feed rate, cooling technique, and cutting tool material. The cutting fluid in MQL machining was supplied to the interface of work piece and cutting tool as pulverize. An orthogonal array was used for the experimental design. Optimum machining parameters were determined by the gray relational grade obtained from the gray relational analysis.

As cutting fluids are widely used in industrial machining operations, and because of their negative effects on health, safety, and environment, legislation and public environmental concerns now have great impacts on their development. Dry machining and minimum quantity lubrication (MQL) machining have been successfully applied in some kinds of machining processes. However, in others, such as grinding, it is very difficult to obtain good results without the help of cutting fluids, because of the high amount of heat generated during grinding. As for MQL machining, although progress is being made, we have a long way to go before this problem is solved in applications workshops. Cryogenic machining, even though proved useful, involves more cost. Therefore, research on the composition, supply techniques, selection, cleaning, and maintenance of cutting fluids is still active at present. However, serious research efforts are going on for developing the new technologies to avoid or minimize the use of cutting fluids.

References

1. Abdulkareem S, Khan AA, Konneh M (2009) Reducing electrode wear ratio using cryogenic cooling during electrical discharge machining. Int J Adv Manuf Technol 45(11–12): 1146–1151
2. Aggarwal A, Singh H, Kumar P, Singh M (2008) Optimization of multiple quality characteristics for CNC turning under cryogenic cutting environment using desirability function. J Mater Process Technol 205(1–3):42–50

3. Aoyama T, Kakinuma Y, Yamashita M, Aoki M (2008) Development of a new lean lubrication system for near dry machining process. CIRP Ann Manuf Technol 57(1):125–128
4. Bell DD, Chou J, Nowag L, Liang SY (1999) Modeling of the environmental effect of cutting fluid. Trib Trans 42(1L):168–173
5. Boisse P, Altan T, Luttervelt VK (2007) Friction and flow stress in forming and cutting. Viva Books Pvt. Ltd
6. Brinksmeier E, Heinzel C, Wittmann M (1999) Friction, cooling and lubrication in grinding. CIRP Ann Manuf Technol 48(2):581–598
7. Bruni C, D' Apolito L, Forcellese A, Gabrielli F, Simoncini M (2008) Surface roughness modeling in finish face milling under MQL and dry cutting conditions. Int J Mater Form 1(1):503–506
8. Chiou RY, Lu L, Chen JSJ, North MT (2007) Investigation of dry machining with embedded heat pipe cooling by finite element analysis and experiments. Int J Adv Manuf Technol 31:905–914
9. De Chiffre L, Andreasen JL, Lagerberg S, Thesken IB (2007) Performance testing of cryogenic CO_2 as cutting fluid in parting/grooving and threading austenitic stainless steel. CIRP Ann Manuf Technol 56(1):101–104
10. Dhar NR, Paul S, Chattopadhyay AB (2002) Machining of AISI 4140 steel under cryogenic cooling—tool wear, surface roughness and dimensional deviation. J Mater Process Technol 123(3):483–489
11. Dhar NR, Kamruzzaman M (2007) Cutting temperature, tool wear, surface roughness and dimensional deviation in turning AISI-4037 steel under cryogenic condition. Int J Mach Tools Manuf 47(5):754–759
12. Dudzinski A, Devillez A, Moufki A, Larrouquere D, Zerrouki V, Vigneau J (2004) A review of developments towards dry and high speed machining of Inconel 718 alloy. Int J Mach Tools Manuf 44:439–456
13. El-Tayeb NSM, Yap TC, Venkatesh VC, Brevern PV (2009) Modeling of cryogenic frictional behaviour of titanium alloys using response surface methodology approach. Mater Des 30(10):4023–4034
14. Firouzdor V, Nejati E, Khomamizadeh F (2008) Effect of deep cryogenic treatment on wear resistance and tool life of M2 HSS drill. J Mater Process Technol 206(1–3):467–472
15. Fratila D (2009) Evaluation of near-dry machining effects on gear milling process efficiency. J Clean Prod 17(9):839–845
16. Gill SS, Singh H, Singh R, Singh J (2010) Cryoprocessing of cutting tool materials—a review. Int J Adv Manuf Technol 48(1–4):175–192
17. Gaitonde VN, Karnik SR, Davim JP (2008) Selection of optimal MQL and cutting conditions for enhancing machinability in turning of brass. J Mater Process Technol 204(1–3):459–464
18. Guleryuz CG, Krzanowski JE, Veldhuis SC, Fox-Rabinovich GS (2009) Machining performance of TiN coatings incorporating indium as a solid lubricant. Surf Coat Technol 203(22):3370–3376
19. Hassan A, Yao ZG (2004) Multi-objective optimization in the milling of titanium alloys using the MQL technique. Int J Mater Form 19(4):503–506
20. Hong SY, Ding Y (2001) Micro-temperature manipulation in cryogenic machining of low carbon steel. J Mater Process Technol 116:22–30
21. Hong SY, Markus I, Jeong WC (2001) New cooling approach and tool life improvement in cryogenic machining of titanium alloy Ti-6Al-4 V. Int J Mach Tools Manuf 41(15): 2245–2260
22. Hua L, Weiping C, Zhixin K, Tungwai N, Yuanyuan L (2005) Fuzzy multiple attribute decision-making for evaluating aggregate risk in green manufacturing. Tsinghua Sci Technol 10:627–632
23. Iqbal A, Ning H, Khan I, Liang L, Dar NU (2008) Modeling the effects of cutting parameters in MQL-employed finish hard-milling process using D-optimal method. J Mater Process Technol 199(1–3):379–390

24. Jayal AD, Badurdeen F, Dillon Jr OW, Jawahir IS (2010) Sustainable manufacturing: Modeling and optimization challenges at the product, process and system levels. CIRP Ann Manuf Technol. doi:10.1016/j.cirpj.2010.03.006
25. Klocke F, Eisenblätter G (1997) Dry cutting. CIRP Ann Manuf Technol 46(2):519–526
26. Khan MMA, Mithu MAH, Dhar NR (2009) Effects of minimum quantity lubrication on turning AISI 9310 alloy steel using vegetable oil-based cutting fluid. J Mater Process Technol 209(15–16):5573–5583
27. Kirillov AK, Vereshchaka AS, Kozlov AA, Robakidze ZY (2009) Dry cutting of hard-to-machine materials, with compensation of the physical functions of the lubricant and coolant fluid. Russian Eng Res 29(4):26–29
28. Kumar KVBSK, Choudhury SK (2008) Investigation of tool wear and cutting force in cryogenic machining using design of experiments. J Mater Process Technol 203(1–3):95–101
29. Li KM (2006) Predictive modeling of near dry machining: mechanical performance and environmental impact. PhD Thesis, Georgia Institute of Technology, Atlanta
30. Li KM, Liang SY (2007) Performance profiling of minimum quantity lubrication in machining. Int J Adv Manuf Technol 35(3–4):226–233
31. Li S, Xie Y, Wu X (2010) Hardness and toughness investigations of deep cryogenic treated cold work die steel. Cryogenics 50(2):89–92
32. Loewen EG, Shaw MC (1954) On the analysis of cutting tool temperature. J Eng Ind 76:217–231
33. Madu CN, Kuei C, Ifeanyi E (2002) A hierarchic metric approach for integration of green issues in manufacturing: a paper recycling application. J Env Manag 64:261–272
34. Marksberry PW, Jawahir IS (2008) A comprehensive tool-wear/tool-life performance model in the evaluation of NDM for sustainable manufacturing. Int J Mach Tools Manuf 48:878–886
35. Mukhopadhyay D, Banerjee S, Reddy NSK (2007) Investigation to study the applicability of solid lubricant in turning AISI 1040 steel. J Manuf Sci Eng 129(3):520–526
36. Nandi AK, Davim JP (2009) A study of drilling performances with minimum quantity of lubricant using fuzzy logic rules. Mechatronics 19(2):218–232
37. Paul S, Dhar NR, Chattopadhyay AB (2001) Beneficial effects of cryogenic cooling over dry and wet machining on tool wear and surface finish in turning AISI 1060 steel. J Mater Process Technol 116(1):44–48
38. Pusavec F, Krajnik P, Kopac J (2010) Transitioning to sustainable production—Part I: application on machining technologies. J Clean Prod 18(2):174–184
39. Pusavec F, Krajnik P, Kopac J (2010) Transitioning to sustainable production—Part II: evaluation of sustainable machining technologies. J Clean Prod. doi:10.1016/j.jclepro.2010.01.015
40. Rao RV (2007) Decision making in the manufacturing environment using graph theory and fuzzy multiple attribute decision making methods. Springer-Verlag, London
41. Rao RV, Patel BK (2009) Decision making in the manufacturing environment using an improved PROMETHEE method. Int J Prod Res. doi: 10.1080/00207540903049415
42. Rao RV, Patel BK (2010) A novel method for decision making in the manufacturing environment. Proc Inst Mech Eng Part B J Eng Manuf
43. Reddy NSK, Rao PV (2006) Experimental investigation to study the effect of solid lubricants on cutting forces and surface quality in end milling. Int J Mach Tools Manuf 46(2):189–198
44. Reddy TVS, Sornakumar T, Reddy MV, Venkatram R (2009) Machinability of C45 steel with deep cryogenic treated tungsten carbide cutting tool inserts. Int J Refra Met Hard Mater 27(1):181–185
45. Sadeghi MH, Hadad MJ, Tawakoli T, Vesali A, Emami M (2010) An investigation on surface grinding of AISI 4140 hardened steel using minimum quantity lubrication-MQL technique. Int J Mater Form, DOI 10.1007/s12289-009-0678-3
46. Sarkis J (1999) A methodological framework for evaluating environmentally conscious manufacturing programs. Comput Ind Eng 36:793–810

47. Shaji S, Radhakrishnan V (2003) Analysis of process parameters in surface grinding with graphite as lubricant based on the Taguchi method. J Mater Process Technol 141:51–59
48. Sharma VS, Dogra M, Suri NM (2009) Cooling techniques for improved productivity in turning. Int J Mach Tools Manuf 49(6):435–453
49. Singh D, Rao PV (2008) Performance improvement of hard turning with solid lubricants. Int J Adv Manuf Technol 38:529–535
50. Sreejith PS, Ngoi BKA (2000) Dry machining: machining of the future. J Mater Process Technol 101(1–3):287–291
51. Sreejith PS (2008) Machining of 6061 aluminium alloy with MQL, dry and flooded lubricant conditions. Mater Lett 62(2):276–278
52. Tasdelen B, Wikblom T, Ekered S (2008) Studies on minimum quantity lubrication (MQL) and air cooling at drilling. J Mater Process Technol 200(1–3):339–346
53. Tawakoli T, Hadad MJ, Sadeghi MH (2010a) Investigation on minimum quantity lubricant-MQL grinding of 100Cr6 hardened steel using different abrasive and coolant-lubricant types. Int J Mach Tools Manuf. doi:10.1016/j.ijmachtools.2010.04.009
54. Tawakoli T, Hadad MJ, Sadeghi MH (2010b) Influence of oil mist parameters on minimum quantity lubrication–MQL grinding process. Int J Mach Tools Manuf 50(6):521–531
55. Tixer J, Dusserre G, Salvi O (2002) Review of 62 risk analysis methodologies of industrial plants. J Loss Prev Process Ind 15:291–303
56. Tosun N, Pihtili H (2010) Gray relational analysis of performance characteristics in MQL milling of 7075 Al alloy. Int J Adv Manuf Technol 46(5–8):509–515
57. Wang ZG, Rahman M, Wong YS, Neo KS, Sun J, Tan CH, Onozuka H (2009) Study on orthogonal turning of titanium alloys with different coolant supply strategies. Int J Adv Manuf Technol 42(7–8):621–632
58. Yildiz Y, Nalbant M (2008) A review of cryogenic cooling in machining processes. Int J Mach Tools Manuf 48(9):947–964

Appendix A
Meta-Heuristic Optimization Techniques: Sample Codes

A.1 Sample Codes for Rough Grinding Process

A.1.1 ABC Code

```
/************  THIS PROGERAMME IS FOR OPTIMIZATION OF ROUGH
GRINDING USING ABC    **********/
#include<graphics.h>
#include<stdlib.h>
#include<stdio.h>
#include<conio.h>
#include<math.h>
#include<dos.h>
void main()
{
int i,j,k,n,ne,no,Nint[10][30],fit[5][15];
float R[15],R1[12][5],R2[12][5],Nfloat[5][15],R4[12][5],fit1[5][15],sumfit[15];
float f[5][15],fi[5][15],sumfi[15],p[5][15],m,q,x1[5][15],x2[5][15];
float x1max,x1min,x2max,x2min,s1,s2,min[5][15],min1[15],minf[15];
float x1new[12][5][15],x2new[12][5][15],fnew[12][5][15],p1[5][15];
float z1[5][15],z2[5][15],z3[5][15],con4[5][15],pc1,pc2,x3[5][15];
float x3new[12][5][15],z1new[12][5][15],con4new[12][5][15];
float R3[12][5],s3,x3max,x3min,x4max,x4min,x4[5][15],Tave[5][15];
float
Tavenew[12][5][15],pc4,x4new[12][5][15],s4,z2new[12][5][15],z3new[12][5][15]
;
float con2[5][15],con2new[12][5][15],WWP[5][15],WWPnew[12][5][15];
/*****************************************************************/
float ap=0.05,De=355,VOL=6.99,dg=0.3,HRC=58,G=60,Kp=0.0869,Rmax=1.8;
/*****************************************************************/
```

```
clrscr();
printf("\For optimum results enter following data:");
printf("\n\nNo.of iterations=65");
printf("\n\nNumber of Employed Bees=5");
printf("\n\nEnter Number of Onlookers Bees=11");
printf("\n************************************************");
printf("\nEnter the No.of iterations:");
scanf("%d",&n);
printf("\nEnter Number of Employed Bees:");
scanf("%d",&ne);
printf("\nEnter Number of Onlookers Bees:");
scanf("%d",&no);
x1min=1000; x2min=10; x3min=0.01; x4min=0.01;
x1max=2023; x2max=22.7; x3max=0.1370; x4max=0.1370;
s1=(x1max-x1min)/6;    s2=(x2max-x2min)/6;    s3=(x3max-x3min)/6;s4=(x4max-
x4min)/6;
//clearviewport();
/***************  INITIAL SOLUTION ***************************/
x1[1][0]=1200;    x2[1][0]=12;   x3[1][0]=0.034;   x4[1][0]=0.130;
x1[2][0]=1400;    x2[2][0]=14;   x3[2][0]=0.058;   x4[2][0]=0.058;
x1[3][0]=1600;    x2[3][0]=16;   x3[3][0]=0.082;   x4[3][0]=0.082;
x1[4][0]=1700;    x2[4][0]=18;   x3[4][0]=0.106;   x4[4][0]=0.106;
x1[5][0]=1900;    x2[5][0]=20;   x3[5][0]=0.130;   x4[5][0]=0.034;
/* Calculate the objective function for each food source */
for(k=0;k<=n-1;k++)
{
minf[k]=999999;
for(j=1;j<=ne;j++)
{
z1[j][k]=(38.2544/x2[j][k])+(0.697/(x4[j][k]*x1[j][k]))+(4.18*x3[j][k])+4.0485;
z2[j][k]=0.0603*(1+(2*x3[j][k]/(3*x4[j][k])))*pow(x4[j][k],0.5789)*pow((x2[j][k
]/x1[j][k]),0.1578)*x1[j][k];
Tave[j][k]=132.023*(1+(x3[j][k]/x4[j][k]))*pow(x4[j][k],0.5925)*pow((x2[j][k]/x
1[j][k]),0.5925);
if(Tave[j][k]>0 && Tave[j][k]<0.254)
z3[j][k]=0.4587*pow(Tave[j][k],0.30);
if(Tave[j][k]>=0.254)
z3[j][k]=0.78667*pow(Tave[j][k],0.72);
WWP[j][k]=(Kp*ap*pow(dg,0.1315)*pow(HRC,1.4210)/(pow(De,(1.2/(VOL-
0.1067)))*pow(VOL,0.38)))*((1+(x3[j][k]/x4[j][k]))*pow(x4[j][k],1.4210)*pow((
x1[j][k]/x2[j][k]),0.1579)*x2[j][k]/(1+(2*x3[j][k]/(3*x4[j][k]))));
con2[j][k]=(z2[j][k]/WWP[j][k])-G;
con4[j][k]=Rmax-z3[j][k];
//
printf("\nz1=%f,con1=%f,con2=%f,con3=%f",z3[j][k],con1[j][k],con2[j][k],con3[
j][k]);
```

```
if(con2[j][k]<0)
pc2=0.10; /* (Original pc2=0.065) */
else
pc2=0;
if(con4[j][k]<0)
pc4=2.9;
else
pc4=0;
// getch();
f[j][k]=0.5*(z1[j][k]/10)-0.5*(z2[j][k]/20)-pc2*con2[j][k]-pc4*con4[j][k];
//  printf("\nValue of objective function of source %d is:%f",j,f[j][k]);
}
for(j=1;j<=ne;j++)
{
if(f[j][k]>=0)   fit[j][k]=1/f[j][k];
if(f[j][k]<0)    fit[j][k]=1+(-1*f[j][k]);
}
/* Calculate the sum of inverse of all objective functions */
for(j=1;j<=ne;j++)
{
fit1[j][k]=fit[j][k];
}
fit1[0][k]=0;
for(j=1;j<=ne;j++)
{
fit1[j][k]=fit1[j][k]+fit1[j-1][k];
}
sumfit[k]=fit1[ne][k];
// printf("\nSum of inverse of all objective function is:%f",sumfit[k]);
// getch();
/* Calculate the cumulative probability of chosing a food source */
for(j=1;j<=ne;j++)
{
p[j][k]=(sumfit[k]);
p1[j][k]=fit[j][k]/p[j][k];
//  printf("\n Probability=%f",p1[j][k]);
}
//  getch();
/* Calculate the number of Onlookrs bees to each food source */
for(j=1;j<=ne;j++)
{
Nfloat[j][k]=p1[j][k]*no;
Nint[j][k]=Nfloat[j][k];
//   printf("\nNumber of Onlookers bees assigned to source %d=%d",j,Nint[j][k]);
}
//  getch();
```

```
for(j=1;j<=ne;j++)
{
for(i=1;i<=Nint[j][k];i++)
{
R1[i][j]=((float)(rand() % 100)/100);
R2[i][j]=((float)(rand() % 100)/100);
R3[i][j]=((float)(rand() % 100)/100);
R4[i][j]=((float)(rand() % 100)/100);
// printf("R1[%d]=%f  and  R2[%d]=%f",k,k,R1[k],R2[k]);
x1new[i][j][k]=x1[j][k]+(s1*(R1[i][j]-0.5));
x2new[i][j][k]=x2[j][k]+(s2*(R2[i][j]-0.5));
x3new[i][j][k]=x3[j][k]+(s3*(R3[i][j]-0.5));
x4new[i][j][k]=x4[j][k]+(s4*(R4[i][j]-0.5));
if(x1new[i][j][k]>x1max) x1new[i][j][k]=x1max; else
x1new[i][j][k]=x1new[i][j][k];
if(x2new[i][j][k]>x2max) x2new[i][j][k]=x2max; else
x2new[i][j][k]=x2new[i][j][k];
if(x3new[i][j][k]>x3max) x3new[i][j][k]=x3max; else
x3new[i][j][k]=x3new[i][j][k];
if(x4new[i][j][k]>x4max) x4new[i][j][k]=x4max; else
x4new[i][j][k]=x4new[i][j][k];
if(x1new[i][j][k]<x1min) x1new[i][j][k]=x1min;  else
x1new[i][j][k]=x1new[i][j][k];
if(x2new[i][j][k]<x2min) x2new[i][j][k]=x2min;  else
x2new[i][j][k]=x2new[i][j][k];
if(x3new[i][j][k]<x3min) x3new[i][j][k]=x3min;  else
x3new[i][j][k]=x3new[i][j][k];
if(x4new[i][j][k]<x4min) x4new[i][j][k]=x4min;  else
x4new[i][j][k]=x4new[i][j][k];
//printf("\n\nNew value of X1=%f, X2=%f,
X3=%f",x1new[i][j][k],x2new[i][j][k],x3new[i][j][k]);
//getch();
z1new[i][j][k]=(38.2544/x2new[i][j][k])+(0.697/(x4new[i][j][k]*x1new[i][j][k]))+
(4.18*x3new[i][j][k])+4.0485;
z2new[i][j][k]=0.0603*(1+(2*x3new[i][j][k]/(3*x4new[i][j][k])))*pow(x4new[i][j
][k],0.5789)*pow((x2new[i][j][k]/x1new[i][j][k]),0.1578)*x1new[i][j][k];
Tavenew[i][j][k]=132.023*(1+(x3new[i][j][k]/x4new[i][j][k]))*pow(x4new[i][j][k
],0.5925)*pow((x2new[i][j][k]/x1new[i][j][k]),0.5925);
if(Tavenew[i][j][k]>0 && Tavenew[i][j][k]<0.254)
z3new[i][j][k]=0.4587*pow(Tavenew[i][j][k],0.30);
if(Tavenew[i][j][k]>=0.254)
z3new[i][j][k]=0.78667*pow(Tavenew[i][j][k],0.72);
```

```
WWPnew[i][j][k]=(Kp*ap*pow(dg,0.1315)*pow(HRC,1.4210)/(pow(De,(1.2/(V
OL-
0.1067)))*pow(VOL,0.38)))*((1+(x3new[i][j][k]/x4new[i][j][k]))*pow(x4new[i][j
][k],1.4210)*pow((x1new[i][j][k]/x2new[i][j][k]),0.1579)*x2new[i][j][k]/(1+(2*x
3new[i][j][k]/(3*x4new[i][j][k]))));
con2new[i][j][k]=(z2new[i][j][k]/WWPnew[i][j][k])-G;
con4new[i][j][k]=Rmax-z3new[i][j][k];
//
printf("\nz1=%f,con1=%f,con2=%f,con3=%f",z3new[i][j][k],con1new[i][j][k],con
2new[i][j][k],con3new[i][j][k]);
if(con2new[i][j][k]<0)
pc2=0.10;  /* (Original pc2=0.065) */
else
pc2=0;
if(con4new[i][j][k]<0)
pc4=2.9;
else
pc4=0;
// getch();
fnew[i][j][k]=0.5*(z1new[i][j][k]/10)-0.5*(z2new[i][j][k]/20)-
pc2*con2new[i][j][k]-pc4*con4new[i][j][k];
// printf("\nNew function value of Onlooker bee %d for source
%d=%f",i,j,fnew[i][j][k]);
// getch();
}
}
//   getch();
for(j=1;j<=ne;j++)
{
min[j][k]=999999;
for(i=1;i<=Nint[j][k];i++)
{
if(fnew[i][j][k]<min[j][k])
{
min[j][k]=fnew[i][j][k];
m=i;
}
}
//printf("\nMin.of all Onlookers bees for source %d is=%f",j,min[j][k]);
//  getch();
if(min[j][k]<f[j][k])
{
x1[j][k+1]=x1new[m][j][k];
x2[j][k+1]=x2new[m][j][k];
x3[j][k+1]=x3new[m][j][k];
x4[j][k+1]=x4new[m][j][k];
```

```
//printf("\nUpdated variables for source
%d=%f,%f,%f",j,x1[j][k+1],x2[j][k+1],x3[j][k+1]);
}
else
{
x1[j][k+1]=x1[j][k];
x2[j][k+1]=x2[j][k];
x3[j][k+1]=x3[j][k];
x4[j][k+1]=x4[j][k];
// printf("\nUpdated variables for source
%d=%f,%f,%f",j,x1[j][k+1],x2[j][k+1],x3[j][k+1]);
}
}
min1[k]=999999;
for(j=1;j<=ne;j++)
{
if(min[j][k]<min1[k])
{
min1[k]=min[j][k];
q=j;
}
}/* previous j loop ends */
min1[-1]=999999;
if(min1[k]<min1[k-1]) min1[k]=min1[k];
else min1[k]=min1[k-1];
printf("\n************************************************************");
  printf("\nMin.function value at the end of iteration %d=%f",k,min1[k]);
  printf("\nBest solution found at the end of iteration %d=%f,%f,%f
%f",k,x1[q][k+1],x2[q][k+1],x3[q][k+1],x4[q][k+1]);
printf("\n************************************************************");
getch();
}   /* k loop ends here */
getch();
}
```

A.1.2 PSO Code

```
/*****OPTIMIZATION OF GRINDING OPERATION USING PSO (ROUGH
GRINDING) ***/
#include<graphics.h>
#include<stdlib.h>
#include<stdio.h>
#include<conio.h>
#include<math.h>
```

```
#include<dos.h>
void main()
{
int i,j,k,gd=DETECT,gm,errorcode,ch;
/*****************************************************************/
float n,np,nv,Xmax[10],Xmin[10],RX[10][30],RV[10][30];
float x[10][10][30],v[10][10][30],w,c1,c2;
float f[10][30],pbest[10][10][30],/*w=0.65,c1=1.65,c2=1.55,*/ RC[5][5][30];
float RD[5][5][30],gbest[5][30],minf[30],leastf[5][30],leastminf[30];
float x0,y0,z1[10][30],z2[10][30],z3[10][30];
float con1[10][30],con2[10][30],con3[10][30],con4[10][30],z[10][30];
/*****************************************************************/
float t1z1,t2z1,M=30,p=1,Lw=300,Le=150,bw=60,be=25,fb=2,aw=0.1,ap=0.05;
float SP=2,pi=3.14,De=355,bs=25,Sd=100,Vr=254,t1=5,tch=30,Nt=12,Nd=20;
float Cs=0.003,Cd=25,Ntd=2000,VOL=6.99,dg=0.3,HRC=58,Ra,Tave[5][30];
float G=60,Kc[5][30],Rem=1,Km=100000,U[5][30];
float Ku=3.937*pow(10,-7),Kp=0.0869,WWP[5][30],Ks[5][30],MSC[5][30];
float Umax[5][30],Ao=0,w1=0.5,w2=0.5,w3=0.5;
float pc1,pc2,pc3,pc4,Rmax=1.8;
/*con=constraint, pc=penalty for constraint*/
/*****************************************************************/
clrscr();
printf("\For optimum results enter following data:");
printf("\n w, c1, and c2 = 0.65,1.65,1.55");
// printf("\nNo.of variables=4");
printf("\n*************************************************************");
n=99;
printf("\nEnter w, c1, and c2:");
scanf("%f%f%f",&w,&c1,&c2);
np=3;
// printf("\nEnter the no.of variables:");
// scanf("%f",&nv);
nv=4;
for(j=1;j<=np;j++)
{
for(i=1;i<=nv;i++)
{
RX[i][j]=((float)(rand() % 100)/100);
RV[i][j]=((float)(rand() % 100)/100);
//printf("\nRX[%d][%d]=%f   RV[%d][%d]=%f",i,j,RX[i][j],i,j,RV[i][j]);
//getch();
} }
for(k=0;k<=n-1;k++)
{
for(j=1;j<=np;j++)
{
```

```
for(i=1;i<=nv;i++)
{
RC[i][j][k]=((float)(rand() % 100)/100);
RD[i][j][k]=((float)(rand() % 100)/100);
//printf("\nRC[%d][%d][%d]=%f
RD[%d][%d][%d]=%f",i,j,k,RC[i][j][k],i,j,k,RD[i][j][k]);
//getch();
} } }
//clearviewport();
/* for(i=1;i<=nv;i++)
{
printf("\nEnter Min.& Max. value of variable%d:",i);
scanf("%f%f",&Xmin[i],&Xmax[i]);
}    */
Xmin[1]=1000; Xmin[2]=10; Xmin[3]=0.01; Xmin[4]=0.01;
Xmax[1]=2023; Xmax[2]=22.7; Xmax[3]=0.1370; Xmax[4]=0.1370;
/***************  INITIAL SOLUTION **********************/
minf[0]=999999;
x[1][1][0]=1200;  x[2][1][0]=20;   x[3][1][0]=0.04;   x[4][1][0]=0.03;
x[1][2][0]=1600;  x[2][2][0]=16;   x[3][2][0]=0.08;   x[4][2][0]=0.07;
x[1][3][0]=2000;  x[2][3][0]=12;   x[3][3][0]=0.12;   x[4][3][0]=0.11;
for(j=1;j<=np;j++)
{
for(i=1;i<=nv;i++)
{
// printf("\nEnter Random numbers RX%d%d & RV%d%d:",i,j,i,j);
// scanf("%f%f",&RX[i][j],&RV[i][j]);
// x[i][j][0]=Xmin[i]+(RX[i][j]*(Xmax[i]-Xmin[i]));
v[i][j][0]=Xmin[i]+(RV[i][j]*(Xmax[i]-Xmin[i]));
pbest[i][j][0]=x[i][j][0];
printf("\nInitial Pbest[%d%d]=%f & V[%d%d]=%f",i,j,pbest[i][j][0],i,j,v[i][j][0]);
}
/*****************************************************************/
z1[j][0]=(38.2544/x[2][j][0])+(0.697/(x[4][j][0]*x[1][j][0]))+(4.18*x[3][j][0])+4.0
485;
z2[j][0]=0.0603*(1+(2*x[3][j][0]/(3*x[4][j][0])))*pow(x[4][j][0],0.5789)*pow((x[
2][j][0]/x[1][j][0]),0.1578)*x[1][j][0];
Tave[j][0]=132.023*(1+(x[3][j][0]/x[4][j][0]))*pow(x[4][j][0],0.5925)*pow((x[2]
[j][0]/x[1][j][0]),0.5925);
if(Tave[j][0]>0 && Tave[j][0]<0.254)
z3[j][0]=0.4587*pow(Tave[j][0],0.30);
if(Tave[j][0]>=0.254)
z3[j][0]=0.78667*pow(Tave[j][0],0.72);
Umax[j][0]=6.2+(1.76*pow(De,0.25)/(pow(ap,0.75)*pow(x[2][j][0],0.5)));
```

```
U[j][0]=13.8+((9.64*pow(10,-4)*x[1][j][0])/(ap*x[2][j][0]))+(6.9*pow(10,-
3)*(2102.4*x[2][j][0])/(De*x[1][j][0]))*(Ao+((Ku*x[1][j][0]*Lw*aw)/(x[2][j][0]
*pow(De,0.5)*pow(ap,0.5))))*(x[1][j][0]*pow(De,0.5)/(x[2][j][0]*pow(ap,0.5)));
con1[j][0]=Umax[j][0]-U[j][0];
WWP[j][0]=(Kp*ap*pow(dg,0.1315)*pow(HRC,1.4210)/(pow(De,(1.2/(VOL-
0.1067)))*pow(VOL,0.38)))*((1+(x[3][j][0]/x[4][j][0]))*pow(x[4][j][0],1.4210)*p
ow((x[1][j][0]/x[2][j][0]),0.1579)*x[2][j][0]/(1+(2*x[3][j][0]/(3*x[4][j][0]))));
con2[j][0]=(z2[j][0]/WWP[j][0])-G;
Kc[j][0]=1000*x[2][j][0]*fb/z2[j][0];
Ks[j][0]=1000*x[1][j][0]*fb/WWP[j][0];
MSC[j][0]=(1/(2*Kc[j][0]))*(1+(x[2][j][0]/(x[1][j][0]*G)))+(1/Ks[j][0]);
con3[j][0]=MSC[j][0]-(Rem/Km);
con4[j][0]=Rmax-z3[j][0];
//
printf("\nz1=%f,con1=%f,con2=%f,con3=%f",z3[j][0],con1[j][0],con2[j][0],con3[
j][0]);
if(con2[j][0]<0)
pc2=0.10;  /* (Original pc2=0.065) */
else
pc2=0;
if(con4[j][0]<0)
pc4=2.9;
else
pc4=0;
// getch();
f[j][0]=w1*(z1[j][0]/10)-w2*(z2[j][0]/20)-pc2*con2[j][0]-pc4*con4[j][0];
printf("\nInitial value of objective function is:%f",f[j][0]);
if(f[j][0]<minf[0])
minf[0]=f[j][0];
}
printf("\nInitial minimum function value is:%f",minf[0]);
for(j=1;j<=np;j++)
{
if(f[j][0]==minf[0])
{
for(i=1;i<=nv;i++)
{
gbest[i][0]=x[i][j][0];
printf("\nInitial gbest[%d%d] is:%f",i,j,gbest[i][0]);
} }}
getch();
clrscr();
/**********ENTRY OF RANDOM NUMBERS*****************/
for(k=0;k<=n-1;k++)
{
for(j=1;j<=np;j++)
```

```
{
for(i=1;i<=nv;i++)
{
printf("\nEnter RC[%d%d%d] & RD[%d%d%d]",i,j,k,i,j,k);
scanf("%f%f",&RC[i][j][k],&RD[i][j][k]);
}}} */
/****PROGRAM WITH ITERATIONS STARTS HERE*********/
for(k=0;k<=n-1;k++)
{
leastminf[0]=minf[0];
minf[k+1]=999999;
for(j=1;j<=np;j++)
{
leastf[j][0]=f[j][0];
for(i=1;i<=nv;i++)
{
//
printf("\nV=%f,RC=%f,pbest=%f,x=%f,gbest=%f",v[i][j][k],RC[i][j][k],pbest[i][j
][k],x[i][j][k],gbest[i][k]);
v[i][j][k+1]=(w*v[i][j][k])+(c1*RC[i][j][k]*(pbest[i][j][k]-
x[i][j][k]))+(c2*RD[i][j][k]*(gbest[i][k]-x[i][j][k]));
x[i][j][k+1]=x[i][j][k]+v[i][j][k+1];
if(x[i][j][k+1]>Xmax[i])
x[i][j][k+1]=Xmax[i];
if(x[i][j][k+1]<Xmin[i])
x[i][j][k+1]=Xmin[i];
else
x[i][j][k+1]=x[i][j][k+1];
//printf("\nNew value of X[%d%d%d]=%f &
V[%d%d%d]=%f",i,j,k+1,x[i][j][k+1],i,j,k+1,v[i][j][k+1]);
//getch();
}
z1[j][k+1]=(38.2544/x[2][j][k+1])+(0.697/(x[4][j][k+1]*x[1][j][k+1]))+(4.18*x[3]
[j][k+1])+4.0485;
z2[j][k+1]=0.0603*(1+(2*x[3][j][k+1]/(3*x[4][j][k+1])))*pow(x[4][j][k+1],0.578
9)*pow((x[2][j][k+1]/x[1][j][k+1]),0.1578)*x[1][j][k+1];
Tave[j][k+1]=132.023*(1+(x[3][j][k+1]/x[4][j][k+1]))*pow(x[4][j][k+1],0.5925)*
pow((x[2][j][k+1]/x[1][j][k+1]),0.5925);
if(Tave[j][k+1]>0 && Tave[j][k+1]<0.254)
z3[j][k+1]=0.4587*pow(Tave[j][k+1],0.30);
if(Tave[j][k+1]>=0.254)
z3[j][k+1]=0.78667*pow(Tave[j][k+1],0.72);
Umax[j][k+1]=6.2+(1.76*pow(De,0.25)/(pow(ap,0.75)*pow(x[2][j][k+1],0.5)));
U[j][k+1]=13.8+((9.64*pow(10,-
4)*x[1][j][k+1])/(ap*x[2][j][k+1]))+(6.9*pow(10,-
3)*(2102.4*x[2][j][k+1])/(De*x[1][j][k+1]))*(Ao+((Ku*x[1][j][k+1]*Lw*aw)/(x[
```

```
2][j][k+1]*pow(De,0.5)*pow(ap,0.5))))*(x[1][j][k+1]*pow(De,0.5)/(x[2][j][k+1]*
pow(ap,0.5)));
con1[j][k+1]=Umax[j][k+1]-U[j][k+1];
WWP[j][k+1]=(Kp*ap*pow(dg,0.1315)*pow(HRC,1.4210)/(pow(De,(1.2/(VOL-
0.1067)))*pow(VOL,0.38)))*((1+(x[3][j][k+1]/x[4][j][k+1]))*pow(x[4][j][k+1],1.
4210)*pow((x[1][j][k+1]/x[2][j][k+1]),0.1579)*x[2][j][k+1]/(1+(2*x[3][j][k+1]/(3
*x[4][j][k+1])));
con2[j][k+1]=(z2[j][k+1]/WWP[j][k+1])-G;
// printf("\nZ2[%d]=%f,WWP[%d]=%f",j,z2[j][k+1],j,WWP[j][k+1]);
Kc[j][k+1]=1000*x[2][j][k+1]*fb/z2[j][k+1];
Ks[j][k+1]=1000*x[1][j][k+1]*fb/WWP[j][k+1];
MSC[j][k+1]=(1/(2*Kc[j][k+1]))*(1+(x[2][j][k+1]/(x[1][j][k+1]*G)))+(1/Ks[j][k
+1]);
con3[j][k+1]=MSC[j][k+1]-(Rem/Km);
con4[j][k+1]=Rmax-z3[j][k+1];
//
printf("\nz1=%f,con1=%f,con2=%f,con3=%f",z3[j][k+1],con1[j][k+1],con2[j][k+
1],con3[j][k+1]);
if(con2[j][k+1]<0)
pc2=0.10;  /* (Original pc2=0.065) */
else
pc2=0;
if(con4[j][k+1]<0)
pc4=2.9;
else
pc4=0;
// getch();
f[j][k+1]=w1*(z1[j][k+1]/10)-w2*(z2[j][k+1]/20)-pc2*con2[j][k+1]-
pc4*con4[j][k+1];
//  printf("\nZ1[%d]=%f,constraint2[%d]=%f,penalty =
%f",j,z1[j][k+1],j,con2[j][k+1],pc2);
//printf("\nValue of objective function is:%f",f[j][k+1]);
// getch();
if(f[j][k+1]<leastf[j][k])
leastf[j][k+1]=f[j][k+1];
else
leastf[j][k+1]=leastf[j][k];
if(f[j][k+1]<leastf[j][k])
{
for(i=1;i<=nv;i++)
{
pbest[i][j][k+1]=x[i][j][k+1];
//printf("\nPbest[%d%d%d] is:%f",i,j,k+1,pbest[i][j][k+1]);
}}
else
{
```

```
for(i=1;i<=nv;i++)
{
pbest[i][j][k+1]=pbest[i][j][k];
//printf("\nPbest[%d%d%d] is:%f",i,j,k+1,pbest[i][j][k+1]);
}}
//getch();
if(f[j][k+1]<minf[k+1])
minf[k+1]=f[j][k+1];
}
printf("\nMinimum function value=%f",minf[k+1]);
// getch();
if(minf[k+1]<leastminf[k])
leastminf[k+1]=minf[k+1];
else
leastminf[k+1]=leastminf[k];
//printf("\nLeastminf[%d]=%f & Least
minf[%d]=%f",k,leastminf[k],k+1,leastminf[k+1]);
//getch();
if(leastminf[k+1]<leastminf[k])
{
for(j=1;j<=np;j++)
{
if(f[j][k+1]==minf[k+1])
{
for(i=1;i<=nv;i++)
{
gbest[i][k+1]=x[i][j][k+1];
printf("\nGbest[%d%d] is:%f",i,j,gbest[i][k+1]);
} }
getch();
}}
else
{
for(i=1;i<=nv;i++)
{
gbest[i][k+1]=gbest[i][k];
printf("\nGbest[%d%d] is:%f",i,j,gbest[i][k+1]);
}
getch();
}
printf("\nMinimum Value obtained at the end of iteration %d =
%f",k+1,leastminf[k+1]);
getch();
}
getch();
/*******PROGRAMME FOR SIMULATION STARTS HERE**********/
```

```
/* clrscr();
initgraph(&gd,&gm,"c:\tc\bgi");
x0=200; y0=300;
setcolor(WHITE);
//circle(x0+3*60,y0-2*60,5);
circle(x0+(gbest[1][n-1]*60),y0-(gbest[2][n-1]*60),5);
getch();
for(k=0;k<=n-1;k++)
{
for(j=1;j<=np;j++)
{
for(i=1;i<=nv-1;i++)
{
setcolor(j+10);
circle(x0+(pbest[i][j][k]*60),y0-(pbest[i+1][j][k]*60),5);
line(x0+(pbest[i][j][k]*60),y0-(pbest[i+1][j][k]*60),x0+(pbest[i][j][k+1]*60),y0-
(pbest[i+1][j][k+1]*60));  delay(800);
// getch();
}}
} */
getch();
}
```

A.1.3 SA Code

```
/* PROGERAMM FOR OPTIMIZATION OF ROUGH GRINDING USING
SA*/
#include<graphics.h>
#include<stdlib.h>
#include<stdio.h>
#include<conio.h>
#include<math.h>
#include<dos.h>
void main()
{
int i,j,n,nv;
float x[5][80],sd[5],T[80],dT,RX[5][80],R[80],f[80],dz[80],pr[80];
float R1[5][80][6],k,pc1,con2[80],z1[80],con4[80],z2[80],z3[80];
float xmax[5],xmin[5];
float WWP[80],pc2,pc4,Tave[80];
/*****************************************************************/
float ap=0.05,De=355,VOL=6.99,dg=0.3,HRC=58,G=60,Kp=0.0869,Rmax=1.8;
/*****************************************************************/
clrscr();
```

```
printf("\For optimum results enter following data:");
// printf("\nNo.of variables=4");
printf("\nInitial values of variables:2000 12 0.12 0.11");
printf("\nNo.of iterations=79");
printf("\nInitial temperature and decrement value:200 0.1");
printf("\n*****************************************");
// printf("\nEnter number of variables:");
// scanf("%d",&nv);
nv=4;
for(i=1;i<=nv;i++)
{
printf("\nEnter Initial values of variable %d:",i);
scanf("%f",&x[i][1]);
/* printf("\nEnter standard deviation for variable %d:",i);
scanf("%f",&sd[i]);*/
}
xmin[1]=1000; xmin[2]=10;          xmin[3]=0.01;     xmin[4]=0.01;
xmax[1]=2023; xmax[2]=22.7;       xmax[3]=0.1370; xmax[4]=0.1370;
sd[1]=(xmax[1]-xmin[1])/6;       sd[2]=(xmax[2]-xmin[2])/6;       sd[3]=(xmax[3]-
xmin[3])/6; sd[4]=(xmax[4]-xmin[4])/6;
printf("\nEnter no.of iterations:");
scanf("%d",&n);
printf("\nEnter initial temperature and decrement value:");
scanf("%f%f",&T[1],&dT);
/*****************************************************************/
for(j=1;j<=n;j++)
{
for(i=1;i<=nv;i++)
{
RX[i][j]=((float)(rand() % 100)/100);
//printf("\nRX[%d][%d]=%f ",i,j,RX[i][j]);
//getch();
} }
for(j=1;j<=n;j++)
{
for(i=1;i<=nv;i++)
{
for(k=1;k<=5;k++)
{
R1[i][j][k]=((float)(rand() % 100)/100);
// printf("\nR1[%d][%d]=%f ",i,j,R1[i][j][k]);
}
for(k=1;k<=5;k++)
{
R1[i][j][k+1]=R1[i][j][k+1]+R1[i][j][k];
}
```

```
RX[i][j]=R1[i][j][5];
// printf("\nRX[%d][%d]=%f",i,j,RX[i][j]);
// getch();
} }
for(j=1;j<=n;j++)
{
R[j]=((float)(rand() % 100)/100);
// printf("\nR[%d]=%f",j,R[j]);
}
/*****************************************************************/
for(j=1;j<=n;j++)
{
/*****************************************************************/
z1[j]=(38.2544/x[2][j])+(0.697/(x[4][j]*x[1][j]))+(4.18*x[3][j])+4.0485;
z2[j]=0.0603*(1+(2*x[3][j]/(3*x[4][j])))*pow(x[4][j],0.5789)*pow((x[2][j]/x[1][j]
),0.1578)*x[1][j];
Tave[j]=132.023*(1+(x[3][j]/x[4][j]))*pow(x[4][j],0.5925)*pow((x[2][j]/x[1][j]),0
.5925);
if(Tave[j]>0 && Tave[j]<0.254)
z3[j]=0.4587*pow(Tave[j],0.30);
if(Tave[j]>=0.254)
z3[j]=0.78667*pow(Tave[j],0.72);
WWP[j]=(Kp*ap*pow(dg,0.1315)*pow(HRC,1.4210)/(pow(De,(1.2/(VOL-
0.1067)))*pow(VOL,0.38)))*((1+(x[3][j]/x[4][j]))*pow(x[4][j],1.4210)*pow((x[1]
[j]/x[2][j]),0.1579)*x[2][j]/(1+(2*x[3][j]/(3*x[4][j]))));
con2[j]=(z2[j]/WWP[j])-G;
con4[j]=Rmax-z3[j];
//
printf("\nz1=%f,con1=%f,con2=%f,con3=%f",z3[j],con1[j][k],con2[j],con3[j][k]);
if(con2[j]<0)
pc2=0.10;  /* (Original pc2=0.065) */
else
pc2=0;
if(con4[j]<0)
pc4=2.9;
else
pc4=0;
// getch();
f[j]=0.5*(z1[j]/10)-0.5*(z2[j]/20)-pc2*con2[j]-pc4*con4[j];
printf("\nFunction value f[%d]=%f",j,f[j]);
for(i=1;i<=nv;i++)
{
x[i][j+1]=x[i][j]+(sd[i]*(RX[i][j]-2.5));
if(x[i][j+1]>xmax[i])
x[i][j+1]=xmax[i];
if(x[i][j+1]<xmin[i])
```

```
x[i][j+1]=xmin[i];
}
z1[j+1]=(38.2544/x[2][j+1])+(0.697/(x[4][j+1]*x[1][j+1]))+(4.18*x[3][j+1])+4.04
85;
z2[j+1]=0.0603*(1+(2*x[3][j+1]/(3*x[4][j+1])))*pow(x[4][j+1],0.5789)*pow((x[
2][j+1]/x[1][j+1]),0.1578)*x[1][j+1];
Tave[j+1]=132.023*(1+(x[3][j+1]/x[4][j+1]))*pow(x[4][j+1],0.5925)*pow((x[2][j
+1]/x[1][j+1]),0.5925);
if(Tave[j+1]>0 && Tave[j+1]<0.254)
z3[j+1]=0.4587*pow(Tave[j+1],0.30);
if(Tave[j+1]>=0.254)
z3[j+1]=0.78667*pow(Tave[j+1],0.72);
WWP[j+1]=(Kp*ap*pow(dg,0.1315)*pow(HRC,1.4210)/(pow(De,(1.2/(VOL-
0.1067)))*pow(VOL,0.38)))*((1+(x[3][j+1]/x[4][j+1]))*pow(x[4][j+1],1.4210)*p
ow((x[1][j+1]/x[2][j+1]),0.1579)*x[2][j+1]/(1+(2*x[3][j+1]/(3*x[4][j+1]))));
con2[j+1]=(z2[j+1]/WWP[j+1])-G;
con4[j+1]=Rmax-z3[j+1];
//
printf("\nz1=%f,con1=%f,con2=%f,con3=%f",z3[j+1],con1[j+1][k],con2[j+1],con
3[j+1][k]);
if(con2[j+1]<0)
pc2=0.10; /* (Original pc2=0.065) */
else
pc2=0;
if(con4[j+1]<0)
pc4=2.9;
else
pc4=0;
// getch();
f[j+1]=0.5*(z1[j+1]/10)-0.5*(z2[j+1]/20)-pc2*con2[j+1]-pc4*con4[j+1];
printf("\nFunction value f[%d]=%f",j+1,f[j+1]);
getch();
dz[j]=f[j+1]-f[j];
printf("\ndz[%d] is:%f",j,dz[j]);
if(dz[j]<0)
{
for(i=1;i<=nv;i++)
{
x[i][j+1]=x[i][j+1];
}
T[j+1]=T[j]-dT*T[j];
}
else
{
pr[j]=exp(-dz[j]/T[j]);
printf("\nProbability of accepting point=%f",pr[j]);
```

```
printf("\nRandom number=%f",R[j]);
if(R[j]<pr[j])
{
for(i=1;i<=nv;i++)
{
x[i][j+1]=x[i][j];
}
T[j+1]=T[j]-dT*T[j];
}
else
{
for(i=1;i<=nv;i++)
{
x[i][j+1]=x[i][j];
}
T[j+1]=T[j];
}
}
for(i=1;i<=nv;i++)
{
printf("\nx[%d][%d]=%f",i,j+1,x[i][j+1]);
}
printf("\n\nTemperature is:%f",T[j+1]);
}
getch();
}
```

Index